MICROWAVE ELECTRONICS

I. LEBEDEV

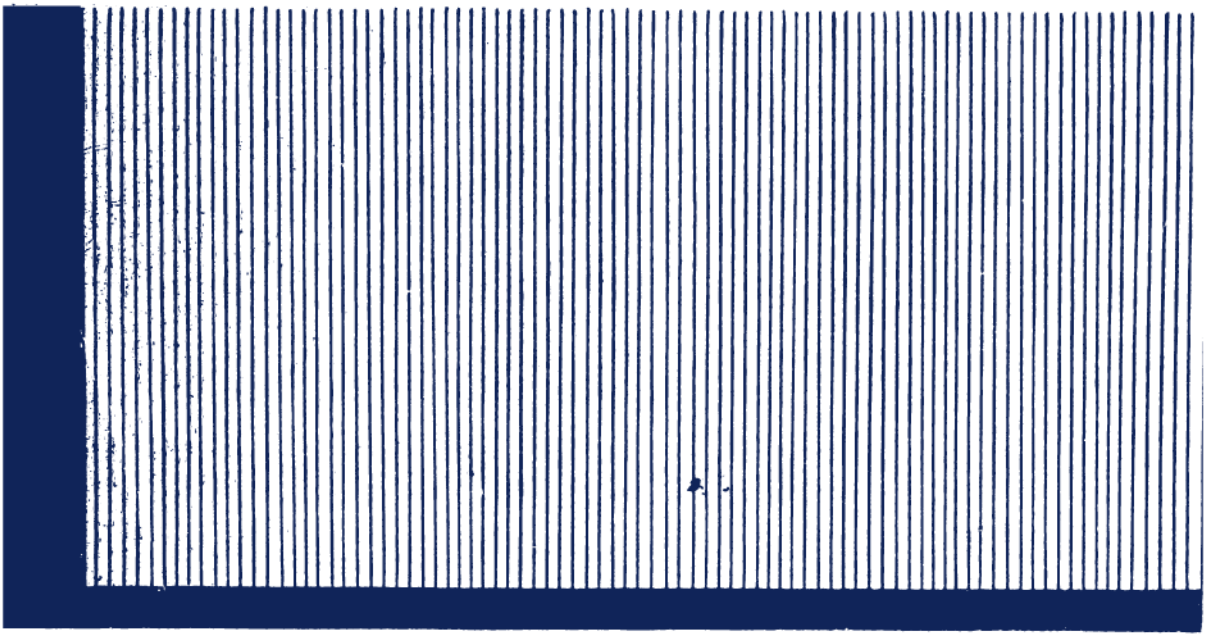

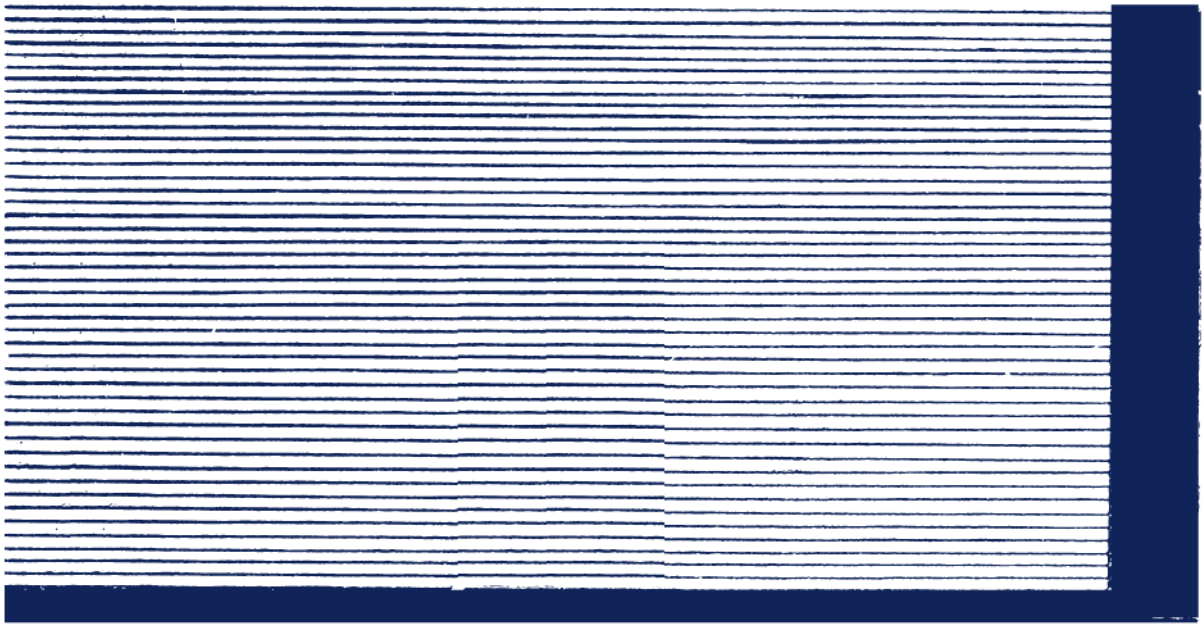

ABOUT THE AUTHOR

I. Lebedev, D. Sc. (Eng.), is professor of the Moscow Power Institute, Deputy Head of the Chair of Electron Devices. He was awarded the State Prize for his scientific and research work in the field of microwave electronics. Over 100 of his scientific papers have been published. Among these are 30 Inventor's Certificates.

ABOUT THE BOOK

This textbook is the second part of the Course in Microwave Engineering and Electronics. The book is devoted to the fundamental physics of microwave electronics and sets out the main types of modern microwave electron devices such as triodes, drift and reflex klystrons, travelling-wave tubes and backward-wave oscillators ot the O-type, oscillators and amplifiers of theM-type as well as microwave discharge devices.

The textbook is intended for the students of power, electrical and radio engineering institutes. It may also be of use to engineers and technicians working in industry and scientific research institutes.

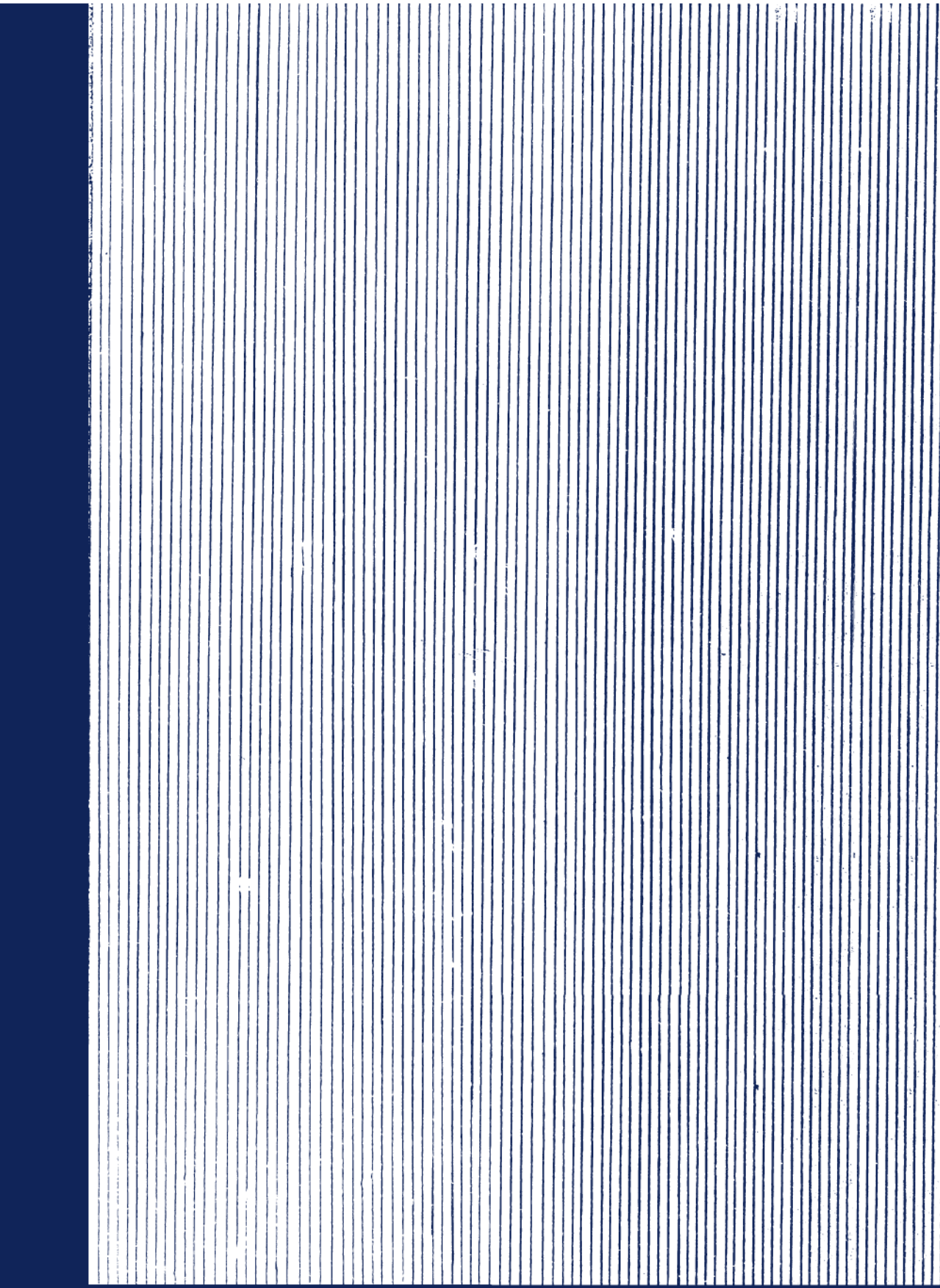

ИЗДАТЕЛЬСТВО
МИР

И. В. ЛЕБЕДЕВ

ТЕХНИКА И ПРИБОРЫ СВЧ

Под редакцией академика Н. Д. Девяткова

Издательство «Высшая школа» • Москва

MICROWAVE ELECTRONICS

I. LEBEDEV

Translated from the Russian by V. Povzner

MIR PUBLISHERS

MOSCOW

First published 1974

Revised from the 1972 Russian edition

The Greek Alphabet

Αα	Alpha	Ιι	Iota	Ρρ	Rho
Ββ	Beta	Κκ	Kappa	Σσ	Sigma
Γγ	Gamma	Λλ	Lambda	Ττ	Tau
Δδ	Delta	Μμ	Mu	Υυ	Upsilon
Εε	Epsilon	Νν	Nu	Φφ	Phi
Ζζ	Zeta	Ξξ	Xi	Χχ	Chi
Ηη	Eta	Οο	Omicron	Ψψ	Psi
Θϑ	Theta	Ππ	Pi	Ωω	Omega

На английском языке

© English translation, Mir Publishers, 1974

CONTENTS

Foreword 7

Chapter One. INTRODUCTION 9

1.1. Peculiarities of Microwave Electron Devices 9
1.2. Evolution of Microwave Generation and Amplification Techniques 10

Chapter Two. GENERAL PROBLEMS OF MICROWAVE ELECTRONICS 13

2.1. Original Concepts 13
2.2. Electron Transit Time and Transit Angle 18
2.3. Current Conduction Through Electron Devices at Microwave Frequencies. Equation of Induced Current 24
2.4. Electron Beam Energy Transfer 34
2.5. Methods of Electron Beam Control at Microwave Frequencies 47
2.6. Oscillation in Positive-Grid Triodes. Retarding-Field Oscillator 52
2.7. Admittance of a Gap Carrying an Electron Beam. Monotron and Oscillating Diode 57
2.8. Electron Beam Control by Velocity Modulation 63
2.9. Waves in Electron Beams 76

Chapter Three. GENERAL PROBLEMS OF MICROWAVE OSCILLATORS AND AMPLIFIERS 83

3.1. Equivalent Circuit of Oscillators with Resonant Oscillatory System. Electron Admittance 83
3.2. Oscillation Amplitude and Frequency in Terms of Electron Beam Conductance 86
3.3. Effects of Load on the Performance of Resonant-Type Microwave Oscillators and Amplifiers 95
3.4. Peculiarities of Performance of Microwave Devices with Non-Resonant Oscillatory Systems 107
3.5. Requirements to Microwave Oscillators and Amplifiers . . . 109
3.6. Review of Microwave Amplifier and Oscillator Types 116

Chapter Four. MICROWAVE TRIODES AND TETRODES . .

4.1. General Considerations 119
4.2. Electronic Processes Under Small-Signal Conditions 123
4.3. Operation of Microwave Triodes Under Large-Signal Conditions 127
4.4. Oscillatory Systems of Triode Oscillators and Amplifiers . . . 136
4.5. Microwave Triode Design Problems 141

4.6. Microwave Tetrodes 145
4.7. Application of Microwave Triodes and Tetrodes 146

Chapter Five. KLYSTRONS 149

5.1. General Problems 149
5.2. Kinematic Theory of Electron Bunching (Drift Method of Modulation Conversion) 151
5.3. Two-Cavity Klystron Amplifiers 163
5.4. Two-Cavity Klystron Oscillators and Frequency Multipliers 169
5.5. Multicavity Amplifier Klystrons 175
5.6. Typical Designs and Parameters of Drift Klystrons 190
5.7. Reflex Klystrons 196
5.8. Electronic and Mechanical Tuning of Reflex Klystrons . . . 212
5.9. Problems of Reflex Klystron Design 221
5.10. Application of Reflex Klystrons 226

Chapter Six. TRAVELLING-WAVE TUBES 230

6.1. General Problems. Principle of Operation of O-Type TWT 230
6.2. Small-Signal Theory of O-Type TWT Amplifier 234
6.3. Effect of Space Charge on TWT Performance 245
6.4. Parameters and Characteristics of O-Type TWT's 248
6.5. Problems of O-Type TWT Design 261
6.6. O-Type Backward-Wave Tubes 271
6.7. Designs and Parameters of Backward-Wave Tubes 282
6.8. Cascaded Amplifiers of the O-Type 285

Chapter Seven. MICROWAVE CROSSED-FIELD ELECTRON DEVICES 287

7.1. Magnetron Oscillators. General Problems 287
7.2. Electron Motion in a Magnetron Under Static Conditions 289
7.3. Properties of Multicavity Oscillatory Systems of Magnetron Oscillators 297
7.4. Electron Motion in the Interaction Space of a Magnetron Oscillator 310
7.5. Conditions of Self-Excitation in a Multicavity Magnetron 315
7.6. Magnetron Efficiency 321
7.7. Operating and Load Characteristics of Magnetrons . . . 327
7.8. Problems of Magnetron Design 331
7.9. Pulsed Operation of Magnetron Oscillators 344
7.10. Forward-Wave and Backward-Wave Tubes of the M-Type 346
7.11. M-Type Amplifiers with Emitting Negative Electrode. Platinotron 357
7.12. Oscillators and Amplifiers Utilizing Cyclotron-Frequency Resonance 371

Chapter Eight. MICROWAVE DISCHARGE DEVICES 380

8.1. Electron-Ion Plasma at Microwave Frequencies 380
8.2. TR and ATR Tubes 392
8.3. TR and ATR Tubes Design Problems 403
8.4. Other Types of Microwave Discharge Devices 412

Chapter Nine. CONCLUSION 417
Index 421

FOREWORD

The present Textbook is based on the course of lectures delivered by the author at the Moscow Power Institute. The complete course consists of two separate but interconnected parts: "Microwave Engineering" and "Microwave Electronics". The first part published in 1973 was devoted to microwave linear transmission lines, such as waveguides, resonant cavities, slow-wave systems and other elements of microwave engineering. The second part of the course deals with the physics, theory and design of microwave electron devices, such as triodes, drift and reflex klystrons, magnetrons, travelling-wave tubes, backward-wave oscillators as well as microwave discharge devices. Particular applications of the devices are only briefly explained and serve in the main for substantiating the choice of the main parameters and design of the respective devices. The book does not cover semiconductor and microwave quantum devices which are in themselves separate scientific and technical entities.

A special feature of the present book is that the first three chapters are devoted to solving general problems of microwave electron devices. Such presentation emphasizes physical fundamentals of the existing devices and should ensure a deeper insight into the operating principles and theory of the microwave devices still to appear. The description of the main types of devices is according to the classification established in practice. It is quite obvious that even in the adopted presentation devices which have many features in common are not always united in the same class.

The author assumes that the reader is familiar not only with the fundamentals of microwave engineering given in the first part of the course and the fundamentals of electrical and radio engineering, but also with the principles underlying conventional electron devices. It would also be useful for the student to familiarize himself with the general principles of radar technique.

The present textbook in which the most necessary material is systematized will be of assistance to the students majoring in electron devices. The book will also be useful for students engaged in similar fields as well as for the young engineers who wish to be specialists in this particular branch of engineering.

CHAPTER ONE
INTRODUCTION

1.1. Peculiarities of Microwave Electron Devices

Electron devices designed to operate at microwave frequencies hold a special position among modern electron and gas-filled tubes. This may be largely attributed to the fact that the microwave frequency range is employed in radar, radio navigation, communications and in many other fields of science and engineering. In addition, in some respects microwave electronics is essentially different from the "ordinary" electronics of conventional (low-frequency) tubes. These differences are first of all due to the specific properties of microwaves, treated in "Microwave Engineering"[1].

The first important feature of microwave electronics is that the *electron transit time in microwave devices is comparable with the period of oscillations.* In conventional electron tubes the electron transit time is of the order of 10^{-8}-10^{-9} s and therefore becomes commensurate with the period of oscillations at frequencies of 10^{8}-10^{9} Hz, i.e. at metric and decimetric waves. With centimetric and millimetric waves the electron transit time may exceed the oscillation period by an order of magnitude and more. At microwave frequencies the electron tube ceases to be a peculiar "inertialess relay", which is in essence the principle of tube operation at lower frequencies. Electron inertia effects greatly disturb or hamper detection, amplification or generation of oscillations, whereas these functions are successfully performed by electron tubes at comparatively low frequencies.

The second main difficulty encountered at higher operating frequencies is associated with "circuitry" problems. To increase the resonant frequency of a circuit the inductance and capacitance of its elements have to be reduced; as a result, beginning with metric wavelengths the *lead inductances and interelectrode capacitances of tubes become comparable with the parameters of the external circuit.* Any further increase in operating frequency, therefore, requires a corresponding reduction of the interelectrode capacitances and lead inductances of the tube.

---

[1] A textbook by the same author, Moscow, MIR Publishers, 1973.

The situation is further aggravated as the *wavelength becomes comparable with the size of the external circuit* and with the size of the tube electrodes and leads. The "classical" tube is designed to be connected to a circuit with lumped constants. The essential drawbacks inherent in such circuits make it imperative to review the design of electron devices operating within the decimetric and, especially, centimetric and millimetric wave bands.

One of the possible ways to overcome these difficulties is miniaturization and microminiaturization of electron tubes: fabrication of tubes with closer interelectrode spacings, smaller geometrical dimensions of the electrodes and shorter leads. This permits reduction of the electron transit time between the tube electrodes, on the one hand, and reduction of the interelectrode capacitances and lead inductances, on the other hand, as well as diminution of the radiation from the circuit incorporating the electron tube. A further reduction of the inductances can be obtained by the use of electrode leads in the form of metal cylinders or discs.

Miniaturization and the use of efficient tube designs make it possible to extend the useful range of low-power electron tubes up to the centimetric wave band without altering their operating principles. The potentialities of this trend have not yet been completely exhausted. However, to extend the use of low-power devices into the wave band below 2-3 cm and to develop high-power devices operating in the entire microwave range it is necessary to change radically the operating principles of microwave devices. In microwave electron devices, the physical problems due to electron inertia are closely interwoven with the equally important problems of electrodynamics of microwave oscillatory systems.

It is the characteristic features of microwave electronics that enabled the development of a modern microwave device which, as a rule, incorporates an oscillatory system and other circuit elements which formerly pertained to the domain of classical radio engineering. A separate treatment of the "tube" proper and the "circuit" becomes quite impossible at microwave frequencies. The development of microwave electron devices necessitates, therefore, a thorough knowledge of the physics and technique of electron devices as well as the knowledge of waveguides, resonant cavities and other elements of microwave devices.

1.2. Evolution of Microwave Generation and Amplification Techniques

When mastering any new frequency range the basic problem is to provide signal amplification and generation. This problem becomes still more serious at microwave frequencies.

In essence, the history of microwave electronics is the evolution of microwave amplification and generation techniques. Other problems, such as signal detection, modulation, etc., were also given due attention, but the problem of producing and amplifying microwave signals remains the main one up to the present time.

Modern radio electronics is mainly concerned with *coherent* oscillations, the coherence concept at microwave frequencies being basically the same as in general physics. By definition, coherence is the congruous course in time and space of several processes. Several oscillations are considered to be coherent if they feature a constant relative phase shift (and are, therefore, of the same frequency) during a time interval considered adequate for observation.

Coherence can be evaluated in terms of *coherent length*, i.e. the maximum difference in path lengths of two signals produced by splitting the output of one source, required for interference effects to become noticeable. A perfectly coherent source produces continuous-wave (c.w.) oscillations of a single constant frequency and thus features an infinite coherent length[1]. Other methods of evaluating the degree of coherence of several signals are also available.

The main way of obtaining coherent microwave oscillations is to pass streams of free electrons through high vacuum. Gas-filled devices have not yet found any significant application as microwave signal sources, except as sources of microwave noise (non-coherent) oscillations; they are also used as switching devices.

Up to the third decade of this century, research and development of microwave devices were confined mainly to the laboratory stage. Rapid progress in microwave electronics has begun with the advent of several basically new devices, *klystrons* and *magnetrons*, and somewhat later, *travelling-wave* and *backward-wave* tubes. Substantial progress was also achieved in the development of more common tube types, such as triodes and tetrodes. In large measure this progress was due to the contributions of the Soviet scientists N. Devyatkov, M. Grekhova, Yu. Katzman, M. Neiman, S. Gvozdover, V. Kovalenko, S. Zusmanovsky and others.

The rapid progress in the development of microwave devices continues at the present time. The number of radically new devices is steadily increased. The requirements for high output powers and a more stable oscillation frequency, as well as other performance parameters of amplifiers and oscillators, become more and more stringent. The field of application of microwave devices becomes increasingly wider: along with radio location and communications, microwave devices (amplifiers and oscillators) have encroached upon such fields as television, radio astronomy, radio control, nucleonics,

---

[1] In case of an ordinary (non-coherent) light source the coherent length does not exceed some 1-3 m.

radio spectroscopy, industrial electronics, biology, medicine and other branches of science and engineering. Space research has opened up extremely wide possibilities for microwave electronics.

Research in the molecular physics and the solid-state physics has demonstrated that the travel of free electrons through vacuum is not the only possible source of microwave oscillations. Due to the works of the Soviet scientists V. Fabrikant, A. Prokhorov and N. Basov, as well as scientists of other countries, *quantum-mechanical oscillators* and *amplifiers* have been created and are now achieving a constantly widening field of application; these devices operate at definite (discrete) frequencies corresponding to changes in the energy levels of atoms and molecules. Great progress has been achieved in the development of *parametric amplifiers* utilizing semiconductor diodes with non-linear capacitance. Transistors capable of operating in the decimetric and even centimetric wave bands have been developed and are being improved. Finally, low-power microwave oscillators and amplifiers utilizing the negative dynamic resistance of certain types of semiconductor diodes have gained recognition as devices capable of competing with electron devices in some cases and are now being rapidly refined.

Even this brief review of progress in the development of non-electronic devices indicates the appearance of several new and independent branches of science and engineering. Nevertheless, electron devices remain unrivalled in the microwave range, excepting, perhaps, some cases of low-power oscillators and low-noise amplifiers. For this reason and because of the great difference in the physical principles of their operation, semiconductor and quantum devices will not be dealt with in the present textbook.

Characteristic of the present state of the art and, in particular, of the techniques of microwave generation and amplification, is a great variety of available electron device types and classes. In the present textbook, therefore, the discussion of definite devices will be preceded by the examination of physical phenomena underlying microwave electronics and the engineering methods of treating the performance of various types of microwave oscillators and amplifiers.

CHAPTER TWO
GENERAL PROBLEMS OF MICROWAVE ELECTRONICS

2.1. Original Concepts

The basic laws governing microwave electronics cannot differ from the general laws of physics, electrical engineering and "ordinary" low-frequency electronics. However, when dealing with microwave electron devices the validity of certain simplifying assumptions adopted when analysing "conventional" electron devices has to be questioned. As will be shown later, many of the familiar concepts used in low-frequency electronics are not in fact generally applicable and are valid only when the electron transit time is negligible as compared to the period of oscillations. The fact that the operating wavelength is commensurable with the geometrical dimensions of the tube and the associated circuit may be of fundamental importance in certain cases.

2.1a. Maxwell's Equations

The most general approach to the electrodynamics at all frequencies (low, high and microwave) is to apply the electromagnetic field theory and Maxwell's equations. From this point of view, the basic equations derived in the analysis of transmission lines and oscillatory systems of the microwave frequency range require only to be supplemented by taking into account the presence of free electric charges (electrons, more rarely, ions) to become applicable to microwave electron devices.

The system of Maxwell's equations for the vectors of electric field intensity $\overline{E}$, magnetic field intensity $\overline{H}$, electric displacement $\overline{D}$ and magnetic induction $\overline{B}$, with the moving free electric charges taken into account, can be presented as follows (here and later, if not otherwise specified, the mksa system of units is employed):

$$\operatorname{curl} \overline{H} = \overline{J}_{tot} = \sigma \overline{E} + \frac{\partial \overline{D}}{\partial t} + \rho \overline{v} \tag{2.1}$$

$$\operatorname{curl} \overline{E} = -\frac{\partial \overline{B}}{\partial t} \tag{2.2}$$

$$\operatorname{div} \overline{D} = \rho \tag{2.3}$$

$$\operatorname{div} \overline{B} = 0 \tag{2.4}$$

where

$$\overline{B} = \mu\mu_0 \overline{H} \tag{2.5}$$

$$\overline{D} = \varepsilon\varepsilon_0 \overline{E} \tag{2.6}$$

Here, as usual, ε, μ and σ denote the relative permittivity, permeability and specific conductivity of the medium, respectively. Since in case of electron devices the working medium is vacuum or rarefied gas, the relative permittivity and permeability may be taken equal to unity and the specific conductivity equal to zero. The permittivity and permeability of vacuum are

$$\varepsilon_0 \cong 0.886 \cdot 10^{-11} \text{A} \cdot \text{s/V} \cdot \text{m}; \quad \mu_0 \cong 1.256 \cdot 10^{-6} \text{V} \cdot \text{s/A} \cdot \text{m} \tag{2.7}$$

The quantities ρ and $\overline{v}$ in equations (2.1) and (2.3) denote the electric charge density and the speed of travel of these free charges, respectively. The product $\rho\overline{v}$ determines the density of the convection current $\overline{J}_{con}$

$$\overline{J}_{con} = \rho\overline{v} \tag{2.8}$$

and is a measure of the time rate at which electric charge is transported through a unit surface normal to the vector of velocity $\overline{v}$. The total current density $\overline{J}_{tot}$ in (2.1) in any cross section at a zero conductivity of the medium is the sum of convection and displacement current densities.

2.1b. Electron Motion Equation

The system of Maxwell's equations is inadequate to obtain solutions to problems involving the presence of free electric charges because the velocity $\overline{v}$ is a function not only of the initial conditions, but of the electric and magnetic field intensities $\overline{E}$ and $\overline{H}$ at each point where the charge under examination is found.

The dependence of the velocity of a charged particle on the electric and magnetic field intensities is described by the equation of particle motion, which, with the Lorentz force taken into account, for the general case is

$$\frac{d(m\overline{v})}{dt} = \overline{F} = q\{\overline{E} + [\overline{v}\overline{B}]\} \tag{2.9}$$

where q is the charge of the particle, assumed, to be a point one in the present case, m is the particle mass and $\overline{F}$ is the force acting on the particle.

If the speed of the charged particle is considerably lower than the velocity of light in free space (c), equation (2.9) can be written as

$$m_0 \frac{d\bar{v}}{dt} = q\{\bar{E} + [\bar{v}\bar{B}]\} \tag{2.10}$$

where m_0 is the rest mass (mass at zero velocity).

In the most common case, when the charged particle under examination is a free electron, q should be taken equal to $-e$. The electron charge and rest mass are

$$e \cong 1.6 \cdot 10^{-19} \text{ coulomb and } m_0 \cong 9.11 \cdot 10^{-31} \text{ kg} \tag{2.11}$$

These values are widely used in actual electron tube design[1].

The equation of electron motion is often applied in the analysis and design of various microwave electron devices. The electric field intensity $\bar{E}$ and magnetic induction $\bar{B}$ in equation (2.10) may both be time-invariable, as well as both feature a variable component. In most cases, however, it is practically sufficient to allow only for the constant values of these quantities and the variable component of the electric field, neglecting the radio-frequency component of the magnetic field. This statement can be illustrated by the example of a section of a transmission line carrying a transverse electromagnetic wave (TEM propagation mode). For the sake of simplicity, the time-invariable fields will be assumed to be zero. In case of vacuum the force acting upon a free electron may be described as

$$\bar{F} = -e\bar{E} - e\mu_0 [\bar{v}\bar{H}] = \bar{F}_E + \bar{F}_H$$

where $\bar{F}_E$ and $\bar{F}_H$ are components of this force, which are due to the action of the electric and the magnetic field, respectively. The maximum value of the Lorentz force $|\bar{F}_H|$ is $e\mu_0 |\bar{v}|\,|H|$, hence

$$\frac{|\bar{F}_H|}{|\bar{F}_E|} \leqslant \mu_0 |\bar{v}| \frac{|\bar{H}|}{|\bar{E}|}$$

The ratio $|\bar{H}|/|\bar{E}|$ is the reciprocal of the characteristic impedance, which in the case under examination is $Z_{TEM} = (\mu_0/\varepsilon_0)^{1/2}$. Substituting this relation and taking into account that $1/\sqrt{\varepsilon_0\mu_0} = c$ yields

$$\frac{|\bar{F}_H|}{|\bar{F}_E|} \leqslant \frac{v}{c}$$

A similar result will be obtained in other cases, as well, for instance, when an electron moves in a waveguide or a resonant cavity.

Thus, if the electron velocity is much less than the velocity of light in free space, the effect of the radio-frequency magnetic field

[1] More precise values are $1.60091 \cdot 10^{-19}$ coulomb and $9.1082 \cdot 10^{-31}$ kg.

as compared to the effect of the radio-frequency electric field can be disregarded. Later it will be demonstrated that the condition of small electron velocities as compared to the velocity of light in free space is satisfied in most modern electron devices designed for the microwave frequency band. However, even in those cases when these velocities are comparable, the action of the radio-frequency magnetic field, as a rule, may be neglected, because it is the electric field that is mainly present in the interaction space. Combining Maxwell's equations (2.1) to (2.4) with the equation of motion (2.9) is attended with certain inherent contradictions. Indeed, equation (2.9) describes the motion of a discrete (point) electric charge q, while the field equations examine an electric charge of a definite density ρ, which is continuously spreading throughout the volume (as is a smoothly flowing liquid). Another contradiction consists in neglecting the quantum nature of energy exchange between an electric charge and the electromagnetic field. Both these circumstances, however, are of no practical significance for the case of microwave devices. The quantum effects have to be taken into account only at considerably higher frequencies, when the quantum of energy becomes comparable with the energy of thermal motion. The discrete nature of electrons is of some practical importance only in the examination of fluctuation effects (noise).

2.1c. Equations of Continuity and Electron Velocity in a Potential Electric Field

Besides the basic equations (2.1) to (2.4) and (2.9) discussed above, two other relations, the so-called equation of continuity and the equation describing the speed of a charged particle moving in a potential electric field, are also of major importance for the analysis of electronic processes.

The equation of continuity follows directly from the Maxwell equations. The density of the total current

$$\bar{J}_{tot} = \rho\bar{v} + \partial\bar{D}/\partial t \tag{2.12}$$

By equation (2.1) the total current is always of a curl nature and therefore

$$\operatorname{div} \bar{J}_{tot} = \operatorname{div} \operatorname{curl} \bar{H} = 0$$

or

$$\operatorname{div}(\rho\bar{v}) + \frac{\partial}{\partial t} \operatorname{div} \bar{D} = 0$$

The equation of continuity is obtained by substitution of the latter relation into (2.3)

$$\operatorname{div}(\rho\bar{v}) = -\partial\rho/\partial t \tag{2.13}$$

Equation (2.13) is especially useful for the analysis of wave processes in electron beams, as in forward-wave and backward-wave tubes. The physical meaning of this equation is the law of charge conservation.

The velocity acquired by an electron in travelling through a potential electric field can be determined proceeding from the law of energy conservation

$$eV = m_0 v^2/2; \qquad v = (2eV/m_0)^{1/2} \tag{2.14}$$

where V is the difference in electric potential between the space point of interest and the point at which the electron velocity is zero.

Substituting the magnitudes of e and m_0 into (2.14) we obtain the design equation

$$v\ (\text{m/s}) \cong 5.95 \cdot 10^5 V^{1/2}\ (\text{V}) \tag{2.15}$$

Formally, equations (2.14) and (2.15) express that it is possible to obtain unlimitedly high electron velocities with an unlimited increase of the accelerating voltage V. This physical contradiction is easily eliminated by taking into account relativistic effects. In the general case, the kinetic energy W_k of an electron should be determined from the condition

$$W_k = mc^2 - m_0 c^2$$

instead of the implied $W_k = m_0 v^2/2$; here $m = \dfrac{m_0}{\sqrt{1-(v/c)^2}}$

Equating the initial potential energy eV to this kinetic energy yields

$$v = c\,\frac{\sqrt{1+\dfrac{2m_0c^2}{eV}}}{1+\dfrac{m_0c^2}{eV}} \tag{2.16}$$

Equation (2.16) may also be written as

$$v = \sqrt{\frac{2eV}{m}}\,\frac{\sqrt{1+\dfrac{eV}{2m_0c^2}}}{1+\dfrac{eV}{m_0c^2}} \tag{2.17}$$

If the accelerating voltage V is not great so that the condition $eV \ll m_0c^2$ is satisfied, the velocity of the charged particle is much lower than the velocity of light and equation (2.17) may be reduced to the more familiar equation (2.14). When using this equation as a design equation for electron devices, the relativistic correction factor for voltages up to about scores of kilovolts can be neglected. As can easily be found, at a voltage of, say, 50 kV, the error in electron velocity calculation by equation (2.14) is less than 8 per cent compared to the results obtained from the more rigorous equa-

tion (2.17). At accelerating voltages of the order of hundreds of kilovolts, however, as is the case with certain types of super-high power klystrons, applying equation (2.14) or (2.15) may result not only in quantitative errors, but even lead to qualitatively erroneous conclusions (v can be found to exceed c!).

It is also very important to point out that equations (2.14) to (2.17) do not allow for a possible change in the magnitude of V during the time of charge travel and therefore, strictly speaking, are applicable to the case of a static electric field, or — approximately—to the case when the time of charge travel is considerably less than the period of voltage variation. When the transit time and the variation period are comparable, the change in voltage and the finite time of particle transit have to be taken into account; this problem is treated in more detail later.

The system of basic equations of microwave electronics discussed above can be solved provided the boundary and initial conditions are preset. Besides the usual conditions describing the electric and magnetic fields at the interface between two media, these conditions include initial electron velocities at fixed surfaces and at specified moments of time. Here lies one of the radical differences between the low-frequency and the microwave electronics: in low-frequency electronics, only the space distribution of electrons is taken into consideration, whereas in microwave electronics, the time-space distribution should equally be considered.

2.2. Electron Transit Time and Transit Angle

2.2a. Electron Transit Time

A very important parameter characterizing microwave electron devices is the *time of electron transit* τ between two specified electrodes of a tube, for instance, between the cathode and anode of a diode, the cathode and grid of a triode, or between two grids in a multigrid tube or klystron, and so forth.

The transit time of an electron, as of any material particle, is determined by integrating a corresponding equation of particle motion. In case when the field intensities $\overline{E}$ and $\overline{H}$ are known and the initial conditions can be determined beforehand, integrating equation (2.10) over any specified time interval yields the electron velocity v at any point in space. Further calculation of the transit time can be reduced to integration of the following form

$$\tau = \int_{s_1}^{s_2} ds/v$$

where s_1 and s_2 are the coordinates of the electrodes of interest,

Another obvious method of determining the transit time is to perform a second integration of equation (2.10) and thus derive the equation of electron motion $s = f(t)$. Substitution of the coordinates of electrodes s_1 and s_2 into this relation gives the transit time τ as the difference between the corresponding time moments t_2 and t_1

$$\tau = t_2 - t_1$$

Consider, as an example, the simplest planar diode whose electrodes are formed by two infinitely extending parallel surfaces *1* and *2* spaced at a distance d (Fig. 2.1). As will be shown later, parallel-plane systems are most widely used in the design of many types of modern microwave devices.

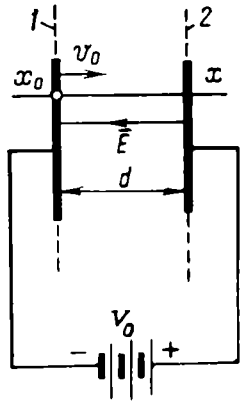

Fig. 2.1. Planar diode

The voltage V_0 will be assumed invariable in time, and the external magnetic field will be taken zero. Relativistic effects will be neglected, assuming $v \ll c$.

In the absence of space charge, the equation of electron motion will then acquire the simplest possible form

$$m\frac{d^2x}{dt^2} = -e\left(-\frac{V_0}{d}\right)$$

(here and later, for the sake of simplicity, the zero subscript at m, denoting that this is a rest mass, will be omitted).

The initial conditions to be used in integration are: at plane $x = x_0$ and at time $t = t_0$, the electron velocity $v = v_0$. Then

$$v = v_0 + \frac{eV_0}{md}(t - t_0) \tag{2.18}$$

$$x = x_0 + v_0(t - t_0) + \frac{eV_0}{md}\frac{(t-t_0)^2}{2} \tag{2.19}$$

The time of electron transit will be determined by the second of the above mentioned methods. Substituting the coordinate of the second electrode $x = x_0 + d$ into equation (2.19) we obtain

$$\frac{eV_0}{md}\frac{\tau^2}{2} + v_0\tau = d$$

With $v_0 = 0$ (which corresponds approximately to the conditions in a conventional diode with a heated cathode), the following simple equation describes the electron transit time under saturation conditions (temperature-limited operation)

$$\tau = d(2m/eV_0)^{1/2} \tag{2.20}$$

Another case of interest for microwave electronics is when $V_0 = 0$ but the initial electron velocity v_0 is different from zero. Such a situation is encountered, for instance, in klystrons, where the electrons enter an interaction gap and are carried through it by their inertia. The electron transit time through such a gap is

$$\tau = d/v_0 \tag{2.21}$$

As mentioned in the Introduction, electron transit time through most of the conventional tubes is about 10^{-8} to 10^{-9} s. Indeed, if the cathode-anode gap of a planar diode is, for instance, 2 mm and the anode voltage is 100 V, then, in accordance with (2.20), the transit time under temperature-limited operation will be $0.68 \cdot 10^{-9}$ s.

The space charge in the interelectrode gap modifies the electron transit time by reducing the accelerating field in the vicinity of the cathode. The transit time of an electron in a planar diode with a heated cathode under space-charge-limited operation can be shown to be 1.5 times higher than in the same diode under saturation conditions and to be governed by the relation

$$\tau = 1.5d\,(2m/eV_0)^{1/2} \tag{2.22}$$

Now consider the transit time in case of a harmonic voltage $v = V_m \sin \omega t$ applied to the electrodes forming a parallel-plane gap (at present the case of a non-sinusoidal voltage is of no practical interest for the microwave frequency range). Disregarding for the time being the wave processes that can take place in the interelectrode gap, i.e. neglecting the possible phase lag of the radio-frequency field, it is possible to write the initial equation of electron motion in the following form (for the sake of simplicity initial electron velocity v_0 and space charge are again not taken into account):

$$m \frac{d^2x}{dt^2} = \frac{eV_m}{d} \sin \omega t$$

The first integration yields

$$\frac{dx}{dt} = \frac{eV_m}{\omega md} (\cos \omega t_0 - \cos \omega t)$$

where t_0 as before denotes the instant of time the electron enters the interaction gap. After the second integration we obtain

$$x = x_0 + \frac{eV_m}{\omega^2 md} [(\omega t - \omega t_0) \cos \omega t_0 - \sin \omega t + \sin \omega t_0] \tag{2.23}$$

As in the preceding case, it is possible to use this equation to determine the electron transit time from the conditions that $x = x_0 + d$ and $\tau = t - t_0$. Without going into the calculation we can note that the transit time is now different for electrons entering

the gap at different instants of time t_0. This circumstance makes it impossible to introduce the concept of a "true" transit time to characterize the gap under discussion at a specified amplitude of a radio-frequency voltage with no direct voltage applied to the same electrodes.

In the general case, when a radio-frequency voltage is superimposed onto a direct voltage across the gap, i.e. when $v = V_0 + V_m \sin \omega t$, the time of electron transit through the gap at comparable values of V_0 and V_m will also depend on the initial time t_0. However, if $V_m \ll V_0$, the small variations of electron transit time due to the radio-frequency component can often be neglected and the "undisturbed" transit time considered as a fair approximation of the electron transit time.

2.2b. Electron Transit Angle

The absolute value of the electron transit time cannot adequately describe electron inertia effects. As mentioned in the Introduction, the behaviour of an electron device depends on whether the electron transit time is comparable with the period of oscillations or not. Therefore, more important is the *ratio* of the electron transit time τ to the period of oscillations T.

In the analysis of inertia effects in electron devices the concept of a *transit angle* θ is generally employed. This angle is proportional to the ratio $\frac{\tau}{T}$ and is defined as

$$\theta = 2\pi\tau/T \tag{2.24}$$

Since the period of oscillations T in this equation and the angular frequency of oscillations are related by $\omega = 2\pi/T$, equation (2.24) can be presented as

$$\theta = \omega\tau \tag{2.25}$$

The transit angle as defined by equations (2.24) and (2.25) is given in radians, but may also be expressed in degrees

$$\theta = 360°\tau/T \tag{2.26}$$

In a physical sense, the transit angle is a measure of the change in phase of the voltage applied between the electrodes during the time of electron transit through the interelectrode gap.

The transit angle may be easily determined from the known electron transit time and operating frequency. Thus, in case of the parallel-plane electrode structure treated above and an infinitesimal radio-frequency voltage superimposed onto a considerable constant voltage, i.e. at $V_0 \gg V_m$, the undisturbed transit angle in the absence of space charge according to equations (2.20) and (2.25) is equal to

$$\theta = \omega d\,(2m/eV_0)^{1/2} \tag{2.27}$$

The undisturbed transit angle by equations (2.21) and (2.25) can be determined as

$$\theta = \omega d/v_0 \tag{2.28}$$

if the interelectrode gap, across which only a small radio-frequency voltage is applied, is pierced by a stream of electrons of high initial velocities v_0. This latter relation is valid only when

$$V_m \ll mv_0^2/2e$$

i.e. when the amplitude of the radio-frequency voltage is far less than voltage V_0 corresponding to electron velocities v_0.

Relations (2.24) to (2.28) are extensively used as design equations for various types of microwave electron devices when *small-signal* conditions are examined. As will be shown later, the small-signal theory is the most universally adopted and simple method of treating the performance of microwave electron devices.

As an example, calculate the transit angle through a planar diode operating under the conditions mentioned above ($V_0 = 100$ V, $d = 2$ mm). In this case the electron transit time is $0.68 \cdot 10^{-9}$ s. At a frequency of 1 MHz (300-m wavelength) the transit angle according to equation (2.26) is $\theta = 0.24°$, while the same diode operating at a frequency of 1 GHz (30-cm wavelength) features a transit angle of 245°.

Thus, if at a frequency of 1 MHz the voltage may be considered as practically constant during the time of electron travel through the interelectrode space, at a frequency of 1 GHz electrons emitted from the cathode, for instance, during the positive halfwave will reach the anode at a retarding r.f. field; in this case electron inertia effects will be quite pronounced.

For the reasons mentioned above, it is impossible to introduce the concept of a transit angle which would unambiguously define electron motion under the action of commensurate direct and radio-frequency voltage components. However, in case $V_0 = 0$ and only a radio-frequency voltage of amplitude V_m is applied across the diode, it is conventionally adopted to use in calculations the value of the transit angle through the same gap at the constant voltage numerically equal to the amplitude of the radio-frequency voltage in the absence of a space charge.

The transit angle thus defined is a *fictitious* angle; it should be considered as a certain generalized parameter with the dimension of a transit angle, which can be used to interrelate the frequency, the amplitude of the voltage across the gap and the spacing between the electrodes of interest.

The fictitious transit angle is denoted by α to distinguish it from the actual transit angle θ corresponding to the small-signal conditions. By analogy with equation (2.27) and in accordance with the defini-

tion given above, the fictitious transit angle can be described as

$$\alpha = \omega d\,(2m/eV_m)^{1/2} \tag{2.29}$$

The conventional nature of the fictitious transit angle should be emphasized; in no case can this fictitious transit angle be considered as a somewhat "averaged" value of the actual transit angle. The fictitious transit angle concept is rarely applied in the design of microwave electron devices.

2.2c. *Motion Diagrams*

The motion of electrons can be illustrated with the aid of graphs representing electron coordinates as functions of time, the so-called *space-time* or *motion diagrams.*

Figure 2.2*a* presents a family of parabolic curves which describe the motion of electrons in a planar diode in the absence of a magnetic

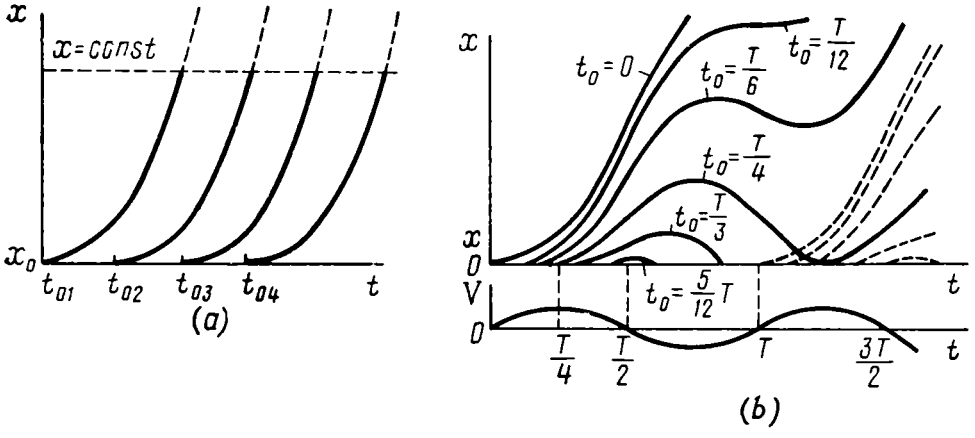

Fig. 2.2. Electron motion in a planar diode
(*a*) in the absence of a radio-frequency voltage ($V_0 > 0$); (*b*) at $V_m > 0$, $V_0 = 0$

field and space charge at zero initial velocity v_0, plotted in accordance with equation (2.19). Only a direct voltage V_0 is applied to the diode. The curves corresponding to different instants of time t_{01}, t_{02}, etc., are identical in pattern, this meaning that electrons emitted from the cathode at equal time intervals will arrive at the anode or at any specified plane x = const also at equal time intervals.

The motion diagram illustrating electron motion under the action of a radio-frequency voltage (in the absence of any direct voltage) can be plotted according to equation (2.23); such a motion diagram is presented in Fig. 2.2*b*, with $v_0 = 0$ and the space charge not taken into account. As can be noted, not all electrons emitted from the cathode arrive at the anode (the anode can be represented by

a straight line $x = \text{const}$). At a great spacing between the electrodes d, or, what is the same, a great fictitious transit angle α, up to half of the emitted electrons return to the cathode, where they dissipate their kinetic energy. Some of the electrons finally arrive at the anode after having made several "swings" in the interelectrode gap.

The motion diagram allows of drawing some other important conclusions. If the curves representing the motion of various electrons are plotted for a sufficiently great number of electrons leaving the cathode at regular time intervals, the density of the curves intersecting a straight line $x = \text{const}$ may be used to evaluate the instantaneous convection current density at a specified distance from the cathode, for instance, at the anode. Tangentials to the curves of a motion diagram are indicative of the instantaneous electron velocities and thus of the kinetic energy of any electron at any specified point in the interelectrode space and at any specified instant of time. The magnitudes of the instantaneous and mean power dissipated by the electrons on the anode and cathode can also be evaluated.

The motion diagram method is widely used in the treatment of transit-time effects in microwave electron devices, including devices employing both electric and magnetic fields.

2.3. Current Conduction Through Electron Devices at Microwave Frequencies. Equation of Induced Current

2.3a. Current Induced by the Motion of Free Charges in a Parallel-Plane Gap

The problem of the interrelation between electron motion inside a tube and the current carried by the external circuit forms the basis of modern electronics. Although the effects taking place at low, high and microwave frequencies have in principle much in common, the physical concepts of current adopted in "low-frequency" electronics prove inadequate for application at microwave frequencies.

At low frequencies, the instantaneous current in the external circuit of a tube electrode is identified with the convection current, i.e. with the arrival of electrons at this electrode. If the common capacitive current, which is independent of free electrons, is disregarded, the current in the external circuit of an electrode, from this point of view, should always be zero if the electrode under treatment does not intercept any electrons. This seemingly obvious statement is generally confirmed at low frequencies, but is at variance with the experimental findings at microwave frequencies.

We shall examine, for simplicity, a parallel-plane vacuum gap (Fig. 2.3) with the external circuit including a source of d.c. or

a.c. voltage V; the internal resistance of this voltage source is assumed to be zero.

In the absence of free electrons, the electrodes of this gap, as the plates of any capacitor, carry surface charges $+Q_0$ and $-Q_0$, which for any instant of time are determined by the Gauss theorem as

$$Q_0 = \varepsilon_0 E_0 A$$

where $E_0 = V/d$, d is the spacing between electrodes and A is their area.

When a charge $+q$ is introduced into the interelectrode gap, surface charges $-q_1$ and $-q_2$ are induced in the electrodes in accordance

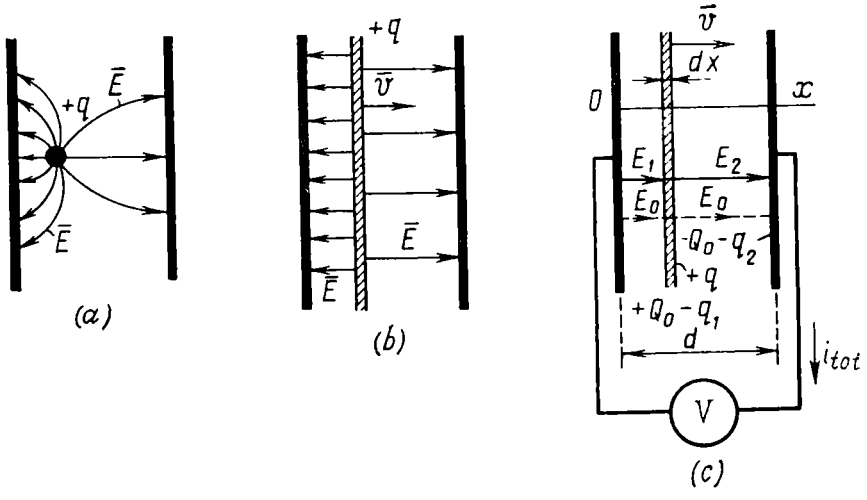

Fig. 2.3. Current induction in the external circuit due to the movement of charge $+q$ in a parallel-plane gap

with the law of electrostatic induction; these charges and the original charge $+q$ are interrelated by the equation of charge conservation

$$q - q_1 - q_2 = 0$$

The pattern of the electric field produced by a point charge or a thin sheet of charge is qualitatively illustrated in Fig. 2.3*a* and *b*. This field is superimposed onto the electric field E_0 present in the gap in the absence of free charge. The field intensities to the left and to the right from the sheet of charge (Fig. 2.3*c*) are

$$E_1 = +(+Q_0 - q_1)/\varepsilon_0 A;\ E_2 = -(-Q_0 - q_2)/\varepsilon_0 A$$

In these relations the signs (polarity) are determined by the direction of the electric lines of force relative to the electrodes of the gap.

Since a voltage V is applied across this gap,

$$E_1 x + E_2 (d - x) = V = E_0 d$$

where x is the independent variable characterizing the coordinate of the sheet of charge, whose thickness is taken to be dx. Expressing E_1, E_2 and E_0 in terms of the corresponding charges, we obtain

$$q_2 (d - x) - q_1 x = 0$$

and applying the equation of charge conservation, interrelating the magnitudes q, q_1 and q_2, we obtain

$$q_2 = qx/d; \; q_1 = q (1 - x/d)$$

Thus, the total instantaneous charge on each of the electrodes is

$$Q_1 = Q_0 - q (1 - x/d); \quad Q_2 = -Q_0 - qx/d$$

The total instantaneous current measured in the external circuit can now be determined as

$$i_{tot} = +\frac{dQ_1}{dt} = -\frac{dQ_2}{dt}; \qquad i_{tot} = \frac{dQ_0}{dt} + \frac{q}{d}\frac{dx}{dt}$$

or

$$i_{tot} = \frac{dQ_0}{dt} + \frac{qv}{d} \tag{2.30}$$

Here v denotes the velocity of charge transfer.

Consequently, the current in the external circuit is made up of the common capacitive current through the gap (dQ_0/dt) and a component produced by the moving electric charges. The physical meaning of this second component can be easily seen from the pattern of electric lines of force emerging from a point charge and terminating at one of the electrodes (Fig. 2.3*a*). The number of these lines of force varies as the charge moves; as a result, the electric charges are transferred from one electrode to the other via the external circuit connecting these electrodes.

A current produced in an external circuit by a moving electric charge is known as the *imposed* or *induced current*. In the case of a parallel-plane gap the magnitude of this current by equation (2.30) is

$$i_{ind} = qv/d \tag{2.31}$$

Equation (2.31) will be extensively used in the subsequent discussions and is the simplest form of a more general equation of imposed current, namely the so-called Ramo equation.

2.3b. Derivation of the General Equation of Induced Current

We shall examine a comparatively simple method of deriving the general Ramo equation applicable to a point charge moving relative to any number of electrodes of arbitrary configuration

and interconnected in an arbitrary manner. Suppose that the charge magnitude $+q$ and the vector of its instantaneous velocity $\bar{v}$ are specified. To determine the current in the circuit of any electrode of interest, say A in Fig. 2.4, imagine voltage V is applied to this electrode relative to all the other electrodes of the structure (including the ground terminal). Denoting the electric field intensity at the place where the charge q is located at the specified time, as $\bar{E}$, we deduce the work carried out by the field in displacing the charge by a distance $d\bar{r}$ during a time interval dt as the scalar product of the vector of force $\bar{F}$ affecting the charge by the vector $d\bar{r}$

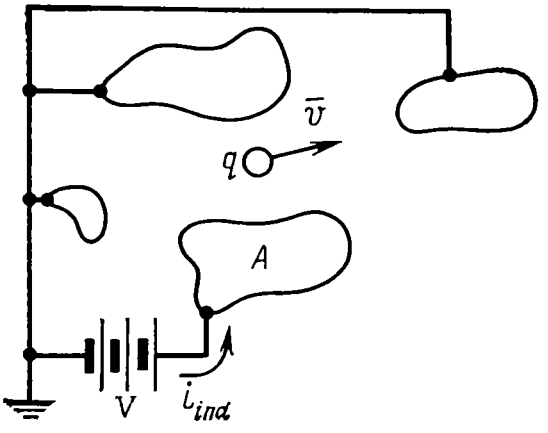

Fig. 2.4. To the derivation of the general equation for induced current

$$dW = \bar{F}\, d\bar{r} = q\bar{E}d\bar{r}$$

On the other hand, the energy drawn from the source of voltage V during the time interval dt is obviously related to the induced instantaneous current through the external circuit as

$$dW = i_{ind}V\, dt$$

According to the law of energy conservation

$$i_{ind}V\, dt = q\bar{E}\, d\bar{r}; \qquad i_{ind} = q\frac{\bar{E}}{V}\frac{d\bar{r}}{dt}$$

Since $d\bar{r}/dt$ is the velocity vector $\bar{v}$ of the charge under examination,

$$i_{ind} = q\frac{\bar{E}}{V}\bar{v} \tag{2.32}$$

Equation (2.32) derived by considering the energy relations in the system, indicates the most general approach to the calculation of induced currents. The magnitude $\bar{E}/V$ in this equation has the dimension of reciprocal length and corresponds to the electric field intensity at the point of charge location at a specified instant of time, provided a unit voltage $V = 1$ is applied to the electrode of interest relative to all the other electrodes. Denoting $\bar{E}/V$ as $\bar{E}_1$, equation (2.32) may be written as

$$i_{ind} = q\bar{E}_1\bar{v} \tag{2.32a}$$

Thus, to calculate the induced current by equation (2.32a) it is necessary to determine the scalar product of the vector of electric field intensity $\overline{E}_1$ by the velocity vector $\overline{v}$, keeping in mind that the magnitude of $\overline{v}$ is a function of the fields actually present in the system and in the general case can be independent of $\overline{E}_1$. When the induced current is at a maximum these vectors are collinear, i.e. the charge under consideration moves along a line of electric force. In case of n charges moving in the system, the total effect is the sum of individual effects, so that the currents induced by all charges are summed up

$$i_{ind} = \sum_n q_n \overline{E}_{1n} \overline{v}_n \tag{2.33}$$

Note, that equations (2.32) and (2.33) are equally applicable to the case of a space charge. The present deduction cannot, however, allow for the effects associated with lagging potentials, as well as for relativistic effects.

Equation (2.32), as can easily be seen, in case of a parallel-plane gap reduces to (2.31). Indeed, in this case $E = V/d$ and therefore $E_1 = 1/d$. Since the vectors $\overline{E}_1$ and $\overline{v}$ are collinear $i_{ind} = q\frac{1}{d}v$, which coincides with (2.31).

The above technique of deriving the Ramo equation is simple as regards the mathematics involved, which is typical of all calculations based on the law of energy conservation. However, the process of current induction is not as fully disclosed as in 2.3*a*.

It should be emphasized, that equations (2.32), (2.33) are applicable at any frequency and may therefore be used to determine the current in the external circuits of any electron or gas-filled device, not necessarily of microwave devices only.

2.3c. Waveform of Induced Current Pulses

The significance of deductions made in discussing the induced-current equation can be more easily appreciated if we consider the waveform of current pulses induced in the circuit of a planar diode by the movement of point charges (electrons) through the diode.

According to equations (2.31) and (2.32), the induced current can be calculated if the velocity of the moving electric charge is known beforehand. In the planar diode gap under consideration the electron velocity in the absence of space charge is determined by (2.18) as

$$v = v_0 + \frac{eV_0}{md}(t - t_0)$$

where t_0 is the instant of time when the electron is at the plane of the first electrode and begins to move through the interelectrode space, and v_0 is its initial velocity at this plane. Substitution of velocity v and charge $q = -e$ into equation (2.31) yields

$$i_{ind} = -\left[\frac{ev_0}{d} + \frac{e^2V_0}{md^2}(t - t_0)\right] \qquad (2.34)$$

Figure 2.5*a* illustrates the waveform of the induced current pulse plotted according to (2.34). In the absence of charge in the gap the induced current is zero. At the instant of time $t = t_0$ the absolute value of the induced current increases drastically up to ev_0/d, and after this the current becomes a linear function of time. Finally, at the moment the electron arrives at the second electrode the induced current abruptly falls off to zero.

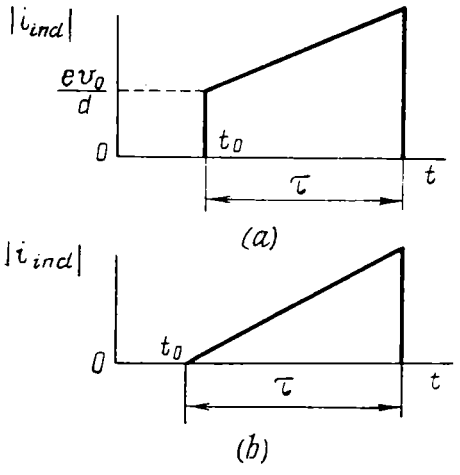

Fig. 2.5. Pattern of induced current pulses, produced by the motion of an electron in a parallel-plane gap free of space charge
(*a*) at $v_0 \neq 0$; (*b*) at $v_0 = 0$

This picture can be observed when current is induced by an electron moving in the grid-anode gap of a triode or tetrode. However, if the first electrode is the cathode, emitting electrons with zero initial velocities, the pulses of induced current are of a triangular waveform (Fig. 2.5*b*). It is just such pulses that make up the current in the external circuit of any diode, provided the device operates under saturation (temperature-limited) condition[1]. Finally, electrons passing with a constant velocity through the gap between two grids produce pulses of induced current of a rectangular waveform. As can easily be seen, in any case the total area of a single pulse produced by a solitary electron, i.e., the total charge transferred by an electron from one electrode to the other, is exactly equal to the electron charge e.

The induced current pulses produced by individual electrons are of a very short duration, which is equal to the time of electron transit τ through the gap under consideration. When the period of oscillations of the applied voltage is long enough, it can, as a first approximation, be considered that the current pulse duration coin-

[1] In case of a space-charge-limited current the pulses of current induced in a planar diode become 1.5 times longer and cease to be strictly triangular in waveform as a result of a reduced intensity of the electric field at the surface of the cathode.

cides with the time of electron impact on the anode. Actually, however, the induced current *disappears* just at this moment, rather than appears. Interception of electrons by an electrode is not a necessary condition of current conduction in the circuit of this electrode; if the second electrode is made "transparent" to electrons but "non-transparent" to the electric field, i.e., is a perfect grid, current induction will take place just the same. This conclusion is of major importance and will be examined in more detail in Section 2.4*c*.

The above argumentation makes it possible to conclude that the total current in the external circuit of *any* electron device is composed of the following two main components:

(1) induced current, which is due to the movement of all electric charges present in the interelectrode space;

(2) displacement current, which is due to a "cold" capacitance between the electrodes and does not depend on the presence of free electric charges.

A third component of the total current corresponds to conduction current (leakage current) and in principle is not essential to the present discussion.

It should be emphasized that the instantaneous current in any electrode circuit is in no way identical to the *convection* current of this electrode. Convection current can never be considered as a component of the total electrode current; it is only a factor determining the appearance of induced current which is actually measured in the external circuit.

As will be demonstrated later, in one particular case only, namely in the absence of an a.c. component or when the transit angle is negligibly small, the current in the external circuit is numerically exactly equal to the convection current appearing at the specified electrode. This circumstance is responsible for the convenient, though strictly speaking inaccurate, conception of the identity of convection current to the current flowing in the external circuit, as adopted in "classical" (low-frequency) electronics. This is the reason why low-frequency electronics does not discuss or even mention the presence of convection and induced currents, though the effects of current induction take place at all frequencies, no matter how low or high.

Thus, the total current flowing in the *external* circuit of a device is always an induced current and is the result of free electric charges moving through the interelectrode gap. This total current, however, has to be of one and the same magnitude in any section of a series circuit, including the space *inside* the gap. Returning once again to Fig. 2.3, it can be noted that inside the gap, at sections where there is no charge at a given instant of time, the total current is represented by the displacement current which is numerically equal to the induced current. Correspondingly, at the place of a

moving charge at a given instant of time, the total current is exactly equal to the instantaneous convection current.

The fact that the total current is constant at any section of a series circuit determines the direction of the induced current. When the current is produced by the moving electrons (negative charges q), the induced current is in the *opposite* direction to the electron movement through the gap.

2.3d. Current Induced by a Density-Modulated Electron Beam Passing Through a Parallel-Plane Gap

Let us examine the process of current induction in the external circuit of a two-grid gap, as presented in Fig. 2.6. In contrast to the case illustrated in Figs 2.3 and 2.4, a *continuous stream* of electrons will be discussed here, and not the transfer of discrete charges q; the electron stream (beam) will be assumed to feature a variable volume density ρ at constant electron velocities v_0.

Suppose the beam density at the input grid varies in accordance with a harmonic law

$$\rho = \rho_0 + \rho_1 \sin \omega t$$

where ρ_0 is the charge density of an unmodulated beam, ρ_1 is the amplitude of the alternating component of charge density.

The convection current through a fixed plane

$$i_{con} = \rho A v_0 = I_0 + I_m \sin \omega t \quad (2.35)$$

where $I_0 = \rho_0 A v_0$, $I_m = \rho_1 A v_0$ and A is the transverse section area of the beam.

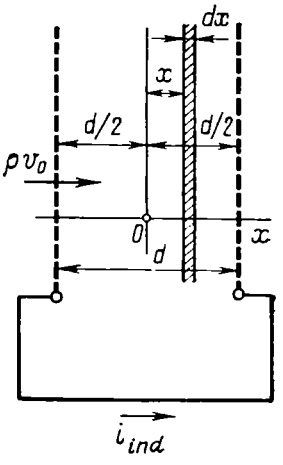

Fig. 2.6. A short-circuited parallel-plane gap carrying a density-modulated electron beam

Applying the general equation of induced current, we can determine the current i_{ind} flowing in the external circuit of this gap, when the grids are short-circuited. Figure 2.6 shows the direction of induced current with the negative sign of electron charge taken into account.

The origin of the x axis can be set at the middle of the gap under consideration. Denoting the instant of time when an elementary sheet of charge passes through the middle of the gap as t_0, we deduce the charge carried in this sheet to be $dq = i_{con}\, dt$, where $dt = dx/v_0$ (i_{con} is the convection current by definition); dx is the thickness of this elementary sheet of charge shown as a shaded area in Fig. 2.6.

Applying equation (2.31) yields the induced current di_{ind} in the external circuit due to the movement of charge dq through the gap

$$di_{ind} = dq \frac{v_0}{d} = i_{con} \frac{dx}{d} \quad (2.36)$$

Electron velocities inside the gap are assumed to be the same as at the gap input, this being obviously valid only in case of an external circuit of zero impedance, corresponding to the absence of an electric field inside the gap.

The total current induced in the external circuit can be determined by integrating the above equation over the entire width of the gap. Substituting equation (2.35) into (2.36) and rearranging results in

$$i_{ind} = \int_{d/2}^{+d/2} \{I_0 + I_m \sin(\omega t_0 + \omega x/v_0)\} \frac{dx}{d} =$$

$$= I_0 + I_m \sin \omega t_0 \frac{\sin \frac{\omega d}{2v_0}}{\frac{\omega d}{2v_0}}$$

The electron transit angle through this gap is $\theta = \omega d/v_0$. We shall denote

$$M = \frac{\sin(\theta/2)}{\theta/2} \tag{2.37}$$

In its final form, the current induced by a density-modulated electron beam, with (2.37) taken into account, will be

$$i_{ind} = I_0 + MI_m \sin \omega t_0 \tag{2.38}$$

The factor M in equation (2.38), defined by (2.37), is usually termed the *gap factor* or *coupling coefficient* and is a measure of the efficiency of electron beam interaction with the electric field inside a gap. The dependence of the gap factor M on the electron transit angle θ is illustrated in Fig. 2.7.

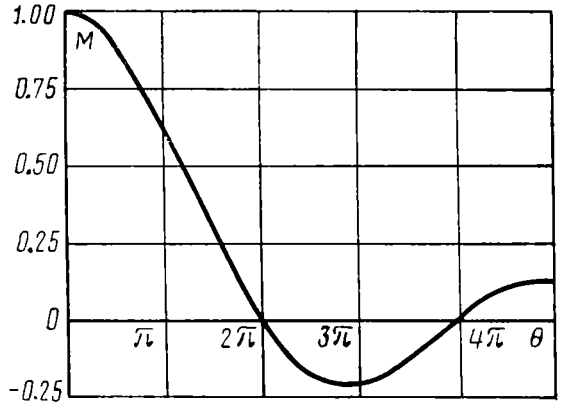

Fig. 2.7. Coupling coefficient of a parallel-plane gap as a function of electron transit angle

At negligibly small transit angles, the gap factor M approaches unity and the induced current turns out to be numerically equal to the convection current through the gap. Indeed, if $\theta \to 0$ equation (2.38) reduces to (2.35). However, an increase in the transit angle results in a reduced amplitude MI_m of the induced current, as follows from (2.38). At $\theta = 2\pi$ the a.c. component of the induced current turns to zero despite the fact that the convection current through the gap remains constant and is, as before, described by equation (2.35).

The gap factor or coupling coefficient M plays an important part in the theory of microwave devices and defines the efficiency of current induction in a gap. The less the transit angle, the larger the amplitude of induced current, which in the extreme case may become equal to that of the convection current. It now becomes more clear why low-frequency electronics can practically disregard the principal difference between the convection and induced currents.

One more conclusion can be drawn from equation (2.38). A parallel-plane gap characterized by a finite magnitude of the transit angle, from the viewpoint of current induction, may be represented by an equivalent gap of zero length placed at the middle of the actual gap, provided the amplitude of the a.c. component of the convection current is reduced by a factor of M; in this case the modulated electron beam can be considered as a current generator driving the gap.

The convection current is often actually of a non-sinusoidal character. In this case the function should be expanded into a harmonic series

$$i_{con} = I_0 + \sum A_n \sin(n\omega t) + \\ + \sum B_n \cos(n\omega t) \qquad (2.39)$$

and equations (2.38) and (2.37) applied to the current harmonic of interest. In the general case the waveforms of convection and induced currents are different because the gap factor M is different for different harmonics.

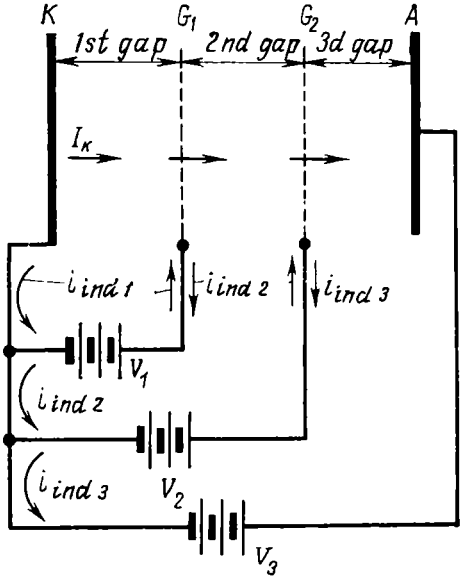

Fig. 2.8. Induced currents in a multielectrode electron device

According to equation (2.38) the d.c. component of the induced current I_0 is independent of the transit angle θ and always equal to the d.c. component of the convection current. Note, however, that the current of any particular electrode, that can actually be measured in its external circuit, should be examined with due regard of the currents of adjacent electrodes. As an example, a system consisting of a thermionic cathode K, two plane grids G_1 and G_2, and anode A (collector) is illustrated in Fig. 2.8; this system can be imagined as made up of three parallel-plane two-electrode gaps, and the above statement holds completely for each of them (for the sake of simplicity, the grids are assumed to be perfect screens for electric fields).

If the electrons are not intercepted by the grids G_1 and G_2, the d.c. components of the induced currents $i_{ind\ 1}$, $i_{ind\ 2}$ and $i_{ind\ 3}$ in the

circuits of all the three gaps should be identical and equal to the direct convection current from the cathode I_k, irrespective of the magnitudes of the d.c. voltages V_1 and V_2 and the presence of alternating voltage and current components.

In the grid leads the induced currents flow in opposite directions; thus the instantaneous values of currents of the first and second grids, respectively, are:

$$i_{g1} = i_{ind\ 1} - i_{ind\ 2}$$

$$i_{g2} = i_{ind\ 2} - i_{ind\ 3}$$

The d.c. component of grid currents turns out to be zero, which is in absolute agreement with the intuitive conceptions adopted in low-frequency electronics. The a.c. components of induced currents, however, do not cancel each other in the general case; this effect is of prime importance, for instance, to the performance of microwave triodes (refer to Section 2.5*a*).

2.4. Electron Beam Energy Transfer

The ultimate purpose of most microwave devices (including amplifiers and oscillators) is the conversion of the energy of a d.c. supply into microwave oscillations. Therefore, the mechanism underlying the process of energy abstraction from an electron beam and the conditions of maximum energy conversion are of prime interest.

2.4a. Energy Abstraction of a Solitary Electron

Once again, consider a plane gap formed between two grids; this gap is supposed to be pierced by a solitary electron or a very short electron bunch.

In the case when the grids are short-circuited by an external circuit there can obviously be no power in this circuit. The presence of an ohmic resistance R in this circuit, however, will change the situation (Fig. 2.9*a*), namely, the resistance dissipates power which is due to the flow of induced current through the external circuit.

Since induced current flows only during electron movement, this resistance will dissipate power only till the electron strikes the second grid or leaves the gap. If the electron is intercepted by the second grid, this in no way interferes with the process of energy abstraction; the only additional effect will be grid heating due to the electron striking its surface.

The mechanism of energy abstraction from a solitary electron can be explained as follows. The induced current passing through the resistor R causes a voltage drop across it with a polarity indicat-

ed in Fig. 2.9*a*. This voltage drop tends to make the potential of the electrode, toward which the electron in question moves, negative. At the instant the electron (or electron bunch) passes through the gap, a *retarding electric field* is set up in this gap. As the electron moves through the retarding field, its velocity decreases, resulting in that the electron kinetic energy at the gap output becomes lower than at the gap input. The difference between these values of electron kinetic energy is exactly the energy transferred into the external circuit and dissipated in resistor R. The rest of the electron kinetic energy is dissipated at the second electrode or at another electrode (collector) located behind the gap.

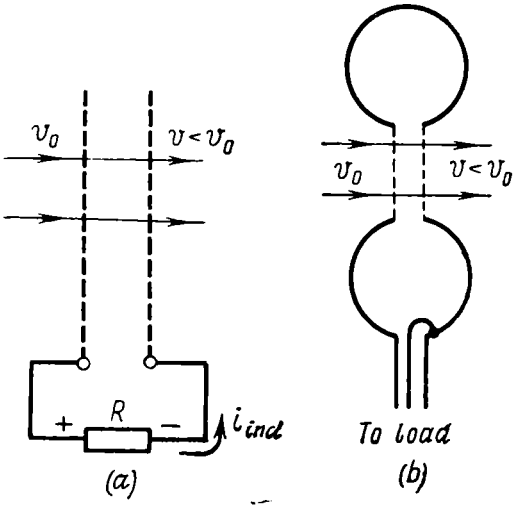

Fig. 2.9. Taking energy off electrons in a parallel-plane gap. The "+" and "—" signs denote the polarity of voltage developed across resistor R by the induced current

The highest magnitude of induced current is obtained when vectors $\overline{E}$ and $\overline{v}$ are collinear. Therefore, in the general case, the maximum energy can be taken off an electron provided it moves along the lines of force of the electric field.

The above argumentation enables one to draw certain important conclusions about the nature of electron interaction with the electric field of a gap. *Energy transfer into an external circuit takes place during electron movement in a longitudinal retarding electric field.* Energy dissipation due to electron bombardment of the electrodes, forming part of the main microwave circuit, is not essential. In principle, therefore, it is possible that functions of tube electrodes be shared between different electrodes, namely, electrodes which catch microwave energy from electrons and pass it to external circuits and electrodes specially designed for collecting the "exhausted" electrons and dissipating the unused part of their kinetic energy. These simple statements, from the point of view of general physics, are the basis for designing the various types of electron devices, that are to be discussed in this textbook.

At microwave frequencies, the ohmic resistor R of Fig. 2.9*a* may be replaced by a matched transmission line. The input impedance of a lossless matched transmission line is purely ohmic in nature and equal to the wave (characteristic) impedance Z_c. Another way of providing an ohmic load at microwave frequencies is the use of a resonant cavity. Indeed, any resonant cavity features

a purely ohmic impedance (equal to the reciprocal of its equivalent conductance G) at the discrete frequencies of natural resonance. An obvious solution is to make the gap, excited by an electron beam, integral with a resonant cavity, as shown in Fig. 2.9*b* for the case of a toroidal cavity. In accordance with the principles outlined above, electrons should be passed through the capacitive part of the cavity, where the radio-frequency electric field is predominantly concentrated.

2.4b. Taking the Energy of a Modulated Electron Beam. Perfect Waveform of Convection Current

A solitary electron or an electron bunch passed through the gap of a resonant cavity (Fig. 2.9*b*) will cause shock excitation of this cavity, and the oscillations thus developed will be damped oscillations. A density-modulated electron beam, i.e. periodic electron bunches, fed into the cavity will compensate for the power loss in the cavity and produce continuous oscillations under steady-state conditions. In this case, as before, the condition of energy transfer from the electron beam to the cavity is that each subsequent electron bunch passes through a retarding field in the gap. It follows, therefore, that *maximum energy will be taken of the electron beam when the resonant frequency of the cavity is equal to the recurrence rate (frequency) of electron bunches.*

For now, we shall restrict ourselves to the case when the electron transit time is considerably less than the period of oscillations. The d.c. electric field in the gap will be assumed to be zero. Now consider qualitatively the optimum waveform of electron bunches, or, in other words, whatkind of time dependence of convection current corresponds to the maximum oscillatory power in the load. Initial electron velocities will be assumed constant and equal to v_0.

Figure 2.10 (*a* and *b*) illustrates graphs of a microwave voltage applied to the gap of a resonant cavity and of a convection current of arbitrary but periodic waveform at the resonant frequency of the cavity equal to the recurrence rate of electron bunches in the beam. The wave pattern is assumed to be sinusoidal, this corresponding to oscillations at a single oscillation mode in a high-Q cavity.

By Ohm's law, the amplitude of the voltage V_m is a function of the induced current amplitude and the magnitude of resistance R "terminating" the gap (Fig. 2.9*a*). At infinitesimal gap widths, however, V_m cannot exceed the constant voltage V_0 which corresponds to electron velocities at the gap input. Indeed, in the opposite case the part of the electrons that enter the gap at a maximum retarding field would not be able to pass through the gap and be repelled. As a result part of the energy stored in the cavity will be expended and thus the amplitude of V_m decreased. In the extreme case, when

$V_m = V_0$, electrons passing through the gap under a maximum retarding field give up their energy completely, and have to stop at the plane of the second grid.

In order to ensure high efficiency it is necessary that the number of electrons crossing the gap during the accelerating halfwave of the applied voltage be much less than during the retarding halfwave,

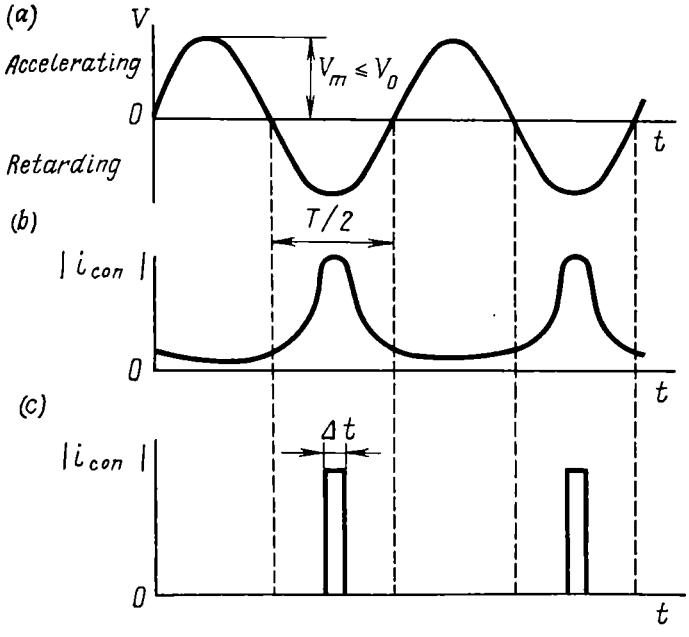

Fig. 2.10. To the problem of optimum convection current waveform, at which the greatest amount of energy is taken off the electron beam

as shown in Fig. 2.10*b*. Furthermore,the electrons should rather pass through the gap when the retarding field is at a maximum. Therefore, it is preferable that an electron beam compressed into bunches of short duration and rectangular waveform be fed through a gap at the instants the retarding field is maximal (Fig. 2.10*c*). During the time intervals between pulses the convection current must be zero.

When the duration of current pulses is much less than the oscillation half-cycle (i.e., when $\Delta t \ll T/2$), the electric field across the gap can be considered as almost constant during the time of electron bunch transit. This means that at $V_m = V_0$ all the kinetic energy carried by the electrons will be completely used up and converted into the energy of microwave oscillations. The efficiency of an electron device in this case (without regard for dissipative loss in the oscillatory system) approximates 100 per cent. This perfect waveform of convection current pulses is described mathematically by the Dirac delta-function.

The period of radio-frequency oscillations can be a multiple of the recurrence rate of electron bunches. This means that convection current pulses (Fig. 2.10*c*) will pass through the gap not during each half-cycle of the retarding field, but will always give up their kinetic energy. The efficiency in this case will also approximate the ideal 100 per cent. These conditions correspond to the operation of a perfect *frequency multiplier*, as distinct from the operation of a perfect amplifier or oscillator.

In practice the ideal waveform of convection current pulses shown in Fig. 2.10*c* cannot be realized. Nevertheless, one of the major problems in microwave electronics is to provide the shortest possible electron bunches of a sharply defined waveform.

To meet the condition that $\Delta t \ll T/2$ it is essential to ensure that the geometrical length of each electron bunch in the direction of beam movement be much less than half the wavelength in free space, even if v_0 approaches c. This requirement imposes considerable restrictions on the development of oscillators and amplifiers for the shortwave part of the microwave range.

It should be noted that the requirement of providing short pulses of convection current to attain high efficiency values is valid for considerably lower frequencies as well. In particular, this condition accounts for the high efficiency of class *C* amplifiers, as well as oscillators used under conditions of a small operating angle. The simplified methods of low-frequency analysis do not, however, provide an adequate notion of the physical effects involved.

2.4c. Use of Resonant Oscillatory Systems to Couple Out the Energy of an Electron Beam

In conventional electron devices designed for use at comparatively low frequencies, abstraction of the energy from electrons and dissipation of the excessive kinetic energy of the electron beam are both the functions of one and the same electrode, the anode. The structure of the anode imposes limits on increasing the operating frequency and output power, as can easily be noticed by examining conventional tubes, triodes in particular. Electrode dimensions have to be reduced with increasing operation frequencies, and this inevitably results in the increased specific power dissipation aggravated by a drop of device efficiency at higher operating frequencies. As a result, the supply power has to be drastically reduced and one has to be content with a very low level of output power. From this point of view, the anode of a conventional tube, which functions both as a high-frequency electrode and an electron collector, is far from being a perfect output assembly.

At microwave frequencies the same functions can be successfully performed by three electrodes, namely a gap with two grids, forming

part of a resonant cavity, and a collector placed behind this gap, as illustrated in Fig. 2.11*a*. In the simplest case, both the grids of the gap and the collector may be kept at the same d.c. voltage; the collector can be completely screened from the action of radio-frequency fields and need not have any microwave connection with the gap, because its only purpose is to gather the "used up" electrons after they have emerged from the gap. On the other hand, the gap

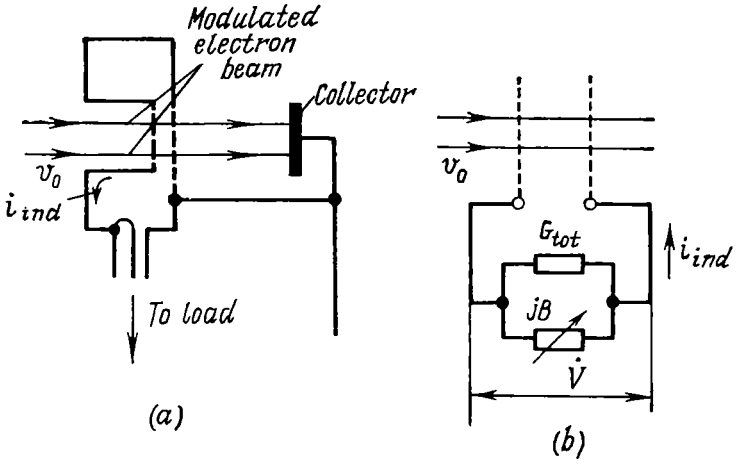

Fig. 2.11. Resonant cavity for coupling out the energy of a density-modulated electron beam and the equivalent circuit

is designed only to "catch" the microwave energy without noticeable interception of the electron beam. This makes the thermal operating conditions of the gap grids more favourable, thus enabling a further increase in the device power level.

The equivalent circuit of a gap incorporated into a resonant cavity excited at one oscillation mode, is presented in Fig. 2.11*b*. In this circuit, the conductance G_{tot} includes both the equivalent conductance of the cavity itself and the conductance of the cavity load, as related to the section of the gap. Around the resonant frequency the cavity susceptance B is a linear function of frequency and is determined by the magnitude of the loaded Q. When the cavity is tuned exactly to the frequency of the induced current, $B = 0$.

The induced current flows along the interior surface of the cavity walls and in the general case can be of a highly non-sinusoidal pattern, because it is a function of the waveform of electron bunches. Despite this, only one harmonic of the induced current need be considered if a resonant cavity is employed, namely the harmonic with a frequency f which is near to the cavity resonant frequency f_0. Energy transfer will take place just at this frequency, the cavity presenting a short to all other harmonics.

Tuning of the resonant cavity will not affect the frequency of oscillations transported into the load, provided the recurrence rate of electron bunches through the gap remains unaltered. The only effect of cavity retuning in this case will be a change in the amplitude of oscillations inside the cavity, and therefore in the microwave output power. The maximum output power can be obtained on condition that $B = 0$. If the cavity is tunable in a wide range of frequencies, another maximum of output power will be observed when the resonant frequency f_0 is raised to a value nearly equal to twice the recurrence rate of electron bunches. The output frequency will be abruptly twice the recurrence rate of electron bunches, and so on. This effect underlies *the frequency multiplication* principle.

The total cavity conductance G_{tot} required for maximum energy transfer from the electron beam can be evaluated proceeding from the following considerations. At an infinitely narrow gap the voltage amplitude V_m across the gap is equal to V_0, if the electron bunches have completely given up their energy, as demonstrated above. The induced current amplitude $I_{ind.m}$ depends on the waveform of convection current and is directly proportional to the d.c. component I_0. Theoretically, the maximum obtainable $I_{ind.\ m}$ is $2I_0$, this being readily confirmed by expanding a rectangular waveform into the Fourier series and assuming $\frac{\Delta t}{T} \to 0$[1].

It will be shown later that in actual electron tubes the maximum value of induced current amplitude, obtainable with density-modulated electron beams, is about (1.0-1.5) I_0. Assuming for simplicity $I_{ind.\ m} = I_0$, the total conductance of the loaded cavity should be

$$G_{tot} = \frac{I_{ind.\ m}}{V_m} \approx \frac{I_0}{V_0} = G_0 \tag{2.40}$$

where G_0 is the d.c. conductance of the electron beam.

Equation (2.40) is sometimes interpreted as the necessity of *matching* the conductances (or resistances) of the electron beam and oscillatory system, though the term is taken here in another, narrower sense than it is used in connection with transmission lines.

Condition (2.40) can be used to determine more stringent requirements that the output oscillatory systems of microwave electron devices should meet. Thus, for instance, at $V_0 = 1$ kV and $I_0 = 50$ mA the conductance G_{tot} should be of the order of $5 \cdot 10^{-5}$ mho,

[1] The same conclusion can be more obvious if we compare the expressions for microwave power P, delivered by the electron beam to the load, and for d.c. power P_0 drawn by the beam from the source of accelerating voltage. Evidently, $P = 0.5\ V_m I_{ind.m}$ and $P_0 = I_0 V_0$. Hence, by the law of energy conservation, in the case of 100 per cent efficiency and with $V_m = V_0$, $I_{ind.m} = 2I_0$.

or in other words, the dynamic resistance of the oscillatory system (at resonance) should be about 20 kohms. Such values cannot be obtained in the microwave range through the use of circuits with lumped constants, so that the necessity of employing resonant cavities is ever more obvious.

For efficient energy transfer, the coupling coefficient has to be made as high as possible, so as to exclude a considerable reduction of the induced current amplitude as compared to the amplitude of the convection current (refer to Section 2.3*d*). Electron transit angles through the gap should not approximately exceed π and in any case should be less than 2π. For this reason most of the electron devices equipped with resonant cavities are conventionally classified

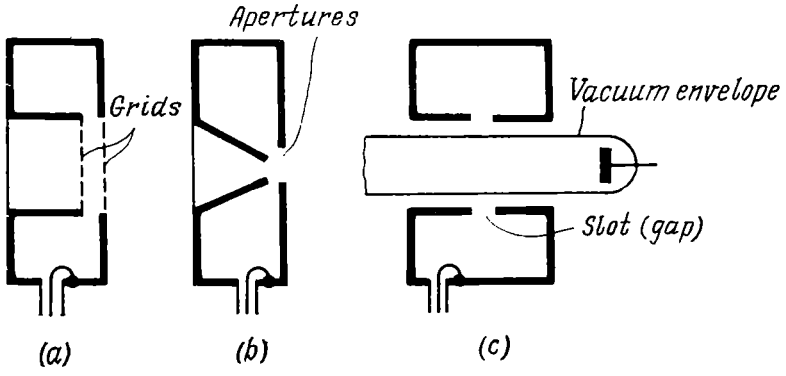

Fig. 2.12. Forms of catcher cavity

among devices with *short-term interaction* of the electron beam with the electromagnetic field (as distinct from long-term interaction). The most suitable in this respect are the nosed-in (reentrant) resonant cavities, toroidal cavities in particular, as well as coaxial and cylindrical cavities with shortening capacitances.

Gaps, forming an integral part of the cavity, can be made in the form of parallel-plane grids or gridless apertures of small diameters, as shown in Fig. 2.12. The output (catcher) cavity need not necessarily be enclosed in the tube envelope since the principle of current induction permits the cavity to be mounted outside the envelope, provided this latter is made of some low-loss dielectric, as of glass. Such an approach, despite its limited practicability because of the gap field being somewhat attenuated in the region carrying the electron beam, is of interest from the physical point of view.

2.4d. Abstraction of Electron Beam Energy with the Aid of Non-Resonant Oscillator Systems

The main limitation of a resonant cavity used for coupling out the energy of an electron beam is its frequency selectivity, more commonly referred to as a *narrow bandwidth*. The range of operating

frequencies can be somewhat widened by a tighter coupling with the load, i.e. by the reduction of the external and loaded Q's of the cavity at the constant unloaded Q_0. This also results in an increase in cavity efficiency. However, in this case the dynamic resistance of the cavity is reduced, i.e. G_{tot} is increased (Fig. 2.11*b*) due to a higher load conductivity as transformed to the gap section. With an invariable beam current I_0, a higher G_{tot} will, in turn, cause a reduction in the intensity of the radio-frequency retarding field across the gap. As a consequence, the amount of energy taken from the electron beam by the gap and hence, the efficiency of the device are reduced.

Another method of increasing the operating bandwidth is to replace the resonant cavity by a transmission line terminating in a matched load and to make the interaction gap an integral part of the transmission line. However, the characteristic (equivalent) impedance of most transmission lines is comparatively low (scores and hundreds of ohms) and it is usually impossible to provide a fair "match" with the electron beam. To utilize the kinetic energy of the electron beam to the utmost, a sufficiently great number of identical gaps should be connected into one common transmission line. Electron bunches should be made to pass through successive gaps at the same phase of the radio-frequency field, namely, when the intensity of the retarding field is highest.

The condition of a constant phase of the radio-frequency field in each gap with respect to the electron bunches means that the phase velocity v_p of the wave propagating along the line connecting the gaps should be approximately equal to the beam velocity v_0, and is ordinarily referred to as *synchronism* of the electron beam with the travelling wave. The beam velocity cannot, however, be equal to the velocity of light in free space and, the more so, cannot exceed it. It follows, therefore, that the transmission line connecting consecutive gaps should feature the properties of a delay line, as indicated in Fig. 2.13*a*.

At microwave frequencies the function of a delay line can be performed by slow-wave structures, such as a helix, a comb line, an interdigital system, etc. The two grids in each gap shown in Fig. 2.13 are not essential, they would only intercept part of the beam current and hinder wave propagation along the slow-wave structure. The longitudinal electric field developed by these gaps can easily be replaced by the edge fields, that are always present in any kind of slow-wave system supporting modes of the electric type.

However, the field intensity of a slow wave diminishes rapidly as the distance from the system surface increases and it is therefore desirable to pass the electron beam as near to the conductors of the slow-wave system as possible. Furthermore, the intensity of the

radio-frequency electric field in a slow-wave structure is the higher, the higher its coupled impedance K. Consequently, to obtain effective interaction between the electron beam and the slow electromagnetic wave it is desirable to use slow-wave structures featuring sufficiently high coupled impedances.

The operating bandwidth of the device under discussion is determined by the dispersion characteristic of its slow-wave structure, i.e., by the phase velocity of the slow wave as a function of frequency. The less pronounced are the dispersive properties, the wider is the frequency band within which the required degree of synchronism of the electron beam with the slow wave can be provided. Helical slow-wave systems are capable of ensuring bandwidths of the order of 50 to 100 per cent of the middle frequency; this extremely useful property is utilized in modern amplifier travelling-wave tubes. For comparison, it is useful to recall that the bandwidth of a single resonant cavity is inversely proportional to the loaded Q and even at moderate values of the latter (about 50 to 100) constitutes but several per cent of the middle frequency.

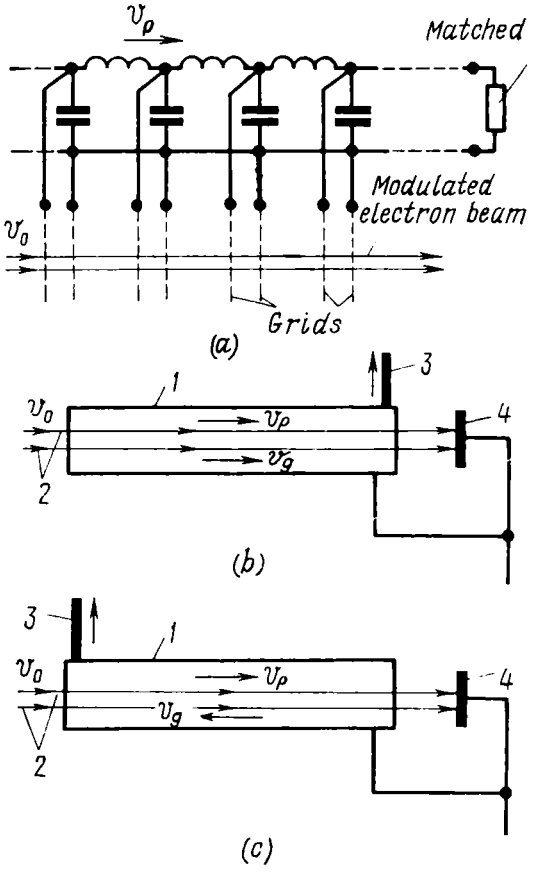

Fig. 2.13. Skeleton diagram of non-resonant catcher with several gaps connected to a common delay line (*a*) and the use of slow-wave structures with forward (*b*) and backward (*c*) dispersion

1—slow-wave structure; *2*—modulated electron beam; *3*—power output; *4*—collector

The place at which the matched load is connected to the line is to a great extent determined by the nature of dispersion in a slow-wave structure. In case of forward (positive) dispersion the directions of the phase and group velocities coincide, while the phase velocity has to be directed along the electron beam to provide for synchronism. Consequently, in this case the power output should be mounted at the end of the slow-wave structure, facing the collector, as shown in Fig. 2.13*b*. When spatial harmonics featuring backward (negative) dispersion are utilized, the energy output should be located at the

slow-wave system end nearest to the source of electrons (Fig. 2.13*c*); this is due to that the phase and group velocities in this case are of opposite directions.

Energy transfer from the electron beam to the travelling-wave field can take place along a considerable part of the slow-wave system and be of a repeated or a continuous nature. Devices utilizing sections of slow-wave structures are therefore classified among devices with *long-term* or *extended interaction* of the electron beam and the electromagnetic field. Representative of this class of electron

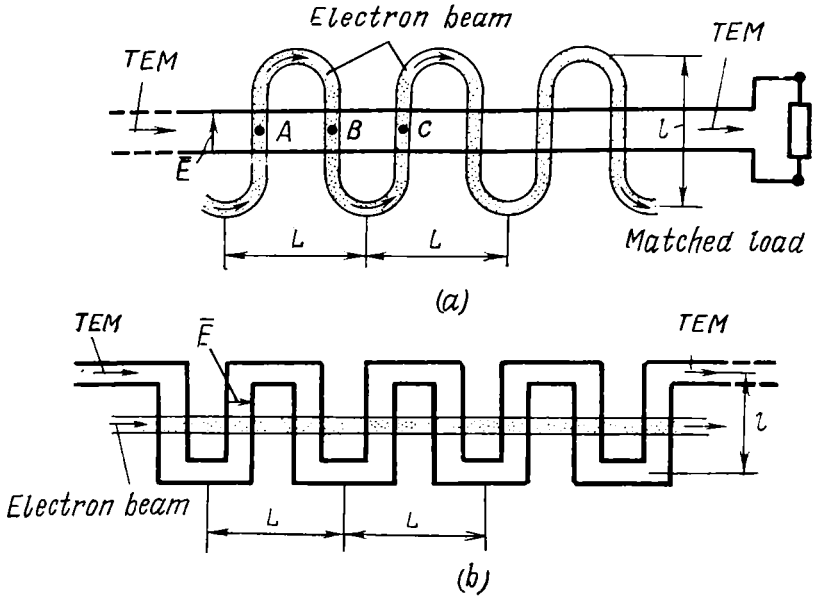

Fig. 2.14. Electron beam interaction with a non-resonant line
a) periodic electron beam interacting with an unretarded wave; (*b*) rectilinear electron beam interacting with a periodic slow-wave structure

devices are the travelling-wave tube (TWT), backward-wave oscillator (BWO), as well as magnetrons, platinotrons and others.

At first glance it may appear impossible to provide long-term interaction of electron beams with fast (not decelerated) waves of the TEM, TM and TE propagation modes, since at $v_p \geqslant c$ the condition of phase synchronism is not met. It is possible to overcome this difficulty by bending the electron beam in a certain fashion and making it interact periodically with the field of the propagating wave. Figure 2.14*a* illustrates, as an example, a two-wire or strip line excited at the TEM mode. A density-modulated electron beam periodically intersects this line and interacts with the electric field of this mode, which is longitudinal relative to the direction of electron motion. Synchronism, i.e. a constant phase of the microwave field when one and the same electron bunch passes in succession through points A, B, C, etc., can be provided by a properly chosen beam geometry (L and l in this Figure).

For comparison, a far more simple solution to the same problem is presented in Fig. 2.14*b*, where a rectilinear electron beam is shown passing through a periodic slow-wave structure in the form of a folded line. The similarity of these problems is quite obvious. In case of a non-rectilinear periodic electron beam the synchronism can be considered as existing between the fast wave propagating along the line and one of the spatial harmonics of the electron beam.

The utilization of such fast waves is of particular interest for devices designed to operate in the millimetre and submillimetre wave bands, where the geometrical dimensions of slow-wave structures become inconveniently small.

2.4e. Generalized Skeleton Diagram of Microwave Oscillators and Amplifiers

The above-discussed methods of converting d.c. energy into the energy of microwave oscillations explain the principles underlying the design of modern microwave electron devices. Figure 2.15 presents general skeleton diagrams of microwave oscillators and amplifiers, differing in the character of electron beam interaction with the electromagnetic field.

The electron beam emitted by cathode K is accelerated by an accelerating electrode A and then enters a *control* (bunching) assembly. The control assembly is designed to modulate the convection current of the beam, i.e. to develop periodic electron bunches along the beam[1]. These electron bunches finally pass through the gap of an output resonant cavity or along a slow-wave structure, inducing microwave currents in these devices and thus giving up part of their kinetic energy to the field. The used-up electrons arrive at the collector and dissipate the rest of their energy on this electrode in the form of heat. In the simplest case the bunching and output (catcher) assemblies and the collector can have a direct d.c. connection with the accelerating electrode.

When the device is an amplifier the control signal is fed from an external source of microwave power. For self-excitation to take place, i.e. to convert an amplifier into an oscillator (self-oscillator), it is sufficient to provide a path of positive feedback between the output and input, as shown in Fig. 2.15 in dashed lines.

The devices of Fig. 2.15 can serve as vivid illustrations of the use of electrons as energy-storing elements and as an "intermediary agent" in converting the d.c. energy of accelerating voltage source V_0 into the energy of microwave oscillations. The conversion condi-

[1] The control assembly providing electron beam bunching should not be confused with control electrodes of certain types of electron devices, where it is used to shape the electron beam with the aid of d. c. fields, as well as for pulse and other kinds of low-frequency modulation.

tions are considered perfect when electrons possess almost zero velocities after having passed the output assembly.

Some modern microwave electron devices, such as multicavity klystrons, employ a circuit exactly coinciding with that presented in Fig. 2.15*a*. The actual design of microwave amplifiers and oscillators can, however, considerably differ in appearance from the circuit described. Thus, the control assembly and accelerating electrode can change places (as is the case with microwave triodes and

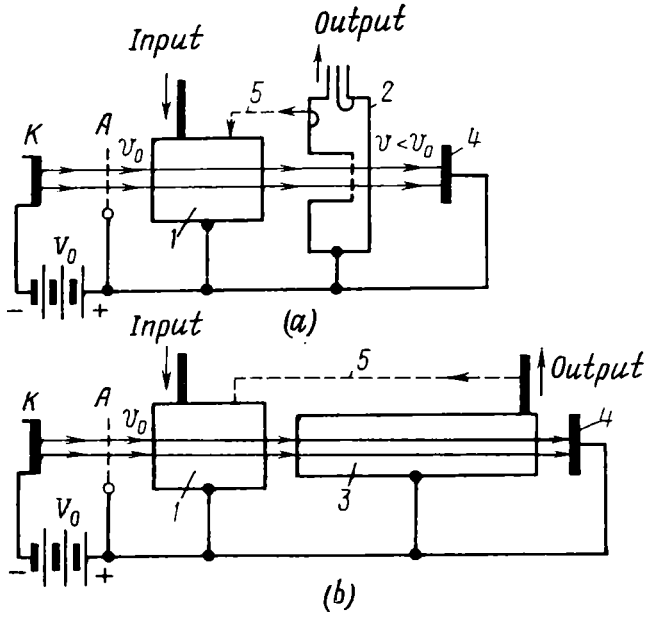

Fig. 2.15. Skeleton diagrams of microwave amplifier and oscillator tubes with short-term (*a*) and extended (*b*) interaction of the electron beam with the field of the catcher

1—buncher; *2*—output resonant cavity; *3*—output slow-wave structure; *4*—collector; *5*—feedback loop

tetrodes). The functions of collecting the used-up electrons and taking the energy of the electron beam can be performed in certain cases by one and the same electrode. It is also possible that the functions of all the elements described above be performed by a single two-electrode gap (as is actually the case with a magnetron or a diode oscillator described in Section 2.7). Nevertheless, even in these simplest designs all the processes examined above, namely, electron acceleration, density modulation of the electron beam and coupling out the energy by making the beam interact with a retarding radio-frequency field, can be discerned.

Here it might be asked why all these principles do not directly apply to low-frequency devices. But, on the one hand, the problem of dissipating power on the output element at low frequencies is not as acute as at microwaves since in principle no restrictions are

imposed on the size and structure of electrodes, and therefore it would be inefficient to use three electrodes (two grids and a collector) instead of one anode, this only complicating the design. On the other hand, utilization of resonant cavities and slow-wave structures for the low-frequency band would only result in unjustifiably great and sometimes even unrealizable size of such elements. These considerations reveal still other characteristic features of microwave electron devices.

2.5. Methods of Electron Beam Control at Microwave Frequencies

2.5a. Electrostatic Control

In the simplest case the control device shown in Fig. 2.15 can function as an instantaneous gate, "cutting" electron bunches out of a continuous electron beam at the required rate, or the microwave frequency. The ideal waveform of convection current is rectangular pulses of short duration (Fig. 2.10*c*), as was demonstrated in Section 2.4. The electron beam after having passed through the control assembly takes the form of equally spaced thin (in the extreme case, infinitely thin) plates or discs of charge moving toward the output assembly.

At low and moderate frequencies the a.c. component of the convection current is usually obtained by an *electrostatic control* method with the aid of a grid that is negative relative to the cathode (Fig. 2.16). In principle, all modern general-purpose amplifier and oscillator tubes utilize this method of controlling the electron beam.

At low frequencies, the convection electron current i_a entering the anode-grid space becomes time-dependent as shown in Fig. 2.17, due to the action of the d.c. grid bias V_{g0} and the a.c. voltage amplitude V_g. Under large-signal conditions (class C operation), the electrostatic control method makes it possible to obtain pulses of convection current in the form of sections of sinusoids sliced at the bottom. Reducing the operating angle Θ by increasing the grid bias V_{g0} and increasing the control voltage amplitude V_g we can obtain electron bunches of short duration.

The most valuable feature of the electrostatic control at low frequencies in tubes employing conventional circuitry is practically zero power consumption from the source of control voltage, provided there is no electron interception by the grid. At microwaves, however, control by means of a negative grid necessitates a certain finite amount of control power, which increases as the operating frequency is increased. This circumstance, as well as other undesirable effects, hampers the development of microwave amplifiers and oscillators with electrostatic beam control for wavelengths shorter than some

3 to 5 cm. The main factor determining lower effectiveness of grid control is a considerable transit angle through the cathode-grid space.

Consider power consumption in the control circuit as a function of the transit angle. To simplify matters, the discussion will be limited to the case of a triode employing a common-cathode connection circuit[1] under small-signal conditions. The conclusions made

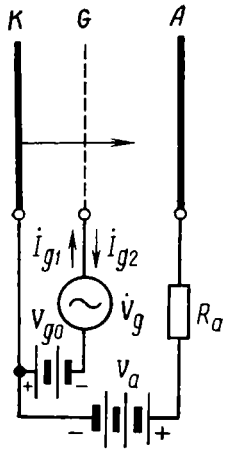

Fig. 2.16. Electrostatic current control in a triode

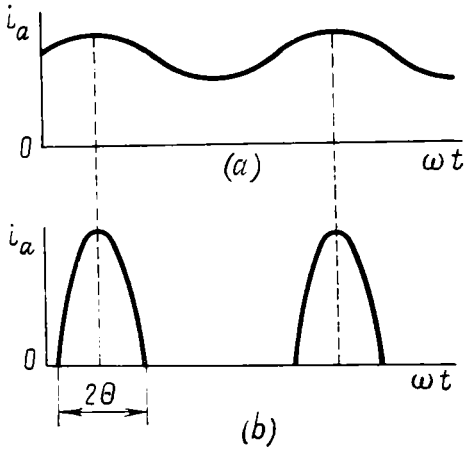

Fig. 2.17. Convection current with electrostatic control in case of a small (*a*) and large (*b*) amplitude of the control signal

are applicable to other types of devices with electrostatic electron beam control, in particular, for microwave tetrodes.

Returning to Fig. 2.16, let us consider a planar triode structure with the grid kept negative relative to the cathode. A small control voltage $\dot{V}_g$ is applied to the grid along with the bias voltage V_{g0}. For simplicity, the effects of anode load resistance will be neglected.

At a small penetration factor (Durchgriff) the entire structure can be considered as consisting of two independent parallel-plane gaps divided by a common electrode, grid, and pierced by one and the same stream of electrons moving from the cathode to the anode. The conclusions made in the course of the above analysis of induced currents are applicable to each of these gaps.

Electron bunches moving in the cathode-grid gap induce a current with a complex amplitude of the first harmonic $\dot{I}_{g1}$ flowing in the direction indicated in Fig. 2.16. As the electron bunches move in the anode-grid gap, a current $\dot{I}_{g2}$ is induced in the grid circuit, and

[1] In an amplifier tube, the common electrode is that which is connected both to the input and the output circuits; refer also to Section 4.4.

therefore, in the general case, the total grid current differs from zero and is the vector difference of currents $\dot{I}_{g1}$ and $\dot{I}_{g2}$

$$\dot{I}_g = \dot{I}_{g1} - \dot{I}_{g2}$$

A similar relation for the instantaneous values of induced currents was discussed earlier in Section 2.3*d*.

With identical vectors $\dot{I}_{g1}$ and $\dot{I}_{g2}$, the total grid current is zero (provided, of course, that the grid does not directly intercept electrons). However, because of the finite time of electron transit in the cathode-grid gap, the maximum of induced current $\dot{I}_{g1}$ lags behind the maximum of grid control voltage. The corresponding phasor diagram is presented in Fig. 2.18.

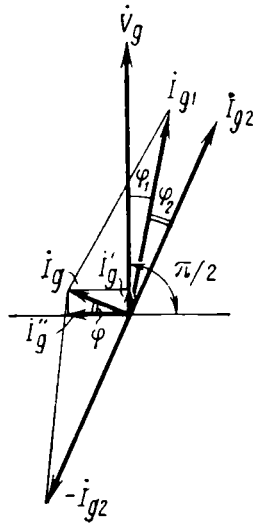

Fig. 2.18. Phasor diagram of induced input currents in the common-cathode circuit with electrostatic control

The phase shift φ_1 between current $\dot{I}_{g1}$ and voltage $\dot{V}_g$ is a unique function of the electron transit angle θ_{gk} through the cathode-grid gap, but these angles are not exactly identical. Indeed, if the electron velocities remained constant, then, according to the findings of Section 2.3*d* the cathode-grid gap could be replaced by an equivalent gap of zero width situated at the middle of the actual gap. In this case the phase shift of current $\dot{I}_{g1}$ would be half the actual transit angle through this gap $\theta_{gk} = \omega\tau_{gk}$. In the general case, therefore, the phase shift of the current should exceed zero, but be less than the transit angle.

Usually, the transit angle through the anode-grid gap θ_{ag} is considerably less than θ_{gk} because of the significantly higher electron velocities due to the action of a high anode voltage. Nevertheless, the induced current $\dot{I}_{g2}$ lags behind $\dot{I}_{g1}$ by a phase angle φ_2, which in general can exceed θ_{ag}. This effect is readily explained if θ_{ag} is assumed to be zero. In this case the current $\dot{I}_{g2}$ should lag behind the voltage $\dot{V}_g$ exactly by θ_{gk}. Taking into account the transit angle through the anode-grid gap, the additional phase lag of the induced current $\dot{I}_{g2}$ is found to be about $\theta_{ag}/2$. Therefore, at $\theta_{ag} > 0$. it can be written that $\varphi_1 + \varphi_2 \geqslant \theta_{gk}$, i.e. $\varphi_2 \geqslant \theta_{gk} - \varphi_1$.

Here θ_{gk} and θ_{ag} are implied to be transit angles as defined by equations of the (2.28) type, i.e. at small values of the a.c. amplitudes of anode and grid voltages.

As seen from Fig. 2.18, the total grid current $\dot{I}_g$ induced in the input circuit differs from zero and at moderate values of φ_1 and φ_2 leads the control voltage $\dot{V}_g$ by a phase angle $\varphi' = \frac{\pi}{2} - \varphi$. As a consequence, the grid circuit draws a current, one component of which ($\dot{I}'_g$) is in phase with the control voltage despite the fact that the grid itself does not intercept any electrons.

Thus it can be considered qualitatively proven that at finite transit angles the input circuit requires active power from the source of control voltage for electrostatic control of the current. Besides this active current component $\dot{I}'_g$, the induced grid current also features a capacitive component $\dot{I}''_g$, which is usually greatly in excess of $\dot{I}'_g$.

The grid current component $\dot{I}'_g$, that is in phase with the control voltage $\dot{V}_g$, can be thought of as a conductive component of the grid admittance, $G_{in} = \dot{I}'_g/\dot{V}_g$. Analysis discloses that under the assumptions adopted and with moderate transit angles θ_{gk} this conductance can be approximated as

$$G_{in} = kg_m\theta_{gk}^2 \tag{2.41}$$

where g_m is the static mutual conductance of the triode and k is a numerical coefficient.

Thus, with electrostatic beam control, the input conductance caused by electron inertia effects in case of a common-cathode circuit is, as a first approximation, in direct proportion to the square of the transit angle through the cathode-grid gap. With all other parameters fixed, this conductance increases, therefore, proportionally to the square of the operating frequency. These deductions have been confirmed experimentally. The input susceptance due to electron inertia is less significant and will not be examined in the present book.

A rise in the loss in the input circuit of a common-cathode amplifier with an increase in the operating frequency limits the application of microwave tubes with electrostatic current control. Thus, for example, at θ_{gk} about 50° the input conductance of general-purpose amplifier and oscillator tubes amounts to 10^{-3} mho and rapidly increases with a rise in frequency. In case of oscillators this means that an ever increasing part of the output power has to be passed to the grid circuit to provide for the proper amount of feedback. Finally, at a certain frequency all the output power has to be used as the feedback to maintain self-excitation. This deprives the load of any power and the oscillator stops functioning.

It may appear strange that there is a considerable amount of power consumption by the input circuit with no electron bombardment of the grid so that it may not be quite clear where all this power is dissipated. Actually, the effects described give rise to an increase in the average kinetic energy of electrons that are passed to the anode, where this energy is dissipated as heat.

2.5b. Dynamic Control

In conventional tubes with electrostatic current control, the electron transit time always is an unfavourable factor. The drawbacks of electrostatic control have motivated the search for other systems, in which the electron transit time would cease to be detrimental to tube operation and could be put to use for density modulation of the electron beam. A mechanism of this kind, where the finite time of electron transit is utilized to advantage, is known as *dynamic control.*

The weak point of current control by means of an ordinary grid at microwave frequencies is that the grid has to produce density modulation of the convection current directly. As demonstrated above, this inevitably leads to different densities of the electric charge to both sides of the grid at every instant of time, this effect in turn resulting in an induced current in which an active component is present. A radical solution of this problem is possible provided the idea of controlling the current directly by varying the charge density is completely rejected.

In the final analysis, the control arrangement is required to provide an electron convection current at a certain plane, corresponding to the plane of the power output (catcher), which would vary in accordance with the law

$$i_{con} = I_0 + i(t)$$

where $i(t)$ is a periodic function of time and I_0 is the d.c. component of the convection current.

Note, that the alternating component $i(t)$ of the convection current does not necessarily have to be produced in the control arrangement itself. It is more expedient, therefore, to use such a mechanism which would provide that, as the electron beam moves in the space between the control device and power output, the electrons be gradually grouped to form dense bunches just at the input to the power output arrangement. At the same time, the charge density at the output of the control system could remain invariable, this being especially important for eliminating the input conductance.

Figure 2.19 presents a hypothetical motion diagram of electrons emerging from the control system at regular intervals. Despite the fact that the electrons leave the control electrode at different ins-

tants t_1, t_2, t_3, etc., their trajectories have to intersect at one point (x_{out}, t_{out}) where they should form a bunch. Obviously, this can be obtained only if the derivatives dx/dt for various electrons are different, i.e. with different electron velocities.

The above elementary argumentation contains a deduction of major importance about the possibility of dynamic control of electron beam by first varying periodically the electron velocities and then converting this velocity modulation into density modulation of the convection current. Such periodic variation of electron velocities in the control system is termed *electron beam velocity modulation* or simply *velocity modulation.*

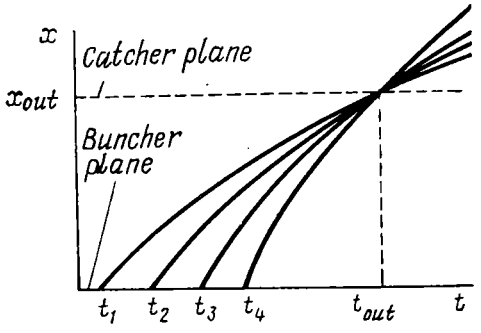

Fig. 2.19. Motion diagram of electron bunching; electrons leave the modulating assembly at different instants of time, but arrive at the catcher simultaneously

With dynamic current control, as illustrated in Fig. 2.19, the transit time of electrons in the space from the control to the output arrangements is put to good use.

A numerous class of microwave devices, namely, *reflex* and *drift* (multicavity) *klystrons* rely for their operation on velocity modulation of the electron beam. The principles of this control are treated in more detail in Section 2.8 and Chapter 5.

With dynamic control, electron bunching is not necessarily produced with the aid of a control arrangement forming a separate and independent element of the microwave electron tube. Even at the early stages of microwave electronics development, systems with implicit ("inherent") automatic control mechanisms of this kind were discovered. In these systems, the electron transit time also plays a useful part and, in particular, determines the frequency of oscillations. As examples of systems with "inherent" dynamic control, triodes with a positive grid (retarding-field oscillators) and monotrons described below, as well as certain other microwave oscillator tubes can be cited.

In a broad sense of the term, dynamic control of electron beams underlies the performance of an overwhelming majority of modern microwave electron tubes.

2.6. Oscillation in Positive-Grid Triodes. Retarding-Field Oscillator

Consider a triode whose grid is fed with a high positive voltage V_g (scores or hundreds of volts) instead of a negative bias. The anode of this tube is at a zero or slightly negative voltage V_a with respect

to the cathode. With such an unusual connection electrons emerging from the cathode are accelerated by the grid and enter a retarding static electric field in the anode-grid gap. The electrons stop short of the anode, reverse and are again accelerated by the grid; as a result the electrons keep oscillating back and forth in a "potential well" shown in Fig. 2.20 until they are intercepted by the grid. The diagram of electron motion in the absence of microwave oscillations is shown in Fig. 2.21*a*.

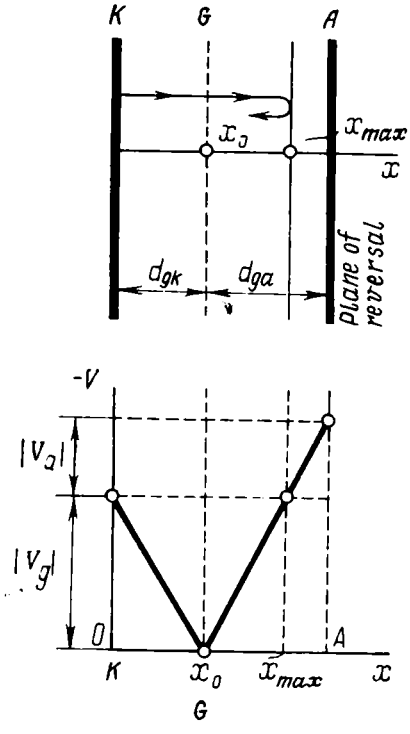

Fig. 2.20. Distribution of d.c. voltage across planar triode with a positive grid under temperature-limited current conditions (in the absence of space charge)

Applying the concept of induced currents to this case, we may conclude that the moving electrons induce currents in the tube electrodes, which vary in time with the frequency of these electron oscillations. The period T of current fluctuations in the grid-anode circuit turns out to be equal to the time of electron transit between the positive grid and the "reverse plane" and back to the grid, i.e.,

$$\tau = T \qquad (2.42)$$

If $V_a \to 0$ the electron transit time τ is proportional to $V_g^{-1/2}$ and therefore the period of induced oscillations should also be a function of the constant grid voltage of the form $T = kV_g^{-1/2}$, where k is a certain constant. Hence, applying the relation of the wavelength to the period of oscillations[1], the following equation is obtained:

$$\lambda^2 V_g = \text{const} \qquad (2.43)$$

This interesting conclusion has been corroborated by experiment. Triodes with positive grids are capable of oscillating at frequencies corresponding to the decimetric and centimetric wave bands; at low values of loaded Q of the oscillatory system, the wavelength is almost independent of the parameters of the external circuit and is described by a relation of the (2.43) type. Sources of microwave

[1] Here and in the following discussion λ is the wavelength in free space, as defined by $\lambda = cT$, where c is the velocity of light in free space, approximately equal to $3 \cdot 10^{10}$ cm/s.

oscillations of this kind are known as *retarding-field oscillators*[1]. The Barkhausen-Kurz and Gill-Morrell oscillators may be cited as examples of actual designs.

Thus, even the simplest train of reasoning leads to a working hypothesis that is capable of providing at least a qualitative explanation of the existence of oscillations in the external circuit of the triode in question. The simple hypothesis of "electron swinging"

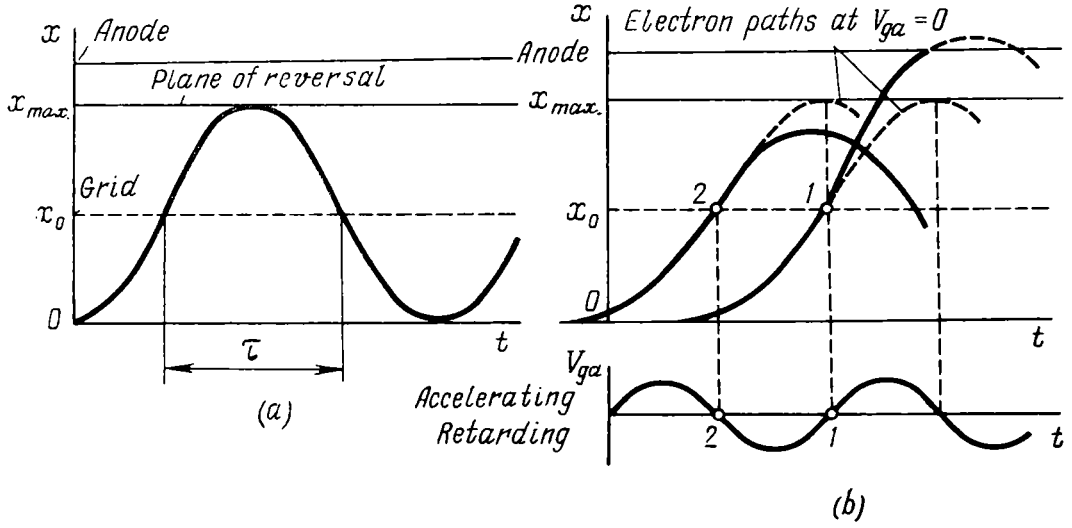

Fig. 2.21. Motion diagram for a positive-grid triode in the absence (*a*) and presence (*b*) of radio-frequency oscillations in the anode-grid space

in the tube is, however, inadequate to provide an exhaustive explanation of the phenomenon. Indeed, it is necessary to allow for the continuous nature of electron emission from the cathode, leading to an equal number of electrons moving to and from the grid in the grid-anode gap at any instant. This should have resulted in a complete cancelling out of the current induced in the external circuit.

Orderly oscillations in the external circuit are possible only if the electron movement is orderly itself, in other words, when the electron stream is density-modulated. In this respect the mechanism of energy transfer from the electrons to the external circuit in retarding-field oscillators must be the same as in the general circuit of Fig. 2.15. Since there is no explicit mechanism of controlling the electron beam in retarding-field oscillator circuits, the internal factors that can be responsible for the effect of beam density modulation should be given a more close scrutiny. The existence of such a mechanism has to be postulated if only to explain oscillations observed in triodes with a positive grid.

[1] The static retarding field in the grid-anode gap of this oscillator should not be confused with the radio-frequency retarding field that interacts with electrons and provides for energy transfer to an external load in this and any other kind of microwave electron amplifier or oscillator (refer to Section 2.4).

Consider a case when an oscillatory circuit is connected only between the grid and anode of a triode. A connection of this kind is possible when the electrode leads constitute a resonator shorted at the other end by a capacitive bridge network.

The following method, widely applied in the analysis of various types of microwave devices, can be used to explain the mechanism of oscillations in this particular case. Assume the oscillations to be already present in the circuit in question and examine the balance of energy exchange between the electron beam and the microwave field. If the action of the microwave field is such that during a period of oscillations electrons deliver more energy to the field (on the average) than acquire from this field, then the oscillations should build up and self-excitation takes place. Conversely, if energy exchange on the average leads to the energy being transferred from the external oscillatory circuit to the electron beam, then the oscillations, even though present due to some reason or other, are damped out. Under these conditions a system consisting of an oscillatory circuit and an electron beam is, therefore, incapable of maintaining oscillations and cannot be self-excited. This kind of approach is physically completely justifiable, because initial oscillations exist in any system in the form of thermal fluctuations and shot-effect, anyway, as well as shock excitation oscillations due to transients when the circuit is turned on.

Thus, oscillations described by equations (2.42) and (2.43) are assumed to be present in the grid-anode circuit. Consider the change in electron motion due to the presence of a radio-frequency component v_{ag} across the anode-grid gap. The corresponding motion diagram for two typical electrons that were emitted from the cathode at different instants is presented in Fig. 2.21*b*.

Electron of type *1* enters the anode-grid gap at the instant of time the radio-frequency field changes from a retarding to an accelerating one and moves toward the anode during the accelerating halfwave, thereby acquiring kinetic energy from the field. As a result, the amplitude of the swing of this electron increases and it approaches the anode surface, overcoming the retarding action of the static electric field. If the amplitude of the radio-frequency voltage is high enough and the static retarding field is not excessive, the electron strikes the anode and its further movement is discontinued.

Thus, electrons of type *1*, which acquire energy from the radio-frequency field and are therefore most "unfavourable" from the point of view of oscillation build-up, can move in the anode-grid gap only during a single halfwave of the radio-frequency oscillation, after which they are intercepted by the anode. A certain amount of d.c. current appears in the anode circuit, despite the fact that this electrode is at a voltage negative with respect to the cathode.

Now, consider the motion of electrons of type *2*, which begin their travel through the anode-grid gap a halfwave earlier or later, i.e., when the radio-frequency field changes to a retarding one (Fig. 2.21*b*). Electrons of type *2* cannot reach even the coordinate of plane $x_{max.}$ (the plane of electron reversal in the absence of oscillations), to say nothing of the anode surface, because they continually lose their energy as a result of the retarding action of the radio-frequency field. The electrons return to the grid and again give up energy since at $\tau \approx T$ the field reverses polarity simultaneously with the reversal of electron motion. Thus, electrons of type *2* give up their energy during two halfwaves of the radio-frequency oscillations; after this they are either intercepted by the grid or enter the cathode-grid gap. They are unable to reach the cathode and again start moving towards the grid. With a properly chosen transit time in the cathode-grid gap, electrons of type *2* can again be injected into the anode-grid gap at the retarding halfwave of the radio-frequency field, where they again give up energy, and so on. From the point of view of sustaining oscillations in the external circuit, electrons of type *2* are the most "favourable".

The above argumentation indicates that electrons with a "favourable" phase are present in the radio-frequency electric field considerably longer than the "unfavourable" electrons of type *1*. The latter are automatically "sorted out" by the anode so that an orderly movement of electrons in the anode-grid gap results. Bunches of electrons with a "favourable" phase return periodically to the grid, moving all the time in a retarding field. The total energy balance inevitably leads to an increase in the energy of oscillations, this revealing the tendency of a positive-grid triode to self-excitation.

The mechanism of development of an orderly electron movement described above is known as *anode sorting* or *anode selection*. This mechanism confirms the existence of dynamic control and density modulation of the electron beam in retarding-field oscillators.

Analysis of the mechanism of oscillations excitation allows one to draw certain conclusions on the part played by the external circuit. Electron movement cannot be discussed without regard for the oscillatory circuit, because only an alternating voltage on the tube electrodes makes the mechanism of electron sorting possible. This radio-frequency voltage is produced by the induced currents flowing through the oscillatory circuit (resonator) connected between the tube electrodes. Thus, electron sorting and self-excitation are feasible only on condition that an oscillatory circuit of rather low conductance is present in the system. Despite the fact that the parameters of this oscillatory circuit are not explicitly present in equation (2.43), oscillations in a retarding-field oscillator are possible only if the "circuit" and the "electronics" are properly matched.

Figure 2.22 illustrates a retarding-field oscillator in which a toroidal resonant cavity is connected between the anode and grid of a triode. This circuit bears a close resemblance to that of a reflex klystron (to be discussed in Chapter 5). Oscillators of this kind are capable of providing output powers of the order of fractions of a watt in the centimetric wave band at efficiencies up to 5 to 7 per cent.

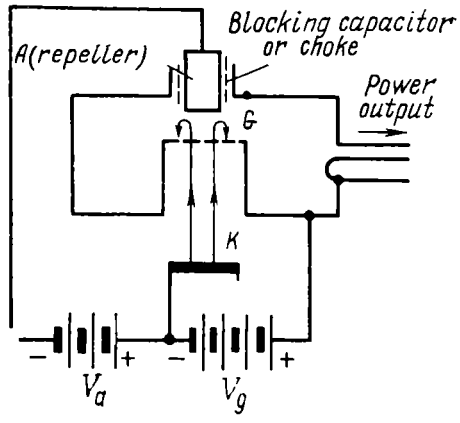

Fig. 2.22. Retarding-field oscillator circuit

Retarding-field oscillators have played an important part in the development of the basic concepts of microwave electronics. In their time, these devices were among the most widely used sources of microwave power for the decimetric and centimetric wave bands. With the aid of similar designs even millimetric waves were obtained. They served as a stepping-stone to the development of magnetron devices, oscillations of the magnetron type being first discovered in retarding-field oscillators. Finally, the development of the reflex klystron is to a great extent due to research carried out with retarding-field oscillators.

At present retarding-field oscillators have become almost obsolete due to the availability of reflex klystrons and other types of low-power microwave oscillators; their wider application in future as sources of centimetric and millimetric waves cannot, however, be totally excluded.

2.7. Admittance of a Gap Carrying an Electron Beam. Monotron and Oscillating Diode

The operation of many types of microwave amplifier and oscillator tubes depends on the travel of an electron beam through a gap to which an external radio-frequency voltage is applied. We shall examine the case when an electron beam from an ordinary electron gun without any preliminary density modulation travels through a parallel-plane gap formed by two grids, as shown in Fig. 2.23. Similar situations may be encountered, for instance, in the circuit of a microwave amplifier or oscillator (Fig. 2.15) if this two-grid gap is used as the control assembly. We shall ignore for the present the motion of the beam after it passed through the gap. For the sake of simplicity a collector may be assumed to be at the output of the gap (Fig. 2.23).

The constant accelerating voltage and the radio-frequency voltage amplitude will be denoted as V_0 and V_m, respectively; the discussion will be restricted to a small-signal case ($V_m \ll V_0$). The grids G_1 and G_2 forming the gap will be assumed ideal, i.e. perfectly transparent to the electron beam and totally opaque to the radio-frequency field.

In cases when the transit angle tends to approach zero, the average energy drawn by the electron beam from the field is also zero. This can easily be explained if we take into consideration that the number of electrons accelerated in the gap during one halfwave of the radio-frequency field is exactly equal to the number of electrons decelerated during the alternate halfwave. At a finite transit angle, however, the situation is reversed, because the transit time of decelerated electrons becomes longer than that of the accelerated electrons.

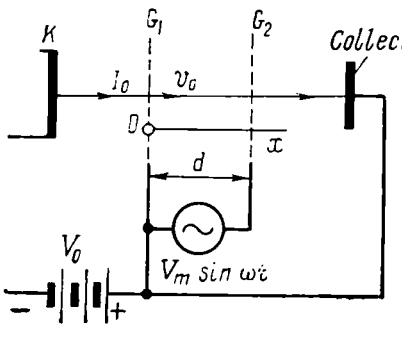

Fig. 2.23. Parallel-plane gap carrying unmodulated electron beam

Consider the balance of energy acquired by the electron beam from the radio-frequency field in the general case. To this end, the equation of current induced in the external circuit by electron motion between the grids has to be derived.

The equation of electron motion in the gap can be presented as

$$m\frac{d^2x}{dt^2} = -eE = e\frac{V_m}{d}\sin\omega t \qquad (2.44)$$

(the positive sign of voltage is conventionally assumed to correspond to electron acceleration along the $+x$ axis).

The first integration of equation (2.44) yields electron velocity v

$$\frac{dx}{dt} = v = v_0 - \frac{eV_m}{\omega md}(\cos\omega t - \cos\omega t_0) \qquad (2.45)$$

where t_0 is the instant of time the electron in question enters the gap and v_0 is the initial electron velocity equal to (neglecting relativistic effects)

$$v_0 = (2eV_0/m)^{1/2} \qquad (2.46)$$

The second integration of (2.44) gives

$$x = v_0(t - t_0) - \frac{eV_m}{\omega^2 md}[\sin\omega t - \sin\omega t_0 - (\omega t - \omega t_0)\cos\omega t_0]$$

The electron transit time through the gap can be determined from the condition that $x = d$ and $\tau = t - t_0$, hence

$$d = v_0\tau - \frac{eV_m}{\omega^2 md}[\sin\omega t - \sin(\omega t - \omega\tau) - \omega\tau\cos(\omega t - \omega\tau)] \qquad (2.47)$$

Here t denotes the instant of time when the electron, that entered the gap at t_0, leaves the gap.

Equation (2.47) is a transcendental one relative to the transit time τ. Its solution can be obtained by taking into account the condition that the radio-frequency amplitude V_m is small as compared to the d. c. accelerating voltage V_0. The electron transit time and the undisturbed transit angle in the absence of a microwave field can respectively be denoted as τ_0 and θ, i.e.,

$$\theta = \omega\tau_0 = \omega d/v_0 \tag{2.48}$$

Then, with $1 \gg V_m/V_0$, we may assume

$$\tau = \tau_0 + \delta\tau; \quad \delta\tau \ll \tau_0$$

Expanding the trigonometric functions into a power series by the small parameter $\omega\delta\tau$ and neglecting all terms with power higher than the first, we arrive at

$$\sin(\omega t - \omega\tau) \approx \sin(\omega t - \theta) - \omega\delta\tau\cos(\omega t - \theta)$$
$$\cos(\omega t - \omega\tau) \approx \cos(\omega t - \theta) + \omega\delta\tau\sin(\omega t - \theta)$$

Substitute these relations into (2.47). Disregarding the terms containing $(\omega\delta\tau)^2$ and the term of the first order of smallness, we find

$$d \approx v_0\tau - \frac{eV_m}{\omega^2 md}[\sin\omega t - \sin(\omega t - \theta) - \theta\cos(\omega t - \theta)] \tag{2.49}$$

This equation, which can be used to determine the transit time τ for any instant of time, is held in reserve, while the general equation for induced current is applied. Suppose the first grid passes an elementary layer of space charge $dq = I_0\,dt_0$ during a time period dt_0 (here I_0 is the d.c. component of the convection current). By equation (2.31), the motion of this elementary charge will induce a current di_{ind} equal to

$$di_{ind} = I_0\,dt_0\,\frac{v}{d}$$

The instantaneous velocity of electrons v can be determined from equation (2.45); the total induced current for any instant t can then be determined by integrating over all the charges present inside the gap at this instant

$$i_{ind} = \int_{t-\tau}^{t} \frac{I_0}{d}\left[v_0 - \frac{eV_m}{\omega md}(\cos\omega t - \cos\omega t_0)\,dt_0 = \right.$$
$$\left. = \frac{I_0}{d}\left\{v_0\tau - \frac{eV_m}{\omega^2 md}[\omega\tau\cos\omega t - \sin\omega t + \sin(\omega t - \omega\tau)]\right\}\right.$$

Again applying the expansion of function $\sin(\omega t - \omega\tau)$ into a series and omitting from now on the sign of approximate equality,

we obtain

$$i_{ind} = \frac{I_0}{d}\left\{v_0\tau - \frac{eV_m}{\omega^2 md}\left[\theta\cos\omega t - \sin\omega t + \sin(\omega t - \theta)\right]\right\}$$

The radio-frequency component of induced current $i_{ind.\ rf}$ can be determined by substituting the magnitude of $v_0\tau$ from (2.49) and rearranging, with equations (2.48) and (2.46) taken into account,

$$i_{ind.\ rf} = \frac{V_m I_0}{2V_0}\left\{F_1(\theta)\sin\omega t + F_2(\theta)\cos\omega t\right\} \tag{2.50}$$

where

$$F_1(\theta) = \frac{2(1-\cos\theta) - \theta\sin\theta}{\theta^2} \tag{2.51}$$

$$F_2(\theta) = \frac{2\sin\theta - \theta(1+\cos\theta)}{\theta^2} \tag{2.52}$$

Equation (2.50) shows that in the general case the radio-frequency component of the induced current in the gap is different from zero and features an active (in-phase with the voltage) component along with a reactive one. Designating the amplitudes of these components as I_{m1} and I_{m2}, we can rewrite equation (2.50) as

$$i_{ind.\ rf} = I_{m1}\sin\omega t + I_{m2}\cos\omega t \tag{2.50a}$$

$$I_{m1} = \frac{V_m I_0}{2V_0}F_1(\theta) \tag{2.53}$$

$$I_{m2} = \frac{V_m I_0}{2V_0}F_2(\theta) \tag{2.54}$$

Now the total admittance of the gap can be easily determined since both the induced current and the voltage applied to the gap ($v = V_m \sin\omega t$) are known. The corresponding components of the admittance at the gap terminals are usually termed the *electron (beam) conductance* and *electron (beam) susceptance*, which are

$$G_e = I_{m1}/V_m \text{ and } B_e = I_{m2}/V_m$$

Applying equations (2.53) and (2.54) we obtain

$$G_e = \frac{I_0}{2V_0}F_1(\theta) \tag{2.55}$$

$$B_e = \frac{I_0}{2V_0}F_2(\theta) \tag{2.56}$$

The functions $F_1(\theta)$ and $F_2(\theta)$ are presented in graphical form in Fig. 2.24.

In the present discussion the beam conductance G_e is of greater interest than the electron susceptance, because it characterizes the energy exchange between the radio-frequency field of the gap and the electron beam. Indeed, the average power P derived by the

electron beam from the radio-frequency field can be presented as

$$P = 0.5 V_m^2 G_e$$

In cases when the electron conductance G_e, which is the load for the external microwave source, is positive, the power is also positive, and, hence, the electron beam absorbs the energy of microwave oscillations. Conversely, at a negative beam conductance the energy consumed by the beam becomes negative, which means that energy is transferred from the electron beam to the external circuit of the gap. Under these conditions the parallel-plane gap passing an unmodulated electron beam can be used as an amplifier or oscillator of microwave signals.

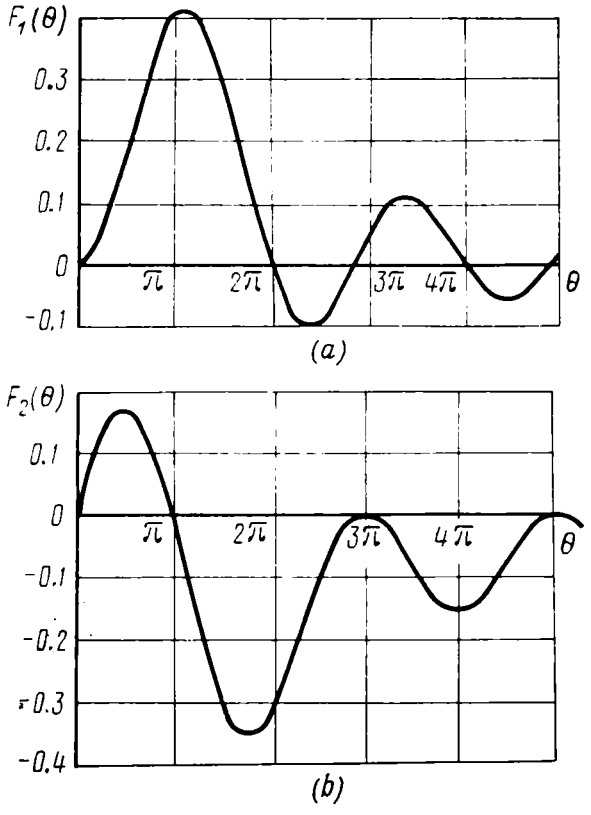

Fig. 2.24. Functions $F_1(\theta)$ and $F_2(\theta)$, determining the input conductance (*a*) and the input susceptance (*b*) of a gap

As shown in Fig. 2.24*a* the first region of negative beam conductance values begins with electron transit angles θ in excess of 2π; the conditions most favourable for self-excitation correspond to an electron transit angle of about $5\pi/2$.

The circuit of a microwave oscillator utilizing the above principle (the so-called *monotron*) is presented in Fig. 2.25*a*. This circuit employs a single resonant cavity with the interaction gap forming an integral part of this cavity. The cavity has to be tuned to the frequency at which the transit angle at the given accelerating voltage through the gap of d width will be equal to

$$\frac{\omega d}{\sqrt{\frac{2eV_0}{m}}} = \frac{5\pi}{2}$$

This relation can be rearranged as

$$\lambda^2 V_0 = 0.32 \frac{mc^2}{e} d^2 = \text{const} \qquad (2.57)$$

if wavelength is substituted for frequency.

Thus, in case of a monotron circuit, just as with a retarding-field oscillator, the product of the square of the wavelength by the accelerating voltage is a constant, determined only by the design parameters of the tube. Such a relation is typical of all tubes with dynamic current control, where the electron transit time is put to good use.

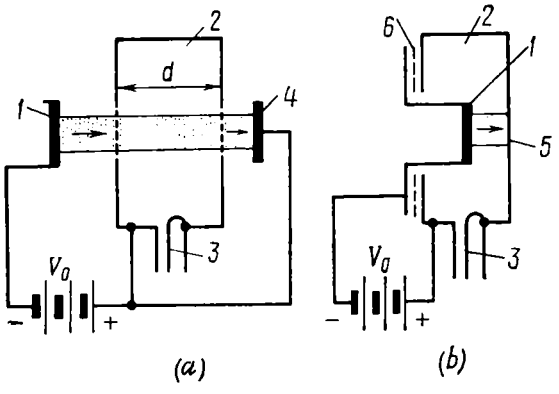

Fig. 2.25. Monotron (*a*) and diode oscillating at considerable transit angles (*b*)
1—cathode; *2*—resonant cavity; *3*—power output; *4*—collector; *5*—anode; *6*—blocking capacitor

Oscillations of the monotron type can be developed not only in an electron-beam diode (monotron), but also in an ordinary diode connected to a resonant cavity, as shown in Fig. 2.25*b*. Figure 2.26 presents without proof the theoretical curve of diode conductance under space-charge-limited current conditions (g_{m0} here is the diode static transconductance). As with a monotron, the diode features regions of negative conductance, where the most favourable conditions for self-excitation are at an undisturbed transit angle of about $5\pi/2$. In the present case, the transit angle θ should be determined with the aid of equation (2.22).

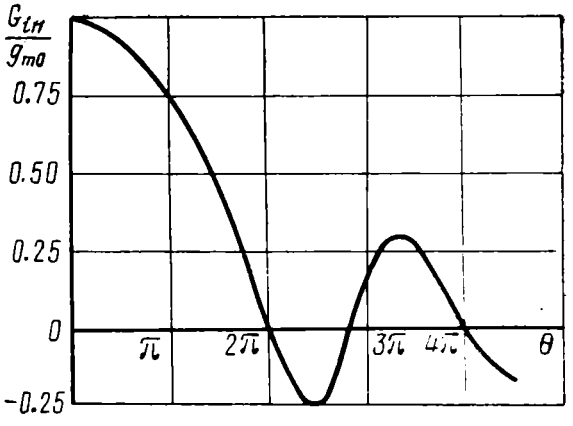

Fig. 2.26. Input conductance of a parallel-plane gap *vs* undisturbed transit angle (small-signal conditions)

The possibility of obtaining microwave oscillations with the aid of a monotron and a vacuum diode employing the circuits of Fig. 2.25 was confirmed by experiment. These devices, however, have not found extensive application despite their apparent simplicity and attractiveness because they feature extremely low efficiency, as compared to other types of microwave oscillators, and this makes their utilization inexpedient[1].

[1] Diodes with heated cathodes may be used as microwave noise sources with a continuous spectrum, provided the electron transit time through the diode is small compared to the period of oscillation. *Noise diodes*, operating on this principle, should not be confused with the diodes described above, where negative conductance at considerable transit angles is utilized.

2.8. Electron Beam Control by Velocity Modulation

2.8a. General Considerations

Dynamic current control which shows up automatically in the systems discussed above does not always lend itself to control with a view to improving its efficiency. Ordinarily, the efficiency of devices with inherent dynamic control is poor.

In Section 2.5*b* it was demonstrated that electron bunches on short durations can be obtained with the aid of velocity modulatiof

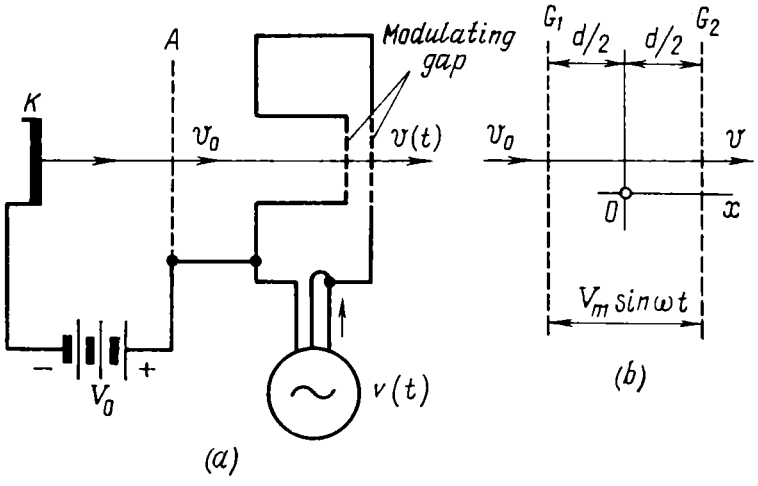

Fig. 2.27. Resonant cavity and perfect two-grid gap for velocity modulation of an electron beam

of the electron beam, i.e. by imposing periodic changes on the velocities of electrons at an original uniform charge density of the beam (refer to Fig. 2.19). The velocity-modulated electron beam will become density-modulated in its further travel. Thus, velocity modulation is a means for obtaining external dynamic control, in which the electron transit time is used to advantage.

The velocities of electrons can be periodically varied with the aid of a resonant cavity excited from an external source of microwave oscillations, as illustrated in Fig. 2.27*a*. The greatest variations of electron velocities will be obtained when the electron beam is passed through that part of the cavity, where the electric field is predominantly concentrated. In case of a toroidal resonant cavity (Fig. 2.27*a*) this region is the capacitive gap, ordinarily formed by two parallel-plane grids. The initial electron velocity v_0 should coincide in direction with the electric lines of force in the gap as much as possible.

Velocity modulation, which takes place when the vectors of the electron velocity and the radio-frequency electric field intensity

are collinear, is of a longitudinal character. So far as the normal (relative to the direction of electron motion) component of the electric field is concerned, it produces transverse velocity modulation, that is of no interest for the present discussion. We can ignore this transverse velocity modulation and assume, for instance, that a permanent longitudinal magnetic field of infinitely high intensity is applied to the system to preclude electron movement in the transverse direction.

2.8b. Equation of Velocity Modulation

At first we shall examine the process of velocity variation by a sine voltage $v = V_m \sin \omega t$ applied to the electrodes forming a parallel-plane gap (Fig. 2.27*b*), while the process of conversion of velocity modulation into density modulation of electron beams will be disregarded for the moment. The case when the applied voltage waveform differs from sinusoidal will be treated later. It should be mentioned, however, that in a high-Q resonant cavity the actual voltage across the gap is always sinusoidal, irrespective of the waveform provided by the driving microwave source.

The origin of coordinates will be placed at the middle of the gap, as was done above when examining the current induced in the output gap. The energy acquired by an individual electron in travelling a path of length dx inside the gap is

$$dW = e \cdot dv = e \frac{V_m}{d} \sin \omega t \, dx \tag{2.58}$$

As in the preceding analysis, the voltage v is assumed to be positive if it provides electron acceleration in the $+x$ direction.

The total incremental energy ΔW acquired by the electron in passing through the entire gap can be determined by integrating equation (2.58) over the gap width, i.e. from $-d/2$ to $+d/2$. The instant the electron passes through the middle of the gap (i.e. through point $x = 0$) will be designated as t_0; neglecting the small increment of velocity inside the gap, we obtain

$$t = t_0 + x/v_0$$

The increment of kinetic energy of the electron can be determined from equation (2.58) by substituting this relation for the time t

$$\Delta W = \int_{-d/2}^{+d/2} \frac{eV_m}{d} \sin (\omega t_0 + \omega x/v_0) \, dx =$$

$$= eV_m \sin \omega t_0 \frac{\sin \theta/2}{\theta/2} = eMV_m \sin \omega t_0 \tag{2.59}$$

The quantity $\theta = \omega d/v_0$ is the undisturbed transit angle through the modulating gap. Here M is the gap factor (coupling coefficient) used above and defined by equation (2.37).

The total kinetic energy of an electron, which enters the gap with the initial velocity $v_0 = (2eV_0/m)^{1/2}$, at the gap output is

$$W = \frac{mv^2}{2} = eV_0 + \Delta W$$

The electron velocity at the gap output can be determined by substituting the energy increment as given by equation (2.59) into the latter relation and rearranging

$$v = \sqrt{\frac{2eV_0}{m}\left(1 + \frac{MV_m}{V_0}\sin \omega t_0\right)} \tag{2.60}$$

We restrict ourselves to the small-signal case when the amplitude of the modulating voltage V_m can be considered small in comparison with the constant accelerating voltage V_0. Expanding equation (2.60) into a power series relative to the small parameter V_m/V_0 and neglecting all terms with powers higher than unity, we obtain

$$v = \sqrt{\frac{2eV_0}{m}}\left\{1 + 0.5\frac{MV_m}{V_0}\sin \omega t_0 - \right.$$
$$\left. - 0.125\left(\frac{MV_m}{V_0}\right)^2 \sin^2 \omega t + \ldots\right\} \approx v_0 + v_1 \sin \omega t_0 \tag{2.61}$$

where

$$v_1 = \frac{MV_m}{2V_0} v_0 \tag{2.62}$$

The equation of velocity modulation (2.61), along with relation (2.62), plays a very important part in the theory of microwave amplifiers and oscillators which employ velocity control of the electron beam. As seen from (2.61), at small amplitudes of the modulating voltage, the velocity modulation produced follows the same law as the modulating voltage. Since $V_m \ll V_0$, the alternating component v_1 of the electron velocity by (2.62) is much less than the initial velocity v_0 acquired by the electron in the accelerating gap (electron gun).

According to (2.62) the greatest amplitude of velocity modulation v_1 is obtained when $M \to 1$, i.e. when $\theta \to 0$. Thus, the coupling coefficient M is a very important factor not only in the process of current induction in the output gaps of microwave tubes, but in control assemblies designed to produce velocity modulation of the electron beam, as well. The greater the transit angle θ (refer to the graph of Fig. 2.7), the lower is the efficiency of the modulation process. At $\theta = 2\pi$, there is no velocity modulation at all; employing still greater values of the transit angle is also practically useless because of the small value of the gap factor M.

We may draw still another conclusion from the examination of equation (2.61). With finite values of the transit angle the parallel-plane gap used for velocity modulation of the electron beam can be

represented by an equivalent gap of zero width located at the middle of the actual gap, provided the amplitude of the modulating voltage across the equivalent gap is taken to be by a factor of M smaller than the actual voltage. The general equations of velocity modulation hold in this case[1].

At transit angles approaching zero, the electron beam at the output of the modulating gap is not yet density-modulated. Therefore, if $\theta \to 0$ the number of electrons accelerated by the gap field is exactly equal to the number of decelerated electrons. Velocity modulation in this case should be accomplished without any power drain from the source of control signal.

The situation will be somewhat different if the finite value of the electron transit angle is taken into account. In Section 2.7 it was demonstrated, that at $0 < \theta < 2\pi$ the gap carrying an unmodulated electron beam features a certain finite conductance G_e, which is positive in this range of transit angle values. This conductance is responsible for the average microwave power taken from the source of input signal.

The gap conductance that is due to the passage of the d.c. component of the convection current I_0 is usually referred to as the *electron load conductance* and designated as $G_{e.l}$. According to equations (2.55) and (2.51), this quantity can be described as

$$G_{e.l} = \frac{I_0}{2V_0} \frac{2(1-\cos\theta)-\theta\sin\theta}{\theta^2} \tag{2.63}$$

This equation can also be presented as

$$G_{e.l} = \frac{I_0}{2V_0}(M^2 - \sin\theta/\theta) \tag{2.63a}$$

In the present case, therefore, a finite value of the transit angle deteriorates the performance of a modulating gap as to both the efficiency of velocity modulation and the input conductance of the gap, just as was the case with electrostatic beam control. It can easily be shown, however, that these harmful effects are considerably less significant than with electrostatic control.

For example, consider the most unfavourable (from the point of view of the $G_{e.l}$ value) transit angle, which is about π. Suppose the accelerating voltage to be 300 V at a beam current $I_0 = 30$ mA. By equation (2.63) the input conductance $G_{e.l} = 2.2 \cdot 10^{-5}$ mho, this being quite a small value as compared to the input conductance in case of electrostatic control, calculated in Section 2.5*a* (to say nothing of the fact, that at such transit angles electrostatic control becomes entirely inoperable).

[1] It should be kept in mind that equations (2.61) and (2.62) describe variations of the velocity of *different* electrons that pass through the modulation gap at different instants of time t_0.

At moderate values of the beam current, the electron conductance with velocity modulation does not usually exceed the actual conductances G of resonant cavities used in conjunction with interaction gaps (a typical value of the resonant cavity G, as referred to the plane of the gap, is about 10^{-3} to 10^{-4} mho). In a number of cases the effects of the input conductance can be completely neglected and the process of velocity modulation considered as dissipationless.

At transit angles equal to π the effectiveness of velocity modulation by (2.62) is diminished in direct proportion to the gap factor M, which is equal to 0.635. Therefore, the effect of a finite transit angle in this case is mainly reduced to the following: in order to maintain the same depth of modulation, the amplitude of the modulation voltage should be increased by about 30 per cent as compared to the "perfect" conditions of a zero transit angle.

An important peculiarity of the velocity modulation technique is that the tube cathode does not form part of the radio-frequency circuit. This allows electron beam acceleration to considerable velocities before it enters the interaction gap. Thus, even with modulation gaps of appreciable width it becomes possible to obtain, at very high frequencies, small values of the transit angle, in any case not exceeding π. On the other hand, removing the cathode from the radio-frequency region of the tube allows the design, dimensions and configuration of this electrode to be chosen on the basis of the required emissivity, beam configuration, convenience of mounting, etc.

2.8c. Conversion of Velocity-Modulated Electron Beam into Density-Modulated Electron Beam

The final goal of introducing velocity modulation is to produce a convection current with as high a radio-frequency component $i(t)$ as possible

$$i_{con} = I_0 + i(t)$$

The process of conversion of the velocity modulation of the beam into density modulation has to take place automatically, outside the modulating gap, in the space between the modulating and the output gaps (the latter are often termed the *buncher* and *catcher*, respectively).

Two techniques for converting a velocity-modulated beam into a density-modulated one are used in modern microwave electronics, namely, the so-called *drift method* and the *retarding-field method*. The first is based on the movement of electrons due to inertia in a space free of any external fields, either static or radio-frequency; the second technique utilizes electron movement in a static longi-

tudinal electric field. Skeleton diagrams of devices carrying out these two methods of conversion are presented in Fig. 2.28.

A diagram of electron motion (velocity) in a system consisting of a cathode K, accelerating electrode A and a velocity-modulating gap formed by two grids G_1 and G_2 (refer to Fig. 2.28*a*) is presented in Fig. 2.29. The output arrangement is placed behind the gap and kept at the same constant voltage. The space between the modulating gap and the output arrangement is known as a *drift space*

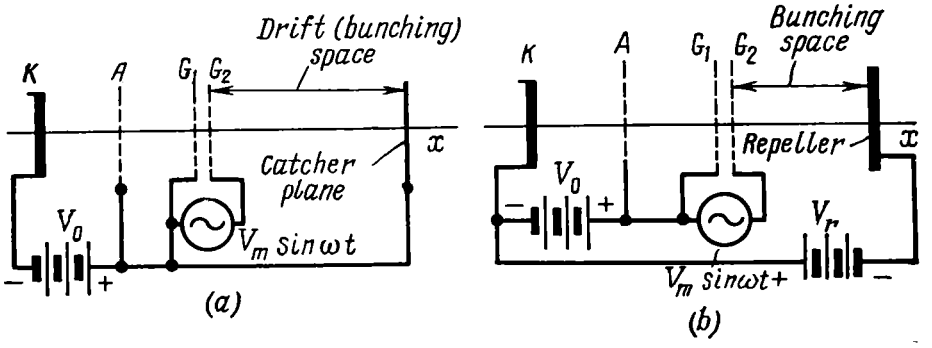

Fig. 2.28. Conversion of velocity modulation into density modulation by means of the drift (*a*) and retarding-field (*b*) methods

or a *bunching space*; this region is free of any static or radio fields. It is just in this space that the conversion in question should take place.

Consider the motion of four typical electrons passing through the modulating gap at different instants t_0. Electrons of types *1* and *2*, which pass the gap at the instants the microwave field is zero, retain their velocities; the velocity of electrons of type *3* is increased in an abrupt manner, while electrons of type *4*, which pass through the gap at a maximum retarding field, are decelerated as compared with electrons *1* and *2*.

Moving in the drift space due to inertia, the "fast" electrons of type *3* gradually catch up with electrons of type *1*, which crossed the gap a quarter of an oscillation period earlier. At the same time, the "slow" electrons (type *4*) lag behind electrons of type *2* which have not changed their velocities. As a result, the beam is compressed into an electron bunch at a certain plane $x = \text{const}$, where the gap of the catcher can be located. Thus, the electron beam has become bunched, i.e. density-modulated with a depth of modulation, as seen from Fig. 2.29, which is a function of the spacing between the buncher and the catcher, i.e. a function of the time of electron transit through the drift space. At specified operating frequency and voltages V_0 and V_m, there is a certain optimal length of the drift space which corresponds to the highest value of the radio-frequency component of convection current in the catcher circuit.

Though it is possible that electrons of types *1*, *3* and *4* arrive simultaneously at one and the same plane as illustrated above, simultaneous arrival at the same plane of all the other electrons, which occupy an intermediate position as regards the time of entering the gap t_0, is not obvious. Indeed, as will be shown later, the simultaneous arrival of all the electrons requires a special waveform of

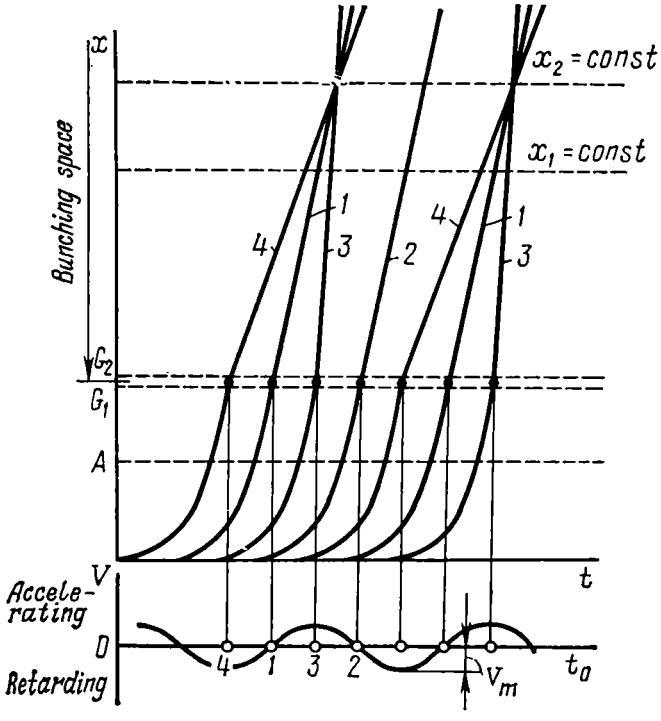

Fig. 2.29. Motion diagram of conversion of velocity modulation into density modulation by the drift method

the modulating voltage across the buncher gap, this waveform differing from a simple sine wave. Nevertheless, even the velocity diagram examined allows certain important qualitative conclusions concerning the laws of electron beam bunching to be drawn. *The electron bunches arriving at the catcher gap are formed around electrons that pass the middle of the buncher gap at a zero radio-frequency field, when the latter changes from a retarding to an accelerating one, if the conversion from velocity to density modulation is accomplished by the drift method.* The rate of recurrence of these electron bunches is exactly equal to the frequency of the modulating voltage. These conclusions should be particularly emphasized, because they will be of importance for the discussion of devices which employ velocity modulation of electron beams.

Consider now the circuit (Fig. 2.28*b*) in which velocity modulation of an electron beam is converted into density modulation with

the aid of the retarding-field technique. In the space behind the modulating (bunching) gap a time-invariable retarding field is developed by means of a special electrode, the *repeller* or *reflector*, to which a voltage negative with respect to the cathode is applied.

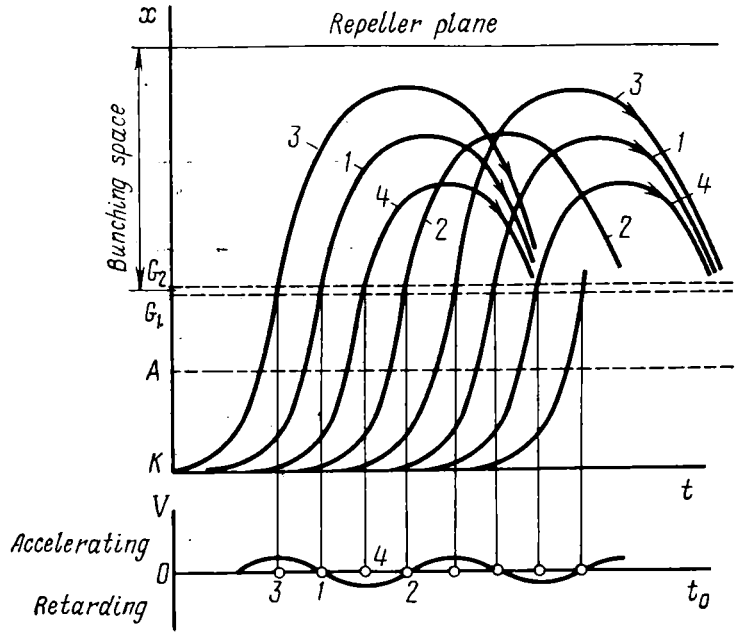

Fig. 2.30. Motion diagram of conversion of velocity modulation into density modulation by the retarding-field method

The space between the modulating gap and the repeller, as in the previous case, is also termed the *bunching space*, but the term "drift" is no longer applicable.

The process of conversion in a retarding static field can be qualitatively examined by means of the motion diagram presented in Fig. 2.30. The motion of electrons in the bunching space is similar to the motion of electrons in a positive-grid triode, discussed above (refer to Section 2.6), the main difference being that in case of a positive-grid triode the regions of static and radio-frequency fields coincide, while in the case under examination the bunching space contains only a static electric field of longitudinal direction.

If the potential of the repeller is set to be nearly equal to that of the cathode, the beam reflected from the repeller may be density-modulated since part of the electrons is intercepted by this electrode. However, a much more effective way is to reverse the motion of electrons before they arrive at the repeller surface. As can be seen from Fig. 2.30, electrons of type *3* and *4*, that pass through the modulation gap at the highest accelerating and retarding fields, respectively, are bunched around electrons of type *1*.

Thus, *in case the conversion from velocity modulation to density modulation is by the retarding-field method, the electron bunches are formed around electrons that pass the middle of the bunching gap at a zero radio-frequency field, when the latter changes from an accelerating to a retarding field.* Here lies the difference between the drift and the retarding-field method.

There is still another peculiarity of these two conversion methods examined, that also merits some attention. In the first case (the drift method) the density modulation can be utilized in a catcher arrangement mounted behind the modulating gap, with the electron beam passing through each of these gaps only once in the forward direction. This method underlies the performance of modern *multicavity klystrons.* In the second case (the retarding-field method), the most suitable time of coupling out the energy of the electron bunches is when they travel back toward the bunching gap, this making it possible to combine the modulating and catcher gaps into one to be placed in a single resonant cavity; in this case electrons travel twice through one and the same gap, but in opposite directions. A system of this kind was first proposed by the Russian scientists N. Devyatkov, Ye. Daniltsev and I. Piskunov in 1940, and by V. Kovalenko. A numerous class of modern microwave devices, *reflex klystrons*, depend for their operation upon this principle.

2.8d. Non-Resonant Arrangements for Velocity Modulation

The modulating assemblies examined above are narrow-band because the buncher gap forms an integral part of a resonant cavity. If the cavity is not tuned exactly to the frequency of the input signal, the amplitude of microwave oscillations will rapidly deteriorate, this resulting in a less deep velocity modulation. A similar situation is found in the output assembly treated in Section 2.4*c*.

To provide wideband velocity modulation, resonant systems with short-term interaction have to be replaced by non-resonant structures with prolonged interaction of the electron beam and the microwave field. As the velocity-modulating system a slow-wave structure (a guiding system supporting a slowed-down wave) can be employed.

Consider a section of a slow-wave system, such as of a helix, to whose input a microwave signal is applied, as shown in Fig. 2.31. The other end of this system terminates in a matched load. An electron beam provided by an ordinary electron gun is passed along the system axis.

For a qualitative explanation of velocity-modulation effects in this system, it is expedient to examine the case of synchronism, i.e. approximate equality of the wave phase velocity v_p to the velocity v_0 of the electron beam, both of these velocities having the same direction. A graph representing the distribution of the longitudinal

component E_z of the travelling wave in a reference plane moving with the wave phase velocity v_p, is shown in Fig. 2.32. Here the slow-wave length is designated as λ_{slow}; the radio-frequency field E_z appears as static in this reference plane.

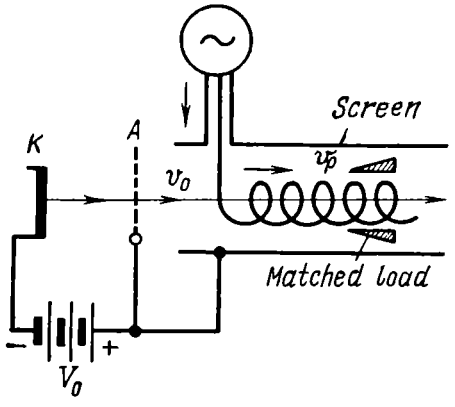

Fig. 2.31. Helix as a velocity-modulating device (the case of positive dispersion)

Electrons of types *1* and *2* (refer to Fig. 2.32) remain immobile relative to the reference plane adopted, provided the condition $v_p = v_0$ is satisfied, because they are located at the points of zero radio-frequency field. Electrons of type *3* are continuously accelerated by the longitudinal electric field and therefore acquire velocities exceeding v_0. Correspondingly, electrons of type *4*, which are located in a maximum retarding field, are decelerated. Thus, the beam acquires periodical velocity modulation with the depth of modulation growing as the beam travels along the slow-wave system.

Note that the electron beam emerging from the slow-wave system is not only velocity-modulated but, to some extent, density-modulated. The centres of the bunches are electrons of type *1* in the regions where the radio-frequency field E_z passes through zero when changing from an accelerating to a retarding field.

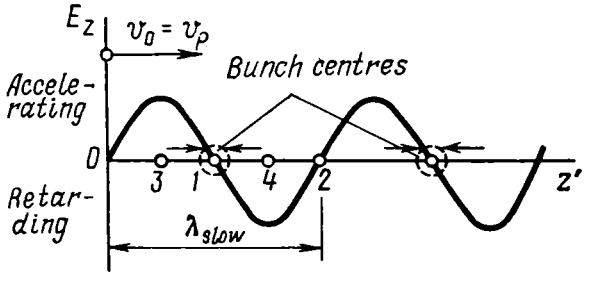

Fig. 2.32. Velocity modulation with prolonged interaction of electron beam with the field of a travelling slow-wave

With forward (positive) dispersion, the input signal should be applied to the gun end of the slow-wave structure, as illustrated in Fig. 2.31; when the electron beam is synchronous with one of the negative (backward) spatial harmonics, the input signal should be fed into the slow-wave structure at the collector end.

The less pronounced the dispersion effects, the wider is the band of frequencies within which the electron beam remains in synchronism with the slow wave at a constant value of the d.c. accelerating voltage V_0. In helical slow-wave systems the operating bandwidth can amount to 50 to 100 per cent of the middle frequency.

The intensity of the longitudinal electric field in a slow-wave structure is considerably lower than in a resonant cavity at the

same level of input power. The electron transit angle through a slow-wave structure, however, is not limited in principle. Therefore the path over which the electron beam acquires modulation from the radio-frequency field in a slow-wave system can be made well in excess of the width of the bunching gap of a resonant cavity. As a result, the radio-frequency component of velocity in the electron beam at the system output can be made of the same order of magnitude as in high-Q resonant systems with short-term interaction.

The modulating travelling-wave arrangement discussed is very much similar to the output system outlined in Section 2.4*d*, just as the resonant buncher and catcher systems resemble each other. Applying the reciprocity principle, all such systems can be treated as *arrangements for coupling* the electron beam to an external circuit.

2.8e. Phase Focussing Concept. Perfect Modulating Voltage Waveform

The motion curves illustrating the process of conversion of a velocity-modulated electron beam into a density-modulated electron beam feature peculiar bends and intersections and somewhat resemble the pattern of rays of light being focussed by an optical lens. This optical analogue is termed *phase focussing*, in contrast to geometrical focussing known from the classical and the electron optics. The gap with two grids, used to produce velocity modulation, can thus be said to function as a *phase lens.*

Consider the waveform $V = f(t)$ of the signal across a gap of infinitesimal width (across a phase lens), that should be applied to produce perfect phase focussing. Assuming as before, that the electrons enter the modulating gap with identical velocities v_0, the kinetic energy of the electrons at the output of this phase lens can be described as

$$\frac{mv^2}{2} = \frac{mv_0^2}{2} + eV$$

Hence, the electron velocity is

$$v = v_0 \left(1 + \frac{2eV}{mv_0^2}\right)^{1/2} \tag{2.64}$$

With the drift method of beam bunching the electrons which are to constitute the centres around which the bunch will be formed, travel through the gap at a zero microwave voltage, when the field changes from retarding to accelerating (refer to Section 2.8*c*). Therefore, the time of travel of the bunch centre as far as the point of focussing (which may properly be termed the *phase focus*) is $\tau_0 = s/v_0$, where s is the spacing between the phase lens and the phase focus.

The time can be reckoned from the instant the central electron of the bunch passes through the phase lens. For any other electron,

passing through the gap at $t \neq 0$ and $V \neq 0$, the transit time is $\tau = s/v$.

The condition that all electrons arrive simultaneously at the phase focus can be described as

$$\tau_0 = \tau + t$$

and taking into account (2.64) this can be presented as

$$\frac{s}{v_0} = \frac{s}{v_0\left(1+\frac{2eV}{mv_0^2}\right)^{1/2}} + t$$

Taking into account the relation $v_0 = \left(\frac{2eV_0}{m}\right)^{1/2}$ gives

$$V = V_0\left[\frac{1}{(1-v_0t/s)^2} - 1\right] \tag{2.65}$$

The perfect waveform of the modulating voltage is illustrated in Fig. 2.33 as a graph plotted in accordance with equation (2.65).

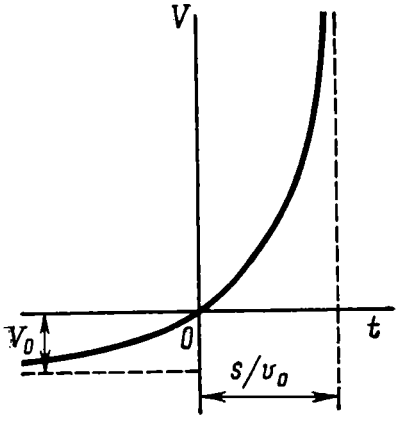

Fig. 2.33. Perfect waveform of modulating voltage

Physically the tendency of the voltage $V = f(t)$ toward V_0 as t approaches $-\infty$ is readily explained by the fact that electrons passing the gap long before the central electron of the bunch have to be practically stopped and should then wait at the phase focus for the central electron to catch up with them. Furthermore, the voltage across the bunching gap should approach infinity at $t = s/v_0$, because at this instant the central electron is exactly at the phase focus and electrons which are in the phase lens should acquire infinitely great velocities to be able to catch up with the central electron (relativistic effects being neglected). Obviously, all electrons entering the gap after s/v_0 cannot be compressed into the electron bunch in question.

In order to obtain periodic electron bunches the voltage across the gap should be of a saw-tooth waveform, as illustrated qualitatively in Fig. 2.34*a*. In this case pulses of convection current of infinitely short duration dt (theoretically, of course) (Fig. 2.34*b*) arrive at the phase focal plane. The d.c. component of this current is finite and exactly equal to the d.c. current from the electron gun at the input to the phase lens. Thus, all electrons emitted from the cathode and entering the two-grid bunching gap turn out to be "favourable".

The above conditions correspond to ideal electron bunching obeying the delta-function law mentioned in Section 2.4*b*. A high

efficiency of the direct-current to radio-frequency energy conversion provided by the accelerating voltage supply can be obtained by passing the electron bunches through an output (catcher) arrangement, mounted at the plane of the phase focus. In this case, however, the efficiency is limited by the spread of electron velocities in the bunch, inherent to this mechanism of current control. To obtain efficiencies approaching the ideal value of 100 per cent, the distribution of electron velocities should obey a delta-function law. Thus, the use of velocity modulation leads to a new contradiction,

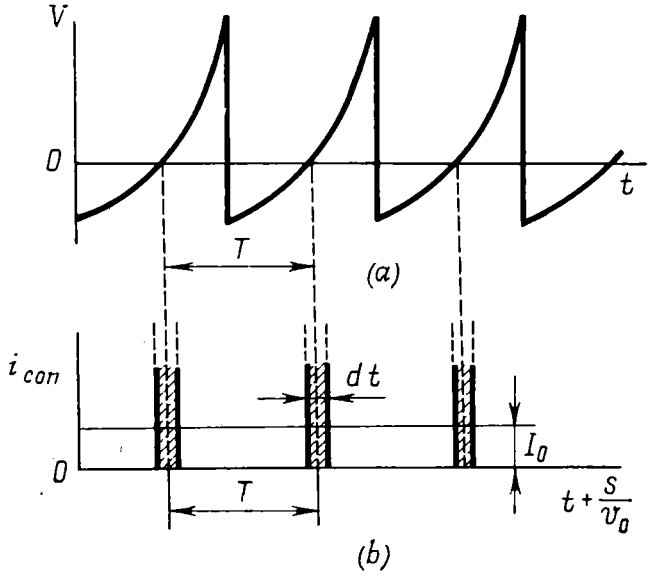

Fig. 2.24. Periodic phase focussing of a continuous electron beam

which can in part be circumvented by reducing the amplitude of the saw-tooth voltage or increasing the value of the d.c. accelerating voltage V_0.

Practically, it is quite a problem to develop a saw-tooth radio-frequency voltage. Ordinarily, the modulating voltage is of a sine waveform, especially if resonant cavities of high Q-factors are employed.

Sinusoidal-law modulation can be considered only as a very rough approximation of the perfect velocity modulation and therefore in principle cannot provide for complete phase focussing of an electron beam, this inevitably resulting in a reduced efficiency of tubes utilizing velocity modulation. Convection current under sinusoidal phase focussing is treated in some detail in Chapter Five, where various types of klystrons are examined.

In the broad sense, phase focussing takes place not only in the case being considered but at any quickly varying electric fields. The term "phase focussing" is sometimes used in the same meaning as "bunching" and implies dynamic control of electron beam.

Concluding this brief discussion of the general problems of velocity modulation, it should perhaps be emphasized that this kind of modulation ordinarily accompanies the usual density modulation employed in triodes, tetrodes and other types of conventional and microwave tubes. Strictly speaking, there is no "pure" density modulation, just as "pure" velocity modulation is almost never encountered. At relatively low frequencies, however, the effects of electron velocity modulation and subsequent density modulation (electron bunching) can, as a rule, be neglected because of the insignificant transit angle. This is also the reason why velocity modulation is not directly applicable to low-frequency electron devices; the dimensions of such tubes at low frequencies would be prohibitive.

2.9. Waves in Electron Beams

Processes in microwave devices, which take place at considerable transit angles, are mainly analysed by examining the laws governing the motion of individual electrons typical for the process in question. Here the effects due to lagging electric potentials may be neglected. The above analysis of velocity modulation can be cited as an example. Another possible approach is to use somewhat different concepts, which treat the electron beam as a peculiar medium, through which electromagnetic waves are propagated.

Consider an electron beam travelling in a drift space, where no external static electric fields are present. Assume for simplicity that the electrons travel only in the $+z$ direction without any transverse motion. Such a situation can be visualized as the result of applying an infinitely strong longitudinal static magnetic field for electron beam focussing.

An electromagnetic disturbance is superimposed onto this beam, for instance, with the aid of the simplest two-grid gap, discussed in Section 2.8. Suppose all the radio-frequency quantities describing the field and the beam (such as field intensities $\bar{E}$ and $\bar{H}$, electron velocity v, charge density ρ and so on) vary in time according to a sinusoidal law with a delay directed along the z axis; this law in complex form can be described by a factor $\exp(j\omega t - \Gamma z)$, where Γ is the propagation constant of the wave in question[1].

Under the assumptions adopted and neglecting the spread in initial electron velocities of the undisturbed beam, the velocity of electrons at any plane of the disturbed beam can be presented as

$$\bar{v} = \bar{e}_z v; \quad v = v_0 + v_1 \exp(j\omega t - \Gamma z) \tag{2.66}$$

[1] In waveguide theory the complex propagation constant is designated by the symbol γ; in the present book the capital Γ is used in the case of an electron beam travelling inside a waveguide.

where v_0 and v_1 are the initial and radio-frequency component of the electron velocity, respectively, and $\bar{e}_z$ is the unit vector along the z axis.

The density of the space charge can also be considered as the sum of a static and a radio-frequency component

$$\rho = \rho_0 + \rho_1 \exp(j\omega t - \Gamma z) \tag{2.67}$$

The wave equation for the vector of electric field intensity $\bar{E}$ can be obtained by applying Maxwell's equations (2.1) to (2.4). Substituting the field intensity $\bar{H}$ from (2.2) into equation (2.1) and assuming a zero specific conductivity of the medium yield

$$\nabla^2\bar{E} + k^2\bar{E} = \frac{1}{\varepsilon_0}\operatorname{grad}\rho + j\omega\mu_0\rho\bar{v} \tag{2.68}$$

where $k^2 = \omega^2\varepsilon_0\mu_0$. The relative permittivity and permeability are taken to be unity because electron movement takes place in vacuum.

Equation (2.68) differs from the ordinary wave equations of transmission lines in that the right-hand side is not zero because of the presence of an electron beam.

First the case of a beam of infinite width without any variations along the transverse section will be examined, this reducing the problem to a one-dimension case, i.e. all quantities characterizing the propagation of the disturbance along the beam are independent of the transverse coordinates. Consequently,

$$\nabla^2\bar{E} = \frac{\partial^2\bar{E}}{\partial z^2} = \Gamma^2\bar{E}$$

In a rectangular system of coordinates equation (2.68), with (2.66) taken into account, can be presented as three equations

$$(k^2 + \Gamma^2)E_x = 0 \tag{2.69}$$

$$(k^2 + \Gamma^2)E_y = 0 \tag{2.70}$$

$$(k^2 + \Gamma^2)E_z = \frac{1}{\varepsilon_0}\frac{\partial\rho}{\partial z} + j\omega\mu_0\rho v \tag{2.71}$$

Equations (2.69) and (2.70) do not depend on the presence of an electron beam and describe ordinary TEM propagation modes for which $\Gamma = \pm jk$, and, therefore, are of no interest for the present discussion.

The term ρv in the right-hand side of equation (2.71) describes the density of the beam convection current. Assume the radio-frequency components of velocity v_1 and charge density ρ_1 to be small as compared to the d.c. components v_0 and ρ_0. Thus we shall restrict ourselves in further treatment to the small-signal case. Neglecting the product of small quantities $\rho_1 v_1$, the approximate

equation based on equations (2.66) and (2.67) can be derived:

$$\rho v = \rho_0 v_0 + (\rho_1 v_0 + \rho_0 v_1) \exp(j\omega t - \Gamma z) \tag{2.72}$$

In the subsequent discussion the d.c. component of convection current density $\rho_0 v_0$ can be disregarded as of no interest for the case in question (for simplicity, this static space charge can be assumed to be compensated by the space charge of positive ions).

The longitudinal component of the radio-frequency electric field in the electron beam may be then presented as

$$E_z = E_{zm} \exp(j\omega t - \Gamma z) \tag{2.73}$$

Thus, taking relations (2.67) and (2.72) into account, the wave equation (2.71) for the radio-frequency component of the convection current reduces to

$$(k^2 + \Gamma^2) E_{zm} = -\frac{\Gamma}{\varepsilon_0} \rho_1 + j\omega\mu_0 (\rho_0 v_1 + \rho_1 v_0) \tag{2.74}$$

The radio-frequency components of charge density and electron velocity in equation (2.74) are functions of the electric field intensity E_{zm}. The above equation should, therefore, be examined in conjunction with the equation of electron motion (2.9) and the equation of continuity (2.13).

In the non-relativistic case ($v \ll c$) the equation of electron motion in a uni-dimensional case reduces to

$$\frac{dv}{dt} = -\frac{e}{m} E_z \tag{2.75}$$

Since the velocity of electrons by (2.66) is a function of two variables z and t, it follows that

$$\frac{dv}{dt} = \frac{\partial v}{\partial t} + \frac{\partial v}{\partial z}\frac{dz}{dt}\,; \quad \frac{dv}{dt} = \{j\omega v_1 - \Gamma v_1 (v_0 + v_1 \exp(j\omega t - \Gamma z)\} \cdot \exp(j\omega t - \Gamma z)$$

Again neglecting the product of small quantities, with relation (2.73) taken into account, equation (2.75) can be presented as

$$v_1 = -\frac{e}{m} \frac{E_{zm}}{j\omega - \Gamma v_0} \tag{2.76}$$

Now it remains only to determine the amplitude of the radio-frequency component of the charge density. We apply the equation of continuity (2.13) and assume $\frac{\partial}{\partial x} = \frac{\partial}{\partial y} = 0$ in an infinitely wide beam. Neglecting the product of small quantities when differentiating by z and t, with the aid of equations (2.66) and (2.67), we obtain

$$\rho_1 = v_1 \frac{\Gamma \rho_0}{j\omega - \Gamma v_0} \tag{2.77}$$

Substitution of (2.76) and (2.77) into the right-hand member of the wave equation (2.74), neglecting the trivial solutions $E_{zm} = 0$ and $k^2 + \Gamma^2 = 0$, after simple rearrangements, yields

$$\frac{e\rho_0}{m\varepsilon_0 (j\omega - \Gamma v_0)^2} = 1 \tag{2.78}$$

This equation may be used to calculate the propagation constant Γ and is known as the *characteristic* or *dispersion* equation of waves in electron beams.

The undisturbed concentration of electrons in the beam, i.e. the number of electrons per unit volume (one cubic metre) in the absence of a radio-frequency field, will be designated as N. Then $\rho_0 = -Ne$ and equation (2.78) can be reduced to

$$\frac{Ne^2}{m\varepsilon_0} \frac{1}{(\omega + j\Gamma v_0)^2} = 1 \tag{2.79}$$

The term $Ne^2/m\varepsilon_0$ in this equation should have the dimension of the frequency squared; denoting it as ω_p^2, we obtain

$$\omega_p = e \left(\frac{N}{m\varepsilon_0} \right)^{1/2} \tag{2.80}$$

This equation (2.80) is extensively used in the theory of microwave electron and gas-filled devices. The quantity ω_p is usually referred to as the *natural frequency of electron plasma oscillations*, or *plasma frequency* for short. In Chapter Eight this quantity will be shown not only to characterize the propagation of waves in electron beams, but to determine the frequency of microwave oscillations spontaneously developed in the plasma of electric gas discharges.

Applying equation (2.80), the characteristic equation (2.79) yields

$$\Gamma = j \frac{\omega \pm \omega_p}{v_0} \tag{2.81}$$

Thus, the propagation constant of waves along electron beams can be of one of two values, corresponding to the different signs in equation (2.81). Designating $\Gamma = j\beta$ (where β is the phase constant of the waves in question), we can determine the phase velocity of waves propagating along electron beams by taking into account that in the general case the phase constant is a function of the angular frequency ω and the phase velocity v_p of the wave $\beta = \omega/v_p$; hence

$$v_p = v_0 \frac{\omega}{\omega \pm \omega_p} \tag{2.82}$$

As usual, the group velocity v_g is determined from the relation $v_g = \frac{d\omega}{d\beta}$. As can easily be demonstrated, by differentiating equation (2.81), the group velocity of both waves is identical and is exactly equal to the undisturbed beam velocity v_0.

The above analysis shows that *two waves* can propagate along an electron beam, the direction of propagation of both waves coinciding with the direction of electron travel. The electron plasma frequency ω_p which determines the velocity of these waves, at current densities and electron concentrations usually encountered in practice, proves to be significantly lower than the frequency ω of the radio-frequency signal. Therefore, the phase velocities of both waves described by equation (2.82) are of the same order of magnitude as the beam velocity v_0.

As follows from equation (2.82), these waves are dispersive and this is a sufficient reason for them not to be classed with TEM modes. The field pattern of these waves differs materially from that of "ordinary" TEM, TE and TM modes propagating along guiding systems in the absence of an electron beam. Indeed, equation (2.81) indicates that these waves are characterized by $\Gamma \neq jk$ and therefore $k^2 + \Gamma^2 \neq 0$. From equations (2.69) and (2.70) it follows that $E_x = E_y = 0$. Examination of the wave equation relative to vector $\overline{H}$ discloses $H_x = H_y = H_z = 0$ and the only field component present is the longitudinal electric field intensity E_z.

The waves under examination should therefore be classified among slow "electric" waves of a special kind; these waves cannot exist without an electron beam. The physical meaning of these waves can easily be understood when examining the variations of charge density along the electron beam. Since $\rho_1 \neq 0$, the electron beam displays periodic compressions of the electron gas and it is just these compressions that are responsible for the existence of a longitudinal electric field E_z. These waves may be properly called compression waves. Very often they are referred to as *waves of space charge* or *electron waves*. Besides, they are similar to the ordinary audio waves in a gas, which are also of a purely longitudinal nature.

The first of these waves of space charge with a phase velocity slightly less than the average beam velocity (according to equation (2.82)) is usually known as the *slow wave*, while the second wave whose phase velocity is somewhat higher than the average beam velocity is called the *fast wave*[1].

Since the constant Γ calculated above is a purely imaginary quantity, neither build-up nor attenuation of the waves of a space charge takes place; oscillations are neither amplified nor generated. The situation changes, however, if there exist electrons having different velocities. Thus, when the motion of two electron beams is parallel and their velocities v_{01} and v_{02} are close but not equal,

[1] Unfortunately, the term "fast wave" is sometimes also used to describe the ordinary transverse electromagnetic wave of the TEM propagation mode; in the present book this term will not be applied to TEM modes so as to exclude possible confusion.

the waves interact so that their amplitudes build up. This principle underlies the operation of *double-stream* electron-wave amplifiers.

It is of interest to find the numerical value of the phase velocities of space charge waves by equation (2.82). The electron concentration N and the density of the d.c. component of convection current are interrelated by $J_0 = -Nev_0$. Hence, examining the absolute value of the convection current we obtain

$$N = \frac{J_0}{e\,(2eV_0/m)^{1/2}} \tag{2.83}$$

where V_0 is the constant voltage accelerating the electron beam.

Substitution of (2.83) into the equation for plasma frequency (2.80) results in

$$\omega_p = \left[\frac{J_0}{\varepsilon_0}\,(e/2mV_0)^{1/2}\right]^{1/2} \tag{2.84}$$

Suppose the beam convection current density to be 1 A/cm^2, i.e. 10^4 A/m^2, and the accelerating voltage $V_0 = 1000$ V. Applying equation (2.84), the phase velocities of the fast and slow waves of space charge for a 10-cm free space wavelength are found to be approximately $1.22v_0$ and $0.85v_0$, respectively.

In actual electron devices the electron beam is obviously of a finite width; it may be enclosed in a metal screen defining a drift space. The above simplified theory has to be modified to allow for the finite dimensions of the electron beam.

The presence of a conducting pipe should lead physically to a decrease in the longitudinal field intensity E_z at the outer boundary of the beam, which is concentric with the metal wall. Thus, the effect of variations of the space charge density is reduced. This can be taken into account by a corresponding reduction of plasma frequency in equations (2.81) and (2.82).

This effective (reduced) electron plasma frequency will be designated as ω_p', this quantity, as mentioned, allowing for the finite cross-sectional dimensions of the electron beam and drift tube. Figure 2.35 presents in graphical form the results of calculations performed for the case of a solid cylindrical beam of radius b and a metal pipe of radius a. Plotted along the y-axis is the ratio of effective plasma frequency ω_p' to the frequency ω_p of an infinitely wide beam, the accelerating voltage V_0 and current density J_0 being the same for both cases. The effective plasma frequency is always lower than ω_p as defined by equation (2.84). The phase velocities of the fast and slow waves of space charge prove to be still closer to the average beam velocity v_0.

In "thick" electron beams higher modes of waves of space charge can exist along with the two simplest modes described above. These higher modes feature variations of the field, space charge density

and electron velocity across the transverse section of the beam, as well as along the beam length. Each higher mode corresponds to two waves of space charge propagating in the direction of electron transfer, with velocities close to the average velocity of the electron beam.

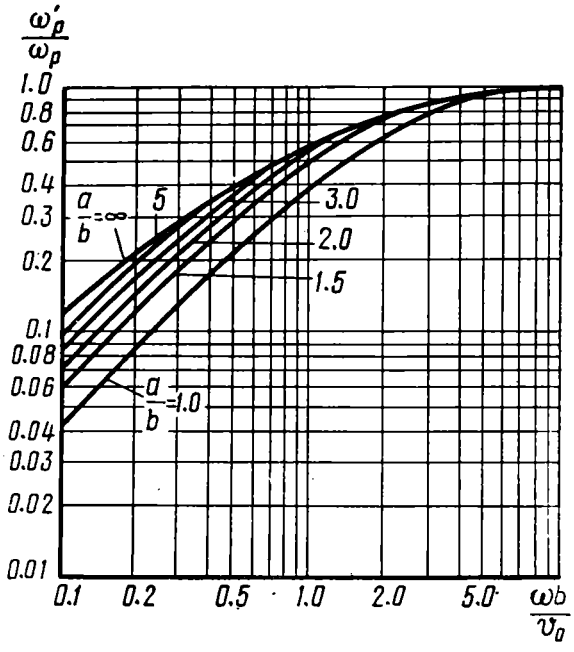

Fig. 2.35. Reduction of electron plasma frequency of a continuous hollow cylindrical electron beam of radius b confined inside a cylindrical metal screen of radius a

The concept of waves of space charge can be applied to explain the effects of velocity modulation and phase focussing, treated above. In this case the modulating gap may be considered as an assembly exciting waves by varying the velocities of electrons; the two space-charge waves thus developed have different velocities, and interference of these waves results in beats of the radio-frequency component of space charge density. The distance between the buncher gap and the point at which the convection current is at a maximum was treated earlier as the phase focus; now this spacing may be determined from the condition of the density beats being at a maximum.

In practice, applying the wave theory to the design of microwave electron devices is somewhat inexpedient. In certain cases, however, the wave concept proves to be extremely useful, as for instance in the treatment of travelling-wave tubes.

Besides waves of space charge, which are longitudinal in nature, electron beams are capable of supporting transverse waves of the cyclotron-frequency mode at finite intensities of the static magnetic field. Some properties of these waves are examined in Section 7.12.

CHAPTER THREE

GENERAL PROBLEMS OF MICROWAVE OSCILLATORS AND AMPLIFIERS

3.1. Equivalent Circuit of Oscillators with Resonant Oscillatory System. Electron Admittance

Operating conditions in microwave electron oscillators and amplifiers are determined by the following three main factors: *properties of the electron beam, parameters of the radio-frequency oscillatory system and characteristics of the load.*

Modern microwave oscillators and amplifiers may be divided into two major categories by the properties of the radio-frequency oscillatory system employed.

The first category includes devices in which the oscillatory system features discrete oscillation modes, i.e. can be considered as a single resonant circuit in the frequency range of interest. This category includes all devices (both existing and being developed) based on short-term interaction of an electron beam with the field of a gap and containing a resonant cavity (or several cavities). Devices with multiple or prolonged interaction, whose slow-wave structure operates under standing-wave conditions and forms an oscillatory system with discrete oscillatory modes, must also be placed into this category. Thus, amplifiers and oscillators of this group can be considered as devices with resonant oscillatory systems, or devices of the *resonant type* for short. Representative of this group of devices are microwave triodes and tetrodes, reflex and multicavity klystrons and magnetron oscillators.

The second category embraces devices with prolonged or multiple interaction, whose oscillatory system does not display resonant properties in the frequency band of interest and operates under travelling-wave conditions. Oscillators and amplifiers of this kind are usually classified among devices with non-resonant oscillatory systems or *non-resonant devices* for short. Forward-wave and backward-wave travelling-wave tubes as well as platinotrons belong to this group.

A convenient way of analysing the performance of oscillators and amplifiers with resonant oscillatory systems is by using equivalent circuits, a method widely used with waveguides and resonant cavities. In this method, the oscillatory system, external load and electron beam are presented as electric circuits with lumped constants. The equivalent circuit method may be used to generalize

many of the important properties of microwave electron devices, regardless of their actual design and purpose.

We shall first examine the "cold" oscillatory system[1] of an electron device, i.e. the resonant structure (cavity) with its load in the absence of an electron beam (or electron-ion plasma, if the device is of the gas-filled type). As is known from microwave engineering, any oscillatory system at frequencies in the vicinity of resonance of one of its oscillatory modes can be represented by a parallel connection of conductance G and susceptance B, as illustrated in

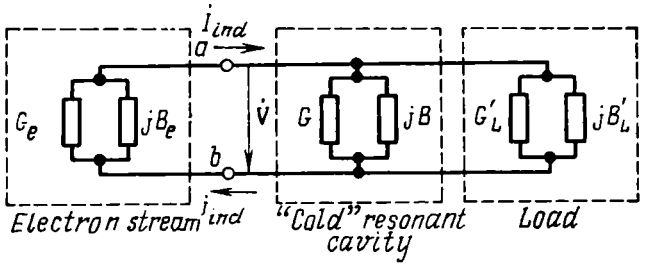

Fig. 3.1. Equivalent circuit of an electron device with a resonant oscillatory system

Fig. 3.1. Here G'_L and B'_L are the conductance and susceptance of the load, respectively, referred to the same section as G and B.

In cases when the resonant cavity is an integral part of an oscillator or amplifier and is excited by a modulated electron beam, the latter should be considered as a generator of induced current $\dot{I}_{ind}$ fed to the system through "terminals" ab. This causes a radio-frequency voltage $\dot{V}$ to be developed across the gap, this voltage in the general case being a complex quantity.

It is convenient to refer the cavity and load conductances and susceptances to the plane of the radio-frequency gap, this resulting in one and the same voltage $\dot{V}$ being applied to the oscillatory system, load and electron beam. Since the elements to the right from section ab in Fig. 3.1 are connected in parallel, it will be convenient to represent the action of the electron beam in terms of a certain *electron admittance* Y_e, connected, from the left, to the same terminals ab

$$Y_e = G_e + jB_e \tag{3.1}$$

The quantities G_e and B_e formally introduced here will be termed the *electron conductance* and *electron susceptance*, respectively.

[1] The "cold" parameters of a device do not imply the actual thermal conditions of the system. However, precise determination of the "cold" conductance of a resonant cavity necessitates that the cavity temperature be the same as in an operating device. Thus, the cavity should not be cold literally.

The concept of electron conductance was already used in the discussion of certain particular oscillators, namely the monotron and diode. Now this concept may be generalized to be used in connection with any electron device with a resonant oscillatory system.

Electron admittance is especially useful in the analysis of microwave oscillators. Returning again to the equivalent circuit of Fig. 3.1, we shall examine the steady-state conditions in the absence of any external (input) microwave signal. Once the oscillations have been built up, the vector sum of voltage drops to the right and left of section *ab* has to be equal to zero, in accordance with the second Kirchhoff law,

$$\frac{\dot{I}_{ind}}{G_e+jB_e}+\frac{\dot{I}_{ind}}{G+G'_L+j(B+B'_L)}=0$$

Hence

$$G+G'_L+G_e+j(B+B'_L+B_e)=0$$

Under steady-state conditions, therefore, the sum of conductances and susceptances in the entire system (oscillatory circuit, load and electron beam) in any self-oscillator should be equal to

$$G+G'_L+G_e=0 \tag{3.2}$$

$$B+B'_L+B_e=0 \tag{3.3}$$

These equations play an important part in the theory and design of microwave electron devices and will often be referred to in the subsequent discussion.

The physical meaning of the electron beam conductance in (3.2) can be explained by examining the energy relations. Designate respectively as P_e and P_c the power drawn from the gap by the electron beam and the circuit, the load included. From the law of energy conservation under steady-state conditions the following relation should be valid

$$P_e+P_c=0 \tag{3.4}$$

P_e and P_c can be related to the amplitude V_m of the voltage and conductances G, G'_L and G_e (Fig. 3.1) as follows

$$P_e=\frac{1}{2}V_m^2G_e; \quad P_c=\frac{1}{2}V_m^2(G+G'_L)$$

Substitution into equation (3.4) yields a relation exactly coinciding with (3.2), provided $V_m \neq 0$. Thus, (3.2) in which the sum of conductances is equal to zero is only a form of presenting the energy conservation law.

Relations (3.2) and (3.3) can be derived in still another way, by considering the circuit of Fig. 3.1 as a complex oscillatory circuit

with total conductance and susceptance

$$G_\Sigma = G + G'_L + G_e; \qquad B_\Sigma = B + B'_L + B_e$$

Free oscillations in a circuit of this kind will be sustained for an unlimited period of time at a constant amplitude if the circuit loss is zero, i.e. if $G_\Sigma = 0$. On the other hand, any parallel oscillatory circuit at its resonant frequency exhibits zero total susceptance, as is known from the circuit theory. This condition gives $B_\Sigma = 0$ which coincides with equation (3.3).

The conductances of the cavity and the load are essentially positive magnitudes. As a consequence, $G_e < 0$ is the condition of any self-oscillator operation. All microwave oscillators of the resonant type may therefore be classified as devices with a *negative conductance* (or *negative resistance*).

3.2. Oscillation Amplitude and Frequency in Terms of Electron Beam Conductance

3.2a. Steady-State Amplitude

The electron beam conductance G_e in equation (3.2) depends on the electronic mechanism involved in each particular case and in the general case can be a function of many parameters of the electron device

$$G_e = f(V_0,\ I_0,\ \theta,\ V_m,\ \ldots)$$

Consider the process of self-excitation, i.e. build-up of oscillations from any infinitesimal fluctuation present in the circuit of Fig. 3.1; all other parameters determining the magnitude of G, except the oscillation amplitude V_m, are assumed to be constant.

For oscillations to build up, the sum of all conductances at section *ab*, should be negative

$$\{G_e(V_m)\}_{V_m \to 0} + G_{tot} < 0 \tag{3.5}$$

where

$$G_{tot} = G + G'_L \tag{3.6}$$

By equation (3.2) any self-oscillator can be described by

$$G_e(V_{m0}) + G_{tot} = 0 \tag{3.7}$$

where V_{m0} is the steady-state amplitude of oscillations.

Operating conditions providing oscillation amplitude gradually increasing from the level of noise fluctuations to its steady-state magnitude are known as "*soft*" *self-excitation*. Comparison of relations (3.5) and (3.7) discloses the condition of soft self-excitation

$$|G_e(V_{m0})| < |G_e(V_m)|_{V_m \to 0}$$

where the function $-G_e(V_m)$ should feature a monotonically drooping pattern, as illustrated in Fig. 3.2*a*.

The steady-state amplitude V_{m0} can be determined from relation (3.7) by graphical techniques. The total conductance G_{tot}, which by (3.6) is the sum of conductances of the cavity and its load, is independent of the oscillation amplitude V_m and therefore V_{m0} may be represented by the point of intersection of the nonlinear function $-G_e(V_m)$ with the horizontal line $G_{tot} = \text{const}$, as illustrated in Fig. 3.2*a*.

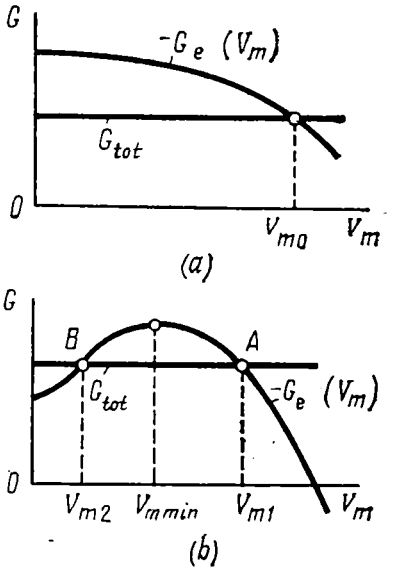

Fig. 3.2. Graphical determination of operating conditions of a microwave oscillator

Certain electron devices may feature a non-monotonic dependence of electron beam conductance on the amplitude of radio-frequency oscillations. Thus, as illustrated in Fig. 3.2*b*, there may be more than one point of intersection of the curve $-G_e(V_m)$ with the line $G_{tot} = \text{const}$. Here arises the problem of oscillation stability at points A and B.

Assume that the oscillator operates under conditions represented by point A and that an external factor causes a change in the amplitude of oscillations by ΔV_m. In case ΔV_m is small the function $G_e(V_m)$ may be approximated by

$$G_e = f(V_{m1} + \Delta V_m) \approx G_e(V_{m1}) + \Delta V_m \frac{\partial G_e(V_m)}{\partial V_m}$$

At a positive derivative $\frac{\partial G_e}{\partial V_m}$, as is the case at point A, any positive increment ΔV_m causes a positive increment to appear in the beam conductance, i.e. produces a lower value of G_e. Since the condition

$$G_e(V_{m1}) + G_{tot} = 0$$

is satisfied at point A, the system will acquire a certain amount of additional loss. As a consequence, the amplitude of oscillations will begin to fall till the initial conditions are restored. With a negative voltage increment the sum of the electron beam and total conductances will become negative, this inevitably leading to an increase in the amplitude of oscillations.

Thus, any change in oscillation amplitude at point A causes a reaction of the system, tending to restore the initial operating conditions (i.e., the magnitude of V_{m1}). From this it is inferred

that in the general case the oscillations will be stable, provided

$$\frac{\partial G_e}{\partial V_m} > 0; \quad \frac{\partial |G_e|}{\partial V_m} < 0 \tag{3.8}$$

which is a conclusion of major importance.

Similar argumentation concerning operating conditions corresponding to point B (Fig. 3.2*b*) discloses that with a negative derivative $\frac{\partial G_e}{\partial V_m}$ any positive voltage increment causes a negative increment in G_e, and the system loss becomes negative. Any fluctuation causing an increase in oscillation amplitude will therefore lead to a still higher amplitude, till a section of the curve $G_e = f(U_m)$ is reached where the derivative becomes positive and condition (3.7) is met again. Operating conditions will abruptly, during a very short time, change from those corresponding to point B to those of point A. Any negative voltage increment will result in the abrupt diminution of the oscillation amplitude down to zero.

Thus, the operating conditions are unstable, if at the point of intersection of curve $-G_e(V_m)$ with the line $G_{tot} = \text{const}$

$$\frac{\partial G_e}{\partial V_m} < 0; \quad \frac{\partial |G_e|}{\partial V_m} > 0 \tag{3.9}$$

The voltage $V_{m\,\min}$, at which oscillations cease to be stable corresponds to the maximum of the curve $-G_e(V_m)$ in Fig. 3.2*b*. Since this voltage is of a finite magnitude, self-excitation here is inevitably accompanied by abrupt changes in oscillation amplitude. These operating conditions are usually referred to as "*hard*" *self-excitation*. As will be shown in Section 3.3*b*, hard self-excitation is accompanied by undesirable hysteresis effects.

A question may arise here on the actual pattern of the curves $G_e = f(V_m)$ in microwave electron oscillators. Obviously, this question can be answered in full only when discussing particular types of oscillator devices (reflex klystrons, magnetrons, etc.), but physically the curve $-G_e(V_m)$ cannot be of a continuously increasing pattern because this would lead to infinite oscillation amplitudes and thus to unlimited increase in power obtainable from an electron beam. As the oscillation amplitude V_m rises, there has to be a fall (in absolute value) in the electron beam conductance, so that the curve somewhere goes through zero and then becomes positive.

3.2b. Start-Oscillation Current

Equation (3.5) can be employed to determine a very important parameter, the *starting current* I_s of an oscillator, provided the function of electron beam conductance is known beforehand, if only

for small-signal conditions. The starting current I_s is defined as the minimum value of electron-stream current (i.e. convection current I_0) through an oscillator at which self-sustained oscillations will appear under specified conditions of loading. At a finite amplitude of oscillations V_m the condition of oscillator operation is

$$I_0 > I_s \qquad (3.10)$$

The output power as a function of the d.c. convection current with all other parameters of the oscillator fixed is of a pattern qualitatively illustrated in Fig. 3.3.

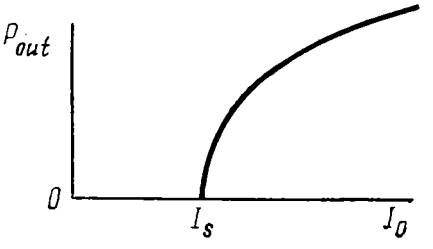

Fig. 3.3. To the problem of oscillator starting current

Consider for example the monotron oscillator. The electron conductance of the gap, according to the findings of Section 2.7, under small-signal conditions is

$$G_e = \frac{I_0}{2V_0} F(\theta)$$

Therefore, by equation (3.5), self-sustained oscillations in a monotron will be set up if

$$0 < G_{tot} \leqslant -\frac{I_0}{2V_0} F(\theta)$$

where G_{tot} is the sum of cavity and load conductances, referred to the plane of the gap. Hence, the starting current of this oscillator is

$$I_s = \frac{2V_0 G_{tot}}{-F(\theta)} \qquad (3.11)$$

Under the most favourable conditions for monotron self-excitation at $\theta \approx \frac{5\pi}{2}$ (refer to Fig. 2.24*a*), $F(\theta) = -0.095$ and $I_s \approx$ $\approx 21.1 V_0 \cdot G_{tot}$. Taking, for example, $V_0 = 300$ V and $G_{tot} =$ $= 10^{-3}$ mho, relation (3.11) yields $I_s \approx 6.33$ A. Even at $G_{tot} =$ $= 10^{-4}$ mho, the monotron starting current will be 0.633 A.

Such high current values in a thin electron stream at comparatively low accelerating voltages are ordinarily unobtainable. This in part accounts for the failure of most experiments aimed at developing practical monotron oscillators. As we see now, the absolute value of negative conductance in a monotron is too small, so that either the conductances of the resonant cavity and its load (as referred to the gap) must be reduced or the convection current greatly increased. Similar situations are encountered in certain other types of microwave devices.

3.2c. Frequency of Oscillations

The frequency of steady-state oscillations can be determined by applying equation (3.3), according to which the sum of susceptances of the system and the load and the susceptance of the electron beam under steady-state conditions is equal to zero. For simplicity, the admittance of the cavity load at the gap will be assumed purely ohmic, i.e. $B'_L = 0$ (the case of a complex load admittance is treated in Section 3.3). Any oscillator with an equivalent circuit of the kind shown in Fig. 3.1 should then have a cavity susceptance exactly equal to the susceptance of the electron beam, but of an opposite sign

$$B = -B_e \tag{3.12}$$

On the other hand, the susceptance B of any "cold" resonant system in the vicinity of the resonant frequency f_0 is related to the loaded Q-factor by

$$Q_L = \frac{f_0}{2G_{tot}} \left(\frac{dB}{df}\right)_{f \approx f_0} \approx \frac{f_0}{2(G+G'_L)} \frac{B}{f-f_0} \tag{3.13}$$

where f is the frequency at which the cavity susceptance is measured. Hence, applying the designations of (3.6), we obtain

$$B = 2Q_L G_{tot} \left(\frac{f}{f_0} - 1\right) \tag{3.14}$$

The frequency f, at which condition (3.12) is satisfied, corresponds to the frequency of steady-state oscillations, provided the values of f_0, Q_L, G_{tot} and B_e are fixed; substitution of equation (3.14) into (3.12) therefore yields

$$f_{osc} = f; \quad f_{osc} = f_0 (1 - B_e/2Q_L G_{tot}) \tag{3.15}$$

The quantity G_{tot}, in this relation, can be replaced by the electron conductance with a negative sign, according to the condition of steady-state amplitude (3.2). The frequency of steady-state oscillations is finally

$$f_{osc} = f_0 \left(1 + \frac{1B_e}{2Q_L G_e}\right) \tag{3.16}$$

Equation (3.16) is of prime importance. It shows that in the general case the frequency of oscillations is defined in the first place by the resonant frequency of the "cold" oscillatory system. The higher the loaded Q-factor of the cavity, i.e. the lower the loss in the cavity and the weaker its coupling with the load, the less is the difference between the frequency of self-sustained oscillations f_{osc} and the resonant frequency f_0.

The frequency of oscillations can be controlled by varying the value of f_0, i.e. by retuning the oscillatory system. It is just for

this purpose that the oscillators of the resonant type are fitted with mechanical tuning arrangements. One of the drawbacks of mechanical tuning is its inherent inertia, which motivated the search for other, faster methods of frequency control.

The resonant frequency of oscillatory systems is determined by their geometry. Therefore, variations of the temperature of these systems will cause corresponding changes in f_0 and, thus, in the frequency of oscillations. Such instabilities of oscillation frequency are usually evaluated in terms of the *temperature coefficient of frequency*, defined as the shift in oscillation frequency per degree change in temperature. Materials and designs, which provide as high a temperature stability of oscillation frequency as possible, are chosen when developing microwave oscillators.

3.2d. Electronic Tuning and Frequency Pushing

The electron susceptance, just as the electron conductance, is a function of the transit angle, constant voltages and direct convection current, as well as of the amplitude of radio-frequency oscillations. Therefore, the ratio B_e/G_e in (3.16) depends on the operating conditions of the oscillator in question

$$\frac{B_e}{G_e} = f(V_0,\ I_0,\ \theta,\ V_m,\ \ldots)$$

Equation (3.16) determining the frequency of steady-state oscillations in any oscillator with a resonant oscillatory system can therefore be presented now as

$$f_{osc} = f_0\left[1 + \frac{1}{2Q_L} f(V_0,\ I_0,\ \theta,\ V_m,\ \ldots)\right] \qquad (3.16a)$$

Thus, the frequency of oscillations within a certain range of values can be controlled by varying the direct convection current I_0 through the oscillator or the constant voltage V_0 applied to it, without having to retune the resonant cavity, i.e. at $f_0 = \text{const}$.

The change brought about in oscillation frequency by variation of the electron-stream current is known as *frequency pushing*. Frequency control by varying one of the constant voltages applied to the tube is termed *electronic tuning* or *voltage tuning*. In a broad sense, the term encompasses all methods of electrical (non-mechanical) frequency control, and is not necessarily restricted to influencing only electron streams but semiconductors, ferrites, etc.

Electronic tuning can easily be demonstrated graphically, as shown in Fig. 3.4*a*. Examine the points of intersection of the B *vs* frequency function with the $-B_e$ *vs* frequency curve, where condition (3.12) is satisfied. A change of the electron conductance from $(B_e)_1$

to $(B_e)_2$ causes a corresponding change in oscillation frequency from $f_{osc\,1}$ to $f_{osc\,2}$.

Electronic (voltage) tuning is an important feature of microwave oscillators; as will be shown later, this property is especially pronounced in devices with non-resonant oscillatory systems. Electronic tuning may be employed for instantaneous frequency control in addition to mechanical tuning, as well as for frequency modulation of a radio-frequency carrier. In cases, when the tuning range is wide enough, as determined by equations (3.16) and (3.16a), electronic tuning can be used instead of mechanical tuning of an oscillator.

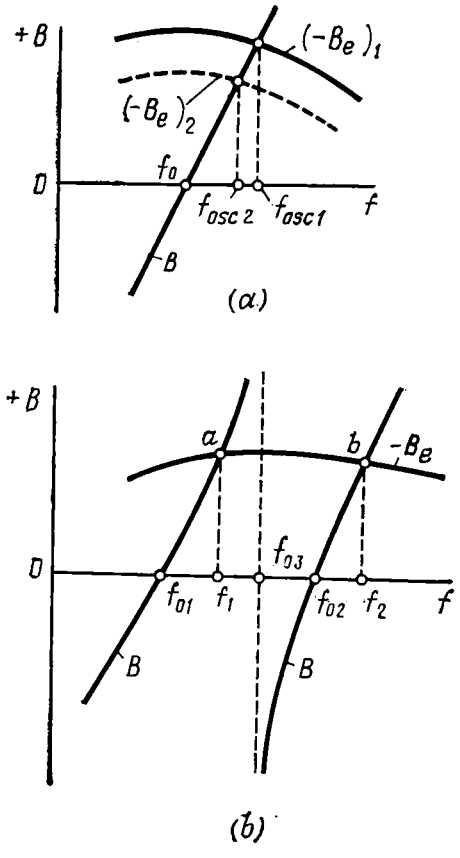

Fig. 3.4. Determining the steady-state frequency of an oscillator with a single (*a*) and two closely spaced (*b*) oscillation modes of the oscillatory system

By (3.16), the electronic tuning range can be increased by reducing the value of Q_L. This can be achieved by increasing the loss in the oscillatory system; in practice, however, a reduction in Q_L is obtained by a tighter coupling of the cavity to the load, which is more preferable from the point of view of device efficiency. As evident from (3.13), this leads to a higher conductance G'_L of the load (as referred to the gap plane). The same conclusion can be arrived at in a more formal manner, by examining the transformation of the load conductance to the plane of the oscillator gap. As we know from the first part of the course "Microwave Engineering" for any resonant cavity the transformed load conductance is

$$G'_L = G\frac{Q_0}{Q_{ext}}$$

where Q_{ext} is the external Q-factor of the resonant system. The total conductance of the cavity and its load is

$$G_{tot} = G + G'_L = G\left(1 + \frac{Q_0}{Q_{ext}}\right) \qquad (3.17)$$

and it may be varied within wide limits by changing Q_{ext} and thus Q_L.

Another important conclusion can also be made from relation (3.16a). A high stability of oscillation frequency at a constant load can be attained by the use of resonant cavities with as high Q_L as practicable, as well as high-stabilization supply sources (voltage V_0 and current I_0). However, in order to obtain high values of Q_L, it is necessary, in the first place, to raise Q_0 of the oscillatory systems by reducing, as far as possible, dissipative loss in the cavity in question. Another way of increasing Q_L is by the use of a looser coupling to the load. Use can also be made of additional (stabilizing) high-Q cavities (called idler cavities), which increase the amount of microwave energy stored in the oscillatory system[1].

So we see that the principles employed when designing voltage-tunable and highly stable oscillators can differ very much. These differences cover not only the oscillatory system and the degree of coupling to the load chosen but the parameters of the electron beam as well. Indeed, by equations (3.15) and (3.16), obtaining a wider range of electronic tuning necessitates variation of B_e within wider limits, while the latter (even from considerations of physical dimensions) must be proportional to the ratio I_0/V_0. Therefore, electronically tunable oscillators, in contrast to oscillators of stable frequencies, should operate at as low supply voltages and as heavy beam currents as practicable.

The difference between the steady-state frequency f_{osc} and the natural frequency f_0 of the resonant system is ordinarily quite slight and, as a first approximation, these frequencies can be considered identical when designing oscillatory systems for microwave devices. The error in calculating resonant cavities is considerably greater than the actual difference between these frequencies, as determined by equation (3.16).

3.2e. Oscillation Modes in Microwave Oscillators

Determination of the steady-state frequency becomes much more of a problem, if the "cold" oscillatory system supports more than one oscillation mode. Indeed, the dependence of system susceptance on operating frequency in this case may differ from a linear function, as can easily be noted, for instance, in Fig. 3.4*b*. Here this function (with an opposite sign) is shown to vary slowly within a certain limited frequency range, where the high-Q oscillatory system features two oscillation modes with resonant frequencies f_{01} and f_{02}. The curve B_e *vs* frequency intersects the susceptance curve of the oscillatory system at two points (*a* and *b*), corresponding to two fre-

[1] To increase the Q-factor the cavity is even sometimes fabricated of a superconducting material and operated at liquid-helium temperatures, this providing values of Q_0 of the order of 10^8 to 10^9 and even higher.

quencies f_1 and f_2. Both these frequencies are within the range of frequencies that are generated by the oscillator in question, provided condition (3.7) for the steady-state amplitude is satisfied in both cases.

In the general case the number of oscillation frequencies is equal to the number of oscillation modes supported by the "cold" oscillatory system in a range of frequencies where G_e remains negative. Each of these oscillation conditions is termed the *oscillation mode* of the oscillator being examined[1].

The term "oscillation mode" should not be confused with the same term which is unfortunately used also to describe oscillations based on different electronic mechanisms and should more properly be termed *oscillation types*. Thus, for instance, magnetrons treated in Chapter Seven are capable of oscillating at three different modes (types). Oscillations of one of these types can in turn be of several different modes when the magnetron operates as a travelling-wave device (so-called travelling-wave modes).

Practically, it is usually desirable to ensure oscillator operation at a single oscillation mode with all other modes suppressed, this problem becoming especially pressing when the resonant frequencies of different oscillation modes are closely spaced. The relative difference between the frequencies of the desired and the nearest (unwanted) mode will be termed *mode separation* (for instance, $(f_{02} - f_{01})/f_{01}$ in Fig. 3.4*b*). The lower the mode separation, the more difficult is it to ensure oscillator operation on a single frequency, corresponding to one of these modes. Various secondary factors, such as the rate of oscillation build-up under transient conditions, the Q_L of the system at these modes, etc., determine which of the modes will finally prevail.

With closely spaced oscillation modes, frequency jumps from one oscillation mode to another may occur, this being a highly undesirable effect in actual applications. This problem is most typical of multicavity systems, employed, for instance, in magnetrons.

Returning once again to Fig. 3.4*b* the following can be noted. In the presence of dissipative loss the curve $-B_e$ *vs* frequency intersects the susceptance curve of the system at a third point, near the frequency of series resonance f_{03}. Condition (3.12) is satisfied at this point as well as at the other two, which would appear to be sufficient testimony to the existence of a third oscillation mode. However, the cavity conductance turns out to be so high at this point that the condition (3.2) of steady-state oscillation amplitude is violated. Moreover, in the vicinity of f_{03} the derivative dB/df

[1] Various oscillation modes are encountered not only in microwave electronics, but in quantum electronics as well, in particular, in laser engineering.

proves to be negative instead of positive. The oscillator operation at this point is unstable. Indeed, any small positive increment $+\Delta f$ will produce an additional negative (i.e. inductive) susceptance in this system, this shifting the frequency to still higher values, till stable oscillations corresponding to f_2 (Fig. 3.4*b*) are established. A negative fluctuation $-\Delta f$ will cause a similar sequence of events, ending in the frequency jumping abruptly to f_1. Thus, oscillations with the frequency f_{03} will not be supported.

3.3. Effects of Load on the Performance of Resonant-Type Microwave Oscillators and Amplifiers

3.3a. Equivalent Circuit of Microwave Oscillator with Power Output Taken into Account

In the preceding treatment the load terminating the oscillator or amplifier was assumed to be constant. In practice, however, the load is often variable; thus, for instance, if the oscillator in question is used to drive a space-scanning radar antenna system, the imperfections present in the rotary joints and other similar factors will cause periodical variations of the input impedance of the assembly. A variable load may also be encountered in microwave measurements in cases of inadequate decoupling of the oscillator, and so on. The problem in such situations is to evaluate the effect of load variations on the frequency and output power of the oscillator at fixed supply voltage or current.

Another important aspect is the choice of an optimal load for a microwave device at the development stage. The load is actually never connected directly to the device, there always being a two-port network with the properties of an impedance transformer between them. This arrangement, ordinarily known as the *power output*, as a rule forms an integral part of the devices and often is mounted inside the vacuum envelope. When designing the power output the effects of the load on the device parameters must be taken into consideration.

As far as possible the power output should be dissipationless. A perfect power output may therefore be considered as a linear two-port network without loss, which transforms the load impedance (or admittance) to the imaginary terminals of the output gap.

The general equivalent circuit of an oscillator including the power output is presented in Fig. 3.5*a*. The manner in which the parameters of the load are transformed to the terminals of the gap was shown earlier in Fig. 3.1. Now it is convenient to refer the parameters of the equivalent circuit to the "output terminals" *cd*, as illustrated in Fig. 3.5*b*. These transformed cavity parameters

G' and B', as well as the conductance G'_e and susceptance B'_e of the electron stream, are determined by multiplying the respective

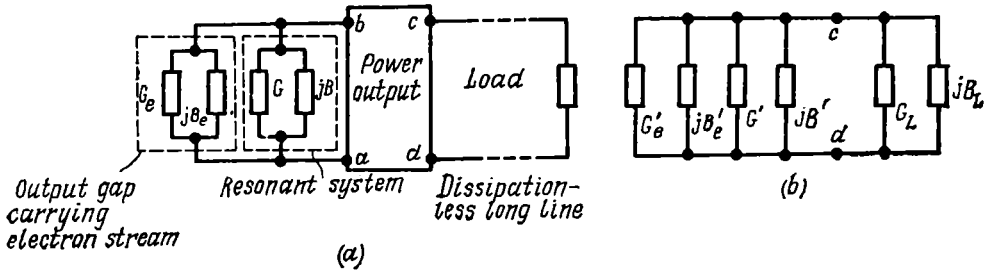

Fig. 3.5. Transformation of equivalent circuit parameters for a device with a resonant oscillatory system

magnitude by the transformation ratio of the power output, this ratio being determined by the coupling of the resonant system to the output guide[1].

3.3b. Output Power vs Load Conductance

Consider the equivalent circuit version presented in Fig. 3.5*b*. Assume that the dependence of beam conductance G'_e on the amplitude of oscillations is of a form shown in Fig. 3.6*a*. At a fixed cavity

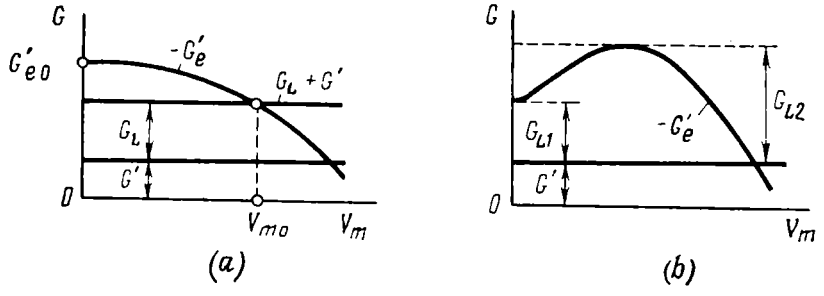

Fig. 3.6. Determining oscillation amplitude as a function of the load conductance

conductance G', variations of the load conductance G_L can be represented by shifting the line $(G_L + G')$ vertically and parallel to the line $G' = \text{const}$.

The output power P_{out} delivered to the external load is

$$P_{out} = 0.5V_{m0}^2 G_L \tag{3.18}$$

where V_{m0} is the steady-state amplitude of oscillations.

[1] This transformation ratio can be shown to be equal to $Q_{ext}Y_0/Q_0G$ where Y_0 is the characteristic (wave) admittance of the output transmission guide.

In turn, this amplitude is a function of the load conductance G_L (refer to Fig. 3.6*a*); at $G_L = 0$ the amplitude of oscillations in the cavity is at a maximum, but the power delivered to the load, by (3.18), is zero. With an increase in the load conductance the oscillation amplitude drops off till a zero amplitude (and therefore zero output power) is set up at $(G_L)_{cr} = |G'_{e0}| - G'$. By Roll's theorem this indicates that the output power has to feature at least

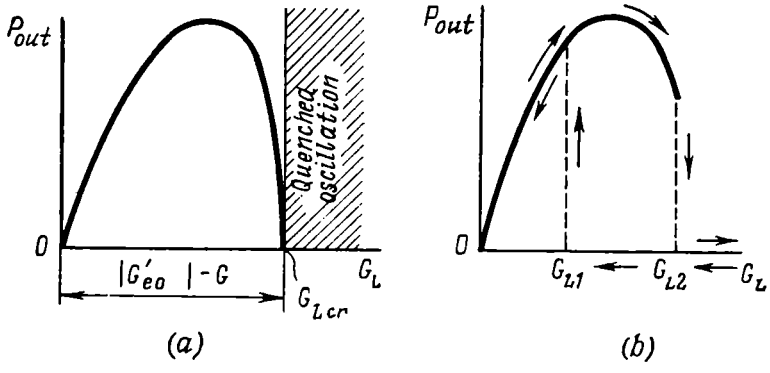

Fig. 3.7. Output power *vs* load conductance. Curves (*a*) and (*b*) correspond to the cases of Fig. 3.6*a* and *b*

one maximum at an intermediate value of the load conductance, this being qualitatively illustrated in Fig. 3.7*a*.

Applying the techniques described above, a non-monotonic dependence $-G'_e$ *vs* V_m (see Fig. 3.6*b*) can easily be demonstrated to produce abrupt variations ("jumps") in output power and hysteresis effects under variable load conductance conditions, as illustrated in Fig. 3.7*b*. In this Figure the output power variations are indicated by arrows.

The argumentation presented shows that with a constant conductance of the resonant system of a microwave oscillator there is an optimal value of the load conductance $(G_L)_{opt}$ at which the power delivered to the load is at a maximum. There is also a critical value $(G_L)_{cr}$ at which the oscillations are damped out. The region where oscillations cease to be self-sustained is shown as a shaded area in Fig. 3.7*a*.

The load conductance G_L in any oscillatory circuit is in reverse proportion to Q_{ext} and therefore the relation of Fig. 3.7*a* can also be presented in terms of Q_{ext}, as shown in Fig. 3.8. At a certain optimal value of $(Q_{ext})_{opt}$ a maximum level of power is delivered to the load.

The output power can be calculated and the requirements to the power output arrangement formulated from the conditions of maximum power level at the load, for instance, if the behaviour of the

electron conductance is known beforehand. In practice, however, it is not always expedient to fulfil this condition, because a tighter coupling of the oscillatory system to the load deteriorates the stability of oscillator frequency. This problem, however, merits a more detailed treatment.

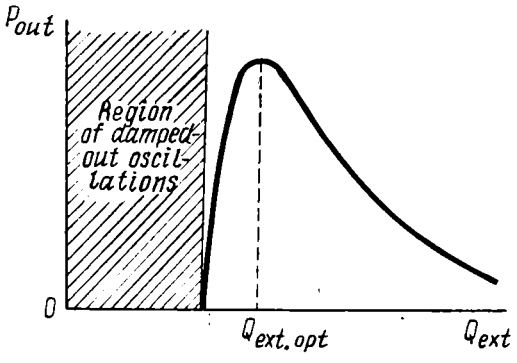

Fig. 3.8. Oscillator output power *vs* Q_{ext} of the oscillatory system (in the absence of hysteresis effects)

3.3c. Frequency Pulling

Variations of the load impedance tend to change the oscillation frequency at fixed d.c. operating conditions of an oscillator. This effect, in contrast to the effects of electronic tuning and frequency pushing discussed earlier, is known as *frequency pulling.*

Again the equivalent circuit of an oscillator with a resonant oscillatory system (Fig. 3.5*b*) may be used to explain frequency pulling. The reference plane *cd*, corresponding to the imaginary terminals of the power output from the transmissions line side, makes it possible to perform the analysis in familiar terms of reduced impedance, conductance and susceptance. Thus, in the following treatment the transformed parameters of the resonant system and electron stream (G', B', G'_e, and B'_e), as well as the parameters of the load G_L and B_L will be assumed to be in terms of the characteristic (wave) impedance, which is taken to be unity.

The appearance of a load susceptance at the *cd* plane can be thought of as a reactance (capacitance or inductance) connected in parallel to the oscillatory system. The frequency of oscillations tends to increase if the load susceptance is negative (inductive) in nature and decrease with a positive (capacitive) susceptance. Thus, a certain invariable value of the oscillation frequency corresponds to every fixed value of B_L.

It is convenient to describe variations of the load input admittance in terms of the VSWR and phase of a standing wave relative to the *cd* reference plane (Fig. 3.5). Conventionally, frequency pulling is evaluated as the maximum change in frequency caused by a specified value of the VSWR at the most unfavourable phase of reflections from the load; during measurements, the phase is usually varied within 180°, thus going through all physically realizable values.

Assume at first that the output transmission guide terminates in a matched load, i.e. VSWR = 1. Then at the *cd* reference plane

in Fig. 3.5*b* $B_L = 0$ and $G_L = 1$. The frequency of oscillations under these conditions is determined by the condition of a zero sum of the cavity and electron susceptances

$$f = f_{match}; \quad B'_e + B' = 0 \tag{3.19}$$

At VSWR > 1 a third term appears in the left-hand side of (3.19), namely the input susceptance B_L of the guide to the load. With small deviations of the frequency, B'_e can be considered invariable, and the only way for regaining a zero sum of susceptances is an automatic change of oscillation frequency, which ensures a change in the susceptance of the system by $\Delta B'$

$$B' + \Delta B' + B'_e + B_L = 0$$

Hence, with (3.19) taken into account,

$$\Delta B' + B_L = 0 \tag{3.20}$$

This increment to the cavity susceptance can easily be related to the change in oscillation frequency by applying the equation for external cavity Q-factor. Since this latter is invariable relative to the reference plane, Q_{ext} at the *cd* plane in Fig. 3.5*b* can be presented as

$$Q_{ext} = \frac{f_0}{2} \left(\frac{dB'}{df} \right)_{f \approx f_0}$$

Hence, keeping in mind the linear behaviour of B' *vs* frequency in the vicinity of resonance,

$$\Delta B' = 2Q_{ext} \frac{\Delta f}{f_0} \tag{3.21}$$

Substitution of this relation into (3.20) and rearrangement yields the change in oscillation frequency

$$\Delta f = \Delta f_{osc}; \quad \Delta f_{osc} = -\frac{f_0}{2Q_{ext}} B_L \tag{3.22}$$

Thus, evaluation of frequency pulling effects necessitates a knowledge of the limits within which the input susceptance of the guide to the load may vary at any phase of reflections from the load with a specified VSWR. The corresponding plot is presented in Fig. 3.9, where circles of constant VSWR are shown in rectangular and polar coordinates on admittance charts.

The easiest way of determining the maximum and minimum values $(B_{in})_{max}$ and $(B_{in})_{min}$ is with the aid of Fig. 3.9*a* because the absolute value of these susceptances is exactly the radius R_0 of the circle VSWR = const. From the theory of admittance charts, this radius is known to be equal to $(S^2 - 1)/2S$, where S is the magnitude of the VSWR.

Note, that the relation for R_0 can be derived without detailed calculations by simply examining the points of intersection of the

circles of constant VSWR with the conductance axis. The coordinates of these points with any type of chart are S and $1/S$, respectively, and therefore the diameter of the circle in rectangular coordinates is $S - 1/S$, this resulting in exactly the same value of R_0 as above.

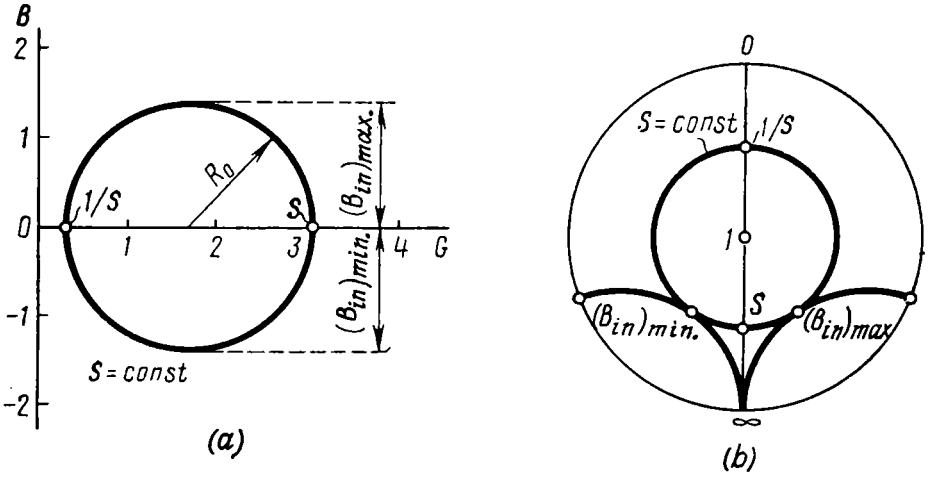

Fig. 3.9. Determining the maximum and minimum input susceptances on the rectangular (*a*) and polar (*b*) impedance charts

The behaviour of the input susceptance as a function of the phase of the standing wave, that can be inferred from Fig. 3.9, is qualitatively illustrated in Fig. 3.10*a*. Here l denotes the length of the

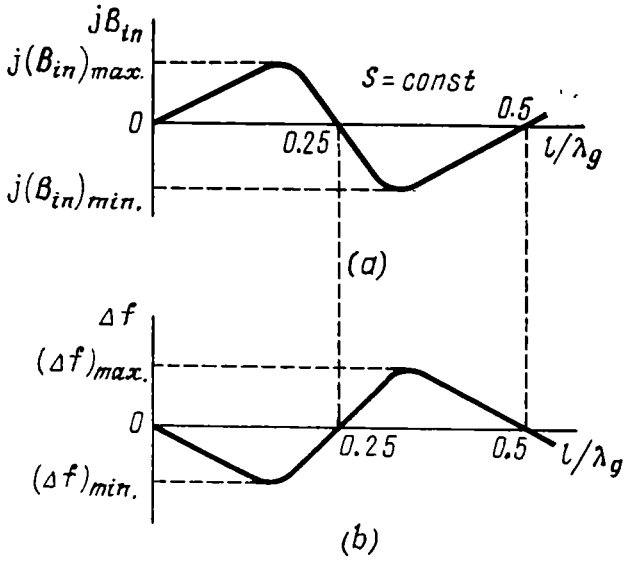

Fig. 3.10. Input susceptance of a mismatched line *vs* the line length and the respective variation of oscillation frequency (frequency pulling)

guide between the oscillator proper and the load and λ_g is the guide wavelength with the effects of dispersion taken into account.

Thus, the maximum and the minimum load susceptances B_L in relative units are

$$(B_L)_{\substack{\text{max.}\\\text{min.}}} = (B_{in})_{\substack{\text{max.}\\\text{min.}}} = \pm (S^2 - 1)/2S \tag{3.23}$$

Substitution of (3.23) into (3.22) results in the maximum frequency shift to both sides of f_{match}

$$(\Delta f_{osc})_{\substack{\text{max.}\\\text{min.}}} = \mp \frac{f_0}{2Q_{ext}} \frac{S^2-1}{2S} \tag{3.24}$$

The pattern of frequency variations with a change in the phase of the standing wave at the oscillator output is shown in Fig. 3.10*b*.

The total change in oscillation frequency is equal to twice the frequency shift described by (3.24)

$$(\Delta f_{osc})_{tot} = \frac{f_0}{Q_{ext}} \frac{S^2-1}{2S} \tag{3.25}$$

where f_0 is the resonant frequency of the "cold" oscillatory system.

The degree of frequency pulling F_p (termed the *pulling figure*) is defined as the greatest change in oscillator frequency caused by any phase of reflections from a load with a VSWR of 1.5 : 1.

Taking $S = 1.5$ in (3.25), we have

$$F_p \approx 0.417\ f_0/Q_{ext} \tag{3.26}$$

The frequency pulling figure is a very important parameter of modern microwave oscillators. The pulling corresponding to any value of the load VSWR is readily determined as

$$(\Delta f_{osc})_S = F_p 1.2\,(S^2 - 1)/S \tag{3.27}$$

The effect of frequency pulling is the less pronounced, the higher is Q_{ext} of the resonant system of the oscillator in question. Thus, the requirements of a low pulling figure and maximum power being delivered to the load are contradictory (refer to Fig. 3.8).

The value of Q_{ext} of a resonant cavity should therefore be selected as a compromise between the output power and stability of oscillation frequency. Depending on the requirements to be met by a particular oscillator, it is sometimes expedient to obtain a higher stability of frequency at a sacrifice in the level of output power, and vice versa. In the majority of modern microwave oscillators Q_{ext} is in excess of 50 to 100 and in certain cases has to be made as high as 300 to 400. Under these conditions the pulling figure does not exceed fractions of one per cent of the operating frequency, such stability being ordinarily considered adequate for most applications (for instance in radar transmitters).

3.3d. Load Characteristics

The dependence of oscillator frequency and output power on the admittance (or impedance) of the load are conventionally termed *load characteristics*. The most convenient way of presenting the load characteristics is by plotting them on a polar diagram, with the reflection coefficient (or the standing wave ratio of the load) and its phase angle used as coordinates. When a Volpert—Smith chart is used for this purpose the resulting contours of constant output

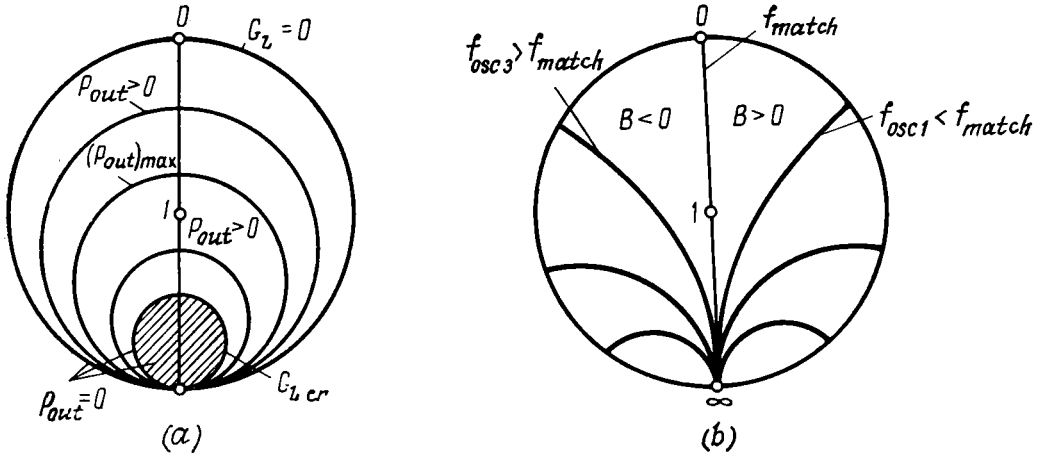

Fig. 3.11. Lines of constant output power (*a*) and constant frequency (*b*) on a polar admittance chart

power and constant oscillation frequency are known as the Rieke diagram. The effects discussed in the preceding sections can be generalized in a very vivid manner by means of such diagrams.

Consider the *contours of constant output power* P_{out} = const on the Rieke diagram. These contours should be drawn through points corresponding to the load admittance at plane *cd* in Fig. 3.5, at which the output power of the oscillator remains invariable.

As seen from Fig. 3.7*a* and equation (3.18) the output power is a function of the load conductance G_L and is independent of the load susceptance B_L. The curves of constant output power on a polar chart are therefore represented by the contours of constant load conductances, i.e. by circles with centres lying on the axis of real quantities.

The region where oscillations are damped out by the load, shown as a shaded area in Fig. 3.7*a*, on the Rieke diagram is presented by the area inside the circle $(G_L)_{cr}$ = const, as illustrated in Fig. 3.11*a*. The output power is also zero on the peripheral circle of purely reactive load admittance. Somewhere between these two circles $(G_L)_{cr}$ and $(G_L) = 0$ is the circle of maximum output power; in the

general case, this circle does not necessarily pass through the chart centre, which corresponds to the conditions of perfect matching.

The *contours of constant oscillation frequency* can be treated in much the same way. As shown earlier, the oscillation frequency is a function of the load susceptance and does not depend on the load conductance. Therefore, the contours of $f = \text{const}$ coincide with the circles of constant load susceptance $B_L = \text{const}$, as illustrated in Fig. 3.11*b*. The left half-plane of the chart corresponds to negative susceptances (inductive loads) and the frequency here

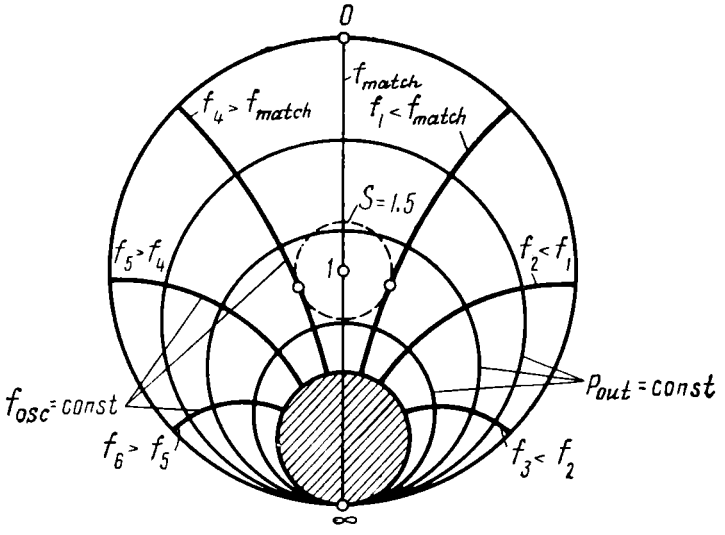

Fig. 3.12. Idealized oscillator load impedance diagram (oscillator of the resonant type)

is slightly higher than when operating onto a matched load. In the right half-plane the load is of a capacitive nature and the frequency is lower than f_{match}, decreasing with an increase in B_L.

The load impedance chart of an oscillator with both the contours of constant frequency and constant output power is presented in Fig. 3.12. Since the families of circles $B_L = \text{const}$ and $G_L = \text{const}$ are mutually orthogonal, in the approximation adopted the contours of constant frequency and constant output power will feature a similar property. The region, where oscillations are damped out, is shown as a shaded area; plotting the contours of constant frequency and constant output power inside this area has obviously no physical meaning.

The circle of constant VSWR = 1.5 : 1 shown in a dashed line in Fig. 3.12 allows of emphasizing once again the meaning of the pulling figure F_p; in this case F_p is determined by the difference between f_4 and f_1, corresponding to points where the circle VSWR = 1.5 : 1 touches the circles $f_4 = \text{const}$ and $f_1 = \text{const}$.

Ordinarily, the load impedance diagrams for practical use are not calculated but measured directly, a mismatch of predetermined magnitude being inserted between a matched load and the oscillator in question to simulate the effects of a variable load[1]. The argumentation presented provides a deeper insight into the behaviour of load characteristics and their connection with the electronic processes taking place in the oscillator tube.

It will be of certain interest to examine the load impedance diagram of an amplifier. Obviously, there is no need of plotting the contours of constant frequency in this case, since the steady-state oscillation frequency is determined only by the input signal (it is only pulling of the output signal phase that can be considered in this case). As regards the contours of constant output power, they are of interest and can be easily measured.

Analysis shows that these curves, as in the case of an oscillator, can be approximated by circles. There is an optimal value of load conductance, at which the output power is at a maximum; the physical meaning of this effect was explained in Section 2.4*c*. However, as distinct from an oscillator, in an amplifier there is no region where the oscillations are completely damped out. This is readily explained by the fact that electron bunching is independent of the process of coupling out the energy of an electron beam.

3.3e. Long-Line Effect

When deriving the equation of frequency pulling, the possibility of the load parameters being frequency-selective was not taken into account; this made it possible to examine the effects of the load on the oscillator performance, with the reverse effects of a variable frequency on the load admittance being neglected. In practice, however, the input admittance of microwave transmission lines is frequency-dependent, even if the load parameters are independent of the frequency.

Consider the steady-state frequency of an oscillator connected to a load via a transmission line of any type, which is long in comparison with the wavelength of oscillations.

As a first approximation, assume the load itself to be independent of frequency, when variations of this latter are within comparatively narrow limits. In this case the variations of the input admittance at the *dc* plane in Fig. 3.5 will be determined only by the electric length of this guide and the VSWR of the load. With an increase in frequency the point corresponding to the input admittance at the *cd* plane on the polar admittance chart will move clockwise along a circle of constant VSWR.

[1] Conventionally, load impedance diagrams (Rieke diagrams) are plotted at a constant d.c. current I_0 through the oscillator.

Suppose that the reflection coefficient of the load is $K = |K| \exp(j\varphi)$. Then the phase of the standing wave ψ at the output terminals of the oscillator will be

$$\psi = \varphi - 2\beta l = \varphi - 4\pi l/\lambda_g \tag{3.28}$$

where l is the length of the guide between the oscillator and the load and β is the phase constant of this guide, $\beta = 2\pi/\lambda_g$.

Omitting for simplicity the effects of dispersion in the guide (dispersion will only make the undesirable effects under treatment more pronounced) and assuming the guide wavelength λ_g to be the same as the wavelength in free space, we obtain

$$\psi = \varphi - \frac{4\pi l}{c} f \tag{3.29}$$

where f is the frequency of oscillations in question and c is the velocity of light in free space. By equation (3.29) the function ψ *vs* frequency is linear, as shown in Fig. 3.13*a*, for guides of various length and different phases of reflection coefficient φ.

On the other hand, variations of the standing wave phase ψ at the oscillator output cause frequency pulling at a constant value

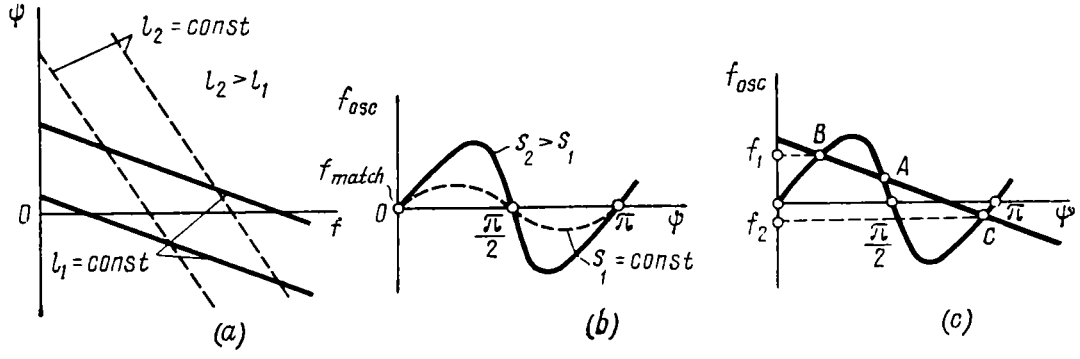

Fig. 3.13. Long-line effect on microwave oscillator performance

of the VSWR. By plotting the contours $S = \text{const}$ on the load impedance diagrams it is possible to obtain curves f_{osc} *vs* ψ as shown in Fig. 3.12*b* (refer also to Fig. 3.10*b*).

Now bring into coincidence both graphs. The steady-state frequency is determined by the points of intersection of the phase line ψ *vs* f with the frequency pulling curve f_{osc} *vs* ψ, as illustrated in Fig. 3.13*c*. There can be either one or several such points of intersection, depending on the length of the guide. In case of several intersections, frequency stability has to be examined.

Point *A* in Fig. 3.13*c* corresponds to unstable frequency conditions, since any positive increment of the frequency causes a change

in phase ψ, which tends to further increase the frequency. A similar sequence of events will take place if the frequency deviates towards lower values. As regards the other two points of intersection of the graphs in question, namely B and C, the oscillation frequency here proves to be stable and the conditions may be equally suitable for oscillation at any of these frequencies so that which of these two frequencies f_1 or f_2 will be sustained is not too clear. (This type of oscillator performance is called frequency-sensitive.)

Experiments and practice evidence that, under such circumstances, with pulsed operation conditions, part of the pulses are generated with a frequency f_1 and the rest, with a frequency f_2. Thus, the oscillator may feature abrupt changes of the output signal frequency (*frequency jumps*) from the desired frequency to a nearly undesired frequency, even with the oscillatory system sustaining a single oscillation mode.

The long-line effect manifests itself not only under pulsed operation conditions, but under continuous-wave (c.w.) conditions as well. The greatest difficulties are encountered when mechanically tunable oscillators are required to operate onto long transmission lines: the tuning characteristic (signal frequency *vs* position of tuning element) ceases to be monotonic and can even become intermittent. In this case highly undesirable tuning hysteresis effects are observed.

The long-line effect takes place only when the electric length of the guide exceeds a certain critical value, as can easily be noted by examining the graphs of Fig. 3.13. This critical length is determined by the derivative of the frequency pulling function at $\psi = \pi/2$. In cases when the function $f_{osc} = f(\psi)$ is a steep one, the two curves in question intersect at one point only and therefore there is only one steady-state frequency.

Long-line effects can be eliminated by:

(1) reducing the guide length to a value less than the critical one and thus ensuring the existence of only one oscillation frequency;

(2) reducing the VSWR of the load, this tending to reduce the slope of the curve $f(\psi)$ at the point $\psi = \pi/2$;

(3) providing a decoupling element (preferably a non-reciprocal pad such as a ferrite isolator or a circulator) between the oscillator and its load.

In practice, depending on the requirements to be met, one or all the three of the above methods are used. Ordinarily, the upper limit to admissible VSWR values of the load is 1.2 : 1 to 1.5 : 1. Note in passing, that limiting the VSWR value of the load is desirable also from the point of view of the electric strength of the power output and microwave guide.

3.4. Peculiarities of Performance of Microwave Devices with Non-Resonant Oscillatory Systems

The performance of microwave amplifiers and oscillators with prolonged interaction is to a great extent dependent on the parameters of the radio-frequency circuit, the slow-wave structure, which does not exhibit pronounced resonant properties.

The main functions of the slow-wave system in microwave electron devices are similar to those of resonant oscillatory systems. Just as a resonant cavity, a slow-wave structure is an intermediate between the electron beam and the load, and is responsible for coupling out the microwave energy and for electron beam bunching. Nevertheless, devices with prolonged interaction feature a number of peculiarities. As a typical example, the effects of the parameters of a slow-wave structure on the frequency of a signal from an amplifier or an oscillator will be examined.

As follows from the qualitative reasoning presented in Sections 2.4 and 2.8, the condition of prolonged interaction between an electron beam and a radio-frequency field is the phase synchronism of this beam with the travelling electromagnetic wave. Designating the beam velocity and phase velocity of the wave as v_0 and v_p, respectively, this condition can be written as

$$v_0 \approx v_p \tag{3.30}$$

In the simplest case v_0 is determined by the constant accelerating voltage V_0 applied to the device, according to an equation of the (2.14) type. On the other hand, the phase velocity v_p of the wave in the general case is frequency-dependent and consequently there is a certain relationship between the constant voltage V_0 and frequency f at which the condition of phase synchronism is satisfied; this relationship is determined by the dispersion characteristic of the slow-wave structure.

The characteristic curve of a slow-wave system with abnormal dispersion (when the absolute value of phase velocity is increased with a rise in frequency) is shown as an example in Fig. 3.14*a*. Depending on the behaviour of $v_0 = f(V_0)$, the frequency *vs* V_0 graph will be of the form shown qualitatively in Fig. 3.14*b*. The curve presented here can be interpreted in the following way. In case of a self-oscillator, the frequency can be controlled by varying the voltage V_0; if the device in question is an amplifier, then a change in the accelerating voltage tends to shift the frequency to a value at which the device will feature a maximum gain. This means that the amplifier has electronic tuning which is similar to the ordinary mechanical tuning of resonant-type amplifiers.

The range of electronic tuning shown in Fig. 3.14 depends first of all on the steepness of the dispersion characteristic curve v_p *vs*

frequency. It depends also on the practically admissible range of V_0 and the degree of allowable reduction of output power.

Thus, from the point of view of voltage-tunability, the part played by the slope of the dispersion characteristic curve is similar to that of the loaded Q_L of a resonant cavity. However, the passband of a slow-wave system can be by an order or two higher than that of a cavity resonator. The electronic tuning range of a device with

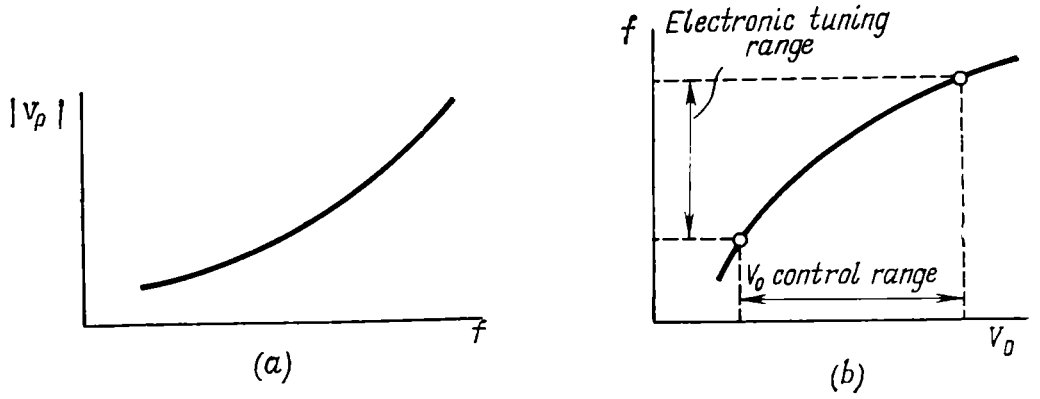

Fig. 3.14. To the problem of determination of the frequency of oscillations, amplified or generated by a microwave device with a non-resonant oscillatory system

a non-resonant oscillatory system does not, therefore, have the same restrictions as inherent to oscillators with resonant cavities, and this feature is one of the major advantages of devices with prolonged interaction.

Another interesting feature of microwave devices with prolonged interaction is the behaviour of their load characteristics. The wave reflected from the external load is dissipated in a matched load terminating the other end of the slow-wave system. This reflected wave does not interact with the electron beam to any noticeable degree, since the condition of synchronism (3.30) is not satisfied. Therefore, these devices feature a much less pronounced frequency pulling; the contours of constant output power in case of amplifiers and oscillators with non-resonant oscillatory systems coincide almost exactly with the circles of constant VSWR. In this case the condition of a maximum power delivered to the load coincides with matching.

The equivalent circuit of electron devices with non-resonant oscillatory systems as a first approximation may be represented by a uniform transmission line with negative attenuation, as shown in Fig. 3.15. The symbols Y_0 and Z_0 here denote the specific admittance and specific impedance of the "cold" line. The distributed shunting electron admittance $(Y_e)_0$ depends on the parameters of the electron beam; in particular, $(Y_e)_0$ is a function of the d.c.

component I_0 of the electron beam convection current, the accelerating voltage V_0, the operating frequency f, and so on. A certain

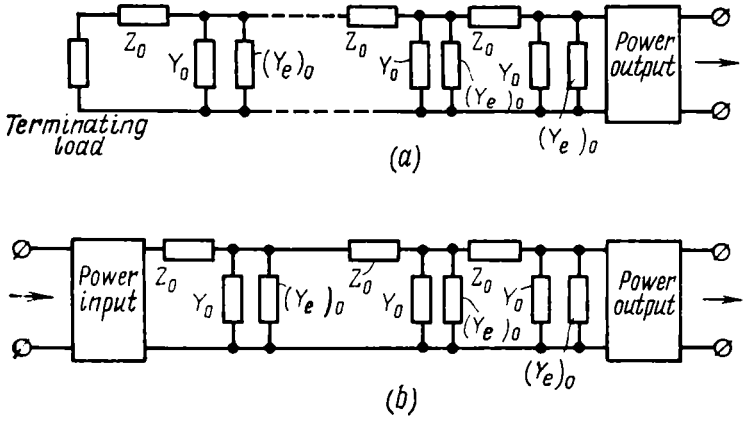

Fig. 3.15. Equivalent circuits of an oscillator (*a*) and an amplifier (*b*) with a non-resonant oscillatory system

analogy between $(Y_e)_0$ and the lumped electron admittance Y_e, discussed earlier in connection with the equivalent circuits of devices with resonant oscillatory systems, may be drawn.

The electron admittance concept used in Sections 3.1-3.4, and the equivalent circuit technique are applicable not only to microwave electron devices but to many other systems consisting of a linear oscillatory network and an active non-linear element coupled to it. In particular, these techniques prove to be extremely useful in the analysis of microwave solid-state devices, such as parametric amplifiers, avalanche and Gunn-effect diodes, etc. Similar methods are widely employed in the research and development of quantum oscillators and amplifiers of the microwave and optical wavelengths, *masers* and *lasers*, despite the essential difference in the physical principles involved.

3.5. Requirements to Microwave Oscillators and Amplifiers

Prior to discussing definite types of microwave devices, the general requirements imposed upon microwave amplifiers and oscillators will be briefly enumerated. The purpose of the device is a decisive factor in formulating these requirements.

3.5a. Microwave Oscillators

The main radio-frequency parameters and characteristics of microwave oscillator devices are the following:

(1) level of output power;

(2) overall efficiency;
(3) range of admissible variation of frequency (or tuning range, either mechanical or electronic, or both) relative to the middle operating frequency and rate of admissible frequency variation;
(4) frequency pulling figure, when operating onto a mismatched load;
(5) stability of oscillation frequency;
(6) possibility of amplitude, frequency or pulse modulation of the carrier;
(7) level of noise in the vicinity of the operating frequency and power of spurious radiation, i.e. unintended oscillations outside the operating frequency range.

In low-power oscillators designed mainly for use in microwave measurements and as local oscillators in microwave receivers, the value of overall efficiency is of comparatively small importance. In these applications the required level of output power is usually so low (of the order of scores or hundreds of milliwatts) that efficiency is not even listed among the device specifications. In this case efficiency is important mostly from the point of view of power dissipation in the device and thermal conditions of operation, and not as a measure of power drawn from the d.c. supply.

Efficiency becomes one of the most significant parameters of a device when the required output power is of a high level; in this case the device can become not only inefficient but even impracticable. Frequency stability, frequency tuning, modulation capabilities and noise parameters are in certain cases less important than the output power and efficiency. A typical example of such a device is a microwave oscillator used for industrial heating. In most applications, however, the requirements of a stable frequency and frequency control are not less, and sometimes even more important, than the available level of output power. This can be explained by the extremely stringent requirements imposed upon modern radio equipment.

Consider as an example a microwave oscillator intended for use in a Doppler radar system; as known from general physics, the frequency of a signal reflected from a moving target differs from the radiated signal frequency by a value which, neglecting relativistic effects, is described by the equation

$$f_d = f_{osc} \frac{2v_r}{c} \tag{3.31}$$

where f_{osc} is the frequency of oscillations radiated by the transmitter, v_r is the radial component of the target velocity in the direction to the transmitter and receiver and c is the free-space velocity of light.

Thus, in coherent systems the magnitude of the Doppler frequency shift is measured to be used to evaluate the speed v_r of the target.

To this end the transmitter signal is mixed with the reflected signal and the beat frequency, corresponding to the difference of these frequencies, is measured.

With radial speeds of the target ranging from 1 m/s to 10 km/s the value of this Doppler frequency shift at a 10 cm operating wavelength ($f = 3$ GHz) is from 20 Hz to 200 kHz. Such extremely small magnitudes of f_d necessitate a highly stable frequency (short-term stability). Depending on the required minimum value of f_d,

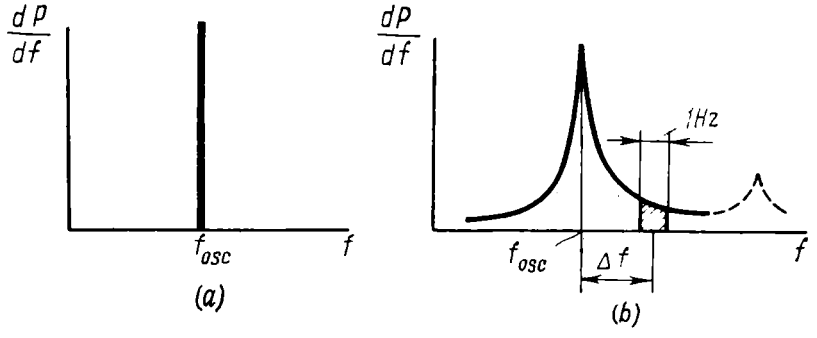

Fig. 3.16. Output signal spectrum of a perfect (*a*) and actual (*b*) c.w. oscillator

the admissible instability of oscillator frequency during a time sufficient for signal processing should not exceed 10^{-6} to 10^{-9} of the carrier frequency.

Reducing the level of noise signal radiated by the transmitter or local oscillator at frequencies ($f_{osc} \pm f_d$) is as important as providing the required frequency stability. In this respect the signal spectrum purity, i.e. the spectral power density as a function of frequency, is of major importance.

Figure 3.16*a* illustrates the spectrum of a signal provided by an ideal oscillator of continuous-wave radiation which is monochromatic (contains but a single frequency) and similar in appearance to the delta-function. The spectrum of the signal of an actual device is shown in an exaggerated form in Fig. 3.16*b*.

The amount of noise and spurious oscillations is conventionally evaluated by the ratio of output power at the desired frequency to the power radiated at a frequency removed from the desired by a specified frequency shift Δf in a frequency band of specified width (ordinarily, 1 Hz or 1 kHz), as illustrated in Fig. 3.16*b*; usually this ratio is given in decibels per hertz or kilohertz, respectively.

Actual oscillator designs provide noise levels of the order of 100 to 170 dB/Hz at frequencies removed from the carrier by frequency shifts from units of hertz to scores of megahertz[1].

[1] Amplitude noise and frequency noise are distinguished, i.e. fluctuations of the signal amplitude and fluctuations of the signal frequency. In modern oscillators the latter are considered most important.

Noise and spurious oscillations, including oscillations far outside the operating frequency range and harmonics of the signal frequency, are highly undesirable not only in connection with the above mentioned Doppler systems, but for a number of other reasons as well. In particular, the *compatibility* of various radio equipment to a considerable extent depends on the mutual interference due to spurious signal radiation. Great attention is therefore being paid to the problem of eliminating or suppressing to acceptable levels the noise and spurious radiation of modern sources of microwave power.

3.5b. Microwave Power Amplifiers

Power amplifiers for the microwave range should be treated in terms of the following radio-frequency characteristics:

(1) output power level;
(2) overall efficiency;
(3) gain;
(4) operating bandwidth, within which the amplifier can be used without resorting to mechanical or electronic tuning;
(5) range of mechanical or electronic tuning;
(6) noise and spurious radiation levels;
(7) phase stability.

The problem of frequency instability caused by variations of the load or supply voltages is practically never encountered, and it is just for this reason that single-stage and multistage amplifiers are finding ever increasing use, replacing power oscillators with self-excitation. Amplifiers used instead of self-oscillators are further advantageous in that they are easily synchronized; a constant phase shift can readily be maintained between several simultaneously operating amplifiers driven by one common source of microwave signal. Problems of this sort are met, for instance, when using phased arrays as the antenna assembly, or with linear electron accelerators.

The *gain* is usually evaluated in decibels and defined as

$$G = 10 \log_{10} \frac{P_{out}}{P_{in}} \text{ dB} \tag{3.32}$$

where P_{out} is the output power delivered to a matched load, and P_{in} is the power fed by the input signal source when the amplifier in question is replaced by a matched load.

The *bandwidth* (passband) B of a microwave amplifier, just as at lower frequencies, is defined as the difference between frequencies f_1 and f_2, at which the gain is reduced by a specified amount (1 dB or 3 dB) compared to the gain provided at the nominal frequency f_0; this definition is illustrated in Fig. 3.17. The tuning of resonant cavities, electric operating conditions and other parameters of the amplifier, except frequency, are assumed to be fixed; to emphasize

this assumption the amplifier operating bandwidth is sometimes referred to as *instantaneous*.

The curve of Fig. 3.17 can be shifted to both sides of the middle frequency f_0 if the amplifier in question has some tuning mechanism. The extreme positions of this curve correspond to the maximum and minimum values of frequency f_{max} and f_{min}, as indicated in dashed lines; the difference between these values is known as the *tuning*

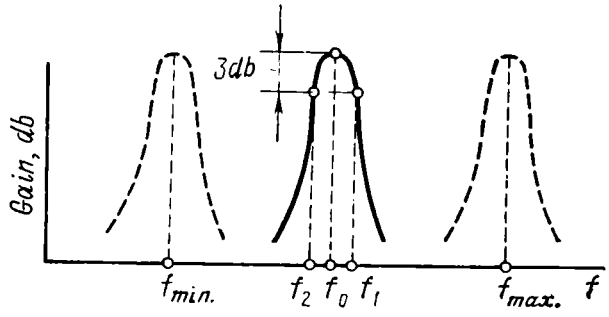

Fig. 3.17. Bandwidth and tuning range of a microwave amplifier

range of an amplifier. Sometimes the bandwidth and the tuning range are specified in per cent of the middle frequency, instead of in frequency units (Hz or MHz).

Power amplifiers have to meet about the same requirements on noise and spurious radiation as oscillators. These parameters should not be confused with the noise figure used to evaluate the performance of low-power input amplifiers and also given in decibels.

3.5c. Amplifiers of Small Signals

Despite their seeming similarity to power amplifiers, amplifiers of small signals (input amplifiers) are required to meet essentially different specifications. The main radio-frequency parameters, by which the performance of input amplifiers is usually evaluated, are as follows:

(1) gain;
(2) noise factor or figure;
(3) bandwidth at fixed tuning.

The absolute level of output power in case of small-signal amplifiers is a secondary consideration, while the efficiency can usually be completely neglected. This is typical not only of microwave amplifiers, but of input amplifiers in general. With an input signal commensurate with the level of inherent amplifier noise, the *signal-to-noise ratio* at the input and output becomes much more important than the amplifier gain. This statement warrants a more detailed examination.

As for any two-port network, the noise factor of microwave amplifiers can be determined by several different though interchangeable methods. The noise power at the amplifier input and output in the frequency band Δf of interest can be designated by $P_{n.in}$ and $P_{n.out}$, respectively. The *noise factor* (or *noise figure*) of the amplifier F may be defined as

$$F = 10 \log_{10} \frac{P_{in}/P_{n.in}}{P_{out}/P_{n.out}} \text{ dB} \tag{3.33}$$

Relation (3.33) describes the change (deterioration) of the signal-to-noise ratio due to the presence of an amplifier. The ratio P_{out}/P_{in}, however, is nothing more than the absolute value of the amplifier gain G_{abs}. The noise at the amplifier output is composed of the amplified noise present at the amplifier input, and the "inherent" noise present at the amplifier output, which are, respectively $G_{abs}P_{n.in}$ and $P_{n.inh}$. Thus, equation (3.33) can be rearranged in the following manner:

$$F = 10 \log_{10} \left(1 + \frac{P_{n.inh}}{G_{abs}P_{n.in}}\right) = 10 \log_{10} \left(1 + \frac{P'_{n.inh}}{P_{n.in}}\right) \text{ dB} \tag{3.34}$$

where $P'_{n.inh}$ is the inherent noise power reduced to the amplifier input and therefore equal to $P_{n.inh}/G_{abs}$.

The noise factor of a perfect amplifier, which itself does not add any noise to the signal being amplified, by (3.34), is zero. The nearer to this value is the noise figure of an actual amplifier, the higher is its quality and the greater are the possibilities of amplifying small signals. The value of F to a considerable extent determines the main performance characteristics of many types of radio equipment, such as the range of target detection in radar, for instance.

The noise at the input of a matched microwave amplifier is due to thermal radiation and is described by the Nyquist equation as

$$P_{n.in} = kT\Delta f \tag{3.35}$$

where k is Boltzmann's constant equal to $1.38 \cdot 10^{-23}$ joules per degree, T is the temperature in degrees absolute and Δf is the bandwidth in hertz.

When calculating the noise factor, the temperature T is conventionally taken to be standard (290°K). Substituting (3.35) into (3.34) yields

$$F = 10 \log_{10} \left(1 + \frac{P'_{n.inh}}{kT_0\Delta f}\right) \text{ dB} \tag{3.36}$$

The noise properties of amplifiers may be evaluated in terms of the effective noise temperature T_n, instead of by the noise figure F. The concept of the noise temperature was treated in the previous

course[1] for the case of passive waveguide networks. The *effective noise temperature of an amplifier* is the absolute temperature of a matched load at the noiseless amplifier input, at which the noise power at the amplifier output is exactly equal to the inherent noise power $P_{n.inh}$ generated by the amplifier

$$P'_{n.inh}=kT_n\Delta f$$

Applying this concept, equation (3.36) can be presented as

$$F = 10 \log_{10} (1 + T_n/T_0) \text{ dB} \tag{3.37}$$

Hence it follows that the noise temperature of an amplifier and its noise factor are interrelated by the simple ratio

$$T_n = 290 (F_{abs} - 1) \text{ (degrees Kelvin)} \tag{3.38}$$

where F_{abs} is the absolute value of the noise factor determined by the term under the logarithm sign in equations (3.33), (3.34) and (3.36).

Historically, the development of microwave electron devices began with self-excited oscillators, amplifiers appearing somewhat later, when the requirements to the stability of microwave oscillations became more stringent. At present power amplifiers are becoming more and more important.

For a long time there have been no satisfactory means whatever for amplifying small radio signals. The level of inherent noise of any device available at that time was prohibitively high. At present low-noise and super-low noise travelling-wave tubes are commercially available, as well as parametric electronic and solid-state amplifiers, and quantum-mechanical amplifiers. For example, typical values of the noise factor of a 10-cm TWT can be as low as 3 dB (T_n = 290°K) and even less. The noise temperature of solid-state amplifiers, operating at liquid helium temperatures, may be as low as some 3-30 degrees absolute.

Besides the main requirements enumerated above, other factors have to be considered when developing microwave amplifier and oscillator electron devices. Very important are the requirements to the d.c. supply sources, in particular, to the value of the supply voltage and its stability. Keeping in mind the sphere of microwave device application, considerable attention must be given to mechanical and climatic (environmental) factors, as well as to the geometrical dimensions and weight. A problem of great importance is the life and reliability of microwave electron devices. Finally, in studying microwave devices and developing new types the

[1] "Microwave Engineering" by the same author, Mir Publishers, 1973.

design, technology and cost problems should receive particular emphasis.

All these practical considerations are in the ultimate the decisive factors in evaluating the scope of practical application of a particular microwave device.

3.6. Review of Microwave Amplifier and Oscillator Types

Figure 3.18 presents a diagram illustrating the present state of affairs in the field of microwave signal generation and amplification. This diagram, while not claiming a complete and thorough covering of the problem, gives a vivid picture of the variety of elaborate techniques and devices that may be employed to provide amplification or generation of radio-frequency signals.

Along with electron oscillators of coherent signals, the diagram shows noise generators of continuous spectrum as well as early types of spark oscillators capable of producing only non-coherent damped oscillations. Solid-state quantum amplifiers and oscillators (masers and lasers) are also included in this diagram together with parametric amplifiers of microwave signals. In this classification solid-state devices include microwave oscillators utilizing the negative resistance of semiconductor diodes and transistor oscillators of the microwave range.

Some of the groups of devices in this diagram are at present of interest only in principle, as for example the monotron and oscillating diode treated in Chapter Two. Electron plasma oscillators and amplifiers, outlined briefly in Chapter Eight, and electron-wave tubes mentioned in Section 2.9 have not as yet found extensive use. The Doppler and Cherenkov effects were repeatedly proposed to be used for generation and amplification of radio-frequency signals, but the development of the devices utilizing these effects is still at the laboratory research stage.

Many other versions of microwave electron devices of the resonant as well as of the non-resonant type, that have not come into wide use, have been omitted from this diagram. However, it is quite possible that these, as well as other types of devices, may gain acceptance in future.

Multicavity magnetrons, reflex and multicavity klystrons, travelling-wave and backward-wave tubes (TWT and BWO) of the O type and platinotrons, which are actually a version of the BWO of the magnetron type, as well as certain special types of triodes and tetrodes are the microwave device types that are the most widely used at present in actual radio equipment. The following chapters will deal mainly with just these device types, which in the diagram are shown in bold lines.

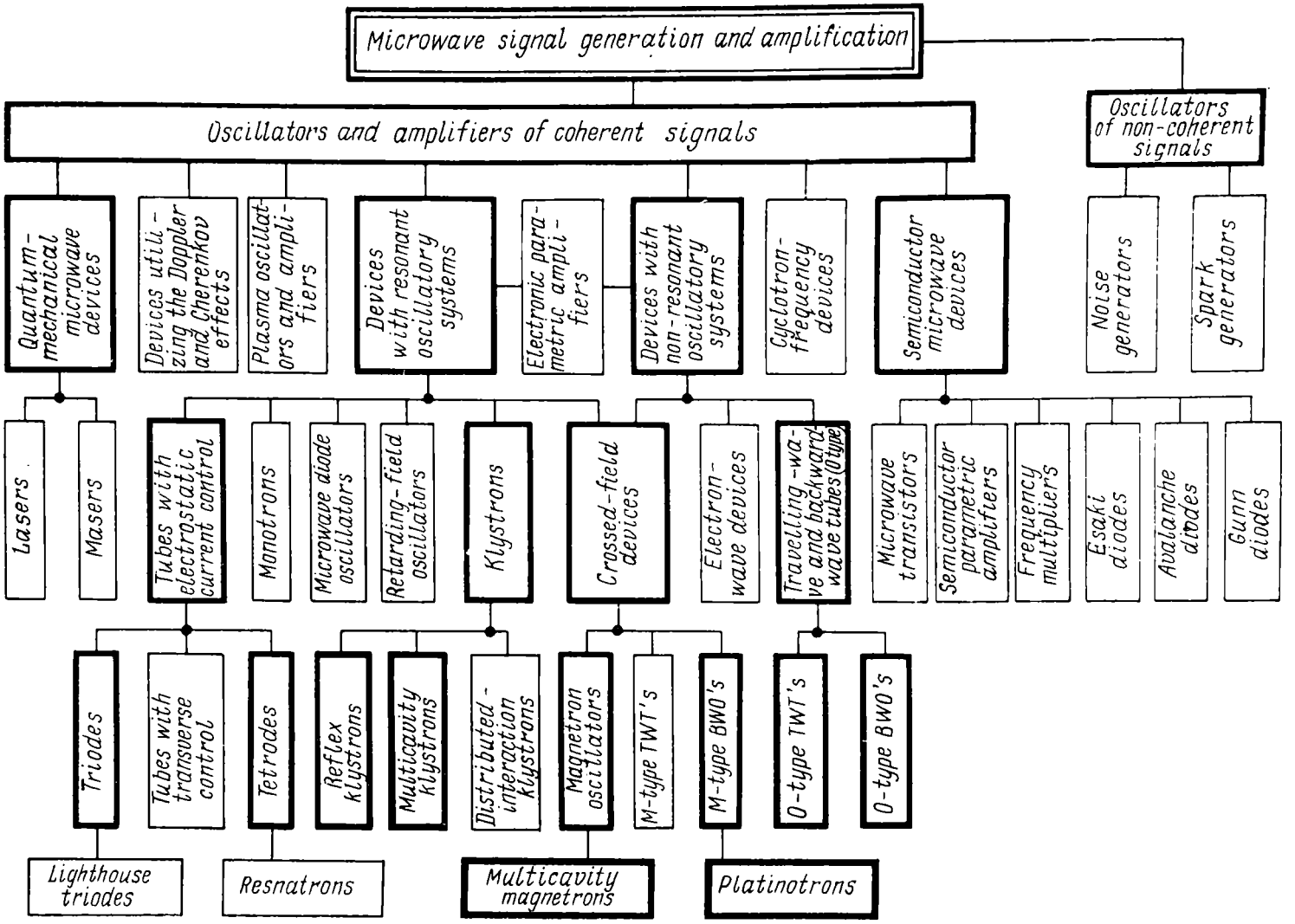

Fig. 3.18. Major trends in microwave signal generation and amplification

It should be emphasized that the classification presented in the diagram is rather conventional and insufficiently rigorous. Certain types of devices classified among different groups in many cases have much in common. This is the case, for example, of multicavity magnetron oscillators and forward- and backward-wave tubes of the O and M types. Klystrons with prolonged interaction and TWT's of the O type also have much in common. Utilization of the Cherenkov effect is similar to the principles underlying the operation of a travelling-wave tube, and so on. This only emphasizes the close interrelation between microwave amplifiers and oscillators, utilizing the same physical principles.

At present certain other types of electron and gas-filled devices (switches, modulators, etc.) not included in the diagram of Fig. 3.18, are also used in radio equipment along with amplifiers and oscillators of the microwave range. These devices will also be given some attention in the following discussion.

CHAPTER FOUR

MICROWAVE TRIODES AND TETRODES

4.1. General Considerations

The main distinguishing feature of microwave triodes and tetrodes is the use of electrostatic control of the electron stream, this being accomplished by varying the control grid voltage and thus affecting the space charge at the cathode. The same principle is known to be the basis of performance of modern low-frequency amplifier and oscillator tubes. This allows a simplified treatment of microwave triodes and tetrodes, considering them as a variety of the "conventional" electron tubes.

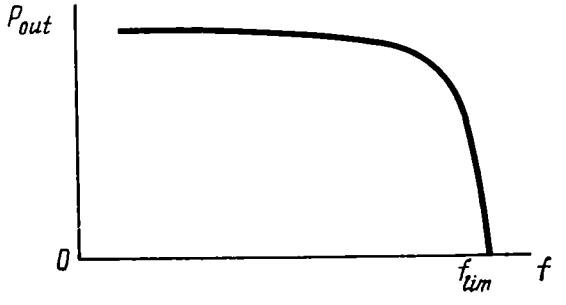

Fig. 4.1. Typical frequency dependence of triode output power

At the early stages of development of microwave triodes and tetrodes, the main efforts were directed at partially adapting the ordinary low-frequency tubes to operation at higher frequencies. It turned out, however, that the output power of oscillators and amplifiers deteriorates rapidly with an increase in operating frequency. A typical dependence of triode oscillator or amplifier output power on frequency is illustrated in Fig. 4.1. The frequency f_{lim} at which the tube practically ceases to function is conventionally known as the *limiting* (*critical*) frequency of this tube.

As in other microwave electron devices, the limiting frequency of triodes is determined by two factors, namely the properties of the oscillatory system and the inertia effects due to a finite time of electron transit through the interelectrode space.

When considering the limiting effects of the oscillatory system, the finite magnitudes of interelectrode capacitances and lead inductances should be taken into account. These capacitances and inductances are comparatively small (in low-power tubes, of the order of several microhenry and several picofarads). It is no problem, however, to calculate that such a tube, even with the leads short-circuited externally, forms an oscillatory circuit with a resonant

wavelength in the decimetric or metric wave bands. This makes it extremely difficult to provide amplification or oscillation of frequencies higher than this resonant frequency.

The obvious method of obtaining a shorter wavelength with such tubes is to reduce interelectrode capacitances and lead inductances. Parasitic tube capacitances may be reduced by mounting the electrode leads at different ends of the tube instead of passing them through a common base. Fair results can be obtained with radial electrode leads (so-called acorn tubes); the interelectrode capacitance can also be reduced by diminishing as much as possible the non-operating parts of the electrodes (cathode, grid and anode). Lead inductances are brought down by making them in the form of short thick bars or by using several parallel leads for one electrode. There are technological methods of eliminating partially the harmful effects of tube inductances and capacitances. This enables extension of triodes application up to the middle of the decimetric wave band in open oscillatory circuits employing lumped constants or in oscillatory circuits composed of sections of two-wire (Lecher) lines.

With a further shortening of the wavelength, especially in the case of power tubes of considerable geometrical dimensions, the defects specific to open oscillatory circuits, such as significant level of energy radiation, greater dissipative loss in metal conductors and dielectric spacers, inadequate mechanical rigidity, etc., become still more pronounced. The Q-factor of an open oscillatory circuit drops off with an increase in operating frequency, the conductance of these circuits increases, resulting in a reduced dynamic impedance. As a consequence, the amplitude of oscillations becomes smaller, and the anode efficiency of the tube drastically reduces. The output power of oscillators and amplifiers deteriorates rapidly with an increase in operating frequency, this making triodes and tetrodes practically useless at frequencies in excess of about 500 to 600 MHz, if they are employed in open oscillatory circuits.

The natural trend of development of oscillatory systems for use with triodes and tetrodes is to employ resonant cavities, which are free of most of the above mentioned drawbacks. The tube design has to be modified, because it becomes desirable to incorporate the tube electrodes into the cavity. The interelectrode capacitances should function as shortening capacitances, for instance in cylindrical or coaxial cavities. Electrode leads have to be made in the form of metal discs or cylinders for direct connection to the cavity walls.

This idea of making a triode integral with a cavity was first proposed and realized in 1938-1941 by N. Devyatkov and collaborators. The use of resonant cavities made it possible to widen the useful range of frequencies for triodes by about an order of magnitude

as compared to that of earlier tube types employed with open oscillatory circuits.

The deterioration of output power of electrostatically controlled tubes, observed experimentally, is due not only to a poorer quality of the oscillatory circuit, but to the effects of electron inertia as well. Now it can be safely stated that the older types of tubes were incapable of operating at microwave frequencies not because of the electron transit angle, but mainly due to the influence of the external circuit and tube design. Nevertheless, the electron transit angle plays an important part in the performance of microwave triodes and tetrodes.

Under direct-current and low-frequency conditions the theory and design of electron devices are based on the Child-Langmuir-Schottky equation (also known as the "3/2 power law"), which determines the static parameters of the tube. However, with quickly varying voltages this equation no more holds. The induced current, flowing in the external circuit of the tube, may differ from the convection current through the tube. Static characteristics, therefore, become meaningless when discussing microwave effects in triodes and tetrodes[1].

With a finite transit angle the phase relationships between the electrode voltages and currents are disturbed. Another manifestation of electron inertia effects is the appearance of an input conductance (refer to Section 2.5): the tube input begins to consume microwave energy, while at lower frequencies in the common-cathode circuit this power consumption may be neglected. This effect considerably impairs the performance characteristics of triode amplifiers and oscillators.

The performance of triodes and tetrodes is also affected by other electronic phenomena at microwaves. Up to the present time, however, there is yet no final solution to the problem of the relation between the limiting frequency and electron transit angle. Despite the seeming simplicity of triode and tetrode designs, a quantitative analysis of drift effects in these tubes is an extremely difficult problem.

The first difficulty is that the interelectrode gaps carry static electric fields along with the radio-frequency field. In certain cases (such as small-signal amplifiers, oscillators with very low efficiencies) the amplitudes of the radio-frequency components can be considered negligible as compared to the d.c. (static) components and in these cases the comparatively simple small-signal theory proves to be applicable. For usual oscillators and power amplifiers, however, large-signal operating conditions are more typical, and the radio-

[1] Naturally, this does not mean that static parameters of microwave tubes cannot be used as one of the ways of checking tube quality during its manufacture and in practical applications.

frequency components turn out to be commensurate in magnitude with the d.c. components. This makes the computation of the tube operating conditions a serious problem.

The second difficulty consists in the existence of a significant space charge in the interelectrode gap between the cathode and grid; under small-signal conditions the distribution of this space charge corresponds to that encountered under static conditions in an equivalent diode. Under large-signal conditions the behaviour of this space charge becomes much more complex. The analysis of electronic effects in the cathode-grid gap of microwave triodes and tetrodes becomes therefore more difficult, than the examination of anode-grid or anode-screen grid gaps.

Despite the above difficulties we can arrive, through qualitative reasoning, at important conclusions about the way in which the performance characteristics of triodes and tetrodes can be improved. These tubes feature the best performance at transit angles tending toward zero. It may therefore be assumed that such devices could be made to operate at microwave frequencies not worse than in the lower frequency ranges, provided the increase in operating frequency could be somehow compensated by a corresponding reduction of the electron transit time. Under these conditions the electron transit angle would remain the same, despite the higher value of frequency.

In principle, the electron transit time can be reduced by either increasing the electrode voltages or reducing the interelectrode spacing.

Experiments show that one and the same tube is capable of operating at higher frequencies if the electrode voltages can be increased. This effect is especially pronounced under pulsed conditions when the supply voltage can be considerably raised without violating the rated power dissipation on the anode, and the cathode emissivity ceases to be a limiting factor. In certain cases, however, increasing the supply voltages proves to be an inefficient measure, especially in case of low-power devices. There are other limitations, too, which restrict the application of this technique.

Another method, consisting in reducing interelectrode spacings, is widely used in the design of microwave triodes. In this respect the most suitable is the planar tube design, which is employed in most modern microwave triodes.

The operating conditions of electron tubes at low frequencies fall mainly into three categories, termed usually class A, B and C. As a rule, this classification is not used to characterize the operation of microwave triodes and tetrodes. It is more convenient to distinguish between the two operating conditions mentioned earlier, the small-signal and large-signal operating conditions. The first can be considered similar to class A operation, the second is somewhat analogous to class B and C conditions.

4.2. Electronic Processes Under Small-Signal Conditions

4.2a. Equivalent Diodes. Transit Angles

An ideal grid may be considered transparent to the electron stream, but opaque to electric fields. Such an assumption is often made in the analysis of various types of microwave electron devices. In actual triodes the penetration factor ("durchgriff") D is ordinarily not in excess of several per cent and therefore this assumption can be considered absolutely justifiable.

A microwave triode can therefore be divided into two diodes that have no coupling by the electric field, but are both pierced by a common electron beam. As mentioned earlier, actual microwave triodes are of a parallel-plane structure; this simplifies the analysis of these two diodes, reducing them to the plane gaps treated in Chapter Two. The operating conditions of each of these gaps will now be examined.

The electron stream entering the first gap from the cathode features thermal velocities of electrons and no initial density modulation. The d.c. component of the convection current through this gap is limited by the space charge and can be described by the usual Child-Langmuir equation, provided the radio-frequency amplitude is much smaller than the static bias applied between the grid and cathode.

The second of these gaps, corresponding to the anode-grid interelectrode spacing, is pierced by an electron stream, in which the radio-frequency component of convection current differs from zero but is considerably less than the d.c. component. Electron velocities at the grid plane can be neglected in comparison with the velocities at the anode; the grid may be considered to function as a sort of cathode, which emits electrons forming a density-modulated beam, though their initial velocities are zero. The space charge may also be neglected, and the field distribution between the grid and anode assumed to be linear.

Thus, the first gap is equivalent to an ordinary diode operating under space-charge limited current and small-signal conditions. The second gap differs from the first one in that there is no space charge and the electron beam at the plane of the equivalent cathode (i.e. at the triode grid) is density-modulated. These gaps are coupled electronically: the convection current at the plane of the equivalent cathode of the second gap is equal to the convection current at the plane of the equivalent anode of the first gap.

One essential circumstance should be noted: all electrons beginning to move toward the grid do not reverse the direction of their motion and inevitably arrive first at the grid plane and then at the anode of the triode. This is one of the distinguishing features of small-

signal performance, as distinct from large-signal operation (refer to Section 4.3).

The radio-frequency properties of a triode are characterized by the electron transit angles through the two equivalent diodes. It is easier to determine the transit angle through the second equivalent diode (grid-anode gap). Assuming this space to be free of space charge and neglecting the static grid bias, by equation (2.27),

$$\theta_{ga} = \omega d_{ga} (2m/eV_a)^{1/2} \tag{4.1}$$

where V_a is the constant anode voltage (relative to the cathode, as usual) and d_{ga} is the spacing between the grid and anode planes.

Substituting the magnitudes of m and e, by (2.11), and replacing the angular frequency by the wavelength reduce equation (4.1) to

$$\theta_{ga} \approx 6.35 \cdot 10^3 \frac{d_{ga}}{\lambda} (V_a)^{-1/2} \text{ radians} \tag{4.2}$$

When calculating the transit angle through the first equivalent diode the initial thermal velocities of electrons emitted from the cathode can usually be neglected. In this case the analysis should be performed taking into account equation (2.28), which was examined in Section 2.2. The transit angle through the cathode-grid gap proves to be

$$\theta_{kg} = 1.5\omega d_{kg} (2m/eV_{eff})^{1/2} \tag{4.3}$$

where d_{kg} is the spacing between the cathode and grid of the triode and V_{eff} is the effective voltage at the grid plane, equal to $V_{eff} = V_g + DV_a$; as usual, D is the triode penetration factor.

For practical purposes equation (4.3) may be reduced to

$$\theta_{kg} \approx 9.53 \cdot 10^3 \frac{d_{kg}}{\lambda} (V_{eff})^{-1/2} \text{ radians} \tag{4.4}$$

At especially close spacings between the cathode and grid, the potential minimum formed at a distance of several microns from the surface of the heated cathode should be taken into account. A still more serious problem is to allow for considerable non-uniformities of the electric field in this gap, resulting in different transit angles and transit times for different electrons. The idea that it is just this spread in transit angles that determines the value of the limiting frequency has been advanced many times.

4.2b. Triode Input Conductance Under Small-Signal Conditions

In the discussion of drawbacks intrinsic to electrostatic current control in Section 2.5*a*, it was shown that increasing the frequency of oscillations in a common-cathode circuit leads to the appearance

of a conductive component in the input admittance, this conductance being approximately in direct proportion to the square of the transit angle θ_{kg} through the cathode-grid gap. The transit angle also affects the input admittance of a triode in a common-grid circuit. As will be shown later, this circuit connection is the most suitable for microwave applications. First we compare the input conductance in these two circuits.

The paths of induced currents when the triode is connected into the common-cathode and common-grid circuits are shown in Fig. 4.2 in dashed lines. In the common-grid circuit, in contrast to the common-cathode connection, the induced current $I_{ind\ 2}$ at the input

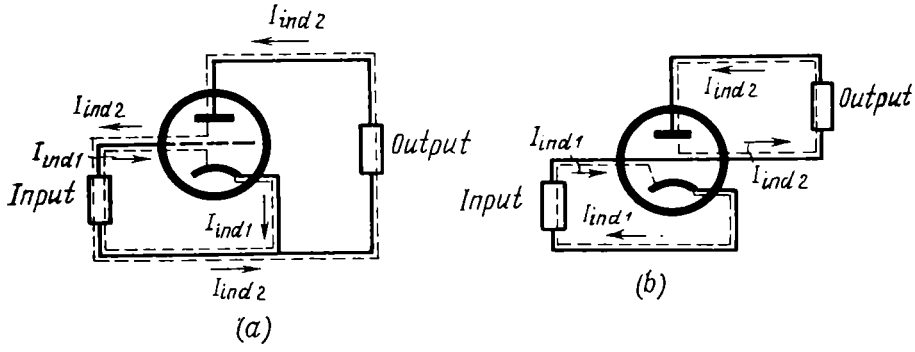

Fig. 4.2. Induced currents with the triode in the common-cathode (*a*) and common-grid (*b*) circuits. The d.c. sources are omitted for simplicity

is not extracted from the current $I_{ind\ 1}$. At low frequencies the induced current $I_{ind\ 1}$ is equal to the convection current through the diode made up of a cathode and a grid. Consequently, at low frequencies a triode in the common-grid circuit has an input conductance that is numerically equal to the static mutual conductance g_m.

What changes in the current, induced in the input circuit of a common-grid circuit, can be caused by an increase in the operating frequency? As before, the current induced in the output circuit does not pass through the input circuit. Consequently, the input admittance in the common-grid circuit should coincide with the admittance of a diode, whose cathode coincides with the cathode of the triode and with the triode grid functioning as the anode of this diode.

The results of calculations of the diode input conductance under small-signal conditions and considerable transit angles were presented in Fig. 2.26. The input conductance of a triode in the common-grid circuit, therefore, is reduced with an increase in transit angle and goes through zero at $\theta_{kg} = 2\pi$. On the other hand, the value of G_{in} of the same triode in the common-cathode circuit by equation (2.41)

increases in direct proportion to the square of the transit angle. The input conductances in both these circuit arrangements can be shown to be identical at a transit angle $\theta_{kg} \approx 5\pi/4$.

Thus, at considerable transit angles the common-cathode circuit loses its main advantage over the common-grid circuit.

4.2c. Restriction of the Limiting Frequency by Cathode Emissivity

Consider equation (4.3) which determines, as a first approximation, the electron transit angle through the cathode-grid gap. The effective static voltage V_{eff} in this equation may be related to the density of the d.c. convection current of the cathode (which is assumed to operate under space-charge-limited conditions) by the usual Child-Langmuir equation

$$J_k = \frac{4}{9} \varepsilon_0 (2e/m)^{1/2} V_{eff}^{3/2} d_{kg}^{-2} \tag{4.5}$$

Calculation of V_{eff} by this equation and substitution of the result into (4.3) yields

$$\theta_{kg} = \omega (6m\varepsilon_0 d_{kg}/eJ_k)^{1/3} \text{ radians} \tag{4.6}$$

The equation thus deduced indicates that it is desirable to increase the specific emission current of the cathode, if a reduction of the transit angle is to be obtained. It goes without saying that the emissive properties of the cathode cannot all by themselves affect the value of the transit angle. The physical meaning of equation (4.6) consists in the statement that with a higher specific emissivity of the cathode it becomes possible to employ higher voltages and, as a consequence, to obtain a smaller transit angle.

An important conclusion can be drawn from equation (4.6). In order that the transit angle remain invariable at increased frequencies it is necessary to provide an increase in cathode specific emissivity proportional to the cube of the frequency, provided the interelectrode spacing remains the same.

The relation derived can be used to roughly estimate the maximum operating frequency of a triode. By experiment, the triode gain is found to be unity or less (under small-signal conditions) at transit angles of the order of 270-300°. Taking the limiting value of θ_{kg} in equation (4.6) to be $3\pi/2$, the limiting frequency of a microwave triode is found to be

$$f_{lim} = 0.75 (eJ_k/6m\varepsilon_0 d_{kg})^{1/3}$$

or

$$f_{lim} \text{ (GHz)} \approx 3.21 (J_k/d_{kg})^{1/3} \tag{4.7}$$

where J_k is in A/cm^2 and d_{kg}, in mm.

For the limiting frequency of microwave triodes to be increased it is necessary to use cathodes with the highest emissivity obtainable This requirement of a high emissivity of the cathode is typical not only of microwave triodes, but of other microwave electron devices as well. In modern triodes the value of J_k amounts to 1 to 2 A/cm^2 under c.w. conditions.

4.3. Operation of Microwave Triodes Under Large-Signal Conditions

4.3a. General Considerations

Under large-signal conditions the constant grid bias may be neglected in comparison with the amplitude of radio-frequency oscillations. Operating conditions of this kind are known to be widely employed in common radio transmitting equipment (when the operating angle of the anode current is approximately 90°).

In the analysis of triode performance, the assumption of a small penetration factor of the grid is again in order, and two planar diodes can again be examined. In contrast to the small-signal conditions, the first of these equivalent diodes (the cathode-grid gap) can be considered energized only by the radio-frequency field; in the second diode, however, both the static and the radio-frequency fields have to be taken into account.

From the point of view of the efficiency and output power of a triode used as an amplifier or oscillator, the first (fundamental) harmonic of the current induced in the output gap is of the greatest interest. In turn, this current depends both on the parameters of the output gap (i.e. the grid-anode circuit) and the cathode-grid gap, too. Indeed, the process of current induction is to a considerable extent dependent on the initial parameters of the electron stream at the grid plane, namely the waveform of the convection current and the electron velocities at different instants of time. The induced current and the output power of the triode can be calculated if the convection current at the grid plane and the electron velocities are known, provided the gap width d_{ga} and the voltage and frequency are specified.

Determination of the convection current and electron velocities at the grid plane necessitates solving the problem of electron motion through the equivalent cathode-grid diode. At the same time, in solving this problem certain other parameters that are important to the performance of a microwave triode amplifier or oscillator can be determined, such as the current induced in the cathode-grid circuit and the convection current at the cathode plane. The time dependence of these parameters can be used as a means for calculating the input admittance of the triode under large-signal conditions,

the maximum emission current of the cathode, the average cathode current, etc.

The analysis of diode performance under large-signal conditions presents considerable difficulties. Only certain qualitative considerations and the results of calculations, which provide a rough idea of the processes taking place in microwave triodes and their effect on the limiting frequency, will be presented in this discussion.

4.3b. Cathode Current Under Large-Signal Conditions

A planar equivalent diode, one electrode of which is a heated cathode, is shown in Fig. 4.3. A radio-frequency voltage $v = V_m \sin \omega t$ is applied to this gap; assume the frequency ω to be so low that electron inertia effects are negligible. In accordance with the Child-Langmuir equation, the convection current supplied by the cathode should then vary relative to voltage as shown in Fig. 4.4*a*, *b*. The duration of a cathode current pulse is exactly equal to half the oscillation period T.

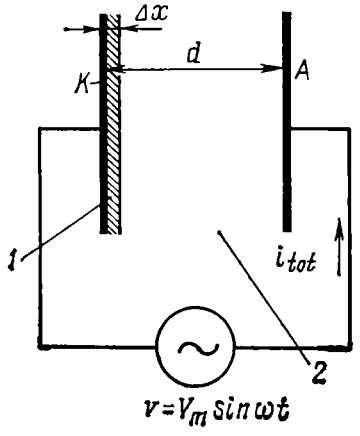

Fig. 4.3. Pattern of current take-off from the cathode at microwaves

Consider now the other extreme case, when the fictitious transit angle, as defined by equation (2.29), is very large. In this case the electrons leaving the cathode will not have time enough to move a considerable distance away from its surface; this means that the thickness of the layer Δx of emitted electrons (refer to Fig. 4.3) during the entire period of current take-off in the course of one oscillation cycle remains much less than the interelectrode spacing d. Let us also assume that to the beginning of the next oscillation cycle the gap, one way or another, is made free of all the electrons emitted earlier, so that their effect on the subsequent process of current take-off can be neglected.

The instantaneous value of the total current i_{tot} through all sections of a series circuit has to be the same. Therefore the total current through the layer of electrons at the cathode surface (shaded area *1* in Fig. 4.3) should be equal to the total current through section *2*, where at this instant no electrons are present, i.e.

$$i_{tot} = i_{con\,1} + i_{d\,1} = i_{con\,2} + i_{d\,2} \qquad (4.8)$$

where i_{con} and i_d are the convection and displacement currents, respectively, at various sections of the gap.

In cases of unlimited emissivity of the cathode, the intensity of the electric field at the cathode surface should be zero at instants of time when the grid voltage is positive, provided the initial electron velocities are assumed to be zero. In the electron layer of Δx thickness, therefore, the displacement current i_{d1} should also be zero

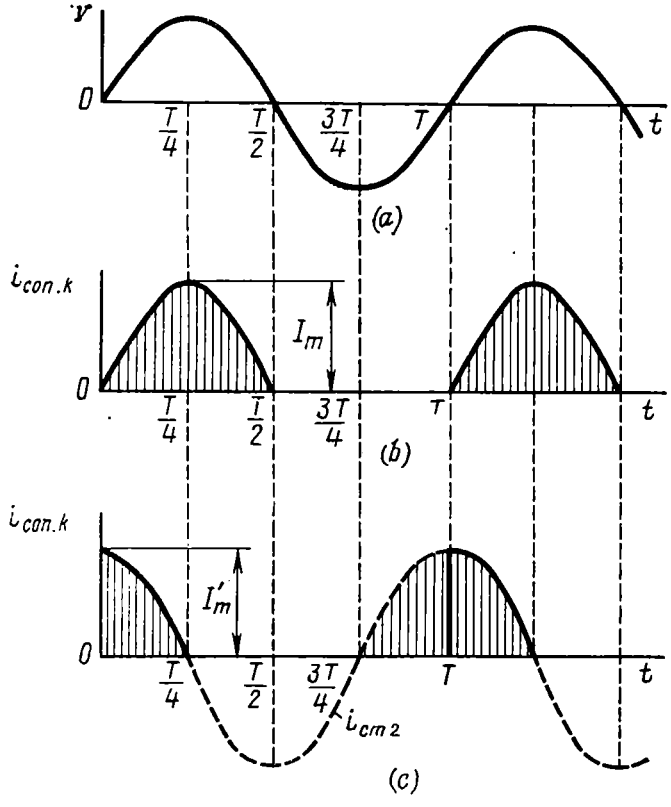

Fig. 4.4. Pattern of cathode convection current at infinitesimal (*b*) and very great (*c*) transit angles, assuming infinite cathode emissivity

and the total current through this section of the gap should be defined solely by the convection current i_{con1} of electrons moving from the cathode to the grid (equivalent anode). In all the rest of the gap there are no electrons, so that $i_{con2} = 0$. Therefore, by equation (4.8),

$$i_{con1} = i_{d2} \tag{4.9}$$

At $\Delta x \ll d$, the displacement current through the second section of the gap may be approximated by the capacitive current through the "cold" gap:

$$i_{d2} \approx C \frac{dv}{dt} = \omega C V_m \cos \omega t \tag{4.10}$$

where C is the interelectrode capacitance of the equivalent diode in the absence of electrons.

The convection current from the cathode at extremely large transit angle conditions will be designated as $i'_{con.k}$ (the prime used to distinguish this current from that described by the Child-Langmuir equation). This current $i'_{con.k}$ is equal to the convection current $i_{con.1}$ through the thin electron layer directly at the cathode surface. Applying equations (4.9) and (4.10), we obtain

$$i'_{con.k} \approx \omega C V_m \cos \omega t \qquad (4.11)$$

Equation (4.11) indicates that the convection current of electrons leaving the cathode under condition of large transit angles is numerically equal to the capacitive current through the same gap in the absence of electrons. However, at negative values of the effective voltage, i.e. at instants $T > t > T/2$, electrons with zero initial velocities are incapable of moving away from the cathode, and the convection current from the cathode at these instants is therefore zero. Furthermore, only the convection current in the positive direction, corresponding to electrons leaving the cathode and moving to the grid (equivalent anode), is of interest when examining cathode emission. From this it follows, that current take-off from the cathode at extremely large transit angles takes place only during the time $T/4 > t > 0$.

A graph illustrating the current $i'_{con.k}$ as a function of time is presented in Fig. 4.4*c*. The shaded areas correspond to electrons being drawn away from the cathode, while the variations of the capacitive current are shown in dashed lines. For convenience, the time scale is the same as in Fig. 4.4*b*, where current flow in accordance with the Child-Langmuir equation is presented.

The first impression is that the results arrived at are somewhat startling — electron take-off from the cathode lasts only a *quarter* of the oscillation cycle at large transit angles, instead of half of a cycle, as in the case of low frequencies. The maximum convection current coincides just with the beginning of the positive halfwave, and not with its middle. Cathode emission starts with an abrupt current surge to the maximum value, this maximum being equal in magnitude to the maximum capacitive current. The current take-off from the cathode ceases just when the effective voltage across the gap is at a maximum.

Physically, however, these peculiarities must be quite obvious if we recall the nature of the total current in different sections of the gap. Every line of force can be also imagined to originate at the anode and terminate in a free electron in the vicinity of the cathode without reaching the surface of the cathode itself; this notion is in absolute accordance with the assumption of a zero field intensity at the cathode surface. Then, the number of electrons drawn away from the cathode at each instant of time is equal to the increment of the number of lines of force in the interelectrode gap. Thus, current

take-off from the cathode will stop at the instant the electric field ceases to increase, despite the radio-frequency voltage remaining an accelerating one during another quarter of the oscillation cycle.

The phenomena in the interelectrode space are further complicated if the time of cathode emission (i.e. a quarter of the cycle) is sufficient for the electrons to be noticeably displaced relative to the cathode or even to pass partially the grid plane. In this case new electrons have to be emitted from the cathode to compensate for the electric field developed at its surface; these electrons have to screen the cathode in just the same way as did the electrons, that have left the interelectrode gap or are approaching the grid plane. The convection current now stops flowing not at the instant the anode voltage goes through a maximum, but somewhat later. If the transit angle is not too excessive, the nature of current flow approximates that under steady-state conditions, and the emission current is governed mainly by the instantaneous value of voltage instead of its time derivative dv/dt.

The maximum currents $I_{max.}$ and $I'_{max.}$ are easily obtained from equations of the (4.5) and (4.11) type (Fig. 4.4). The current $I'_{max.}$ can be shown to exceed the amplitude $I_{max.}$ (as defined by the Child-Langmuir equation) at transit angles greater than about 51°. Thus, the emissivity of cathodes designed for use in tubes of the decimetric and centimetric wave bands (sometimes even for the metric band) has to be increased, as compared to the requirements imposed at lower frequencies.

The conclusions made above about the nature of cathode current under large transit angle conditions are applicable not only to diodes and triodes but to tetrodes and other types of tubes employing electrostatic current control, in other words, to devices with cathodes directly affected by the radio-frequency field.

4.3c. Drift Effects in the Cathode-Grid Space

It is convenient to apply the concept of the fictitious transit angle to the treatment of drift effects in the cathode-grid gaps of microwave triodes operating under large-signal conditions; the fictitious transit angle was defined earlier by equation (2.29) as

$$\alpha_{kg} = \omega d_{kg} (2m/eV_m)^{1/2} \tag{4.12}$$

where V_m is the amplitude of the control voltage applied between the grid and cathode and d_{kg} is the spacing between these electrodes.

First, an intentionally simplified case will be examined, when the cathode operates under saturation conditions (i.e. the current is temperature-limited) and there is thus no space charge in the cathode-grid gap. The electron motion diagram in this case is of the same pattern as examined in Section 2.2*c* for the case of a planar

diode (refer to Fig. 2.2*b*). On this diagram, the triode grid corresponds to the horizontal line x = const. The greater the transit angle α_{kg}, the higher should this line be plotted.

As transit angles α_{kg} approach zero, all electrons leaving the cathode will arrive at the grid plane and move further to the anode. This group of electrons is useful and essential to the performance of triode amplifiers and oscillators. Electron bunches formed with a properly functioning electrostatic current control are composed of just such electrons (refer to Fig. 2.17). However, an increase in the transit angle causes the appearance of a group of electrons that are emitted from the cathode at the end of the positive halfwave and, not being able to reach the grid plane, are returned to the cathode.

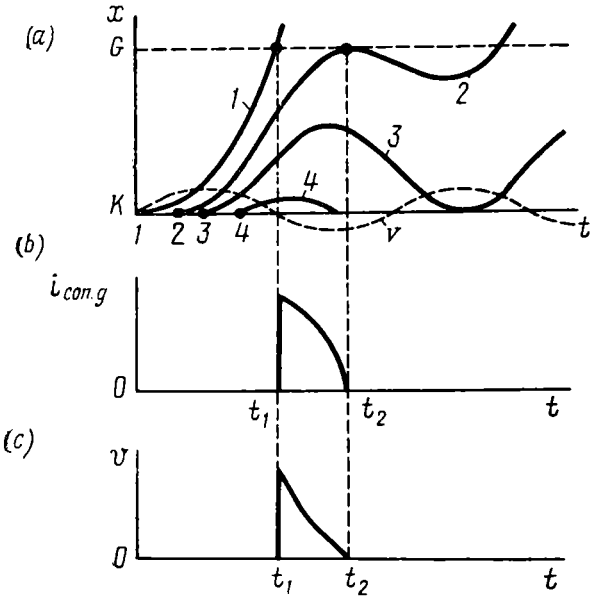

Fig. 4.5. Electron motion in cathode-grid gap under large-signal conditions (*a*), convection current waveform at the grid plane (*b*) and electron velocities at the same plane (*c*)

For the sake of clarity, Fig. 4.5*a* presents the motion diagram for the case of a large transit angle α_{kg}. It shows the trajectories of four typical electrons that are emitted from the cathode at different instants of time during the positive voltage halfwave.

Electrons of type *1* are emitted from the cathode at the instant the field passes through zero in changing from a retarding to an accelerating one. These electrons turn out to be in the leading edge of the electron bunch which passes through the grid plane; they arrive at this plane at the instant of time t_1, having acquired a considerable velocity. Electrons of type *4*, which have left the cathode not long before the end of the voltage halfwave under examination, are returned to the cathode. When striking the cathode surface the electrons have finite velocities, as evidenced by the angle of inclination of the electron trajectory to the cathode surface in Fig. 4.5*a*. Thus, electrons of type *4* dissipate a certain amount of energy, acquired from the radio-frequency field, on the cathode surface, this resulting in additional heating of this surface.

A very important characteristic of large-signal operation of a microwave triode is these electrons returning to the cathode,

as distinct from small-signal operation conditions at which electrons do not reverse their motion in the interelectrode spacing.

Examine now the motion of electrons of type *3*, emitted from the cathode at the instant the radio-frequency field was at a maximum (Fig. 4.5*a*). These electrons can oscillate infinitely in the interelectrode spacing, returning to the cathode with zero velocities exactly after a period of the radio-frequency field. By analyzing equation (2.23) it can easily be shown that the condition that electrons of type *3* never pass the grid plane is α_{kg} equal to, or greater than, 2 radians. Thus, at $\alpha_{kg} \geqslant 2$ radians, half of the electrons emitted from the cathode (i.e. all electrons emitted during the second half of the accelerating halfwave) will not reach the grid plane and be returned to the cathode.

The rest of the electrons (those emitted during the first half of the positive halfwave) will arrive into the grid-anode space. Part of these electrons, however, will pass into the grid-anode gap only after performing one or several oscillations in the cathode-grid gap, as illustrated by the trajectory of electron *2* in Fig. 4.5*a*, where this electron is shown arriving at the grid plane at the instant of time t_2 with a zero velocity.

The trajectories shown in Fig. 4.5*a* can be used to plot the qualitative pattern of convection current and velocities of electrons passing through the grid plane (Fig. 4.5*b* and *c*, respectively). Disregarding the oscillatory movement of electrons, the duration of the convection current pulse at the grid plane is determined by the instants of time t_1 and t_2. Electrons in the bunch have different velocities, zero velocities being featured by electrons that are the last to pass through the grid plane. As will be shown later, this spread in electron velocities is responsible for the deterioration of the microwave triode efficiency.

In actual microwave triodes, cathodes with temperature-limited emission are almost never employed. Detailed analysis reveals that the main features of electron motion in the cathode-grid gap also hold in the presence of a space charge at the cathode surface.

One of the obvious consequences of the drift phenomena in the cathode-grid gap is that the pulses of convection current at the grid plane lag behind the radio-frequency control voltage. Figure 4.5 indicates that electron bunches may pass through the grid plane even at the beginning of the retarding halfwave of the control voltage, provided the transit angle is great enough.

This effect of lagging current pulses does not affect the performance of amplifiers to any noticeable extent. Indeed, in passing through the grid-anode space the electron bunches induce a current in the external circuit of this gap. If the external circuit connected to this gap is tuned exactly to the fundamental of the induced current, i.e. the dynamic impedance of this circuit is purely ohmic, a retard-

ing electric field is built up across this gap automatically at the instant the electron bunches pass through the gap (refer to Section 2.4). Thus, the efficiency with which the electron bunches give up their energy to the radio-frequency field of an amplifier is independent of the phase shift between the convection current and the control voltage. However, this phase shift plays an important part in oscillator performance, because the conditions, which hold at low frequencies, that the convection current and grid voltage be in phase and the grid and anode voltages be in antiphase are no more satisfied. The phase of the feedback at radio frequencies has to differ from π and may approach 2π. An increase in the fictitious transit angle α_{kg} also results in a higher conductance of the cathode-grid gap. Besides the effects qualitatively examined in Sections 2.5*a* and 4.2*b*, the microwave loss due to electron bombardment of the cathode becomes noticeable under large-signal conditions.

Another important consequence is the change in the convection current waveform and a lower amplitude of the convection current fundamental. The average convection current at the grid plane also diminishes. Analysis shows, nevertheless, that the ratio of the amplitude of convection current fundamental to the d.c. component of this current does not fall with an increase in transit angle α_{kg}, but is even slightly increased. This indicates that there are no principal limitations to effective current control by means of a triode grid at the transit angles α_{kg} not greater than 120-126° (no data are available at present on triode performance at greater transit angles). However, the amplitude of the feedback signal has to be increased to provide proper oscillator performance; the gain of a microwave triode as an amplifier proves to be lower than at moderate frequencies.

It is of interest to know which of the drift processes discussed exerts the most deteriorating influence on microwave triode performance and defines, in the final analysis, the limiting frequency of the triode. As will be shown later a marked effect on the limiting frequency of a triode can be produced by the processes in the grid-anode gap, as well as in the cathode-grid gap; the same is true both of the tube design and the oscillatory system. Experience shows, nevertheless, that modern microwave triodes are capable of providing satisfactory performance at transit angles up to about 120°, i.e. $2\pi/3$. The value $\alpha_{kg} \approx 2\pi/3$ can be considered as critical for large-signal conditions.

4.3d. Electronic Processes in the Grid-Anode Gap

Spike pulses of convection current entering the grid-anode space induce a current in the external circuit of the triode. In this respect, the current induction is analogous to that in a gap discussed in

Section 2.3*d*. It should be remembered, however, that the grid-anode space is under the action of both a static and a radio-frequency field so that the velocity of each electron does not remain invariable. Electrons entering the gap also have different velocities. As in the analysis of effects in the cathode-grid gap, the main method of examination here is the grapho-analytical method.

The finite transit time through the grid-anode gap results first of all in a greater duration of the induced current pulse as compared to the duration of the pulse of convection current. Indeed, the beginning of the induced current pulse coincides with the instant the first electron enters this gap, and the end of the pulse corresponds to the instant the last electron of the bunch strikes the anode surface.

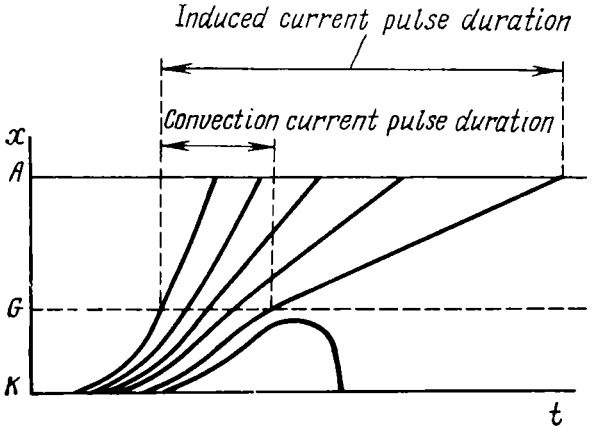

Fig. 4.6. Electron motion diagram in the grid-anode gap of a triode under large-signal conditions

The pulse of induced current is also stretched out because the trailing edge of each electron bunch passing the grid plane contains electrons of very low velocities (Fig. 4.5*c*). The fact that electron bunches have to move in a retarding field so as to give up their energy to this field, also tends to increase the induced current pulse duration. Since the amplitude of the radio-frequency voltage under large-signal conditions is commensurate with the d. c. anode voltage, electron bunches are accelerated but slightly in the grid-anode gap. Electron trajectories acquire, therefore, a fan-shaped pattern, as illustrated qualitatively in the motion diagram of Fig. 4.6.

A greater duration of the induced current pulse results in a lower amplitude of the fundamental, as well as a lower amplitude of all the other harmonics exciting the oscillatory circuit of the triode. Consequently, the output power of triode oscillators and amplifiers, as well as frequency multipliers, should deteriorate with an increase in the transit angle through the grid-anode gap, even if the output gap is excited by electron bunches of perfect waveform. As a result, the efficiency of triodes operating in the microwave band of frequencies is considerably lower than of those operating at moderate frequencies. Thus, at wavelengths of about 7 to 10 cm, triode efficiencies do not exceed 20 to 30 per cent. The efficiency and output power rapidly fall off with a further increase in frequency.

4.4. Oscillatory Systems of Triode Oscillators and Amplifiers

4.4a. Circuit Connection of Microwave Oscillators and Amplifiers

A triode as a circuit element can be considered as an active three-terminal network. Therefore, in the general case the external circuit of a triode can also be reduced to a three-terminal equivalent network shown in Fig. 4.7*a*. The impedances Z_1, Z_2 and Z_3 in this circuit

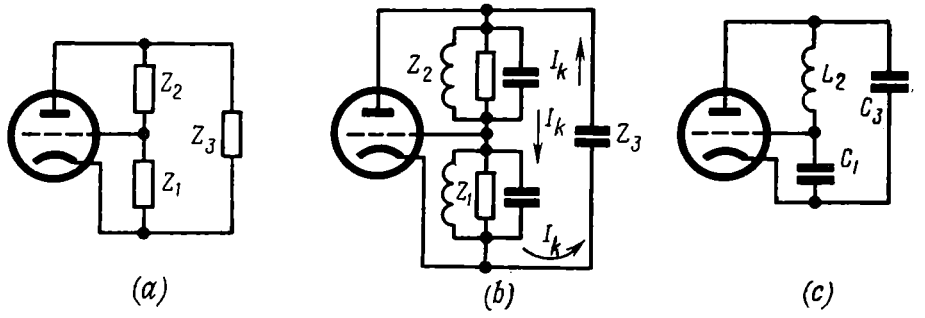

Fig. 4.7. Generalized equivalent circuit of triode connection (*a*) and common-grid triode oscillator circuit (*b*, *c*)

include the external network, interelectrode capacitances and lead inductances of the triode; in the general case each of these impedances can be composed of one or more oscillatory circuits.

In the microwave range the *common-grid* (or *grid-separation*) circuit of a triode with *two resonant cavities* is almost exclusively used. In this circuit (Fig. 4.7*a* and *b*) the elements Z_1 and Z_2 are resonant cavities. The required feedback is provided via element Z_3, which is ordinarily non-resonant in the frequency band of interest and ensures the proper coupling between elements Z_1 and Z_2. If we remove element Z_3, the circuit is converted to a common-grid amplifier, also extensively used at microwaves.

The main advantages of a common-grid circuit connection at microwave frequencies are as follows.

1. Internal feedback in this circuit arrangement is due to the finite inductance L_g of the grid lead and the interelectrode capacitance between the cathode and anode C_{ak}. In any triode this capacitance is the lowest, as compared to the other two interelectrode capacitances. The inductance of the grid lead can be minimized by employing a disc-seal grid (refer to Section 4.5). Therefore, the parasitic internal feedback in the common-grid circuit proves to be lower than in the other two possible connections. This feature is especially important when designing triode amplifiers, which tend

to become self-excited at high and microwave frequencies. In oscillators, it is also useful to weaken the uncontrollable internal feedback, which simplifies the selection and adjustment of the external feedback.

2. The common-grid circuit is especially convenient and suitable for the design of microwave triode amplifiers and oscillators. Indeed, a triode may be connected to two independent resonant cavities without the cavities intersecting each other only if the grid plane separates these cavities from one another (hence, the second designation "grid-separation"), as shown in Fig. 4.8. One of these cavities proves to be connected between the grid and cathode, the second, between the grid and anode of the triode. The tube electrodes are integral elements of the resonant cavities.

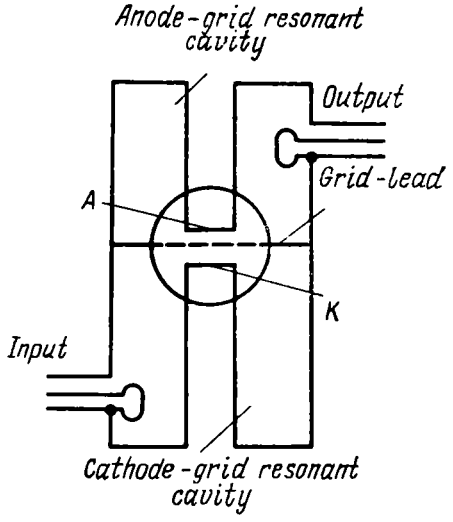

Fig. 4.8. Relative positions of resonant cavities and tube in a common-grid triode oscillator

The disadvantage of the common-grid circuit is a high input conductance and, as a result, a lower gain. However, as demonstrated in Section 4.2*b*, at higher frequencies the input conductance in the common-cathode circuit tends to approach that of the common-grid circuit and therefore this drawback cannot be considered essential at microwave frequencies. At present a vast majority of microwave triode oscillators and amplifiers are designed with the common-grid circuit connection.

4.4b. Some Characteristic Features of Common-Grid Triode Oscillators

We shall now analyze the oscillation frequency and the role of the resonant cavities making up the external circuit of a triode oscillator. In accordance with the general principles (refer to Section 3.2) the oscillation frequency of any microwave oscillator with a resonant oscillatory system as a first approximation can be considered equal to the resonant frequency of its oscillatory system. For simplicity, electron inertia effects for the moment will be disregarded.

When the entire oscillatory system is at resonance, the currents in the right-hand and left-hand branches of the complex tuned circuit of Fig. 4.7*b* are equal in magnitude and opposite in direction (parallel resonance or antiresonance). The circuit current I_c produces a voltage drop across element Z_3 and the cathode-grid tuned circuit. To provide

antiphase fields in the cathode-grid and the grid-anode gap, the reactance of element Z_3 should be of the same nature as the reactance of the cathode-grid tuned circuit.

If element Z_3 is a capacitance, as in Fig. 4.7*b* and *c*, the cathode-grid circuit should also feature a capacitive (positive) reactance at the oscillation frequency. It means that the oscillation frequency, and the corresponding resonant frequency of the entire system must be higher than the resonant frequency of the cathode-grid cavity.

On the other hand, with two circuit elements (Z_1 and Z_3) featuring a capacitive reactance at the operating frequency, the anode-grid cavity has to exhibit an inductive reactance so as to ensure resonance at this frequency. It follows that the grid-anode cavity should be tuned to a frequency slightly higher than the oscillation frequency. The equivalent circuit of the oscillator in question acquires the form shown in Fig. 4.7*c*. The resonant frequency ω_0, which is approximately the oscillation frequency ω_{osc}, can be determined from the obvious relation

$$\omega_0 = \left(L_2 \frac{C_1 C_3}{C_1 + C_3}\right)^{-1/2} \tag{4.13}$$

(L_2, C_1 and C_3 are clear from Fig. 4.7).

Tuning the cathode-grid cavity causes a change in its susceptance, this resulting in a corresponding change in the radio-frequency voltage $\dot{V}_g$ applied between the grid and cathode of the triode. The ratio of this voltage to the voltage between the anode and cathode is known as the *feedback factor*. Thus, tuning the cathode-grid cavity affects not only the resonant frequency of the entire system, but the feedback factor of a triode oscillator. Voltage $\dot{V}_a$ is, however, higher in absolute value than $\dot{V}_g$ and therefore the equivalent capacitance C_1, which represents the cathode-grid cavity at the oscillation frequency, should be greater than C_3 (refer to Fig. 4.7*c*).

Equation (4.13) indicates that at $C_1 > C_3$ the frequency is but slightly dependent on C_1; in other words, tuning the cathode-grid cavity leaves the oscillation frequency almost unchanged. The function of this cavity is mainly to adjust the feedback and thus control the output power. Thus, tuning the cathode-grid cavity causes the output power to vary within wide limits and go through a maximum at a certain frequency

$$\omega_{osc} \approx \omega_{02} \approx (L_2 C_3)^{-1/2} \tag{4.14}$$

though the oscillation frequency remains almost constant.

The feedback factor is defined not only by the tuning of the cathode-grid cavity, but by the feedback impedance Z_3 as well; in the case under treatment this element features a capacitive reactance. Ordinarily, this impedance is fixed to simplify the process of oscil-

lator tuning in the frequency band of interest. The value of C_3 is selected as low as practicable, so as not to impair the dynamic resistance of the oscillatory system at the oscillation frequency. Therefore the equivalent inductance L_2 turns out to be considerable and the oscillation frequency approximates the resonant frequency of the grid-anode cavity.

Several conclusions can be drawn from the argumentation presented. In a common-grid two-cavity oscillator, the oscillation frequency is determined mainly by the tuning of the grid-anode cavity. Tuning the cathode-grid cavity is necessary to provide the proper feedback factor, i.e. to ensure the maximum output power.

From this point of view, a two-cavity oscillator should be equipped with two tuning arrangements. At first the required frequency is coarsely set by tuning the grid-anode cavity, then the maximum power is obtained by tuning the cathode-grid cavity, and finally the oscillator is precision-tuned to the required oscillation frequency by means of the grid-anode cavity.

Drift effects in the triode make the relations discussed much more elaborate. As shown in Section 4.3, transfer of the energy of electron bunches to the microwave field is effective when the phase shift between the anode and grid voltages is in excess of 180° and may approach 2π. The value of this phase shift depends on electron transit angles and, therefore, on the constant voltages applied to the tube electrodes, as well as on the oscillatory conditions. Furthermore, the cathode-grid interelectrode gap acquires an input admittance, which is also a function of these voltages. It is therefore desirable that the feedback phase, as well as its magnitude, be controlled continuously.

Continuous control of the feedback phase is possible only if the elements constituting the voltage divider (elements Z_1 and Z_3 in Fig. 4.7) have a conductive component. It is not necessary however in this case to introduce any additional external resistors, because the input admittance of the triode features a significant conductive component. Thus, as before, the cathode-grid resonant cavity can control both the magnitude and the phase of the feedback. Operation in the vicinity of the limiting frequency, however, proves to be very sensitive to feedback tuning.

4.4c. Elements of Triode Amplifiers and Oscillators

Triode amplifiers and oscillators are designed mainly with coaxial cavities, loaded by the tube interelectrode capacitances[1]. Two versions of two-cavity systems are possible, i.e. double-ended and single-ended; they are illustrated in Fig. 4.9.

[1] The oscillatory systems of subminiature triode amplifiers and oscillators also employ stripline (microstrip) elements.

In a triode amplifier the input signal is fed into the cathode-grid cavity, and the amplified signal is coupled out of the anode-grid cavity by means of a loop or probe that terminate the feeder

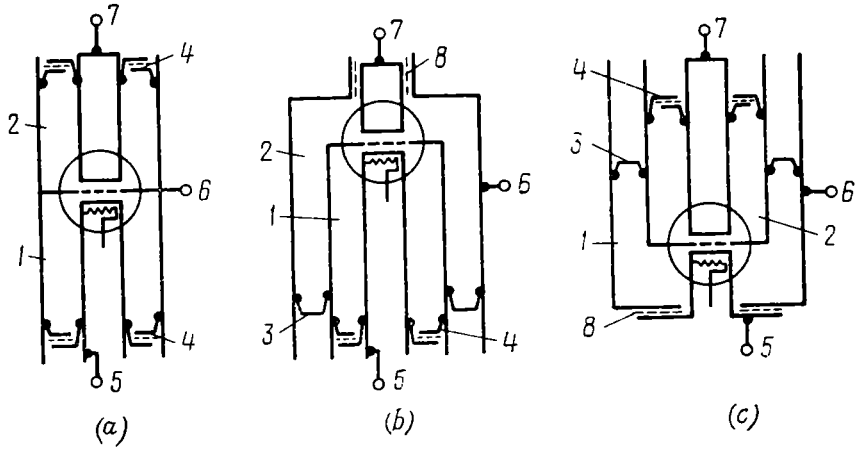

Fig. 4.9. Double-ended (*a*) and single-ended (*b*, *c*) forms of mounting a triode in coaxial cavities

1—cathode-grid cavity; *2*—grid-anode cavity; *3*—tuning plunger; *4*—tuning plungers with blocking capacitors; *5*, *6*, *7*—cathode, grid and anode d.c. leads, respectively; *8*—blocking capacitor

line, as shown in Fig. 4.8. At shorter wavelengths, where microwave triodes are applied at present (3 to 5 cm), use is also made of waveguide power output arrangements.

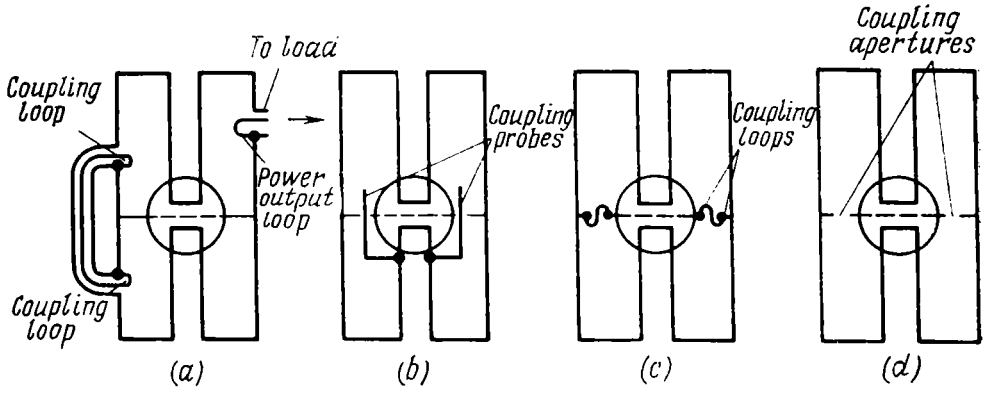

Fig. 4.10. Feedback arrangements in microwave triode oscillators

(*a*) inductive feedback via two loops and a coaxial line; (*b*) conductive-capacitive feedback via probes; (*c*) inductive coupling via two loops; (*d*) feedback via an aperture in the common wall

Usually, in oscillators the load is coupled to the anode-grid cavity; feedback is provided by means of loops, probes or apertures between the cavities, as shown in Fig. 4.10 for the case of a double-ended oscillator version.

Tuning the resonant cavities of triode amplifiers and oscillators is ordinarily accomplished with the aid of movable tuning plungers of the contact (spring), choke or capacitive types, as illustrated in Fig. 4.9. In case of a moderate tuning range (about several per cent) the use of tuning screws mounted on the side walls of the cavities, becomes possible. Movable plungers provide a much wider tuning range, up to an octave and even more.

The electrodes of a triode must be fed with three voltages, namely the d.c. anode voltage V_a, the d.c. grid bias V_g and the d.c. or a.c. heater voltage V_h. Blocking elements (chokes and capacitors) are usually provided in triode amplifiers and oscillators for d.c. separation of these voltages as well as to exclude radio-frequency power leakage or bring it down to an acceptable minimum. Possible arrangements of these blocking capacitors are shown schematically in Fig. 4.9. Ordinarily these capacitors employ mica or some other dielectric with low radio-frequency loss, featuring adequate breakdown capabilities (for instance, teflon film). The magnitude of the capacitance usually required to provide a low reactance at the operating frequency (as compared to the characteristic impedance of the corresponding coaxial line) does not exceed some hundred picofarads. An excessive capacitance is undesirable since it hampers the amplitude and especially pulse modulation of a triode oscillator or amplifier.

We shall now touch the problem of grounding the triode oscillator. It should be emphasized that connecting any of the tube electrodes to ground cannot in any way influence the radio-frequency performance of an amplifier or oscillator. Indeed, the use of resonant cavities ensures that the radio-frequency fields are confined within these cavities. In practice, selection of the electrode that should be grounded is mainly determined by the considerations of safety and the convenience of manufacturing d.c. supplies and modulating devices.

Usually, it is desirable to ground the electrode which is directly connected to the external massive metal parts and has d.c. connection with the signal input or output. Note that the choice of the electrode to be grounded in other types of microwave devices, such as klystrons, magnetrons, etc., is made from similar considerations.

4.5. Microwave Triode Design Problems

4.5a. General Considerations

When discussing the trends in designing microwave triodes there arises the problem, the same as with many other microwave electron devices, of mounting the oscillatory system either inside or outside the vacuum envelope of the tube. Correspondingly, in the following

discussion the respective designs will be referred to as *internal* and *external*.

Reduction of the operating wavelength results in smaller linear dimensions of the resonant cavities, and therefore these latter can be mounted inside the tube envelope. This becomes feasible even at decimetric wavelengths, but is especially justified at centimetric and millimetric wavelengths, where the cavities turn out to be very small. With the internal cavity design, the cavity walls simultaneously form the vacuum envelope of the tube. The tube becomes all-metal, so that a dielectric envelope is no longer necessary, this in turn reducing microwave power loss.

Internal arrangement of the cavities may even provide certain advantages in operation, because the tube need not be linked mechanically to external cavities. The power output, feedback arrangement and other elements of the oscillatory system in this case are also inside the tube envelope and have to be adjusted and fixed in the process of tube manufacture. No further adjustment is necessary.

Tube designs with internal cavities possess essential drawbacks that should also be kept in mind. The range of mechanical tuning of the internal cavities rarely exceeds 10 to 20 per cent of the middle frequency, because it is difficult to provide considerable plunger displacement without deterioration of vacuum. Tubes with internal cavities are of more complex designs and are more difficult to produce, hence their higher cost. At the same time, the device becomes less versatile. Indeed, tubes with internal cavities can be used only within a narrow frequency band. To ensure operation in the entire microwave frequency range, a great many electron device types have to be produced.

In contrast to microwave devices of other classes, such as klystrons, magnetrons, etc., the electronics underlying the triode performance does not set any definite limit to their utilization at lower frequencies. In principle, microwave triodes can be used at any frequency beginning with d.c. and up to the limiting frequency which is determined by the effects examined above. From this point of view it would be inexpedient to make triodes less versatile by incorporating an internal cavity into their design. It should also be remembered that triodes are incapable of operating at millimetric wavelengths, where internal cavities become indispensable. In most cases, therefore, triodes with external cavities are used, internal designs being employed sometimes in power tetrodes (*resnatrons*) treated in Section 4.6 and in triodes for use with wavelengths shorter than 3 cm.

4.5b. Typical Triode Designs and Parameters

Figure 4.11 shows three typical microwave triodes of the low and medium power levels. Glass or ceramics are used as materials for vacuum envelopes. Radio-frequency leads are made in the form

Table 4.1

Parameters of Typical Microwave Triodes

No.	Triode type	Maximum operating frequency, GHz	Maximum output power at the design frequency, W	V_a, V	I_a, mA	Gain, dB	Noise figure, dB	Notes
1	Low power glass-to-metal lighthouse triode (Fig. 4.11*a*)	3.4	0.035 400	250 2500	15 —	— —	— —	C.w. oscillator Pulsed oscillator
2	Low power ceramic-to-metal triode	6.0	2	350 350	60 60	13* —	— —	C.w. amplification C.w. oscillator
3	Medium power ceramic-to-metal triode (Fig. 4.11*b*)	3.3	120** 12,000	1500 9000	225 7500	— —	— —	C.w. oscillator Pulsed oscillator
4	Low power titanium-to-ceramic triode (Fig. 4.11*c*)	6.0	0.025	200	10	— 15***	— 10***	C.w. oscillator C.w. amplification

* At a frequency of 2GHz in the band of 30 MHz
** At a frequency of 600 MHz
*** At a frequency of 4 GHz

of metal discs or cylinders, which are connected to external cavities by means of spring contacts.

In certain cases the tube includes elements which are specific to the resonant system, such as blocking capacitors and feedback arrangements. Thus, a mica capacitor is placed between the radio-frequency and d.c. leads of the cathode of a lighthouse triode shown

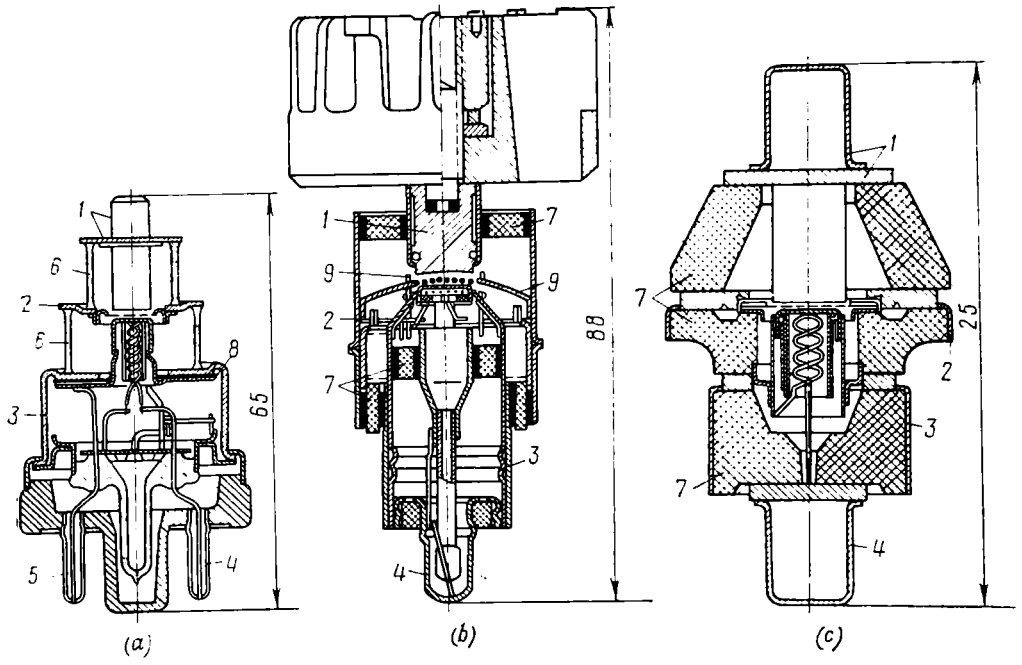

Fig. 4.11. Disc-seal triodes of the glass-to-metal and ceramic-to-metal variety (*a* and *c*, respectively) and a ceramic-to-metal triode with cylindrical electrode leads (*b*)

1—anode lead; *2*—grid lead; *3*—cathode lead; *4*—heater lead; *5*—d.c. cathode lead; *6*—glass; *7*—ceramics; *8*—mica blocking capacitor; *9*—conductive-capacitive feedback probes

in Fig. 4.11*a* (compare to Fig. 4.9*c*). The triode shown in Fig. 4.11*b* contains internal feedback probes, which are schematically shown in Fig. 4.10*b*. A triode with internal feedback probes can only be used as an oscillator and is obviously unsuitable for microwave amplifier applications. On the contrary, triodes without an internal feedback can be used as microwave oscillators or amplifiers, provided the required feedback in the former case is external.

Table 4.1 presents data on several types of low and medium power triodes. Metal-to-ceramic designs of considerably higher power levels are also available; they are mostly for the 400 to 600 MHz band with water cooling of the anode and output power levels up to 300 kW c.w. or up to 5 MW pulsed operation. The efficiency of such triodes is up to 60 per cent at the design frequency. The gain provided by these and most other triode types, however, is usually not in excess of 10 to 15 dB in the common-grid circuit.

4.6. Microwave Tetrodes

The drawbacks of microwave triodes under large-signal conditions can be partially eliminated by placing a screen grid between the control grid and the anode. The input oscillatory circuit is as before connected between the first (control) grid and the cathode, while the output circuit is connected between the anode and the screen grid, as illustrated in Fig. 4.12. In many respects this circuit is similar to the common-grid circuit of a triode, which was discussed in Section 4.4. The gap between the control and the screen grid should be made free of radio-frequency field. To this end, blocking capacitors or sections of transmission lines equivalent to them are used to connect these grids.

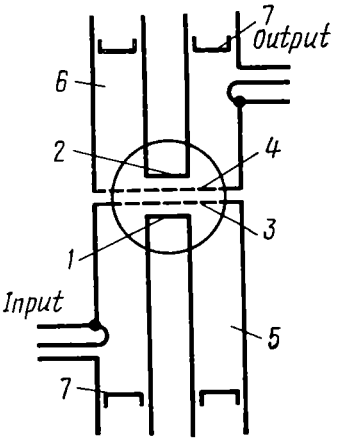

Fig. 4.12. Microwave tetrode in two-cavity oscillatory system

1—cathode; *2*—anode; *3*—control grid; *4*—screen grid; *5*—input resonant cavity; *6*—output resonant cavity; *7*—tuning plungers

In the circuit in question the parasitic feedback may be via the cathode-anode interelectrode capacitance which couples the output and the input cavities. Due to the screening action of the second grid this capacitance proves to be reduced. Thus the tetrode can be used as an amplifier with a greatly reduced tendency to self-excitation. Obviously, an amplifier of this kind is easily converted into an oscillator by simply including the necessary feedback elements between the input and output cavities.

Tetrodes are used mainly under large-signal conditions (class C operation). The electronic processes in the cathode-control grid gap of a tetrode cannot differ to any noticeable extent from those in the corresponding gap of a triode; the main difference and advantages of a tetrode are due to the effects taking place in the output gap between the anode and the screen grid.

Electron bunches passing through the control grid plane arrive into the output gap only after having acquired a considerable degree of acceleration in the strong static electric field between the two grids. Owing to this, the spread in electron velocities, which causes stretching out of the convection current pulse in triodes, produces a considerably less pronounced harmful effect in tetrodes. Furthermore, the transit angle through the output gap is also reduced, this also tending to shorten the pulse of induced current in the output circuit. A shorter pulse of induced current in tetrodes as compared to that in a triode (Figs 4.13 and 4.6) ensures a higher amplitude of the current fundamental and, thus, a higher efficiency. Tetrodes

are therefore suitable for use as high power microwave amplifiers and oscillators, with efficiencies exceeding those obtained with similar triode designs.

As with triodes, microwave tetrodes can also have internal or external cavities. The former are used in super-high power tubes known as *resnatrons* (resonant-cavity tetrodes) while the latter

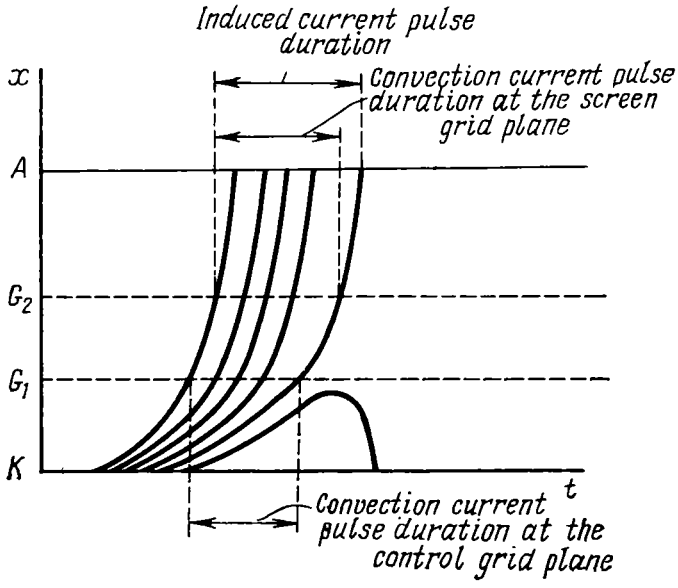

Fig. 4.13. Electron motion diagram in a tetrode under large-signal conditions (compare to Fig. 4.6)

employ glass-to-metal or ceramic-to-metal seals to which external cavities are connected with the aid of spring contacts.

Resnatrons are capable of providing c.w. output power levels up to scores and hundreds of kilowatts at wavelengths in the 40 to 200 cm range; their overall efficiency can be up to 60-75 per cent. Gains above some 8 to 10 dB, however, have not yet been realized. As mentioned, this drawback is common to all devices with electrostatic current control.

4.7. Application of Microwave Triodes and Tetrodes

The main fields of application of microwave triodes are the following:

(1) input amplifiers of small signals in microwave receivers;

(2) laboratory oscillators of low and medium power levels for measurements;

(3) oscillators and amplifiers of medium power levels for use in television, navigation, relay, communications transmitters, etc.;

(4) pulsed oscillators of medium and high power designed for radar transmitters.

Besides, microwave triodes are also used as frequency converters and multipliers; the shortest wavelength obtained with the aid of a triode frequency multiplier is about 1.5 cm.

The application of tetrodes is restricted mainly to high power oscillators and amplifiers for use as the final stages of radio transmitters, in radio countermeasure equipment, television and communications.

Devices designed to function as input amplifiers must have a low level of inherent noise. Experience shows that the noise figure of low-power microwave triodes is 9 to 10 dB at a 25-cm wavelength and 10 to 15 dB at a 10-cm wavelength. Such noise figures make microwave triodes incapable of competing with superheterodyne receivers of the centimetric wave band, in which the crystal mixer forms the receiver input. Travelling-wave tubes, treated in Chapter Six, also feature a better noise figure than microwave triodes. For these reasons, microwave triode input amplifiers are ordinarily used at wavelengths longer than some 10 to 15 cm.

As compared to other amplifier devices (travelling-wave tubes, multicavity klystrons, etc.) microwave triodes and tetrodes exhibit a considerably lower gain in conjunction with a comparatively narrow band of operating frequencies.

At the same time, triodes have a number of advantages, too, among which are the absence of external elements for focussing the electron beam, which are of considerable dimensions and weight. Furthermore, triodes operate with comparatively low supply voltages and provide a greater stability of the phase characteristic when used as amplifiers. As oscillators, triodes are advantageous from the point of view of oscillation frequency stability with respect to variations of the supply voltage. Thus, the frequency stability of triode oscillators can be dozens of times higher than that of similar oscillators employing reflex klystrons. The low cost of triodes as compared to other more complex electron devices is also worthy of notice.

It is of interest to examine the future trends in the development of microwave triodes and tetrodes. The opinion that the potentialities of improving the perfomance characteristics of this class of devices are already exhausted and that only essentially new types of oscillators and amplifiers can be of practical interest was proclaimed time and again. Each time such statements were disproved by actual practice. Such was the case with the advent of klystrons and the development of travelling-wave tubes and magnetrons, and recently — with the appearance of solid-state microwave devices (transistors, avalanche diodes, Gunn diodes, etc.). Progress in the development of these devices has each time served as an additional

impetus to the improvement of microwave triodes and tetrodes on a new and a more perfect basis.

Further improvement of microwave triodes and tetrodes can be expected to follow along the following lines:

(1) further reduction of the interelectrode spacings and providing a more uniform field in the gaps;

(2) increasing the cathode emissivity;

(3) development of designs capable of operating at elevated temperatures without deterioration of vacuum;

(4) general miniaturization, development of triodes with internal cavities and creation of integrated microwave assemblies.

An important part in solving these problems is to be played by vacuum tube technology. In future higher operating frequencies of microwave triodes and tetrodes, as well as higher output powers, longer life and higher reliability may be expected.

CHAPTER FIVE
KLYSTRONS

5.1. General Problems

Klystrons are classified among electron-beam devices with dynamic current control. The circuit schematic of a *two-cavity klystron*[1] is illustrated in Fig. 5.1*a*.

The first (input) resonant cavity of the klystron is designed to velocity-modulate the electron beam and is termed the *buncher*.

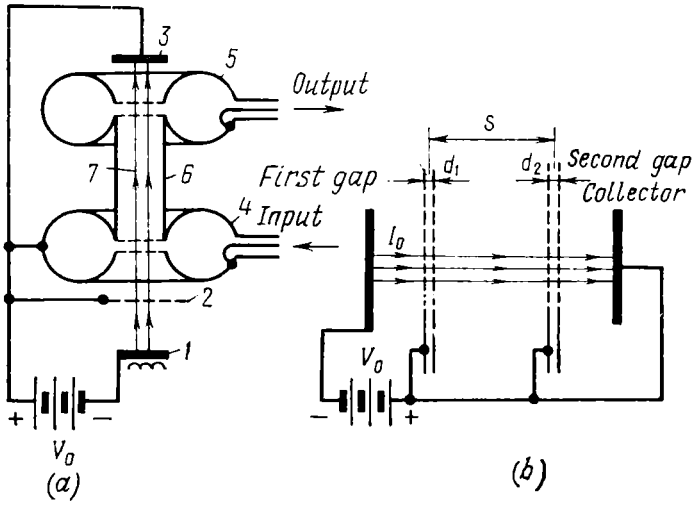

Fig. 5.1. Design (*a*) and idealized circuit (*b*) of a two-cavity klystron
1—cathode; *2*—accelerating electrode; *3*—collector; *4*—input cavity (buncher); *5*—output cavity (catcher); *6*—drift tube; *7*—electron beam

The second (output) cavity is designed to couple out the energy of a density-modulated electron beam and is termed the *catcher*. The metal tube mounted between these cavities screens the *drift* (*bunching*) *space* from external static and alternating fields; at the design frequency this drift tube features the properties of a waveguide under cut-off conditions. It is just in this drift tube that the process of conversion of velocity modulation into density modulation takes place. The action of magnetic fields can be disregarded in the

[1] The term klystron originates from the Greek "klyso" which means surf.

analysis of klystron performance, except for the action of a permanent longitudinal magnetic field, which is employed to provide focussing of the electron beam.

The principles of performance of a two-cavity amplifier klystron can be briefly described in terms of the effects discussed in Sections 2.4 and 2.8. The unmodulated electron beam from the cathode enters the buncher cavity, whose gap carries a longitudinal radio-frequency electric field. This field modulates the velocities of electrons in this beam. Moving in the drift space, the electrons are compressed into bunches which arrive at the output resonant cavity with a repetition rate equal to the frequency of the input signal and induce a current on the inner surface of this cavity walls. The radio-frequency field thus developed across the gap proves to be a retarding one relative to the electron bunches; the kinetic energy acquired by the electron beam from the source of accelerating voltage V_0 is thus converted into the energy of a microwave field and is delivered to the load via the power output arrangement. After passing through the catcher gap, the electron beam is intercepted by the collector, where the rest of the kinetic energy of the beam is dissipated in the form of heat.

The main features by which a klystron differs from conventional low-frequency tubes are as follows:

(1) the use of dynamic current control, based on velocity-modulation of electron beam with subsequent conversion of this velocity modulation into density modulation, instead of electrostatic current control; the electron transit time through the drift space is put to good use;

(2) utilization of the principle of current induction in the output gap and separation of the functions of the output gap and collector;

(3) the use of resonant cavities with the input and output gaps made integral with these cavities which are most suitable for microwave applications;

(4) isolation of the cathode from the microwave circuit and placing the accelerating electrode in front of the modulating (buncher) gap.

At the same time klystrons have much in common with microwave devices employing electrostatic current control. The fact that the tube itself and the cavities constitute one indivisible unit is not characteristic of klystrons only, the same is true of modern microwave triodes and tetrodes as well. There is a striking similarity between the circuit of a two-cavity klystron amplifier and the two-cavity circuits of common-grid triode and tetrode amplifiers and oscillators (refer to Figs 4.8 and 4.12). Thus, in discussing klystrons one should take into account the properties of other types of microwave devices.

As any other amplifier, the klystron of Fig. 5.1*a* can be made to oscillate by providing a positive feedback between the catcher and buncher cavities. Furthermore, this amplifier can be converted into a frequency multiplier by tuning the output cavity to a frequency, which is an exact multiple of the input signal frequency.

Further development of the principles of klystron amplifiers has resulted in the appearance of *cascaded multicavity klystrons*, in which one or more intermediate (idler) cavities are mounted between the buncher and catcher cavities. As will be demonstrated in Section 5.5, multicavity klystron designs ensure a considerable increase in the gain, efficiency and output power, as compared to the two-cavity design.

Another version of a klystron, that is also very extensively used, is the so-called *reflex klystron*; these devices are used mainly as low power oscillators. In this kind of klystrons, which was first proposed by N. Devyatkov, Y. Daniltzev and I. Piskunov and nearly simultaneously by V. Kovalenko (1940), only one resonant cavity is employed, with the same electron beam passing through this cavity twice (refer to Fig. 5.24). The reversal of electron beam is performed by a special electrode, a reflector or repeller, to which a negative voltage relative to the tube cathode is applied. A certain similarity between the reflex klystron and the retarding-field oscillator discussed earlier may be noted; one of the main differences is that the reflector of a klystron does not function as a radio-frequency electrode.

A common feature of all klystron tubes is the use of velocity modulation with subsequent conversion of this modulation into density modulation of the electron beam. All the kinematic calculations of velocity modulation and phase focussing effects, discussed in Chapter Two, are therefore applicable to klystrons. The processes taking place in klystrons can also be treated by the electron-wave theory methods, examined in Section 2.9.

5.2. Kinematic Theory of Electron Bunching (Drift Method of Modulation Conversion)

5.2a. Initial Relations

The peculiarities of the drift method were examined in Section 2.8, where the laws governing the process of electron bunch formation were disclosed, and the equations of velocity modulation by a small sinusoidal signal were derived. Now a more detailed analysis of the effects taking place in the drift space of a two-cavity klystron will be presented.

An idealized circuit of a two-cavity klystron is shown in Fig. 5.1*b*. The buncher and catcher gaps are represented by two pairs of perfect parallel-plane grids that are transparent to the electron beam but

absolutely opaque to the electric field. The spacing between these grid pairs is d_1 and d_2, respectively. Electrons are accelerated by a constant voltage V_0 and then move under the action of inertia (all the grids are d.c. connected to one another). The electron beam is velocity-modulated in the first (buncher) gap by a radio-frequency voltage with an amplitude V_1 which, as before, is assumed to be much smaller than V_0.

The instant of time the electron in question passes the middle of the buncher gap will be denoted as t_1 (in the following treatment all quantities related to the buncher gap will be given the subscript "1", while those of the catcher gap, the subscript "2"). Thus, the instantaneous modulating voltage across the buncher gap can be described as

$$u = V_1 \sin \omega t_1; \quad 1 \gg V_1/V_0$$

The electron velocity v at the output of the buncher gap is determined by the equations of velocity modulation (2.61) and (2.62). With the designations adopted, we have

$$v = v_0 + v_1 \sin \omega t_1 \tag{5.1}$$

$$v_1 = v_0 M_1 V_1 / 2V_0 \tag{5.2}$$

where

$$v_0 = (2eV_0/m)^{1/2} \tag{5.3}$$

The gap factor M_1 determines here the degree of interaction of the electron beam with the radio-frequency field of the buncher gap and is defined in terms of the transit angle θ_1 through the buncher gap by equation (2.37) as

$$M_1 = \frac{\sin(\theta_1/2)}{\theta_1/2} \tag{5.4}$$

where $\theta_1 = \omega d_1/v_0$.

Ignoring the effect of space charge and assuming electron motion inside the drift tube to be purely inertial, the time of arrival t_2 at the catcher gap of the electron, which passed the middle of the buncher gap at t_1, will be

$$t_2 = t_1 + s/(v_0 + v_1 \sin \omega t_1) \tag{5.5}$$

where s is the length of the drift space between the middles of the buncher and catcher gaps (refer to Fig. 5.1*b*).

Rearranging equation (5.5), keeping in mind the fact that v_1 is considerably less than the average beam velocity v_0, results in

$$t_2 = t_1 + \frac{s}{v_0}\left(1 + \frac{v_1}{v_0}\sin \omega t_1\right)^{-1} \approx t_1 + \frac{s}{v_0} - \frac{sv_1}{v_0^2}\sin \omega t_1 \tag{5.6}$$

Multiplying both sides of this equation by the angular frequency and omitting the sign of approximate equality yield

$$\omega t_2 - \frac{\omega s}{v_0} = \omega t_1 - \frac{\omega s v_1}{v_0^2}\sin \omega t_1 \tag{5.6a}$$

The following abbreviation will be introduced:

$$X = \frac{\omega s v_1}{v_0^2} \tag{5.7}$$

This dimensionless quantity X is termed the *bunching parameter* and plays an important part in klystron theory. Equation (5.7) using (5.2) can be represented as

$$X = \frac{\omega s}{v_0} \frac{M_1 V_1}{2V_0} = \Theta \frac{M_1 V_1}{2V_0} \tag{5.8}$$

Here Θ is the transit angle through the drift space for the electron whose velocity has remained unaltered. The magnitude of Θ is

$$\Theta = \omega s / v_0 \tag{5.9}$$

Thus, the bunching parameter X is in direct proportion to the transit angle through the drift space, and to the ratio of modulating voltage to constant accelerating voltage.

Using the designations (5.7) and (5.9), relation (5.6a) can be rewritten as:

$$\omega t_2 - \Theta = \omega t_1 - X \sin \omega t_1 \tag{5.10}$$

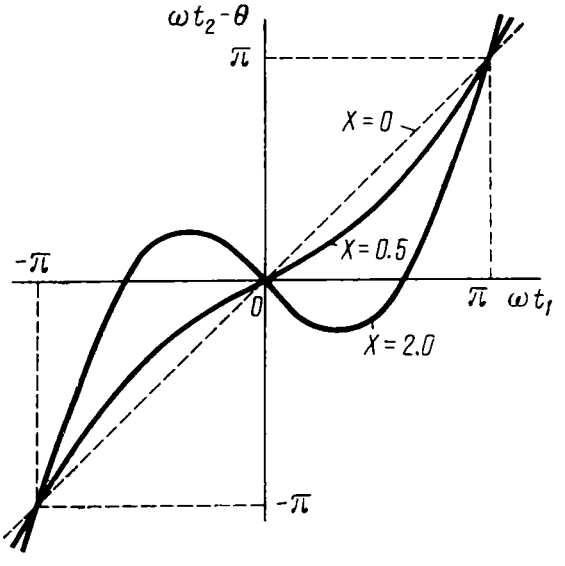

Fig. 5.2. Phase of electron arrival at the catcher cavity as a function of phase of passage of the buncher cavity

This equation, describing the phase of arrival of an electron at the catcher gap, should be examined in more detail. At $X = 0$, i.e. in the absence of a modulating voltage across the buncher gap, $\omega t_2 - \Theta = \omega t_1$. The phase of electron arrival at the catcher gap is a linear function of the phase at which the same electron passed the middle of the buncher gap. Obviously, there is no electron bunching in this case. If $V_1 \neq 0$ and $M_1 \neq 0$, at a finite transit angle the bunching parameter must also differ from zero. The dependence of the phase of arrival at the output gap on the phase at which the buncher gap was crossed ceases to be linear, according to (5.10). This means that periodic compressions of the electron beam take place, i.e. bunching.

The effect of bunching, when the "fast" electrons catch up with the "slow" ones, was explained with the aid of the motion diagram

of Fig. 2.29. Equation (5.10) provides a deeper insight into the effects of electron bunching in case of a small modulating signal; Fig. 5.2 presents a graph plotted by equation (5.10) for three different values of the bunching parameter X.

The greater the magnitude of X, the greater is the departure of the function describing the phase of electron arrival from a straight line. The fact that at a certain value of X the function $t_1 = f(t_2)$ can become ambiguous also merits attention; this effect will be examined in more detail somewhat later.

Now we shall discuss the main characteristics, namely the waveform of the convection current in the catcher gap and the maximum electronic efficiency of a two-cavity klystron.

5.2b. Convection Current Waveform in the Drift Space and Catcher Gap

Earlier it was assumed that, being perfect, the grids of the gap intercept no current. Now, in addition, interception of electrons by the drift tube walls will also be assumed negligible, supposing the electron beam to be focussed by an infinite static magnetic field. Thus, the average convection current can be considered as identical in any section of the electron beam. Applying the law of charge conservation,

$$dq_1 = dq_2;\ i_1 dt_1 = i_2 dt_2$$

where i_1 and i_2 are the instantaneous values of the beam convection current at the middle of the buncher and catcher gaps, respectively. Therefore, the convection current delivered to the second (catcher) cavity is

$$i_2 = i_1 \frac{dt_1}{dt_2} = I_0 \frac{dt_1}{dt_2} \tag{5.11}$$

since there is yet no density modulation of the beam at the middle of the buncher gap and therefore $i_1 = I_0$.

Thus, the instantaneous value of the convection current can be determined, if the derivative dt_1/dt_2 is known.

By equation (5.6)

$$\frac{dt_2}{dt_1} = 1 - \frac{\omega s v_1}{v_0^2} \cos \omega t_1 = 1 - X \cos \omega t_1$$

Substitution into equation (5.11) results in

$$i_2 = \frac{I_0}{dt_2/dt_1} = \frac{I_0}{1 - X \cos \omega t_1} \tag{5.12}$$

For convenience of analysing the function $i_2 = f(t_2)$, the following designations can be introduced:

$$\omega t_1 = \varphi$$

$$1 - X \cos \omega t_1 = y \tag{5.13}$$

$$\omega t_2 - \Theta = x \tag{5.14}$$

Equations (5.12) and (5.10) can then be presented as

$$i_2 = I_0/y \tag{5.15}$$

$$y = 1 - X \cos \varphi \tag{5.16}$$

$$x = \varphi - X \sin \varphi \tag{5.17}$$

At first glance, introducing new variables has only complicated the calculations, but this is not so. Equations (5.16) and (5.17) bear resemblance to the equation of a trochoid in parametric form, that is a curve described by a point at a fixed distance from the centre of a circle rolling along a plane without sliding (the same is true of a cycloid).

The corresponding geometrical plot in rectangular coordinates is illustrated in Fig. 5.3. The point of interest A is at a distance r from the circle centre, the radius of this circle being R. Assume point A to coincide initially with the y axis, as shown in Fig. 5.3 in dashed lines. After the circle turns without sliding along the x axis through an angle φ the coordinates of point A' can be determined from the obvious geometrical considerations

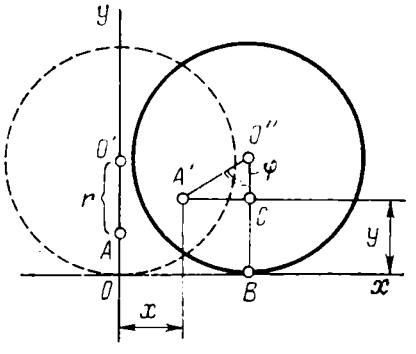

Fig. 5.3. To the equation of a trochoid (in connection with the calculation of klystron convection current)

$$x = OB - A'C; \quad OB = \varphi R; \quad A'C = r \sin \varphi$$

$$y = O''B - O''C; \quad O''B = R; \quad O''C = r \cos \varphi$$

The final equations of a trochoid in parametric form are

$$x = \varphi R - r \sin \varphi; \quad y = R - r \cos \varphi$$

These relations are identical to (5.16) and (5.17), provided $R = 1$ and $X = r$.

Thus, by (5.15) the current i_2 is described by a function, reverse to a trochoid, at a unit radius of the rolling circle. The independent variable is x, which by (5.14) is a linear function of time t_2; this

means that in the following analysis it will be sufficient to examine the function $y^{-1} = f(x)$ instead of $i_2 = f(t_2)$.

Three typical cases are possible, depending on the magnitude of the bunching parameter X. At $X < 1$, i.e. at $r < R$, point A which traces the trochoidal curve is inside the rolling circle (Fig. 5.4*a*). Curve $y = f(x)$ is always above the x axis and does not come into

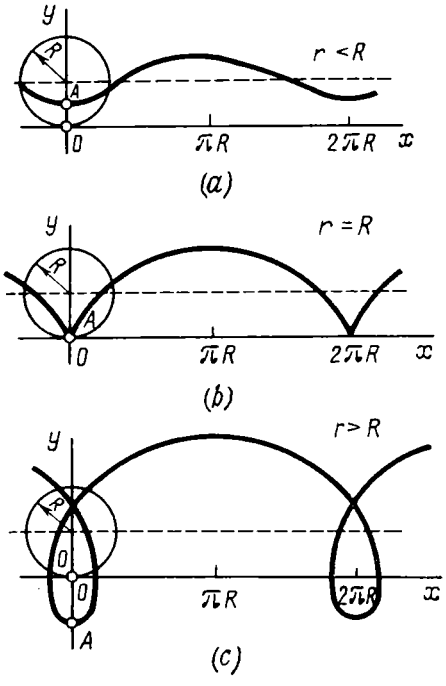

Fig. 5.4. Three typical cases determining the waveform of current through a klystron

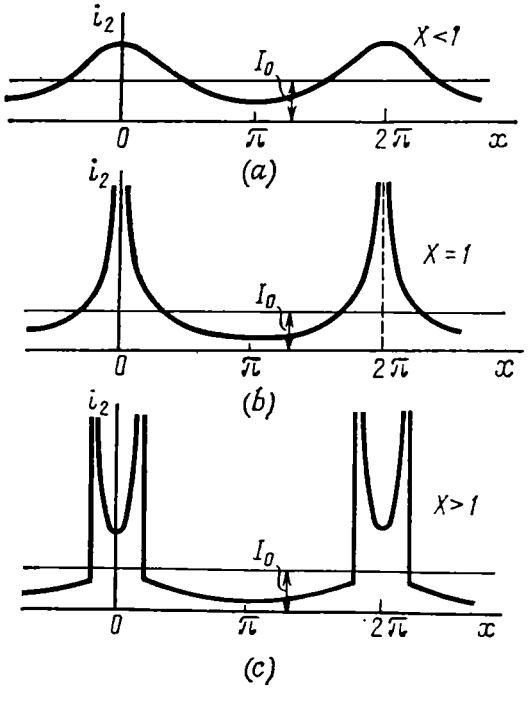

Fig. 5.5. Waveform of convection current in a two-cavity klystron at three typical values of the bunching parameter X

contact with it at any point; the current $i_2 = f(t_2)$ is therefore finite at any value of x, as illustrated in Fig. 5.5*a*. When $X = 1$ the point of interest is on the circle with radius R; the curve produced is an ordinary cycloid (Fig. 5.4*b*). The points at which this curve contacts the abscissa axis correspond to current $i_2 = f(x)$ featuring peaks of infinite magnitude, as shown in Fig. 5.5*b*. If the bunching parameter X exceeds unity (i.e. at $r > R$), the curve intersects the x axis twice during each revolution of the circle (Fig. 5.4*c*). This means that the current must have two infinitely sharp peaks, with the spacing between these peaks increasing with a higher value of the bunching parameter.

The case of $X > 1$ seems to present certain difficulties in determining the reverse function $i_2 = f(t_2)$. As can be seen from Fig. 5.4*c*, in a certain range of values the function $y = f(x)$ is ambiguous

and may have two, or even three roots; the circumstance that one of these roots is negative can make the case ever more complicate.

The ambiguity of the function $y = f(x)$ is easily explained by examining again Fig. 5.2. Physically, this ambiguity corresponds to several electron bunches leaving the buncher at different instants of time, but passing through the output gap simultaneously. Thus, some electron bunches *overtake* other bunches and these bunches are superimposed in the output gap. Note, that no such effect can take place at $X \leqslant 1$. This overtaking is due to the sinusoidal form of the bunching voltage, which in the ideal case should be of a sawtooth waveform (refer to Section 2.8*e*).

The convection current in the catcher gap at $X > 1$ can be determined by adding up the currents developed by each individual bunch. Since the direction of electron motion in the gap is invariable, summation of only the absolute values of $1/y$ should be performed. Strictly speaking, at $X > 1$ equations (5.11) and (5.15) should be presented as

$$i_2 = I_0 \sum \left| \frac{dt_1}{dt_2} \right| = I_0 \sum |y^{-1}| \qquad (5.18)$$

The convection current waveform at $X > 1$ is qualitatively illustrated in Fig. 5.5*c*.

Thus, in the general case the radio-frequency component of the convection current, developed as a result of electron bunching, is extremely non-sinusoidal in waveform. In a reference plane situated in the middle of an electron bunch and moving with the average beam velocity v_0 the electron concentration will appear to increase. The pattern of these electron compressions gradually changes in accordance with the increase in bunching parameter X.

It should be remembered that the current i_2 in Fig. 5.5 characterizes only electron bunching in the beam. The value of the current induced in the catcher gap should be determined with the properties of this gap taken into account.

5.2c. Electronic Efficiency of a Two-Cavity Klystron

Suppose the output gap of an amplifier, multiplier or oscillator klystron to be carrying an electron beam with a radio-frequency current component as determined by equations (5.16) to (5.18). Let us find the power delivered to the load of this gap and the klystron efficiency.

The solution to this problem is to be obtained by applying the general principles of current induction, discussed earlier in Sections 2.3 and 2.4. Owing to the non-sinusoidal waveform of this current, it must be represented by means of a Fourier series. The output cavity of a klystron is a high-Q system and therefore it

will be sufficient to examine only one harmonic of the convection current—that whose frequency approximates the resonant frequency of the catcher cavity. The finite width of the output gap necessitates that the interaction coefficient (gap factor) be taken into account.

The convection current of the electron beam in a klystron is an even function of time (variable x) and therefore only the cosine terms of the series need be examined:

$$i_2(x) = A_0 + \sum_{n=1}^{\infty} A_n \cos nx$$

where $A_0 = \frac{1}{\pi}\int_0^{\pi} i_2(x)\,dx$; $A_n = \frac{2}{\pi}\int_0^{\pi} i_2(x)\cos nx\,dx$.

Differentiating equation (5.14) yields

$$dx = \omega dt_2 \tag{5.19}$$

Substitute (5.11) and (5.19) into the equation for the d.c. component of the Fourier series:

$$A_0 = \frac{1}{\pi}\int_0^{\pi} I_0 \frac{dt_1}{dt_2}\,\omega\,dt_2 = I_0$$

As one would expect, under the assumptions adopted, the constant component of the expansion is the d.c. component of convection current of the beam entering the buncher gap of the klystron.

Now determine the coefficients A_n. Again applying equations (5.11) and (5.19), as well as (5.17), results in

$$A_n = 2I_0 \frac{1}{\pi}\int_0^{\pi} \cos(n\varphi - nX\sin\varphi)\,d\varphi$$

This integral has no solution in terms of elementary functions, but has the form familiar in the theory of Bessel functions. Comparison with the integral form of the Bessel function of the first kind[1] readily yields

$$A_n = 2I_0 J_n(nX)$$

The final expansion of the instantaneous convection current of a klystron into a Fourier series is

$$i_2(x) = I_0 + 2I_0 \sum_{n=1}^{\infty} J_n(nX)\cos nx \tag{5.20}$$

[1] The integral form of the Bessel function of the first kind of order n at a whole number of n is $J_n(z) = \frac{1}{\pi}\int_0^{\pi} \cos(n\varphi - z\sin\varphi)\,d\varphi$.

Thus, the n-th harmonic of the electron convection current at the input to the catcher gap has an amplitude

$$I_{2n} = 2I_0 J_n (nX) \tag{5.21}$$

The amplitude of the current induced in the catcher cavity is equal to the amplitude of the convection current I_{2n}, multiplied by the interaction coefficient between the electron beam and the gap at the frequency of the harmonic in question (this gap factor will be designated as M_{2n}). The power delivered to the output cavity by the n-th harmonic of the electron beam cannow be determined by the common relations known in electrical engineering

$$P_{2n} = 0.5 V_{2n} M_{2n} I_{2n} \cos \psi \tag{5.22}$$

where V_{2n} is the amplitude of the n-th harmonic developed across the output gap and ψ is the phase shift between the induced current and the voltage developed across the gap due to this current flowing along the cavity walls.

Substitution of the equation for convection current (5.21) into (5.22) results in

$$P_{2n} = V_{2n} M_{2n} I_0 J_n (nX) \cos \psi \tag{5.23}$$

The d.c. power drawn by the accelerating gap (electron gun) from the d.c. supply source is $P_0 = I_0 V_0$. In the absence of a microwave signal all this power is dissipated on the collector, provided this latter is under the same d.c. voltage (refer to Fig. 5.1).

The *electronic* efficiency η_e will be defined as the ratio of P_{2n}, given up by the electron beam to the microwave field of the catcher cavity, to the applied d.c. power P_0. With (5.23) taken into account this leads to

$$\eta_e = \frac{P_{2n}}{P_0} = \frac{M_{2n} V_{2n}}{V_0} J_n (nX) \cos \psi \tag{5.24}$$

Conditions of obtaining maximum efficiency can be determined by considering the cofactors in (5.24) as mutually independent.

The last cofactor $\cos \psi$ cannot exceed unity. Physically $\psi = 0$ corresponds to electron bunches passing through the gap during the time of maximum retarding field.

The factor $M_{2n} V_{2n}$ in (5.24) represents the voltage amplitude across an equivalent gap of zero width placed at the middle of the actual catcher gap (refer to Section 2.8*b*). By Ohm's law the amplitude V_{2n} is a function of the induced current amplitude and the admittance of the loaded resonant cavity. At first glance it appears possible to obtain a high efficiency by simply reducing the total admittance of the cavity and its load (as referred to the output gap plane), because this leads to an increase in V_{2n} and, thus, to a higher ratio $M_{2n} V_{2n} / V_0$. However, the simple physical argumentation of Section 2.4*b* shows the existence of a certain upper limit.

To provide that the electrons are not repelled back from the gap, the voltage across the gap of infinitesimal width should not exceed the value of V_0, or more strictly, the value $(V_0 - V_1)$, where V_1 is the voltage amplitude across the buncher gap. The spread in electron velocities due to velocity modulation in the buncher gap

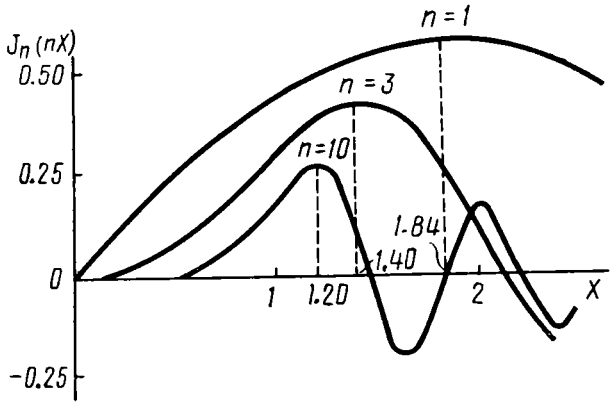

Fig. 5.6. Graphs of Bessel functions determining the amplitude of the fundamental, third and tenth harmonics of convection current through a two-cavity klystron

is here neglected, i.e. it is again assumed that v_1 is much less than the average beam velocity v_0. Thus, the maximum value of $M_{2n}V_{2n}/V_0$ is unity.

The last cofactor in (5.24) to be examined is $J_n(nX)$. The graphs presented in Fig. 5.6 illustrate the behaviour of the Bessel function $J_n(nX)$ for three different values of n. As can be noted, the Bessel function features a maximum at a certain magnitude of X.

Thus, since two of the cofactors cannot exceed unity, the maximum electronic efficiency of a two-cavity klystron at the n-th harmonic is

$$\eta_{e.\,max.} = [J_n(nX)]_{max.} \qquad (5.25)$$

The maximum values of electronic efficiency of a klystron and the corresponding magnitudes of the bunching parameter $X_{max.}$ for different harmonic numbers n are listed in Table 5.1.

Table 5.1

Maximum Electronic Efficiency of a Two-Cavity Klystron and Optimum Bunching Parameter with the Output Gap Operating at the n-th Harmonic of the Input Signal

n	$\eta_{e.\,max.}$, per cent	$X_{max.}$	n	$\eta_{e.\,max.}$, per cent	$X_{max.}$
1	58.2	1.84	8	32.0	1.22
2	48.7	1.53	...	...	...
3	43.4	1.40	16	26.0	1.13
...	...	...			

The maximum theoretical electronic efficiency of a two-cavity klystron at the fundamental, according to the argumentation presented, proves to be 58.2 per cent. The optimum value of the bunching parameter $X_{max.}$ exceeds unity for any harmonic and at $n = 1$ equals 1.84. Thus, the optimum waveform of the convection current in a two-cavity klystron should be of the double-peak pattern, as shown in Fig. 5.5*c*[1].

A reduction in the value of parameter X, for instance, because of a lower input signal amplitude V_1 or higher accelerating voltage V_0, will result in an *underbunched* electron beam. The electronic efficiency and output power in this case are correspondingly reduced. An *overbunched* electron beam, when the bunching parameter exceeds the optimum value, is also responsible for a poorer efficiency.

The actually realizable values of electronic efficiencies in two-cavity klystrons are lower than might be expected from analysis, this being due to the interception of some electrons by the grids. The overall efficiency of a klystron, as with any other type of device, is the product of electronic efficiency by the efficiency of the oscillatory system (resonant cavity, in the present case) with the microwave loss in the oscillatory system taken into account

$$\eta_{tot} = \eta_e \eta_{cav} \tag{5.26}$$

The value of η_{cav} is a function of the ratio of unloaded to loaded Q-factor of the output cavity and can be of the order of 60 to 80 per cent. Therefore, the overall efficiency of conventional klystrons is usually not in excess of some 25 to 30 per cent.

5.2d. Electron Beam Debunching in the Drift Space

With considerable densities of the electron beam the effects of space charge can no longer be neglected. The most interesting is the effect of the radio-frequency component of the space charge, which cannot be cancelled by the space charge of positive ions at the frequencies being considered.

The space charge exerts two kinds of influence on the process of electron beam bunching in klystrons:

(1) electron beam bunching results in the development of an electric field which tends to spread out over the transverse section of the beam. This effect is known as *transverse debunching* and resembles beam defocussing in ordinary electron-beam devices. Transverse debunching can lead to that part of the electrons of an electron

[1] It should be emphasized once again that the above statement is valid only for the case of a sinusoidal modulating voltage. A more suitable form of convection current is short pulses of rectangular waveform (refer to Section 2.4*b*), but this requires a special waveform of the modulating voltage, as was demonstrated earlier in Section 2.8*e*.

bunch are intercepted by the walls of the drift tube. This kind of debunching may be eliminated or at least greatly reduced by increasing the static longitudinal magnetic field; in the following discussion transverse debunching effects will be considered negligible;

(2) more typical for klystron performance is the effect of *longitudinal debunching*, which is due to that a longitudinal field is developed in the beam itself in the space between subsequent electron bunches. Electrons, tending to approach the bunch middle under the action of the acquired velocity modulation and thus to form more compact bunches, are subject to the retarding action of the space charge of the bunches already formed. As a result, the pattern of the electron bunches becomes less abrupt (more spread out). The amplitude of the fundamental (and of all the other harmonics) diminishes, and thus a drop in the output power results.

The effects of longitudinal debunching may be evaluated by calculating the intensity of the electric field developed by the radio-frequency component of the space charge, applying Poisson's equation to this end. Electron motion can be analysed using a reference plane, which moves along the beam with the average beam velocity v_0, and taking into account the debunching field intensity, as determined earlier.

Analysis shows that the effects of space charge can be allowed for by employing an effective bunching parameter X', which is lower than parameter X calculated for the case when the space charge effects can be neglected. The interrelation between these parameters is given by

$$X' = X \frac{\sin hs}{hs} \tag{5.27}$$

where s is the length of the drift space and h is a new parameter of the space charge, defined as

$$h = \frac{\omega_p}{v_0} = \frac{2\pi f_p}{v_0} \tag{5.28}$$

Here the natural frequency of electron plasma oscillations is designated as f_p (in Hz), ω_p being the angular frequency.

The ratio v_0/f_p has the dimension of length and is conventionally termed the *plasma wavelength* λ_p. For the case, when relativistic effects can be considered negligible, with equation (2.84) taken into account, this wavelength is

$$\lambda_p = \frac{v_0}{f_p} = 2\pi \left[\frac{2\varepsilon_0 V_0}{J_0} (2eV_0/m)^{1/2} \right]^{1/2} \tag{5.29}$$

where V_0 and J_0 are the constant accelerating voltage and the d.c. component of the density of the electron beam convection current, respectively.

The effect of longitudinal debunching sets an upper limit on the increase in gain of a klystron, that can be obtained by increasing the length of the drift tube. Indeed, by equation (5.27) at $hs = \pi$, i.e. at a drift length equal to half the plasma wavelength, the electron beam becomes completely debunched ($X' = 0$) and the output power of the klystron falls off to zero. As will be demonstrated, there is an optimum length of the drift space corresponding to the maximum gain obtainable with two-cavity klystrons.

5.3. Two-Cavity Klystron Amplifiers

The advantages of two-cavity klystrons as amplifiers, in comparison with devices utilizing electrostatic current control, are as follows:

(1) a higher efficiency in the centimetric wave band;

(2) a low level of power required for electron beam bunching, and as a consequence, a higher gain;

(3) ability to operate at higher frequencies.

At present, two-cavity klystrons have become practically obsolete and are replaced by other microwave devices with still better parameters, such as multicavity klystrons and travelling-wave tubes. Nevertheless, two-cavity klystrons merit consideration as a separate class of devices, because many of the properties of these tubes are common to all klystron amplifiers and a thorough knowledge of the physics underlying the performance of these devices is essential for a complete understanding of multicavity klystrons, which are of particular interest as regards their application and design principles.

5.3a. Amplifier Output Power vs Input Power

The equivalent circuit of the buncher resonant cavity of a klystron, shown in Fig. 5.7*a*, contains a conductance G_{eL1}, i.e. the electron load conductance which is due to the gap of this cavity carrying an unmodulated electron beam (refer to Section 2.8), along with an equivalent conductance G_1 which describes the dissipative loss in the "cold" cavity.

Ordinarily, the electron transit angle through the interaction gaps of a klystron ranges from $\pi/2$ to π[1]. The magnitude of G_{eL1} is therefore positive and at high d.c. beam conductances (equal to I_0/V_0) determines the major part of the power dissipated in the buncher cavity.

---

[1] Note, that the transit angle through a gap should not approach 2π because this leads to a rapid decrease of the interaction coefficient M and therefore, to a lower efficiency of klystron performance.

The coupling between the input line and the buncher cavity should provide a maximum energy transfer from the source of input signal to the buncher gap, assuming the output impedance of the signal source to be matched with the input line. The most suitable from this point of view are the critical coupling conditions, i.e. matching the "hot" cavity with the input line at the operating frequency.

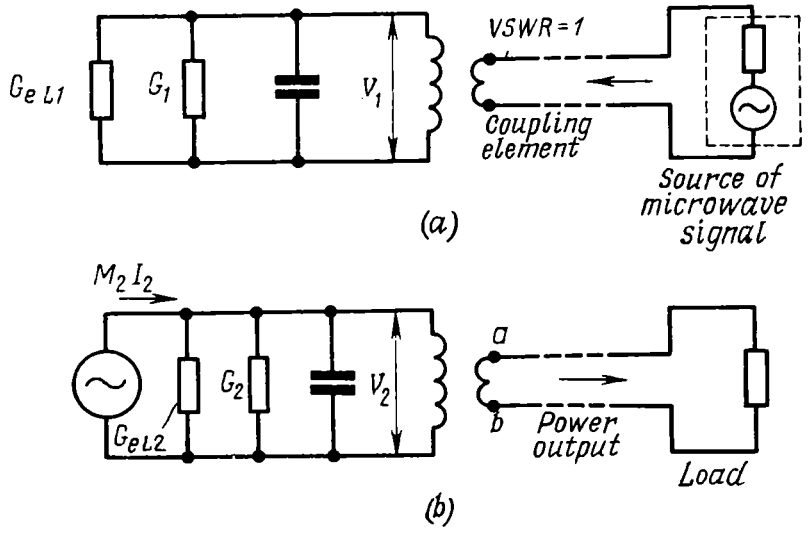

Fig. 5.7. Equivalent circuit of the input (*a*) and output (*b*) resonant cavities of an amplifier klystron

The power of the input signal is thus related to the voltage amplitude across the modulating gap of a klystron by

$$P_{in}=0.5V_1^2(G_1+G_{eL1})$$

provided this match is ensured. For convenience, V_1 will be expressed in terms of the bunching parameter X. According to equation (5.8)

$$V_1=\frac{2V_0}{M_1\Theta}X; \quad P_{in}=\frac{2V_0^2(G_1+G_{eL1})}{M_1^2\Theta^2}X^2 \tag{5.30}$$

Now consider the power given up by a modulated electron beam to the field of the catcher cavity of a klystron; the equivalent circuit is presented in Fig. 5.7*b*. The catcher cavity is assumed to be tuned to nearly the frequency of the convection current fundamental ($n = 1$). The output cavity gap with the bunched electron beam can be considered as a current generator with a complex amplitude $M_2\dot{I}_2$. The amplitude of the voltage $\dot{V}_2$ developed across the catcher gap can then be described as

$$\dot{V}_2=\frac{M_2\dot{I}_2}{(G_2+G'_L+G_{eL2})+j(B_2+B'_L)} \tag{5 31}$$

Here G'_L and B'_L denote the conductance and susceptance of the load, respectively, as transformed to the plane of the gap from section ab; G_2 and B_2 are the conductance and susceptance of the catcher cavity. Note, that in the general case the electron load G_{eL2} may differ from the above electron load of the buncher cavity, this being to a considerable extent due to non-linear effects developed under large-signal conditions. Furthermore, the electron load can be affected by the presence of secondary electrons which can be generated in the vicinity of the output gap.

The output power of the amplifier P_{out} is determined by the power dissipated in the transformed load conductance G'_L, i.e.

$$P_{out} = 0.5 \, | \dot{V}_2 |^2 \, G'_L$$

Applying equations (5.31) and (5.21) and disregarding for the time being the effects of beam debunching due to space charge, we obtain

$$P_{out} = 2M_2^2 I_0^2 [J_1(X)]^2 \frac{G'_L}{(G_2 + G'_L + G_{eL2})^2 + (B_2 + B'_L)^2} \qquad (5.32)$$

Note, that equation (5.32) agrees with the relation (5.23) derived earlier. The equation (5.32) can be applied only in case the output gap displays the properties of a current generator, i.e. when $V_2 < V_0$.

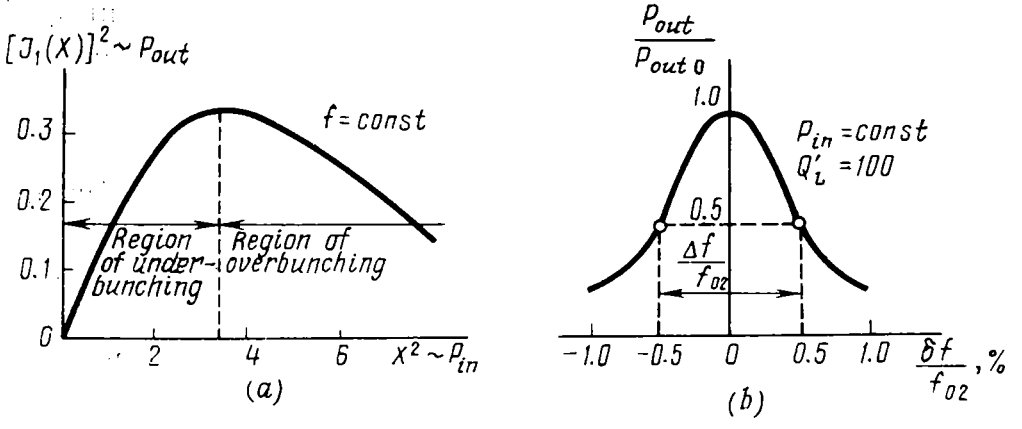

Fig. 5.8. Output power *vs* input power (*a*) and output power *vs* frequency (*b*) for a two-cavity klystron

Equations (5.30) and (5.32) indicate that, all other conditions being equal, the output and input power of a klystron amplifier can be interrelated in terms of the bunching parameter

$$P_{in} \sim X^2; \quad P_{out} \sim [J_1(X)]^2$$

The graph $[J_1(X)]^2 = f(X^2)$, determining the dependence of P_{out} on P_{in} (in relative units) for a two-cavity klystron amplifier

is plotted in Fig. 5.8*a*. The behaviour of this "amplitude" characteristic can be explained from the standpoint of physics as follows. The initial linear section of this curve, which is gradually bended with an increase in parameter X, corresponds to underbunched beam conditions, i.e. $X < 1.84$. Under optimum bunching ($X = 1.84$) the output power of the klystron in question is at a maximum. A further increase in the input power ($X > 1.84$) causes overbunching of the electron beam and, as a consequence, a reduced output power. At still greater values of X (not shown in the Figure) the output power varies periodically between the maximum value and zero, the values of these maxima rapidly decreasing at greater X magnitudes.

The maximum gain at minimum non-linearity distortions is obtained when the operating conditions correspond to the initial section of the curve $P_{out} = f(P_{in})$, these conditions being typical for input (low-power) amplifier applications. On the contrary, if the object is to obtain a maximum output power and the non-linearity distortions are of no or small consequence, the operating conditions of the klystron should be near to the maximum of the curve $P_{out} = f(P_{in})$, this being typical for power amplifier applications.

Thus, two distinct kinds of operating conditions can be discerned when discussing the performance of klystrons, namely maximum gain conditions and maximum output power and efficiency conditions. Similar differentiation is often resorted to when examining the operation of other types of microwave amplifier devices.

5.3b. Gain of a Two-Cavity Klystron

By the general definition of gain given in Section 3.5, the gain of a klystron (in decibels) is defined as

$$G = 10 \log_{10} \frac{P_{out}}{P_{in}} \tag{5.33}$$

Substituting the above equations for the input and output power (5.30) and (5.32) into (5.33) and allowing for the mutual repulsion of electrons in the space charge by replacing X by X', defined by (5.27), in equation (5.32) yield the gain provided by a two-cavity klystron.

The gain as a function of the load admittance will be at a maximum when

$$B_2 + B'_L = 0; \quad G'_L = G_2 + G_{eL2}$$

i.e. with conjugate matching of the load with the catcher cavity of the klystron. Designating the gain under these conditions as G_0,

$$G_0 = 20 \log_{10} \left[\frac{M_1 M_2 I_0 \Theta}{2V_0 (G_1 + G_{eL1})^{1/2} (G_2 + G_{eL2})^{1/2}} \frac{J_1(X')}{X} \right] \tag{5.34}$$

Under small-signal conditions, on the linear section of the $P_{out} = f(P_{in})$ curve when $X' \ll 1$ and $J_1(X')$ is approximately $X'/2$, the gain G_0 is maximum maximorum and equal to

$$G_{0\,max.} = 20 \log_{10}\left[\frac{M_1 M_2 I_0 \Theta}{4V_0 (G_1 + G_{eL1})^{1/2} (G_2 + G_{eL2})^{1/2}} \frac{X'}{X}\right] \qquad (5.35)$$

This latter relation seems to indicate that it is possible to attain as high a value of gain as desired with an increase in the transit angle Θ. Physically this would mean that a higher gain could be obtained simply by increasing the length s of the drift space. Actually, however, an unlimited increase in $G_{0max.}$ is restricted by debunching effects.

Applying equation (5.27), which defines the bunching parameter X', to relation (5.35), i.e. taking into account the space charge parameter h (also referred to as the wave number of the space charge), results in

$$G_{0\,max.} \sim \sin(hs)$$

Thus, the condition of maximum gain is $hs = \pi/2$; the optimum length of the drift space should be one quarter of the plasma wavelength

$$s_{opt} = \frac{\pi}{2h} = \frac{\lambda_p}{4} \qquad (5.36)$$

This is practically a strict limitation of the maximum gain obtainable with two-cavity klystrons, and actual realization of designs with gains in excess of some 10 to 15 dB is usually out of the question.

5.3c. Effects of Detuning the Input and Output Cavities. Operating Bandwidth

Under steady-state conditions the frequency of the output signal is determined only by the frequency of the signal applied to the buncher cavity. Any detuning, therefore, at all other parameters remaining unaltered, can affect only the amplitude of the output power and the klystron gain.

The simplest is the examination of effects due to detuning the catcher cavity, because this cavity does not influence the process of electron beam bunching. Under operating conditions the loaded Q of the output cavity (i.e. "hot" Q, allowing for the presence of the electron beam) will be designated as Q'_L. At not too great detuning, with an input signal frequency f, the susceptance of this cavity by equation (3.13) is

$$B_2 = 2Q'_L G_{tot} \frac{f - f_{02}}{f_{02}} = 2Q'_L G_{tot} \frac{\delta f}{f_{02}}$$

where f_{02} is the natural frequency of this cavity and G_{tot} denotes the total conductance at the plane of the catcher gap, in the present case equal to $G_2 + G_{eL2} + G'_L$.

Substituting these values of B_2 and G_{tot} into equation (5.32), which describes the output power of the klystron, and assuming for simplicity the load susceptance B'_L to be zero, we obtain

$$P_{out} = 2M_2^2 I_0^2 [J_1(X)]^2 \frac{G'_L}{G_{tot}^2 \left[1 + 4Q_L'^2 \left(\frac{\delta f}{f_{02}}\right)^2\right]}$$

With all other parameters, including the input power and bunching parameter X, remaining invariable, the maximum output power and maximum gain correspond to the case of zero detuning, i.e. $\delta f/f_{02} = 0$. Designating the output power for this case as $P_{out\,0}$,

$$P_{out} = \frac{P_{out\,0}}{1 + 4Q_L'^2 \left(\frac{\delta f}{f_{02}}\right)^2} \tag{5.37}$$

Equation (5.37) indicates that the output power of a klystron amplifier deteriorates rapidly with the output cavity being detuned relative to the input signal frequency, or what is the same, with a variable frequency of the input signal and fixed tuning of the catcher cavity (refer to Fig. 5.8*b*). The gain *vs* frequency dependence is of the same character; this dependence is usually referred to as the *amplitude-frequency characteristic*. The lower the "hot" loaded Q-factor Q'_L, the less critical is the tuning of the catcher cavity.

Equation (5.37) may be used to evaluate the operating bandwidth of a klystron amplifier $\Delta f/f_{02}$, as determined by the output cavity. Ordinarily, the operating bandwidth is evaluated by a 3 dB decrease in the output power (refer to Section 3.5*b*); therefore, taking $P_{out\,0} = 2P_{out}$ and keeping in mind the fact that δf in (5.37) allows for the frequency shift to any side of the central frequency f_{02}, after obvious rearrangements the operating bandwidth is found to be

$$\frac{\Delta f}{f_{02}} = (Q'_L)^{-1} \tag{5.38}$$

An increase in bandwidth may be obtained by reducing the value of Q'_L, i.e. by using a tighter coupling to the output guide at a constant Q_0, in other words, by reducing the external Q-factor. It should be remembered, however, that a lower Q_{ext} results in a higher G'_L at the output gap plane (refer to equation (3.17)), leading to violation of the conditions of optimum loading and, therefore, to a lower output power and gain at the design frequency.

From this it follows that widening the bandwidth by significantly reducing Q'_L is obtained at the expense of output power and gain. The product of gain by bandwidth remains practically constant.

The effects of input cavity detuning relative to the input signal frequency are somewhat different. Variations of the resonant frequency f_{01} of the buncher cavity at a constant frequency of the input signal result in variation of the cavity input admittance and thus lead to reflection of part of the input power. Examination of the circuit of Fig. 5.7*a* readily discloses that the power delivered to the buncher cavity is

$$P_{in} = \frac{P_{in\,0}}{1 + Q_{ext}^2 (\delta f/f)^2} \tag{5.39}$$

where Q_{ext} is the external Q-factor of the buncher cavity, $\delta f = f - f_{01}$ and $P_{in\,0}$ is the power delivered into the buncher cavity under conditions of matching at the design frequency (i.e. at VSWR = 1 : 1).

As seen from (5.39) detuning the input cavity at a constant level of input power is equivalent to reducing the input power. In the discussion to follow the results obtained in Section 5.3*a* can be used. The curve of the output power *vs* relative detuning of the buncher cavity proves to be similar to that of Fig. 5.8*b* and has a maximum at the frequency $f = f_{01}$.

This curve, however, can easily be proved to feature a double-hump pattern, provided parameter X is high enough at the design frequency $f = f_{01}$.

The analysis presented shows that it is necessary to tune accurately both the buncher and the catcher cavity of a two-cavity klystron amplifier. At practicable Q-factors of these cavities, the operating bandwidth is quite narrow and usually does not exceed fractions of a per cent of the middle frequency. This drawback, along with an inadequate gain, is to a considerable extent responsible for the restricted field of application of two-cavity klystron amplifiers.

Nevertheless, these devices are sometimes used in the centimetric wave band, where they are capable of providing output power levels of the order of units or dozens of watts under c.w. conditions. As an example, the parameters of one type of a two-cavity klystron are cited in Table 5.2 (refer to Section 5.6)

5.4. Two-Cavity Klystron Oscillators and Frequency Multipliers

5.4a. Main Features of a Two-Cavity Klystron Oscillator

The design of a two-cavity klystron oscillator is schematically shown in Fig. 5.9. The main difference between this circuit and that of an amplifier (Fig. 5.1*a*) is the presence of elements constituting a path of positive feedback. These elements may resemble the arrange-

ments described in Section 4.4c for the case of a triode oscillator in a common-grid circuit.

The feedback loop is designed such as to provide for a certain phase relationship between oscillations in the catcher and buncher

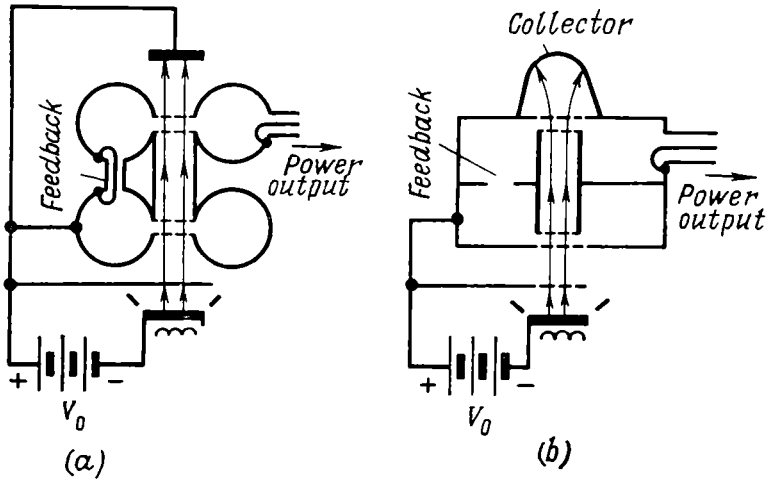

Fig. 5.9. Two-cavity klystron oscillator with a coaxial feedback line (*a*) and a coupling aperture in the wall common to both cavities (*b*)

cavities, this ensuring that the phase condition of self-excitation is satisfied.

Figure 5.10 presents graphs of the voltages developed across the buncher and the catcher gap of a two-cavity klystron oscillator;

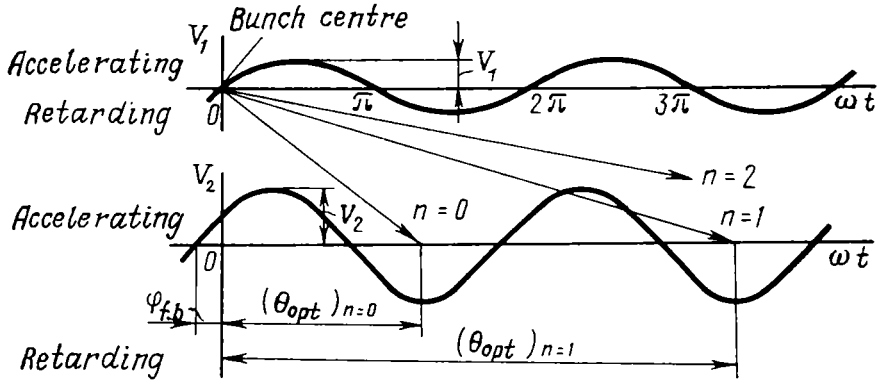

Fig. 5.10. Optimum transit angles through the drift space of a two-cavity klystron oscillator

the phase shift provided by the feedback assembly is designated here as φ_{fb}. As usual, electron bunches are formed around electrons passing the middle of the buncher gap at the instant the radio-frequency field changes from retarding to accelerating. Maximum

energy transfer from the electron bunches to the microwave field is ensured if the electron bunches pass through the catcher gap during the maximum retarding field. Figure 5.10 shows that the optimum transit angle through the drift space should be

$$\Theta_{opt} = 1.5\pi - \varphi_{fb} + 2\pi n; \quad n = 0;\ 1;\ 2;\ \ldots$$
$$\Theta_{opt} = 2\pi\,(n + {}^3/_4) - \varphi_{fb} \qquad (5.40)$$

On the other hand, the drift angle Θ, according to the designations adopted, is equal to

$$\Theta = \frac{\omega s}{(2eV_0/m)^{1/2}}$$

Substitution of this quantity into equation (5.40) results in

$$\frac{\omega s}{(2eV_{0\,opt}/m)^{1/2}} + \varphi_{fb} = 2\pi\,(n + {}^3/_4) \qquad (5.41)$$

Condition (5.41) is similar in meaning to the phase condition of self-excitation of other kinds of microwave devices discussed in Chapter Two, the monotron and retarding-field oscillator. At a fixed value of n in this relation, it is reduced to the familiar form $\lambda^2 V_0 = \text{const}$; V_{0opt} in (5.41) denotes the optimum anode (accelerating) voltage, at which the electron bunches arrive into the catcher gap at a maximum retarding field, this corresponding to the maximum output power.

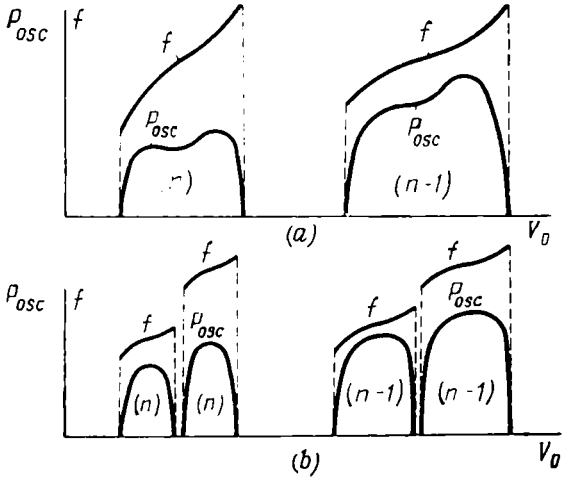

Fig. 5.11. Output power and frequency *vs* accelerating voltage in a two-cavity klystron oscillator

(*a*) loose coupling between cavities; (*b*) tight coupling

Therefore, variation of the voltage V_0 should lead to the appearance of a series of *zones of oscillation*, each zone corresponding to a certain integer value of n. The output power drops off to zero between these oscillation zones, as illustrated in Fig. 5.11*a*. This latter circumstance can easily be understood by examining the diagrams of Fig. 5.10; in this case the electron bunches arrive into the catcher gap during the accelerating radio-frequency field.

The number of the oscillation zone n is the higher, the greater is the time of electron bunch transit through the drift space. The

zero oscillation zone ($n = 0$) is the first one to be encountered when the accelerating voltage is reduced from the highest value down.

The distinguishing feature of two-cavity klystron oscillators is the presence of two oscillation modes in the system, these modes having closely spaced resonant frequencies ω_{01} and ω_{02}. Indeed, any oscillatory system consisting of N coupled tuned circuits in the general case features N oscillation modes, provided each resonant cavity (tuned circuit) sustains only one oscillation mode. With identical resonant cavities these modes differ by the phase of the microwave field in each cavity. Equation (5.41) should in fact be divided into two separate relations of identical form, differing from one another by the value of the resonant frequency (ω_{01} or ω_{02}). The number of regions of a two-cavity klystron oscillator (oscillation zones) is therefore increased twofold in the general case, i.e. two optimum values of the accelerating voltage correspond to each value of n. Depending on the degree of coupling between the resonant cavities, the oscillation zones can be of different patterns, as indicated qualitatively in Fig. 5.11*a* and *b*.

Within each of these doubled oscillation zones the frequency can be varied by changing the accelerating voltage, i.e. the device is voltage-tunable. Physically, the electronic tunability of a klystron oscillator is accounted for by variations of the phase of current induced in the output gap with variations of the accelerating voltage. We shall not present here the calculations involved and shall only point out that the electronic tuning range of two-cavity klystron oscillators is rather narrow; at a frequency of 3 GHz (10-cm wavelength) typical values of the electronic tuning range are several MHz. Ordinarily, the rate of electronic tuning does not exceed some dozen kHz per volt of accelerating voltage.

Electronic tuning in a two-cavity klystron amplifier necessitates a considerable amount of power consumption from the source of tuning voltage. This is a very serious drawback so that this kind of voltage tuning is of no practical importance.

The output power and efficiency of two-cavity klystron oscillators are of the same order of magnitude, as those of amplifiers. Two-cavity klystrons are therefore unsuitable for use as high power sources of microwave signal and cannot compete with such devices as multicavity klystrons, magnetrons, etc. As microwave power sources for measurement purposes they cannot stand up to reflex klystrons because of the elaborate design and tuning procedure. Two-cavity klystrons may nevertheless be sometimes used as pump oscillators for parametric amplifiers, as well as output stages of relay transmitters and in Doppler systems at power levels of the order of units or dozens of watts. The main advantage of two-cavity klystron oscillators is their comparatively high long-term frequency

stability, low level of noise in the vicinity of the signal frequency and a higher output power as compared, for instance, with reflex klystrons treated in Section 5.7.

5.4b. Two-Cavity Klystron Frequency Multiplier

The convection current of a two-cavity klystron has sharp peaks and is therefore rich in higher harmonics. A device of this kind is therefore suitable for use not only as an oscillator or amplifier, but as a frequency multiplier as well.

The skeleton diagram of a two-cavity klystron frequency multiplier is presented in Fig. 5.12. The catcher cavity in this case is of significantly smaller dimensions than the buncher cavity and is tuned to a frequency n times higher than the input signal. The buncher cavity is sometimes provided with a shortening capacitance of increased magnitude to reduce the dimensions of this cavity and thus obtain a more compact design; in all other respects the design resembles that of a usual two-cavity klystron amplifier.

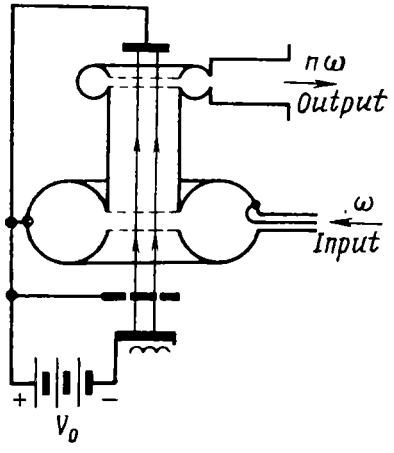

Fig. 5.12. Two-cavity klystron frequency multiplier

As was demonstrated in Section 5.2, the theoretical maximum efficiency of a two-cavity klystron falls off gradually with an increase in operating frequency. When the two-cavity klystron is used as a multiplier the range of optimum values of the bunching parameter is from 1.84 to 1; the higher the frequency multiplication factor, the nearer is the value of X to unity. Physically this means that to obtain the greatest possible amplitude of induced current at the n-th harmonic, it is necessary to reduce the spacing between adjacent peaks of the beam convection current (refer to Fig. 5.5), without, however, letting these peaks merge into one, as would take place at $X = 1$.

As can be seen from the graph of Bessel functions $J_n(nX)$ shown in Fig. 5.6, the optimum value of parameter X for frequency multiplication purposes is considerably more critical than in case of amplification at the fundamental. This means that a two-cavity klystron frequency multiplier is very sensitive to variations of the input power and buncher cavity tuning, as well as changes in the accelerating voltage.

One of the characteristic properties of a frequency multiplier is a considerably higher input power, as compared to a klystron amplifier with the same signal frequency and output power. This

may be qualitatively explained in the following way. Assume the input signal frequency to be varied in steps of ω_2/n at a fixed value of the output signal frequency ω_2. The bunching parameter

$$X = \frac{\omega_1 s v_1}{v_0^2} = \frac{\omega_2 s v_1}{n v_0^2}$$

will fall off rapidly. This reduction in the magnitude of X can be compensated for either by increasing the length s of the drift space, or by increasing the magnitude v_1, i.e. by increasing the input power.

Application of the first of these two methods is greatly limited by the effect of beam debunching. The forces of mutual repulsion are especially strong at the regions where the electron bunches are most compact, which correspond to the peaks of convection current. As a result, these sharp peaks are flattened out, this first of all affecting the harmonic content. Because of this, the drift space in frequency multiplier klystrons is even somewhat shortened, instead of being lengthened. Consequently, the necessary bunching conditions can be ensured only by increasing the input power level. Since the input signal v_1 should be increased approximately in direct proportion to n, the necessary increase in input power has to be made proportional to n^2.

It should be noted that the argumentation presented above is rather rough, because at high modulating voltages in the buncher cavity the simplified theory employed here no longer holds. However, the conclusions arrived at mainly agree well with practical findings.

As compared to the types of electron devices discussed earlier, klystron frequency multipliers do not open up new possibilities for obtaining oscillations of the shorter wavelengths. Indeed, all the limitations typical of drift klystrons and other types of devices with resonant oscillatory systems based on short-term interaction of the electron beam with a microwave field, are inherent in klystron frequency multipliers as well. The main field of application of klystron frequency multipliers is microwave systems, where a high degree of frequency stability is imperative. Klystrons can be used as a means for obtaining centimetric and shorter wavelengths from a crystal-controlled (or standard-cavity controlled) source of lower frequency[1].

In commercially available types of frequency-multiplier klystrons the output power does not exceed scores or hundreds of milliwatts at multiplication factors from 3 to 10.

---

[1] The shortest wavelength obtained in laboratory conditions from a two-cavity klystron frequency multiplier at present is 0.4 mm at $n = 20$.

5.5. Multicavity Amplifier Klystrons

5.5a. Qualitative Description

One of the ways in which a higher gain can be obtained is by connecting several two-cavity klystrons in cascade, as shown in Fig. 5.13. The principle of cascade connection is known to be widely used and it is quite justified at lower frequencies. It is equally

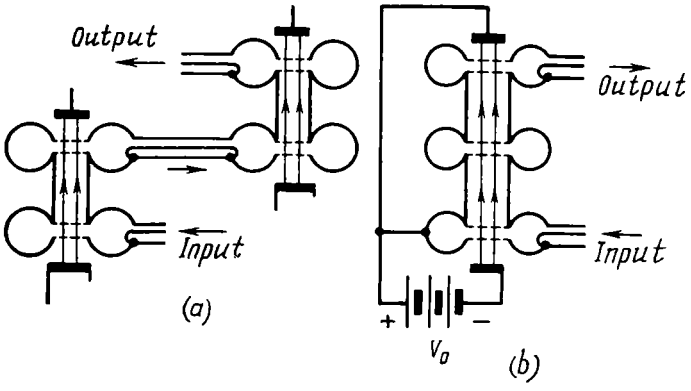

Fig. 5.13. Cascade connection of two-cavity klystrons (*a*) and three-cavity klystron amplifier (*b*)

applicable and suitable at microwaves. However, the design, tuning procedure and voltage supply of a chain of amplifier devices become more complicated.

When examining Fig. 5.13*a*, the idea may occur of combining the output cavity of the first stage with the input cavity of the second stage and utilizing one common electron beam for both these klystrons as shown in Fig. 5.13*b*. In the most general case, N resonant cavities divided from each other by drift spaces can be the final klystron design.

If the operation mechanism of each stage of the "unified" klystron remained unaltered, this design would have the following advantages over a chain of individual amplifiers of a two-cavity klystron, connected in series:

(1) a higher gain due to a smaller number of cavities and lower microwave loss in the intermediate cavities;

(2) a lower power drain from d.c. voltage sources due to the utilization of a common electron beam;

(3) a simpler tuning procedure due to a smaller number of cavities that have to be tuned.

As will be shown later, multicavity klystrons have some more very important advantages which completely justify the intricate design of these devices.

The process of electron bunching in a multicavity klystron is conventionally known as *cascade bunching*; in the general case, the bunching process in a multicavity klystron may differ somewhat from that in the drift space of a two-cavity device.

For simplicity, a three-cavity klystron will be examined (Fig. 5.13*b*). Suppose that the intermediate (idler) cavity separating the input and the output cavity is tuned exactly to the frequency of the input signal (the effects of cavity detuning will be examined later). The electron beam from the electron gun is velocity-modulated in the first (input) cavity. With a low value of the modulating voltage, the second (intermediate) cavity is excited by an under-bunched electron beam, as in the case illustrated in Fig. 5.5*a*.

In a multicavity klystron, the cavities do not have any direct electromagnetic coupling, and therefore an unmodulated electron beam will produce no oscillations in the idler cavity. However, when this cavity is excited by electron bunches, its inner surface will conduct induced radio-frequency current, as with the catcher cavity of a two-cavity klystron. This current will be quite small, but it may, nevertheless, develop a significant voltage across the gap of this cavity, that will be considerably greater than the signal voltage across the gap of the input cavity. To a considerable extent this effect is due to the intermediate cavity carrying no external load so that the total conductance of this cavity is defined only by the microwave loss in the cavity walls and the electron beam load of its gap.

Under steady-state conditions the induced current and voltage developed across the gap of the intermediate cavity are of exactly the same frequency as the input signal. Furthermore, the susceptance of this cavity is zero, provided it is tuned exactly to the frequency of the input signal. As was shown in Section 2.4, under these conditions electron bunches automatically develop an electric field which is maximally retarding to these bunches.

The corresponding diagram is presented in Fig. 5.14, where the motion diagram for four most typical electrons is illustrated. Note that with the drift method of beam bunching, electron bunches are formed around electrons of type *1* which pass through the modulating gap when the field goes through zero changing from retarding to accelerating (refer to Section 2.8).

The voltage developed across the gap of the intermediate cavity in turn modulates the electron beam, this additional velocity modulation lagging behind the modulation of the input gap by a phase angle of $\pi/2$. In other words, electrons of type *1* cease to be the central electrons of the bunch after passing the second gap. Now the bunch tends to be compressed around electrons that pass through the gap of the idler cavity a quarter of the oscillation cycle later.

This change in electron motion may also be traced by examining the behaviour of electrons of type *4*, which were the most unfavourable for bunching in the drift space between the input and the intermediate cavities. After acceleration in the second gap these electrons tend to gradually approach the middle of the new electron bunch being formed.

Similar processes take place in each drift space of a multicavity klystron. Thus, the analysis of cascade bunching becomes very

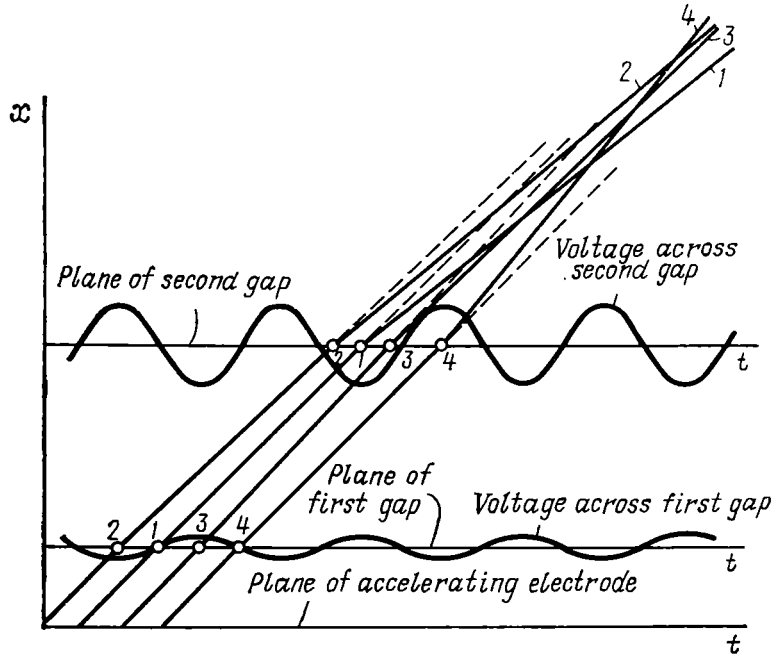

Fig. 5.14. Motion diagram of electron bunching in three-cavity klystron with intermediate cavity tuned exactly to the signal frequency. Electron trajectories in the absence of the intermediate cavity are shown in dashed lines

cumbersome. The waveform of convection current arriving at the output cavity can differ considerably from the pattern shown in Fig. 5.5*c*.

The analysis of cascaded klystrons can be significantly simplified if the modulation acquired by the electron beam when passing through the preceding cavity can be considered negligible as compared to the modulation produced in the cavity in question. In this case an N-cavity klystron may be divided into $(N - 1)$ simple two-cavity amplifiers. Thus, the intermediate cavity in a three-cavity design can be considered to function as the output cavity relative to the input resonant cavity and as the buncher relative to the output cavity. In the general case all the resonant cavities, except the output one, should be considered as a multicavity buncher assembly that determines the convection current of the electron beam, which excites the output cavity.

5.5b. Kinematic Theory of Cascade Bunching. Gain of Multicavity Klystrons

Consider cascade bunching for the simplest case of a three-cavity klystron, neglecting at first the effects of space charge and restricting, as earlier, the analysis to the case of small signals in all cavities except the output one. The voltage developed across the input gap shall be assumed to be

$$u_1 = V_1 \sin \omega t_1; \quad V_1 \ll V_0$$

Under these assumptions the motion of the electron beam through the first drift space, by analogy with (5.6), can be described as

$$t_2 = t_1 + \frac{s_{12}}{v_0 + v_1 \sin \omega t_1} \approx t_1 + \frac{s_{12}}{v_0} - \frac{s_{12} v_1}{v_0^2} \sin \omega t_1$$

$$\omega t_2 = \omega t_1 + \Theta_1 - X_{12} \sin \omega t_1 \tag{5.42}$$

where

$$X_{12} = \frac{\omega s_{12} v_1}{v_0^2} = \Theta_1 \frac{M_1 V_1}{2V_0} \tag{5.43}$$

$$\Theta_1 = \frac{\omega s_{12}}{v_0} \tag{5.44}$$

Here X_{12} is the bunching parameter of the beam entering the second interaction gap of the klystron, s_{12} is the length of the drift space between the centres of the input and intermediate cavity gaps and Θ_1 is the undisturbed transit angle through the first drift space. The rest of the designations are the same as in Section 5.2.

The maximum of the retarding field across the intermediate cavity gap can be shifted by a phase angle φ relative to the time of electron bunch arrival, this phase shift depending on the tuning of the second cavity as shown in Fig. 5.15. The voltage developed across the second gap should thus be described as

$$u_2 = -V_2 \cos (\omega t_2 - \Theta_1 + \varphi)$$

In the particular case of a purely conductive admittance of the second cavity, this phase shift is zero and, as mentioned, the maximum retarding field is developed across this gap just at the instant the electron bunch passes through the gap.

The kinetic energy acquired by an electron at the output of the second gap is

$$\frac{mv^2}{2} = e \{V_0 + M_1 V_1 \sin \omega t_1 - M_2 V_2 \cos (\omega t_2 - \Theta_1 + \varphi)\}$$

Hence, the velocity of the electron beam in the second drift space can be determined as

$$v=\left\{\frac{2eV_0}{m}\left[1+\frac{M_1V_1}{V_0}\sin\omega t_1-\frac{M_2V_2}{V_0}\cos(\omega t_2-\Theta_1+\varphi)\right]\right\}^{1/2}$$

The factor M_2V_2/V_0, as follows from the principle of klystron amplifier performance, can always be assumed less than unity,

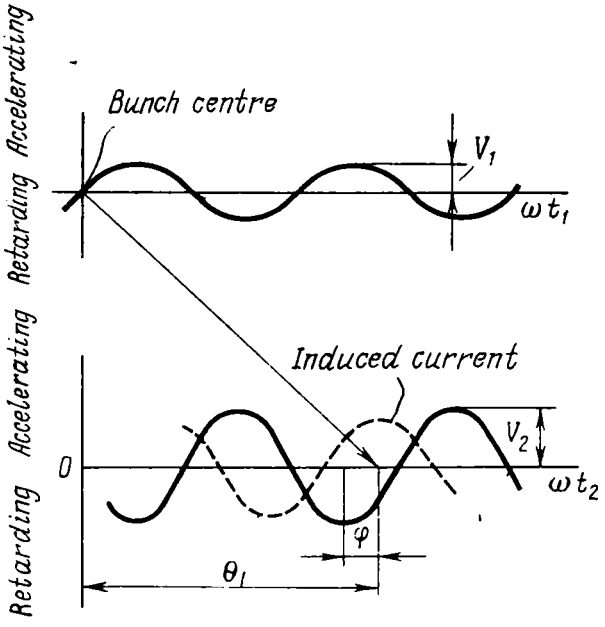

Fig. 5.15. Phase shift between induced current and voltage developed across the second gap in a three-cavity klystron

this making it possible to approximate the later equation by

$$v=v_0\left[1+\frac{M_1V_1}{2V_0}\sin\omega t_1-\frac{M_2V_2}{2V_0}\cos(\omega t_2-\Theta_1+\varphi)\right]$$

The instant the bunch arrives at the middle of the third interaction gap can be determined from the condition

$$t_3=t_2+\frac{s_{23}}{v}\approx t_2+\frac{s_{23}}{v_0}\left[1-\frac{M_1V_1}{2V_0}\sin\omega t_1+\frac{M_2V_2}{2V_0}\cos(\omega t_2-\Theta_1+\varphi)\right]$$

where s_{23} is the length of the second drift space. Multiplication of this relation by the angular frequency yields

$$\omega t_3=\omega t_2+\Theta_2-\Theta_2\frac{M_1V_1}{2V_0}\sin\omega t_1+\Theta_2\frac{M_2V_2}{2V_0}\cos(\omega t_2-\Theta_1+\varphi) \quad (5.45)$$

where Θ_2 denotes the undisturbed transit angle through the second drift space:

$$\Theta_2=\frac{\omega s_{23}}{v_0} \quad (5.46)$$

The phase of electron bunch arrival at the third gap can be expressed in terms of the phase with which the bunch passed through the input gap by substituting equation (5.42) into (5.45). Applying the designations

$$X_{13}=(\Theta_1+\Theta_2)\frac{M_1V_1}{2V_0} \tag{5.47}$$

$$X_{23}=\Theta_2\frac{M_2V_2}{2V_0} \tag{5.48}$$

results in

$$\omega t_3=\omega t_1+\Theta_1+\Theta_2-X_{13}\sin\omega t_1+ \\ +X_{23}\cos(\omega t_1-X_{12}\sin\omega t_1+\varphi) \tag{5.49}$$

X_{13} and X_{23} may be treated as the bunching parameters for an electron beam which would enter the third cavity from only the first or only the second cavity (with the other of them absent but at the same lengths s_{12} and s_{23} of the drift spaces).

Expansion into a series of the terms $\cos(X_{12}\sin\omega t_1)$ and $\sin(X_{12}\sin\omega t_1)$, neglecting terms higher than the first at $X_{12}^2/2$ much less than unity, results in the transformed equation (5.49)

$$\omega t_3-\Theta_1-\Theta_2=\omega t_1-X_{13}\sin\omega t_1+ \\ +X_{23}\cos(\omega t_1+\varphi)+X_{12}X_{23}\sin\omega t_1\sin(\omega t_1+\varphi) \tag{5.50}$$

This equation determines the nature of electron bunching in three-cavity klystrons, just as equation (5.10) describes this process in two-cavity klystrons. From comparison of (5.10) and (5.50) it is apparent that cascade bunching processes are very complicate.

Consider an approximate solution of (5.50) for the case when the last term can be neglected (i.e. when X_{12} is negligible as compared to unity). The bunching parameters X_{13} and X_{23} can be of one and the same order of magnitude, comparable to unity. After simple rearrangements, we obtain

$$\omega t_3-\Theta_1-\Theta_2=\omega t_1-[\sin\omega t_1(X_{13}+X_{23}\sin\varphi)- \\ -X_{23}\cos\omega t_1\cos\varphi]$$

The last two terms inside the brackets can be represented as

$$\sin\omega t_1(X_{13}+X_{23}\sin\varphi)-X_{23}\cos\omega t_1\cos\varphi=X'\sin(\omega t_1+\varphi')$$

The new constants X' and φ' are determined from the obvious relations

$$X'\cos\varphi'=X_{13}+X_{23}\sin\varphi \tag{5.51a}$$

$$X'\sin\varphi'=-X_{23}\cos\varphi \tag{5.51b}$$

Thus, the equation of electron bunching may be reduced to

$$\omega t_3-\Theta_1-\Theta_2=\omega t_1-X'\sin(\omega t_1+\varphi') \tag{5.52}$$

For convenience of comparison, equation (5.10) for a two-cavity klystron is written here

$$\omega t_2 - \Theta = \omega t_1 - X \sin \omega t_1$$

Both these equations can be made similar in appearance if quantity φ' is added to both parts of equation (5.52)

$$\omega t_3 - (\Theta_1 + \Theta_2 - \varphi') = (\omega t_1 + \varphi') - X' \sin (\omega t_1 + \varphi') \qquad (5.53)$$

Consequently, the bunching process can in the main be considered as governed in both cases by similar laws, except for the fact that the bunching parameter X for the two-cavity case should be replaced by an effective bunching parameter X' and the phase should be taken as $(\Theta_1 + \Theta_2 - \varphi')$ instead of Θ. Without performing again the calculations of Section 5.2, the convection current in the third resonant cavity by analogy with (5.20) can be described as

$$i_3 = I_0 + 2I_0 \sum_{n=1}^{\infty} J_n (nX') \cos \{n [\omega t_3 - (\Theta_1 + \Theta_2 - \varphi')]\} \qquad (5.54)$$

Under the approximations adopted the current waveform proves to be the same as in a two-cavity klystron.

The amplitude of the convection current fundamental in the third cavity will be designated as I_3. Equation (5.54) then yields

$$I_3 = 2I_0 J_1 (X') \qquad (5.55)$$

The condition of a maximum value of the fundamental is $X' = 1.84$, just as in a two-cavity klystron; in this case $I_{3\max} = 1.164\, I_0$ and the maximum efficiency should be 58.2 per cent.

What changes are then produced by introducing a third, intermediate cavity into the design of a two-cavity klystron? Let us examine the gain provided by the three-cavity klystron. The output power can be determined by the methods used in the analysis of two-cavity klystron amplifiers. Assuming the output cavity to be tuned exactly to the signal frequency and the load to be purely conductive, by analogy with equation (5.32),

$$P_{out} = 2M_3^2 I_0^2 [J_1 (X')]^2 \frac{G'_L}{(G_3 + G'_L + G_{eL3})^2} \qquad (5.56)$$

Here G_3 and G_{eL3} are the conductance and electron load of the third (output) cavity as referred to the gap plane, M_3 is the gap factor of the third interaction gap. Note, that X' here has a somewhat different meaning than in equation (5.27) and does not take into account space charge effects.

The input power to the klystron (assuming matched conditions at the input) can be described as

$$P_{in} = \frac{2V_0^2 (G_1 + G_{eL1})}{M_1^2 (\Theta_1 + \Theta_2)^2} X_{13}^2 \tag{5.57}$$

This latter relation can be easily derived by techniques similar to those used to obtain equation (5.30).

The gain provided by a three-cavity klystron at the design frequency with a matched load terminating the output cavity, with relations (5.56) and (5.57) taken into account, proves to be

$$G_0 = 20 \log_{10} \left[\frac{M_1 M_3 I_0 (\Theta_1 + \Theta_2)}{2V_0 \sqrt{(G_1 + G_{eL1})(G_3 + G_{eL3})}} \frac{J_1 (X')}{X_{13}} \right] \tag{5.58}$$

(in this case the condition of output matching is $G'_L = G_3 + G_{eL3}$).

It will be useful to compare the relation thus obtained with the corresponding equation for a two-cavity klystron (5.34). For convenience of comparison both devices will be assumed to be of identical electric length, i.e. $\Theta = \Theta_1 + \Theta_2$. In this case the difference in gain provided by a three-cavity klystron and a two-cavity klystron is the greater, the greater the difference between the corresponding bunching parameters X' and X_{13}.

The system of equations (5.51a) and (5.51b) yields

$$X' = (X_{13}^2 + X_{23}^2 + 2X_{13}X_{23} \sin \varphi)^{1/2} \tag{5.59}$$

Hence it follows that X' (the effective bunching parameter) exceeds the value of X_{13}, which would characterize the klystron operation in the absence of an intermediate cavity. It is interesting to note that X' is dependent on the angle φ, which in turn is a function of the tuning of the intermediate cavity (refer to Section 5.5*d*).

At high Q-factors of the intermediate cavity the voltage amplitude developed across the second gap can be quite high and the difference between the bunching parameters X' and X_{13} significant. The increase in X' with cascade bunching is obtained without having to increase the length of the drift space. Due to this a higher gain is not in contradiction with the above effect of beam debunching due to the forces in the space charge[1]. The gain of a three-cavity klystron is greatly in excess of that provided by two-cavity designs and in actual devices is up to 30 to 35 dB. Thus, one of the main drawbacks of the two-cavity design, a low gain, is eliminated.

A further increase in device gain can be obtained by simply including other intermediate cavities, each additional stage increasing

[1] The optimum length of each drift space, at which the gain is at a maximum, according to the findings of Section 5.3*b* is a quarter of the plasma (space charge) wavelength.

the overall gain by some 20 to 25 dB. The following empirical relation can be used to estimate the gain of an N-cavity klystron:

$$G_0 \approx 15 + (N-2)\,20 \text{ dB} \tag{5.60}$$

Physically, an increase in the gain of a multicavity klystron at fixed values of the d.c. voltage and current is obtained not as a result of increased output power or higher efficiency, but by reducing the input power required to control the electron beam.

In principle, increasing the number of cavities to 5-7 and even more huge gains in excess of 100 dB can be obtained. In practice such extremely high gains are ordinarily undesirable. It should also be kept in mind that at extremely high gains the klystron tends to become self-excited since various paths of stray radiation provide the parasitic feedback. In modern multicavity klystron designs the number of cavities is increased not to obtain higher gains, but rather to widen the bandwidth by tuning the cavities in a special way, as will be shown in Section 5.5*d*.

5.5c. *Efficiency of Multicavity Klystrons*

Cascade bunching permits of increasing not only the gain but also the efficiency of multicavity klystrons above the theoretical maximum of 58.2 per cent, characteristic of two-cavity designs.

Analysis of the convection current entering the output gap of a multicavity klystron discloses that the amplitude of the fundamental exceeds the value of $1.164I_0$, arrived at earlier when examining equation (5.55). Thus, in a three-cavity klystron the amplitude of the fundamental can attain the value of $1.48I_0$ and even higher. The above operating conditions can be achieved if we lift the restriction that X_{12} should be much less than unity, i.e. the amplitudes of the input signal will be considerable. Thus, with cascade bunching, the ideal waveform governed by the delta-function law, can be approximated more closely than in the case of an ordinary two-cavity klystron.

A higher amplitude of the convection current fundamental results in a higher electronic efficiency of a cascaded klystron at higher input signal levels. If the output cavity is assumed to operate at maximum allowable amplitudes equal to V_0[1], the maximum efficiency of a three-cavity klystron proves to be 73.8 per cent instead of the 58.2 per cent of the two-cavity and three-cavity devices operating with small input signals.

---

[1] With the finite transit angle through the output gap taken into account, the optimum voltage amplitude across the gap is (1.2-1.3) V_0. For comparison, note that the voltage amplitude across the last but one gap is about (0.3-0.4) V_0.

When increasing the number of resonant cavities, still higher efficiencies can be obtained, the improvement being due to a better beam bunching and approaching the theoretical maximum of convection current amplitude in the output gap equal to $2I_0$ (refer to Section 2.4). Note, that at high voltage amplitudes across the preceding gaps the electron bunch entering the output gap may feature a considerable spread in electron velocities. To obtain a maximum efficiency it is desirable to keep this spread as low as possible.

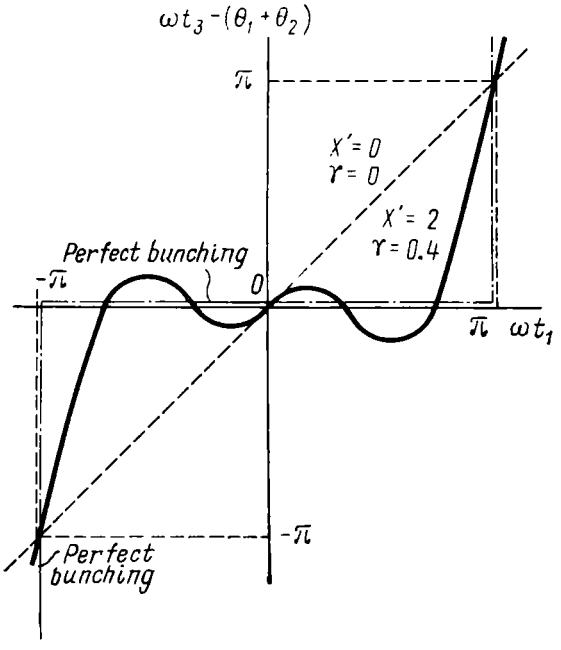

Fig. 5.16. Phase of electron arrival at the third cavity *vs* the phase of passage through the first cavity under cascade bunching (Fig. 5.2)

The calculated phase of electron arrival at the third gap as a function of the phase, at which the electron passed the middle of the first gap, is shown as a graph in Fig. 5.16. The bunching parameter X' and the phase shift φ between the induced current and the voltage across the gap of the intermediate cavity are here assumed to be 2 and $+\pi/2$, respectively, while γ denotes the ratio $X_{13}X_{23}/2X'$.

A distinguishing feature of the graph in Fig. 5.16, as compared to that of Fig. 5.2, is that the curve of electron arrival intersects the abscissa axis at four finite values of the phase ωt_1 instead of two. Many of the electrons, "unfavourable" for ordinary bunching, in this case acquire an "improved" phase and give up their energy to the field of the output resonant cavity. Dependence of this kind is typical for velocity modulation in the presence of the second harmonic.

For comparison, total (perfect) bunching in accordance with the delta-function law is illustrated in the same graph by a dot-and-dashed line. As can be noted by comparing Fig. 5.16 and Fig. 5.2, cascade bunching is a closer approximation of the ideal bunching conditions than the process taking place in a two-cavity klystron.

The improvement in bunching characteristics in the case of a multicavity klystron can be treated as a result of the ordinary two-cavity system being driven by a certain non-sinusoidal voltage whose waveform as if approximates the ideal saw-tooth pattern discussed in Section 2.8*e*.

A still further increase in the efficiency of multicavity klystrons can be obtained with the aid of *recuperative deceleration* of the electron beam at the collector (so-called depressed collector operating conditions). The electronic efficiency can be described as

$$\eta_e = \frac{P_{out}}{P_0} = \frac{P_{out}}{P_{out} + P_{diss.\,col} + P'_{diss}} \tag{5.61}$$

where P_0 is the power consumed from the d.c. supply sources, $P_{diss.\,col}$ and P'_{diss} are powers dissipated as heat by the collector and by the cavity walls, drift tubes and interaction gaps, respectively.

Equation (5.61) indicates that in principle it is possible to obtain a significant improvement in efficiency by reducing the power dissipated by the collector (ordinarily, $P_{diss.\,col}$ is greatly in excess of P'_{diss}), even if the electron beam gives up only part of its kinetic energy to the field of the output gap. Physically, this may be accomplished by slowing down the electron beam after it has left the output gap, so that it arrives at the collector with an almost zero velocity.

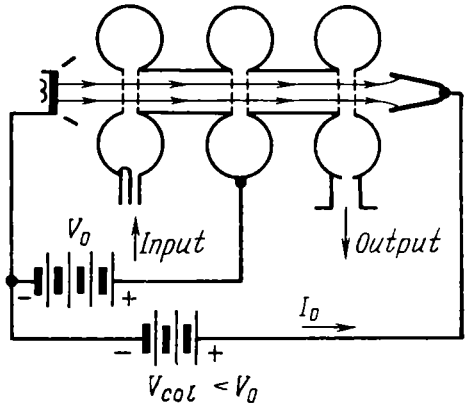

Fig. 5.17. Single-step recuperation with depressed collector voltage (cf. Fig. 5.13*b*)

The electron beam can be slowed down by means of a retarding static electric field in the space between the output resonant cavity and the collector. The collector should thus be kept under a voltage V_{col} (relative to the cathode, of course) that is lower than the accelerating voltage applied to the resonant system, as shown in Fig. 5.17 (hence the designation "depressed collector"). The energy acquired by the electron beam from the source of accelerating voltage and not given up to the output gap field is thus recuperated (returned) to the d.c. source[1].

In this case the power consumed from the sources of d.c. voltage is

$$P_0 = V_0 I'_0 + V_{col} I_{col}$$

where I'_0 is the current of the resonant system and I_{col} is the collector current (d.c. values). The equation for electronic efficiency under depressed collector conditions can then be presented as

$$\eta_{e\,(recup)} = \frac{\eta_e V_0 I_0}{V_0 I'_0 + V_{col} I_{col}} \approx \frac{\eta_e}{V_{col}/V_0} \tag{5.61a}$$

[1] A certain analogy can be drawn between these operating conditions and the recuperative deceleration employed in electric traction systems and accomplished by changing the conditions from electric drive to generator.

provided the condition $I_0' \ll I_{col}$ is satisfied; η_e denotes here the electronic efficiency without energy recuperation, i.e. when $V_{col} = V_0$.

The ratio V_{col}/V_0 can be made the lower, the higher are the electron velocities at the output of the catcher gap and the lower is the value of η_e. The limit to collector voltage depression is set by the effect of electron beam reflection back to the output gap. Actually, after passing through the output gap and giving up there a considerable part of their kinetic energy, electrons of the beam feature a significant spread in velocities. In the ideal case it would be necessary to section up the collector into separate areas and feed each area with a different d.c. voltage; electrons with the highest velocities would then be made to arrive at the section with the most negative voltage.

Besides providing a higher efficiency, the depressed collector operating conditions offer additional advantages in that the collector cooling becomes less of a problem and that the source of the greatest d.c. power (collector voltage) may be regulated to a smaller degree (Fig. 5.17).

Sectioning the collector is a technique rarely used, because it makes the design of the device itself and its supply arrangement much more complicated. Utilization of depressed collector conditions is also hampered by the fact that part of the electrons (those with the lowest velocities) are repelled from the collector and arrive back into the drift space of the resonant system. These electrons, along with secondary electrons ejected from the collector surface, can be the cause of self-excitation effects, instability of device gain and a reduction of electronic efficiency.

Practically, modern multicavity klystrons with single-step collector voltage depression can operate with collector voltages depressed by not more than some 20 per cent relative to the accelerating voltage, this providing quite a slight improvement of the overall device efficiency. Nevertheless, depressed collector conditions are of a considerable practical interest, especially in cases when the interaction of the electron beam with the output gap field is of insufficient effectiveness. This kind of operation is applicable to other types of microwave devices as well, first of all to travelling-wave tubes of the O type, treated in Chapter Six.

5.5d. Effect of Cavity Tuning on the Characteristics of a Multicavity Klystron. Operating Bandwidth

Detuning the *output* cavity of a multicavity klystron does not affect the process of beam bunching. The conclusions arrived at in Section 5.3*c* are applicable to multicavity klystrons as well.

Detuning the *input* cavity, as in the case of a two-cavity klystron, results in partial reflection of the input power and a lower voltage developed across the input gap; this effect, therefore, can be examined in terms of the dependence of klystron gain and output power on the input signal power.

The effect of detuning the *intermediate* cavities is a more specific one. This effect will be examined by taking as an example the detuning of the second cavity in a three-cavity device.

A change in the resonant frequency f_{02} of the intermediate cavity (relative to the frequency f of the input signal) affects the phase shift φ between the induced current and the voltage, developed across the gap by this current in the idler cavity (refer to Fig. 5.15). Detuning the second cavity can make this phase angle vary in the range from $-\pi/2$ to $+\pi/2$ and is thus capable of exerting a marked influence on the process of electron beam bunching. These effects can be shown by shifting the sinusoid $u_2(t)$ to both sides with respect to the instant of bunch arrival, obviously independent of cavity tuning.

A qualitative treatment of the change in effective bunching parameter X' produced under small-signal conditions by variations of the angle φ discloses that at $+\pi/2$ the centre of the electron bunch enters the second gap when the radio-frequency field changes from retarding to accelerating. The additional bunching action of the intermediate cavity tends to further compress the electron bunch around the same centre, so that a deeper velocity modulation of the beam results. On the contrary, if the angle $\varphi = -\pi/2$ the field of the second gap tends to debunch the electron beam and to form new electron bunches shifted from the initial ones by a phase angle π.

Thus, an increase in the effective bunching parameter can be obtained by detuning the intermediate cavity in such a manner, as to produce a phase shift of about $+\pi/2$ (at a constant X_{23}). The same conclusion can be drawn in a more formal manner by examining equation (5.59).

A voltage leading the current by an angle of $\varphi = +\pi/2$ can be developed only if the susceptance of the cavity is of an inductive character. Thus, the intermediate cavity should be detuned to a frequency *slightly higher than the input signal frequency* f (f_{02} should exceed f)[1].

Actually, however, detuning the intermediate cavity causes not only a change in the phase angle φ, but is also accompanied by a reduction of the voltage amplitude V_2 due to the cavity admittance rapidly increasing with detuning. In turn, this decrease in V_2 causes a lower bunching parameter X_{23} (refer to (5.59)). Ignoring the calculations involved, it is possible to conclude that the magnitude

[1] This statement is based on the behaviour of a parallel resonant circuit: the susceptance around the resonant frequency is a linear function of frequency and goes through zero at resonance, with a positive derivative dB/df.

of X' and the total gain of the klystron will be at a maximum at a certain optimum detuning of the intermediate cavity.

Figure 5.18 presents a qualitative illustration of the behaviour of effective bunching parameter X' as a function of the relative detuning $\frac{\delta f}{f} = \frac{f_{02} - f}{f}$. When detuning is negative, parameter X' features a minimum with a subsequent asymptotic increase in magnitude approaching X_{13}. The same asymptotic limit is set for X' at considerable positive detuning of the intermediate cavity.

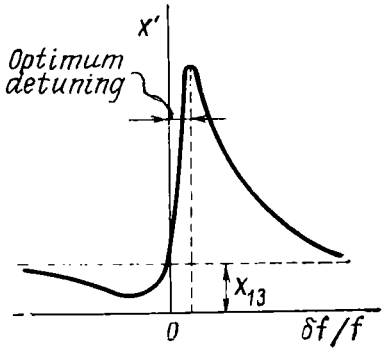

Fig. 5.18. Effect of detuning the intermediate cavity of a three-cavity klystron on bunching parameter X'

The lower the input signal level and the lower the value of parameter X_{13}, the slighter is the direct effect of the angle φ and the lower, therefore, should the detuning be. In cases of very small input signals the electron bunching process is almost entirely determined by parameter X_{23}; the intermediate cavity should be tuned to practically the signal frequency. Such conditions are conventionally known as *synchronous tuning*.

At a higher input signal, detuning of the intermediate cavity becomes more pronounced. However, in this case, the required relative detuning also proves to be quite small (fractions of a per cent) because the intermediate cavity, not being loaded by any external load, features a very high Q-factor, of the order of 1000 and even higher.

The main drawback of synchronous tuning in a multicavity klystron is the extremely narrow instantaneous bandwidth, usually not exceeding several MHz. This drawback can be partially eliminated by detuning the intermediate cavities to both sides of the middle frequency, similar to detuning stagger-tuned circuits when bandpass filters are designed. Increasing the number of intermediate cavities and detuning them in an appropriate manner prove to be effective in obtaining a wider bandwidth up to several per cent of the middle frequency at the cost of the maximum obtainable gain. It is, however, desirable to tune the last but one resonant cavity of the klystron to a frequency slightly higher than the input frequency, so as to provide electron bunches of better waveform and thus obtain a higher efficiency.

The operating bandwidth of a klystron is also a function of the loaded Q of its output cavity (refer to Section 5.3*c*). To realize the bandwidth provided by the preceding cavities, which may be considered as constituting a complex buncher (under detuning this bandwidth can be up to 5 to 10 per cent of the middle frequency), the

output cavity, by equation (5.38), may have a comparatively low loaded Q, of the order of 10 or 20 and even less.

To ensure that such a value of the loaded Q does not impair the efficiency of energy exchange between the microwave field of the output cavity and the electron beam (refer to Section 2.4), it is necessary to increase the ratio I_0/V_0, in other words, to use beams of high perveance[1]. With all other parameters invariable, the operating bandwidth obtainable is increased approximately in direct proportion to the beam perveance. A higher beam perveance is also advantageous from the point of view of reducing the magnitude of the accelerating voltage at a given output power level.

Another way of obtaining a wider bandwidth is the use of several tightly coupled cavities as the output assembly, instead of a single cavity. Finally, the resonant output devices can be rejected altogether in favour of a section of non-resonant slow-wave system as the output assembly of a multicavity klystron. "Hybrid" microwave devices of this kind have been developed known as *twistrons*, they have much in common with power travelling-wave tubes of the O type (refer to Chapter Six).

5.5e. Other Problems of Multicavity Klystrons

The dependence of output power and gain of a klystron on the input signal power will first be examined.

If we gradually increase the input power from zero upward (by tuning intermediate cavities to a maximum output power at each value of the input signal), the magnitude of the X_{12} parameter first seems to be quite small. As was shown in Section 5.5*b* with X_{12} considerably less than unity, a cascaded klystron features the same properties as a two-cavity device, but a much higher gain. Therefore, the initial section of the curve $P_{out} = f(P_{in})$ is qualitatively similar to the curve of Fig. 5.8*a*. The slope of the linear section of this characteristic is, however, considerably steeper than that of a similar two-cavity klystron.

The difference in behaviour between a two-cavity and a multicavity klystron becomes especially pronounced at large input signal levels, when an increase in fundamental of the beam current specific to cascade bunching shows up. As a result, the output power continues to increase gradually, instead of falling off, as it was in the case of a two-cavity klystron. The corresponding graph is shown in Fig. 5.19, the smooth maximum of output power being determined by optimum cascade bunching conditions.

As the ordinary two-cavity klystrons, cascaded klystrons are thus capable of operating under two distinctly different kinds of

---

[1] *Perveance* is the factor in the Child-Langmuir equation $I_0 = kV_0^{3/2}$; often the concept of microperveance (i.e. $k \cdot 10^6$) is used.

conditions, namely linear conditions of maximum gain and nonlinear conditions of maximum output power and maximum efficiency. The difference between these operating conditions is even more pronounced with multicavity klystrons. "Saturation" conditions, as indicated by the graph $P_{out} = f(P_{in})$, tend to reduce amplitude modulation of the output frequency-modulated signal.

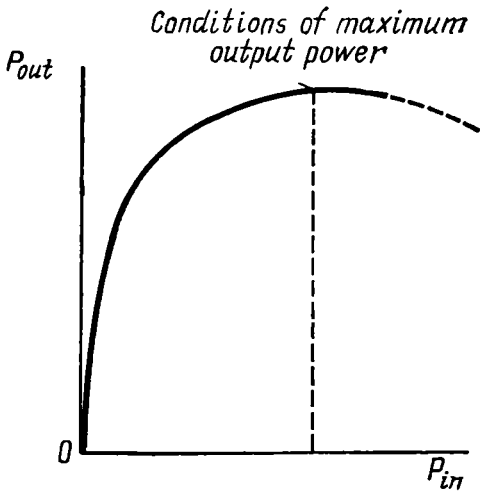

Fig. 5.19. Output power *vs* input power in a multicavity klystron (intermediate cavities are tuned to maximum output power conditions)

Most of the rest of the cascaded klystron characteristics are in principle similar to the corresponding characteristics of a two-cavity klystron.

Multicavity klystrons have the following properties, which contribute to output powers of exceedingly high levels:

(1) the cathode is removed from the radio-frequency circuit and this lifts the restrictions typical for such devices as microwave triodes, tetrodes and magnetrons;

(2) the collector circuit does not form a part of the radio-frequency system of the device, this also circumventing many of the problems associated with dissipating high power levels;

(3) an almost unlimited possibility of increasing the accelerating voltage.

Attaining high power levels is also assisted by the increase in efficiency obtained due to cascade bunching. Finally, the considerable maintenance advantages offered by amplifiers as compared to oscillators (such as stability of frequency and phase, simple synchronization and possibility of connecting several amplifiers to a common load) should also be kept in mind.

The main field of application of multicavity klystrons is as amplifiers of medium, high and super-high output power levels, employed as the output stages of radar, television and telecommunications transmitters. Pulse klystrons with extremely high output powers are used in nuclear physics to drive linear electron accelerators.

5.6. Typical Designs and Parameters of Drift Klystrons

Development of power amplifier klystrons necessitates the solution of a number of serious problems; among them are:

(1) obtaining and shaping a heavy rectilinear electron beam which

should pass through a successive series of gaps and drift spaces with as low a current loss as practicable;

(2) providing an adequate breakdown capability of the interelectrode gaps and insulators at extremely high accelerating voltages;

(3) dissipating a high power level on the collector;

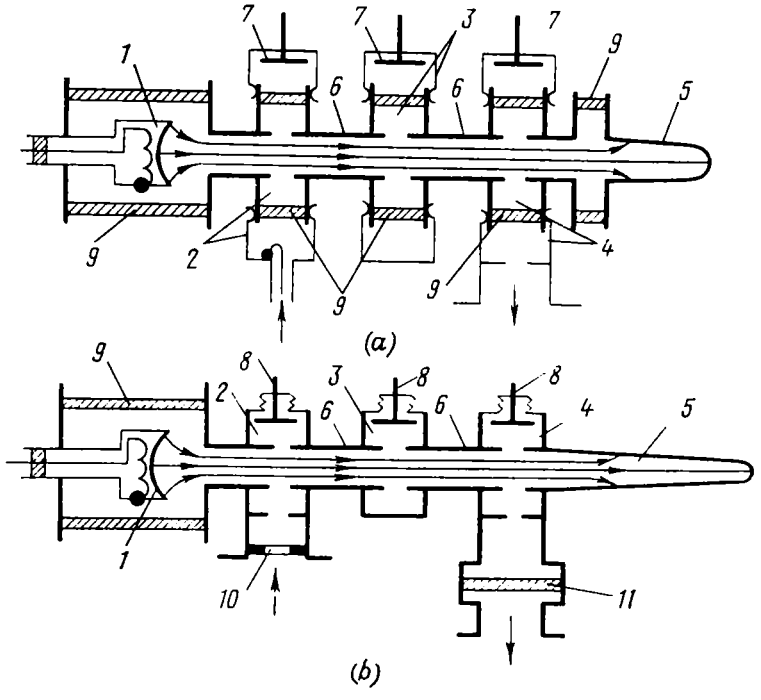

Fig. 5.20. Diagram of three-cavity power amplifier klystrons with external (*a*) and internal (*b*) resonant cavities; focussing and other auxiliary elements are omitted

1—cathode; *2*, *3*, *4*—input, intermediate and output cavities, respectively; *5*—collector; *6*—drift tubes; *7*—tuning arrangement mounted outside the vacuum envelope; *8*—tuning arrangement inside the tube envelope; *9*—ceramic tubes; *10*—input window; *11*—output window

(4) designing an output power assembly which would withstand considerable output power without breakdown;

(5) designing resonant cavities with a tuning arrangement which meets all the requirements of operation at high power levels.

When designing multicavity klystrons the choice between the *internal* and *external* mounting of resonant cavities has to be made; this problem was already discussed in Section 4.5*a* in connection with microwave triodes and tetrodes. Klystrons designed for the decimetric wave band are often provided with removable cavities of the rectangular waveguide type, that are mounted outside the vacuum envelope of the tube; these devices are designed mostly for c.w. operating conditions. This kind of design is illustrated schematically in Fig. 5.20*a*. The evacuated part of the cavity is made

up of sections of ceramic pipes and the gaps of these tubes are usually in the form of apertures without grids.

In high-power pulse klystrons designed for the 10-cm band and higher frequencies the internal cavity design is most common, the cavities being ordinarily of the rectangular waveguide type and the gaps made as apertures without grids. The resonant cavities are entirely enclosed inside the vacuum envelope of the tube, with the metal walls of the cavity and drift tubes functioning as part of the vacuum envelope. This design version is schematically shown in Fig. 5.20*b*. The cavities are tuned with the aid of movable plungers which are driven through vacuum-tight bellows (sylphons). It should be mentioned, that a considerable part of the commercially available klystrons are made with a fixed tuning and are not designed to be retuned during maintenance. In this case the device is tuned to the required frequency band only once—during manufacture.

The spacings between the middles of the cavities, as in a two-cavity klystron, have to be made approximately a quarter of the electron plasma wavelength. As a first approximation, the effects of the conducting walls, surrounding the drift spaces, can be taken into account by introducing the coefficient of plasma frequency reduction, discussed in Section 2.9. Actually, however, the charge density in the electron bunches is greatly in excess of the charge density of an unmodulated beam and the wave properties of the electron beam under these non-linear conditions are described by much more complex relations. The optimum spacing between cavities is usually reduced as the collector end of the tube is approached and in typical power klystrons is from 0.2 to 0.1 of the electron plasma wavelength.

Vacuum-tight output windows for waveguide power outputs of klystrons with internal cavities are of interest. Practice shows that these windows can be damaged due to heat dissipated as a result of dielectric loss in the window material, secondary electron bombardment and electric breakdown caused by a high electric field intensity. The best results are obtained with ceramic windows, in particular, when beryllium ceramics is used as the dielectric. In high and super-high power klystrons conical and "pot" window designs are extensively employed, as well as halfwave designs.

Electron guns intended for use in power klystrons should feature a high d.c. conductance I_0/V_0 and a high-perveance beam. The most widely used are the axially-symmetrical designs with magnetic screens, commonly known as Pierce guns, and versions of this design with beam convergence about 10-50 and more. The maximum value of specific power of the electron beam in a klystron may be up to 1 MW per square centimetre of cathode area.

A typical value of the microperveance of electron guns designed for use in power pulse klystrons with a continuous cylindrical electron beam is about 2 to 3 $\mu A/V^{3/2}$. Hollow beams can be used as

a means of increasing the microperveance up to 10 to 20 $\mu A/V^{3/2}$ and even higher. In this connection the use of electron guns of the *magnetron type* is of considerable promise, this type of gun having a conical configuration of the cathode and anode. The devices with such electron guns have much in common with the crossed-field devices treated in Chapter Seven. *Multibeam* designs can also be used and find a certain field of application; in this case each cavity is made with several interaction gaps so that each of these gaps interacts with a separate electron beam. All these beams are connected in parallel and accelerated by the voltage of a single d.c. source.

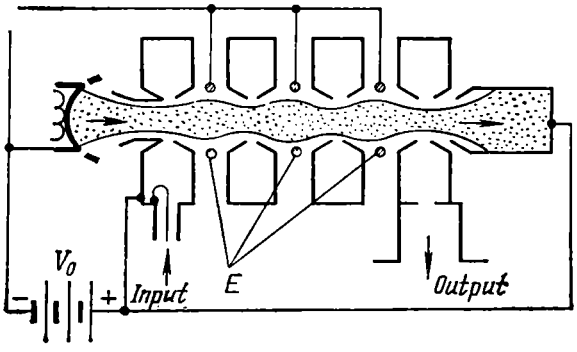

Fig. 5.21. Four-cavity amplifier klystron with electrostatic focussing (*E*—ring-shaped focussing electrode)

Ordinarily, the electron beam of a klystron is focussed by means of a static longitudinal magnetic field provided by a solenoid or a permanent magnet. The development of electrostatically focussed klystrons is of particular interest, this providing great savings in weight and dimensions. An example of this kind of design is schematically illustrated in Fig. 5.21. The electrostatic lenses shown here are in the form of rings mounted between the resonant cavities and d.c. connected to the tube cathode. It will be of interest to note that the electronic efficiency of klystrons with electrostatic focussing is superior to that of devices with magnetic beam focussing.

One of the important problems encountered when designing power pulse klystrons, as well as during their maintenance, is that of a pulse modulator; a similar problem is encountered with magnetrons (refer to Chapter Seven). Ordinarily, anode pulse modulation is utilized; it resides in that the anode or collector is d.c. connected to ground and short pulses of negative polarity applied to the device cathode.

High-power pulse modulators, with pulse voltages of the order of 100 to 400 kV at peak powers of 100 MW and more, are extremely

cumbersome devices[1]. This problem can be somewhat alleviated by including a special *modulating electrode* into the design of the electron gun in power klystrons, this modulating electrode being mounted between the cathode and the main accelerating electrode (the resonant system). In this case the operation of the klystron can be controlled by means of a pulse of considerably lower amplitude applied to this modulator electrode; the resonant system is maintained under the nominal high accelerating voltage. Obviously, the power requirements to the modulator in this case are considerably lower, because the current of the modulating electrode is much less than the electron beam current.

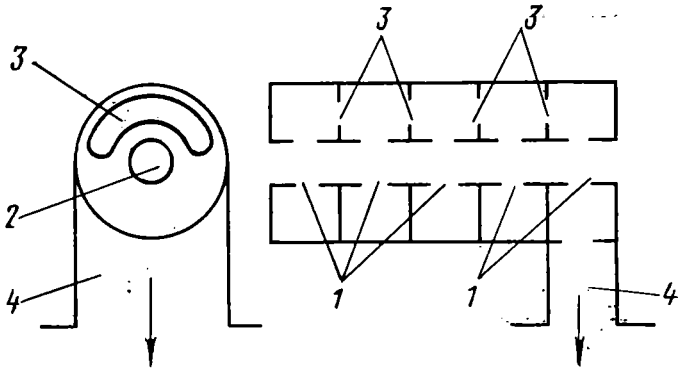

Fig. 5.22. Multigap cavity for power and super-high power klystrons
1—gridless gap; *2*—drift channel; *3*—coupling aperture; *4*—power output assembly

In conclusion of the present brief review of the aspects of multicavity klystron design, one more important trend should be mentioned. Figure 5.22 is an illustration of the design of a multigap resonant cavity, composed of a series of single-gap cavities coupled by means of apertures in the common cavity walls. A chain of cavities of this kind consisting of from 2 to 5 individual cavities (sometimes more) may be treated as a resonant section of a slow-wave structure of the periodically-loaded waveguide type. The electron beam passing through such a multigap cavity interacts periodically with the radio-frequency field, effectively giving up kinetic energy to this field.

Multigap cavities can be advantageously employed as the output cavities of a klystron, all the other cavities of which are of the "ordinary" single-gap design. It is also possible to design multicavity klystrons with the input, intermediate and output cavities of the kind shown schematically in Fig. 5.22. The advantage of multicavity klystrons with this kind of distributed interaction is a higher

[1] With such extremely high values of the accelerating voltage, relativity effects have to be taken into account when designing the klystron; in the above discussion these effects have been omitted.

efficiency and a greater gain-bandwidth product; multigap cavities are also advantageous from the point of view of obtaining high output power levels.

At present the efficiency of multicavity klystrons with magnetic beam focussing, designed for use as power and super-high power amplifiers, is in the range of 50 to 60 per cent, rarely—higher, at pulse powers of 30 to 50 MW. Under c.w. conditions the highest level of

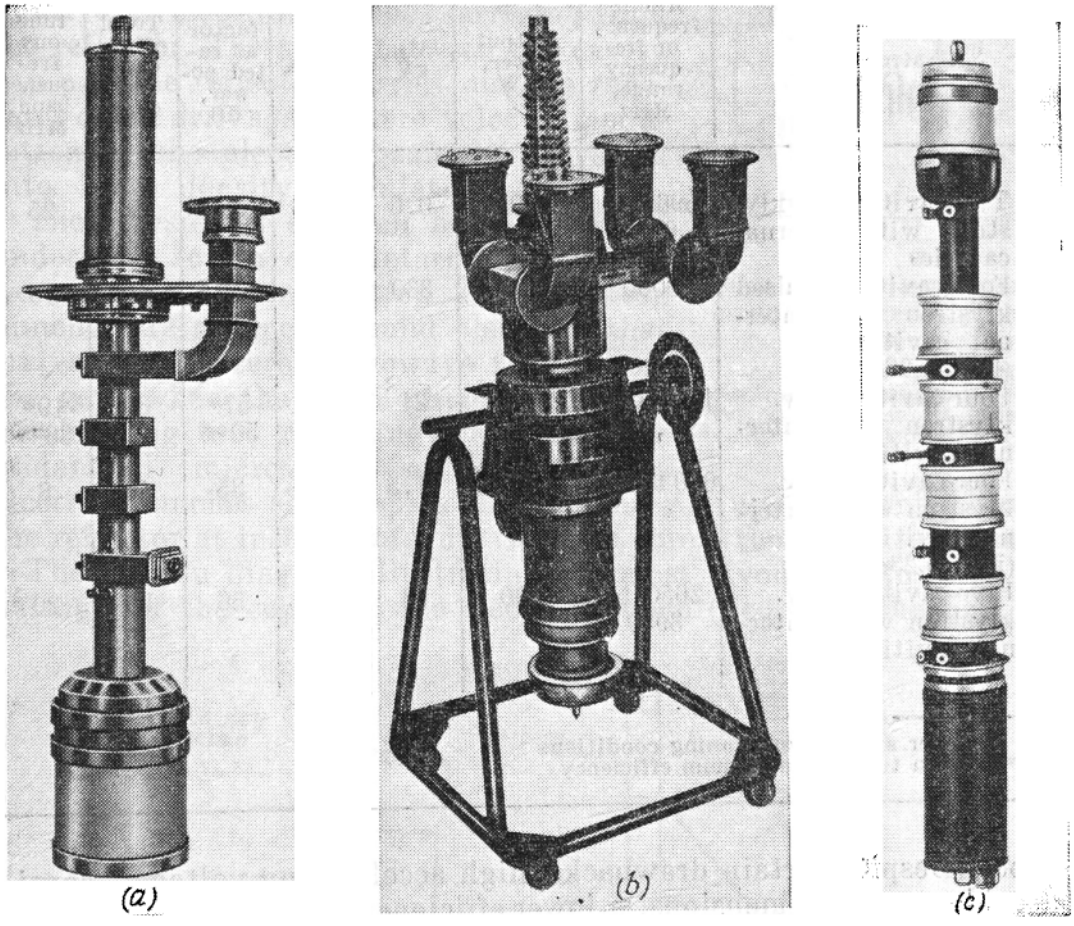

Fig. 5.23. Four-cavity klystron amplifiers with internal (*a*, *b*) and external (*c*) cavities

output power attained at present is about 1 MW. Electrostatically focussed klystrons are still at the output pulse power level of units of megawatts.

The main parameters of several typical multicavity klystrons (c.w. and pulse) are listed in Table 5.2 with the parameters of a typical two-cavity amplifier klystron presented in this Table for comparison. The external appearance of a typical multicavity klystron is presented in Fig. 5.23.

Parameters listed in this Table emphasize the peculiarities of multicavity klystrons as sources of high microwave power levels. In this respect klystrons have no equal among microwave devices, including devices of the magnetron type and power travelling-wave

Table 5.2

Parameters of Typical Amplifier Klystrons

Klystron type	Middle frequency or frequency range, MHz	Output power, kW	V_0, kV	I_0, A	Gain factor at rated power, dB	Total efficiency, per cent	Instantaneous frequency band, MHz
1. Two-cavity c. w. klystron with internal cavities	5965 to 6385	0.004	0.6	0.16	7 to 10	5	25
2. Four-cavity pulsed klystron with internal cavities (Fig. 5.23*b*)	3000	30,000	330	300	57	40	15
3. Four-cavity c.w. klystron with internal cavities	10,000 to 11,000	20	21	3.1	57* 50**	30	19* 30**
4. Four-cavity c.w. klystron with external cavities (Fig. 5.23*c*)	680 to 985	11	11.5	2.3	35	40	8
5. Five-cavity c.w. klystron with internal cavities	2650 to 3950	500	63	140	56	56	20

* Under synchronous tuning conditions
** When tuned to maximum efficiency

tubes. Despite certain drawbacks (high accelerating voltages, considerable overall dimensions, a lower efficiency than that of crossed-field devices) multicavity klystrons are extensively used and are finding ever increasing application as high-power devices.

5.7. Reflex Klystrons

5.7a. Qualitative Description. Phase Condition of Self-Excitation

Reflex klystrons are designed mainly as low-power sources of microwave signals. The basic diagram of a reflex klystron is presented in Fig. 5.24. The idealized diagram is shown in Fig. 5.25, where the distribution of d.c. voltages is also shown.

Reflex klystrons have but one resonant cavity that is pierced by the electron beam twice. Reversal of the electron beam and its return to the resonant cavity is the function of a special electrode, the repeller or reflector, which is maintained at a d.c. voltage negative relative to the tube cathode. The resonant cavity thus functions both as a buncher to the electron beam entering the cavity from the cathode side and as a catcher relative to electron bunches arriving from the reflector. The space between the cavity gap and the reflector carries out the functions of the drift space where velocity modulation of the electron beam is converted into beam density modulation.

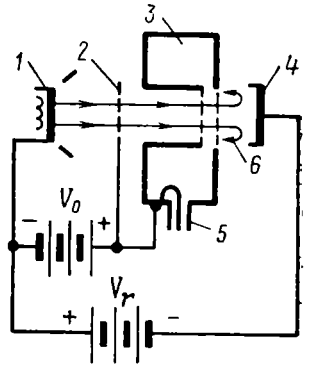

Fig. 5.24. Diagram and circuit of a reflex klystron

1—cathode; *2*— accelerating electrode; *3*—resonant cavity; *4*—reflector; *5*—power output; *6*—electron beam

The physics of electron beam bunching under the action of a retarding d.c. field were examined in Section 2.8*c*. Electron bunches are grouped around electrons that arrived into a zero microwave field across the gap, when the field changes from an accelerating to a retarding one. To provide undamped microwave oscillations, the electron bunches should pass through the gap upon returning from the reflector at instants of time the field across the gap is retarding.

The motion diagram illustrating the most favourable instants of passage for the centre of the electron bunch (i.e. when the field is

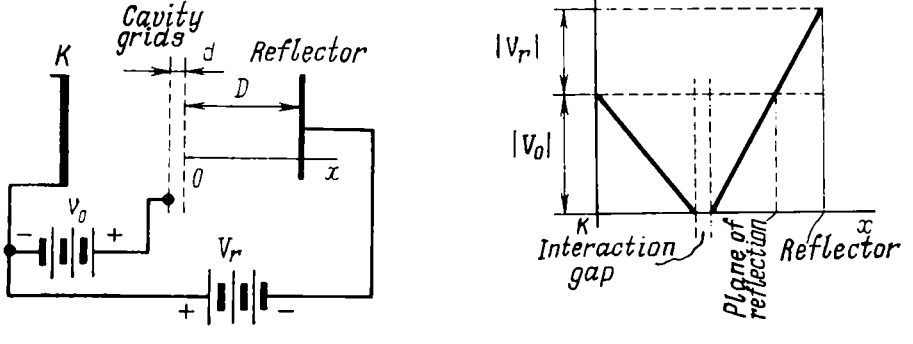

Fig. 5.25. Idealized circuit and voltage distribution in a reflex klystron; the cavity potential is set at ground (zero)

maximally retarding) is presented in Fig. 5.26. When plotting such diagrams, reversal of electron motion should be taken into account, because it leads to accelerating and retarding fields changing places as regards the nature of their action on the electrons.

As seen from Fig. 5.26, the optimum time of travel of the centre of the electron bunch in the bunching space relative to the middle of the interaction gap in the general case can be described as

$$\tau_{opt} = \frac{3}{4}T + nT = T\,(n + {}^3/_4) \tag{5.62}$$

where T is the period of radio-frequency oscillations and n is any integer, including zero.

The total time of electron travel in the bunching space as a function of the interelectrode spacing and the constant voltages applied to the klystron can be calculated from the following considerations

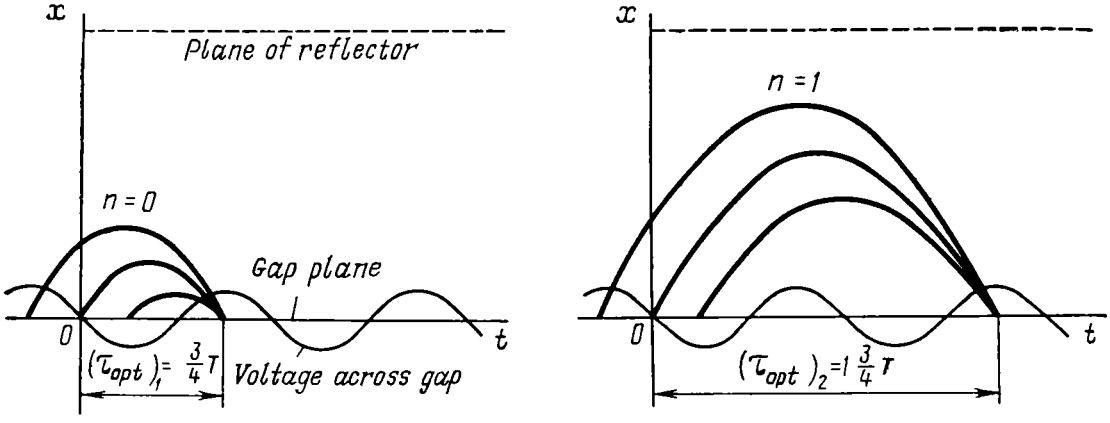

Fig. 5.26. Motion diagrams for two values of the optimum transit time through the bunching space

(Fig. 5.25). All the tube electrodes will be considered as parallel planes; edge effects and the effect of space charge will be neglected. The klystron will be assumed to oscillate under steady-state conditions. Under these assumptions the instantaneous value of the radio-frequency voltage across the interaction gap can be presented as

$$u = -V_1 \sin \omega t \tag{5.63}$$

with V_1 being much lower than the d.c. accelerating voltage V_0. This means that all the following argumentation will be restricted to the small-signal case, as was done in all the previous instances. The frequency of oscillations ω is supposed to be approximately equal to the natural frequency ω_0 of the resonant cavity at the oscillation mode utilized. The minus sign in equation (5.63) indicates that the origin of the time axis coincides with the electron that will afterwards be the centre of the electron bunch (refer to Fig. 2.30 and Fig. 5.26).

The moment of electron transit through the middle of the gap in the "forward" direction (i.e., when entering into the cavity from the

cathode side) can be denoted as t_1; electron velocities at the gap output can then be determined from the equation of velocity modulation (with the above relation (5.63) taken into account) as

$$v = v_0 - v_1 \sin \omega t_1 \tag{5.64}$$

where

$$v_0=(2eV_0/m)^{1/2}; \quad v_1=v_0MV_1/2V_0 \tag{5.65}$$

In the bunching space between the second grid and the reflector the electron motion is described as

$$m\ddot{x} = -eE$$

where E is the static field intensity, equal (according to Fig. 5.25) to

$$E=\frac{|V_0|+|V_r|}{D}=\frac{V_0-V_r}{D} \tag{5.66}$$

The first integration of the motion equation yields the electron velocity (with the electron velocity v at the gap output taken into account) as

$$\dot{x}=v-\frac{eE}{m}(t-t')$$

where t' is the instant of time when the electron passes the gap grid nearest to the reflector. In what follows t'' will be used to denote the instant of time the same electron comes back to this grid under the action of the reflector field.

The time of electron transit through the bunching space can be determined as $(x)_{t=t''} = 0$. Performing the second integration and placing the axis origin at the plane of the second grid yield

$$x=v(t-t')-\frac{eE}{m}\frac{(t-t')^2}{2} \tag{5.67}$$

and applying the above condition we arrive at two possible solutions

$$t''-t'=0; \quad \frac{eE}{m}\frac{t''-t'}{2}-v=0$$

The first of these solutions is a trivial one, corresponding to the instant of time the electron leaves the gap; the second solution describes the time of electron travel in the retarding static field as

$$t'' - t' = 2mv/eE \tag{5.68}$$

The time of electron travel thus determined has to be increased by twice the transit time $d/2v$ through the space between the equivalent gap of infinitesimal width (placed at the middle of the actual gap) and the output grid. Thus, the total time of travel of an arbitrary

electron from the middle of the interaction gap to the plane of reflection and back turns out to be

$$\tau = \frac{d}{v} + \frac{2m}{eE} v \tag{5.69}$$

The time of electron bunch travel can be determined from this relation by substituting v_0 for v, because the velocity of the central electron, around which the bunch is grouped, remains unaltered when passing the gap in the "forward" direction.

Substituting the equation for total electron transit time into equation (5.62), which determines the optimum time of bunch travel, and replacing the oscillation period T by the frequency $f = 1/T$ result in

$$n + \frac{3}{4} = f (m/e)^{1/2} \left(\frac{d}{(2V_0)^{1/2}} + \frac{D (8V_0)^{1/2}}{V_0 - V_r} \right) \tag{5.70}$$

The first term inside the brackets can often be neglected, provided $D \gg d$, this reducing the relation to

$$n + \frac{3}{4} = \frac{fD (8mV_0/e)^{1/2}}{V_0 - V_r} \tag{5.70a}$$

Equations (5.70) and (5.70a) describe the phase conditions of electrons giving up a maximum amount of their kinetic energy to the field of the klystron cavity. These relations are similar to equation (5.41), which determines the conditions of self-excitation for a two-cavity klystron.

Just as the two-cavity klystron, a reflex klystron has discrete zones of oscillation: at a fixed value of the accelerating voltage the output power as a function of the reflector voltage is of a pattern qualitatively illustrated in Fig. 5.27, with each oscillation zone corresponding to a definite value of n[1]. As distinct from the two-cavity klystron oscillator, the oscillation zones of a reflex klystron are not split into two. The frequency f in equation (5.70), as a first approximation, can be considered equal to the resonant frequency of the klystron cavity, coupled to the electron beam by the interaction gap.

The middles of the oscillation zones (at a fixed value of the acceleration voltage V_0 — points A, B, C, D in Fig. 5.27) can be determined with the aid of equation (5.70) or (5.70a); however, the configuration of these oscillation zones and the magnitude of the output power remain to be determined. The zones $n = 1$ and $n = 0$, not

[1] These oscillation zones should in no case be confused with the oscillation *modes* of klystron oscillators: various oscillation zones differ from one another only by the time of electron bunch travel in the bunching space at an identical pattern of the radio-frequency field inside the resonant cavity, independent of the integer n.

shown in Fig. 5.27, correspond to still higher values of the negative reflector voltage.

Consider a numerical example. The cavity of the reflex klystron is tuned to a frequency $f_0 = 9375$ MHz (wavelength 3.2 cm). With a 300 V accelerating voltage and a 3 mm spacing D between the

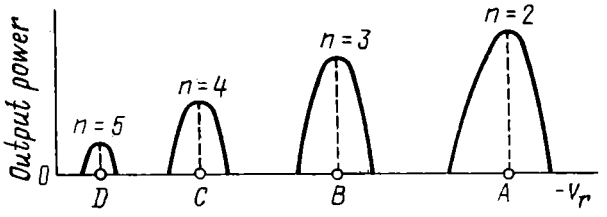

Fig. 5.27. Oscillation zones in a reflex klystron

reflector and the second grid, the reflector voltage by equation (5.70*a*) in the mksa system of units proves to be

$$V_r = 300 - 3270/(n + 3/4) \text{ V}$$

and the values of the reflector voltage for different values of n are as follows

n	0	1	2	3	4	5	6	7	8	9	10	11
V_r, V	−4060	−1570	−890	−571	−388	−268	−185	−122	−74	−35	−5	+21

At n greater than 10 the potential of the reflector in this klystron relative to the tube cathode becomes positive. In this case, however, the electrons will be attracted to the reflector and will therefore not be returned to the cavity. Thus, in principle, the klystron in question can operate on 11 different oscillation zones. Actually measured values of the reflector voltage are in reasonable agreement with the approximate voltages cited in this example.

5.7b. Convection Current in Reflex Klystrons

The analysis of convection current in reflex klystrons is in many respects similar to that of Section 5.2 for drift klystrons. The law of charge conservation can be used to derive the instantaneous beam current i_2 arriving at the middle of the interaction gap from the bunching space (without taking into account the reversal of the direction of electron motion) as

$$i_2 = I_0 \frac{dt_1}{dt_2} \tag{5.71}$$

where t_1 and t_2 are the instants of time one and the same electron passes through the middle of the gap and I_0 is the d.c. component of the beam convection current. For the time being the effect of electron interception by the gap grids and the reflector may be disregarded. Multiple passage of the electron through the gap will also be neglected, assuming that the beam after having passed through the gap from the reflector side is in some way or other intercepted by the cavity walls.

Consider the function $t_2 = f(t_1)$. Applying equation (5.69) which determines the time of electron travel from the middle of the gap into the bunching space and back yields

$$\tau = t_2 - t_1 = \frac{d}{v} + \frac{2mv}{eE}$$

Substituting equations (5.64) and (5.66) and multiplying both sides by the angular frequency, we arrive at

$$\omega(t_2 - t_1) = \frac{\omega d}{v_0 - v_1 \sin \omega t_1} + \frac{2m}{e} \frac{\omega D}{V_0 - V_r} (v_0 - v_1 \sin \omega t_1)$$

The amplitude of velocity modulation v_1 is much smaller than the average beam velocity v_0 because V_1 is considerably less than V_0. Expanding the first term into a series and neglecting all the resulting terms except the first two, after rearrangement yield

$$\omega(t_2 - t_1) = \frac{\omega d}{v_0} + \frac{2m}{e} \frac{\omega D v_0}{V_0 - V_r} - v_1 \left(\frac{2m}{e} \frac{\omega D}{V_0 - V_r} - \frac{\omega d}{v_0^2} \right) \sin \omega t_1 \qquad (5.72)$$

The first term in the right-hand side of relation (5.72) is the undisturbed transit angle through the interaction gap of the klystron. In the future this angle will be denoted by the symbol θ:

$$\theta = \frac{\omega d}{v_0} \qquad (5.73)$$

The second term in the right-hand side of (5.72) is the undisturbed transit angle through the bunching space, or in other words, the transit angle of the bunch centre from the second grid to the plane of reflection in the bunching space and back to the second grid, as is easily confirmed by setting $v_1 = 0$. This transit angle is designated by the symbol Θ and is equal to

$$\Theta = \frac{2m}{e} \frac{\omega D v_0}{V_0 - V_r} \qquad (5.74)$$

This latter relation can also be represented as

$$\Theta = \frac{\omega D}{V_0 - V_r} (8mV_0/e)^{1/2} = \frac{\omega D}{v_0} \frac{4}{1 - V_r/V_0} \qquad (5.74a)$$

Equation (5.72), with relations (5.73) and (5.74) taken into account, can be presented in a form that will emphasize its similarity to that used in the theory of two-cavity klystrons

$$\omega t_2 - (\Theta + \theta) = \omega t_1 - X \sin \omega t_1 \tag{5.75}$$

Here X is the bunching parameter known in the theory mentioned and in the present case equal to

$$X = v_1 \left(\frac{2m}{e} \frac{\omega D}{V_0 - V_r} - \frac{\omega d}{v_0^2} \right) = \frac{v_1}{v_0} (\Theta - \theta) \tag{5.76}$$

Taking into account relation (5.65) reduces this latter equation to

$$X = \frac{MV_1}{2V_0} (\Theta - \theta) \tag{5.76a}$$

As usual, M here denotes the interaction coefficient (gap factor) of the electron beam with the field of the gap, as defined by equation (2.59), i.e.,

$$M = \frac{\sin (\theta/2)}{\theta/2}$$

Note the similarity between equations (5.75) and (5.10) for the convection current in a reflex and a two-cavity klystron. The same degree of similarity can be noted to exist between the equations for the bunching parameter (5.76a) and (5.8), differing only in that the equation for a reflex klystron contains the *difference* in transit angles ($\Theta - \theta$), instead of the transit angle through the drift space Θ of a two-cavity klystron. This fact is explained by that electron bunches in a reflex klystron are grouped around different electrons inside the interaction gap and in the retarding field of the bunching space, shifted relative to each other by half the oscillation period.

Further calculation of the convection current is performed in the same way as for a drift klystron. The convection current i_2 entering the resonant cavity from the bunching space is

$$i_2 = I_0 \frac{dt_1}{dt_2} = \frac{I_0}{1 - X \cos \omega t_1} \tag{5.77}$$

provided electron interception by the reflector may be neglected.

Thus, in the general case, the waveform of convection current in a reflex klystron is of the same pattern as in a two-cavity klystron and is shown in Fig. 5.5.

Because of the similarity of equations (5.77) and (5.12), the expansion of current i_2 into a series can be represented by equation (5.20). However, the impossibility of utilizing the higher current harmonics in a reflex klystron of conventional design should be taken into account. Indeed, since one and the same resonant cavity is responsible both for beam bunching (velocity modulation) and energy coupling out of the bunched beam, the external circuit of this cavity

is a practical short-circuit for all other current harmonics except the fundamental. This means that only the fundamental need be taken into account and the instantaneous value of this fundamental is

$$(i_2)_1 = 2I_0J_1(X)\cos[\omega t_2 - (\Theta + \theta)] \tag{5.78}$$

Here the presence of the sum of transit angles $(\Theta + \theta)$ is due to the left-hand side of equation (5.75) acting as the parameter x, defined for a two-cavity klystron by equations (5.14) and (5.17).

The main parameters of a reflex klystron (output power, efficiency, tuning range) will be determined on the basis of the above kinematic calculations; the electronic tuning range mentioned is perhaps one of the most important parameters of this class of devices. One of the most effective techniques of analysis, as with any microwave oscillator, is with the aid of the electron admittance concept.

5.7c. Electron Admittance of the Interaction Gap in a Reflex Klystron

According to the reasoning presented above, the current induced in the resonant cavity and the voltage developed across the gap as a result of the passage of an electron bunch through the gap can be described as

$$i_{ind} = -M \cdot 2I_0J_1(X)\cos[\omega t_2 - (\Theta + \theta)] \tag{5.79}$$

$$u = -V_1 \sin \omega t_2 \tag{5.80}$$

The negative sign in equation (5.79) allows for the reversal of electron motion which takes place in the bunching space; the reason for the minus sign in equation (5.80) was already explained in connection with the choice of an origin for the phase[1].

Equation (5.80) can be rewritten as

$$u = V_1 \cos(\omega t_2 + \pi/2)$$

this form being more convenient for the use of the complex form of currents and voltages. These latter can now be described as

$$\dot{V} = V_1 \exp(j\pi/2)$$

$$\dot{I}_{ind} = -M2I_0J_1(X)\exp[-j(\Theta + \theta)]$$

By using the expressions deduced, determine the complex electron conductance of the gap

$$Y_e = \frac{\dot{I}_{ind}}{\dot{V}} = \frac{2MI_0J_1(X)}{V_1}\exp[-j(\Theta + \theta - \pi/2)] \tag{5.81}$$

---

[1] The choice of any other origin would only have made the comparison of the equations for the reflex and the two-cavity klystrons more complicated.

For convenience of the following calculations, the voltage amplitude V_1 is to be expressed in terms of the bunching parameter X. Applying equation (5.76a) results in

$$V_1 = 2V_0X/M\ (\Theta - \theta) \tag{5.82}$$

Substitution of (5.82) into (5.81) results in

$$Y_e = G_e + jB_e = \frac{M^2I_0}{2V_0}(\Theta - \theta)\,F(X)\exp[-j(\Theta + \theta - \pi/2)] \tag{5.83}$$

where

$$F(X) = \frac{2J_1(X)}{X} \tag{5.84}$$

The function $F(X)$ is shown as a graph in Fig. 5.28.

By equation (5.83) the gap conductance and susceptance prove to be

$$G_e = \frac{M^2I_0}{2V_0}(\Theta - \theta)\,F(X)\sin(\Theta + \theta) \tag{5.85}$$

$$B_e = \frac{M^2I_0}{2V_0}(\Theta - \theta)\,F(X)\cos(\Theta + \theta) \tag{5.86}$$

With fixed values of the accelerating and reflector voltages the value of the bunching parameter X for the design specified is determined only by the amplitude of oscillations V_1. Therefore the graph $F(X)$ of Fig. 5.28 can be considered as actually representing the electron conductance and susceptance of the gap (in relative units) as functions of the radio-frequency voltage across the gap. Thus, the analysis of self-excitation conditions in a reflex klystron can now be performed with the aid of the techniques of Chapter Three.

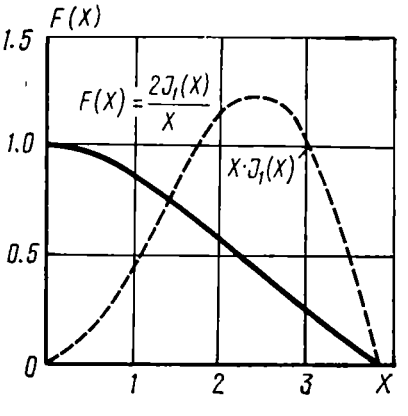

Fig. 5.28. Functions $F(X)$ and $XJ_1(X)$ which determine the electron admittance and electronic efficiency of a reflex klystron

It should be borne in mind that the electron conductance of the gap and the electron susceptance of the gap are implicit functions of frequency, because the transit angles Θ and θ are frequency-dependent. This dependence, however, is not too marked; within a frequency band of several per cent the functions $G_e(\omega)$ and $B_e(\omega)$ can be considered as slowly varying. This particular case corroborates the assumptions of the electron gap admittance being only slightly frequency-dependent, adopted earlier in Section 3.2.

5.7d. Self-Excitation Condition

The necessary, though inadequate, condition of any microwave oscillator being self-excited is the presence of a negative conductance.

According to equation (5.85), the electron conductance is maximum negative value when $\sin(\Theta + \theta) = -1$, hence

$$\Theta + \theta = 2\pi (n + 3/4) \tag{5.87}$$

where n is any integer, including zero.

This relation corresponds to the condition (5.62), which ensures that the electron bunches encounter a maximum retarding microwave field when entering the interaction gap, as can easily be confirmed by multiplying both sides of equation (5.62) by the angular frequency and taking into account the fact that $\omega\tau_{opt} = \Theta + \theta$. Thus, equation (5.87) may be used to determine the middles of the oscillation zones of a reflex klystron. The optimum transit angles from the middle of the interaction gap to the plane of reflection and back prove to be $3\pi/2$; $7\pi/2$; $11\pi/2$ and so on.

The transit angle θ through the interaction gap of a reflex klystron is usually set to be

$$\theta \approx (0.5 - 0.8)\,\pi \tag{5.88}$$

just as in drift klystrons.

This value of the transit angle θ is arrived at as a compromise between the reduction in gap factor M due to an increase in the gap width d, on the one hand, and higher microwave loss and higher equivalent cavity conductance G due to an increase in cavity capacitance as a result of a narrower gap, on the other hand.

The transit angle through the bunching space proves to be well in excess of the transit angle through the interaction gap for all oscillation zones, except $n = 0$. This justifies the neglection of θ in all the above equations and substitution of Θ determined from (5.74) for the sum or difference of these transit angles.

A more detailed examination of self-excitation conditions can be made by analysing the equivalent circuit of a reflex klystron, as of any other oscillator with an oscillatory system of the resonant type (refer to Fig. 3.1). Points *ab* here correspond to the grids of the interaction gap of the klystron; the effects of an alternating component of the convection current may be described by the electron conductance G_e discussed earlier and electron susceptance B_e (refer to the previous Section). The fact that the interaction gap in a reflex klystron carries the d.c. component of the convection current can be allowed for by including into the circuit of Fig. 3.1 of a doubled electron load conductance G_{eL}, as defined by equation (2.63). The double increase in electron load conductance in this case is necessary

since one and the same gap carries the beam with an I_0 d.c. component twice.

By the general criteria of self-excitation (refer to Section 3.1), the necessary and adequate condition for oscillations to build up is that the sum of all the circuit conductances be equal to zero

$$G + G'_L + G_e + 2G_{eL} = 0 \qquad (5.89)$$

In low-power reflex klystrons the electron load conductance G_{eL} may often be considered negligible. For brevity, this magnitude in the following discussion will be omitted, assuming it to be allowed for, in case of need, in the value of the cavity conductance G.

At the edges of the oscillation zones (Fig. 5.27) the power of the radio-frequency oscillations and their amplitude V_1 tend toward zero, and therefore $X \to 0$. In this case $J_1(X) = X/2$ and the function $F(X)$, which determines the electron conductance G_e by equations (5.84) and (5.85), tends to become unity. Thus, the condition of self-excitation (5.89) at the zone edges reduces to

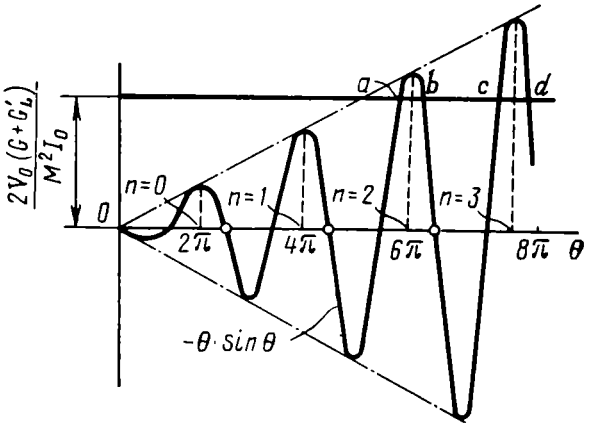

Fig. 5.29. Graphical solution of self-excitation equation for a reflex klystron. Points a, b, c, d correspond to edges of oscillation zones shown in Fig. 5.27

$$-\Theta \sin \Theta = (G + G'_L)\, 2V_0/M^2 I_0 \qquad (5.90)$$

provided the transit angle θ is negligible; G'_L here is the conductance of the external load referred to the plane of the klystron gap (Fig. 3.1).

The solution of equation (5.90) is presented in graphical form in Fig. 5.29, this graph indicating that the width of the oscillation zones measured by the points of zero output power, is a function of the load as well as of the values of the d.c. voltages and beam current. Indeed, the condition of self-excitation is represented in Fig. 5.29 by the points of intersection of a horizontal line with an "involuting" sinusoid, the former describing the right-hand side of equation (5.90) and the latter, the left-hand side of the same equation. The greater the load conductance G'_L, the higher is this horizontal line above the abscissa axis and the narrower (in terms of the transit angle Θ, and, thus, of the reflector voltage) is the oscillation zone. At high values of the total conductance, corresponding to small transit angles Θ, oscillation zones may disappear completely, as is the case for the $n = 0$ and $n = 1$ zones in Fig. 5.29.

The behaviour of the electron conductance as a function of the radio-frequency voltage is determined by $F(X)$; the corresponding graph is presented in Fig. 5.28. As demonstrated in Section 3.1, such a pattern of $G_e = f(V_1)$ corresponds to soft self-excitation and hence there should be no hysteresis effects[1].

5.7e. Oscillatory Power and Electronic Efficiency in Reflex Klystrons

The total radio-frequency power delivered by the electron beam to the resonant cavity and the load under steady-state conditions can be described in terms of the voltage amplitude V_1 and the total conductance G_{tot} of the interaction gap, this latter being

$$G_{tot} = G + G'_L$$

By the common relation, known in electrical engineering, this power is

$$P = 0.5V_1^2 G_{tot}$$

Under steady-state conditions, however, the condition

$$G_{tot} + G_e(V_1) = 0$$

has to be satisfied. Applying equation (5.85) results in

$$P = -0.5V_1^2 G_e = \frac{M^2}{4} V_1^2 \frac{I_0}{V_0} F(X)(\Theta - \theta)\sin(\Theta + \theta)$$

The voltage amplitude V_1 can be described in terms of the bunching parameter X. By equation (5.82)

$$P = -V_0 I_0 \frac{\sin(\Theta + \theta)}{\Theta - \theta} 2XJ_1(X) \tag{5.91}$$

The d.c. power drawn by the klystron from the source of accelerating voltage is $I_0 V_0$. The electronic efficiency of a reflex klystron is readily determined from equation (5.91) as

$$\eta_e = -\frac{\sin(\Theta + \theta)}{\Theta - \theta} 2XJ_1(X) \tag{5.92}$$

The radio-frequency power and the electronic efficiency at the centre of an oscillation zone will be designated as P_1 and η_{e1}, respectively. Applying the condition (5.87) which determines the transit

---

[1] With electrons passing through the interaction gap of a reflex klystron more than twice the function $G_e = f(V_1)$ may cease to be monotonic, in this case a klystron features electronic hysteresis effects, especially at the edges of the oscillation zones, where they are most pronounced.

angle at the centre of an oscillation zone, and neglecting the transit angle through the interaction gap θ, yield

$$P_1 = I_0 V_0 \frac{XJ_1(X)}{\pi (n+3/4)} \tag{5.93}$$

$$\eta_{e1} = \frac{XJ_1(X)}{\pi (n+3/4)} \tag{5.94}$$

Both the output power and the electronic efficiency depend on the product $XJ_1(X)$; this function in graphical form is presented in Fig. 5.28 by a dashed line and goes through a maximum at $X \approx \approx 2.41$. Thus, the maximum electronic efficiency of a reflex klystron by equation (5.94) is

$$\eta_{e\,max.} = \frac{2.41 J_1(2.41)}{\pi (n+3/4)} = \frac{0.398}{n+3/4} \tag{5.95}$$

Calculation of the maximum electronic efficiency by (5.95) yields the following results:

n	0	1	2	3	...	7	...
η_e max., %	53.1	22.7	14.5	10.6	...	5.1	...

The above equations, however, should be applied with a certain amount of discretion, since all the above theory is valid only for the small-signal case, when V_1 is considerably less than V_0. It will be useful to check how this condition is satisfied for various oscillation zones. By equation (5.82) the amplitude V_1 corresponding to the optimum value of 2.41 of the bunching parameter X is

$$V_1 = \frac{0.767 V_0}{M (n+3/4)} \tag{5.96}$$

In case of a unity gap factor M, equation (5.96) for the zero oscillation zone ($n = 0$) yields $V_1 = 1.02\, V_0$, this result being in obvious contradiction with the initial assumption of a small (as compared to the d.c. accelerating voltage) radio-frequency amplitude[1]. At $n = 3$ the amplitude V_1 calculated by (5.96) should be $0.204 V_0$ and at $n = 6$ we have $V_1 = 0.113 V_0$. Thus, the theory presented is not

[1] In any case it is imperative that V_1 should not exceed $V_0/2$ to ensure that the electrons are not stopped and turned back during their second passage through an infinitesimally narrow gap. At the zero oscillation zone this obvious physical requirement is also not met if the theory presented here is applied.

applicable to the case when $n = 0$[1]. The error introduced due to the inaccuracy of the theory presented diminishes with an increase in zone number.

The above calculations reveal two peculiarities of the reflex klystron operation. In contrast to drift klystrons, the electronic efficiency of reflex klystrons turns out to be different for different oscillation zones and decreases with a rise in zone number. Correspondingly, the lower the reflector voltage (in absolute value), the lower is the output power at the zone centre (refer to Fig. 5.27). Furthermore, the maximum electronic efficiency of reflex klystrons proves to be lower than that of drift klystrons (comparatively high value of electronic efficiency at the zero oscillation zone cited above should not be taken into account for the reasons stated above).

These conclusions are not unexpected. The main reason for low electronic efficiency is the use of one and the same interaction gap both to produce velocity modulation of the electron beam and to couple out the energy of the resulting density-modulated beam; both these processes have to take place, therefore, at one and the same magnitude of radio-frequency voltage. At considerable transit angles through the bunching space the amplitude of the microwave voltage has to be kept small and inevitably falls off with an increase in the zone number, this resulting in a lower oscillatory power even under optimum bunching conditions.

In addition to the operating conditions corresponding to maximum electronic efficiency and output power (at $X = 2.41$), consider conditions corresponding to maximum overall efficiency. As usual, the overall efficiency is defined as the product of electronic efficiency by the efficiency of the resonant cavity with regard to the cavity loss. The magnitude of the bunching parameter X can be shown to be slightly less than the optimum value obtained earlier, and the maximum overall efficiency, to correspond to X from 1.84 to 2.41, depending on the conductance of the klystron cavity.

In the above analysis the effect of electron interception by the grids of the interaction gap has been neglected. Actually, with electron beam interception by the gap grids and microwave loss in the cavity taken into account, even at the "optimum" oscillation zones the overall efficiency does not exceed some 1 to 3 per cent. Therefore the reflex klystrons cannot be employed as power oscillators. Such devices would have to operate under extremely difficult thermal conditions, even if the great power drain from the d.c. source could be tolerated.

A low overall efficiency does not, however, prevent their extensive use as sources of low-level microwave power such as local oscillators,

---

[1] Detailed calculations disclose that the maximum electronic efficiency at the $n = 0$ zone is up to 25 per cent.

in measuring gear and so on. The output power of typical reflex klystrons treated in Section 5.9 ranges from dozens of milliwatts to several watts.

5.7f. Starting Current of Reflex Klystrons

The starting current of a reflex klystron oscillator can be determined by applying the general principles of microwave oscillator self-excitation, discussed in Chapter Three. Under the designations adopted here, equation (3.5) becomes

$$(G_e)_{V_1 \to 0} + G + G'_L < 0$$

Substitution of the value of electron conductance under small-signal conditions, as defined by equation (5.85) at $F(X) = 1$, into this relation results in

$$-\frac{M^2 I_0}{2V_0}(\Theta - \theta)\sin(\Theta + \theta) > G_{tot}$$

where $G_{tot} = G + G'_L$.

In case of a reflex klystron oscillator the starting current should be just enough to ensure self-excitation at the zone centres with the most favourable phase of electron arrival into the interaction gap, i.e. when $(\Theta + \theta) = 2\pi(n + 3/4)$. Thus, assuming as earlier Θ to be well in excess of θ, the start-oscillation current $I_{s.o}$ may be determined from the relation

$$I_{s.o} = \frac{V_0 G_{tot}}{M^2 \pi (n + 3/4)} \tag{5.97}$$

The oscillations in a reflex klystron will build up under condition that I_0 exceeds $I_{s.o}$.

On the basis of equation (5.97) certain important conclusions can be drawn. The starting current of such an oscillator is the lower, the lower is the total conductance of the resonant cavity and its load. This starting current proves to be different for various oscillation zones, self-excitation being facilitated with a higher zone number. Finally, the current necessary to provide self-sustained oscillations in a reflex klystron is the lower, the lower the value of accelerating voltage V_0.

Precise calculations of the starting current by equation (5.97) are hampered by the necessity of determining the value of G_{tot}, which can only be roughly found analytically. A numerical example will be useful. The magnitude of G_{tot} in equation (5.97) may be taken as 10^{-4} mho, such an order of magnitude being realizable in actual devices (under no-load conditions and in the absence of an electron-load conductance, klystron cavities ordinarily feature a conductance

in the range from 10^{-4} to 10^{-5} mho). Suppose $V_0 = 300$V, $\theta = 0.7\pi$, this resulting in $M = 0.8$. Substitution of the zone numbers yields:

n	0	1	2	3	...	7	...	10	...
$I_{s.\,o}$, mA	19.4	8.32	5.3	3.88	...	1.88	...	1.35	...

It should be remembered, that the actual values of starting current should be in excess of these calculated values, because the present analysis does not take account of the effect of current interception by the grids as well as certain other effects, impairing the performance characteristics of reflex klystrons. Even under these reservations, the values of starting current prove to be practically acceptable. It is of interest to compare these results with those of a similar calculation for the case of a monotron (Section 3.2*b*). The advantages of reflex klystrons over monotrons as regards the conditions of self-excitation become especially obvious.

Note, that in a reflex klystron the zero oscillation zone is much more difficult to be excited than the other zones with higher zone numbers. Physically this is explained by that the bunching conditions, to be optimum at $n = 0$, require a greater amplitude of the radio-frequency voltage so that a greater amount of microwave power is dissipated in the load. The power given up by the electron beam has, therefore, to be increased so as to maintain the power balance, and this necessitates a heavier electron beam current.

5.8. Electronic and Mechanical Tuning of Reflex Klystrons

In principle, electronic tuning is intrinsic in all microwave oscillators, because variations of the supply voltages inevitably lead to changes of the electron admittance. However, the effect of electronic tuning in reflex klystrons merits a more detailed examination. For a number of reasons, which will be discussed later, the ability of reflex klystrons to be tuned electronically is one of their most valuable features and is of the utmost practical importance.

5.8a. Frequency of Oscillations Under Steady-State Conditions

The dependence of the frequency of steady-state oscillations on the parameters of the resonant cavity and electron beam is determined from the general relation (3.16). Substitution of the conductance and susceptance, as determined by equations (5.85) and (5.86), results in

$$f_{osc} = f_0\left[1 + \frac{1}{2Q_L}\tan^{-1}(\Theta + \theta)\right] \qquad (5.98)$$

At the centre of each oscillation zone the frequency is identical to the natural frequency of the klystron resonant cavity f_0, because here $(\Theta + \theta) = 2\pi\,(n + 3/4)$ and therefore $\tan^{-1}(\Theta + \theta) = 0$. Examine now the change in oscillation frequency produced by the transit angle $(\Theta + \theta)$ deviating from the optimum value within the oscillation zone of a reflex klystron. Assume

$$\Theta + \theta = 2\pi\,(n + {}^3/_4) + \delta\Theta$$

where $\delta\Theta$ is the increment to the total transit angle due to a change in the accelerator voltage V_0 or reflector voltage V_r. In this case equation (5.98) can be presented as

$$f_{osc} = f_0\left(1 - \frac{\tan\delta\Theta}{2Q_L}\right) \qquad (5.98a)$$

For practical use, it is much more convenient to present the oscillation frequency in terms of one of the static voltages applied to the klystron electrodes. Thus, electronic tuning of a reflex klystron can be expressed in terms of the accelerating voltage

$$f_{osc} = f\,(V_0) \text{ at } V_r = \text{const}$$

or reflector voltage

$$f_{osc} = f\,(V_r) \text{ at } V_0 = \text{const}$$

assuming the load and beam current to be invariable.

The method of varying the oscillation frequency by changing the accelerating voltage has a serious disadvantage in that it is accompanied by a considerable power consumption from the source of control signal. Electronic tuning in this case is essentially the same as in two-cavity klystron oscillators; in the following this kind of electronic tuning will not be given any attention, as practically inefficient.

Tuning the klystron frequency by varying the reflector voltage is a much more convenient way, because the reflector current is practically zero, provided the negative reflector voltage is high enough (in absolute value) and this kind of frequency control is therefore accomplished without any power consumption. Consider electronic tuning by varying the reflector voltage in some detail.

Let us examine the variations of the transit angle produced by changing the reflector voltage relative to its value at the centre of the oscillation zone. At the centre of each oscillation zone the transit angle $(\Theta + \theta) = 2\pi\,(n + 3/4)$; the transit angle through the interaction gap θ is independent of the reflector voltage. At $\delta\Theta \ll \Theta$, with (5.74) taken into account,

$$\delta\Theta = \frac{\partial\Theta}{\partial V_r}\,\delta V_r = \frac{\Theta}{V_0 - V_r}\,\delta V_r$$

or

$$\delta\Theta = \frac{2\pi\,(n+3/4)-\theta}{V_0-V_r}\,\delta V_r$$

Ignoring the small value of θ at n greater than zero, by equation (5.98a) we finally arrive at

$$f_{osc} = f_0\left\{1-\frac{1}{2Q_L}\tan\left[\frac{2\pi\,(n+3/4)}{V_0-V_r}\,\delta V_r\right]\right\} \qquad (5.99)$$

Equation (5.99) shows that the oscillation frequency varies within the limits of an oscillation zone following a tangensoidal law; an increase in the absolute value of the reflector voltage (i.e. at a negative δV_r) results in a higher oscillation frequency as illustrated in Fig. 5.30*a*. Physically, such a pattern of the frequency *vs* reflector voltage dependence is easily accounted for by the electron bunches passing through the interaction gap some time before the retarding field is at a maximum, and an increased (in absolute value) reflector voltage thus results in the induced current lagging behind the voltage. In effect this is equivalent to the appearance of an inductive component of the induced current; the frequency, therefore, has to increase.

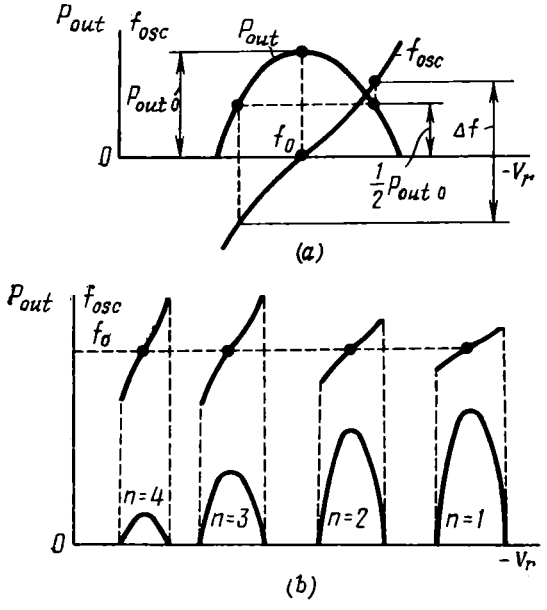

Fig. 5.30. Oscillation frequency *vs* reflector voltage

The physical analogy to this effect is the oscillations of a pendulum when it is pushed slightly before the pendulum weight is in its uppermost position. The frequency of such forced oscillations is known to exceed the natural frequency of pendulum oscillations.

5.8b. Electronic Tuning Sensitivity

A very important parameter of reflex klystrons is the *electronic tuning sensitivity* (also known as the *electronic tuning rate*) on the linear section of the tuning range around the frequency corresponding to the oscillation zone centre. Electronic tuning sensitivity is defined as the rate of change of oscillator frequency per 1 volt of change of the reflector voltage.

At small variations δV_r of the reflector voltage the tangent in equation (5.99) can be replaced by its argument. Designating the relative change in oscillation frequency as δf, by equation (5.99), we have

$$\frac{\delta f}{\delta V_r} = -f_0 \frac{\pi (n + 3/4)}{Q_L (V_0 - V_r)} \qquad (5.100)$$

The maximum tuning sensitivity is obtained at the highest possible zone numbers; with smaller zone numbers the tuning rate falls off, as shown in Fig. 5.30*b*.

Equation (5.100) indicates that the electronic tuning sensitivity of "low-voltage" reflex klystrons, operating with low accelerating and reflector voltages, is higher than that of "high-voltage" devices. Furthermore, the tuning rate is the higher, the higher is the operating frequency and the lower the loaded Q-factor of the klystron cavity. Thus, with a tighter coupling of the klystron cavity to the load, i.e. with an increase in the load conductance G'_L, the electronic tuning sensitivity becomes higher. Remember, however, that this will result in a corresponding change in the output power and the zone width (refer to Section 5.7*d*). The tighter this coupling, the narrower is the oscillation zone $P_{out} = f(V_r)$; with an increase in the tightness of coupling the output power at the zone centre first increases, then goes through a maximum and then gradually falls off, as illustrated in Fig. 5.31.

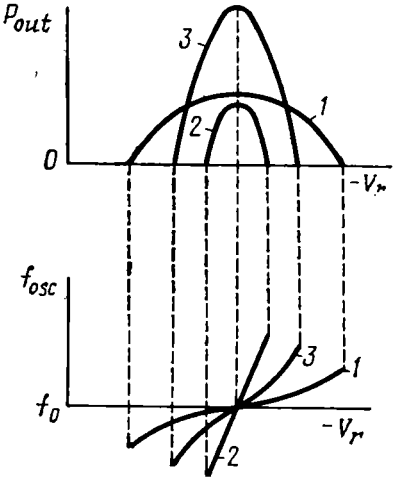

Fig. 5.31. Output power and electronic tuning at one of the oscillation zones of a reflex klystron

1—loose coupling to the load (a high Q_L); *2*—tight coupling (a low Q_L); *3*—intermediate coupling corresponding to maximum output power

The order of magnitude of electronic tuning sensitivity can be illustrated by a numerical example. Assume $V_0 = 300$V, $f_0 = 9375$ MHz and the loaded Q-factor $Q_L = 200$, this being a typical value for actually employed resonant cavities; the reflector voltage will be supposed to correspond to the value calculated in Section 5.7*a* for the case $D = 3$ mm in a 3-cm reflex klystron. Calculations of the tuning sensitivity yield the following results:

n	0	1	2	3	4	5	6	7	8	9
$-V_r$ (V)	4060	1570	890	571	388	268	185	122	74	35
$-\delta f/\delta V_r$ (MHz/V)	0.025	0.138	0.34	0.632	1.02	1.49	2.05	2.70	3.44	4.27

Practice confirms the conclusions arrived at and the results of calculations. The parameters of certain representatives of the class of reflex klystrons are discussed in Section 5.9.

5.8c. Electronic Tuning Range

In a number of practical applications the maximum possible variation of the oscillation frequency within one oscillation zone is of the utmost interest. The fact that these frequency variations are inevitably accompanied by variations of the output power and that usually only a certain part of the zone can be utilized should be taken into account; as a rule, the allowable power variations are confined to 3 dB (i.e. to half the output power at the centre of the oscillation zone). The *range of electronic tuning* is therefore defined as the frequency range of continuous tuning between two points of minimum output power, the reference points being set as half-power points (refer to Fig. 5.30*a*)[1].

Once again equation (5.91) describing the power given up by the electron beam to the resonant cavity, will be examined. The increment to the total transit angle ($\Theta + \theta$), acquired at the half-power points, as compared to the transit angle at the zone centre, will be designated as $\Delta\Theta$. The power delivered by the electron beam at the edges of the tuning range (assuming θ to be negligible as compared to Θ) will then be

$$P_{1/2} = -V_0 I_0 \frac{\sin[2\pi(n+3/4)+\Delta\Theta]}{2\pi(n+3/4)+\Delta\Theta} 2X_{1/2}J_1(X_{1/2})$$

where $X_{1/2}$ is the bunching parameter at the half-power points.

In any case, the increment $\Delta\Theta$ to the transit angle cannot exceed $\pm\pi/2$ and therefore this term can be omitted in the denominator of the latter relation if compared to the transit angle Θ at n exceeding zero. The bunching parameter may also be considered as a function of the oscillation amplitude V_1 only, neglecting the effects of a varying transit angle. Then, by equation (5.76a), at the half-power points

$$X_{1/2} = X_0 2^{-1/2}$$

where X_0 is the bunching parameter at the zone centre.

The equation for the electronic power at the edges of the electronic tuning range acquires the form

$$P_{1/2} = V_0 I_0 \frac{\cos\Delta\Theta}{2\pi(n+3/4)} X_0 2^{1/2} J_1(X_0 2^{-1/2}) \qquad (5.101)$$

[1] These reference points frequently, but not necessarily, correspond to a 3 dB drop in the output power; in some cases the electronic tuning range is evaluated by a reduction in output power by 5 dB, sometimes 1 dB, depending on application requirements.

By equations (5.101) and (5.91) and applying the condition that at the edges of the electronic tuning range the output power drops off by 3 dB, we obtain

$$\cos \Delta\Theta = 2^{-1/2} \frac{J_1(X_0)}{J_1(X_0 2^{-1/2})}$$

Thus, the magnitude of the increment to the transit angle, corresponding to the half-power points at a specified value of the bunching parameter X, is determined. Substitution of this magnitude into equation (5.98) for the electronic tuning range results in (assuming $\delta\Theta = \Delta\Theta$):

$$f_{1,2} = f_0 \left\{ 1 \pm \frac{1}{2Q_L} \sqrt{2 \left[\frac{J_1(X_0 2^{-1/2})}{J_1(X_0)} \right]^2 - 1} \right\}$$

The frequencies f_1 and f_2 correspond to the edges of the electronic tuning range; the difference between these frequencies (i.e. the electronic tuning range) thus proves to be

$$\Delta f = f_2 - f_1 = \frac{f_0}{Q_L} \sqrt{2 \left[\frac{J_1(X_0 2^{-1/2})}{J_1(X_0)} \right]^2 - 1} \qquad (5.102)$$

Equation (5.102) can be somewhat rearranged to present the dependence of the electronic tuning range on the beam current and accelerating voltage in explicit form. The condition of a stationary amplitude at the zone centre yields

$$G_{tot} + G_e = 0$$

$$G_{tot} = \frac{M^2 I_0 (\Theta - \theta)}{V_0} \frac{J_1(X_0)}{X_0}$$

Substitution of the value of G_{tot} in this relation into the equation for the loaded Q-factor of a resonant cavity results in

$$Q_L = \frac{\omega_0 C}{G_{tot}} = \frac{f_0 C V_0}{M^2 I_0 (n + 3/4)} \frac{X_0}{J_1(X_0)}$$

where C is the equivalent capacitance of the resonant cavity. Note that in the general case C is not necessarily equal to the capacitance of the interaction gap, but with toroidal cavities such an equality can safely be assumed.

Substituting the equation for the loaded Q-factor into (5.102) and neglecting the transit angle through the interaction gap, we finally arrive at:

$$\Delta f = \frac{M^2 I_0 (n + 3/4)}{C V_0} \sqrt{\left[\frac{J_1(X_0 2^{-1/2})}{X_0 2^{-1/2}} \right]^2 - \left[\frac{J_1(X_0)}{X_0} \right]^2} \qquad (5.103)$$

Equations (5.102) and (5.103) indicate that the electronic tuning range may be widened by

(1) increasing the beam current I_0 and reducing the operating accelerating voltage V_0 (in other words, using high-perveance guns);

(2) using resonant cavities or other more complicated oscillatory systems with as low loaded Q as practicable and low equivalent capacitance C;

(3) operating at high numbers of oscillation zones.

Some of these recommendations are mutually contradictory. In particular, reduction of the capacitance of the interaction gaps of resonant cavities would call for the use of wider gaps, this would lead to a lower gap factor M or would require an increase in the accelerating voltage V_0. The third recommendation is in obvious contradiction with the requirements of maximum output power and maximum efficiency. The number of the oscillation zone to be used is selected as a compromise between the amount of output power and the range of electronic tuning, depending on which of these two factors is the most important for the particular application in view.

In some applications of reflex klystrons the most important parameter is the linearity of the frequency as a function of the reflector voltage; roughly, the linear part of this dependence can be considered as the electronic tuning range. The lower the loaded Q-factor and the heavier the beam current I_0, the closer does this dependence approximate the ideal linear function.

Consider now the order of magnitude of actually realizable electronic tuning ranges. As was demonstrated in Sections 5.7*d* and 5.7*e*, reflex klystrons operate with maximum efficiency when the bunching parameter is equal to 2.41. In the general case depending on the amount of cavity loss, the bunching parameter value should range from 2.41 to 1.84. With the aid of equation (5.102), the passband of the cavity can be shown to be almost exactly equal to the range of electronic tuning at $X = 1.84$. Setting for example $Q_L = 200$ and $f_0 = 9375$ MHz, the electronic tuning range is found to be about 36 MHz, or less than half per cent of the operating frequency. Thus, electronic tuning cannot completely replace mechanical tuning in reflex klystrons and can only be employed as a means for precise and non-inertial frequency control[1].

Ordinary reflex klystrons commercially available at present feature electronic tuning ranges of about 15 MHz in the 10-cm wave band and 30 to 50 MHz in the 3-cm band. Thus, theoretical predi-

[1] Strictly speaking, under transient conditions the oscillation frequency is not attained instantaneously. Despite the fact that the discussion of transients falls outside the scope of the present treatment, it is obvious that the time required for forced oscillations to be established in a reflex klystron is of the order of magnitude of the ratio of loaded Q-factor to the operating frequency. Thus the time necessary for a process in a reflex klystron to become steady can be neglected in comparison, for instance, with pulse duration of the order of microseconds.

ctions are in fair agreement with the experimental findings in this case. An example of the practical application of electronic tuning is presented in Section 5.10.

Electronic tuning may be a drawback and not only an advantageous feature. Ripples of the d.c. voltage applied to the reflector and accelerating electrode of a reflex klystron produce undesired frequency modulation of the output signal (hum). For instance, a 1 per cent ripple and voltage instability of the reflector voltage source will cause a frequency instability of the output signal of 3.7 MHz (which is ordinarily intolerable) at a 2 MHz/V tuning sensitivity with a —185 V voltage at the zone centre (refer to the numerical example in Section 5.8*b*). High stabilization sources are, therefore, required for the reflex klystrons. In actual practice they are supplied from rectifiers ensuring output voltage stability not worse than 0.1 per cent.

5.8d. Mechanical Tuning Range

The oscillation frequency of a reflex klystron is first of all determined by the oscillatory system, i.e. by the range of the mechanical tuning of the resonant cavity. However, in case of an *external* resonant cavity (refer to Section 5.9) the mechanical tuning range can be made exceedingly wide so that it becomes limited by the electronic effects in the interaction gap and in the bunching space.

The high-frequency limit which is due to a reduction of the gap factor can easily be understood. Indeed, an increase in the operating frequency will cause an increase in the transit angle (at a fixed spacing between the gap grids) and thus a lower interaction coefficient M. By equation (5.85) which contains the cofactor M^2, a rapid decrease in output power is to be expected as the transit angle through the interaction gap θ approaches 2π. At the middle frequency this transit angle is about π. Hence, the highest oscillation frequency should in any case be less than twice the frequency at the middle of the tuning range.

Drift effects in the bunching space also set a limit on possible frequency variations. The total transit angle $(\Theta + \theta)$ should be equal to $2\pi\ (n + {}^3/_4)$ when the klystron operation corresponds to the middle of the oscillation zone. The reflector voltage should be adjusted in such a way as to ensure a maximum output power for any position of the mechanical tuning knob. Indeed, at a lower oscillation frequency the transit angle through the bunching space tends to decrease. For $(\Theta + \theta)$ to be equal to $2\pi\ (n + {}^3/_4) = \text{const}$ the transit time through the bunching space has to be made longer by reducing the reflector voltage (in absolute value). Similarly, at higher oscillation frequencies the middle of the oscillation zone tends toward higher (in absolute values) reflector voltages.

It follows that with a fixed spacing D between the reflector and the grid nearest to it, the range of frequency variation is restricted by the allowable values of the reflector voltage.

Applying equation (5.74a), which determines the transit angle Θ through the bunching space and neglecting the transit angle θ through the gap, the relation describing reflex klystron operation at the centre of an oscillation zone will be

$$\frac{V_r}{V_0} = -\left[\frac{\omega D}{v_0}\frac{2}{\pi\left(n+{}^3/_4\right)} - 1\right] \tag{5.104}$$

Designating the highest and lowest oscillation frequencies as $\omega_{max.}$ and $\omega_{min.}$, respectively, the corresponding reflector voltages $|V_r|_{max.}$ and $|V_r|_{min.}$ by equation (5.104) are related as

$$\frac{\omega_{max.}}{\omega_{min.}} = \frac{1+|V_r|_{max.}/V_0}{1+|V_r|_{min.}/V_0} \tag{5.105}$$

at a fixed value of the zone number, of course.

In any case the minimum reflector voltage should not be zero. To exclude the possibility of appearance of a reflector current, the absolute minimum value of the reflector voltage should at least exceed some 10 to 20 per cent of the accelerating voltage. On the other hand, the maximum absolute value of the reflector voltage is also limited by maintenance considerations (it is highly undesirable to employ high voltages), as well as by deterioration of klystron performance due to distortion of electron trajectories. At considerable reflector voltages electron bunching takes place in the immediate vicinity of the output grid, where the field is far from uniform. The common trend, therefore, is to operate with reflector voltages not in excess (in absolute values) of the accelerating voltage.

Thus, it becomes possible to take approximately

$$|V_r|_{max.} \leqslant V_0; \quad |V_r|_{min.} \geqslant 0.2V_0$$

Based on the above limits, the ratio of the highest to the lowest oscillation frequency by equation (5.105) should not exceed 1.67. In other words, at $n = \text{const}$ the maximum range of mechanical tuning of a reflex klystron constitutes about ± 25 per cent of the middle frequency. The mechanical tuning range of reflex klystrons can be made wider (up to an octave and even more) by changing from one oscillation zone to another[1].

---

[1] An octave corresponds to a frequency ratio of two.

5.9. Problems of Reflex Klystron Design

5.9a. General Considerations

Reflex klystrons designed for the 3 to 5 centimetre and shorter wavelengths as a rule have a resonant cavity mounted inside the vacuum envelope of the tube. At 7 to 10 centimetre wavelengths and longer the "external" design version is more common. The entire design of the tube is governed by the choice between these two possible versions.

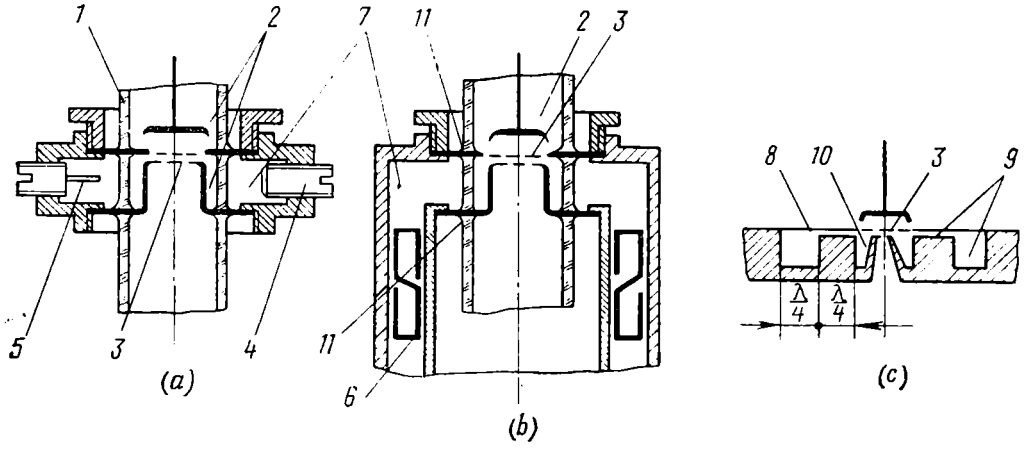

Fig. 5.32. Design of resonant cavities in reflex klystrons with inductive (*a*, *b*) and capacitive (*c*) mechanical tuning

1—glass envelope; *2*—evacuated part of the tube; *3*—grids of the interaction gap; *4*—tuning screw; *5*—tuning vane; *6*—tuning plunger; *7*—part outside the envelope; *8*—elastic membrane; *9*—quarterwave chokes; *10*—main cavity; *11*—disc-seal leads

In case the klystron is designed to operate within a comparatively narrow band of frequencies (about ± 5 to ± 10 per cent of the middle frequency), the resonant cavity is usually of a toroidal configuration or of a cylindrical configuration with a shortening capacitance excited at the E_{010} mode. At wider frequency ranges (of the order of ± 20 per cent and more) the coaxial and rectangular waveguides are employed.

Reflex klystrons may be mechanically tuned by using three different techniques: inductive tuning, capacitive tuning and by means of an additional tunable cavity.

Inductive tuning can be used in cases when the resonant cavity is mounted outside the tube envelope, because in this case it is necessary to provide considerable shifting of the tuning plungers. The klystron is ordinarily provided with disc-seal leads through the glass envelope, and the external cavity is connected to these leads by means of special fasteners. Frequency variation within comparatively narrow limits may be accomplished with the aid of tuning screws inserted

into the cavity; in wideband cavities the tuning is achieved by plungers of the spring-contact or choke types. Examples of the corresponding designs are schematically illustrated in Fig. 5.32*a* and *b*.

Capacitive tuning is accomplished by deformation of an elastic membrane, which forms one of the cavity walls, or by varying the spacing between the grids of the interaction gap itself. Besides the comparatively narrow tuning band obtainable, this kind of tuning arrangement is disadvantageous in that the interaction of the electron beam with the radio-frequency field of the cavity deteriorates when the spacing between the gap grids is varied. Assume, for instance, that the transit angle through the interaction gap is about (0.7-0.8) π at the middle frequency. The capacitance between the grids has to be reduced, i.e. the spacing between them has to be increased, to produce a frequency shift toward higher values. Even if the operating frequency were to remain unaltered, a greater spacing between the grids would result in a greater transit angle. With this kind of capacitive tuning, therefore, the rate of deterioration of the gap factor with an increase in operating frequency is higher than in case the spacing between the gap grids remains constant. As a result there is a rapid decrease in the output power as the frequency is shifted into the shortwave part of the tuning range.

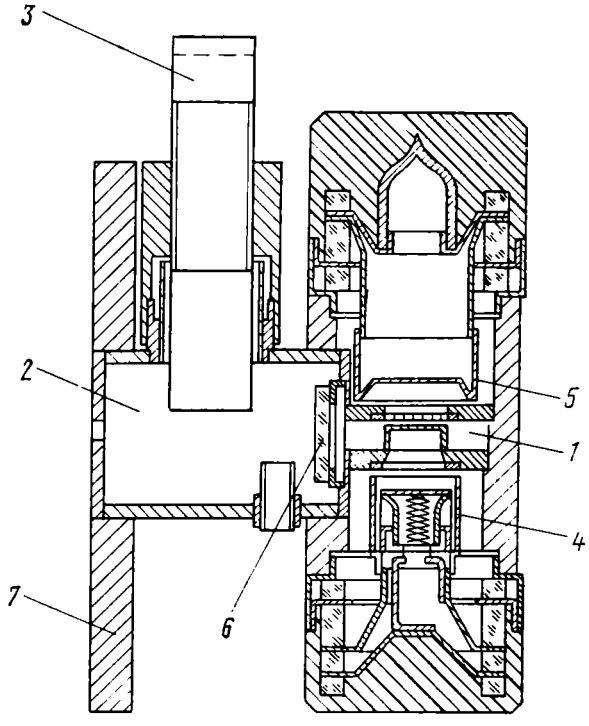

Fig. 5.33. Reflex klystron with idler tunable cavity

1—"active" toroidal cavity; *2*—"passive" (idler) rectangular waveguide cavity; *3*—tuning stub; *4*—electron gun; *5*—reflector; *6*—vacuum-tight window; *7*—output waveguide flange

At very short wavelengths the geometrical dimensions of toroidal cavities become inconveniently small and it becomes very difficult (if not altogether impossible) to make the elastic membrane which should provide the required mechanical variations of the spacing between the gap grids and at the same time retain adequate mechanical properties. Reflex klystrons designed for the millimetric band, therefore, employ a capacitive tuning arrangement schematically illustrated in Fig. 5.32*c* in which quarterwave chokes of the radial-

line type provide a considerable increase of the elastic membrane diameter.

The frequency stability and vibration strength of reflex klystrons can be improved by coupling an additional tunable "passive" cavity (sometimes termed the idler cavity) to the main ("active") cavity of the klystron, this latter not being equipped in this case with any kind of tuning arrangement. A klystron of this kind is shown in Fig. 5.33. Here the tuning element is a metal stub which is inserted into the idler cavity mounted outside the vacuum envelope of the tube.

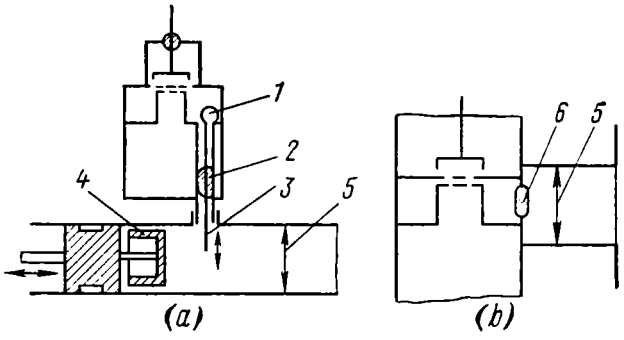

Fig. 5.34. Coaxial-to-waveguide (*a*) and waveguide (*b*) power outputs for reflex klystrons

1—coupling loop; *2*—vacuum-tight seal in coaxial line; *3*—exciting probe in waveguide; *4*—adjusting plunger; *5*—narrow wall of waveguide; *6*—non-resonant coupling aperture

The power output is an inherent element of the klystron design if the resonant cavity is completely enclosed in the vacuum envelope. With "external" resonant cavities the power output assembly can be of various designs, depending on application requirements, for one and the same klystron tube.

One of the most often used is the coaxial power output terminating in a coupling loop which is introduced into the inductive portion of the cavity. This kind of design is often used to excite rectangular waveguides; in this case the central conductor of the coaxial line is passed into the waveguide and functions as an exciting probe (Fig. 5.34*a*). The dimensions of the coupling loop and its location determine the tightness of coupling to the load and, thus, the transformation of the load admittance and the values of the loaded and external Q-factors of the resonant cavity. Ordinarily, the power output arrangement is designed to deliver a maximum amount of power to a matched load; in this case the loaded Q of the klystron cavity should be about 200 to 300.

At wavelengths shorter than some 2 to 3 cm waveguide power outputs are the most suitable; this design is illustrated in Fig. 5.34*b*

(refer also to Fig. 5.33). The butt end of the cavity terminates in a waveguide of rectangular cross section, which supports the H_{10} propagation mode. A vacuum-tight seal is obtained with the aid of a glass, ceramic or mica window.

5.9b. Typical Designs and Parameters of Reflex Klystrons

The main parameters of several typical reflex klystrons are presented in Table 5.3.

A typical reflex klystron with removable external cavities is a 10-cm klystron with a glass envelope, provided with disc-seal leads of the gap grids (No. 1 in the Table). This klystron is schematically shown in Fig. 5.32*a* and *b*; its external appearance is shown in Fig. 5.35*a*. Similar designs prove to be advantageous at wavelengths ranging from about 5-7 cm to 30-50 cm.

Table 5.3

Parameters of Typical Reflex Klystrons

No.	Klystron type	Operating frequency range, GHz	Output power, mW	V_0, V	I_0, mA	$-V_r$, V	Electronic tuning range, MHz	Rate of electronic tuning, $\frac{\text{MHz}}{\text{V}}$	Number of operating zone
1	Glass 10-cm klystron with external cavity (Fig. 5.35*a*)	1.15-3.75	80-140	300	30	110-230	20	0.60-0.85	2 or 3
2	Metal 3-cm klystron with internal cavity (Fig. 5.35*b*)	8.5-9.6	20-30	300	25	130-185	55	2.2	6 or 7
3	Metal 7.5-cm klystron of increased power	3.5-4.3	2700	750	80	800	20	0.09	—
4	Metal klystron of millimeter wave band	48-60	15-30	600	25	150-450	60-180	—	4 or 5

A typical 3-cm reflex klystron (No. 2 in the Table) is of the all-metal kind, its external appearance is illustrated in Fig. 5.35*b*. This klystron is equipped with a coaxial power output assembly designed for capacitive excitation of waveguides of rectangular cross section, as shown in Fig. 5.34*a*. The depth of insertion of the probe into the waveguide and the spacing between the probe and the butt end of the waveguide are adjusted so as to obtain klystron matching to the load. Klystrons of this kind are provided with capacitive mechanical tuning arrangements, but their relative tuning range is considerably narrower than that of glass klystrons with external cavities, that are inductively tuned.

A reflex klystron with a waveguide power output and an idler tunable cavity is illustrated in Fig. 5.35*c*.

Recently the trend has appeared to develop reflex klystrons with output powers of the order of watts (instead of scores and hundreds of milliwatts, considered as typical for the common klystrons discussed formerly); the parameters of one such klystron are given in Table 5.3 (No. 3).

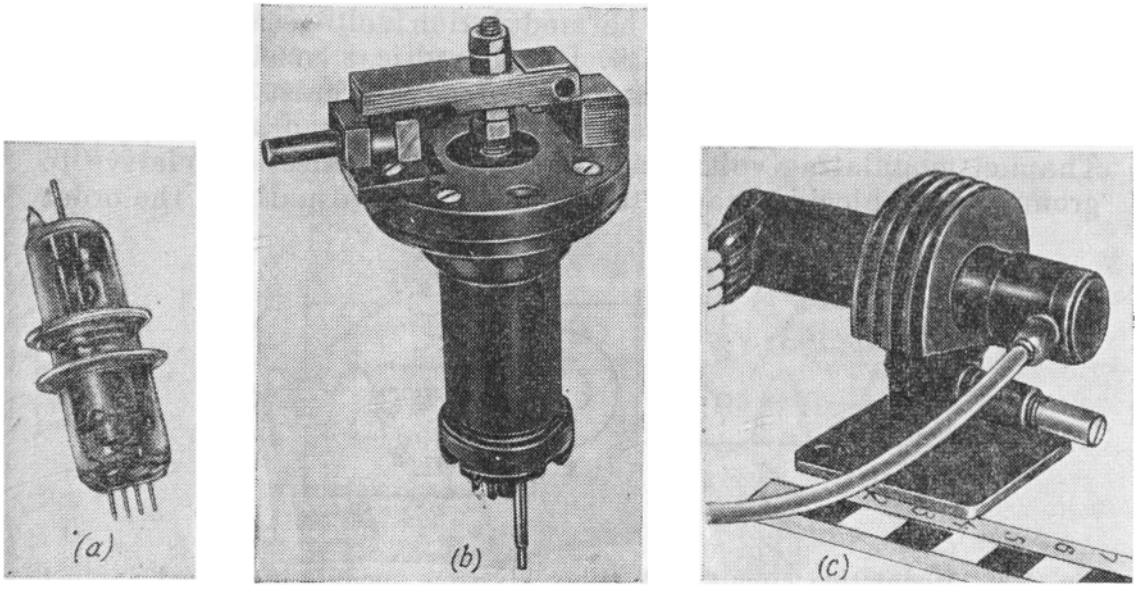

Fig. 5.35. Typical reflex klystrons

(*a*) glass 10-cm klystron (external resonant cavity removed); (*b*) metal 3-cm klystron with capacitive mechanical tuning; (*c*) 3-cm klystron with waveguide output (mechanical tuning with the aid of an idler cavity)

The development of reflex klystrons for the millimetric wave band is of considerable interest. A typical device of this group of reflex klystrons is cited in the same Table. A still further increase in the operating frequency calls for the manufacture of miniature resonant cavities with grids of inconveniently small dimensions (it should be remembered that the cavity diameter with the shortening effect of the grid capacitance taken into account should be less than half the free-space wavelength). Certain difficulties are encountered in the manufacture of other elements of the klystron tube, in particular, in the design of electron guns capable of providing extremely high current densities (up to 30 A/cm^2 and more) in thin electron beams. The shortest wavelength obtained at present with the aid of reflex klystrons is about 1.5 mm.

5.10. Application of Reflex Klystrons

5.10a. Amplitude and Frequency Modulation in Reflex Klystrons

The most convenient and, therefore, most extensively used method of modulating the output signal of a reflex klystron is by varying the reflector voltage since this electrode draws practically no current. The accelerating voltage and the beam current in this case remain invariable.

The simplest circuit with the modulation voltage applied to the reflector is shown in Fig. 5.36. From practical considerations the accelerating electrode and the resonant cavity must be connected directly to ground; to both these electrodes a d.c. voltage is applied. The a.c. modulating voltage is applied to the reflector (relative to ground) via a blocking capacitor C. Resistor R (usually of the order

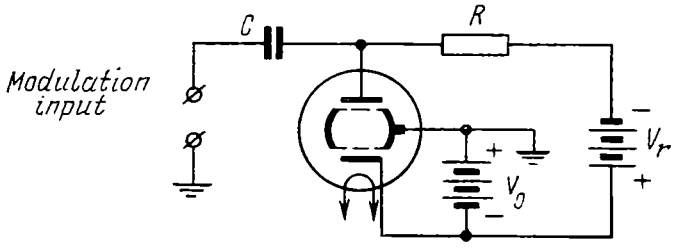

Fig. 5.36. Modulation circuit of a reflex klystron (modulating signal applied to the reflector)

of 50 to 100 kohm) prevents the supply of modulating voltage from being excessively loaded by the reflector voltage source, while capacitor C blocks the d.c. voltage from appearing at the modulating voltage source. The magnitude of this capacitance is selected with due regard for the frequency and waveform of the modulating voltage; the source of modulating signal and the reflector voltage source turn out to be connected in series.

Graphs, illustrating the performance of reflex klystrons with various kinds of modulation are presented in Fig. 5.37 (transients are not treated in the present discussion). As can be easily noted, amplitude modulation of the output signal will not be accompanied by frequency modulation only if the modulating voltage waveform is strictly rectangular (meander). The amplitude of the modulating voltage and the d.c. voltage have to be adjusted so as to ensure that the klystron oscillate only at the peaks of the modulating signal; with too small amplitudes the klystron will oscillate at two points corresponding to one and the same oscillation zone, while at too great

amplitudes "jumping" from one oscillation zone to another becomes possible. In both cases the klystron will oscillate at two frequencies, which is ordinarily highly undesirable.

Pulse modulation by rectangular pulses differs from meander modulation only by the pulse duty factor (with meander modulation the duty factor, i.e. the ratio of average pulse duration to the average pulse spacing or, what is the same, with strictly rectangular pulses—the ratio of average output power to peak power, is 1/2, provided the modulating meander is a symmetrical one). Amplitude modulation by a sinusoidal signal is undesirable.

Generally speaking, frequency modulation of the output signal is inevitably present with any waveform of the modulating signal except the strictly rectangular one. In case frequency modulation should be accompanied by the smallest possible distortions, the range

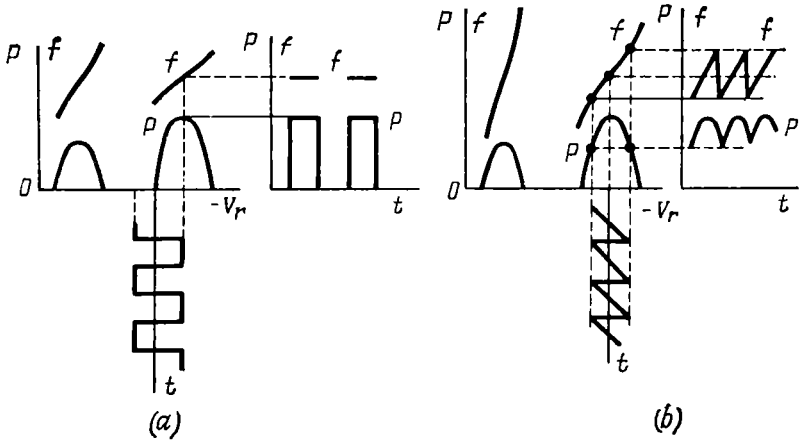

Fig. 5.37. Amplitude (*a*) and frequency (*b*) modulation of a reflex klystron

of modulating voltage values has to be restricted to the linear section of the electronic tuning curve. The same condition will keep the accompanying amplitude modulation to not more than 3 dB. In this case a modulating signal of any waveform may be employed, not necessarily the saw-tooth pattern of the modulating voltage shown in Fig. 5.37*b*.

The frequency of the modulating signal can vary within extremely wide limits, from audio frequencies up to scores of megahertz. The limit to increasing the modulating frequency is set by transients in the reflex klystron.

All the three kinds of modulation mentioned—amplitude by a symmetrical meander, pulse and frequency—are widely employed in actual microwave equipment. Sometimes other kinds of modulation

are used, such as pulse modulation of the accelerating voltage. This kind of modulation allows of increasing significantly the output pulse power at a constant value of the average output power.

5.10b. Applications of Reflex Klystrons

The main advantages of reflex klystrons over other types of low-power microwave oscillators are that they are simple in design and are easily tuned. They feature good modulation characteristics and provide electron tuning that does not require any power consumption. Besides, they are highly reliable and mechanically rigid.

The most typical application of reflex klystrons is as local oscillators in microwave receiving equipment and as microwave low-power sources in measuring gear, used at the laboratory research and development stages as well as for testing microwave equipment. The use of reflex klystrons in radio relay equipment, radio-navigation and television as low-power transmitters, as well as sources of pump signal for microwave parametric amplifiers, should also be mentioned.

The power required for proper performance of crystal mixers is ordinarily about 20 mW. It is just this or somewhat higher output power that is characteristic for most reflex klystrons (No. 2 in Table 5.3).

A very important parameter of oscillator tubes is the level of inherent noise generated at Doppler frequencies and at frequencies removed from the carrier by the value of the intermediate frequency (in microwave receivers this latter ordinarily amounts to some scores of megahertz). Local oscillator noise may exert a marked effect on the overall characteristics of a microwave receiver, noticeably deteriorating the receiver sensitivity. A typical value of the noise generated by modern reflex klystrons at frequencies removed from the carrier frequency by 10 to 100 MHz is about 165 to 175 dB/Hz of bandwidth.

In measuring equipment applications the output power of reflex klystrons is required to be somewhat higher than in local oscillator applications, usually, it is about some hundreds of milliwatts. Finally, the output power of reflex klystrons designed for use in radio relay transmitters is of the order of several watts (refer to No. 3 in Table 5.3).

Reflex klystrons are among the mass-produced microwave tubes. Nevertheless, in the immediate future they are expected to become competitive with the rapidly developing solid state microwave oscillators, namely transistor oscillators with frequency multipliers, Gunn oscillator diodes, avalanche diodes and the like. The great advantage of these solid-state devices is the low supply voltage value and, as a result, reduced weight and dimensions, as well as high anticipated reliability. At the same time, reflex klystrons feature a lower noise level (one or two orders of magnitude lower than that of solid-state

devices mentioned) and a number of other advantages which are due to such factors as simplicity of tuning, frequency range and so on.

It may safely be stated that the problem of choice between a reflex klystron and a solid-state device as the microwave power source for this or that application will to a great extent be influenced by the type of equipment, in which the oscillator in question is to be employed. Advances in solid-state technique also provide an additional impetus to research and development aimed at improving the parameters and characteristics of reflex klystrons.

CHAPTER SIX

TRAVELLING-WAVE TUBES

6.1. General Problems. Principle of Operation of O-Type TWT

In a broad sense, the mechanism underlying the performance of amplifier and oscillator devices of the travelling-wave type is the prolonged interaction of an electron beam with an electromagnetic wave propagating along an oscillatory system of the non-resonant type. Thus, the basic difference between travelling-wave devices and other kinds of microwave devices (such as triodes, klystrons and magnetrons) is the non-resonant character of the oscillatory system. It was demonstrated in Sections 2.4*d*, 2.8*d* and 3.4 that in travelling-wave tubes the same electronic effects as in other kinds of microwave amplifier and oscillator devices take place, namely: electron bunching and the transfer of energy acquired by the electron beam from a static electric field to a microwave field. In this respect there is a strong similarity between magnetrons (treated in Chapter Seven) and travelling-wave tubes.

The great advantage of travelling-wave tubes as amplifier devices is their *wideband characteristics*. Indeed, in all microwave amplifier devices with resonant oscillatory systems the operating bandwidth is limited by the magnitude of the loaded Q-factor of the cavity or the system of cavities. This basic restriction is obviously lifted in devices utilizing non-resonant oscillatory systems. The same property manifests itself in devices with prolonged interaction, when they are used as microwave oscillators: their main advantage is a *wide range of electronic tuning*, that is considerably wider than that obtained with most oscillators of the resonant type.

If prolonged interaction of electrons with the field of an electromagnetic wave is to be obtained, the condition of *phase synchronism* has to be satisfied, i.e. the velocity of the electrons in the beam v_0 has to be made approximately equal to the phase velocity of the electromagnetic wave v_p

$$v_0 \approx v_p \tag{6.1}$$

At the same time it is taken that the direction of electron movement coincides with that of the phase velocity of the wave. Condition (6.1) is easily obtained from Figs 2.13, 2.31 and 2.32 of Chapter Two,

which illustrate non-resonant elements for velocity-modulating an electron beam and coupling out the energy of a bunched beam in a travelling-wave field.

Since electron velocities are always lower than the speed of light in free space, condition (6.1) presupposes the phase velocity of the travelling wave, which interacts with the electron beam, to be also lower than c. This means that the electrons of the beam have to move in the field of a *slowed down* electromagnetic wave. In most travelling-wave tubes special slow-wave structures, wave-guiding systems, meeting the requirement that $v_p < c$, are used. Typical values of the c/v_p ratio range from 2 to 50.

The field of periodic slow-wave structures is known to contain an unlimited number of simultaneously present forward and backward *spatial harmonics*, characterized by different phase velocities and propagating along the structure in opposite directions—in the direction of electromagnetic energy transfer and opposite to it. By properly selecting electron velocity v_0 and the direction of electron movement it is possible to satisfy condition (6.1) for one of the spatial harmonics. Thus, the electron beam can be made to interact with the *forward* or *backward* spatial harmonic of interest[1].

Electron devices, in which the electron beam is intended to interact with the fundamental forward slow wave or the positive spatial harmonic, are termed *forward-wave travelling-wave tubes* or simply *travelling-wave tubes* (abbreviated usually as TWT), though all devices of the type under discussion should in a broad sense of the term be called travelling-wave tubes. Devices in which the desired effect is interaction of the electron beam with one of the negative spatial harmonics (with backward waves, in other words) have been developed somewhat later and are conventionally known as *backward-wave oscillators* (BWO).

A distinguishing feature of forward-wave tubes is the coincidence of the directions of electron beam movement and energy transfer along the slow-wave structure. In backward-wave tubes the electron beam moves in a direction opposite to that of microwave energy transfer; these peculiarities determine the arrangement of the microwave signal input and output: in forward-wave tubes the signal output is placed on the side of the collector, while in backward-wave devices the signal output is at the end of the slow-wave structure facing the electron gun (refer to Fig. 2.13).

Forward-wave and backward-wave tubes are subdivided into two main groups, depending on the direction and designation of the static magnetic field. The first of these groups is conventionally termed

[1] Note, that these forward and backward waves (spatial harmonics) should in no case be confused with the *incident* and *reflected* waves that propagate in any transmission line and correspond to two energy streams, those transferred from the generator to the load and in the opposite direction.

O-type devices, they utilize a *longitudinal* static magnetic field, which is intended only to provide focussing of the rectilinear electron beam. The function of this field is similar to that in amplifier klystrons discussed in Chapter Five. That is why klystrons are classed with O-type devices along with TWT's and BWO's. The second group of devices, known as *M-type* TWT's and BWO's, utilizes a *transverse* static magnetic field. In M-type devices electrons move in crossed static electric and magnetic fields, just as in common magnetron oscillator tubes. TWT's and BWO's of the M type are treated in Chapter Seven, where crossed-field devices are examined[1].

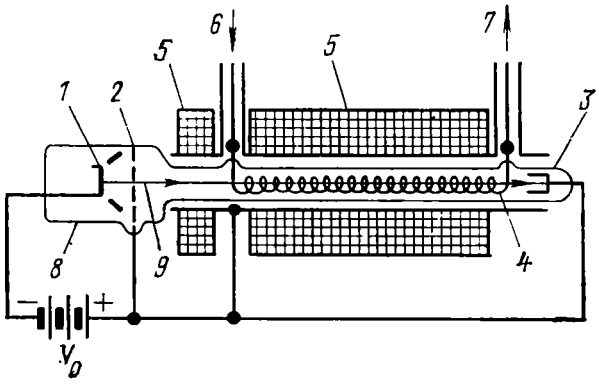

Fig. 6.1. Design of an O-type amplifier TWT in a coaxial fixture

1—cathode; *2*—accelerating electrode; *3*—collector; *4*—helix; *5*—solenoid; *6*—input; *7*—output; *8*—glass envelope; *9*—electron beam

The most typical representative of the class of travelling-wave devices is the O-type amplifier TWT, schematically illustrated in Fig. 6.1. This particular tube features a helical slow-wave structure with a coaxial input and output. The required synchronism of electron movement with the propagation of the slow wave is provided by an accelerating voltage V_0; the radio-frequency wave is slowed down to a velocity of about 0.1 c. Energy transfer along the slow-wave structure is in the same direction as electron beam movement. The electron beam is focussed by a static magnetic field produced by a solenoid; this field is directed along the device axis, as is often the case in amplifier klystrons.

The initial part of the helical slow-wave system functions as an element providing velocity modulation of the electron beam, as shown in Figs 2.31 and 2.32. Electron bunches are formed as the beam moves along the tube axis, these bunches in turn inducing current in the helix and thus developing a retarding radio-frequency field. Signal amplification and transfer of energy from the electron beam are provided due to this retarding microwave field. Thus, the general idea of the TWT design is the same as of any microwave amplifier (as outlined in Fig. 2.15), notwithstanding the absence of strictly defined regions of electron beam bunching and energy transfer.

The condition determining the maximum gain of a TWT with a

[1] The "O" and "M" designations of electron devices with longitudinal and transverse static magnetic field are borrowed from French terminology.

helical slow-wave structure as a function of the accelerating voltage V_0 (refer to Fig. 6.1) can be obtained from the following elementary train of reasoning. The c/v_p ratio of the wave propagating along the slow-wave system as a first approximation can be considered equal to the ratio of helix turn length to pitch. Designating the mean radius of the helix as a, the phase velocity of the fundamental slow-wave can be described as

$$v_p = c \frac{p}{\sqrt{(2\pi a)^2 + p^2}} \approx c \frac{p}{2\pi a} \tag{6.2}$$

where p is the helix pitch. This relation can also be presented as

$$v_p = c \sin \psi \tag{6.2a}$$

where ψ is the pitch angle defined as

$$\sin \psi = \frac{p}{[(2\pi a)^2 + p^2]^{1/2}}$$

The electron beam velocity v_0 is determined by the value of the accelerating voltage V_0 and, with the relativistic effects neglected, is

$$v_0 = (2eV_0/m)^{1/2} \tag{6.3}$$

The optimum accelerating voltage $(V_0)_{opt}$ may be determined from equations (6.2) and (6.3) by the condition of synchronism $v_0 \approx v_p$

$$(V_0)_{opt} = \frac{mc^2 p}{8\pi^2 e a^2} \approx 0.65 \cdot 10^4 (p/a)^2 \tag{6.4}$$

This equation does not allow for the effects of dispersion, which are present in the slow-wave structure of the helical type, as well as for the effects of the dielectric supports of the helix, both of these factors affecting the phase velocity. Nevertheless, equation (6.4) can be used to evaluate approximately the operating accelerating voltage of a travelling-wave tube. Thus, in case of $a = 2$ mm and $p = 1$ mm, $(V_0)_{opt}$ proves to be 1625 V.

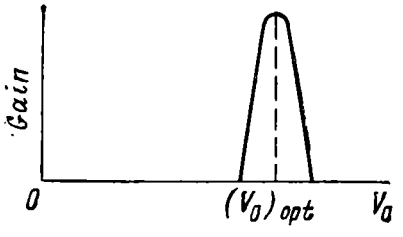

Fig. 6.2. Dependence of the gain of an O-type TWT on the accelerating voltage at fixed frequency

The TWT gain as a function of the accelerating voltage V_0 is qualitatively illustrated in Fig. 6.2. The maximum of this curve corresponds to the optimum accelerating voltage defined by equation (6.4). The dependence of this kind was borne out by experiment, at least under small-signal operating conditions. Any change in the magnitude of $(V_0)_{opt}$ tending to disturb the condition of synchronism will cause a decrease of the output power.

Among devices with prolonged interaction and non-resonant oscillatory systems, travelling-wave tubes of the O-type are most numerous and most widely used, both as small-signal (input) and power amplifiers.

6.2. Small-Signal Theory of O-Type TWT Amplifier

6.2a. Basic Conceptions

Consider the interaction of a slow electromagnetic wave with a rectilinear electron beam moving along the axis of this system at approximately synchronous velocity (Fig. 6.3), without reference to any particular type of slow-wave system.

Several simplifying assumptions will be made. First of all, the discussion will be restricted to the case of small radio-frequency amplitudes, this being the method universally adopted in the analysis of various kinds of microwave devices. For the present case, small-signal conditions will be defined as those at which all the alternating (radio-frequency) magnitudes characterizing the electron beam (such as electron velocities, space charge density, beam convection current) are much less than the d.c. components of the corresponding quantities.

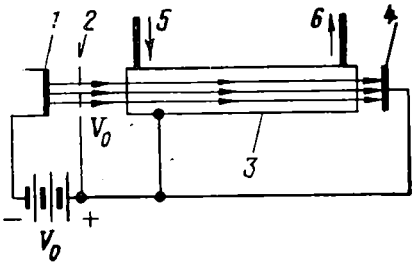

Fig. 6.3. General circuit of an O-type amplifier of the forward travelling-wave kind

1—cathode; *2*—accelerating electrode; *3*—slow-wave structure; *4*—collector; *5*—input; *6*—output

Only the axial movement of electrons through the tube will be taken into account, assuming that any transverse motion of electrons can be eliminated with the aid of a longitudinal static magnetic field of adequate strength. Other simplifying assumptions such as negligible spread in electron velocities, negligible effects of mutual electron repulsion in the space charge, negligible relativistic effects and quantum theory relations are also implied. "Cold" microwave loss in the slow-wave system and interception of part of the electron beam by the slow-wave structure will also be neglected for the time being.

Variations of the radio-frequency field across the transverse section of the electron beam will not be taken into account. To meet this condition, an electron beam in the form of vanishingly thin hollow pipe has to be postulated, if the slow-wave structure employed is a cylindrical one. In case of a flat slow-wave system the electron beam should be in the form of a thin flat strip to make the effect of these variations negligible.

Under the conditions adopted the electron beam velocity and the space charge density in any section of the beam may be described in terms of the respective d.c. and radio-frequency components

$$v = v_0 + v\,(z,\ t);\quad \rho = \rho_0 + \rho\,(z,\ t)$$

where the quantities with zero subscripts characterize the static electron beam (i.e. in the absence of a radio-frequency signal) and are independent both of time and displacement along the z axis of the tube.

Suppose the radio-frequency components of the electron velocity and space charge to be described as travelling waves

$$v\,(z,\ t) = v_1 \exp\,(j\omega t - \Gamma z) \tag{6.5}$$

$$\rho\,(z,\ t) = \rho_1 \exp\,(j\omega t - \Gamma z) \tag{6.6}$$

with the amplitudes v_1 and ρ_1 being smaller by far than v_0 and ρ_0, respectively.

The propagation constant Γ in equations (6.5) and (6.6) in the general case can be a complex quantity and may differ from the propagation constant Γ_0 along the "cold" slow-wave structure due to the effect of the electron beam. A similar approach to the problem of space charge waves, seeking the solution in the form of travelling waves, was already used earlier (Section 2.9).

In a slow-wave structure, the longitudinal radio-frequency field interacting with an electron beam also takes the form of a travelling wave. This field has to be *self-matched*, i.e. the influence of this field on the electron beam should produce such changes in electron movement that the currents induced by electron movement cause exactly the same field pattern; the wave propagation constants in the slow-wave structure and the electron beam, therefore, must be identical. Thus, the radio-frequency longitudinal field of the system may be presented as

$$E_z = E_{zm} \exp\,(j\omega t - \Gamma z) \tag{6.7}$$

The problem of interaction between a travelling electromagnetic wave and an electron beam will be considered in two stages. First, electron bunching under the action of a travelling wave will be examined, disregarding the changes caused in the system by the presence of an electron beam. After this, the process of exciting an electromagnetic wave in a slow-wave structure by the passage of a density-modulated electron beam along its axis will be discussed. The effects taking place in an amplifier travelling-wave tube can then be evaluated by simultaneously allowing for both these processes, the ultimate aim being the calculation of TWT gain under small-signal conditions.

6.2b. Electron Bunching Under the Action of a Travelling Wave

Electrons moving along the slow-wave structure by inertia forces are affected by the longitudinal component E_z of the radio-frequency field. Considering electrons as points of negative charge, the common electron dynamics equation yields

$$m\frac{dv}{dt} = -eE_z \tag{6.8}$$

Applying the rules for differentiating a function of several variables and taking into account relation (6.5) we obtain

$$\frac{dv}{dt} = \frac{\partial v}{\partial t} + \frac{\partial v}{\partial z}\frac{dv}{dt} = j\omega v_1 \exp(j\omega t - \Gamma z) - \\ - \Gamma v_1 \exp(j\omega t - \Gamma z)\cdot[v_0 + v_1 \exp(j\omega t - \Gamma z)]$$

Omitting the product of small quantities yields

$$\frac{dv}{dt} = (j\omega v_1 - \Gamma v_1 v_0)\exp(j\omega t - \Gamma z)$$

Thus, equation (6.8) which describes electron movement can be used to determine the radio-frequency component of the electron velocities in the beam as

$$v_1 = \frac{eE_{zm}}{mv_0\left(j\frac{\omega}{v_0} - \Gamma\right)} \tag{6.9}$$

The density of the electron beam convection current in the presence of a travelling wave can now be determined: the current density J can be calculated as the product of the space charge density by the electron velocity. Neglecting the product of small quantities (radio-frequency components) and allowing for (6.5) and (6.6) result in

$$J = \rho_0 v_0 + (\rho_0 v_1 + \rho_1 v_0)\exp(j\omega t - \Gamma z) \tag{6.10}$$

Thus, the radio-frequency component of the convection current in the beam is

$$J(z, t) = (\rho_0 v_1 + \rho_1 v_0)\exp(j\omega t - \Gamma z) = \\ = J_1 \exp(j\omega t - \Gamma z) \tag{6.11}$$

where J_1 is the amplitude of the convection current density

$$J_1 = \rho_0 v_1 + \rho_1 v_0 \tag{6.12}$$

The magnitude of v_1 was already determined and is described by equation (6.9). Thus, the convection current can be determined if the radio-frequency component of the space charge density ρ_1 is known.

Up till now we have not used in the calculations the law of charge continuity, discussed in Chapter Two. In the case in question the equation of continuity (2.13), taking into account the uni-dimensional character of electron movement, may be written as follows

$$\frac{\partial J}{\partial z} = -\frac{\partial \rho}{\partial t}; \quad -\Gamma J_1 \exp(j\omega t - \Gamma z) = -j\omega \rho_1 \exp(j\omega t - \Gamma z)$$

whence

$$\rho_1 = -j\frac{\Gamma}{\omega} J_1 \tag{6.13}$$

Substitution into relation (6.12) of the quantities ρ_1 and v_1 determined from equations (6.13) and (6.9), taking into account that $v_0^2 = 2eV_0/m$, results in

$$J_1 = -j\frac{\rho_0 v_0 \omega / v_0}{2V_0\left(j\frac{\omega}{v_0} - \Gamma\right)^2} E_{zm} \tag{6.14}$$

The quantity ω/v_0 in this equation has the dimension of a phase constant of a wave moving with a v_0 velocity; in what follows it will be termed the electron phase constant β_e and defined as

$$\beta_e = \omega/v_0 \tag{6.15}$$

According to equation (6.10) the quantity $\rho_0 v_0 = J_0$ represents the d.c. component of the current density in the electron beam. Therefore, the equation for the radio-frequency component of the convection current density in its final form will be

$$J_1 = -j\frac{J_0 \beta_e}{2V_0 (j\beta_e - \Gamma)^2} E_{zm} \tag{6.16}$$

Hence, the amplitude of the convection current may be obtained by taking into account the area of the beam transverse section

$$I_1 = -j\frac{I_0}{2V_0}\frac{\beta_e}{(j\beta_e - \Gamma)^2} E_{zm} \tag{6.17}$$

where I_0 is the d.c. component of the electron beam current. The convection current of the electron beam can be written in complex form as

$$I_{con} = I_1 \exp(j\omega t - \Gamma z) \tag{6.18}$$

Equations (6.17) and (6.18) may be considered as describing the action of a longitudinal radio-frequency field on the convection current of an electron beam, if the reverse effect of the electron beam on the field of this wave travelling in the slow-wave system is neglected.

6.2c. The Influence of a Density-Modulated Electron Beam on the Field in a Slow-Wave Structure

Electron bunches moving along a slow-wave structure induce radio-frequency currents in the latter. This induced current is superimposed onto the current of the travelling wave, propagating along the slow-wave system, bringing about a change in the intensity of the field of this wave.

The equivalent circuit of a slow-wave structure is presented in Fig. 6.4*a*. The actual system is presented here as a uniform dissipationless transmission line with ideal gaps, the properties of this line

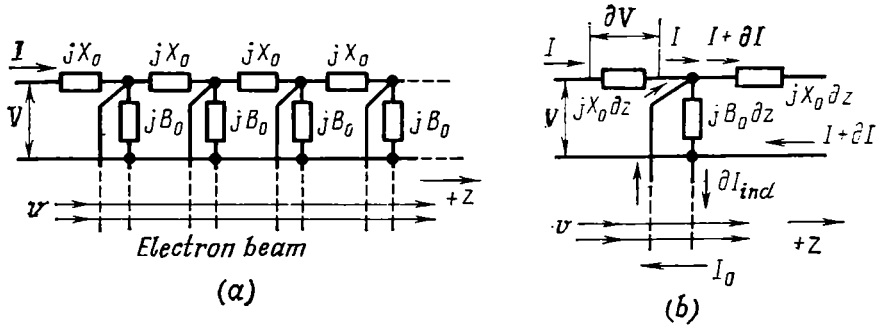

Fig. 6.4. Equivalent circuit of a lossless slow-wave system supporting electron beam (*a*), and current and voltage distribution at the system section of length *dz*, with induced current taken into account (*b*)

approximating those of the slow-wave structure in question. Suppose the radio-frequency voltage V in Fig. 6.4 to correspond to the longitudinal component of the synchronous wave propagating along the actual slow-wave structure, as measured at the electron beam level. A further requirement is that the phase velocity in the equivalent line be equal to the phase velocity of the actual wave and that the characteristic impedance of the line coincide with the coupled impedance K[1], defined at the level of the electron beam.

The object is to derive the differential equations describing the current and voltage in the equivalent line, taking into account the effects of the induced current I_{ind}, caused by the passage of a convection current I_{con} along the slow-wave system. Physically, the induced current is due to displacement currents between electron bunches and conductors of the slow-wave structure.

As was shown in Section 2.3*d*, the induced current is numerically equal to the convection current, provided the gap width may be considered infinitesimal. The direction of the induced current is determined with the negative charge of electrons taken into account (refer

[1] The concept of the coupled impedance is treated in Section 11.3 of "Microwave Engineering" by the same author (MIR Publishers, Moscow, 1973).

to Section 2.3*c*); the d.c. current component I_0 is also directed along the $-z$ axis (Fig. 6.4*b*). Thus, in a line element of ∂z length and at specific reactance jX_0 and specific susceptance jB_0 (i.e. per unit line length) we have

$$\partial V = -IjX_0\,\partial z;\ \partial I = -VjB_0\,\partial z + \partial I_{con}$$

where ∂I_{con} is the increment to the convection current of the beam. These equations can be used to describe the current and voltage in the equivalent line; obvious rearrangements result in

$$\frac{\partial V}{\partial z} = -jX_0 I \tag{6.19}$$

$$\frac{\partial I}{\partial z} = -jB_0 V + \frac{\partial I_{con}}{\partial z} \tag{6.20}$$

Taking into consideration the fact that the voltage V and the currents I and I_{con} vary in time and along the line length z, following exp $(j\omega t - \Gamma z)$ law, yields

$$\Gamma V = jX_0 I \tag{6.21}$$

$$\Gamma I = jB_0 V + \Gamma I_{con} \tag{6.22}$$

All the subsequent reasoning is quite similar to that used in transmission line equations. Thus, substitution of the current, defined by (6.21), into equation (6.22) results in

$$V(B_0X_0 + \Gamma^2) = jX_0\Gamma I_{con} \tag{6.23}$$

In the absence of an electron beam (i.e. when $I_{con} = 0$), the line in question is described by its "cold" parameters determined from the condition

$$B_0X_0 + \Gamma_0^2 = 0;\ \ \Gamma_0 = j(B_0X_0)^{1/2} \tag{6.24}$$

where Γ_0 is the propagation constant of the "cold" line. Thus, equation (6.23) may be presented as

$$V = -j\frac{\Gamma X_0 I_{con}}{\Gamma_0^2 - \Gamma^2} \tag{6.25}$$

The quantity X_0 in equation (6.25) can be expressed in terms of the "cold" characteristic impedance of the equivalent line. By (6.21) and (6.22) the incident wave (assuming $I_{con} = 0$) can be described as

$$\frac{V}{I} = \left(\frac{X_0}{B_0}\right)^{1/2}$$

In this relation the voltage V corresponds to the longitudinal voltage in the slow-wave system, and therefore the meaning of the ratio

V/I is that of the coupled impedance K, which is known from the theory of slow-wave structures and is equal to

$$K=\left(\frac{X_0}{B_0}\right)^{1/2} \tag{6.26}$$

It should be remembered that the magnitude of K should be measured at a certain specified distance from the surface of the slow-wave structure, corresponding to the location of the actual electron beam.

Simultaneous solution of equations (6.24) and (6.26) gives the magnitude of X_0; substitution of this magnitude into (6.25) results in

$$X_0=-jK\Gamma_0;\quad V=-\frac{\Gamma\Gamma_0 KI_{con}}{\Gamma_0^2-\Gamma^2} \tag{6.27}$$

Thus, the above relation describes the voltage developed across a line due to the passage of a density-modulated convection current, if the reverse action of the field thus developed upon the electron beam may be neglected.

6.2d. Self-Matched Field Under Approximate Synchronism Conditions

For a simultaneous solution of equations (6.27) and (6.17) the voltage V should be expressed in terms of the intensity of the longitudinal electric field in the slow-wave structure. Assuming

$$V = V_1 \exp(j\omega t - \Gamma z) \tag{6.28}$$

the amplitude V_1 of this voltage can be related to the amplitude E_{zm} of the longitudinal field intensity by

$$E_z=-\frac{\partial V}{\partial z}=\Gamma V;\quad E_{zm}=\Gamma V_1 \tag{6.29}$$

Substituting the magnitude of convection current, as determined by equations (6.18) and (6.17), into relation (6.27), and taking into account (6.28) and (6.29), we obtain the characteristic (dispersion) equation of a TWT in the form of

$$j\frac{KI_0}{2V_0}\frac{\Gamma^2\Gamma_0\beta_e}{(\Gamma_0^2-\Gamma^2)(j\beta_e-\Gamma)^2}=1 \tag{6.30}$$

In this equation the most interesting quantity is the propagation constant in the presence of an electron beam. Indeed, the behaviour of the wave (its build-up or decay) is determined by the real part of the propagation constant. However, since this equation is somewhat unwieldy, reasonable assumptions must be adopted for its simplification.

Qualitative argumentation showed that the case of the greatest interest for the present discussion is when the average electron beam velocity v_0 approximates the phase velocity of the wave. On the other

hand, it can be intuitively presupposed that the propagation constant in the presence of an electron beam cannot differ greatly from the propagation constant Γ_0 in a "cold" system. It follows that a more detailed examination of the characteristic equation (6.30) under condition that Γ, Γ_0 and $j\beta_e$ are approximately equal is in order.

Suppose the electron phase constant to be precisely equal to the phase constant of the "cold" system, i.e.

$$\Gamma_0 = j\beta_e \tag{6.31}$$

Thus, the following analysis will be based on the assumption that the initial electron beam velocity has been made exactly equal to the phase velocity in the slow-wave structure in the absence of an electron beam. Suppose also that the presence of an electron beam affects but slightly the magnitude of the propagation constant, i.e.

$$\Gamma = \Gamma_0 + \xi \tag{6.32}$$

where ξ is a small quantity that in the general case may be complex.

Substitution of the assumed magnitudes of Γ and Γ_0 into equation (6.31) results in

$$\frac{KI_0}{2V_0}\,\frac{\beta_e^2(-\beta_e^2+2j\xi\beta_e+\xi^2)}{\xi^2(2j\xi\beta_e+\xi^2)}=1$$

Since ξ is taken to be small, the terms containing its second power may be neglected; the term $2j\xi\beta_e$ in the numerator will also be neglected. After obvious rearrangements we arrive at

$$\xi=\beta_e\left(\frac{KI_0}{4V_0}\right)^{1/3}(j)^{1/3}$$

A dimensionless *gain parameter C* will be introduced and defined as

$$C=\left(\frac{KI_0}{4V_0}\right)^{1/3} \tag{6.33}$$

Assuming $(j)^{1/3} = \delta$, the above relation can be written as

$$\xi = C\beta_e\delta \tag{6.34}$$

Equations (6.34) and (6.32) simultaneously determine the propagation constant in the slow-wave structure in the presence of an electron beam. The quantity δ can take three values

$$\delta_1=\frac{\sqrt{3}}{2}+j0.5;\quad \delta_2=-\frac{\sqrt{3}}{2}+j0.5;\quad \delta_3=0-j1$$

Therefore, in the presence of an electron beam and under the assumptions adopted, the slow-wave structure may support *three waves*, which are characterized by an identical field pattern but feature different propagation constants. Substitution of the above roots of δ

into equation (6.34) yields the three propagation constants, if equation (6.32) is applied, in the form of

$$\Gamma_1=\Gamma_0+C\beta_e\left(\frac{3^{1/2}}{2}+j0.5\right)$$

$$\Gamma_2=\Gamma_0+C\beta_e\left(-\frac{3^{1/2}}{2}+j0.5\right)$$

$$\Gamma_3=\Gamma_0-jC\beta_e$$

In the general case the propagation constants Γ and Γ_0 should be considered complex numbers

$$\Gamma=\alpha+j\beta;\ \Gamma_0=\alpha_0+j\beta_0$$

However, travelling waves are excited in a "cold" slow-wave system and, as was postulated from the very beginning of the present discussion, the system itself is dissipationless. It follows, therefore, that $\alpha_0 = 0$ and a purely imaginary magnitude $j\beta_0$ should be substituted for Γ_0. Under these assumptions, according to equation (6.31), β_0 should be taken equal to β_e (i.e. $\beta_0 = \beta_e$). This reduces the above equations for the three propagation constants to

$$\Gamma_1=\alpha_1+j\beta_1=j\beta_e(1+C/2)+\frac{3^{1/2}}{2}C\beta_e \tag{6.35}$$

$$\Gamma_2=\alpha_2+j\beta_2=j\beta_e(1+C/2)-\frac{3^{1/2}}{2}C\beta_e \tag{6.36}$$

$$\Gamma_3=\alpha_3+j\beta_3=j\beta_e(1-C) \tag{6.37}$$

As can easily be noted, the phase constants of the first two waves (β_1 and β_2) are greater than β_0, and β_e. Phase constants, however, are related to the wave and beam phase velocities as follows

$$\beta_0=\omega/v_{p0};\ \beta_{1,2}=\omega/v_{p\,1,2};\ \beta_e=\omega/v_0$$

Hence the phase velocities of the first and second waves v_{p1} and v_{p2} are somewhat lower than the phase velocity v_{p0} in the "cold" slow-wave structure; on the contrary, the third wave features a phase velocity somewhat higher than that of the "cold" system.

Thus, the first wave propagates at a phase velocity slightly *slower* than that of the electron beam and features a *positive* attenuation ($\alpha_1 > 0$). The second wave also travels slightly *slower* than the electron beam, but is characterized by a *negative* attenuation ($\alpha_2 < 0$). The third wave is an *unattenuated* ($\alpha_3 = 0$) one and travels somewhat *faster* than the electron beam. The wave of the greatest interest from the point of view of amplification effects in travelling-wave devices is the second one, whose amplitude is build up along the line, following an exponential law.

The above analysis shows that it is impossible to describe formally the operation of a travelling-wave tube in terms of only one travelling wave. Of course, a unitary wave process propagates along the slow-wave system, but the propagation of this wave process along the TWT axis is characterized by a varying propagation constant; this is just the meaning of three or more waves being formally present in a TWT.

The reasoning presented shows that to obtain amplification the electron beam is required to travel slightly *faster* than the wave, despite the postulate of precise synchronism of the beam with the wave in a "cold" system. Under strictly synchronous movement the electron bunches, as was demonstrated in Section 2.8*d*, would be compressed around points of zero intensity of the longitudinal radio-frequency field, where the field changes from an accelerating to a retarding one (refer to electrons of type *1* in Fig. 2.32). The induced current would feature a phase shift of $\pi/2$ relative to the voltage, i.e. would be purely reactive. However, under these conditions the wave velocity would be somewhat reduced since the induced current leading the radio-frequency voltage by a phase angle of $\pi/2$ causes additional capacitive loading of the slow-wave structure. This results in a slightly lower phase velocity (relative to the average beam velocity) and all electrons of the beam begin to move slowly forward relative to the wave, the speed of this relative movement being equal to the difference between the velocities of the electron beam and the wave. In a reference plane moving with the electron beam, the centres of the electron bunches would appear shifted forward, i.e. into the regions of a retarding radio-frequency field. This causes the electrons to give up part of their kinetic energy to the wave, which starts to build up following an exponential law.

Wave amplification in a TWT can be compared to the development of gradually increasing waves on a water surface when the speed of the wind, producing these waves, is higher than the phase velocity of the waves. A deeper physical analogy can be made between wave amplification in a TWT and the Cherenkov effect which resides in the radiation of optical waves by electrons moving with velocities slightly higher than the velocity of light in the media specified. The function of the medium carrying the electromagnetic wave in case of a TWT is performed by the slow-wave structure.

6.2e. Equation of TWT Gain

First the examination will be restricted to the wave which builds up in moving along the system, following an exponential law. In virtue of equations (6.7) and (6.36), the intensity of the electric field of the second wave (assuming circuit loss to be negligible) varies in

accordance with the following law:

$$E_{z2}=(E_{z\,in})_2 \exp(j\omega t-\Gamma_2 z)=$$

$$=(E_{z\,in})_2 \exp[j\omega t-j\beta_e(1+C/2)] \exp\left(\frac{3^{1/2}}{2}C\beta_e z\right) \quad (6.38)$$

where $(E_{z\ in})_2$ is the intensity of the second wave at the input of the slow-wave structure.

Denoting the geometrical length of the slow-wave system along the tube axis as l and the intensity of the second wave at the system output as $(E_{z\ out})_2$, the gain G_2 of this wave provided by the TWT, with the coupled impedance invariable along the tube axis, can be described as

$$G_2=20\log_{10}\frac{(E_{z\,out})_2}{(E_{z\,in})_2}\,\text{dB} \quad (6.39)$$

After obvious rearrangements and using (6.38) we arrive at

$$G_2=20\log_{10}\exp\left(\frac{3^{1/2}}{2}C\beta_e l\right)=8.68\frac{3^{1/2}}{2}C\beta_e l$$

It will be convenient to replace the electron phase constant β_e in this relation by the phase constant of the "cold" slow-wave system $\beta_0 = \Gamma_0/j$. By equation (6.31) it should be postulated that

$$\beta_e=\beta_0=2\pi/\lambda_{slow}$$

where λ_{slow} is the length of a slow wave in the "cold" slow-wave structure. Thus, the gain of the TWT with only one increasing wave taken into account is

$$G_2 = 47.3Cl/\lambda_{slow} = 47.3CN \text{ dB} \quad (6.40)$$

where N is the number of slow-wave lengths accommodated along the slow-wave system:

$$N = l/\lambda_{slow} \quad (6.41)$$

Actually, the radio-frequency signal applied to the TWT input excites not only this increasing wave, but the other two waves mentioned, as well. These two waves take no part in signal amplification at all and only produce a certain amount of signal loss (termed the launching loss). The amplitude of the input signal is distributed equally between all the three waves, i.e. the field intensity of the increasing wave at the TWT input $(E_{z\ in})_2$ is by a factor of 3 less than the intensity of the electric field of the input signal $E_{z\ in}$. At a considerable distance from the input, the electric field becomes predominantly that of the increasing wave and, consequently, the launching loss can be determined as

$$L = 20\log_{10}(1/3) = -9.54 \text{ dB} \quad (6.42)$$

Therefore, the equation for "electronic" gain G, neglecting the effects of space charge, circuit loss, loss due to signal reflection from a mismatched load, etc., and taking into account relations (6.40) and (6.42), at considerable tube lengths can be presented as

$$G = L + G_2 = -9.54 + 47.3\ CN \text{ dB} \tag{6.43}$$

The above equation can be considered as a first-order approximation of the TWT gain at the maximum of the curve shown in Fig. 6.2. Equation (6.43) can be generalized to take into account the effect of the initial mismatch between the velocities of the beam and the slow wave of a "cold" slow-wave system ($V_0 \neq V_{0\,opt}$) by introducing a factor B, which characterizes the difference between these velocities

$$G = L + BCN \text{ dB} \tag{6.44}$$

(B is equal to or less than 47.3 dB)

It should be emphasized that the above analysis is valid only under small-signal conditions, when the radio-frequency components of all the quantities involved remain small as compared to the respective d.c. components. The large-signal theory of TWT performance involves the solution of cumbersome equations, which are nonlinear differential equations and falls outside the scope of the present analysis.

6.3. Effect of Space Charge on TWT Performance

The effect of space charge on the gain provided by a TWT can be taken into account by including the longitudinal space charge field E_s into the initial equation (6.8), which describes electron motion. This space charge field is developed between electron bunches due to mutual repulsion and it affects the process of electron bunch formation; a similar problem was discussed in Section 5.2 *d*, when analysing debunching effects in klystrons.

The intensity of the space charge field E_s can be determined from Poisson's equation. By (2.3) with the adopted unidimensional model of electron movement taken into account, we obtain

$$\varepsilon_0 \frac{\partial E_s}{\partial z} = \rho; \quad E_s = -\rho/\varepsilon_0 \Gamma \tag{6.45}$$

where ρ is the volume density of the space charge in the electron beam and Γ is the propagation constant in equation (6.7)[1].

The radio-frequency component of the space charge density ρ_1 can be related to the convection current density J_1 by equation (6.13).

[1] Strictly speaking, the electric field of the electron bunches does not exactly correspond to the field of a single wave propagating along the slow-wave structure of a TWT; here this circumstance will be neglected.

Thus, taking into account (6.45) and (6.13), the amplitude of the space charge field in the electron beam of a TWT may be expressed as

$$(E_s)_m = j\frac{J_1}{\omega\varepsilon_0} \tag{6.46}$$

Substitution of the sum of complex magnitudes E_{zm} and $(E_s)_m$ for E_{zm} in equation (6.16) and combining equations (6.46) and (6.16) after some simple rearrangements results in

$$J_1\left[1-\frac{J_0}{2V_0\omega\varepsilon_0}\frac{\beta_e}{(j\beta_e-\Gamma)^2}\right]=-j\frac{J_0}{2V_0}\frac{\beta_e}{(j\beta_e-\Gamma)^2}E_{zm} \tag{6.47}$$

Since $J_0 = \rho_0 v_0$ and $\rho_0 = -Ne$ (where N is the number of electrons per unit beam volume), equation (6.47) after multiplication by the cross-sectional area of the electron beam can be presented in terms of the convection current amplitude as

$$I_1\left[1+\frac{Ne^2}{m\varepsilon_0}\frac{\beta_e^2}{\omega^2(j\beta_e-\Gamma)^2}\right]=-j\frac{I_0}{2V_0}\frac{\Gamma\beta_e}{(j\beta_e-\Gamma)^2}V_1 \tag{6.48}$$

In this equation the quantity $Ne^2/m\varepsilon_0$ can be replaced by the square of the electron plasma frequency in a uniform limitless electron beam, as defined by equation (2.80). Therefore, the effect of an input signal on the electron beam, neglecting the reverse effect of a bunched electron beam on the field of the slow wave, can be described as

$$I_1\left[1+\frac{\omega_p^2}{\omega^2}\frac{\beta_e^2}{(j\beta_e-\Gamma)^2}\right]=-j\frac{I_0}{2V_0}\frac{\Gamma\beta_e}{(j\beta_e-\Gamma)^2}V_1 \tag{6.48a}$$

Further analysis can be carried out using equation (6.27) which describes the longitudinal voltage V in the system, with the induced currents taken into account. Substituting (6.27) into (6.48a) and allowing for the amplitudes of convection current I_1 and voltage V_1 yield

$$j\frac{KI_0}{2V_0}\frac{\Gamma^2\Gamma_0\beta_e}{(\Gamma_0^2-\Gamma^2)(j\beta_e-\Gamma)^2}=1+\frac{\omega_p^2}{\omega^2}\frac{\beta_e}{(j\beta_e-\Gamma)^2} \tag{6.49}$$

The characteristic equation thus deduced in terms of the propagation constant differs from (6.30) by the presence of a more complicated right-hand member. In the absence of space charge ($N \to 0$; $\omega_p \to 0$) equation (6.49) is reduced to (6.30).

The effects of space charge may be allowed for more fully if the restrictions adopted (equality of initial beam velocity v_0 to the phase velocity in the "cold" system, as defined by condition (6.31)) are lifted. A dimensionless *velocity parameter b* will be introduced and defined as:

$$v_0 = v_{p0}(1 + bC) \tag{6.50}$$

where C is the gain parameter as defined by equation (6.33). Still another concept, that of the *space charge parameter* QC, will also be introduced; this parameter is defined as the product of the gain parameter C by a dimensionless quantity Q, which is a function of the ratio ω_p/ω

$$QC=\frac{1}{4C^2}\frac{\omega_p^2}{\omega^2} \tag{6.51}$$

The gain parameter C in the denominator of this equation describes the intensity of beam interaction with the field of the travelling wave. On the other hand, the higher the ratio of electron plasma frequency to the signal frequency, the greater are the effects of mutual electrostatic repulsion in the electron bunches. The space charge parameter QC, therefore, is indeed a measure of the relation between the debunching and bunching tendencies in the electron beam of a TWT. The finite dimensions of the beam can be allowed for by replacing the electron plasma frequency in equation (6.51) by its reduced value ω_p' (refer to Section 2.9).

Equation (6.49) may be solved graphically, with (6.50) and (6.51) taken into account.

The graphs in Fig. 6.5 illustrate the behaviour of the factor B in equation (6.44) as a function of the space charge parameter QC at the velocity parameter b corresponding to maximum gain. In the absence of space charge ($QC = 0$) factor B is 47.3, this being in agreement with the results obtained in Section 6.2. An increase in the space charge causes a slight reduction of the value of B which determines the maximum gain of the increasing wave in a TWT. Calculations show a simultaneous reduction of the value of the launching loss L in equation (6.44), as illustrated in Fig. 6.5.

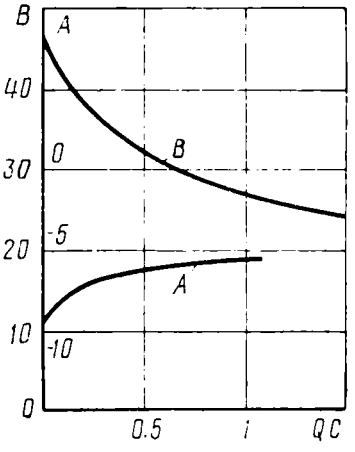

Fig. 6.5. Parameters A and B *vs* the space charge parameter QC; parameters A and B determine the small-signal gain of a TWT according to (6.44)

Analysis indicates that the optimum value of velocity parameter b increases with a rise in the space charge parameter QC and attains a value approximately up to 2 at $QC = 1$[1]. This means that an increase in the electron beam density (higher values of ω_p and QC) causes the maximum of the curve shown in Fig. 6.2 to be shifted toward the re-

[1] Typically, in actual TWT designs the value of parameter QC does not exceed 0.25 to 0.5.

gion of higher accelerating voltages. The initial beam velocity v_0 should exceed the phase velocity v_{p0} to allow for the effect of space charge, but this difference in velocities is not too great. As can easily be noted from examining equation (6.50) even at $b = 2$ and $C = 0.1$, for instance, the beam should outspeed the travelling wave at the initial section of the system only by 20 per cent. The condition of approximate synchronism (6.1) remains valid for power travelling-wave tubes as well, despite the fact that the influence of space charge in these devices is considerably more pronounced.

6.4. Parameters and Characteristics of O-Type TWT's

6.4a. Gain and Bandwidth

The gain of a TWT is in direct proportion to the gain parameter C, as is evident from equation (6.43). In turn, by equation (6.33) parameter C is the higher, the higher the coupled impedance of the slow-wave system; by definition this latter is

$$K = \frac{|E_{zm}|^2}{2\beta^2 P} = \frac{|E_{zm}|^2}{2\beta^2 W_1 v_g} \tag{6.52}$$

where P and W_1 are the power of the travelling wave and energy per unit of slow-wave structure length, respectively, and v_g is the wave group velocity; β is the phase constant of the slow-wave system $\left(\beta = \frac{2\pi}{\lambda_{slow}} = \frac{\omega}{v_p}\right)$.

In actual slow-wave structures the coupled impedance is generally of the order of scores or hundreds of ohms; typical values of parameter C range from about 0.02-0.05 to 0.2. Therefore, at adequate lengths l of the active part of a TWT structure, for instance at N about 10 to 30, the gain, by equation (6.43), can be up to 40 to 60 dB and even higher.

Analysis of equation (6.43) may give an impression that an unlimited increase in the length l of the slow-wave structure (i.e. increasing the number of slow-wave lengths N) can be used as a means for attaining as high gains as desired. Actually, there exist certain limits which are due to that signal is amplified because electrons of the beam give up part of their kinetic energy to the radio-frequency field. The electron velocities drop off as the beam travels along the slow-wave structure. As a result the condition underlying TWT performance that the beam should travel at a velocity slightly higher than the phase velocity of the travelling wave is violated. A further increase in the system length would result in a lower rather than a higher output signal. The impossibility of unlimited increase in the output signal intensity is also quite obvious from purely energetical

considerations: the energy acquired by the electron beam from a source of accelerating voltage is finite.

The magnitude of gain attainable in a TWT is to a certain extent limited also by the tendency of these devices to become self-excited, this being due to imperfections of matching at the input and output of the slow-wave structure. As will be shown, slow-wave structures have to be provided with lumped or distributed dissipative loads (attenuators) or severs to suppress parasitic self-excitation effects, with the total gain of the device G_{tot} reduced by a certain amount, depending on the type and design of attenuator (sever) employed. Thus, taking account of the loss introduced into the slow-wave structure, equation (6.43) can be rewritten as

$$G_{tot} = -9.54 + 47.3CN - L \text{ dB} \tag{6.53}$$

where L is the loss in the slow-wave system.

Usually, the attenuators and severs of slow-wave structures introduce from 4 to 10 dB loss and thus the actual gains obtained with TWT's are quite high, of the order of 30 to 50 dB.

A particularly attractive feature of forward-wave travelling-wave tubes is their considerable bandwidth. At a fixed value of the accelerating voltage the TWT gain can be almost constant in a very wide band of frequencies, namely about 20 to 50 per cent of the middle frequency and often even much wider. This is a great advantage of travelling-wave tubes as compared to amplifier klystrons, which, as demonstrated earlier, are capable of providing extremely high gains but in a significantly narrower band of frequencies.

Partly, the operating bandwidth of a TWT is determined by the dispersion effects which take place in the slow-wave structure, i.e. by changes in the phase velocity of the slow wave as a function of frequency. At a fixed value of the accelerating voltage V_0 the electron velocity v_0 remains constant and, consequently, the less the dispersion effects of the slow-wave structure, the wider is the band of frequencies within which the condition of synchronism of the beam and the travelling wave will be satisfied.

Among the great variety of slow-wave structure types available, the widest bandwidth is provided by a simple helix. Employing a helical slow-wave system makes it possible to almost completely discount bandwidth limitations due to the effects in the slow-wave structure. Slow-wave structures of the coupled-resonator type, which are employed in power TWT's, feature considerably more pronounced dispersion characteristics.

Besides this, other factors also affect the operating bandwidth of a TWT. An increase in the operating wavelength brings about a reduction in the number of slow-wave lengths accommodated along the slow-wave structure; on the other hand, an increase in the signal frequency results in a greater rate of decay of the radio-frequency field

across the transverse section of the slow-wave structure. Since the position of the electron beam with respect to the slow-wave structure remains the same, the coupled impedance (and therefore the gain parameter C) should fall off with a rise in operating frequency. Thus, a simultaneous change in the values of parameters C and N in equations (6.48) and (6.53) should result in a reduction of the gain both at the higher and the lower frequencies.

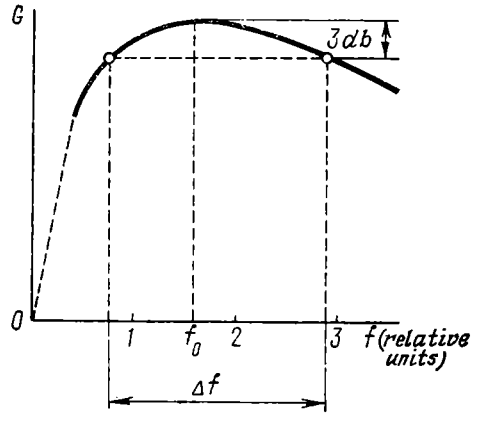

Fig. 6.6. Frequency dependence of TWT gain

In case of a helical slow-wave system the dependence of TWT gain on frequency, governed by changes in parameters C and N, features the pattern illustrated in Fig. 6.6. The maximum gain corresponds to a frequency f_0, at which a slow-wave length accommodates from 4 to 10 turns of the helix[1].

The maximum of the curve G *vs* f is a rather broad one. As can be noted from Fig. 6.6, a 3 dB reduction in gain corresponds to about an octave bandwidth. Practice shows the actual bandwidth to be limited to a considerable extent by the possibility of obtaining wideband matching at the input and output of the TWT.

6.4b. TWT Efficiency

The kinetic energy and velocity of electrons in the beam decrease as the electrons give up their energy to the radio-frequency field. The condition of TWT operation becomes violated, that is the average beam velocity ceases to be approximately equal to the phase velocity of the slow wave. Here lies the main factor limiting the efficiency of O-type TWT's residing in that the electrons cannot give up all the kinetic energy to the radio-frequency field since the electron bunches are displaced from the region of retarding radio-frequency field into the region where this field is accelerating.

The lower limit to the average beam velocity is set by the phase velocity of the slow wave. Physically, therefore, the efficiency should be the higher, the greater is the excess of the initial beam velocity over the phase velocity of the slow wave. However, an excessive difference between these velocities will result in poorer electron beam

[1] This relation is a function of the c/v_p ratio and therefore of the power provided by the TWT. Thus, the maximum gain with 4 helix turns per each slow-wave length corresponds to a pitch angle of about 10 degrees.

bunching at the input section of the slow-wave structure, this leading to a rapid deterioration of the TWT gain (Fig. 6.2). The requirements of maximum efficiency and high gain in a TWT of the O-type are thus contradictory.

The problem of electronic efficiency of a travelling-wave tube cannot be completely solved within the simplified small-signal theory. Indeed, this theory is inadequate to determine the allowable difference between the electron beam and slow wave velocities and therefore the maximum energy level that can be given up by the electron beam to the radio-frequency field.

The non-linear (large signal) theory and certain simplified arguments reveal that the maximum electronic efficiency of an amplifier forward-wave travelling-wave tube is of the order of

$$\eta_e = kC \tag{6.54}$$

where C is the gain parameter defined by equation (6.33) and k is a dimensionless factor of a value ranging from 2 to 8. The highest value of factor k corresponds to the maximum permissible excess of the initial electron beam velocity over the phase velocity of the wave in a "cold" slow-wave structure.

The validity of a relation of the (6.54) type can be demonstrated by the following train of reasoning. Equation (6.17) may be used to describe the intensity of the longitudinal electric field E_{zm} in terms of the amplitude of the beam convection current I_1. Under conditions of "cold" synchronism ($\Gamma = j\beta_e + \xi$) we have

$$E_{zm} = j \frac{2V_0\xi^2}{I_0\beta_e} I_1 \tag{6.55}$$

In Section 2.4 it was shown that the amplitude of the radio-frequency component of convection current I_1 cannot exceed $2I_0$ even under perfect bunching conditions. Furthermore, the parameter ξ for the increasing wave in a TWT, according to the findings of Section 6.2, is equal to

$$\xi = \xi_2 = C \frac{\omega}{v_0} \left(-\frac{3^{1/2}}{2} + j0.5 \right)$$

Applying equation (6.52) which relates the power flux in a slow-wave structure to the coupled impedance, and substituting equation (6.55) with the above magnitudes of I_1 and ξ, we obtain

$$P = \frac{|E_{zm}|^2}{2(\omega/v_0)^2 K}; \quad P = 2CI_0V_0 \tag{6.56}$$

This relation describes the power of a TWT at the output section of its slow-wave structure, where the electron bunches acquire the ideal pattern, corresponding to the delta-function law.

The power drawn by the electron beam from the source of accelerating voltage (under non-depressed collector conditions) is I_0V_0 and therefore the maximum electronic efficiency for the case under treatment is

$$\eta_{e.\ max.} = 2C \tag{6.57}$$

Thus, the parameter C describes not only the TWT gain, but its maximum attainable efficiency as well.

Therefore, to obtain a high electronic efficiency it is desirable to reduce the d.c. anode resistance of the electron gun (equal to V_0/I_0) and increase the coupled impedance of the slow-wave structure.

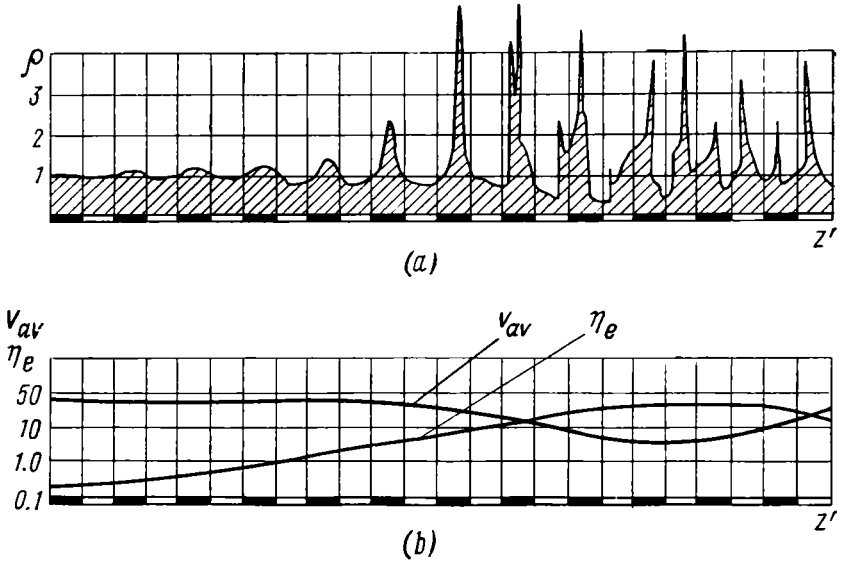

Fig. 6.7. Electron beam bunching in a power TWT (*a*) and pattern of variation of the average beam velocity and electronic efficiency along the axis of slow-wave structure (*b*) with dark areas of the scale indicating regions of retarding radio-frequency field

The pattern of electron bunches and their arrangement relative to the slow wave are of a complex character and affect the magnitude of attainable electronic efficiency to a considerable degree. Figure 6.7*a* illustrates a typical pattern of variation of the space charge density along the beam length, as obtained from non-linear numerical analysis. The scale along the abscissa axis is in distances z' from the TWT input in a reference system moving with a speed equal to that of the slow wave. As can be noted, the electron bunches take the form of sharp peaks, similar in appearance to the current peaks in amplifier klystrons.

First the bunches are compressed around electrons which are located at regions of maximum retarding field, but at the output end of the TWT the middles of the electron bunches are gradually displaced to the points of zero field intensity where the radio-frequency field

changes from an accelerating to a retarding one. This effect is largely due to the electron bunches being slowed down as a result of giving up part of their kinetic energy to the field. After this the electron bunches are transferred into the regions of accelerating field.

Thus, increasing the slow-wave structure length beyond a certain optimum value brings about an increase rather than a decrease in the average beam velocity (Fig. 6.7*b*). The electronic efficiency at first goes through a saturation region and then begins to fall off.

The actual values of efficiency in travelling-wave tubes are commonly somewhat lower than those obtained in power multicavity klystrons and usually constitute about 30 to 40 per cent.

The efficiency of travelling-wave tubes can be increased by gradually reducing the phase velocity of a slow wave along the axis of the slow-wave structure (so-called velocity tapering). In this case the electron bunches can be made to remain approximately in synchronism with the slow wave and thus to continue giving up their kinetic energy to the radio-frequency field. The development of TWT's with such *velocity tapering* is very attractive, though it necessitates the solution of extremely difficult design and development problems; only the advent of computer analysis has made it possible to design slow-wave structures with a varying ("programmed") c/v_p ratio.

Another possible method of increasing the efficiency is by a gradual or abrupt increase of electron bunch velocity as it moves towards the output end of the slow-wave structure. In this case, as in velocity-tapered TWT's, the average beam velocity at the input end can be made approximately equal to the phase velocity in a "cold" slow-wave structure, while at the output end, where the conditions correspond to large-signal amplification, the initial beam velocity is is made higher than the wave phase velocity by a certain value, which ensures a high efficiency. Obviously, in this case the slow-wave structure has to be sectioned into separate parts and each such section fed with a different accelerating voltage (relative to the tube cathode); the c/v_p ratio along the structure may remain constant. It is also possible to reduce abruptly the wave phase velocity at the output end of the slow-wave system at a constant d.c. accelerating voltage throughout the system.

Another and a more easy way of increasing the tube efficiency is by depressing the collector voltage below the value of the accelerating voltage (*depressed collector operation*), which is applicable to TWT's of the O-type just as to amplifier klystrons discussed earlier: this method is illustrated in Fig. 5.17. Analysis shows that it is possible to raise the efficiency up to about 50 per cent and even higher with depressed collector conditions, bringing down the collector voltage to (0.3-0.5) V_0. In this case the configuration of the collector is quite of a problem, since it should exclude the possibility of electron

movement back into the interaction channel of the slow-wave structure.

Depressed collector operation offers more advantages when applied to travelling-wave tubes, as compared to amplifier klystrons; this is due to a less effective mechanism of electron beam interaction with the radio-frequency field, as well as to a lower spread in electron velocities at the output end of the interaction space in TWT's. This explains why depressed collector conditions are extensively employed in TWT's, especially, in medium power tubes. Depressed collector conditions in conjunction with tapered slow-wave structures or abrupt velocity variation have already provided efficiency values up to 50 per cent in experimental models. A further considerable increase in efficiency of O-type TWT's is believed to be possible.

Another completely different way of obtaining high efficiency values is to utilize the *potential* energy of the electron beam, instead of its *kinetic* energy. This principle is used to great advantage in modern magnetron oscillators of the travelling-wave type, as well as in travelling-wave tubes of the magnetron type (M-type TWT's) treated in Chapter Seven.

In conclusion it should be emphasized that the efficiency of a travelling-wave tube is mainly of interest in power TWT's, which are employed as output stages. In case of input tubes (low-noise amplifiers of small signal) this problem is hardly of any significance.

6.4c. Noise in Travelling-Wave Tubes of the O-Type

The problem of employing a TWT as an amplifier of small signals is tightly connected with the problem of reducing the inherent noise level of this device. In a TWT the main sources of noise are:

(1) fluctuations of the convection current density and electron velocities (shot noise);

(2) current redistribution between the tube electrodes due to part of the electron beam being intercepted by the slow-wave structure.

Ion noise due to the presence of residual gas in the tube may also contribute to the overall noise of a TWT.

Fluctuations of the electron density and velocity are the lower, the lower the operating cathode temperature and the more uniform is its emitting surface. This kind of noise is also affected by the ratio of cathode current to cathode emissivity; research discloses this noise to be minimum at about unity values of this ratio. Finally, this kind of noise is a function of the pattern of d.c. field distribution at the cathode, where a major part of electron acceleration takes place: the smoother this pattern, the lower the fluctuation noise.

Considerable attention has been given to the problem of a theoretical minimum of TWT noise, but the answer is yet to be found. Research reveals some interesting possibilities of "cooling" electron be-

ams and thus developing travelling-wave tubes with super-low noise figures[1]. In particular, the fluctuations of current densities and electron velocities turn out to be variable along the beam axis according to a periodic law associated with the space charge waves (Section 2.9).

The noise factor of a TWT can be considerably reduced by placing the input of the slow-wave structure in a node of the noise standing wave; low noise factors are obtained by using electron guns of special multianode designs with a drift tube directly at the input of the slow-wave structure. An example of a gun of this kind is presented in Fig. 6.17.

The use of a thin well focussed electron beam enables significant reduction of the noise due to current redistribution. In low-noise TWT's beam focussing is accomplished by means of a high-intensity longitudinal static magnetic field, which ensures that electron trajectories be almost perfectly rectilinear. The absence of grids, in contrast to triodes and certain types of amplifier klystrons, also tends to reduce the overall noise figure of TWT's.

To a certain extent the inherent noise in a TWT is a function of the radio-frequency loss in the slow-wave structure. The noise signal generated in any transmission line is in direct proportion to the absolute temperature of the system and the amount of microwave loss in it. Therefore, the noise can be reduced by cooling the entire tube (for instance, by immersion in liquid nitrogen). As known from practice, to reduce the noise figure it is also necessary to provide a slow-wave structure as uniform as possible, which in the case of a helix means a highly constant pitch.

Modern super-low noise TWT's of the decimetric and centimetric wave bands are successfully manufactured with noise figures of 3 to 4 dB and even less, this making attractive their use as input amplifiers in microwave receiving equipment. Typical parameters of a 10-cm super-low noise TWT are presented in Section 6.5.

It should be noted that the techniques of noise reduction in travelling-wave tubes are equally applicable to other types of electron-beam devices of the microwave range, including amplifier klystrons. However, the extremely wide bandwidth of TWT's in conjunction with the possibility of obtaining low noise levels make this type of device particularly attractive as small-signal amplifiers.

6.4d. Transfer and Phase Characteristics of TWT's

A typical pattern of the TWT gain and output power *vs* the input signal power is qualitatively shown in Fig. 6.8. The initial section of this transfer characteristic curve $P_{out} = f(P_{in})$, as in most radio-frequency amplifiers (refer, for instance, to Section 5.3*a*), is

[1] For definition of noise figure refer to Section 3.5*c*.

linear and the TWT gain here is at a maximum. However, the maximum efficiency treated in Section 6.4*b* is attained on the nonlinear part, in the vicinity of the maximum of the transfer characteristic curve.

The existence of a maximum and a subsequent drooping section of the transfer characteristic curve can be qualitatively explained by the following train of reasoning. Obviously, the level of output power obtainable is limited by the d.c. power delivered to the electron beam. The gain at high levels of input signal cannot, therefore, remain as high as at low input signals. Under saturation (at the maximum of the transfer characteristic curve) the middles of the electron bunches are shifted out of the regions of maximum retarding field into regions of zero field intensity of the travelling wave (Fig. 6.7*a*) and the induced current turns out to be shifted in phase relative to the voltage by an angle of $\pi/2$.

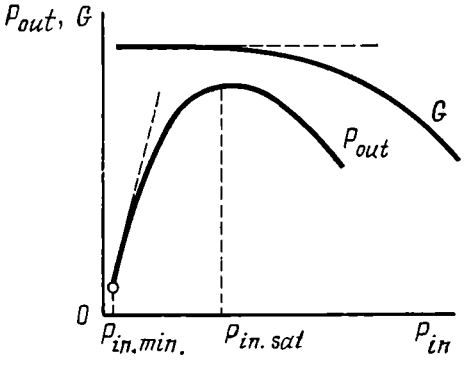

Fig. 6.8. Output power and gain of a TWT *vs* input power

The linear section of the transfer characteristic curve is the most important one if the TWT is designed to be used as an input amplifier. At the same time, it is ordinarily desirable to have as wide a *dynamic range* of input signals as possible, this range being defined as the difference in decibels between the noise level and the overload level of a system (in the case under discussion between the input signal corresponding to saturation and the input signal corresponding to a certain level of TWT noise). The wider the dynamic range and the more linear the transfer characteristic curve $P_{out} = f(P_{in})$, the lower are the crosstalk distortions introduced by a TWT amplifier employed in multichannel communications equipment.

In low and medium power TWT's the dynamic range can be quite considerable, up to some 60 to 90 dB. On the other hand, power and high-power TWT's designed for use as the output stages, are commonly employed at operation conditions set to the maximum efficiency, i.e. at the maximum of the transfer characteristic curve.

The phase of the output radio-frequency signal is a function of the d.c. accelerating voltage and the input signal power. Physically, the phase of the output signal depending on the accelerating voltage is due to variations of the beam average velocity v_0 causing corresponding changes in the propagation constant Γ of the wave process travelling along the slow-wave structure of the TWT. The time of electron bunch transit as well as the time of wave travel along the system do not remain constant.

The dependence $\varphi_{out} = f(P_{in})$ can be explained by an increase in the portion of kinetic energy given up by the electron bunches when the input signal power is increased. A certain reduction of the average beam velocity at the same time results in a longer transit time of the electron bunches and a change in the phase of induced current at the TWT output (Fig. 6.7*b*). Note in passing, that this effect is also responsible for the undesired conversion of amplitude modulation of the input signal into phase modulation of the output signal.

The total time of electron transit along the TWT system is considerable and equal to the period of radio-frequency oscillations multiplied by the number of slow-wave lengths N along the system (refer to Section 6.2*e*). This means that even comparatively small variations in the value of V_0 and P_{in} will produce quite considerable changes in the phase of the output signal. Typically, the change in the phase of the output signal is about 10 degrees per each per cent of accelerating voltage variation and about 2 to 4 degrees per decibel of input power variation.

The dependence of the output signal phase on the operating conditions of a TWT makes application of these devices more difficult, especially if a considerable number of amplifiers are simultaneously operated to drive multielement phased arrays in radar or communications equipment. Multicavity klystrons feature the same or similar phase characteristics; devices of the M-type (treated in the following Chapter) are somewhat better in this respect. In general, it should be emphasized that modern microwave electronics imposes more and more stringent requirements on the phase stability of microwave devices.

6.4e. Suppression of TWT Self-Excitation

Practice shows that amplifier travelling-wave tubes tend to become self-excited under certain conditions. Since this effect is highly undesirable in any kind of amplifier, it will be expedient to examine the possible causes of TWT self-excitation and means for suppressing these parasitic oscillations.

As in any amplifier, the positive feedback necessary for TWT self-excitation can be developed by stray external coupling paths between the device input and output. Furthermore, this parasitic positive feedback may be developed in the TWT itself due to reflections from the tube output caused by imperfect matching; this latter type of feedback is the most typical and therefore merits a more detailed examination.

Practically, it is impossible to attain a perfect match at the input and output of the slow-wave system in the entire range of operating frequencies and so much the more at frequencies outside this range. Therefore, a certain amount of wave reflection from the output dis-

continuity is inevitable and this reflected wave will travel along the slow-wave structure towards the input[1]. After being again reflected from the imperfect match at the input terminals of the system, this wave begins to travel along the slow-wave structure in the forward direction, as indicated in Fig. 6.9*a*.

The TWT will become self-excited if the following two conditions are satisfied:

(1) the amplitude of this "secondary" (i.e., twice reflected) wave at the tube input is at least equal to the amplitude of the "primary" (initial) wave;

(2) the phase of this "secondary" wave after two reflections and two travels through the slow-wave structure is shifted relative to that of the "primary" wave by $2\pi n$, where n is any integer.

This second condition automatically determines the frequency of steady-state parasitic oscillations.

For simplicity the phase shift due to reflection from both ends of the slow-wave structure will be assumed to be zero, and the change in the wave phase velocity under the effect of the electron beam will be considered negligible. Under these assumptions the phase condition of a positive feedback is

$$l = n\lambda_{slow}/2 \tag{6.58}$$

where l is the geometrical length of the slow-wave structure and λ_{slow} is the slow-wave length. The factor n, which determines the mode of oscillation in this TWT oscillator, thus proves to be $2N$.

On the other hand, the relation

$$\frac{\lambda_{slow}}{\lambda} = \frac{v_p}{c}$$

should hold for any slow-wave structure and therefore condition (6.58) can be presented as

$$l = n\frac{\lambda}{2}\frac{v_p}{c} \tag{6.58a}$$

Applying the condition of synchronism of the beam with the wave ($v_0 \approx v_p$), we deduce the wavelength and frequency of these parasitic oscillations

$$\lambda_{par} = \frac{2cl}{nv_p} = \frac{cl}{n}(2m/eV_0)^{1/2};\quad f_{par} = \frac{n}{l}(eV_0/2m)^{1/2} \tag{6.59}$$

Thus, a TWT tends to become self-excited at a series of discrete oscillation modes. Equation (6.59) may be taken as a formal indication of the possible existence of an unlimited multitude of parasitic

[1] The present argumentation does not take into account the possibility of electron beam interaction with one of the backward spatial harmonics.

oscillation frequencies, differing from each other by the magnitude of the factor n in this relation. Some of these parasitic frequencies may happen to be within the range of operating frequencies of the tube, when this latter is employed as an amplifier.

Actually, the TWT is prevented from being self-excited at the longest and shortest wavelengths by a considerable decrease in TWT gain; another factor, that also exerts a marked effect on the process of self-excitation, is the inherent loss in the slow-wave system, this loss increasing with a rise in frequency. Therefore, with no special

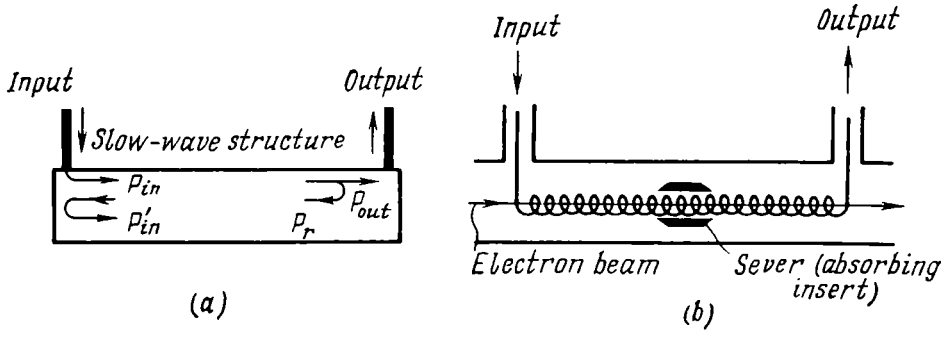

Fig. 6.9. To the problem of TWT self-excitation

measures taken, parasitic oscillations are usually encountered at the long-wave edge of the operating band-width and at the edges of the slow-wave structure band-width.

One of the most effective methods of suppressing parasitic oscillations in a TWT is the introduction of a lumped or distributed dissipative loss into the "cold" slow-wave structure (this technique is also referred to as "severing" the slow-wave structure).

The most expedient is the use of a lumped dissipative pad placed somewhere near the middle of the slow-wave structure (Fig. 6.9*b*). The effect of this pad may be qualitatively explained by examining the simplest case of a pad featuring infinite "cold" loss. In this case all the power of the incident wave travelling from the TWT input will be dissipated in this pad and the same is obviously true of the wave reflected from the TWT output. If the pad (or sever) is matched at both sides, the possibility of TWT self-excitation will be completely eliminated. The two sections of a slow-wave structure to both sides of the sever are, however, coupled via the electron beam, which has acquired velocity and density modulation in the input section; this beam will again induce three waves in the second section of the slow-wave structure, one of which is the increasing wave appearing at the TWT output as the amplifier signal.

Thus, a dissipative pad, which is essentially a reciprocal device, offers different amounts of loss for the signal travelling in the direction of electron beam movement and in the opposite direction, i.e.

acts as a non-reciprocal element. The reduction in TWT gain due to circuit loss L in equation (6.53), caused by this pad, can be shown to be about 3.5 dB at an infinitesimal pad length and up to 8 to 10 dB at a greater pad length.

The minimum value of "cold" loss introduced by this pad so as to ensure that the slow-wave structure be effectively severed into independent sections (coupled only by the electron beam) and thus ensure stability of TWT operation, should at least be numerically equal to the TWT gain. As a confirmation of this statement, examine a signal P_{in} applied to the input section of the slow-wave structure (Fig. 6.9*a*). The amplified signal at the slow-wave system output is $P_{out} = G_{tot}P_{in}$, where G_{tot} is the actual overall gain defined by equation (6.53) with the introduced loss being taken into consideration. If the conditions at the system output are described by a reflection coefficient K_{out}, the power of the reflected signal will be

$$P_{ref} = |K_{out}|^2 P_{out} = |K_{out}|^2 G_{tot} P_{in}$$

The power carried by the reflected wave, after having traversed the tube in the backward direction and being again reflected from the input, can be described as

$$P'_{in} = |K_{in}|^2 \frac{P_{ref}}{L_{tot}} = P_{in} \frac{G_{tot}}{L_{tot}} |K_{in}|^2 \cdot |K_{out}|^2$$

where K_{in} is the reflection coefficient from the tube input and L_{tot} is the value of the "cold" loss introduced by the pad (sever).

The condition of operation stability is P'_{in} being less than P_{in}, i.e.

$$\frac{G_{tot}}{L_{tot}} |K_{in}|^2 \cdot |K_{out}|^2 < 1 \qquad (6.60)$$

The most unfavourable conditions are when both ends of the slow-wave structure are completely mismatched, i.e. when $|K_{in}| = |K_{out}| = 1$. Therefore, absolutely guaranteed stable operation is obtained if condition

$$L_{tot} > G_{tot} \qquad (6.61)$$

is satisfied. To improve gain uniformity throughout the operating range, it is common for the "cold" loss of the sever L_{tot} to be set at about 10 to 20 dB higher than is required by condition (6.61), this uniformity being deteriorated by regenerative effects.

To prevent the tube efficiency from being significantly reduced, the length of the slow-wave structure between the sever and the output of the tube has to be sufficient to provide at least a 20 dB gain. In this case the sever dissipates not more than 1 per cent of the output power. It is undesirable to have too high a gain in this output section, since this could call for an extremely good match of the sever and this output section to prevent instability effects in the section itself.

6.5. Problems of O-Type TWT Design

6.5a. TWT Slow-Wave Structure

The main trend in the development of forward-wave travelling-wave tubes is to produce wideband amplifiers for the decimetric, centimetric and partly for the millimetric wave bands.

Conventionally, travelling-wave tubes are subdivided into *low-power* (input), *medium-* and *high-power* (*output*) devices, the latter being termed simply *power tubes*. The first group includes low- and super-low noise tubes with output power levels usually not in excess of several milliwatts. They are designed to amplify signals fed to the receiver inputs in radar, communications and other such equipment. The second group embraces TWT's with a somewhat higher level of output power (up to hundreds of milliwatts) and less stringent requirements as regards the noise figure. Finally, placed into the third group are power TWT's with output power levels in excess of 1 watt; among this group are a somewhat special class of devices with c.w. power levels from hundreds of watts to kilowatts or pulse powers up to several megawatts.

Low-power and low-noise TWT's usually employ slow-wave systems of the simple helical type operating on the fundamental forward slow wave. This type of system provides the widest bandwidth at a sufficiently high coupled impedance, if the c/v_p ratio is high enough and corresponds to accelerating voltages not in excess of 10 kV. At the same time, the helix features a simple design and provides wideband matching both at the input and output ends.

It is common practice to manufacture the helix from a non-magnetic material, such as tungsten or molybdenum wire. At both ends of the helix the pitch is gradually increased so as to facilitate matching. The phase velocity of the wave and the respective value of the d.c. accelerating voltage for the uniform section of the helix can be determined from the dimensions of the helix with the aid of the approximate equations (6.2) and (6.4).

The shorter the operating wavelength, the lower should the helix radius be (at a specified value of the c/v_p ratio), because the radio-frequency field diminishes rapidly with the distance from the surface of the structure, this being true of any kind of a slow-wave structure. This decrease in field intensity becomes quite significant at distances of the order of half the slow-wave length, while this latter is the shorter, the shorter is the wavelength in free space. When the radius of the helix approaches the value of the slow-wave length (and much more so, exceeds it) the field at the helix axis becomes very weak and its effect on the electron beam, correspondingly small.

On the other hand, an exceedingly small helix diameter is undesirable both from practical design considerations and because this

imposes strict limitations on the allowable beam current that can be passed along the axis of this system at a specified value of the current density. Thus, there is an optimum helix diameter at each value of the operating frequency, which is ordinarily selected with a view to obtaining the maximum gain at the middle of the operating bandwidth.

For most TWT's, the helix radius is selected to be within the following limits

$$a \approx (0.2\text{-}0.4)\ \lambda_{slow} = (0.2\text{-}0.4)\ \lambda v_p/c \qquad (6.62)$$

Under conditions of synchronism the ratio c/v_p in this equation can be expressed in terms of the accelerating voltage V_0

$$v_p \approx v_0 = (2eV_0/m)^{1/2};\quad (c/v_p) \approx 505V_0^{-1/2} \qquad (6.63)$$

Equations (6.62) and (6.63) can be used to estimate the helix radius a at a specified wavelength λ and accelerating voltage V_0.

In the millimetric wave band the helix radius becomes inconveniently small; thus, at a wavelength of 5 mm and even at a comparatively high accelerating voltage of 7 kV, the average diameter of the helix by (6.62) and (6.63) proves to range from 0.33 to 0.66 mm, which is within the possibilities of modern technology. In such cases the helix is wound of a wire or band 0.05 mm thick with a pitch of about 0.3 mm; a tube with such a helix is actually manufactured and is described later (Section 6.5*e*). Any further shortening of the wavelength, however, makes the use of helical slow-wave systems an extremely difficult problem, and millimetre-wave TWT's often employ slow-wave structures of the comb or interdigital types.

A comb slow-wave system operated at the first positive spatial harmonic makes it possible to significantly increase the system pitch as compared to that required for operation with the fundamental slow-wave. As an example, the design of a millimetre-wave TWT with a comb slow-wave system is illustrated in Fig. 6.10; this type of slow-wave system displays a greater mechanical rigidity than the helix, as well as higher heat-dissipating capabilities.

The insufficient heat dissipation of a helix becomes one of its main drawbacks when considering the type of a slow-wave structure to be employed in the design of a power TWT. At the decimetric and centimetric wavelengths this drawback may be partly compensated by fabricating the helix of a hollow metal tube and passing a coolant through it.

Another drawback of the simple helix, which makes it unsuitable for high-power applications, is the necessity of increasing the accelerating voltage as higher and higher power levels are to be obtained. This leads to a higher phase velocity of the slow-wave and thus to a lower c/v_p ratio. At the fundamental wave this results in a lower coupled impedance, which tends to approach zero as the c/v_p ratio appro-

aches unity[1]. At high accelerating voltages helix TWT's become prone to self-excitation at spatial harmonics. This effect underlies the operation of *backward-wave oscillators*, where it is used to advantage (refer to Section 6.6), but makes it impracticable to develop amplifier TWT's with helical slow-wave structures, which should operate at accelerating voltages in excess of some 10 kV. The maximum level of output power obtainable with helix TWT's at actually realizable values of the electron beam perveance is thus restricted to units of kilowatts. It will be pointed out for comparison that megawatt output power levels correspond to accelerating voltages of the hundred kilovolt range.

Far more advantageous for power TWT applications is the *modified helix*, the ring and bar structure which is capable of providing c/v_p ratios down to about 2 to 3. Finally, at very high power levels slow wave structures of the periodically-loaded waveguide type, produced by dividing a circular waveguide supporting the E_{01} mode into separate coupled cavities by means of diaphragms, are extensively used. The slow waves here are due to periodic discontinuities in the form of metal diaphragms with a central hole to accommodate the electron beam. The passband of such systems can be made wider by providing peripheral apertures in the diaphragms, these apertures serving to increase the coupling between individual cavities[2].

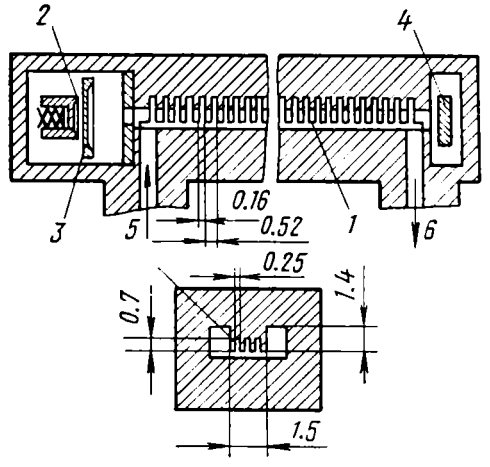

Fig. 6.10. A millimetre-wave TWT with a comb slow-wave structure

1—comb structure with longitudinal groove to accommodate the electron beam; *2*—cathode; *3*—control electrode; *4*—collector; *5, 6*—waveguide input and output, respectively

Typical of this kind of slow-wave systems is the "clover-leaf" design shown in Fig. 6.11 along with a mode transducer to a waveguide of rectangular cross section; the term "clover-leaf" has its origin in the pattern of magnetic lines of force, which is shown in the same Figure in dashed lines. This is a mechanically rigid design capable

[1] As $c/v_p \to 1$ the helix turns into a straight wire conductor carrying the TEM mode, and the longitudinal electric field intensity E_z approaches zero.

[2] Linear electron accelerators can in a sense be considered as devices utilizing a mechanism, opposite to that used in travelling-wave tubes; in these accelerators periodically-loaded waveguides with diaphragms not equipped with additional coupling apertures, are used. Under synchronism the travelling wave gives up its energy to the electron beam, this resulting in electron velocities of the order of scores and hundreds of mega-electron-volts. In some unique models of linear electron accelerators electrons are accelerated to velocities of the order of scores of giga-electron-volts.

of dissipating considerable amounts of heat and having adequate coupled impedances to the fundamental forward wave at beam velocities corresponding to accelerating voltages of the order of 50

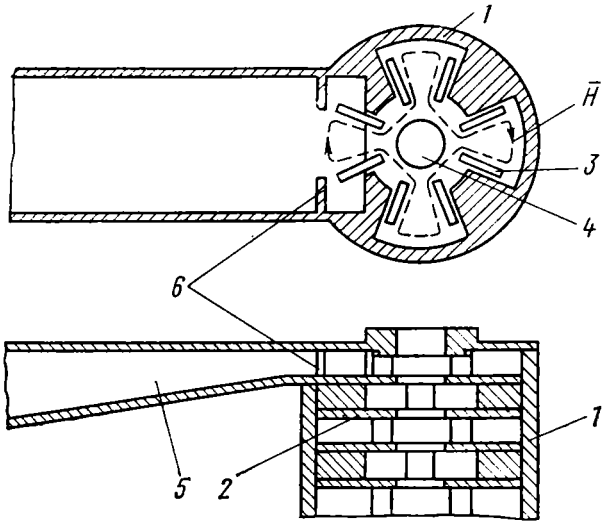

Fig. 6.11. "Clover-leaf" slow-wave structure

1—circular waveguide; *2*—metal plates; *3*—inductive coupling slots; *4*—electron beam channel; *5*—transducer to waveguide of rectangular cross section supporting the H_{10} mode; *6*—inductive iris

to 100 kV. These features account for the extensive use of the "clover-leaf" slow-wave structures in amplifier forward-wave travelling-wave tubes of the centimetric wave band at extremely high levels

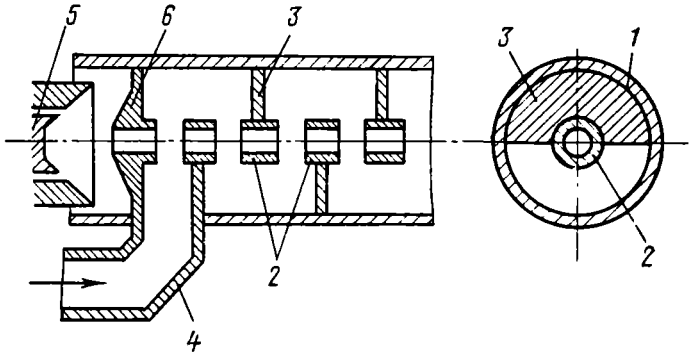

Fig. 6.12. A periodically-loaded waveguide slow-wave structure with partitions of the interdigital type and drift tubes

1—circular waveguide; *2*—drift tube; *3*—metal semidisc; *4*—rectangular input waveguide; *5*—cathode; *6*—accelerating electrode

of pulse power, in excess of about 1 MW. However, the operating bandwidth of these slow-wave structures is considerably inferior to that of the helix and is ordinarily not in excess of some 15 to 20 per cent of the middle frequency.

Another example of the slow-wave structure for power TWT applications is presented in Fig. 6.12. Here the electron beam is passed through gaps between sections of drift tubes in a circular waveguide. A slow-wave structure of this kind can be compared to the meander line discussed in Section 6.6. Operation in this case has to be confined to the first positive spatial harmonic ($p = +1$).

The stack of resonant cavities and other elements of the wave guiding system, including the signal input and output assemblies, of a power TWT bear a striking resemblance to the structure of a multicavity klystron. However, there is an essential difference between the slow-wave structure of a power TWT and the system of klystron cavities. In klystrons, there is practically no coupling between the cavities, except that provided via the electron beam, while in a "cold" slow-wave structure of a power TWT a travelling wave can propagate between the input and output assemblies in both directions. On the one hand, this property is responsible for the greater tendency of the TWT to self-excitation, so that the slow-wave structure of power TWT's has to be equipped with a sever to ensure operational stability, as in the case of a helix tube. On the other hand, working with propagating waves makes the operating bandwidth of a power TWT considerably wider than that of a multicavity klystron; for instance, the bandwidth of a 10-cm pulse power TWT of the megawatt power range may constitute about 10 to 15 per cent of the middle frequency, while with a multicavity klystron it will be but some 1 to 5 per cent.

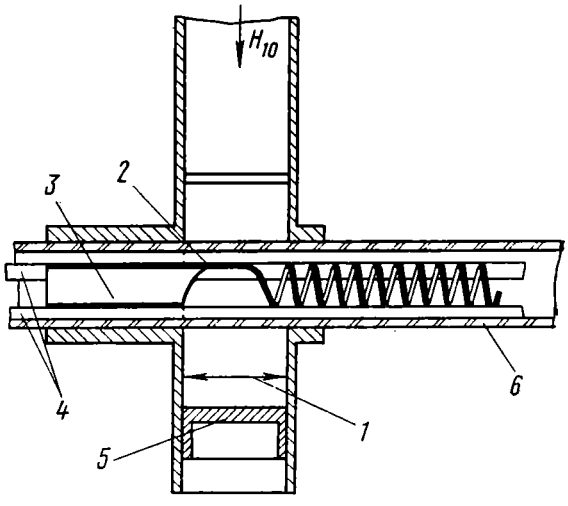

Fig. 6.13. Waveguide-to-helix transducer
1—narrow wall of waveguide; *2*—probe; *3*—quarterwave choke; *4*—dielectric supports of the helix; *5*—tuning plunger; *6*—glass envelope of the TWT

6.5b. Transducers and Severs

When designing a TWT of any kind, much attention should be given to the input and output transformers which are required to provide a fair match of the slow-wave system with the coaxial or waveguide feeder lines, by which the TWT is connected into a circuit. Examples of such designs have been treated in Section 11.9 of the textbook "Microwave Engineering". In case of a helix system the most common type of transducer is formed of a rod or tube terminating the helix and protruding into a waveguide through its wide wall to

serve as an exciting probe. A shorting plunger in the waveguide (Fig. 6.13) makes transducer tuning possible and enables optimum matching at the middle of the frequency band of interest.

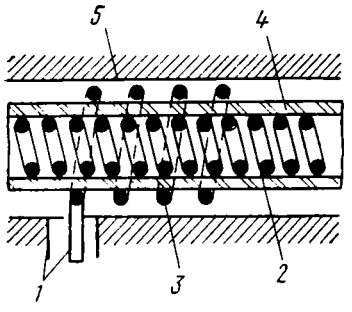

Fig. 6.14. Coupled helices as the input and output impedance transformers in a TWT
1—coaxial line; *2*—main helix; *3*—section of external helix; *4*—glass envelope; *5*—screen

The rectangular waveguide forming the TWT input and output is ordinarily made with a slightly smaller dimension of the narrow wall (for instance, the cross-sectional dimensions of a waveguide used for this purpose with 10-cm TWT designs are 10×72 mm) as compared to the standard dimensions. This is done with a view to improving wideband matching to the helix and, at the same time, reducing the distortions of the static magnetic field set up by a solenoid, a permanent magnet or a system of magnets for beam focussing.

Another extensively used version of compact tunable transducer utilizes coupled helices. In this case the input and output guides of the TWT are in the form of coaxial lines, as shown in Fig. 6.14. The outer helices encompass the main helix (the slow-wave system) but are usually located outside the tube envelope. Analysis and practice show that transducers of this kind are capable of providing extremely wideband matching (VSWR not in excess of about 1.5:1 in an octave bandwidth) if the coupling and slow-wave helices are contrawound.

Examples of transducer designs for power TWT's with the periodically-loaded waveguide type of slow-wave structure are presented in Figs 6.11 and 6.12.

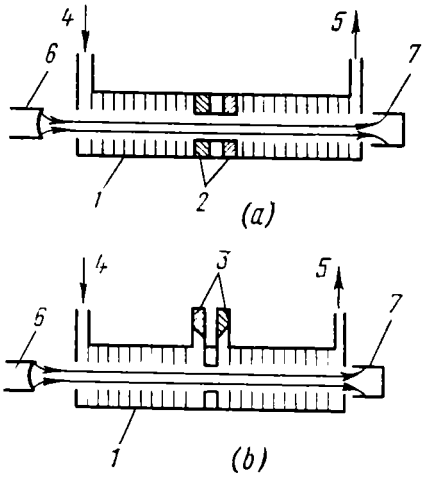

Fig. 6.15. Power TWT with internal (*a*) and external (*b*) sever load to prevent self-excitation
1—slow-wave structure of the ridge-waveguide type; *2*—absorber; *3*—matched waveguide load; *4*, *5*—input and output; *6*—cathode; *7*—collector

Earlier (Section 6.4*e*) it was shown that the slow-wave structure of a TWT has to be equipped with a sever to ensure performance stability. At low power levels this sever (pad) is usually in the form of a dissipative material coating (aquadag) on the dielectric supports of the helix, this providing "cold" loss of at least 50 dB. In medium power tubes this pad is a separate element and the loss is introduced via a coupling helix, mounted outside the tube envelope. Finally, in power

tubes with slow-wave structures of the periodically-loaded waveguide type, blocks of carbonized ceramics are placed between the diaphragms (Fig. 6.15*a*) near the middle of the system to function as pads; at very high power levels external loads terminate the sever provided in the slow-wave structure and are mounted outside the envelope, as shown schematically in Fig. 6.15*b*. There is ordinarily no need to provide severs or pads for the slow-wave structures of millimetre-wave TWT's, because the inherent circuit loss is usually adequate to prevent self-excitation effects.

6.5c. Typical Design Features and Parameters

The parameters of five typical forward-wave amplifier tubes of different output power levels, designed for application in various classes of microwave equipment, are listed in Table 6.1. The first of these

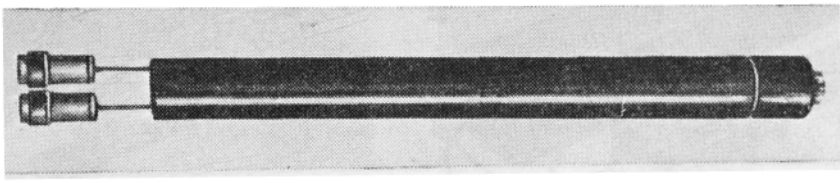

Fig. 6.16. Low-noise 10-cm TWT

tubes is of the low-power, low-voltage class of helix TWT's with a focussing solenoid; the external appearance of a typical low-noise TWT is shown in Fig. 6.16. These tubes are provided with a multianode electron gun (Fig. 6.17) employed to reduce the noise figure.

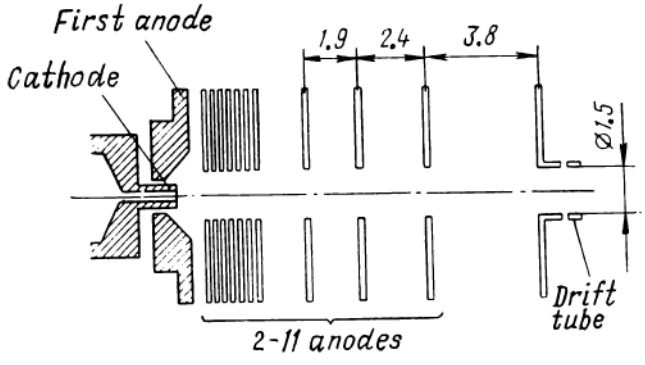

Fig. 6.17. Electron gun of low-noise TWT (dimensions in millimetres)

A typical output TWT of medium power level of the helix type with a waveguide input and output is shown in Fig. 6.18*a*; the parameters of such tubes are given in the Table (No. 2), the parameters of a millimetre-wave helix tube of relatively high output power level (up to 0.5 W) are given for comparison (No. 3).

Table 6.1

Parameters of Typical Amplifier TWT's

No.	Tube type, middle wavelength	Operating bandwidth, per cent	Accelerating voltage	Collector current	Gain, dB	Output power	Noise factor, dB	Efficiency, per cent	Focussing magnetic field, tesla	Design of input and output	Type of slow-wave system
1	Input low-noise TWT of the 10-cm band (Fig. 6.16)	8	370 V	0.2 mA	25	1 mW	4	—	0.04-0.08	Coaxial lines and coaxial cavities	Helix
2	Output TWT of the 7.5-cm band (Fig. 6.18*a*)	33	2.5 kV	30 mA	30	10 W	—	13	0.065	Coaxial-to-waveguide transducers	Same
3	Medium power TWT of the 5-mm band	20	7 kV	3 mA	30	0.5 W	—	2.5	0.15	Waveguides	Same
4	Power TWT for the 3-cm band (c.w. device)	5	20-30 kV	0.9-1.5 A	15	5 kW	—	22-30 (depressed collector)	0.1	Same	"Clover-leaf"
5	High-power pulsed TWT for the 10-cm band (Fig. 6.19)	10	100 kV	90 A	35	3 MW (pulse duration of 2 μs)	—	34			Same

The drawbacks of ordinary focussing solenoid coils (Fig. 6.18*a*) are their considerable dimensions and weight, as well as a separate supply source. These drawbacks are avoided by using periodic *focussing systems of permanent magnets*, this being at present the main means for beam focussing in TWT's[1]. The external appearance of a helix TWT with a focussing system of periodic permanent magnets (abbreviated usually as PPM) is shown in Fig. 6.18*b*; this tube is designed to operate in the 5.6-10.4 GHz frequency range with a c.w.

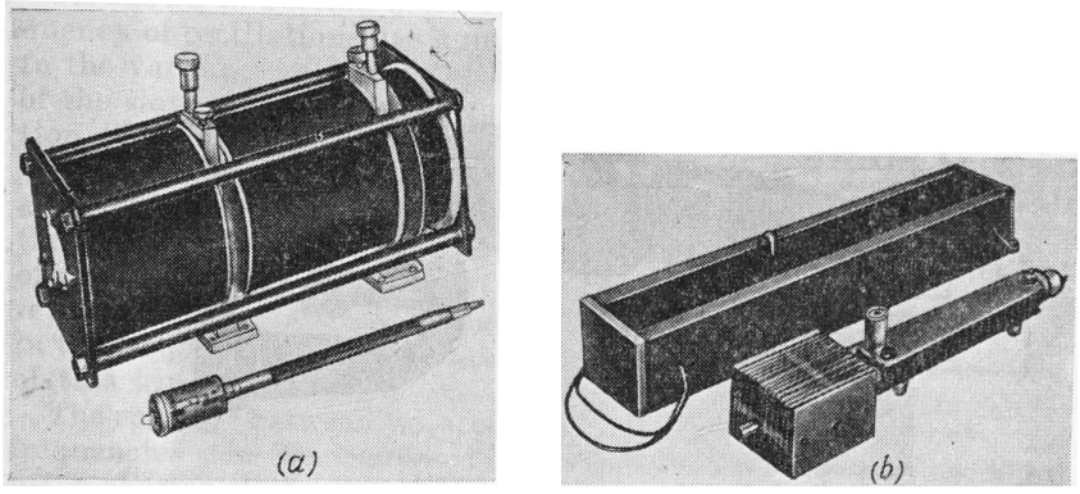

Fig. 6.18. Typical helix TWT
(*a*) with a glass envelope and focussing solenoid (medium power tube; note the input and output waveguides with tuning plungers); (*b*) metal-to-ceramic power TWT with periodic system of permanent magnets for focussing

output power of about 500 W. This tube is of the metal-to-ceramics design with coaxial input and output, it requires forced-air cooling of the collector.

Focussing systems of the electrostatic and ion types are also of interest, being advantageous from the point of view of further reducing the TWT weight. However, up to the present time these types of focussing systems have not found any noticeable application in practical TWT designs.

The tubes listed in Table 6.1, Nos 4 and 5, are typical power amplifiers provided with a "clover-leaf" slow-wave structure (refer to Section 6.5*a*). The external appearance of a 10-cm pulse TWT is presented in Fig. 6.19; as can be noted, these tubes are in many respects similar to multicavity klystrons.

---

[1] The theory and analysis of electron beam focussing systems constitute the subject of a course in electron-beam devices and are not treated in the present textbook.

TWT's of the O-type are finding an ever widening use, ranging from wideband amplifiers in microwave receivers to high-power output stages of pulsed and c.w. transmitters. One of the most extensive fields of TWT applications is in multichannel telecommunication systems, both in radio relay and in satellite equipment. Power TWT's are used to drive phased arrays of radar installations with tunable directivity patterns, these antenna arrays containing a great number (up to several thousand) radiating elements.

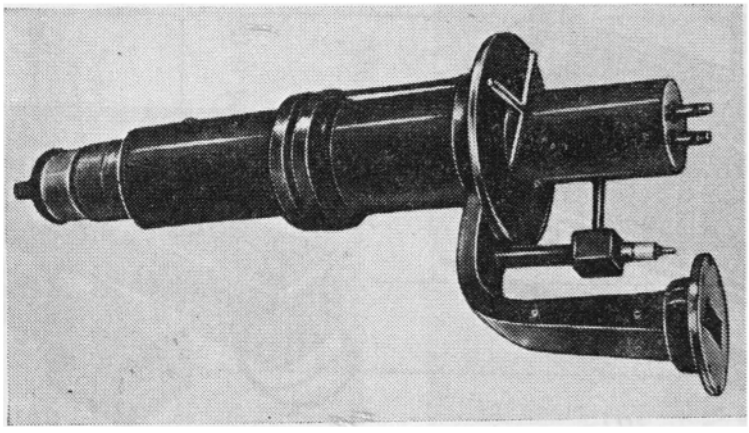

Fig. 6.19. High-power pulse TWT of the 10-cm band

At the same time TWT's are used also as frequency converters and frequency multipliers, phase modulators and as sources of pulses of extremely short duration. TWT applications as noise sources in radar countermeasures systems and in measuring equipment are also of interest.

Among the unusual but nevertheless quite actual problems is the development of TWT devices with *photo*-cathodes or *photo*-multipliers instead of the ordinary thermionic cathode; such designs may prove to be very useful in receivers of the optical band of wavelengths where a carrier signal provided by a laser and modulated by a microwave frequency has to be processed.

Further development of O-type TWT's will to a considerable extent be aimed at reducing their weight and dimensions and improving their mechanical properties. Progress in beam focussing techniques can be expected to become quite an important factor; as an example, the use of permanent magnets fabricated of samarium-cobalt alloys may be cited. Further reduction of the noise figures in input TWT's and an increase in the output power level and efficiency of power devices may also be expected.

6.6. O-Type Backward-Wave Tubes

6.6a. TWT Oscillator and Backward-Wave Tube

In principle, the forward-wave travelling-wave tubes described in the previous Sections can be employed as oscillators as well as amplifiers; to this end it is necessary only to provide a path of positive feedback between the TWT output and input. This path of positive feedback can be either an external or an internal one.

As shown in Section 6.4*e*, with internal positive feedback the frequency of oscillations has a number of discrete values corresponding to the various oscillation modes of the slow-wave system. Equation (6.59) can be used to demonstrate that these frequencies are quite closely spaced due to the considerable electric length of the TWT slow-wave structure, this causing abrupt changes in the frequency of an oscillator of this kind.

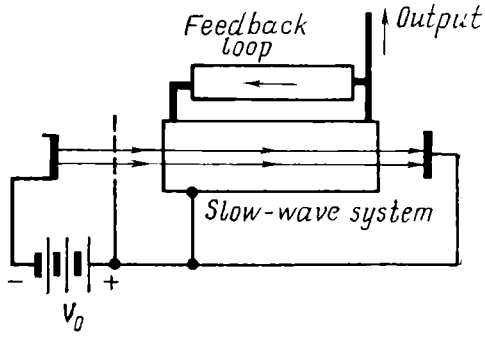

Fig. 6.20. TWT oscillator with external feedback loop

The spacing between adjacent frequencies can be increased by using shorter slow-wave structures, or by using an external feedback assembly, which features a shorter electric length at the same geometrical dimensions. The diagram of an oscillator of this kind is shown in Fig. 6.20; the external feedback here may be simply a section of guide (coaxial or waveguide) with a phase shifter. By including a band-pass filter into the feedback assembly it is possible to avoid self-excitation at unwanted frequencies.

The geometrical length and phase constant of the external feedback path will be designated as $l_{f.b}$ and $\beta_{f.b}$, respectively: $\beta_{f.b} = \omega/(v_p)_{f.b}$, where $(v_p)_{f.b}$ is the phase velocity of the wave in the feedback assembly. The phase condition of self-excitation of this system can be determined by summing up the phase shifts in its separate portions and equating the sum to a multiple of 2π

$$\beta_{f.b} l_{f.b} + \beta l = 2\pi n; \quad \frac{\omega l_{f.b}}{(v_p)_{f.b}} + \frac{\omega l}{v_p} = 2\pi n \qquad (6.64)$$

where β is the wave phase constant in the slow-wave structure of the TWT and l is the length of this structure; in the general case n can be any positive integer, including zero.

Equation (6.64) describes the condition of the feedback signal being in phase with the initial signal at the TWT input. In the general case, the phase velocity of the wave in the TWT and its phase

constant β are functions both of the frequency and the accelerating voltage V_0. Variations of this latter will therefore cause corresponding changes in the frequency of oscillations at each oscillation mode, i.e. this TWT oscillator displays electronic tuning properties.

To obtain wideband operation, the phase of the feedback signal should be made independent of frequency, this condition corresponding to

$$\frac{d}{d\omega}(\beta_{f.b}l_{f.b}+\beta l)=0; \quad l_{f.b}\frac{d\beta_{f.b}}{d\omega}+l\frac{d\beta}{d\omega}=0$$

or

$$\frac{l_{f.b}}{(v_g)_{f.b}}+\frac{l}{v_g}=0 \tag{6.65}$$

where $(v_g)_{f.b}$ and v_g are the group velocities (the rate of energy transfer) in the respective sections of the circuit under treatment

$$(v_g)_{f.b} = d\omega/d\beta_{f.b}; \quad v_g = d\omega/d\beta$$

Equations (6.64) and (6.65) provide an insight into the main drawbacks peculiar to oscillators designed with forward-wave tubes. Under normal positive (forward) dispersion, both terms in (6.65) are positive, this resulting in both phase angles in (6.64) changing in unison with frequency variations. Thus, it becomes impossible to provide a zero total group delay of the signal, as required by (6.65), this limiting the range of electronic tuning of TWT oscillators, as with devices having resonant oscillatory systems.

The actual range of electronic tuning of a TWT oscillator is from tenths to units of a per cent of the middle frequency, i.e. is of the same order of magnitude as in reflex klystrons. It should be noted, however, that a TWT oscillator is far more complex in design, supply arrangement and maintenance. Because of this and due to the advent of backward-wave tubes with extremely wide voltage tuning ranges, TWT oscillators are not used in practice to any significant extent.

Thus, despite its wideband properties when used as an amplifier, a TWT is incapable of providing high quality performance characteristics as a voltage-tunable oscillator.

The range of electronic tuning could be appreciably widened if the group velocities v_g and $(v_g)_{f.b}$ in equation (6.65) could be made to be of opposite directions. This can be accomplished only by using either a slow-wave structure or a feedback loop with *negative dispersion properties*; in this case the group and phase velocities of the wave are of opposite directions and the group velocity is therefore negative.

The dispersion of all ordinary transmission lines is normal and positive, i.e. v_g is positive and $dv_p/d\omega$ is negative; transmission lines are therefore unsuitable for the purpose in question. The situation changes, however, if a *periodic slow-wave structure* with no exter-

nal feedback is employed. All the following argumentation is based on the utilization of beam synchronism with one of the backward (negative) spatial harmonics, when the phase velocity and the group velocity are of opposite directions.

6.6b. Operating Principle of O-Type BWO

The circuit diagram of a backward-wave oscillator of the O-type is presented in Fig. 6.21. In general the design of this oscillator tube resembles that of the forward-wave TWT of the O-type, the difference being in the location of the power output (refer to Fig. 6.3). Since this tube is designed as an oscillator rather than an amplifier, the circuit of a BWO can also be compared with that of a TWT oscillator presented in Fig. 6.20.

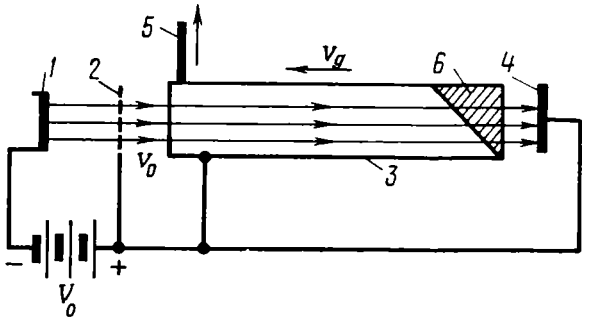

Fig. 6.21. Circuit of the O-type backward-wave oscillator

1 — cathode; *2* — accelerating electrode; *3*—periodic slow-wave structure; *4*—collector; *5*—power output; *6*—matched load

The principles governing backward-wave oscillator performance can be explained by assuming a radio-frequency signal to be injected in some way into the slow-wave structure of a TWT *from the collector end*, this resulting in a signal travelling from right to left with a group velocity v_g.

If the slow-wave structure were perfectly uniform and its field contained no spatial harmonics, the direction of the phase velocity would coincide completely with that of energy transfer, i.e. would be opposite to the direction of electron beam travel. In this case there would be no effective interaction between the electron beam and this wave. If, however, the slow-wave structure is a periodical one, its electromagnetic field may be considered as the sum of an infinite multitude of waves (spatial harmonics) with phase constants β_n depending on the number n of the spatial harmonic. The phase velocities of these harmonics are directed both in the direction of energy transfer (forward waves) and in the opposite direction (backward waves). In the case under treatment (Fig. 6.21) the direction of electron beam travel coincides with that of the phase velocities of the backward waves.

Suppose the accelerating voltage V_0 to be adjusted so as to provide synchronism of the electron beam with one of the slow backward waves, i.e.

$$v_0 \approx |v_p|_n; \quad n < 0 \tag{6.66}$$

Electrons of the beam will then encounter one and the same phase of the longitudinal radio-frequency field, while passing in turn the discontinuities of the structure, and will interact with the field of the synchronous harmonic as if there were present only one slow wave. In this case part of the kinetic energy of the beam will be transferred to the radio-frequency field of the wave.

As is known from electrical engineering, the phase constant of this spatial harmonic is a function of the spatial periodicity of the slow-wave structure L and the number of the harmonic in question n

$$\beta_n = \beta_0 + 2\pi n/L \tag{6.67}$$

where β_0 is the phase constant of the fundamental wave.

The phase velocity of the spatial harmonic $(v_p)_n$ can be determined from

$$(v_p)_n = \omega/\beta_n \tag{6.68}$$

Thus, the general condition of electron beam interaction with the field of a backward wave, with (6.66), (6.67) and (6.68) taken into account, will be

$$\left|\frac{\omega}{\beta_0 + 2\pi n/L}\right| = (2eV_0/m)^{1/2}; \quad n < 0 \tag{6.69}$$

where V_0 is the accelerating voltage (Fig. 6.21).

An essential feature of this interaction is the existence of *inherent feedback*, which is responsible for the device becoming self-excited. Indeed, the slow-wave structure and the electron beam constitute a feedback loop. In the electron beam the direction of energy transfer coincides with the direction of electron bunches movement, whose average velocity is v_0. In the slow-wave structure the energy is transferred in the opposite direction at *coincident* directions of the phase velocity $(v_p)_n$ and beam velocity v_0, as illustrated in Fig. 6.22; for comparison, the directions of the electron beam and wave velocities in a forward-wave tube are shown in the same Figure.

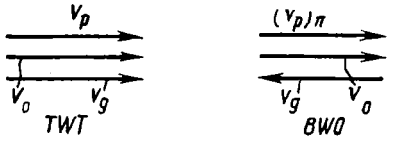

Fig. 6.22. Electron beam velocity, phase velocity and group velocity in forward-wave and backward-wave tubes

It is again assumed that a radio-frequency signal propagates along the slow-wave structure towards the electron gun end of the BWO shown in Fig. 6.21; the electron beam will then be velocity-modulated due to interaction with the synchronous spatial harmonic. The beam will then become density-modulated and, moving towards the collector, induce radio-frequency currents in the slow-wave structure. However, since the energy of the wave interacting with the electron beam is transferred in a direction opposite to the electron

beam, the wave will build up towards the electron gun end of the slow-wave structure, producing a radio-frequency signal at the tube output which is greater than the initial signal. Thus the tube acquires the properties of an oscillator.

The geometrical length of the electron beam is exactly the same as the length of the slow-wave structure. This circumstance, together with the opposite directions of group velocities (i.e. speeds of energy transfer) in the two sections of the feedback loop, provides that condition (6.65), determining a wide range of voltage tuning, be satisfied.

Thus, the electron beam in a backward-wave tube performs two functions, that of an energy source and that of an element of a positive feedback loop. This feature is inherent in the BWO performance and is essentially unavoidable, as distinct from other types of microwave oscillators.

In cases when the output of a backward-wave oscillator (i.e. the electron gun end of the slow-wave structure) terminates in a matched load, the degree of matching at the other end of the structure is of no importance. Not so, however, if the external load is mismatched—the wave reflected from this load will again appear in the slow-wave structure, but there can be no interaction of this reflected wave with the electron beam. Nevertheless, a mismatch at the collector end will cause re-reflection of this wave, this twice reflected wave being capable of interacting with the beam, thereby changing the level of output power.

To avoid these undesirable effects the collector end of the slow-wave structure ordinarily terminates in a matched load (absorber) as illustrated in Fig. 6.21. As a rule, this load is mounted inside the tube envelope, thus being an integral part of the structure, and does not, obviously, affect the tube operation, provided the useful load is fairly matched.

6.6c. Oscillation Zones in an O-Type Backward-Wave Oscillator

The electron beam at the input to the slow-wave structure of a BWO is uniform and free of any density or velocity modulation. At the electron gun end of the structure (at the power output) the beam interacts with the longitudinal radio-frequency field E_z which produces, under synchronism, velocity modulation gradually changing into density modulation of the electron beam. As demonstrated in Section 2.8*d*, the electron bunches are grouped around electrons which enter the interaction space at the region where the field intensity E_z changes from accelerating to retarding.

As in a TWT, the average velocity of the beam v_0 should slightly exceed the phase velocity of the wave $(v_{ph})_n$ so as to ensure that the electron bunches effectively give up their energy to the wave. In

a moving reference plane the electron bunch will appear under these conditions as slowly drifting through the entire halfwave of the retarding field during its time of transit along the length of the system. This means that the phase shift of the wave along the system length relative to the electron transit angle should be π. Conditions are also possible, when this difference will be $\pi(2p+1)$

$$\frac{\omega l}{|v_{ph}|_n} - \frac{\omega l}{v_0} = (2p+1)\pi$$

where p is any integer, including zero.

Physically, $p = 1$ means that the electron bunch moves 1/3 of the total transit time in a retarding field, another third, in an accelerating field and the last third, again in a retarding field.

This equation can be rewritten as

$$(m/2eV_0)^{1/2} = \frac{1}{|v_{ph}|_n} - \frac{p+1/2}{fl} \tag{6.70}$$

by taking into account the common relation between the average electron velocity and the accelerating voltage; here f is the frequency of the signal being amplified or generated ($f = \omega/2\pi$).

From this equation it follows that a backward-wave tube has several broad oscillation *zones* $P = f(V_0)$, each of them characterized by a certain number p ($p = 0; 1; 2; 3; \ldots$). The $p = 0$ zone features the highest output power because in this case the slow-wave structure length is utilized most efficiently.

Equation (6.70) describes not only the oscillation zones of a backward-wave tube, but the conditions of *regenerative amplification*, as well. Indeed, as any other oscillator, backward-wave tubes are characterized by a certain value of the starting current I_s. At low electron beam current values I_0, the amplitude condition of self-excitation is no longer satisfied. However, the positive internal feedback is the characteristic property of the mechanism of BWO operation, and therefore the gain of this tube can become unlimitedly high as the beam current approaches the value of starting current.

The dependence of output power and gain of a backward-wave tube on the value of the d.c. convection current in the beam is qualitatively shown in Fig. 6.23. In principle, a backward-wave amplifier differs from a backward-wave oscillator only in the presence of a signal input, which is at the collector end of the slow-wave structure instead of the matched load shown in Fig. 6.21.

The starting current of higher-order zones is considerably higher than that for the zero zone, as shown in Fig. 6.23. The reason for this is the above mentioned lower efficiency of utilization of the slow-wave structure length at increased zone numbers.

Only oscillations at the zero zone are of practical interest. To exclude the possibility of simultaneous oscillations at the zero and the $p = 1$ zones at different frequencies, the operating beam current is ordinarily set to be from 2 to 5 times higher than the starting current for the zero zone, but lower than the starting current for the $p = 1$ zone (Fig. 6.23).

Electron beam interaction with the backward wave is sometimes the cause of parasitic oscillations appearing in forward-wave tubes. In contrast to oscillations produced by wave reflection (refer to Section 6.4*e*), this kind of parasitic instability is completely independent of the matching at the tube terminals.

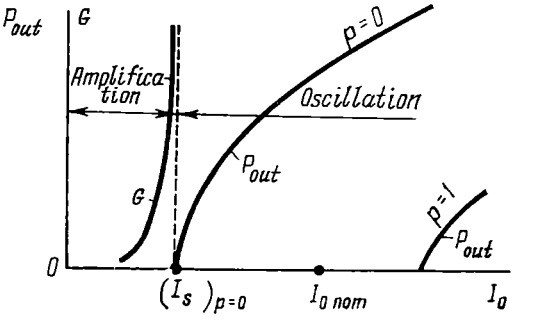

Fig. 6.23. BWO output power and gain *vs* starting current at $V_0 = \text{const}$

The intensity of a spatial harmonic decreases with the distance from the slow-wave structure conductors the faster, the higher is the number of this harmonic. Instability effects due to self-excitation are therefore usually encountered only at the first backward harmonic ($n = -1$); this makes it possible to limit the present discussion of the properties of backward-wave tubes to only this spatial harmonic.

6.6d. Electronic Tuning in a BWO of the O-Type

The existence of a wide voltage tuning range is the main advantage of backward-wave tubes, and therefore this problem is worth being examined in more detail.

Physically, the existence of electronic tuning, i.e. the dependence of the oscillation frequency on the value of the accelerating voltage applied, can easily be accounted for. The condition for a positive feedback in the system is that the beam is in approximate synchronism with the first backward harmonic ($n = -1$). Variations of the accelerating voltage should therefore cause changes in the velocity of this backward wave; since the slow-wave structure exhibits dispersive properties, variations in the accelerating voltage should result in changes of the oscillation frequency (refer to Fig. 3.14), i.e. the device should be voltage-tunable. The rate and polarity of electronic tuning depend on the shape of the dispersion characteristic curve of the slow-wave structure.

Spatial harmonics in slow-wave structures of the periodic type always feature *anomalous* dispersion, i.e. the absolute value of the phase velocity $|v_p|_n$ increases with a rise in frequency. This may

be easily confirmed by examining equation (6.68) and (6.67)

$$(v_p)_n = \frac{\omega}{\beta_0 + 2\pi n/L} = \frac{1}{\dfrac{1}{(v_p)_0} + \dfrac{2\pi n}{\omega L}} \tag{6.71}$$

where $(v_p)_0$ is the phase velocity of the fundamental wave (zero harmonic).

It follows that under synchronism with a backward wave the frequency of oscillations of a BWO should *increase* with a rise in the d.c. accelerating voltage. Corresponding graphs and qualitative explanations were presented in Section 3.4 in the treatment of microwave oscillators with non-resonant oscillatory systems.

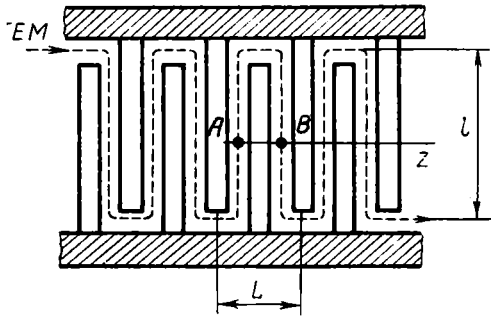

Fig. 6.24. Wave propagation along the interdigital slow-wave structure

Consider, as an example, a slow-wave structure of the interdigital type, which is widely used in backward-wave tubes. Suppose that a TEM wave propagates in the gaps between the digits in the direction indicated in Fig. 6.24 by a dashed arrow. The rectilinear electron beam passes parallel to the surface of the digits along the middle line of the system and has an average velocity v_0. First assume the electron beam to travel in the $+z$ direction; in this case the electrons periodically pass through a radio-frequency field E_z which is concentrated in the spaces between the digits. The rest of the time the electrons drift due to inertia, as in the drift space of an amplifier klystron.

To obtain phase synchronism with the wave, it is necessary to ensure that the electron transit time between points A and B in Fig. 6.24 be equal to the sum of the wave transit time and a halfcycle of the radio-frequency oscillations (because the electron beam intersects the folded line at point B in a direction opposite to that at point A). Addition of any whole number of oscillation periods T will not disturb synchronism

$$\tau = \frac{l + L/2}{c} + \frac{T}{2} + nT; \quad n = 0; \pm 1; \pm 2; \ldots$$

where c is the velocity of light in free space.

Since $\tau = L/2v_0$,

$$v_0 = c\,\frac{L}{2l + L + (2n+1)\lambda} \tag{6.72}$$

where λ is the free-space wavelength.

Velocity v_0, as defined by equation (6.72), will ensure that the electrons of the beam pass each gap between the digits of the slow-wave structure at a constant phase of the radio-frequency field. Therefore, the system can be imagined to carry a slow wave along the z axis with a phase velocity described by equation (6.72). This kind of intermittent interaction of the beam with the field of a radio-frequency wave can be compared to the stroboscopic effect: the beam appears as "stationary" relative to the field.

At $n = -1$ the synchronous beam velocity and the corresponding wave phase velocity are maximum and equal to

$$v_0 = (v_p)_{-1} = -\frac{cL}{\lambda - (2l + L)} \tag{6.73}$$

It is just this wave, which is the fundamental one in an interdigital slow-wave structure, that is utilized in backward-wave tubes.

The negative sign before the right-hand member in equation (6.73) indicates that the electron beam should be passed in a direction opposite to $+z$, i.e. opposite to the direction of energy transfer along the line, to obtain synchronism with the $n = -1$ spatial harmonic. Taking this into account, as well as the beam velocity in devices of the O-type, as described by equation (2.14), results in

$$(2eV_0/m)^{1/2} = c\frac{L}{\lambda - (2l + L)} \tag{6.74}$$

and hence the wavelength of the amplified or generated signal can be determined as a function of the accelerating voltage V_0 as

$$\lambda = 2l + L + cL\,(2eV_0/m)^{-1/2} \tag{6.75}$$

assuming the tube geometry (i.e. l and L) is given.

This equation, together with the dispersion characteristic of the interdigital system, as described by equation (6.73), can be used to plot the electronic tuning characteristic curve of a BWO; the results for the case when $L = 2$ mm and $l = 9$ mm are presented in Fig. 6.25. As can be noted, a backward-wave tube is capable of providing a voltage tuning range of the order of an octave and even more at practicable variations of the accelerating voltage. The tuning characteristic curve, however, is far from linear. To obtain an octave (two-fold) change in the operating

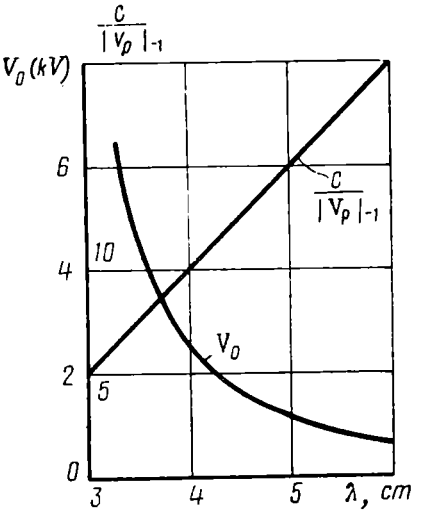

Fig. 6.25. Dispersion characteristic and electronic tuning of a BWO of the O-type with an interdigital slow-wave structure ($L = 2$ mm, $l = 9$ mm)

wavelength and frequency, the accelerating voltage has to be changed by a factor of about ten.

Frequency tuning is accompanied by variations of the output power. The graph of dependence of the output power on the accelerating voltage resembles the oscillation zone curve in a reflex klystron but is even more irregular (output power variations inside one zone can be up to 10 dB and even more if the external and internal loads are not properly matched). This irregularity of the output power within an oscillation zone is one of the main drawbacks of a BWO, because in most practical applications an approximately constant level of output power is one of the common requirements.

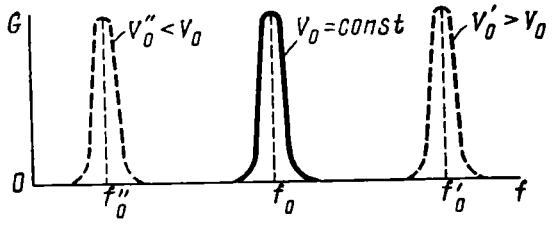

Fig. 6.26. Gain of a regenerative backward-wave amplifier *vs* frequency at three fixed values of the accelerating voltage

A backward-wave tube retains its voltage-tunable properties when used as an amplifier, too. This can be illustrated by examining the frequency dependence of a BWO gain at a constant accelerating voltage, as shown in Fig. 6.26. The function G *vs* frequency is in the form of sharp resonant peaks with the middle corresponding to synchronism; variations of the accelerating voltage will shift this curve along the horizontal axis, as indicated in the Figure in dashed lines.

Thus, a backward-wave tube may be used as a high-Q resonant amplifier with wideband electronic tuning of the resonant frequency f_0. This is one of the essential peculiarities of backward-wave tubes. in which they differ from amplifiers of the forward-wave type, as well as from "true" resonant amplifiers of microwave signals such as multicavity klystrons, for instance.

6.6e. Methods of Analysing the Performance of a BWO of the O-Type

The linear (small-signal) theory of backward-wave tubes can be based on the self-consistent field method examined in Sections 6.2 and 6.3 for the case of forward-wave devices; it is only necessary to take into account the change in direction of energy transfer along the slow-wave structure when deriving the equation of a long line, in which a density-modulated electron beam induces radio-frequency currents. The dispersion characteristic of a BWO, by analogy with equation (6.30), can be presented as

$$\frac{KI_0}{2V_0}\,\frac{\Gamma^2\Gamma_0\beta_e}{(\Gamma_0^2-\Gamma^2)(j\beta_e-\Gamma)^2}=-1 \qquad (6.76)$$

with the same symbols, as in Section 6.2.

Analysing this equation by the same methods, it is again possible to examine three waves with propagation constants nearly approximating that of the fundamental (in the present case—the $n = -1$ spatial harmonic) in the slow-wave structure. The initial conditions at the place the electron beam enters the slow-wave structure should allow for the fact that the sum of the intensities of all three waves is the intensity of the *output*, rather than the input signal. At this

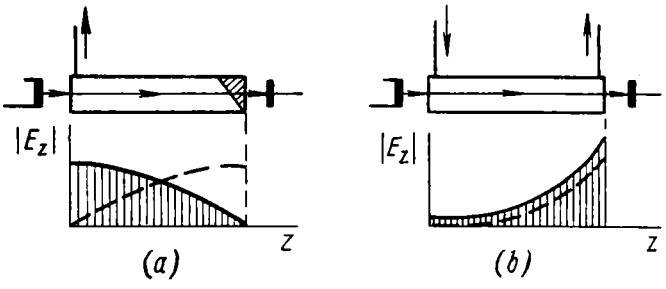

Fig. 6.27. Pattern of radio-frequency field distribution along the slow-wave system of a BWO and TWT. Distribution of the radio-frequency component of beam convection current is indicated in dashed lines

section of the structure the total velocity and density modulation of the electron beam is zero, as in a TWT. Furthermore, the total intensity of the three waves at the collector end of the slow-wave structure in case of a backward-wave tube should also be zero.

Calculations of the starting current for this oscillator and the electronic efficiency, when the device is excited at the zero oscillation zone ($p = 0$), yield

$$I_s \approx 0.124 V_0/KN^3 \tag{6.77}$$

$$\eta_e \approx 0.84C \tag{6.78}$$

Thus, the electronic efficiency of a BWO is determined by the gain parameter C, as in forward-wave tubes, but is somewhat lower than in these latter.

These conclusions have been confirmed by experiment. The total efficiency of BWO's of the O-type is usually units of per cent. Therefore, these devices can be mainly used as low-power local oscillators.

The self-matched field method also gives an idea of other peculiarities of backward-wave tube performance, in particular, of the field distribution along the axis of the slow-wave structure. A graph illustrating qualitatively the total electric field intensity is presented in Fig. 6.27*a* with a similar graph for the slow-wave structure of a TWT (following from the theory of Section 6.2) shown in Fig. 6.27*b* for comparison. In contrast to a TWT, the output signal of a BWO cannot be considered with regard to only one increasing wave. The

graph of field distribution along the structure of a BWO should therefore be considered as the effect of interference of all the three waves, while the field in the vicinity of the TWT output approaches an exponential pattern.

The lower rate of field build-up and "saturation" effects in the vicinity of the BWO output may be explained physically by the electron beam in this region featuring the lowest density modulation. The radio-frequency component of convection current approaches zero at the system output, but is at a maximum at the collector end, where the radio-frequency field is zero.

A simplified method of calculation is widely used to design backward-wave tubes, along with the strict solution; this method is based on approximating the radio-frequency *field specified.* By this technique, the law of distribution of the radio-frequency oscillations along the slow-wave structure is presupposed ("guessed") and the interaction of the electron beam with this field is calculated. A cosine function, roughly approximating the curve $|E_z| = f(z)$ in Fig. 6.27*a*, may be used to estimate this distribution. Other functions for approximating the field in a BWO are also used and provide various degrees of accuracy in design calculations of this type of microwave devices.

6.7. Designs and Parameters of Backward-Wave Tubes

Backward-wave tubes are mostly designed to operate as wideband voltage-tunable oscillators with output power levels about scores of milliwatts or units of watts. The devices have much design features in common with low-power TWT's. As mentioned, a characteristic outward property of a BWO, as compared to a TWT, is that the power output is located at the electron gun end, while the collector end of the BWO slow-wave structure terminates in a matched load (absorber).

The slow-wave structure of a BWO is of the periodic type with the backward-wave as the fundamental, or systems with a pronounced backward spatial harmonic (in the latter the fundamental wave is a forward one). Operation with the fundamental wave is preferable since the field of the fundamental wave features the highest amplitude. The coupled impedance at the fundamental wave is higher than with other spatial harmonics.

Among the systems with a fundamental backward wave are the interdigital systems (Fig. 6.24), the twin-helix system, the ladder systems and the "helix-in-a-screw-groove" system (schematically illustrated in Fig. 6.28); all these types are extensively used in actual designs.

The main parameters of three typical low-power backward-wave oscillator tubes are listed in Table 6.2 with the external appearance

of the first of these tubes and its mounting into a cylindrical permanent magnet shown in Fig. 6.29. This tube is of the glass envelope variety and features a coaxial power output; the electronic tuning range of this particular type comes to an octave.

Backward-wave tubes of the O-type open up wide possibilities for operation at the shorter millimetric waves, as well as for the

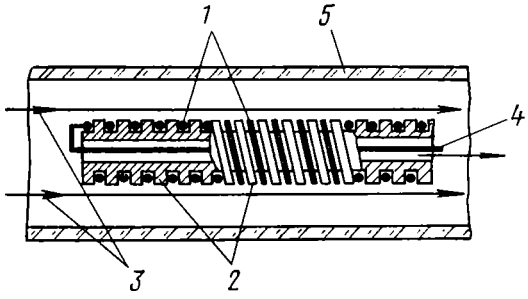

Fig. 6.28. Slow-wave structure of the "helix-in-a-screw-groove" type with coaxial power output

1—wire helix; *2*—screw ridge; *3*—hollow electron beam; *4*—power output; *5*—glass envelope of the BWO

submillimetric wave band. In this respect these devices are superior to reflex klystrons and other sources of coherent radio-frequency oscillations of such frequencies available at present. Typical of

Table 6.2

Parameters of Typical BWO's

No.	Tube type	Operating frequency range, GHz	Accelerating voltage, kV	Beam current, mA	Output power, mW	Efficiency, per cent	Focussing magnetic field, tesla	Slow-wave system type	Power output
1	10-cm BWO (Fig. 6.29)	2.4-4.8	0.17-1.4	40	50-500	1-2	0.06	Interdigital	Coaxial line
2	2-mm BWO	140-150	3.3-4.6	45	5	—	0.4	Comb	Rectangular waveguide 0.75×1.50 mm
3	0.5 mm BWO	485-615	2-4	50	1-7	—	1.0-1.2	Interdigital	Multimode waveguide of the 1.8×3.6 mm cross section

such devices is the tube given in Table 6.2 (No.3), which provides several milliwatts of output power at a 0.5-mm wavelength; such a power level is sufficient for carrying out various studies in the submillimetric wave band.

At present the shortest wavelength obtained with a BWO is 0.2 mm. It is of interest to note, that the longest wavelength obtainable with gas lasers is about 0.77 mm. Thus, the development of the BWO has bridged the frequency gap between electron tubes and quantum oscillators.

Backward-wave tubes can be designed to operate not only at centimetric, millimetric and submillimetric wavelengths, but for

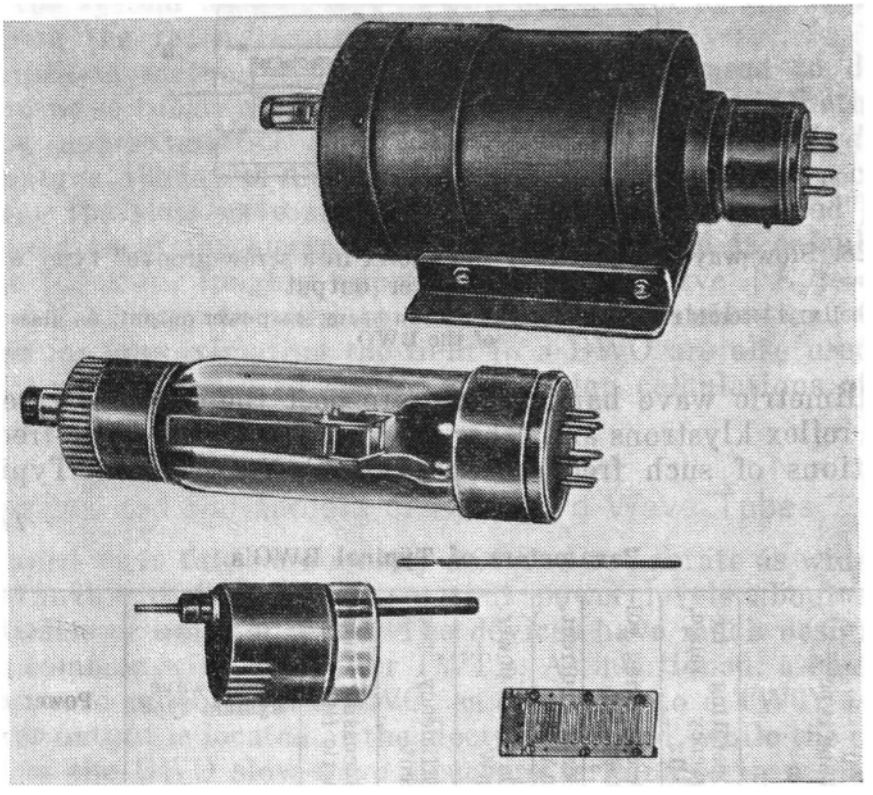

Fig. 6.29. Centimetric-wave BWO with interdigital slow-wave structure (tube in fixture, slow-wave structure and coaxial power output can be seen)

the decimetric and even metric wave bands, too. The slow-wave structures of these "long-wave" devices are made with lumped reactances (inductances and capacitances) forming delay lines, this reducing their dimensions to acceptable.

A variety of the BWO—the *resonant* backward-wave tube—is of interest by itself. In these devices there is no matched load at the collector end of the slow-wave structure and the power output is also mismatched relative to the slow-wave structure. This endows the system with resonant properties, so that a distributed cavity with a length accommodating an integer of slow-wave lengths is obtained.

Because of the resonance effects the radio-frequency field in the slow-wave structure is greatly enhanced. As a result, the starting current can be considerably reduced and the tube itself made shorter. At the same time, the tube efficiency is raised and the width of the magnetic gap reduced, this providing a significant saving in tube weight and dimensions.

The drawback of a resonant BWO is the discontinuities inside the oscillation zone and in the tuning characteristic curve. Indeed, operation of this tube is possible only in the vicinity of resonance frequencies of the "cold" slow-wave structure; in this respect a resonant BWO resembles drift klystrons.

Despite this drawback, resonant BWO's and their various modifications are employed when there is no need of a wide continuous frequency range. An example is the *laddertron*, in which a section of the ladder slow-wave structure is used; devices of this kind are capable of providing several watts of output power at millimetric wavelengths.

The main field of application of the O-type backward-wave tubes is as oscillators for measurements, especially as swept-frequency sources with extremely wide voltage tuning ranges. The demand for oscillators of this kind has considerably increased, which is particularly due to the development and extensive use of automatic reflectometers utilizing frequency-sweeping techniques, as well as other measuring gear based on similar methods, this providing great savings in man-hours as compared to point-by-point measurements.

Backward-wave tubes of the O-type are also employed as local oscillators in certain types of microwave receivers. A drawback of BWO's in this application is a higher level of inherent noise and higher d.c. supply voltages as compared to reflex klystrons.

6.8. Cascaded Amplifiers of the O-Type

In the design of the O-type amplifiers the principle of cascade connection of separate sections of slow-wave structures similar in a sense to cascade connection of resonant cavities in multicavity klystrons, can be employed to advantage. The simplest case of a two-stage backward-wave tube amplifier is schematically illustrated in Fig. 6.30*a* as an example. In this device the electron beam travels through two periodic slow-wave structures one after the other; each of the structures interacts with the beam and operates at the first backward harmonic and each of the structures terminates in a matched load. Between these structures a drift tube with the properties of a cut-off waveguide can be mounted.

The obvious advantage of such a cascaded backward-wave tube, as compared to the ordinary amplifier tubes, is the separation of the

amplifier input from its output. In essence, the same principle is used in travelling-wave tubes, when a sever is introduced into the slow-wave system to ensure operation stability and exclude self-excitation effects. Among other peculiarities of cascaded amplifiers of this kind, a greater bandwidth should be mentioned; this can be obtained by applying a biasing voltage V_0' to the second section of the slow-wave structure (refer to Fig. 6.30*a*). This voltage will cause a change in the conditions of synchronism in the second section, which in effect will be similar to stagger-tuning the cavities of a multicavity klystron. At the same time a greater gain (up to 30-40 dB) is obtained at an adequate spacing from the threshold of self-excitation.

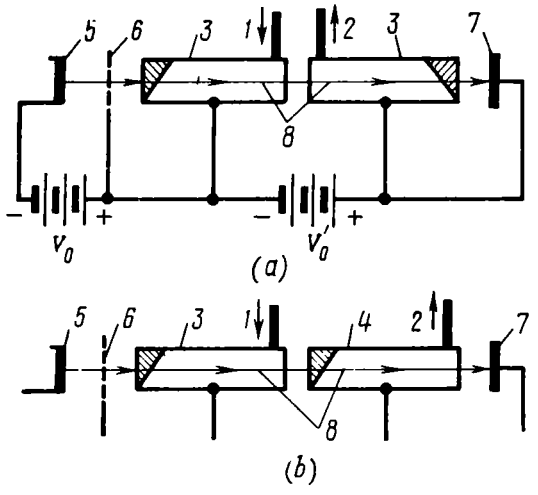

Fig. 6.30. Cascaded amplifiers of the BWO—BWO and BWO—TWT kinds

1—input; *2*—output; *3*—slow-wave system section operating under backward-wave conditions; *4*—section of slow-wave system operating with a forward wave; *5*—cathode; *6*—accelerating electrode; *7*—collector; *8*—electron beam

Cascaded amplifiers can be designed with other circuit configurations as well, utilizing sections of slow-wave systems working with forward and backward waves in various combinations. As an example a cascaded amplifier of the BWO—TWT type is shown in Fig. 6.30*b*. The reader is invited to examine other possible combinations in such hybrid devices, for instance devices of the TWT—BWO kind.

CHAPTER SEVEN
MICROWAVE CROSSED-FIELD ELECTRON DEVICES

7.1. Magnetron Oscillators. General Problems

The magnetron oscillator, which is at present one of the most extensively used microwave electron devices, has a long and complicate development history.

Diode behaviour in the presence of a static magnetic field has been the subject of much investigation from the very beginning of the development of the first electron tube. Microwave oscillations in such diodes were discovered in 1920-1924. Successful experiments with retarding-field oscillators were responsible to a considerable extent for research being launched just in this direction.

Three major oscillation modes, differing from one another in the electronic mechanism involved, have been found in oscillators of the magnetron type:

(1) cyclotron-frequency oscillations;
(2) oscillations of the negative resistance type (dynatron mode);
(3) travelling-wave oscillations.

Oscillations of the travelling-wave mode are practically most important. Multicavity magnetrons, first proposed in 1938-1940 by N. Alekseyev and D. Malyarov, rely for their operation on these oscillations. In the following treatment this oscillation mode will be given particular attention.

Progress of multicavity magnetrons has resulted in the development of high-power and high-efficiency oscillators that play an important part in microwave engineering. At the same time research in, and development of, magnetron oscillators have led to the appearance of a numerous class of microwave electron devices of the magnetron type, such as *M-type travelling-wave tubes*, *backward-wave tubes of the magnetron type* and *platinotrons*. A feature common to all magnetrons and M-type devices is the presence of crossed static electric and magnetic fields in the interaction space.

A typical design of a multicavity magnetron is schematically illustrated in Fig. 7.1. The anode of this device is a solid copper block divided into segments by radial slots. These slots constitute an element of resonant cavities, which are evenly spaced around the anode circumference. A cylindrical cathode is mounted axially relative to this anode structure.

The static magnetic field B is directed along the device axis, i.e. is normal to the second projection plane in Fig. 7.1. A d.c. or pulsed anode voltage is applied between the cathode and anode, thus producing a static radial electric field normal to the static magnetic field. It is common to mount the power output in one of the magnetron cavities and to provide the coupling, for instance, by means of a coupling loop and a coaxial line.

Analysis of multicavity magnetron operation discloses that their performance can be described in terms of travelling waves

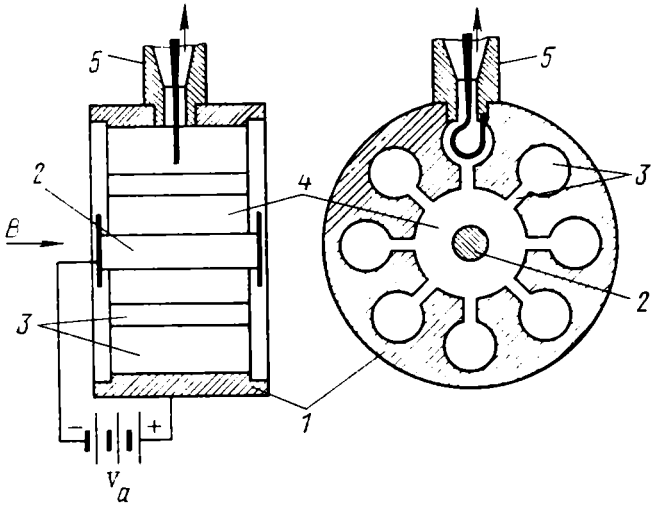

Fig. 7.1. Design and circuit connection of a magnetron oscillator
1—anode block; *2*—cathode; *3*—slot-and-hole resonant cavity; *4*—interaction space; *5*—power output

propagating along the inner surface of the anode structure, which faces the device cathode—hence the designation "travelling-wave mode".

All the electronic processes taking place in any microwave amplifier or oscillator, namely electron beam control, bunch development and coupling out of the energy contained in the electron bunches by a microwave field, occur *in the interaction space* of a magnetron, this space confined between the cathode and the anode structure. Unlike a klystron, in a magnetron there is no way of dividing up this interaction space into separate regions in which one of the above mentioned processes could be predominant. This, along with a complex nature of electron motion, makes the analysis of magnetron electronics a more difficult problem; however, applying the concepts of oscillation modes and equivalent circuit techniques in conjunction with the analysis of electron motion, the general methods examined in Chapter Three prove to be applicable in the case as well.

7.2. Electron Motion in a Magnetron Under Static Conditions

7.2a. Basic Conceptions

Before turning to the treatment of the problem of exciting self-sustained oscillations in a magnetron, the motion of electrons in crossed static electric and magnetic fields in the absence of radio-frequency oscillations has to be examined.

As a rule, the magnetron cathode is a cylinder mounted coaxially with respect to the anode structure which is also a cylinder. Neglecting for the time being the distortions of the electric

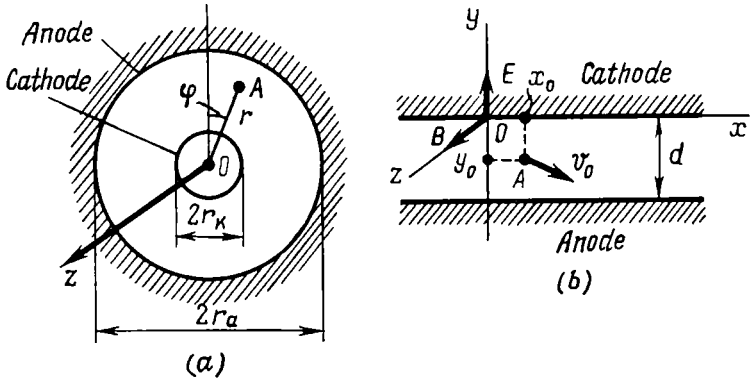

Fig. 7.2. To the analysis of electron motion in a cylindrical and a planar magnetron with a smooth anode under static conditions. The electron is located at point *A*

field due to the presence of slots on its inner surface, the system will be assumed to have a solid anode (Fig. 7.2*a*). The static magnetic field is supposed to be directed along the z axis and the space charge of the electrons moving in the interaction space will be considered negligible.

The effects of the space charge (mutual repulsion of electrons) should be neglected with certain precaution, because in magnetrons these effects can be significantly increased due to the action of the static magnetic field. As will be demonstrated, rigorous analysis of many of the important properties of magnetron devices can be made without taking into account the presence or absence of space charge, while a strict solution to the problem with space charge effects taken into account is not always obtainable.

From the outset, the initial electron velocities, at which they are emitted from the cathode, will be neglected as small. However the general solution with the initial electron velocities allowed for, proves to be useful for the treatment of other microwave electron devices with crossed fields. The initial electron velocities should

also be considered in the analysis of electron sorting processes in magnetron oscillators in the presence of radio-frequency oscillations.

We shall begin computation of electron motion with the simplest case of the parallel-plane system of Fig. 7.2*b*, and the results obtained will then be extended to cover the case of a cylindrical electrode configuration. It is useful to consider the parallel-plane system not only from the point of view of simplicity of mathematics involved; as will be demonstrated later, most modern magnetrons are of the large-diameter variety, this making the parallel-plane approximation fairly justifiable.

7.2b. Electron Motion in a Planar Magnetron

To solve this problem the general Lorentz equation should be applied, which describes the motion of an electron in static electric and magnetic fields. By equation (2.9), with relativistic effects considered to be negligible, the electron motion can be described as

$$m\frac{d\bar{v}}{dt} = -e\{\bar{E} + [\bar{v}\bar{B}]\} \tag{7.1}$$

Resolving the vectors $\bar{v}$, $\bar{E}$ and $\bar{B}$ and laying the components off along the axes of a rectangular system of coordinates and expanding the vector product in equation (7.1), we obtain

$$[\bar{v}\bar{B}] = \begin{vmatrix} \bar{i} & \bar{j} & \bar{k} \\ v_x & v_y & v_z \\ B_x & B_y & B_z \end{vmatrix} = \bar{i}(v_yB_z - v_zB_y) + \\ + \bar{j}(v_zB_x - v_xB_z) + \bar{k}(v_xB_y - v_yB_x)$$

where

$$v_x = dx/dt; \quad v_y = dy/dt; \quad v_z = dz/dt$$

Thus, in a rectangular system of coordinates the scalar equations of electron motion acquire the following form:

$$\frac{d^2x}{dt^2} = -\frac{e}{m}\left(E_x + B_z\frac{dy}{dt} - B_y\frac{dz}{dt}\right) \tag{7.2}$$

$$\frac{d^2y}{dt^2} = -\frac{e}{m}\left(E_y + B_x\frac{dz}{dt} - B_z\frac{dx}{dt}\right) \tag{7.3}$$

$$\frac{d^2z}{dt^2} = -\frac{e}{m}\left(E_z + B_y\frac{dx}{dt} - B_x\frac{dy}{dt}\right) \tag{7.4}$$

It will be convenient to orient the system of coordinates relative to the magnetron electrodes in such a way that the vectors $\bar{E}$ and $\bar{B}$ be of the positive direction. According to Fig. 7.2*b* it can be written

$$E_x = E_z = 0; \quad E_y = E = V_a/d; \quad B_x = B_y = 0; \quad B_z = B$$

where V_a is the anode voltage applied to the magnetron, and d is the spacing between the cathode and anode.

In the final form the equations of electron motion in crossed static electric and magnetic fields are

$$\frac{d^2x}{dt^2} = -\frac{eB}{m}\frac{dy}{dt} \tag{7.5}$$

$$\frac{d^2y}{dt^2} = -\frac{eE}{m} + \frac{eB}{m}\frac{dx}{dt} \tag{7.6}$$

$$\frac{d^2z}{dt^2} = 0 \tag{7.7}$$

Note, that similar equations can be obtained in a less formal manner, without resorting to the use of equation (7.1). Applying the common "left-hand rule" which determines the direction of force applied to a current-carrying conductor in the presence of a static magnetic field is sufficient to arrive at the same results.

The simplest is the solution to equation (7.7)

$$\frac{dz}{dt} = v_{z0}; \quad z = z_0 + v_{z0}t \tag{7.8}$$

where v_{z0} is the initial electron velocity in the direction of the z axis and z_0 is its initial coordinate at the instant of time $t = 0$.

Integration of equation (7.5) yields

$$\frac{dx}{dt} = -\frac{eB}{m}y + C_1$$

Suppose the electron in question to begin its travel from the coordinate $y = y_0$ at the instant of time $t = 0$. Assuming the component of electron velocity along the x axis to be initially v_{x0} we get

$$\frac{dx}{dt} = v_{x0} - \frac{eB}{m}(y - y_0) \tag{7.9}$$

Substitution of (7.9) into (7.6) results in

$$\frac{d^2(y-y_0)}{dt^2} + \left(\frac{eB}{m}\right)^2 (y - y_0) = -\frac{eE}{m} + \frac{eB}{m}v_{x0} \tag{7.10}$$

The general solution to an equation of the (7.10) type without the right-hand member is

$$y - y_0 = C_2 \exp(j\omega_c t) + C_3 \exp(-j\omega_c t)$$

where ω_c is the angular *cyclotron frequency*:

$$\omega = eB/m \tag{7.11}$$

Assuming the particular solution to equation (7.10) to be $y - y_0 = C_4$ and substituting it into (7.10) result in

$$C_4 = -\frac{eE}{m\omega_c^2} + \frac{v_{x0}}{\omega_c}$$

Thus, the total solution to equation (7.10) is

$$y - y_0 = (C_2 + C_3)\cos \omega_c t + j(C_2 - C_3)\sin \omega_c t - \frac{eE}{m\omega_c^2} + \frac{v_{x0}}{\omega_c}$$

C_2 and C_3 can be determined from the boundary conditions: at the instant of time $t = 0$ the electron in question is at $y = y_0$ and has the velocity component along the y axis equal to v_{y0}. Substitution of these conditions into the latter relation yields

$$C_2 + C_3 = \frac{eE}{m\omega_c^2} - \frac{v_{x0}}{\omega_c}\ ;\ C_2 - C_3 = v_{y0}/j\omega_c$$

and after simple rearrangements we obtain

$$y - y_0 = -\frac{mE}{eB^2}(1 - \cos \omega_c t)\left(1 - \frac{B}{E}v_{x0}\right) + \frac{v_{y0}}{\omega_c}\sin \omega_c t \quad (7.12)$$

The equation of electron motion along the x axis may be derived by substituting (7.12) into relation (7.9)

$$\frac{dx}{dt} = v_{x0} + \frac{E}{B}(1 - \cos \omega_c t)\left(1 - \frac{B}{E}v_{x0}\right) - v_{y0}\sin \omega_c t$$

Integration of this relation results in

$$x = v_{x0}t + \frac{E}{B}\left(1 - \frac{B}{E}v_{x0}\right)t + \frac{E}{B\omega_c} \times$$

$$\times \left(1 - \frac{B}{E}v_{x0}\right)\sin \omega_c t + \frac{v_{y0}}{\omega_c}\cos \omega_c t + C_5$$

Again applying the boundary condition, which describes the initial location of the electron at $t = 0$, we deduce the constant C_5 to be

$$C_5 = x_0 - \frac{v_{y0}}{\omega_c}$$

Thus, the final form of the equation describing electron movement along the x axis is

$$x = x_0 + \frac{E}{B}t - \frac{mE}{eB^2}\left(1 - \frac{B}{E}v_{x0}\right)\sin \omega_c t - \frac{v_{y0}}{\omega_c}(1 - \cos \omega_c t) \quad (7.13)$$

The system of equations (7.8), (7.12) and (7.13) is adequate to describe the motion of a solitary electron, which at the instant of time $t = 0$ is at a point (x_0, y_0, z_0) and features initial velocity components along the axes equal to v_{x0}, v_{y0} and v_{z0} (refer to Fig. 7.2*b*).

In case of a magnetron oscillator with a cathode at the $y = 0$ plane as the source of electrons the coordinate y_0 should be taken

$y_0 = 0$. Neglecting the initial electron velocities, at which they leave the cathode

$$x = x_0 + \frac{E}{B} t - \frac{mE}{eB^2} \sin \omega_c t \tag{7.14}$$

$$y = -\frac{mE}{eB^2} (1 - \cos \omega_c t) \tag{7.15}$$

$$z = z_0 \tag{7.16}$$

Thus, electron trajectories are in the form of curves in the $z = z_0 = \text{const}$ plane with the initial coordinate x_0 only shifting the particular trajectory along the x axis.

Analysis of equations (7.14) and (7.15) reveal that they describe a particular case of a trochoid, a cycloid, in parametric form; this

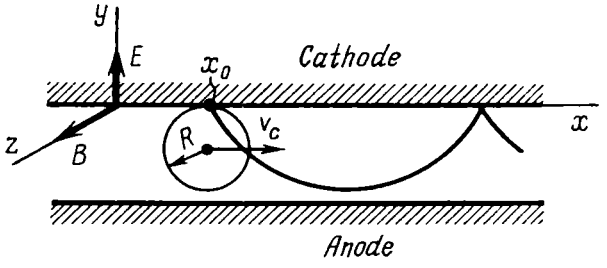

Fig. 7.3. Cycloidal electron motion in crossed static fields in the absence of microwave oscillations; the electron enters the interaction space at point x_0 with a zero initial velocity

curve is shown in Fig. 7.3. Indeed, the general equation of a trochoid, which was discussed in Section 5.2*b*, can be represented as

$$x = v_c t - r \sin \varphi; \quad y = R - r \cos \varphi \tag{7.17}$$

where v_c is the speed of the uniform rolling movement of the circle (of the point O'' in Fig. 5.3) and R as before denotes the circle radius, while r is the spacing of the point of interest from the circle centre and φ is the angle of rotation.

Comparison of equations (7.14) and (7.15) with (7.17) shows the electron trajectories to be cycloids, i.e. trochoidal curves for the particular case when $r = R$ and is equal to

$$R = \frac{mE}{eB^2} \tag{7.18}$$

The speed of the circle centre proves to be

$$v_c = \frac{E}{B} \tag{7.19}$$

The negative sign of the right-hand member in equation (7.15) is defined by the choice of the origin for the coordinate system (refer to Fig. 7.3, where the circle is shown as rolling below the cathode surface).

The physical meaning of the cyclotron frequency defined by equation (7.11) becomes now obvious: this quantity describes the frequency of the angular movement of this rolling circle and thus the angular velocity of electron motion along the cycloidal trajectory. This frequency may be used to determine the total time of electron transit from the cathode to the peak of the cycloid and back to the cathode

$$\tau = \frac{2\pi}{\omega_c} = \frac{2\pi m}{eB} \tag{7.20}$$

The cyclotron frequency is an important characteristic of the performance of most electron devices of the magnetron type, as well

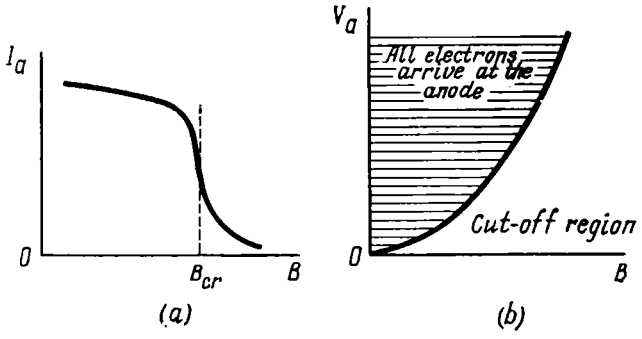

Fig. 7.4. D.c. anode current of a magnetron *vs* static magnetic induction B at V_a = const (*a*) and the cutoff conditions parabola (*b*)

as other microwave electron devices, and will be extensively used in the discussion to follow.

Increasing the static magnetic induction B at a fixed value of the anode voltage V_a = const will cause a gradual reduction of the radius R of the rolling circle, determined from equation (7.18). The electron trajectories, which are normal to the surfaces of the cathode and anode when $B = 0$, become curved and at $d = 2R$ they only touch the anode surface at the peaks of the cycloidal curve. Finally, at d in excess of $2R$ electrons begin to perform multiple oscillations along the cycloid, this resulting in an abrupt fall-off of anode convection current I_a, as illustrated in Fig. 7.4*a*; the corresponding magnitude of the magnetic induction in the interaction space of a magnetron is termed the *critical induction* B_c (the strict definition of this quantity is the smallest theoretical value of a steady magnetic flux at a steady anode voltage, that would prevent an electron emitted from the cathode at zero velocity from reaching the anode). The finite decrease of current around $B = B_c$ and the presence of a small current I_a at $B > B_c$ are due to electron diffusion to the anode as a result of collisions with molecules of residual gas, as well as to initial electron velocities and spontaneous

electron oscillations in the space charge of a magnetron. The end-region effects, a certain degree of inevitable electrode asymmetry and the presence of surface non-uniformities in the form of slots also contribute to the appearance of a small anode current at fields exceeding the critical value.

Thus, the critical magnetic field at which the anode current of a planar diode is practically cut off to zero at a fixed value of the anode voltage V_a is determined with the aid of (7.18) from the conditions that

$$B = B_c; \quad d = 2R; \quad E = V_a/d$$

whence $B_c = \frac{1}{d}\,(2mV_a/e)^{1/2}$ (7.21)

A somewhat different argumentation is also possible. At a fixed value of the static magnetic field intensity B, there is a certain anode voltage $V_{a.\,c}$, below which the anode current will be cut off. By equation (7.21) this critical voltage is

$$V_{a.c} = \frac{eB^2d^2}{2m} \tag{7.22}$$

This relation describes the *critical (cutoff) operating conditions parabola*, shown in Fig. 7.4*b*; the shaded area above this parabola depicts here conditions, in which a magnetron conducts direct current. Note, that the points on this critical parabola correspond to a constant ratio of the anode voltage to the square of the static magnetic induction, this being a constant for the given diode

$$\left(\frac{V_a}{B^2}\right)_c = \frac{ed^2}{2m} \tag{7.23}$$

In the above analysis the effects of space charge were neglected; despite this fact, the equations for B_c and $V_{a.c}$ are absolutely rigorous ones and are in excellent agreement with experimental findings. The equation for cutoff conditions may also be derived by examining the energetics involved, without considering the electric field intensity and disregarding the particular form of electron trajectories.

The critical magnetic induction B_c and anode voltage $V_{a.\,c}$ are important parameters which characterize the behaviour of a magnetron under dynamic conditions (i.e. in the presence of radio-frequency oscillations) as well as under static conditions. As will be demonstrated, the region below the critical parabola, where the static magnetic field exceeds the critical one and the anode voltage is lower than critical, is the region of operation of M-type oscillators and amplifiers.

7.2c. Electron Motion in a Cylindrical Magnetron

Strictly speaking, the above relations hold only for a planar magnetron. At a small value of the cathode-to-anode diameter ratio the trajectories of electrons should be examined using the cylindrical system of coordinates.

We shall omit the cumbersome calculations involved and only point out that under the assumptions adopted in Section 7.2*a* electron trajectories in this case acquire the pattern of cardioid curves and resemble the cycloidal electron trajectories in the planar magnetron. The cutoff conditions in a cylindrical magnetron are described as

$$B_c = \frac{(8mV_a/e)^{1/2}}{r_a\left(1-\frac{r_k^2}{r_a^2}\right)} \tag{7.24}$$

As elsewhere in the present textbook, here the mksa (Giorgi) system of units is used: the magnetic induction should be taken in tesla units (i.e. webers per square metre). Equation (7.24) may be reduced to

$$B_c = \frac{6.75\cdot 10^{-4} V_a^{1/2}}{r_a\left(1-\frac{r_k^2}{r_a^2}\right)} \text{ (tesla)} \tag{7.24a}$$

by expressing the linear dimensions in centimetres and the voltage in volts. As in the case of a planar configuration, equations (7.24) and (7.24*a*) are quite rigorous and independent of the pattern of electron trajectories.

Returning to the problem of the "actual" pattern of electron trajectories, the incomplete character of this part of magnetron theory of the parallel-plane and cylindrical configurations should be pointed out. The cycloidal and loop-shaped trajectories discussed are indicative of two electron streams present simultaneously which move in the opposite radial directions. Theory points also to the possibility of *single-stream* conditions in magnetrons with electrons moving along non-intersecting circles, along with such a *double-stream* movement of the electron cloud. This single-stream state (known as Brillouin flow) is also a useful model for a number of magnetron design computations. Up to the present, however, the existence of the single-stream state in magnetron devices has not been corroborated experimentally. The following treatment will be mainly based on the simplest cycloidal (loop) pattern of electron trajectories.

This pattern of electron trajectories can be even visually observed in magnetron models at sufficiently high pressures of residual gas inside the tube. This method is open to argument since the presence of ions in such high concentrations can cause significant distortions in the distribution of space charge; other indirect experimental confirmations of the cycloidal pattern of electron trajectories in actual magnetron designs are, however, available.

7.3. Properties of Multicavity Oscillatory Systems of Magnetron Oscillators

7.3a. General Problems

The design and performance characteristics of multicavity magnetrons differ significantly from those of microwave oscillators examined earlier, such as triodes, two-cavity klystrons, reflex klystrons, etc. First of all, the oscillatory system of a magnetron consists of a considerable number (from 8 to 120) of mutually coupled resonant cavities, which interact with an electron stream via an equal number of gaps, in this case, slots in the surface of the anode. Furthermore, as already mentioned, electron trajectories in a magnetron are of a considerably more complex pattern than in the case of a simple electron beam in a klystron and many other types of microwave electron tubes. A strict analysis of electron motion in an oscillating magnetron is thus far among the unsolved problems of microwave electronics.

Despite these difficulties, a number of important conclusions about the performance characteristics of magnetron devices can be drawn by applying the general principles of performance of microwave oscillators with resonant oscillatory systems (refer to Sections 3.2 and 3.3) to the case in hand.

The frequency of oscillations is mainly a function of the resonant frequency of the system employed. One of the most important problems is thus the determination of the resonant properties of the "cold" oscillatory system of a magnetron at different oscillation modes. Furthermore, the distribution of the radio-frequency field in the *interaction space* between the cathode and anode which accommodates the electron stream, is also important to the analysis of electronic effects and processes taking place in an oscillating magnetron. Thus, the radio-frequency field, "sagging out" of the resonant cavities into the interaction space in the present case is of rather more interest than the field inside the cavities.

Both these problems—that of determining the resonant frequencies and that of the pattern of the radio-frequency field in the interaction space—may be treated independently of the properties of the electron stream.

7.3b. Oscillation Modes in the Anode Structure of a Magnetron

Consider a closed chain of N resonant cavities evenly spaced over the inner surface of an anode block of a magnetron (Fig. 7.1); at first the kind of cavity actually employed will be disregarded, assuming only all the cavities to be identical and to support only one (dominant) oscillation mode in the frequency band of interest. A system of this kind can be considered as a periodic slow-wave structure folded to form a closed loop, the system being a version of the interdigital system with a metal sole.

The condition of resonance in any looped system is that an integer of wavelengths is accommodated along the loop length. Designating the slow-wave length as λ_{slow}, the condition of resonance will acquire the form

$$2\pi r_a = n\lambda_{slow}; \quad n = 0; 1; 2; \ldots \tag{7.25}$$

where r_a is the radius of the magnetron anode.

The same condition can be described in terms of the phase shift of oscillations in adjacent resonant cavities. The total phase shift along the entire inner surface of the anode block should be a multiple of 2π and therefore

$$\varphi N = 2\pi n; \quad n = 0; 1; 2; \ldots \tag{7.26}$$

It follows that the phase shift between adjacent cavities should vary in discrete steps of

$$\varphi = 2\pi n/N \tag{7.27}$$

The oscillation modes of the anode structure can be described by the number n or directly by the value of the phase shift between successive cavity openings into the interaction space. For example, the phase shift between adjacent cavities in a 8-cavity magnetron by (7.27) can be

n	0	1	2	3	4	5	6	7	8
φ	0	$\pi/4$	$\pi/2$	$3\pi/4$	π	$5\pi/4$ ($-3\pi/4$)	$3\pi/2$ ($-\pi/2$)	$7\pi/4$ ($-\pi/4$)	2π (0)

As can easily be noted, beginning with $n = N$ any further increase in the value of n does not cause the appearance of oscillation modes physically different from those corresponding to n in the range from zero to $(N - 1)$. The same is true of negative n values, these only producing a change in the polarity of the phase shift. The same statements hold also for the general case, when the examination is not

restricted to any definite number of resonant cavities N. It follows that in the general case the anode structure can feature N oscillation modes.

The case $n = 0$ corresponds to in-phase excitation of all the cavities, while at $n = N/2$ adjacent cavities are excited in antiphase, i.e. the phase shift between successive cavities is π. This oscillation mode (conventionally termed the π mode) is the main mode of magnetron operation for a number of reasons. Note in passing, that the π mode can be excited in an anode structure only when the number of resonant cavities is even—this is the reason why anode structures with odd numbers of resonant cavities do not find application in magnetron oscillator devices.

The absolute value of the phase angle φ determines the length of the coupling path between cavities; the coupling may be, for instance, via the magnetic fields of the cavities, with the magnetic lines of force of one cavity being completed into closed loops in the other cavity. This causes the oscillation modes of an anode structure to feature somewhat different resonant frequencies at different values of $|\varphi|$, even if each of the individual cavities resonates at exactly the same frequency.

Oscillation modes corresponding to $n = 1$ and $n = 7$ in the above example ($N = 8$) differ only in the polarity of the phase shift which is equal in this case to $\pm \pi/4$. The distribution of the field (i.e. the pattern of the electric and magnetic lines of force) for these oscillation modes should therefore be identical; it follows that these modes must have identical resonant frequencies, i.e. that modes corresponding to $n = 1$ and $n = 7$ are *degenerate*. The same is obviously true of oscillation modes $n = 2$ and $n = 6$, just the same as for $n = 3$ and $n = 5$. The only non-degenerate modes are those corresponding to $n = 0$ and $n = N/2$ (π mode).

This qualitative treatment discloses that an N-cavity magnetron can have only $(N/2 + 1)$ different resonant frequencies. Operation with degenerate modes is usually avoided, because the resonant frequencies of these degenerate modes may cease to be identical due to discontinuities in the anode structure. To ensure stable operation at one of the two closely spaced frequencies proves to be quite a problem (refer to Section 3.2*c*). That is why the non-degenerate π mode is used in most types of modern magnetron devices.

7.3c. Pattern of Radio-Frequency Field in the Interaction Space. Travelling Waves

Suppose a "cold" multicavity anode structure to be excited at approximately one of its resonant frequencies. The electric field of the cavities sags out of the slots into the interaction space and thus a finite electric field is set up at the cathode surface.

The electric field in a slot-and-hole type of cavity is qualitatively illustrated in Fig. 7.5*a*. At each point of the interaction space the vector of the electric field intensity $\bar{E}$ may be resolved into a radial component E_r and a tangential component E_t, the latter being of particular importance to magnetron operation.

A strict analysis of the field in the interaction space is a serious problem, but, as will be shown later, it is sufficient to examine only

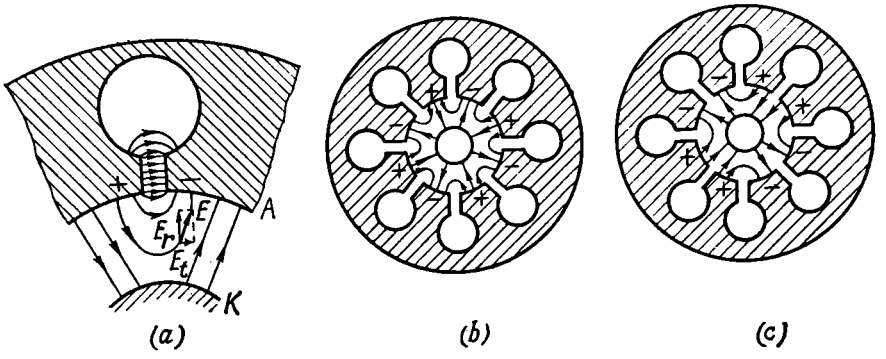

Fig. 7.5. Distribution of microwave electric field in the interaction space in the vicinity of a slot-and-hole cavity (*a*) and in an 8-cavity magnetron at π and $\pi/2$ oscillation modes (*b*) and (*c*)

the general laws governing field distribution over the surface of the anode structure.

At any fixed time the pattern of the standing wave in the interaction space is determined by the number of azimuthal variations of this field, which is equal to the number of the oscillation mode n. Indeed, by (7.25) and (7.26), the number n determines the number of complete spatial periods of the radio-frequency field accommodated along the circumference of the interaction space.

As an example, the pattern of the electric field for the π and $\pi/2$ modes is presented in Fig. 7.5*b* and *c*. The reader is invited to determine the field pattern for the other oscillation modes (that is, for $n = 0$, $n = 1$ and $n = 3$) for the case in question ($N = 8$). In particular, it is possible to state that the electric field at $n = 0$ is mainly characterized by electric lines of force in the form of closed circles concentric relative to the cathode and anode of the magnetron. The radio-frequency magnetic field in the interaction space can be omitted from the discussion, because this field pattern is of interest only for the analysis of electron motion given below. As follows from the findings of Section 2.1*b*, the influence of the radio-frequency magnetic field is much less than that of the electric field, providing electron velocities are considerably lower than the velocity of light.

The patterns of the tangential component of the electric field for the π and $\pi/2$ modes ($n = 4$ and $n = 2$) are qualitatively shown

in Fig. 7.6; both graphs correspond to the instant of time the field in cavity *1* is at a maximum. Similar graphs can be plotted for the radial field component: the maxima of the radial component are shifted by a quarter of the spatial period along the x axis (i.e. in the azimuthal direction) relative to those of the tangential component.

Graphs of this kind can be obtained experimentally with the aid of rotating probes in a "cold" anode structure, with oscillations induced from an external oscillator operating at a frequency near to the frequency of the oscillation mode being investigated. Oscillographic testing methods, used to check anode structures during the research and manufacturing stages are based on this technique.

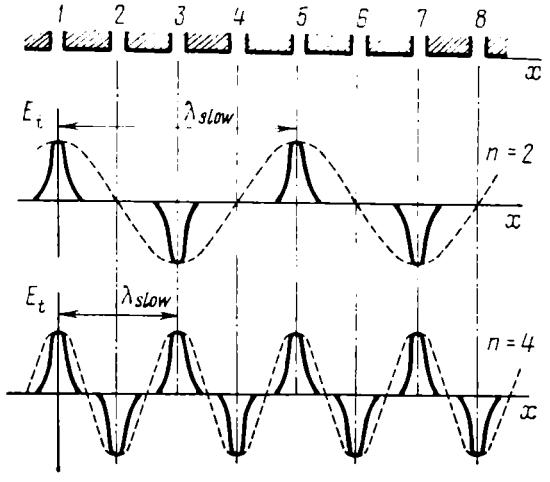

Fig. 7.6. Distribution of tangential component of the E-field along the surface of a magnetron anode block ($N = 8$). The corresponding standing wave is shown in dashed lines

Physically, the field shown in Figs 7.5 and 7.6 may be treated as pulsating and considered to have the pattern of a standing wave. For convenience and clarity, this field can be thought of as the sum of two travelling waves propagating in the space between the cathode and anode of a magnetron.

The slow-wave system of the anode block is a periodic one; the length of the spatial period over the anode surface is equal to $L = 2\pi r_a/N$. The phase velocities of the waves propagating in this system can be determined from the general relations (6.67) and (6.68), with the spatial harmonics taken into account. Magnetron performance can then be treated in much the same way as that of travelling-wave and backward-wave tubes.

The same conclusions can be drawn in a more obvious manner. The phase velocity of the fundamental wave can be determined from the condition that the time Δt required for the wave to travel between adjacent cavities (i.e. the length $L = 2\pi r_a/N$) and the phase shift between these cavities are interrelated as $\varphi = \omega \Delta t$ (where ω is the angular frequency of oscillations, which closely approximates the resonant frequency of the n mode). Applying relation (7.27) and designating the phase velocity of the wave at the n mode as $(v_p)_n$ yields

$$(v_p)_n = \frac{2\pi r_a}{N} \frac{\omega}{\varphi} = \frac{\omega r_a}{n} \tag{7.28}$$

The corresponding angular frequency of wave rotation in a cylindrical multicavity magnetron is then

$$\Omega_n = \frac{(v_p)_n}{r_a} = \frac{\omega}{n} \tag{7.29}$$

To allow for the effect of spatial harmonics imagine an observer moving along the anode surface at a constant speed and registering the magnitude of the radio-frequency field at each successive cavity slot. Such an observer will note an identical phase of this field if the time of travel between successive slots for this observer and the wave are interrelated as

$$t_2 - t_1 = \Delta t + pT = \frac{2\pi n}{\omega N} + pT$$

(here t_1 and t_2 are instants of time when the observer is at the middles of two successive slots, p is any integer including zero with different signs corresponding to opposite directions of the observer motion and Δt is the time of wave travel).

The speed, at which this observer should move, is

$$v = \frac{2\pi r_a}{N(t_2 - t_1)} = \frac{\omega r_a}{n + pN}$$

The fact that the radio-frequency field noted by the observer is of a constant phase can be considered as an indication of the existence of travelling waves with phase velocities

$$(v_p)_{np} = \omega r_a/(n + pN) \tag{7.30}$$

Thus, the actual pulsating field is resolved into two sets of waves rotating in the interaction space in opposite directions. The angular velocity of the p-th spatial harmonic of the n-th oscillation mode, with relation (7.30) taken into account, is equal to

$$\Omega_{np} = \frac{(v_p)_{np}}{r_a} = \frac{\omega}{n + pN} \tag{7.31}$$

At $p = 0$ equation (7.31) reduces to (7.29); the higher the number of the oscillation mode and the higher the number of the spatial harmonic, the lower are the velocities of the forward and backward rotating waves in the interaction space. The wave corresponding to $p = 0$ at a given oscillation mode features the highest phase velocity and is therefore the *fundamental wave* of this oscillation mode.

The magnitude of the phase velocity $(v_p)_{np}$ can be significantly lower than the speed of light in free space. Equation (7.30) readily yields

$$\frac{c}{(v_p)_{np}} = \frac{\lambda(n + pN)}{2\pi r_a} \tag{7.32}$$

where λ is the operating wavelength in free space.

Using again the example of an 8-cavity structure, the $c/(v_p)_{np}$ ratios for the case $p = 0$, $p = \pm 1$, $r_a = 0.5$ cm and $\lambda = 10$ cm turn out to be as listed in Table 7.1; these values were calculated by (7.32). As can easily be noted, waves of the π-mode feature the highest c/v_p ratios.

Table 7.1

Rated Values of c/v_p Ratios in 8-Cavity Magnetron at $r_a = 0.5$ cm; $\lambda = 10$ cm

p	$\frac{c}{(v_p)_{np}}$				
	$n = 0$	$n = 1$	$n = 2$	$n = 3$	$n = 4$ (π mode)
0	0	3.18	6.36	9.54	12.7
+1	25.5	28.7	31.8	35.0	38.2
−1	−25.5	−22.3	−19.1	−15.9	−12.7

The concept of travelling (rotating) waves makes it considerably easier to examine the interaction between an electron cloud and a radio-frequency field and analyse the conditions of magnetron self-excitation.

7.3d. Frequency Spectrum of an Oscillation Mode

The next step in the treatment of "cold" oscillatory systems of magnetrons is the determination of the resonant frequencies at each of the oscillation modes. Analysis of this kind, however, necessitates a precise knowledge of the character of intercavity coupling. Omitting a strict treatment by the field theory methods we shall examine the results of calculations of an equivalent circuit for the case of an *equicavity* magnetron (i.e., a magnetron with N identical cavities).

The resonant wavelength at the n-th oscillation mode can be shown to be

$$\lambda_n = \lambda_0 \left[1 + \frac{C'}{2C\,(1 - \cos 2\pi n/N)}\right]^{1/2} \tag{7.33}$$

assuming the cavities to be intercoupled only via the capacitances C' between an anode segment and the cathode; here C is the equivalent capacitance of an individual cavity and λ_0 is the resonant wavelength of a single cavity. The corresponding equivalent circuit of a section of the magnetron is shown in Fig. 7.7 under the assumption of negligible dissipative loss. The resonant frequencies may be determined as usual by equating to zero the sum of admittances to both sides of any plane dividing the system. In the present case it proves

to be most convenient to examine the input admittance of the interaction space and the input susceptance presented by an individual cavity at the *ab* plane.

The radio-frequency currents entering the i-th, $(i-1)$-st and $(i+1)$-st resonant cavities can be presented in complex form as

$$\dot{I}_{i+1}=\dot{I}_i \exp(\pm j\varphi);\ \dot{I}_{i-1}=\dot{I}_i \exp(\mp j\varphi)$$

where φ is the phase shift as defined by relation (7.27). Applying the common equations known from the circuit theory, we arrive at

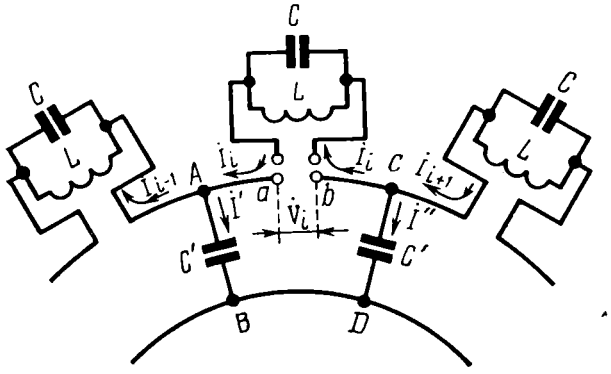

Fig. 7.7. Equivalent circuit of a section of the anode and cathode of a rising-sun magnetron with the capacitance between the anode segment and cathode taken into account

$$\dot{I}_i=\dot{I}'+\dot{I}_{i-1};\ \dot{V}_{AB}=$$

$$=\dot{I}'/j\omega C'$$

$$\dot{I}_{i+1}=\dot{I}_i+\dot{I}'';\ \dot{V}_{CD}=$$

$$=\dot{I}''/j\omega C'$$

$$\dot{V}_i=\dot{V}_{AB}-\dot{V}_{CD}$$

(The designations are taken from Fig. 7.7.)

Hence, the voltage $\dot{V}_i$ across the i-th slot (at points *ab*) is

$$\dot{V}_i=\frac{2\dot{I}_i(1-\cos\varphi)}{j\omega C'}$$

and the input admittance of the interaction space at points *ab* from the cavity side is

$$(Y_{in})_{ab}=\frac{\dot{I}_i}{\dot{V}_i}=\frac{j\omega C'}{2(1-\cos\varphi)}$$

On the other hand, the input admittance of the resonant cavity itself is

$$Y_{in}=j(\omega C-1/\omega L)=j\omega C(1-\omega_0^2/\omega^2)$$

The condition of resonance at the frequency $\omega=\omega_n$ is

$$Y_{in}+(Y_{in})_{ab}=0$$

Hence, the resonant frequency

$$\omega_n=\frac{\omega_0}{\left[1+\dfrac{C'}{2C(1-\cos\varphi)}\right]^{1/2}}$$

Applying equation (7.27) and replacing the resonant frequency for the resonant wavelength, results in equation (7.33).

Equation (7.33) confirms that the oscillation modes of the $(N/2 - 1)$ and $(N/2 + 1)$, etc., kind are twice degenerate. Indeed, in an 8-cavity magnetron the resonant wavelengths for the $n = 3$ and $n = 5$, $n = 2$ and $n = 6$, $n = 1$ and $n = 7$ oscillation modes prove to be identical.

The results of calculation of the resonant wavelengths for the case of an 8-cavity anode structure at different values of C' are presented in Fig. 7.8*a*. For clarity, points corresponding to one and

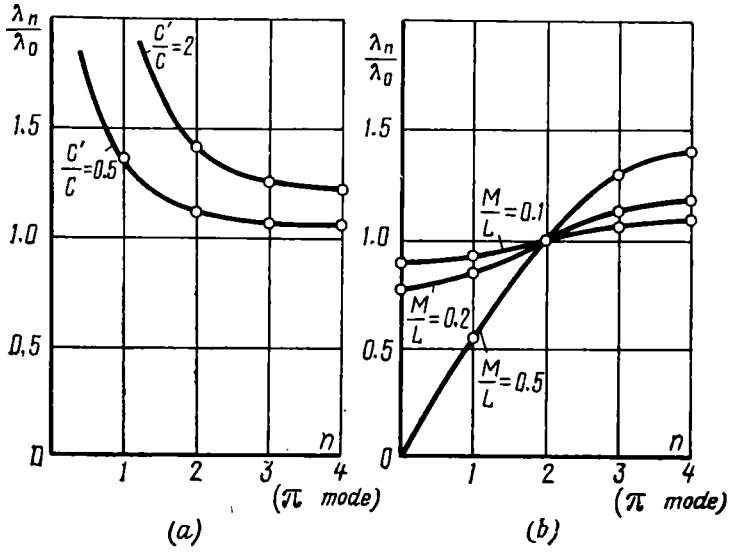

Fig. 7.8. Oscillation modes in an 8-cavity magnetron with coupling via capacitance between segments (*a*) and mutual inductance between cavities (*b*)

the same value of C' are connected by a solid curve, despite the obvious fact that in a reentrant system only integer values of n can be of any physical meaning.

The continuous curve $\lambda = f(n)$, or what is the same $\lambda = f(\varphi)$, represents the *dispersion characteristic* of a non-resonant slow-wave system, corresponding to the anode structure in question. Since the phase angle φ is in inverse proportion to the wave phase velocity, it can be inferred from Fig. 7.8*a* that in this case the dispersion is *normal*.

The spectrum of the oscillation modes presented in Fig. 7.8*a* is such that the resonant wavelength of the π mode only slightly differs from the resonant wavelength of the nearest $n = (N/2 - 1)$ oscillation mode. Ordinarily, the spacing between these frequencies is known as *mode separation* and evaluated in per cent of the π mode frequency

$$\frac{\Delta f}{f_\pi} = \frac{\Delta\lambda}{\lambda_\pi} = \frac{|(\lambda)_{N/2} - (\lambda)_{N/2-1}|}{(\lambda)_{N/2}} \qquad (7.34)$$

The greater the mode separation, the more stable the magnetron operation.

In the case discussed at $N = 8$ the mode separation proves to be quite close, about 1 per cent at C'/C equal to 0.5. It follows from equation (7.33) that a greater number of cavities in the structure will result in a still closer mode separation; the greater the cathode diameter and the greater the segment area (i.e. the higher the capacitance C'), the greater is the mode separation between the $N/2$ and $(N/2-1)$ modes.

The graphs of Fig. 7.8*a* do not present the precise pattern of resonant frequencies of an anode structure. In actual fact the coupling between cavities is of a much more complex nature than was assumed when deriving equation (7.33). At small height of the anode block the coupling is via the magnetic fields at the butt ends rather than via C'.

If the coupling is supposed to be only via the magnetic field (via mutual inductance M between successive cavities in the equivalent circuit) and capacitive coupling can be assumed negligible, the resonant wavelength for different oscillation modes in an equicavity magnetron may be shown to be

$$\lambda_n = \lambda_0 \left(1 - \frac{2M}{L} \cos \frac{2\pi n}{N}\right)^{1/2} \tag{7.35}$$

where L is the equivalent inductance of an individual resonant cavity.

Resonant frequencies corresponding to different oscillation modes are shown in Fig. 7.8*b* for various values of the ratio M/L. As evidenced by this graph, the dispersion in the slow-wave structure in this case (predominantly magnetic coupling between cavities) is *abnormal* in nature.

Thus, the resonant frequencies at the π oscillation mode may be both higher and lower than the resonant frequencies at other oscillation modes and the resonant frequency of individual cavities. In both cases the separation between the frequencies at the $N/2$ and the $(N/2-1)$ modes proves to be small and falls as the number of resonant cavities increases.

Experiments show that the magnetron oscillation spectrum approximates that of Fig. 7.8*b* at axial heights of about (0.1-0.2) λ. At considerable axial dimensions the spectrum shown in Fig. 7.8*a* proves to be more typical.

7.3e. Mode Separation in Multicavity Magnetrons

To ensure stable magnetron operation it is desirable to provide a mode separation of about some 10-20 per cent between the π mode and the $(N/2-1)$ oscillation mode nearest to it. In any case, the

mode separation should at least exceed the operating bandwidth of the anode structure at the π oscillation mode, this bandwidth being equal to the inverse of the loaded Q (in most designs this latter is about 100 to 500). However, as demonstrated earlier, mode separation in a symmetrical anode structure even at $N = 8$ does not exceed some units of per cent and diminishes with a greater number of resonant cavities.

There are two possible ways of increasing the mode separation: (1) by using *strapping arrangements* in *equicavity* anode blocks; (2) by employing anode blocks with *cavities of different dimensions* and therefore different resonant frequencies.

Magnetron cavities are strapped together by means of metal wire or band rings or bars, connecting only the odd or only the even

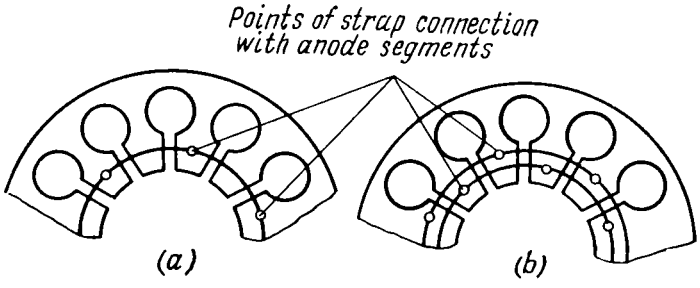

Fig. 7.9. Single (*a*) and double (*b*) ring straps used to increase oscillation mode separation in magnetrons

anode segments, respectively. Two versions of a strapping arrangement are illustrated in Fig. 7.9; the straps are mounted at the butt ends of the anode block and hold the polarities of the anode segments in groups, so that all the segments strapped together follow the same voltage variations. This ensures antiphase oscillations in adjacent segments, which is peculiar to the π mode, and considerably disturbs the oscillations of other modes, for which the phase shift differs from π.

The effect of strapping on the spectrum of oscillation modes will now be considered. With the anode structure excited at the π mode the straps connect points that are under the same radio-frequency voltage and therefore carry no microwave current, the strapping arrangement in this case only increases the electric energy stored in the system by introducing an additional capacitance (between the straps and between the straps and anode segments).

Without a strapping arrangement the entire anode structure at the π mode can be represented by a parallel tuned circuit with an equivalent inductance L and equivalent capacitance C; the resonant frequency of the anode structure is then

$$\omega_\pi = (LC)^{-1/2}$$

The additional capacitance introduced by the strapping arrangement C_{st} will reduce this frequency to

$$\omega_\pi = [L(C + C_{st})]^{-1/2}$$

and therefore, the greater C_{st}, the lower is the resonant frequency of the anode block as compared to the case when there is no strapping arrangement.

The presence of a strapping arrangement affects the resonant frequencies of oscillation modes with low n numbers in essentially a different way. At n less than $N/2$ the points at which the straps are

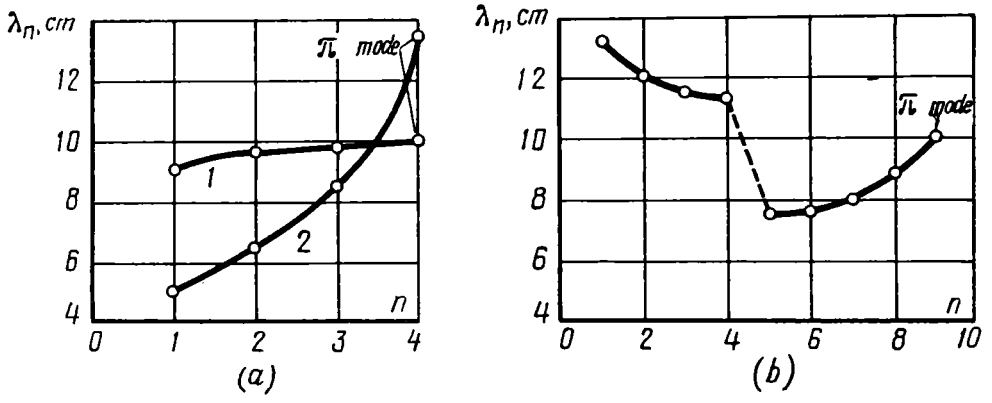

Fig. 7.10. Oscillation modes of 10-cm magnetron anode blocks
(*a*) short equicavity block with and without straps, $N = 8$; (*b*) rising-sun design, $N = 18$; *1*—without straps; *2*—with straps at both butt ends

connected to the anode segments are under different radio-frequency voltages and therefore the straps carry balancing currents; at the same time the inductance of the straps turns out to be connected in parallel to the equivalent tuned circuit. On the other hand, the lower the number of the oscillation modes, the less pronounced is the effect of capacitance C_{st}, introduced into the system by the strapping arrangement. Obviously, both these effects should result in an increase of the resonant frequency at oscillation modes with small mode numbers.

The effect of introducing a strapping arrangement, as observed experimentally, is illustrated in Fig. 7.10*a*; as seen from this graph, the presence of straps increases the mode separation between the π mode and the $(N/2-1)$ mode. With double ring straps at both butt ends of an axially short anode structure the mode separation is up to some 15 to 20 per cent and even more. In magnetrons designed for the decimetric wave band, mode separation in excess of 60 per cent has been achieved.

Obviously, the effect of introducing a strapping arrangement into axially long devices will be less pronounced than in short anode

blocks. Furthermore, straps become less effective with an increase in strap length, as this dimension becomes comparable with the operating wavelength.

Strapping arrangements are effective in increasing the mode separation, but at the same time they tend to impair the non-loaded Q of a multicavity anode structure. This increase in dissipative loss is especially pronounced at wavelengths shorter than some 3 cm. The design difficulties arising with strapping arrangements at the shorter centimetric and especially millimetric waves should also

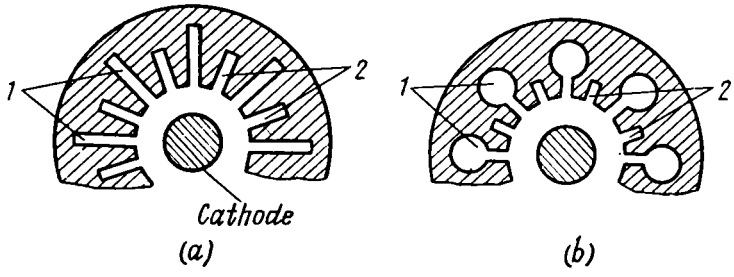

Fig. 7.11. Rising-sun designs of anode blocks
1—long-wave cavities; *2*—short-wave cavities

be taken into account, the geometrical dimensions of anode structures become inconveniently small at these shorter wavelengths and it becomes more expedient to employ multicavity anode structures with *cavities of different size.*

The design of a magnetron block of this kind (commonly known as the rising-sun anode) is schematically shown in Fig. 7.11. The cavities distributed uniformly along the circumference of the anode block are of different dimensions and constitute two distinct groups of alternating design, namely "large" or long-wave and "small" or short-wave resonant cavities.

The results of calculations performed for the oscillation mode spectrum of rising-sun designs are illustrated in Fig. 7.10*b*; these results are in fair agreement with experimental findings. In this case the resonant frequencies fall into two distinct groups, corresponding to the "short-wave" and "long-wave" cavities. At the same time, the resonant frequency of the π mode proves to be between these two groups and turns out to be adequately separated from adjacent oscillation modes.

The greater the difference between resonant frequencies of the two groups of cavities in the rising-sun design, the greater is the mode separation obtained. From this point of view it appears advantageous to increase the ratio of resonant frequencies, corresponding to the "small" and the "large" cavities. However, this is accompanied by a deterioration of the field distribution in the interaction space,

as seen from Fig. 7.12. The distribution of microwave currents along the walls of two successive slot cavities can be shown to result in the appearance of ring currents since the resonant frequency at the π mode is higher than that of the "long-wave" cavity, but lower than that of the "short-wave" group of cavities.

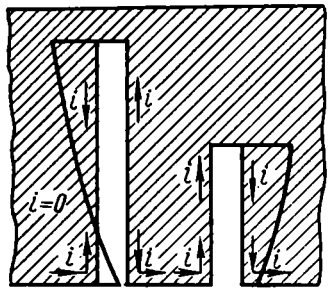

Fig. 7.12. Direction and distribution of microwave currents along the walls of adjacent cavities in the rising-sun magnetron at π oscillation mode

An azimuthal current with no variations along the anode surface produces a field of the zero mode ($n = 0$) in the interaction space, this field being superimposed onto that of the desired π mode. As will be demonstrated in Section 7.5, such a "pollution" of the π mode field by the zero mode field results in a poorer electronic efficiency. Therefore, the ratio of resonant frequencies of the "large" and "small" cavities has to be chosen as a compromise between these factors and is generally not in excess of 1.8 to 2.0.

Another method of obtaining adequate mode separations at high numbers of resonant cavities is by the use of the *coaxial* and *inverted coaxial* designs, which are treated later (Section 7.8).

7.4. Electron Motion in the Interaction Space of a Magnetron Oscillator

7.4a. Electron Sorting at the Travelling-Wave Oscillation Mode

Now we shall qualitatively analyse electronic processes in a multicavity magnetron oscillator under steady-state conditions. Assume the oscillations at one of the modes of the anode structure to be already established; the character of electron motion can then be determined by taking into account the combined action of three fields, the static electric field, the static magnetic field and the radio-frequency electric field.

In the absence of microwave oscillations, electron motion in the interaction space is governed by the laws examined in Section 7.2. With a parallel-phase electrode structure the electron trajectories are cycloids; in the ideal case, at $B > B_c$, there is no convection current. The changes caused by the appearance of radio-frequency oscillations of a small amplitude will now be studied.

Interaction between an electron and microwave field is most effective when their relative phase remains constant during a considerable time. The fact that in a planar magnetron electrons simultaneously perform two kinds of motion should also be taken into

account: electrons move progressively along the cathode surface (this corresponding to the displacement of the circle centre) and perform a rotary motion with the cyclotron frequency. On the other hand, the radio-frequency field in the interaction space may be represented by waves travelling between the anode and cathode of the magnetron. Therefore, the condition of the electron featuring a constant phase relative to the microwave field can be considered in terms of the phase velocity of one of these waves coinciding with the average velocity of the circle centre v_c

$$v_c = (v_p)_{np} \tag{7.36}$$

where $(v_p)_{np}$ is the phase velocity of the p-th spatial harmonic at the n-th oscillation mode of the anode structure.

Relation (7.36) is similar to the condition of synchronism (6.1) and (6.66), which underlie the performance of forward-wave and

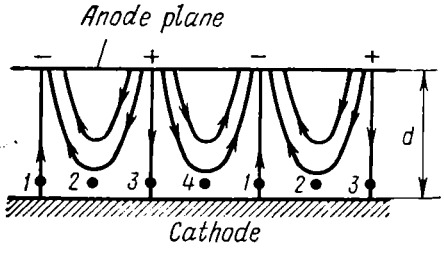

Fig. 7.13. Electric field of a travelling wave in the interaction space of a magnetron

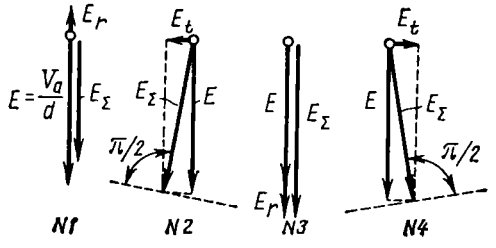

Fig. 7.14. Resulting electric field affecting electrons of type *1*, *2*, *3* and *4* (Fig. 7.13); the position of the plane along which the circle, determining the cycloidal trajectories of electrons, should roll is shown in dashed lines

backward-wave tubes of the O-type. The effect produced by all the other waves may be neglected, provided the condition of synchronism (7.36) is satisfied, because their phase velocities differ considerably from the average electron velocity v_c.

Assume a reference plane to move with one of the waves described by equation (7.30) at a velocity $(v_p)_{np}$. The electric field of this wave appears as static in this reference plane. Suppose, that in the absence of a radio-frequency signal the average electron velocity $v_c = \frac{E}{B} = \frac{V_a}{Bd}$ coincides with the phase velocity $(v_p)_{np}$ of the wave in question. It will be useful to examine the behaviour of several typical electrons, located at various points of the interaction space, as shown in Fig. 7.13. The resulting vectors of electric field intensity, obtained by summing up the static and radio-frequency electric fields at the four points, where the typical electrons *1*, *2*, *3* and *4* are located, are presented in Fig. 7.14.

The resulting electric field E_Σ acting on electrons of type *1*, remains invariable in direction, but features an alternating amplitude. The speed of the rolling circle centre, which determines the electron trajectory in a static reference plane and which is now equal to E_Σ/B, is lower than this speed under purely static conditions. As a result, electrons of type *1* tend to lag behind the travelling wave and are gradually shifted toward electrons of type *4*. Electrons of type *3* experience similar changes; the resulting electric field affecting these electrons is slightly greater than the static field, this tending to accelerate the motion of electrons of type *3*, so that they gradually catch up with electrons of type *4*.

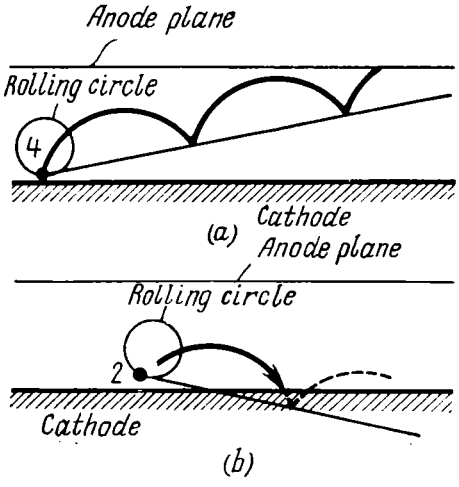

Fig. 7.15. Trajectories of electrons of type *2* and *4* relative to a static reference plane under synchronism with the travelling wave

Electrons of type *4* are forced to move in a resulting electric field that in absolute magnitude is almost the same as the static electric field, but is sloped relative to the latter (Fig. 7.14). This slope means that the circle producing the cycloidal curve should no longer roll parallel to the cathode surface, as discussed in Section 7.2*b*; this rolling movement has to be along a line normal to vector E_Σ, i.e. inclined toward the anode. The corresponding trajectory of electrons of type *4* is illustrated in Fig. 7.15*a*, where the reference plane is assumed stationary: electrons are gradually displaced toward the anode, though they remain in synchronism with the travelling wave.

It follows that electrons of type *4* remain under the action of a maximum retarding tangential field during a considerable time period. With each cycloidal revolution these electrons deliver up part of their potential energy to the radio-frequency field and move closer to the anode; the rotary energy of these electrons remains approximately unchanged.

Physically, electrons of type *4* are the most favourable for sustaining oscillations in a magnetron. As was shown, electrons of types *1* and *3* gradually "improve" their phase relative to the microwave field and, after being shifted into a retarding tangential field, also become favourable.

Not so, however, with electrons of type *2*, which were emitted from the cathode into an accelerating tangential field (refer to Figs. 7.13 and 7.14). The plane, along which the rolling movement

is performed, is inclined in this case toward the cathode. After the first cycloidal oscillation, these electrons, having consumed a certain amount of energy from the radio-frequency field, strike the cathode and are no more existent in the interaction space, as shown in Fig. 7.15*b*. Electrons of type *2* are unfavourable from the point of view of sustaining oscillations, but since they are quickly removed from the interaction space, the latter contains almost exclusively the favourable electrons.

Thus, the microwave field automatically produces electron sorting, the favourable electrons giving up more energy to the radio-frequency field than is consumed by the unfavourable electrons. As a result, the amplitude of microwave oscillations will build up from the small value satisfying condition (7.36), i.e. self-sustained oscillations will be established.

The above argumentation accounts also for such experimentally observed phenomena as considerable convection current in the presence of microwave oscillations, though the static magnetic field is maintained at values in excess of the cutoff field. Under purely static conditions (in the absence of oscillations) this current, as previously mentioned, is ordinarily quite small. Furthermore, the unfavourable electrons which bombard the cathode cause additional heating of this electrode, thereby producing substantial secondary electron emission. Both these effects play an important part in actual design and maintenance procedures of magnetron devices.

7.4b. Alternating Space Charge in Magnetrons. Electron Spokes

The process of electron sorting in the interaction space results in the formation of electron bunches around electrons, which begin to move in a maximum retarding tangential field. Thus, the electron stream is automatically density-modulated without any control electrode. The radial component of the microwave electric field is mostly responsible for the process of electron bunching (phase focussing), while the energy exchange between the electrons and microwave field is mainly via the tangential field component.

A graphic way of examining the process of electron bunching is with the aid of a reference plane moving at the velocity of the slow wave. The centres of the rolling circles, which describe the actual trajectories of electrons, will appear as stationary in this system of coordinates in the absence of a microwave field; in this case each electron moves along a closed circular path, as illustrated in Fig. 7.16*a*.

The presence of a radial and tangential electric field leads to a displacement of the circle centres for electrons of types *1*, *2*, *3* and *4*, as shown in Fig. 7.16*b* in dashed lines. Electrons of type *1* and *3* are

compressed around electrons of type *4*, the resulting electron bunch gradually "rises" toward the anode, while the unfavourable electrons of type *2* "sink" to the cathode.

The entire electron cloud rotating around the cathode with an angular frequency Ω_{np} (provided the condition of synchronism is met) becomes separated into bunches, *spokes*, extending from the space charge around the cathode to the anode. The envelope of electron

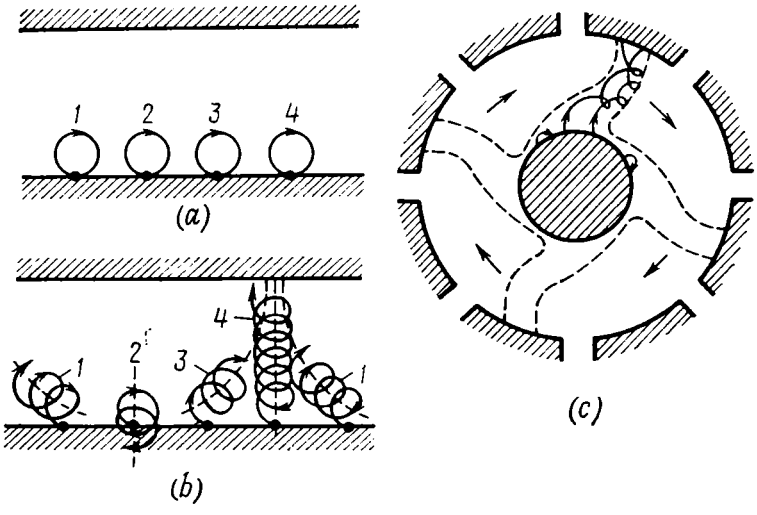

Fig. 7.16. Motion of typical electrons in a reference plane moving synchronously with the slow wave in the absence (*a*) and presence (*b*, *c*) of radio-frequency oscillations

spokes in a cylindrical magnetron for a fixed instant of time is shown in Fig. 7.16*c*; this configuration was obtained by numerical calculation of electron trajectories.

The configuration of space charge spokes resembles that of the spokes of a flywheel with the cathode and the space charge surrounding it acting as the wheel hub. It may also be compared to the rotor of a synchronous motor with the resonant system of the magnetron functioning as the stator.

The number of electron spokes rotating around the cathode may be determined by taking account of the fact that each spoke of space charge is formed around one maximum of the retarding tangential field. By condition (7.25), at the fundamental harmonic ($p = 0$) the number of slow-wave lengths is exactly equal to the number of the oscillation modes n. Thus, at $n = 1$ there will be only one space charge spoke, $n = 2$ corresponds to the presence of two electron spokes, and so on. The maximum number of electron spokes is obtained with the π oscillation mode and is $N/2$; at the same time, the speed of spoke rotation in this case is minimum.

In cases the electron cloud is synchronous with one of the spatial harmonics ($p \neq 0$), the number of electron spokes in principle should be equal to $(n + pN)$ with a corresponding reduction of the speed of spoke rotation. Note, however, that the fields of the spatial harmonics diminish rapidly in the radial direction with an increase in the spacing from the surface of the anode. Therefore magnetron excitation even at $p = \pm 1$ cannot be fully described by the above mechanism of electron spoke formation.

7.5. Conditions of Self-Excitation in a Multicavity Magnetron

As with other microwave oscillators, the self-excitation of magnetrons may be analysed with the aid of the general equations of the (3.2) and (3.3) type and the generalized equivalent circuit of Fig. 3.1. The use of this circuit presupposes that the electron admittance $Y_e = G_e + jB_e$ is known beforehand.

Analysing the electron admittance in a magnetron is not such a simple matter as it was with reflex klystrons. Indeed, the electrons inside the space charge spoke induce currents in anode segments due to spoke rotation, the process of current induction following the general laws of microwave electronics. In the present case, however, the general equation of induced current $i_{ind} = -e(\bar{E}\bar{v})$ is hardly directly applicable because of the complicate nature of electron motion and elaborate pattern of microwave field.

Similar difficulties are encountered when trying to calculate the power given up by the electrons to the radio-frequency field in the interaction space. The argumentation given below is therefore based mainly on the concept of a rotating space charge, as qualitatively discussed in the preceding Sections.

7.5a. Elementary Derivation of Self-Excitation Conditions

We shall first consider the case when the ratio of anode to cathode radii approaches unity (i.e. when the entire structure can be approximated by a parallel-plane one). Assume that the condition of electrons delivering the maximum amount of energy to the radio-frequency field is that the phase velocity of the travelling wave is equal to the average electron velocity in the absence of microwave oscillations, i.e. condition (7.36). In this case any initial disturbance in the anode structure should lead to the build-up of oscillations, this process being finally limited by the onset of non-linear effects.

The phase velocity of the wave at the n-th oscillation mode with the p-th spatial harmonic can be determined from equation (7.30). The averaged condition of synchronism of the wave and electrons may be obtained by replacing the anode radius r_a in (7.30) by the main radius of the interaction space $r_{av} = (r_a + r_k)/2$.

Thus, the average phase velocity of the wave in the interaction space is

$$(v_p)_{np\ av} = \frac{\omega (r_a + r_k)}{2 (n + pN)}$$

By (7.19) the average electron velocity is $v_c = E/B$; hence, the condition of synchronism (7.36) can be presented as

$$v_c = (v_p)_{np\ av}; \quad \frac{E}{B} = \frac{\omega (r_a + r_k)}{2 (n + pN)}$$

In the system in question the intensity of the static electric field may be approximated by $E \approx V_a/(r_a - r_k)$; substituting this relation into the above equation and allowing for the fact that the oscillation frequency is mainly determined by the resonant frequency of the oscillation mode in question (i.e. assuming $\omega \approx \omega_n$) results in

$$V_a = \frac{\omega_n (r_a^2 - r_k^2)}{2 (n + pN)} B \qquad (7.37)$$

According to this relation, the anode voltage at which a multicavity magnetron becomes self-excited at a specified spatial harmonic

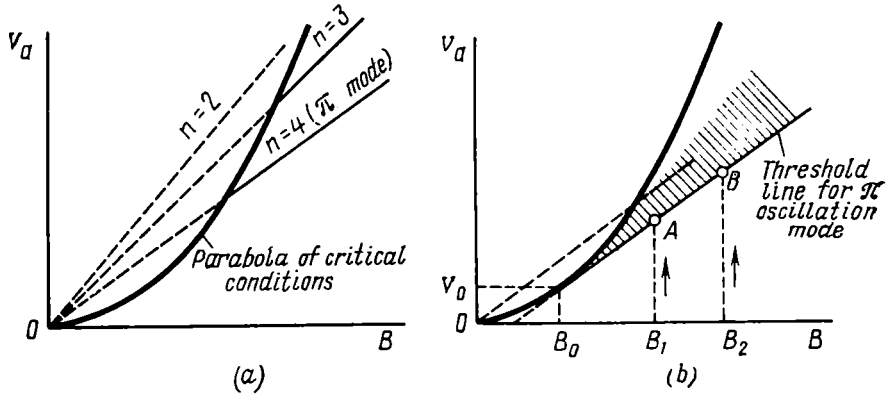

Fig. 7.17. Magnetron self-excitation: according to the simplified equation (7.37) at $N = 8$ (*a*); by equation (7.38) at the π oscillation mode

p is a linear function of the static magnetic field B for each oscillation mode n. The ratio V_a/B is a constant for the given magnetron at fixed values of p and n.

Corresponding graphs for three oscillation modes in an 8-cavity magnetron at $p = 0$ are presented in Fig. 7.17*a* along with the critical conditions parabola discussed in Section 7.2*b*.

The straight lines plotted by (7.37) start from the coordinate origin and intersect the parabola of critical conditions. Physically it is obvious that at V_a in excess of $(V_a)_c$ there can be no oscillations of the travelling-wave type, because all electrons arrive at the anode

not later than after a half-cycle of the cycloidal oscillation. Therefore, only the sections of the straight lines beneath the parabola of critical conditions (shown in Fig. 7.17*a* in solid lines) correspond to regions where self-excitation conditions are satisfied.

The self-excitation graphs presented cannot claim any great accuracy. Proceeding from equation (7.37) and the graphs of Fig. 7.17*a* it can be only stated that there are certain optimum relations between the constant anode voltage and static magnetic induction for every oscillation mode. However, this does not mean that oscillations at points of the (V_a, B) plane not belonging to the straight lines shown are utterly impossible. Increasing the anode voltage at a fixed magnitude of the static magnetic induction causes the output power to go through a maximum and then drop off as the spacing from the straight line of equation (7.37) is increased. A still further increase in the anode voltage may lead to synchronism with the wave of the next oscillation mode with a lower number n. It is natural to assume the existence of an intermediate region of unstable oscillations, where small variations of the anode voltage result in abrupt stepwide transitions ("jumps") from one oscillation mode to another.

Disregarding for the time being the possibility of magnetron excitation at spatial harmonics, it can be stated that the π mode is excited at the lowest possible anode voltage. This peculiarity of the π mode is of special importance in pulse magnetrons. At the same time, it is possible to state that the π mode is separated from the other oscillation modes not only in frequency, but in the magnitude of anode voltage as well.

7.5b. A More Strict Determination of Self-Excitation Condition for Oscillations of the Travelling-Wave Type. Threshold Anode Voltage

The presence of a convection current in the anode circuit of a magnetron is indicative of the existence of oscillations. Indeed, the favourable electrons inevitably move toward the anode in the presence of a radio-frequency field, as seen from Fig. 7.15.

The constant anode voltage V_a at which an infinitesimal amplitude of radio-frequency oscillations in the resonant structure warrants electron arrival at the anode (provided B is greater than the critical value) is conventionally termed the *threshold anode voltage* V_{th} of a magnetron. A more detailed examination of the self-excitation conditions in a cylindrical multicavity magnetron discloses the threshold anode voltage to be related to the static magnetic induction B, the radii of device anode and cathode, the number of oscillation mode and number of spatial harmonic by the Hartree equation

$$V_{th}=\frac{\omega_n (r_a^2-r_k^2)}{2(n+pN)} B-\frac{mr_a^2}{2e}\left(\frac{\omega_n}{n+pN}\right)^2 \qquad (7.38)$$

(in the present treatment the derivation of the Hartree equation is omitted).

Comparison of equations (7.38) and (7.37) discloses their general similarity. Indeed, the first term in the Hartree equation is exactly the same as the right-hand member of equation (7.37), i.e. the threshold voltage is again a linear function of the static magnetic induction B. At fixed values of n and p the line $V_{th} = f(B)$ is parallel to the line of self-excitation $V_a = f(B)$ as determined by (7.37); the threshold line is shifted toward the range of lower voltage values at the same magnitude of B and does not go through the origin of the coordinate system. The threshold line can easily be shown to have only one point of intersection with the parabola of critical conditions, the coordinates of this intersection point being

$$V_0 = \frac{mr_a^2}{2e}\left(\frac{\omega_n}{n+pN}\right)^2; \quad B_0 = \frac{2m}{e(1-r_k^2/r_a^2)}\frac{\omega_n}{n+pN}$$

The Hartree equation can be presented in a more convenient form for the case of magnetron operation at the fundamental wave ($p = 0$), which is the most common in the majority of magnetron devices

$$V_{th} = 1.01 \cdot 10^7 \left(\frac{r_a}{n\lambda}\right)^2 \left[B\left(1-\frac{r_k^2}{r_a^2}\right)\frac{n\lambda}{1.07} - 1\right], \text{ V} \qquad (7.39)$$

where B is in tesla, the wavelength, in centimetres and the voltage, in volts.

The threshold line $V_{th} = f(B)$ is plotted in Fig. 7.17*b* by equation (7.38). The constant anode voltage V_0 corresponding to the point where this line is tangent to the parabola of critical conditions, is sometimes known as the synchronization voltage and carries a simple physical meaning, namely, at $V_a = V_0$ all electrons moving near the anode parallel to its surface prove to be synchronous with the field of the travelling wave.

The zone of magnetron oscillation is confined between the Hartree line and the parabola of critical conditions; this is shown as a shaded area in Fig. 7.17*b*. From this point of view the operating anode voltage should meet the condition $V_a \gtrsim V_{th}$.

Actually observed oscillation zones resemble that of Fig. 7.17*b*, the main difference being in that their lower boundary is somewhat lower and parallel to the Hartree line. The width of the oscillation zone is determined by the loading of the resonant system at the operating oscillation mode, as well as by the cathode emissivity. This circumstance, along with the other peculiarities mentioned points to the complicate character of magnetron electronics and the approximate nature of the present theory.

7.5c. Some Considerations on the Nature of Electron Admittance in Magnetrons. Frequency Pushing

Now the conditions of electron spoke formation in a magnetron of the travelling-wave type under large-signal conditions will be treated qualitatively. The argumentation will be restricted to the case of a parallel-plane structure. Suppose the oscillation amplitude

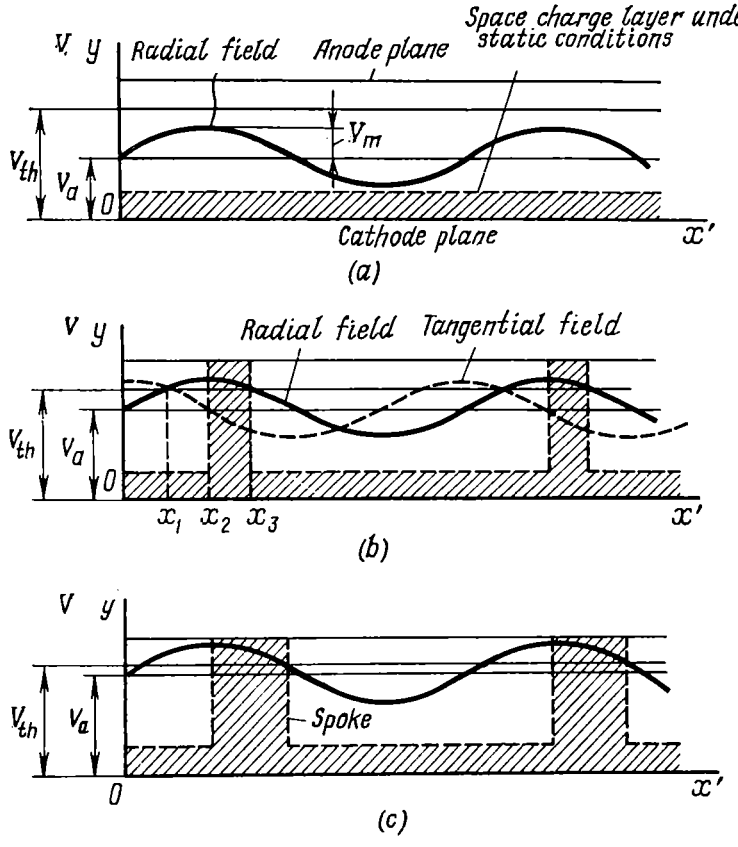

Fig. 7.18. Space charge spoke formation in a planar magnetron relative to a moving reference plane

to be independent both of the constant anode voltage and the d.c. current, such conditions corresponding, for instance, to the magnetron being excited from an external source at the frequency of the oscillation mode specified.

Graphs illustrating the behaviour of the radial component of the fundamental harmonic, which is in approximate synchronism with the electrons, are presented in Fig. 7.18 along with the threshold voltage V_{th} and the constant anode voltage V_a. The total anode voltage in a reference plane moving with the wave, is the sum of the constant voltage V_a and the radial radio-frequency voltage, which has a finite magnitude of the amplitude V_m.

Gradually increasing the static voltage V_a causes the entire curve to be shifted upward on this graph. The appearance of oscillations and the beginning of anode current flow correspond to this summary voltage being tangent to the line of threshold voltage; a finite value of the anode current corresponds to the case when $V_a + V_m$ is in excess of V_{th}.

Figure 7.18*a* illustrates the case when the amplitude of microwave oscillations and the constant anode voltage are insufficient to produce electron spokes. Increasing V_a can make the total voltage exceed the threshold value in the interval x_1x_3, as shown in Fig. 7.18*b*. It should be kept in mind, however, that the interaction space contains also a tangential field component (shown in Fig. 7.18*b* in dashed lines) and the direction of this component in the interval x_1x_2 is such that electrons are forced back towards the cathode, rather than to the anode as in Fig. 7.15*b*. The actual pattern of the electron bunch gradually moving to the anode will therefore be limited to x_2x_3. These electron bunches constitute the spokes discussed in Section 7.4*b*. The higher the constant anode voltage, the wider is the interval x_2x_3 in Fig. 7.18*c* and the wider is the spoke of space charge. The width of electron spokes can be considered approximately proportional to the mean anode current.

It becomes now possible to make an important conclusion about the position of the space charge spoke in respect to the field of the travelling wave. As seen from Fig. 7.18, the middle of the spoke *lags behind* the maximum of the retarding tangential field, this phase lag constituting $\pi/2$ at an infinitesimal anode current and decreasing with a rise in the d.c. anode voltage. The above argumentation also shows that the anode current is possible and the oscillations can be self-sustained at V_a lower than the threshold value under large-signal conditions. This accounts in part for the effect of shifting the lower boundary of the oscillation zone relative to the Hartree line, mentioned earlier. The currents induced in the anode segments by electrons in each space charge spoke lag behind the retarding tangential field by an angle of $\pi/2 \geqslant \varphi \geqslant 0$. Since it is just this field that is responsible for energy exchange with the electrons, the electron admittance in a magnetron in the general case can be said to feature a capacitive susceptance along with a negative conductance. It follows that the oscillation frequency should be slightly *lower* than the resonant frequency of the anode structure at the oscillation mode in question. An increase in anode voltage and current will cause this capacitive susceptance to be reduced, this resulting in a *higher* oscillation frequency.

Thus, it may be stated that magnetrons are voltage tunable and display frequency pushing effects, as other kinds of microwave oscillators (refer to Section 3.2*d*). Since the anode current of a magnetron cannot ordinarily vary independently of the anode voltage

both these effects show up simultaneously. However, with temperature-limited cathode emission or if the electron stream is made to arrive at the anode structure in such a way that the anode current becomes independent of the magnitude of anode voltage, electronic tuning effects can be separated from frequency pushing. Just this circumstance is used to advantage in voltage-tunable magnetrons (VTM or *mitrons*), which are treated later in Section 7.8*c*.

In general, the conclusions made above are confirmed by experimental data. Ordinarily, the oscillation frequency of a magnetron is slightly lower (by fractions of a per cent) than the resonant frequency of its "cold" anode structure. This is due to the heating of the anode block during actual operation, and is in part also due to the capacitive loading effect of the rotating space charge. In magnetron design, however, the oscillation frequency can, as a first approximation, be considered equal to the resonant frequency of the "cold" anode block at the π mode and the final frequency adjustments may be based on the results of "hot" measurements.

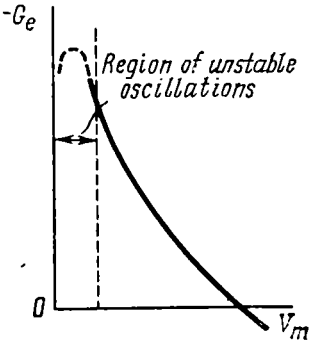

Fig. 7.19. Behaviour of magnetron electron conductance *vs* amplitude of radio-frequency oscillations at $B =$ = const

The dependence of the oscillation frequency on the magnitude of anode current (frequency pushing) is practically evaluated by the frequency shift per ampere of anode current variation. The typical value of frequency pushing for modern magnetron oscillators is from hundreds of kilohertz to several megahertz per 1 ampere. Note, that at low anode currents (near the threshold) frequency pushing effects may become quite significant, much more pronounced than under normal operating conditions.

The curve of electron conductance as a function of the microwave voltage across the segments of a magnetron block obtained experimentally is presented in Fig. 7.19. As should be expected, the dependence—G_e *vs* V_m is mainly of a drooping character. At small amplitudes, the absolute magnitude of electron conductance apparently features a maximum; in this region magnetron operation proves to be unstable (refer to Section 3.2*a*). At the main drooping section of the characteristic $-G_e = f(V_m)$ magnetron operation is similar to that of other microwave oscillators with resonant oscillatory systems.

7.6. Magnetron Efficiency

The difficulties encountered when attempting to directly calculate the amount of microwave power delivered by electrons prove to be so great that up to the present time there is yet no strict method of

evaluating the electronic efficiency of a magnetron oscillator of the travelling-wave type. Under these circumstances it appears suitable to determine the power dissipated by the electrons after interacting with the microwave field and then apply the law of energy conservation.

Examine the kinetic energy of an electron at the instant it arrives at the device anode; the electron in question has thus given up a considerable part of its potential energy to the radio-frequency field in the interaction space.

As was qualitatively demonstrated in Section 7.4, when discussing the process of electron sorting, the cycloidal trajectory of a favourable electron under small-signal conditions is inclined towards the anode, remaining in general the same as under static conditions. By (7.18), the radius of the rolling circle in a planar magnetron is

$$R=\frac{mE}{eB^2}=\frac{m}{eB^2}\frac{V_a}{d}$$

where d is the spacing between the cathode and anode.

The velocity at which the electron strikes the anode surface depends on the time the electron strikes this electrode. From the point of view of efficiency, the most unfavourable case is when the electron strikes the anode surface at the apex of the cycloidal trajectory. Rotation is around a point of tangency of the circle with the plane along which this circle rolls; the radius of electron rotation is thus $2R$. The maximum electron velocity is readily determined from the angular velocity

$$v_{\max.}=\omega_c 2R=2\frac{E}{B}=\frac{2V_a}{Bd}$$

The same result can be obtained by examining the speed of the circle centre which is equal to E/B.

The maximum amount of energy that can be dissipated by this electron on the anode is

$$W_{diss.\,\max.}=\frac{mv^2_{\max.}}{2}=\frac{2mV_a^2}{B^2d^2}$$

The same electron possessed a potential energy relative to the anode (when leaving the cathode) equal to $W_{pot}=eV_a$ at a zero kinetic energy. From the law of energy conservation it follows that the energy delivered to the radio-frequency field is $W_{pot}-W_{diss.\,\max.}$

Thus, the efficiency of the individual electron in question is

$$\eta_e=\frac{W_{pot}-W_{diss.\,\max.}}{W_{pot}}=1-\frac{V_a}{B^2}\frac{2m}{ed^2} \qquad (7.40)$$

This relation can be rearranged by expressing the quantity $2m/ed^2$ in terms of the critical parameters $(V_a)_c$ and B_c. Applying (7.23)

results in

$$\eta_e = 1 - \frac{V_a}{(V_a)_c}\left(\frac{B_c}{B}\right)^2 \tag{7.41}$$

Equation (7.41) discloses the relation existing between the electronic efficiency and the static electric and magnetic fields. The electronic efficiency is zero if the static electric and magnetic fields are equal to their critical values, this being in complete agreement with the assumptions adopted. The greater the difference between the operating and the critical conditions, the higher should the electronic efficiency be. It is of particular interest to note that no theoretical limit is set to the magnitude of electronic efficiency by the above equations.

The dependence of electronic efficiency on the magnitude of the magnetic field can be made especially obvious if the conditions of synchronism at any specified oscillation mode are taken into account. Applying the simplified condition of synchronism (7.37) yields

$$\frac{V_a}{B} = \frac{\omega_n (r_a^2 - r_k^2)}{2(n + pN)};$$

$$\eta_e = 1 - \frac{1}{nB}\frac{m\omega_n}{e}\frac{1+\sigma}{1-\sigma} \tag{7.42}$$

assuming $d \approx r_a - r_k$ in a cylindrical system; here σ is the cathode-to-anode radius ratio ($\sigma = r_k/r_a$).

Taking the magnetic induction in tesla and introducing the resonant wavelength at the n-th oscillation mode ($\lambda_n = 2\pi c/\omega_n$), after substitution of the magnitudes e and m, as defined by (2.11), result in

$$\eta_e = 1 - \frac{1.07(1+\sigma)}{n\lambda B(1-\sigma)} \tag{7.42a}$$

where the wavelength is in centimetres.

As an example, the electronic efficiency of an 8-cavity 10-cm magnetron designed to operate at the π oscillation mode with a static magnetic induction of 0.18 tesla (1800 Gs) is about 70 per cent by equation (7.42a), if we take the typical ratio r_k/r_a equal to 1/3.

Equations (7.42) and (7.42a) ordinarily provide efficiency values slightly in excess of actually attainable ones. In part this discrepancy results from neglecting the loss due to unfavourable electrons bombarding the cathode[1], as well as not taking into account the unproductive loss of electrons at the side caps of the magnetron and certain other factors. Typically, the efficiency of modern commercially available magnetron oscillators of the centimetric wave band

[1] Experimental data indicate the power of electron bombardment of the cathode to be from 1.5 to 4 per cent of the output power of a magnetron.

ranges from about 50 to 70 per cent, sometimes even higher. This is the reason why magnetrons are considered to be the most suitable high power microwave oscillators.

At specified wavelength and magnetron design equation (7.42) may be reduced to

$$\eta_e = 1 - \frac{\text{const}}{nB} \tag{7.42b}$$

The equation thus obtained corresponds to efficiencies calculated for points of one of the self-excitation lines on the (V_a, B) plane (refer to Fig. 7.17*a*). The corresponding graphical representation of the dependence $\eta_e = f(B)$ for the case of an 8-cavity magnetron is shown in Fig. 7.20*a* where the curves describing efficiency are sections of hyperbolae. The lower the number n of the oscillation mode, the lower is the electronic efficiency at a specified value of the magnetic induction B. In other words, the π oscillation mode is characterized by the lowest intensity of the static magnetic field, at one and the same value of electronic efficiency.

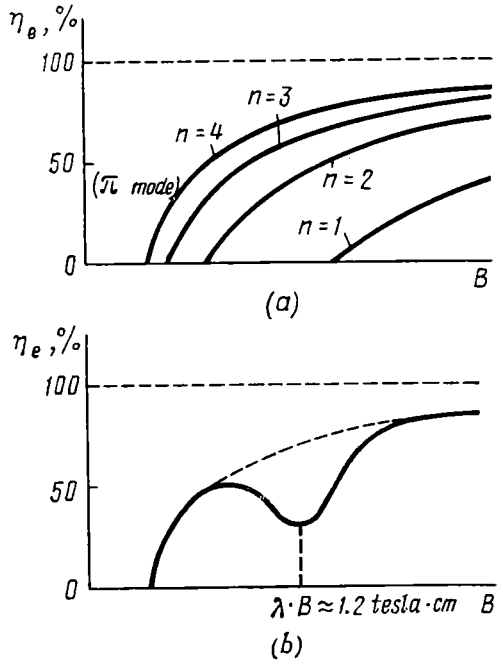

Fig. 7.20. Electronic efficiency of a magnetron *vs* static magnetic field induction at V_a/B = const

The increase in electronic efficiency at higher static magnetic fields (and correspondingly higher static electric fields) is readily explained physically by the unlimited reduction of the radius of the rolling circle and by a reduction of the amount of energy dissipated by the electrons at the anode. Similar tendencies are characteristic of other devices of the magnetron type (refer to Sections 7.10 and 7.11). In this respect the peculiarities and advantages of magnetron devices over devices of the O-type are particularly obvious. In devices of the M-type electrons deliver their *potential* energy to the microwave field, and not the kinetic energy as in devices of the O-type. The average speed of electron transfer remains unaltered, this resulting in undisturbed synchronism with the field of the travelling wave.

At high intensities of the static magnetic field, the period of a single cycloidal oscillation, as determined by equation (7.20), may become considerably shorter than the period of microwave oscilla-

tions. In this case the radio-frequency field can be considered approximately constant during the time of electron travel from the cathode to the anode. Thus, under intense static fields, the operation of multicavity magnetrons can be treated in terms of the static approximation, instead of considering the field of a travelling wave.

Analysis discloses the presence of a negative resistance in case of time-invariable voltages between the anode segments, this effect manifesting itself as an increase in the current drawn by the segment under the lowest voltage. Oscillations of this kind are termed *negative-resistance* (or *dynatron mode*) and were mentioned earlier (Section 7.1).

Oscillations of the negative-resistance kind can be considered as the extreme case of travelling-wave oscillations at the period of cycloidal oscillations much less than the period of operating frequency, in other words, at frequencies considerably lower than the cyclotron frequency. The argumentation presented shows that the electronic efficiency of these oscillations can be exceedingly high; however, the condition that the operating frequency be by far lower than the cyclotron frequency at practicable static magnetic fields can be realized only in the long-wave part of the microwave range. Apparently, oscillations of the negative-resistance type are of no practical importance.

In general, experimental data confirm the behaviour of the efficiency *vs* magnetic induction curve at a constant ratio V_a/B as presented in Fig. 7.20*a*. However, a valley in the efficiency curve in a certain range of magnetic induction values is observed with the rising-sun design (Fig. 7.20*b*). Research has disclosed that all magnetrons at the middle of this "dip" feature a constant product of the magnetic induction (taken in tesla) by the wavelength (in centimetres), approximately equal to 1.2 tesla·cm.

The presence of this "dip" in the efficiency of rising-sun designs can be qualitatively explained in terms of *cyclotron resonance effects*, which take place at $\omega \approx \omega_c$. As mentioned in Section 7.3*e*, the interaction space of a rising-sun magnetron contains a component of the $n = 0$ mode field along with that of the π mode. With the operating frequency approximately equal to the cyclotron frequency the pattern of electron trajectories can be disturbed. The fact that the field of the zero mode diminishes much more slowly than that of the π mode as the distance from the anode increases is also very important. The configuration of the space charge spokes and their interaction with the field of the π mode are impaired. Cyclotron resonance effects will be elaborated in some detail in Section 7.12.

It is common to set the operating static field in rising-sun magnetrons at values lower than that corresponding to the middle of the

"dip"; intense magnetic fields shifting the operating point to the region beyond this "dip" are usually impracticable.

The electronic efficiency of a magnetron is to a considerable degree a function of the mode separation. Apparently, the presence of "polluting" fields in the interaction space deteriorates the conditions of space charge spoke formation. The electronic efficiency may also be impaired by the effect of straps mounted at the magnetron butt ends, because the fields of the straps, not having any azimuthal variations, affect the space charge in about the same way as the zero-mode field in the rising-sun design. Such harmful effects are usually eliminated by mounting the strapping arrangement inside ring grooves at the butt ends, thus screening the fields of the straps.

Electronic efficiency is also a function of the cathode diameter, as evident from (7.12), which points to an increase in efficiency at lower ratios r_k/r_a. However, the conditions of synchronism cannot be completely satisfied at low values of the ratio r_k/r_a, because the intensity of the static electric field is the highest immediately at the cathode surface and drops with a greater distance from this electrode. Usually, the lowest value of this ratio, at which an adequate stability of oscillation modes is still secured, is the most suitable for magnetron design and is recommended with a view to obtaining the maximum efficiency.

Various empirical relations are used to evaluate the optimum value of the r_k/r_a ratio, for instance

$$\sigma=(N-4)/(N+4) \quad \text{or} \quad \sigma=\exp(-8/N) \tag{7.43}$$

where N is the number of cavities. Note, however, that the efficiency $\eta_e = f(\sigma)$ is not too critical and considerable deviations from the values determined by equations of the (7.43) kind are admissible.

It will be recalled in conclusion that the overall efficiency of a magnetron is also a function of the efficiency of its resonant structure

$$\eta_{tot}=\eta_e\eta_{res} \tag{7.44}$$

As known from microwave engineering, the efficiency η_{res} is a function of the unloaded, loaded and external Q-factors of the oscillatory system in accordance with

$$\eta_{res}=1-\frac{Q_L}{Q_0}=\frac{Q_0}{Q_0+Q_{ext}} \tag{7.45}$$

The allowable degree of magnetron frequency pulling sets a limit to the exernal Q-factor (refer to Section 7.7*b*), and ordinarily this factor is taken to be not less than one or two hundred. It is desirable to have as high a non-loaded Q as practicable; in centimetre-wave magnetrons Q_0 is typically of the order of 1000. Thus, by (7.45),

the efficiency of the resonant structure can range from 90-95 per cent to 60-65 per cent at the shorter wavelengths. Typical values of the overall efficiency constitute from 60-70 per cent at decimetric wavelengths to 20-30 per cent at wavelengths of about 1 cm.

7.7. Operating and Load Characteristics of Magnetrons

Two families of characteristic curves are used to describe the maintenance properties of magnetrons. The first family consists of voltampere characteristic curves plotted at a constant load corresponding to the case of the magnetron output terminating in a matched load. Parameters for this family of curves $V_a = f(I_a)$ are the static magnetic induction B, output power P_{out}, oscillation frequency f and overall efficiency η_{tot}. The second family of characteristic curves contains the dependences of output power and oscillation frequency on the load impedance (admittance) and when plotted on a polar chart are known as the Rieke diagrams.

Magnetron voltampere characteristic curves plotted for the case $B = \text{const}$, $P_{out} = \text{const}$, $f = \text{const}$ and $\eta_{tot} = \text{const}$ are called the *operating* (or *operational*) *characteristics.* It is common to plot them in rectangular coordinates with the vertical axis carrying the d.c. anode voltage scale.

Load characteristics $P_{out} = f(Z_L)$ and $f = f(Z_L)$ at $I_a = \text{const}$, as with any other microwave oscillator, are usually presented in the form of graphs plotted in a polar system of coordinates on the complex plane of impedances.

As a rule, the operating and load characteristics of magnetrons are directly measured, rather than determined analytically. Nevertheless, the behaviour of these characteristics is a direct corollary of the physical processes taking place in the device and can therefore be qualitatively evaluated by a train of simple reasoning.

7.7a. Operational Characteristics

The discussion of idealized operational characteristic curves will be based on the above described properties of travelling-wave magnetrons.

The family of curves of constant output power can be obtained from the following argumentation. As with any electron device, the output power of a magnetron is a function of the applied d.c. voltage, the d.c. anode current and the device efficiency according to the relation $P_{out} = V_a I_a \eta_{tot}$. This relation may also be presented as

$$V_a = P_{out}/\eta_{tot} I_a$$

It follows that the voltampere curves of constant output power would be equilateral hyperbolae, provided the magnetron efficiency could be made independent of the anode current. However, the electronic efficiency of a magnetron diminishes slightly with an increase in anode current due to the increase in oscillation amplitude leading to an increase in the fraction of power dissipated on the anode at the last revolution of the cycloidal electron trajectory. Since the efficiency of the resonant structure obviously remains unaffected, the curves of constant power deviate from the precise hyperbolic form

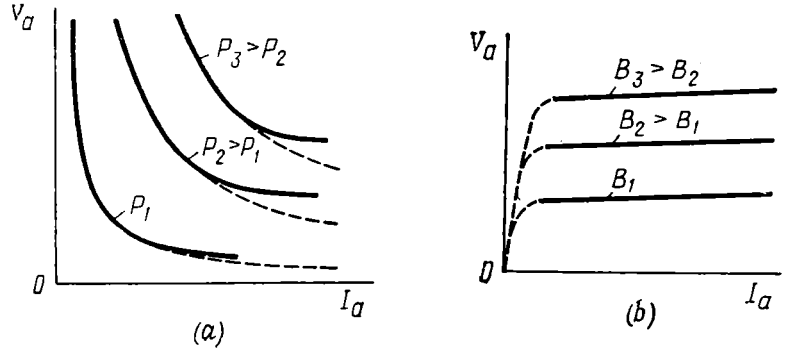

Fig. 7.21. Idealized performance characteristics of a magnetron oscillator

and are slightly elevated at heavier anode currents, as illustrated in Fig. 7.21*a*. The higher the output power, the higher and more to the right is the shift of the P_{out} = const curves.

The behaviour of the curves of constant static magnetic induction can be explained with the aid of the Hartree diagram of Fig. 7.17*b*. We shall take the static magnetic field $B = B_1$ and vary the d.c. anode voltage from zero upwards.

At V_a lower than the threshold value, the anode current should be quite low because the magnetron is under cutoff conditions and there are no radio-frequency oscillations as yet (the reasons for a finite magnitude of the anode current under such conditions were treated in Section 7.2*b*). At point A (Fig. 7.17*b*) or in its vicinity, the anode voltage attains the threshold value and this results in self-excitation of the magnetron and a rapid increase in the anode current. After this, increments of the anode voltage lead to the anode current attaining a maximum value, which is determined by the emissive properties of the cathode.

A similar train of reasoning can be presented for the case when the static magnetic field is increased to $B = B_2$ (refer to Fig. 7.17*b*). Point B corresponds to the condition in which considerable anode current starts flowing, this will take place at a higher value of the anode voltage.

Thus, the voltampere characteristics of a magnetron at B = const are a family of curves with a steep initial section, as shown in

Fig. 7.21*b* in dashed lines. At a certain value of the anode current the curves experience a sharp bend ("knee") and then become almost horizontal, with a slight inclination to the abscissa axis; it is just this last section that characterizes a magnetron under operating conditions (in the presence of microwave oscillations).

Typical operational characteristics of a 10-cm pulse magnetron are presented in Fig. 7.22. The graph contains families of curves of constant efficiency and constant oscillation frequency, along with the

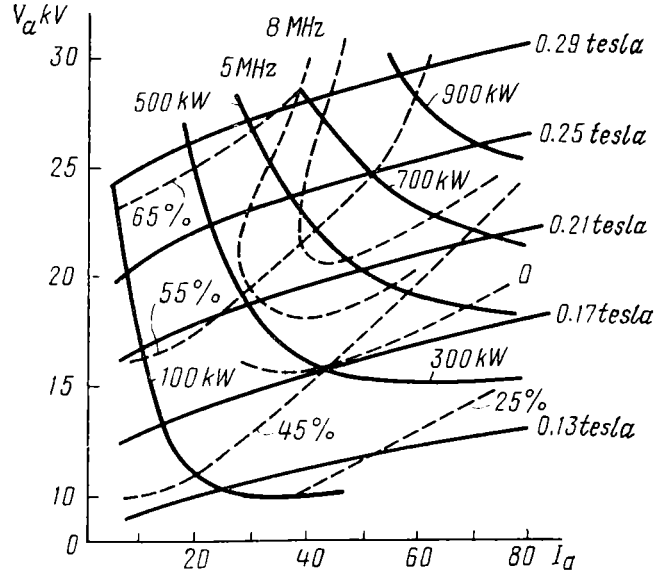

Fig. 7.22. Example of actual performance characteristic of a high-power pulse magnetron; frequency pushing effects are indicated by lines of constant frequency relative to the nominal frequency (2800 MHz)

curves P_{out} = const and B = const. The operating point of the magnetron is in the upper right-hand part of these graphs.

The graphs of Fig. 7.22 indicate that these curves obtained experimentally are in fair agreement with idealized behaviour discussed above. This agreement can be taken to mean that the main qualitative assumptions adopted in the examination of magnetron performance are valid.

7.7b. Magnetron Load Characteristics

The load characteristics of a magnetron resemble those of other microwave oscillators with resonant oscillatory systems, for instance, those of reflex klystrons. This general similarity of device behaviour is due to frequency pulling effects ordinarily being significantly smaller than the mode separation. Magnetron load characteristics have all the main peculiarities discussed in Section 3.3*d*.

It is common to plot the load characteristic curves at nominal values of the static magnetic induction B and d.c. anode current I_a. Sometimes (with particularly high power levels) measurements are carried out at output power levels lower than the nominal so as to avoid breakdown at considerable reflection coefficients; the phase of the standing wave is usually referred to the output flange of the magnetron.

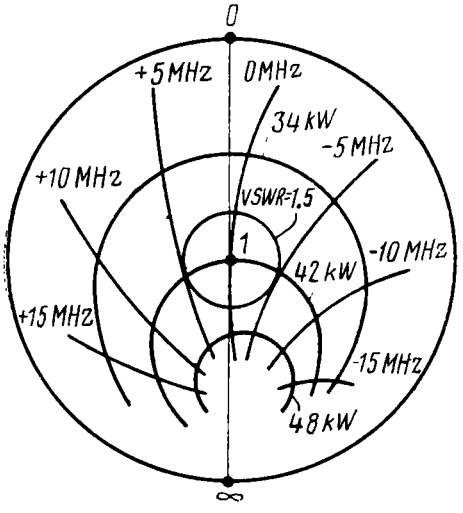

Fig. 7.23. Example of actual load characteristic (Rieke diagram) of a pulse 3-cm magnetron at $B = 0.55$ tesla, $I_a = 10$ A. Zero frequency pulling line corresponds to nominal frequency 9375 MHz

A typical load characteristic curve of a pulse magnetron designed for the 3-cm band is presented in Fig. 7.23. The contours of constant output power are nearly circular, approximating the circles of constant load conductance. The curves of constant oscillation frequency are of a fan-like pattern and closely resemble the curves of constant susceptance on a polar impedance chart.

A very important parameter, characterizing magnetron performance, is the *degree of frequency pulling*, which is conventionally evaluated at a VSWR = 1.5:1 (refer to Fig. 7.23). This parameter, used to evaluate oscillator performance in general, becomes especially important in case of magnetrons, which are often connected directly to the load, without any decoupling arrangement. Frequency pulling of magnetron oscillators is ordinarily some 10 to 15 MHz for 10-cm devices and up to 15 to 20 MHz for 3-cm tubes. The allowable value of frequency pulling is largely a function of the properties of the automatic frequency control system of the receiver in which the local oscillator (usually a reflex klystron) provides for electronic tuning.

The corresponding values of the external Q of a magnetron at the operating oscillation mode can be determined from the general equations describing frequency pulling effects, as treated in Section 3.3*d*. By equation (3.26)

$$Q_{ext} \approx 0.417 f_0 / F_p \tag{7.46}$$

where f_0 is the oscillation frequency, approximately equal to the resonant frequency of the "cold" anode structure at the oscillation mode specified. Ordinarily the fact that the contours of constant output power and constant frequency intersect at an angle differing

from $\pi/2$ is taken into account by introducing an additional empirical factor of about 1.05 into the right-hand side of equation (7.46).

As an example, the external Q-factor of a magnetron designed to operate in the 3-cm band (at a wavelength of 3.2 cm) should be about 200 if frequency pulling is to be limited to not more than 20 MHz. Modern magnetrons typically feature just such or slightly higher (up to 300-500) values of Q_{ext}.

7.8. Problems of Magnetron Design

Modern magnetrons consist of the following main design units:
(1) anode structure with a resonant system and arrangement for mode separation;
(2) frequency tuning arrangement;
(3) power output;
(4) cathode with corresponding leads;
(5) vacuum envelope and cooling system;
(6) magnetic circuit.

In most magnetron designs the entire resonant structure, the tuning mechanism and a substantial portion of the power output unit are mounted inside the vacuum envelope and constitute an integral part of the tube design; this fact to a great extent influences the design of each of the units mentioned.

7.8a. Anode Block and Tuning Mechanism

Most modern magnetrons, excluding perhaps only some millimetre wave devices, operate with the π mode of oscillations of the resonant structure. Earlier it was demonstrated that this mode exhibited a number of peculiarities and advantages, as compared to other oscillation modes. Among these advantages are the absence of degeneracy, the lowest anode voltage at the same intensity of the static magnetic field (disregarding excitation of other oscillation modes at spatial harmonics) and the highest efficiency at a fixed value of the static magnetic field. Yet another advantage of operating with the π mode is the simple design of the oscillatory system.

When choosing the number N of resonant cavities for the anode structure the following factors should be taken into account. First of all, to sustain the π oscillation mode, N has to be an even number. At higher numbers of resonant cavities the mode separation tends to become narrower, but the anode voltage (at a fixed value of the static magnetic field B and fixed anode diameter) also tends to become lower. This is readily confirmed by equation (7.39) if n is set at $N/2$, which corresponds to the π mode. A greater number of resonant cavities allow also compensation for an increase in the r_a/λ

ratio, this increase being necessary when the level of output power is increased or the operating wavelength shortened.

Common magnetrons of the 10-cm band are provided with from 8 to 12 resonant cavities, while in 3-cm devices this number is increased to 12-18. At millimetric wavelengths the number of cavities can be up to 24-38 and even more. Coaxial magnetrons (to be treated later) hold a somewhat peculiar position; in this design a considerably greater number of resonant cavities can be used.

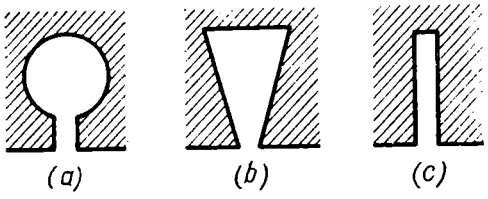

Fig. 7.24. Most common types of magnetron cavities

At wavelengths longer than about 3 cm the slot-and-hole structure and the vane structure are the most common (refer to Fig. 7.24*a* and *b*). In the millimetric wave band slot cavities (Fig. 7.24*c*) are extensively used and with the rising-sun design combinations of different cavity types can be employed.

Practice shows that when the magnetron cavities are strapped together, the maximum value of the diameter of the anode aperture d_a, the operating axial length l_a of the anode block and the wavelength are interrelated by the approximate empirical relations

$$\frac{d_a}{\lambda} \leqslant 0.3; \quad \frac{l_a}{\lambda} \leqslant 0.3$$

and in case of the rising-sun anode design the maximum values of these ratios can be significantly increased

$$\frac{d_a}{\lambda} \leqslant (0.6\text{-}1.0); \quad \frac{l_a}{\lambda} \leqslant (0.6\text{-}0.8)$$

At millimetric wavelengths, especially at wavelengths shorter than 1 mm, the ratio d_a/λ is increased to 1.5 and even up to 2. In this case it becomes suitable to operate the magnetron at oscillation modes other than π and utilize synchronism with the $p = +1$ or $p = -1$ spatial harmonics (refer to Sections 7.3*c* and 7.4*b*) so as to avoid a drastical increase in the number of resonant cavities of the structure or in the magnitudes of the static electric and magnetic fields.

Rising-sun anodes with "multilayer" straps distributed uniformly along the length of the structure can be manufactured with considerable axial dimensions (up to 2 wavelengths), this enabling a considerable increase in the length of the cathode and thus in the output power level.

Mechanical tuning of the oscillation frequency of magnetrons is based on varying the resonant frequency of the anode block at the oscillation mode in question. The presence of several oscillation modes with closely spaced resonant frequencies hampers the mecha-

nical tuning of magnetron oscillators. With any kind of tuning arrangement it is most important to maintain an adequate mode separation and approximately constant non-loaded and external Q-factors of the anode structure in the operating range of frequencies. Any unwanted resonance effects, except the main resonance at the oscillation mode specified, are inadmissible.

The most common arrangement is symmetrical mechanical tuning. All cavities of the structure are simultaneously inductively or

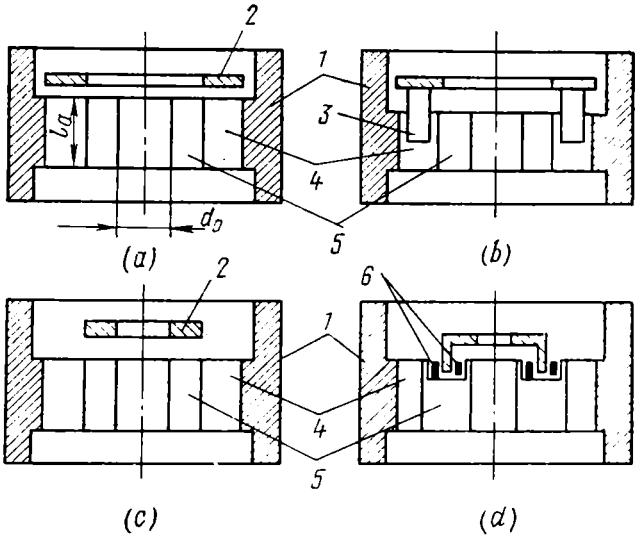

Fig. 7.25. Symmetrical mechanical tuning of a magnetron by an inductive ring (a) and inductive crown (b) and capacitive ring and crown (c, d)
1—anode block; *2*—metal ring; *3*—metal bar; *4*—cavity hole; *5*—cavity slot; *6*—straps

capacitively tuned by means of metal rings, rods or caps moved inside the cavities or at the butt-ends of the magnetron. Several such systems providing a tuning range of up to 3 to 6 per cent of the middle frequency, are illustrated schematically in Fig. 7.25.

With inductive tuning by means of a metal *ring* (Fig. 7.25*a*), most influenced is the radío-frequency field passing the butt-end region. Bringing the ring closer to the butt-end of the anode block tends to reduce the equivalent inductance of all the cavities and, therefore, to increase the resonant frequency of each of the cavities and the entire anode assembly. When the magnetron is to be tuned by affecting the microwave magnetic field of the cavities proper, the tuning arrangement makes use of metal *caps* ("crowns") provided with metal stubs, as shown in Fig. 7.25*b*. Capacitive tuning is accomplished in a similar way with the aid of a metal ring or crown (refer to Fig. 7.25*c* and *d*) mounted in the space containing a predominantly electric radio-frequency field near to the anode segments or strapping arrangement. Sometimes a wider range of mechanical tuning is obtai-

ned by using both inductive and capacitive tuning techniques simultaneously.

An interesting form of magnetron systems is a coaxial magnetron, in which a *coaxial resonant cavity* is used to envelope a multicavity anode structure, with the cylindrical surface of the anode proper functioning as the inner conductor of this coaxial cavity. Alternate

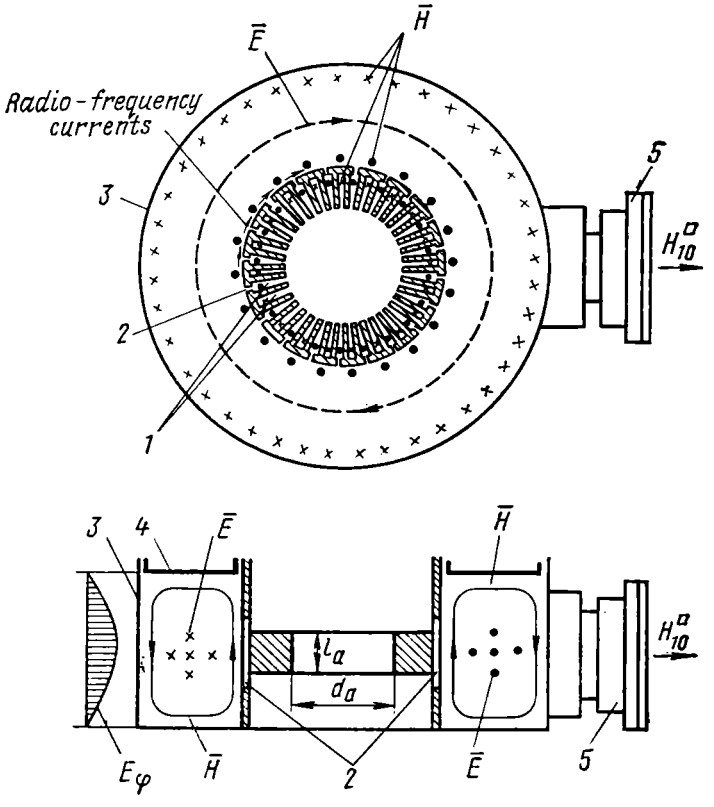

Fig. 7.26. Coaxial magnetron design

1—magnetron cavities; *2*—coupling slots; *3*—external wall of coaxial cavity; *4*—mechanical tuning plunger; *5*—power output (rectangular waveguide)

cavities of the anode block are coupled to the coaxial cavity via longitudinal slots in the cylindrical surface of the anode structure, as illustrated in Fig. 7.26. The coaxial cavity is operated at the H_{011} resonant mode, which is characterized by the electric lines of force and the paths of the wall currents forming closed circles[1]. A similar field pattern and current distribution correspond to the anode structure being excited at the π oscillation mode, because the alternate cavities coupled to the coaxial resonator via slots feature in-phase oscillations with a relative phase shift of 2π.

[1] The H_{011} resonant mode in a coaxial cavity corresponds to halfwave resonance of the H_{01} propagation mode in a coaxial waveguide.

Oscillations in the anode block differing from the π mode correspond to oscillations in the coaxial cavity also different from the H_{011} resonant mode. These unwanted oscillations can easily be damped out, as by means of dissipative inserts or ring slots, the latter disturbing the paths of currents of all resonant modes except the H_{011} mode. This feature can be utilized to great advantage to design such coaxial magnetrons with greater anode diameters and greater numbers of resonant cavities without deteriorating mode separation. An increase in anode diameter makes possible a considerably higher output power.

Coaxial magnetrons have some other important advantages. Storing a considerable amount of microwave energy in the high-Q coaxial cavity tends to increase the non-loaded Q of the entire assembly and thus provides for a higher stability of the oscillation frequency. Making the coupling to the load looser significantly reduces the degree of frequency pulling and at the same time increases the external Q-factor, this being accompanied by an improvement of the efficiency of the resonant system. Furthermore, a greater mode separation makes it possible to reduce the amplitude of the radio-frequency voltage in the interaction space, which results in higher electronic efficiency. These and other merits of coaxial magnetrons make them most promising among magnetron oscillators.

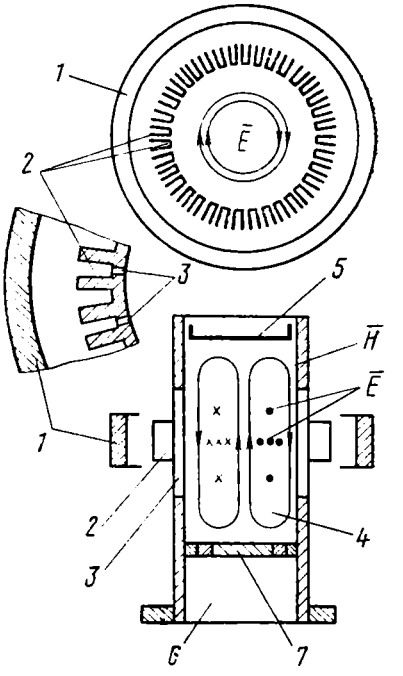

Fig. 7.27. Inverted coaxial magnetron with enlarged section of the interaction space shown at the left

1—cathode; *2*—magnetron cavities; *3*—coupling slots; *4*—stabilizing cylindrical cavity (with the pattern of microwave field shown); *5*—tuning plunger; *6*—power output (circular waveguide at the H_{01} propagation mode); *7*—coupling iris

Another form of the coaxial magnetron — the *inverted coaxial magnetron* — is schematically illustrated in Fig. 7.27. Here the cathode is made to enclose the multicavity anode block, instead of being mounted inside it, and the stabilizing resonant cavity is located inside the anode block and coupled to the latter via slots cut through the walls of alternate cavities, as in the coaxial magnetron discussed above.

The inner coaxial cavity again operates at the H_{011} resonant mode, which has no azimuthal variations of the microwave field; owing to this, mode selectivity is again provided, permitting the number of cavities to be increased up to several hundred. The power output is either directly a cylindrical guide carrying the H_{01} propagation mode or a standard rectangular waveguide at the H_{10} mode.

Coaxial magnetrons, both direct and the inverted forms, are tuned by means of a tuning plunger in the stabilizing cavity.

Inverted coaxial magnetrons are widely employed in the short-wave part of the centimetric wave band and in the millimetric wave band at high levels of output power (refer to Table 7.2). They are comparatively simple in design, as compared to "classical" magnetrons; the development of these devices necessitates, in particular, solution of the problem of suppressing certain parasitic oscillation modes.

7.8b. Power Output. Other Units of a Magnetron

The power output arrangement of a magnetron is required to provide the necessary transformation of the load impedance in the entire

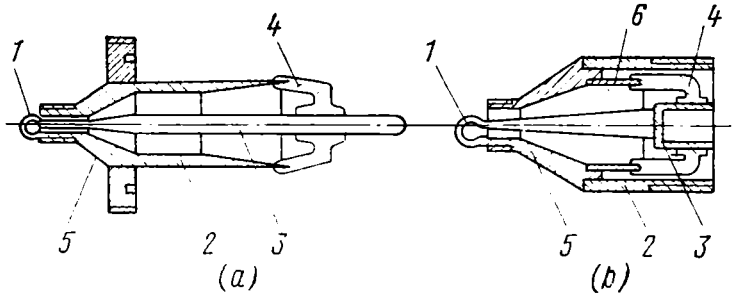

Fig. 7.28. Coaxial power output designs for 10-cm magnetrons of low and medium power levels

1—loop; *2*, *3*—coaxial line conductors; *4*—glass; *5*—copper; *6*—covar

band of operating frequencies, with the inevitable compromise between the amount of output power and the allowable degree of frequency pulling taken into due account. This means that the power output has to be of adequate *bandwidth*. In case of a tunable magnetron, approximately constant output power and frequency pulling in the band of operating frequencies can be ensured only with the aid of a wideband output power arrangement. The same property proves to be of advantage in fixed-frequency devices as well: with a wideband power output the oscillatory system of a magnetron turns out to be tightly coupled to the load not only at the π oscillation mode, but at the other (unwanted) modes as well, this providing for additional suppression of these parasitic modes as the oscillations are being set up.

Typical coaxial and waveguide power output designs are illustrated in Figs. 7.28 and 7.29. The coupling loop is ordinarily mounted at the place of a predominantly magnetic microwave field and the main load impedance transformation (which determines the magnitude of Q_{ext}) is a function of the loop geometry.

Coaxial designs with subsequent transducers to waveguides of a rectangular cross section, with the entire assembly being rigidly mounted to the magnetron, are commonly used at moderate power levels in the short-wave part of the centimetric wave band. At higher power levels, as well as at shorter wavelengths, waveguide power outputs are generally chosen. It is common to provide a quarterwave waveguide transformer between the anode structure and the standard rectangular waveguide (Fig. 7.29), this transformer being responsible for the 100 to 200 times reduction in load impedance. Multistep quarterwave and exponential transducers are also used for this purpose.

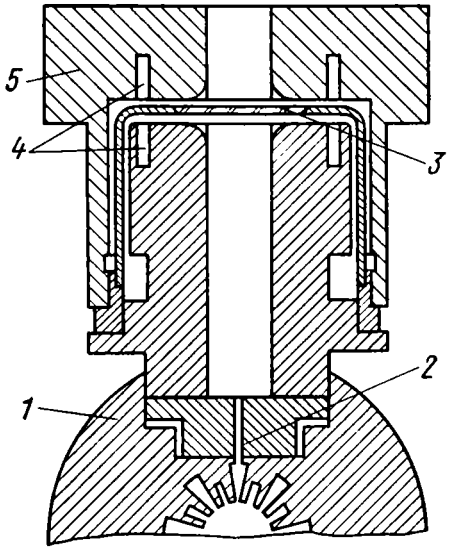

Fig. 7.29. Waveguide power output (with single-step quarterwave transformer) of a 3-cm magnetron

1—anode block; *2*—transformer; *3*—round glass or ceramic window; *4*—choke; *5*—output flange

Magnetron characteristics are much more critical to cathode operation than in other microwave electron devices. The geometrical dimensions (length and diameter) of the cathode in the "classical" magnetron are limited by considerations of the anode axial length l_a, anode diameter d_a and the ratio r_k/r_a (refer to Sections 7.6 and 7.8*a*). Thus, the requirement for specific emissivity of the cathode in a magnetron becomes even more stringent. For example, the typical value of pulse emissivity of a 10-cm magnetron is required to be not less than 10 A/cm^2, while the cathode of a 3-cm magnetron is required to provide about a 30 A/cm^2 current density; a further shortening of the operating wavelength leads to still higher values of the required cathode emissivity.

An additional requirement to be met by magnetron cathodes is that they provide an adequate life span under conditions of considerable bombardment by the electrons returned to the cathode. Since the presence of secondary electron emission from the cathode surface exerts a noticeable effect on the operational characteristics of a magnetron, the magnetron cathode is further required to exhibit high secondary electron emissivity.

The problems of cathode and cathode leads design play an important part in the development of magnetrons. The two main versions of cathode design with *axial* and *radial* leads are schematically illustrated in Fig. 7.30. The axial version with the cathode and heater leads mounted coaxially is the more convenient one; in this case the

leads are passed through an aperture in the magnetic pole piece, which forms an integral part of the vacuum envelope.

Despite the progress achieved, the cathode is still one of the main problems of modern magnetron design: the main reason for magnetron failures is the significant deterioration of cathode characteristics, while all the other magnetron assemblies as a rule completely retain their operational abilities. Further research into and development of cathodes will be conducive to improving magnetron parameters and characteristics.

In conclusion, we shall dwell upon the peculiarities of the magnetic system of a magnetron device. The required magnitude of the static

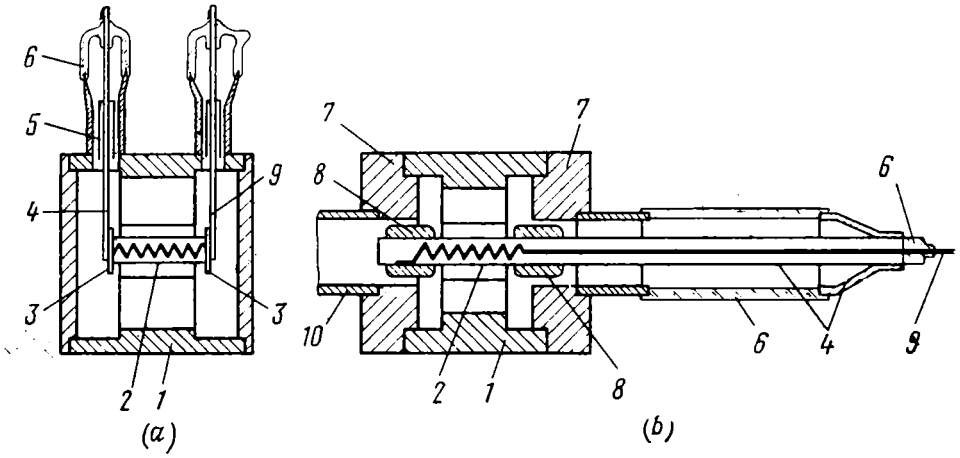

Fig. 7.30. Radial (*a*) and axial (*b*) cathode and heater leads in magnetrons
1—anode block; *2*—cathode; *3*—cathode butt-end discs; *4*—cathode and heater leads; *5*—cathode choke; *6*—glass or ceramics; *7*—iron pole piece; *8*—permendure pole piece; *9*—heater lead; *10*—exhaust tube

magnetic induction is the higher, the shorter is the operating wavelength. Typical values of B for devices of the 10-cm band constitute some 0.12-0.25 tesla, while in the 3-cm band devices the static magnetic induction is required to be about 0.3 to 0.5 tesla. Thus, in the millimetric, and the more so in the submillimetric wave bands the problem of reducing the necessary static magnetic induction becomes one of the most serious. This is just one of the reasons why such magnetrons have to be sometimes operated at spatial field harmonics instead of at the π oscillation mode.

Electromagnets are usually considered inconvenient due to their great size, weight and power consumption; permanent magnets are almost exclusively used in modern magnetrons. Under laboratory conditions and during the research and development stages, however, electromagnets prove to be more suitable due to the possibility of varying the static magnetic field in a wide range. The configuration of the magnetic circuits used with electromagnets and permanent magnets

is selected with a view to obtaining the lowest possible stray magnetic field; several versions are shown in Fig. 7.31.

Magnetrons, as well as most other electron devices of the microwave range, are made mostly as *stacked* devices, with the permanent magnet forming an integral part of the tube and mounted by the manufacturer. As a rule, the permanent magnet is of a special alloy, such as

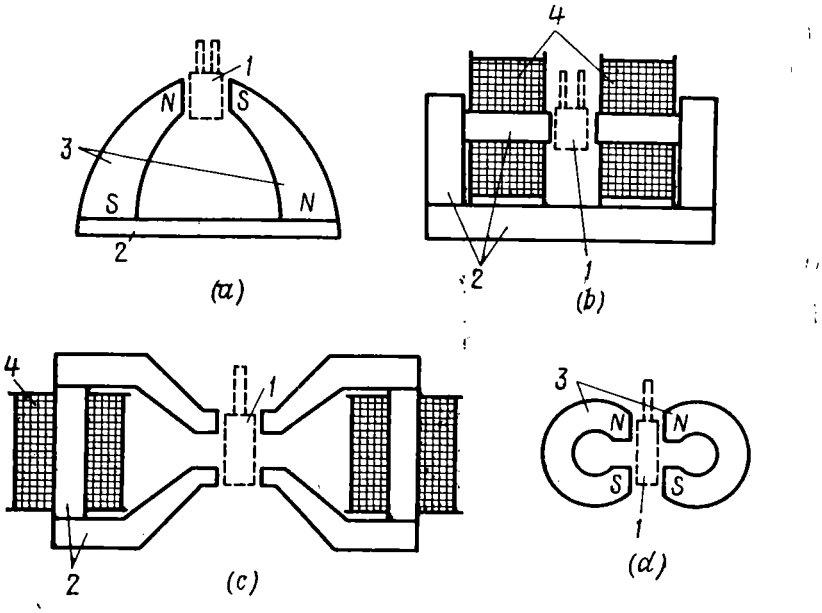

Fig. 7.31. Permanent magnets and electromagnets for magnetrons with radial (*a*, *b*) and axial (*c*, *d*) cathode leads

1—magnetron; *2*—magnetic circuit; *3*—material with high coercive force; *4*—electromagnet coil

alnico, magnico, etc., which displays a high coercive force and high residual induction. The design and manufacture of permanent magnets is a separate problem of considerable importance.

7.8c. Typical Magnetron Designs and Parameters

The main field of application of modern pulse magnetrons is in radar transmitters, less frequently—in transmitters of other services, such as pulsed communication systems, radio telemetry, radio navigation aids, etc. Magnetrons are also employed as high power oscillators for linear accelerator installations. C.w. magnetrons are finding an ever widening field of application in industrial and commercial microwave heating equipment.

The output power of pulse magnetrons ranges from dozens of watts to 10 MW, while c.w. magnetrons feature output power levels from fractions of a watt to scores of kilowatts.

The design of two typical pulsed magnetrons is shown in Figs. 7.32 and 7.33, with the parameters of these devices listed in Table 7.2

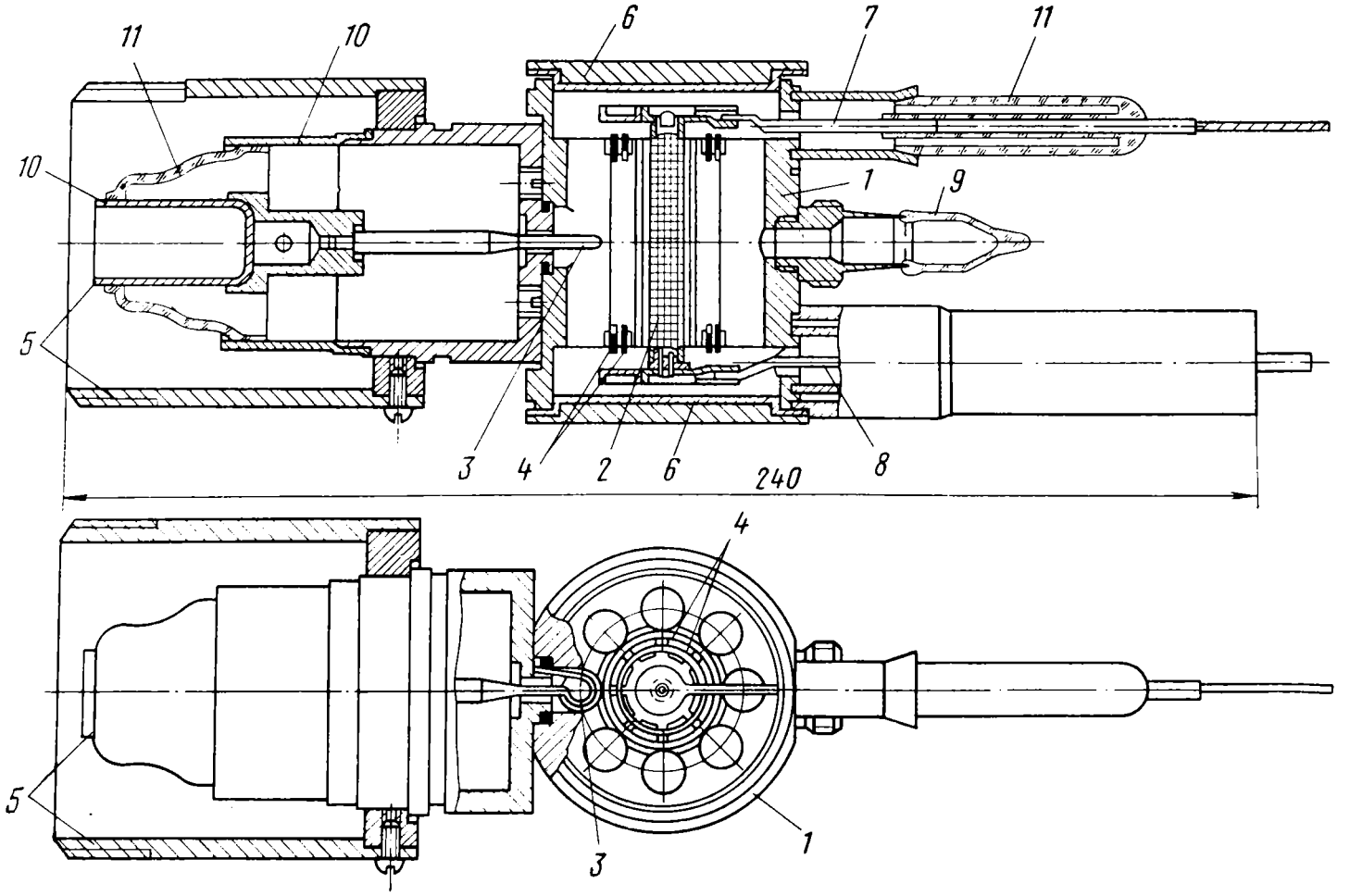

Fig. 7.32. Typical 10-cm fixed frequency magnetron

1—anode block; *2*—cathode; *3*—output power loop; *4*—double ring straps; *5*—coaxial power output; *6*—side caps; *7*—cathode and heater lead; *8*—heater lead; *9*—exhaust tube; *10*—covar; *11*—glass

Table 7.2

Parameters of Typical Magnetrons

Magnetron type	Operating frequency range, GHz	Maximum output power, kW	V_a, kV	I_a, A	B, tesla	η_{tot}, per cent	Frequency pulling, MHz	Number and type of cavities	Mode separation, per cent	Maximum pulse duration, μs
1. Pulsed fixed-frequency magnetron of 10-cm band (Fig. 7.32)	2.72-2.89 (series of models)	1,100	27	65	0.29	63	10	8 (hole and slot)	10	1
2. Pulsed fixed-frequency magnetron of 3-cm band (stacked) (Fig. 7.33)	9.375	280	22	27	0.56	36	13.5	16 (hole and slot)	14	2
3. Pulsed coaxial magnetron of 3-cm band (stacked) (Fig. 7.34)	9.375	1,500	33	83	—	50	5	40 (vane)	16	1
4. Pulsed inverted coaxial magnetron of 8-mm band	33.5-35.5	100	22	21	—	22	—	120 (vane)	—	2
5. C.w. magnetron for commercial and industrial heating	2.45	2.5	5	0.85	0.15	60	—	—	—	—
6. C.w. 10-cm voltage-tunable magnetron of metal-to-ceramics design (Fig. 7.35)	2.5-4.1	0.002	1.3 at 3GHz	0.01	0.25	—	12	—	—	—

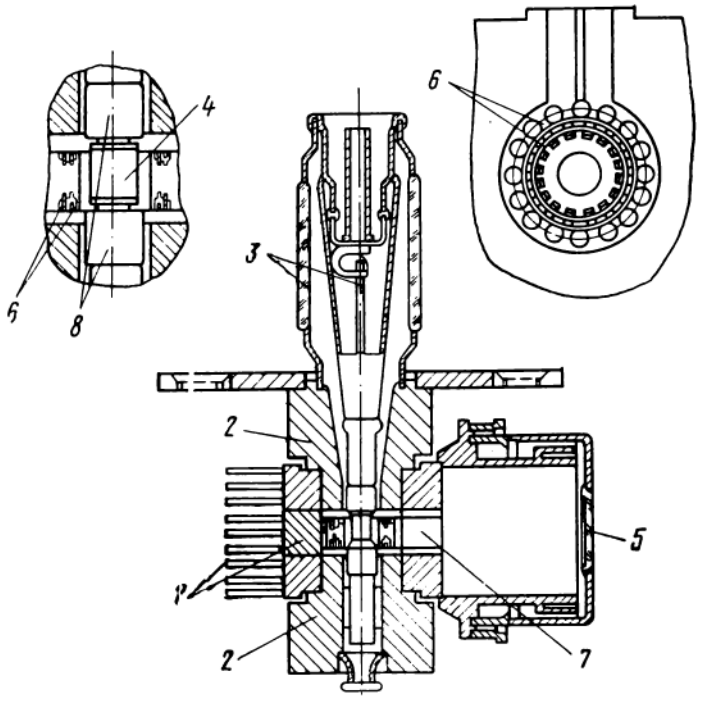

Fig. 7.33. Typical 3-cm magnetron (without permanent magnet); enlarged views of the cathode, straps and anode block are presented

1—anode block with radiator; *2*—pole piece; *3*—cathode assembly; *4*—cathode; *5*—power output window; *6*—straps; *7*—H-type quarterwave transformer; *8*—permendure pole piece

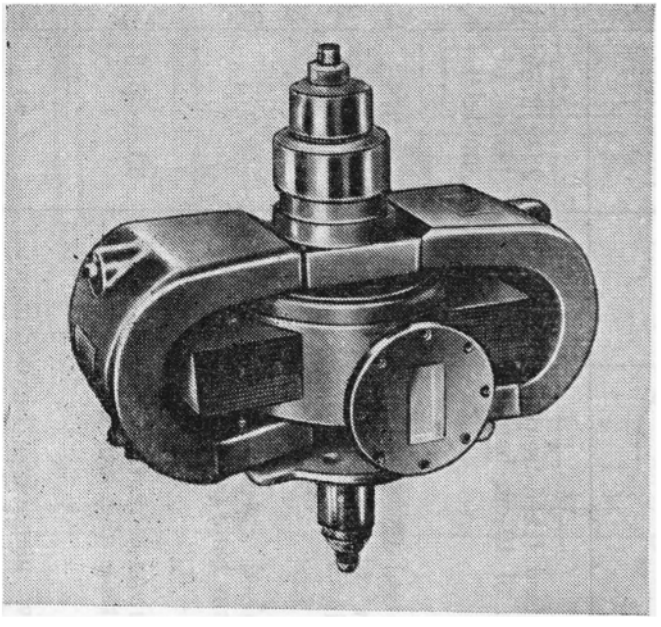

Fig. 7.34. 3-cm pulsed coaxial magnetron of packaged design

(Nos. 1 and 2). Parameters of typical coaxial and inverted coaxial magnetrons are listed in the same Table (Nos. 3 and 4); the external appearance of a coaxial magnetron is presented in Fig. 7.34.

Typical parameters of a c.w. magnetron designed for use in a microwave heating installation (oven) are presented in Table 7.2 (No. 5).

The parameters of a low-power c.w. voltage-tunable magnetron (VTM) are listed at the end of Table 7.2 with the design of this device illustrated in Fig. 7.35. The main peculiarity of a VTM is an extremely wide range of electronic tuning; in these devices the cathode is removed from the interaction space and is mounted along the axis at one of the butt-ends. The cathode is additionally enclosed in a cone-shaped anode which functions as the control electrode, this assembly constituting the electron gun (of the Kayno—Taylor type) of the voltage-tunable magnetron. A negative electrode—cold cathode—is mounted coaxially with the resonant structure and provides the necessary radial static electric field across the interaction space, functioning as the cathode of an ordinary magnetron.

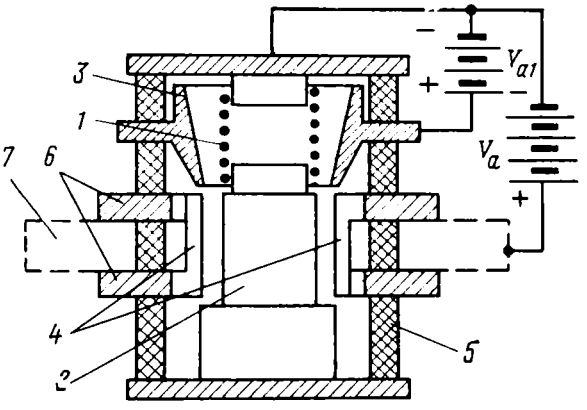

Fig. 7.35. Voltage-tunable magnetron

1—thermionic cathode; *2*—negative electrode; *3*—conical control electrode; *4*—anode vanes (interdigital slow-wave system); *5*—ceramics; *6*—anode rings for connection to external part of cavity; *7*—external cavity

The electron beam in the form of a hollow tube is injected into the interaction space of a VTM and interacts with the field of the π oscillation mode. At V_{a1} = const (refer to Fig. 7.35) the anode current proves to be practically independent of the magnitude of the static anode voltage V_a, this making it possible to use electronic tuning, because this effect is not masked by any accompanying frequency pulling. The loaded Q-factor of a voltage-tunable magnetron is brought down to 2-10 to realize the potentially available wide range of electronic tuning. The VTM shown in Fig. 7.35 is of the interdigital-structure design, with two metal rings connecting the oscillatory system to the external low-Q resonant cavity.

Low-power voltage-tunable magnetrons are capable of covering a bandwidth up to an octave wide. At B = const the oscillation frequency is a linear function of the anode voltage, this function being adequately described by equation (7.37). Thus VTM's successfully compete with backward-wave oscillators of the O-type. An additional advantage of voltage-tunable magnetrons is their high efficiency,

which varies from 25-30 per cent in wideband devices to about 70 per cent in VTM's with electronic tuning ranges of 10 to 20 per cent of the middle frequency.

7.9. Pulsed Operation of Magnetron Oscillators

Magnetron oscillators are widely used under pulse and pulse-code modulation operating conditions. Typical pulse duration is

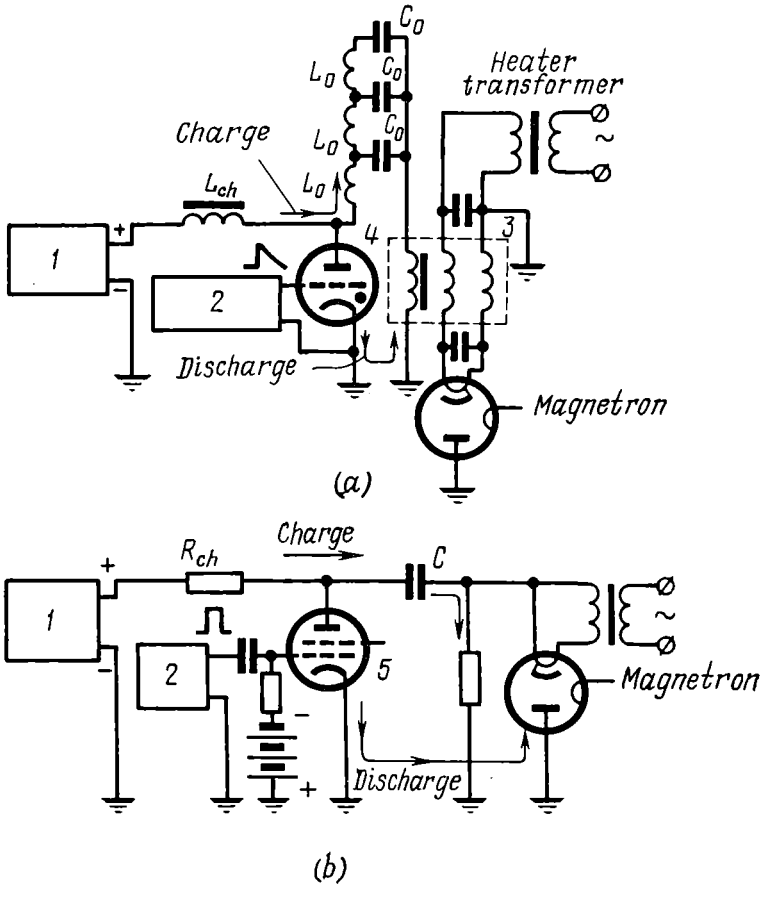

Fig. 7.36. Simplified pulse modulator circuits with complete (*a*) and partial (*b*) discharge of the energy storage unit. Direction of the charging and discharging currents shown by arrows

1—high voltage supply; *2*—pulse timer; *3*—pulse transformer; *4*—pulse thyratron; *5*—modulator tetrode

about one microsecond at pulse reccurence rates from several hundred to several thousand pulses per second.

The high power d.c. pulse of nearly rectangular waveform is provided by a pulse modulator, the simplest circuit versions of this modulator being presented in Fig. 7.36*a* and *b*. The performance of pulse

modulators[1] is based on periodically discharging the d.c. energy stored from a high voltage source, onto a load, a magnetron in the present case or the primary winding of a pulsed transformer, whose secondary terminates in the magnetron leads. Switching from one state to another is accomplished with the aid of a pulsed thyratron or modulator tetrode.

With a pulsed thyratron the duration and waveform of the output pulse are determined by the energy storing device, usually an artificial delay line of 4 to 6 L_0C_0 networks, for instance. In the circuit of Fig. 7.36*a* the storing device is *completely discharged* during the pulse. The circuit shown in Fig. 7.36*b* is based on *partial discharging* of the storing device (capacitor C). The pulsed transformer shown in this circuit is used to match the comparatively high d.c. anode resistance of the magnetron (ordinarily, some 500 to 1000 ohms) to the low resistance of the delay line, besides providing a step-up of the pulse voltage and a reversion of the pulse polarity.

The duration of the operating pulse cannot be chosen arbitrarily and is commonly limited within a comparatively narrow range of values, which are determined, on the one hand, by the time of oscillation build-up in the magnetron, and by the effects of sparking, cathode emission deterioration and the possibility of appearance of unwanted oscillation modes ("frequency jumping"), on the other hand. In most magnetrons of the centimetric band the maximum pulse duration should not exceed some 2 to 5 μs, while the minimum pulse duration is usually of the order of 0.1 μs.

It should not be taken for granted that the modulator quality is the highest and the magnetron performance the best, the nearer the modulating pulse waveform approximates the perfect rectangle, i.e. the steeper the pulse leading and trailing edges. The proper rate of voltage increase at the pulse leading edge should correspond to the build-up of the desired oscillation mode, while passing as quickly as possible the range of voltages where unwanted oscillation modes may arise. With an excessive rate of voltage increase at threshold values of the π mode, this oscillation mode may not be established at all—the magnetron can "skip" the desired oscillation mode or be excited at one of the high-voltage modes corresponding to the upper part of the Hartree diagram. With these effects taken into account, the rate of voltage increase around the threshold value of the π oscillation mode should ordinarily not exceed about 100 to 200 kilovolts per microsecond.

It should be noted, that distortions of the envelope of the output microwave pulse (and, therefore, a wider spectrum of the output signal) may be due not only to an inadequate quality of the magne-

[1] Similar modulators are employed to drive pulsed klystrons and TWT's, examined in Chapters Five and Six.

tron oscillator or its modulator, but to a mismatch at the output magnetron guide as well. The operating conditions of a magnetron oscillator are considerably improved by providing a ferrite isolator or circulator at the magnetron output.

7.10. Forward-Wave and Backward-Wave Tubes of the M-Type

7.10a. General Principles

Magnetrons treated in the previous Sections of the present Chapter are self-oscillators. However, there are certain limitations to using an oscillator as the final stage of a high-power installation, though the numerous advantages of such an arrangement are evident. In many cases the radio transmitter has to be designed as a train of amplifiers driven by a low-power source of highly stable frequency provided by a master oscillator; such amplifier trains have become especially popular with the advent of coherent radio location techniques, as well as with the development of phased arrays for use as antenna systems with controllable directivity.

Self-excitation in a magnetron oscillator is due to the presence of positive feedback in a closed (reentrant) resonant system and to the electron beam. Therefore, to eliminate this positive feedback and, thus, convert the oscillator into an amplifier, the slow-wave structure has to be severed from the electron beam and some kind of arrangement provided at both ends to serve as the signal input and output.

The amplifier thus produced (the TWT of the M-type) is schematically illustrated in Fig. 7.37. The radio-frequency circuit of this tube consists of a parallel combination of a flat slow-wave structure and a flat metal plate, between which a transverse static electric field is developed by the d.c. voltage sources $V_{n.e}$ and V_a. The spacing between these electrodes (of a width d) functions as the interaction space, where the energy of the electron beam is to be converted into the energy of a microwave field. A static magnetic field is imposed onto the entire assembly in a direction normal to the plane of the diagram, as shown in Fig. 7.37. Thus, the electron beam is made to travel through the interaction space in the presence of crossed static electric and magnetic fields, just as in common magnetron oscillator.

First the discussion will be simplified by assuming the electron beam to be injected into the interaction space parallel to the axis of the slow-wave structure by means of an electron gun of the ordinary type, which is removed from the interaction space and additionally fitted with a magnetic screen, as shown in Fig. 7.37. The initial beam velocity v_0, at which the beam enters the interaction space, is determined by the magnitude of the d.c. accelerating voltage V_0:

$$v_0 = (2eV_0/m)^{1/2}$$

The lower plate is kept at a potential negative relative to the tube cathode and is hence commonly known as the *negative electrode* or, less suitably, as the cold cathode, the latter term borrowed from voltage-tunable magnetron terminology.

The trajectories of electrons in devices of the kind shown in Fig. 7.37 will again be examined with the aid of the general equations describing electron motion in crossed static electric and magnetic fields (refer to Section 7.2*b*). In the present case electrons arrive into

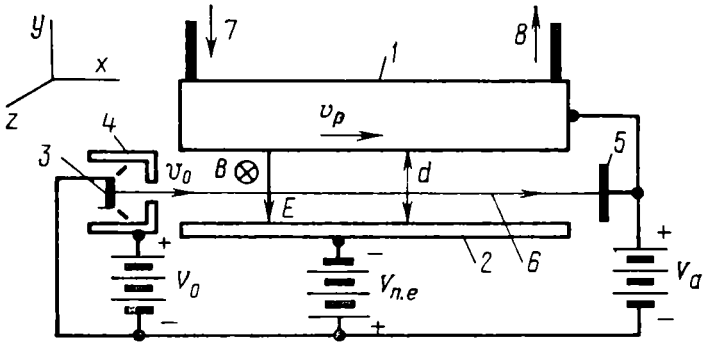

Fig. 7.37. Basic circuit of M-type TWT

1—slow-wave structure; *2*—negative electrode; *3*—cathode; *4*—accelerating electrode and magnetic screen; *5*—collector; *6*—electron beam; *7*, *8*—input and output

the interaction space at an initial velocity v_0 which differs from zero, with the plane of arrival not coinciding with the position of the negative electrode. Equations (7.12) and (7.13) which correspond to such conditions, indicate that the electron trajectories will be trochoidal.

It is of interest to examine the case when a trochoidal trajectory will degenerate into a straight line. Indeed, the right-hand member of (7.12) turns into zero when

$$1-\frac{B}{E}v_{x0}=0 \tag{7.47}$$

$$v_{y0}=0 \tag{7.48}$$

The same conditions turn the last two terms of equation (7.13) into zero as well, and the equations of electron motion acquire the simplest form

$$y=y_0; \quad x=x_0+\frac{E}{B}t \tag{7.49}$$

where E is the intensity of the static electric field in the interaction space, which (neglecting the effects of space charge) is

$$E=\frac{V_a+|V_{n.e}|}{d} \tag{7.50}$$

(The d.c. voltage sources V_a and $V_{n.e}$ are shown in Fig. 7.37.)

According to equation (7.49) the speed of electron transfer along the slow-wave structure in the direction of the x axis is

$$\frac{dx}{dt}=\frac{E}{B}=v_c \tag{7.51}$$

i.e. is precisely equal to the velocity of the centre of the rolling circle which describes the trochoidal trajectory in an ordinary magnetron. It can be stated that the point describing the electron trajectory in the present case coincides with the centre of the rolling circle treated in Fig. 7.3. The physical meaning of this rectilinear electron path is the complete concelling of the transverse force, which affects the electron due to the presence of a static field, by the Lorentz force generated by the static magnetic field.

The condition (7.47), with (7.51) taken into account, can be presented as

$$v_{x0} = v_c \tag{7.52}$$

Since the initial velocity is determined by the accelerating voltage V_0 at the electron gun, condition (7.52) can in turn be given as

$$\sqrt{(2eV_0/m)}=(V_a+|V_{n.e}|)/Bd \tag{7.53}$$

by allowing for (7.50).

Equation (7.53) relates the d.c. accelerating voltage of the electron gun to the other two voltages on the electrodes (Fig. 7.37) and to the static magnetic field B. Thus, the trajectory of the electron beam in the absence of a radio-frequency signal will be the same as in a travelling-wave tube of the O-type, provided the static fields are properly adjusted. The electron beam travels along the slow-wave structure and all of it finally arrives at the collector.

Consider now the effect of a microwave signal applied to the input end of the slow-wave structure. The electric field of this wave travelling along the structure has both a longitudinal and a transverse component (refer to Fig. 7.38*a*). In a travelling-wave tube of the O-type the transverse component of this microwave field is usually of no practical importance due to the presence of an intense longitudinal static magnetic field. In devices of the M-type the situation is different. Under synchronism of the electron beam with the slow wave, the radial radio-frequency field is either added to, or extracted from, the static electric field applied between the slow-wave system and the negative electrode. As a result, the electron movement is either accelerated or retarded relative to the slow wave and thus electron bunches are formed at the regions where the microwave field is a maximum retarding one.

As in common magnetron oscillators (refer to Figs. 7.14 and 7.15), the retarding tangential field determines the slope of the resulting

electric field relative to the tube electrodes. Thus, the circle whose centre describes the electron trajectory, begins to roll along a plane that is inclined upwards. Electrons in the electron bunches are brought nearer to the upper electrode, which is under the highest static potential. Electron bunches take the pattern shown in Fig. 7.38*b*.

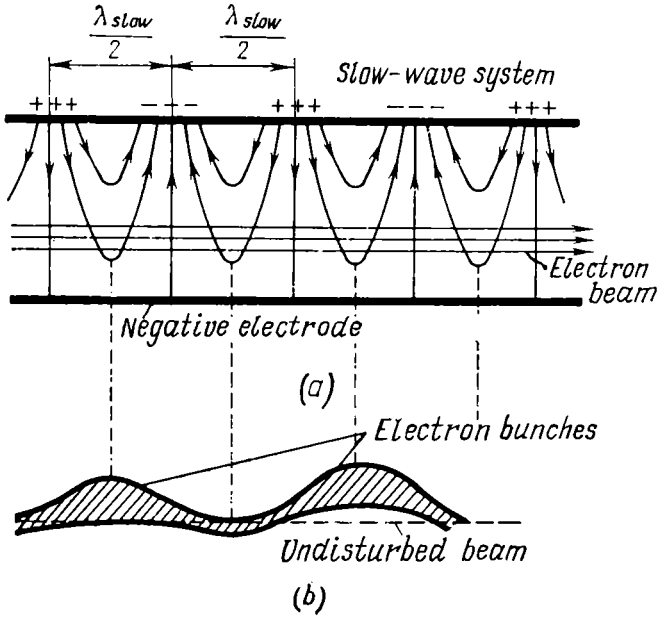

Fig. 7.38. Field distribution of the travelling wave and electron beam bunching in a magnetron amplifier

In contrast to devices of the O-type, electron bunching in the present case is not accompanied by a denser space charge and is mainly a result of charge redistribution in the interaction space, i. e. is mainly due to a change in the configuration of the electron beam.

The process described is quite similar to that of space charge spoke formation in the interaction space of a magnetron oscillator. The average electron velocity v_0 during interaction with the wave remains unaltered. The electrons give up their potential energy to the field developed between the anode (slow-wave structure) and the negative electrode during their gradual movement up towards the anode. At a sufficient length of the system, the electrons arrive at the slow-wave structure and dissipate their kinetic energy here instead of at the collector, this kinetic energy being taken by the electron beam from the source of d.c. accelerating voltage V_0.

Thus, the process of signal amplification in a device of the M-type differs from that in an O-type amplifier in the following:

(1) the most favourable interaction of the electron beam with the travelling wave under small-signal conditions, i.e. the most effective energy exchange between the electron beam and the wave takes place

when the average electron velocity in an M-type amplifier is exactly identical to the phase velocity of the wave; on the contrary, in O-type devices the beam velocity should be slightly greater than the phase velocity of the slow wave;

(2) in travelling-wave tubes of the O-type the electrons give up only their *kinetic* energy to the microwave field, this redundant energy corresponding to the difference in velocities of the beam and wave. In this case the efficiency is limited by the allowable difference in these velocities; the energy transferred to the field is provided by the source of accelerating voltage V_0. On the contrary, in magnetron amplifiers the kinetic energy of the electrons, drawn from the source of

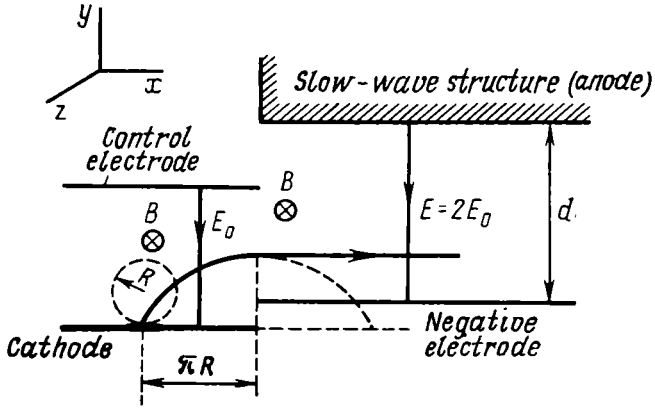

Fig. 7.39. Obtaining a rectilinear electron beam in M-type devices with the aid of the short-optics system

accelerating voltage, remains invariable and only the *potential* energy delivered to the electron beam by the source of d.c. voltage V_a (refer to Fig. 7.37) is converted into microwave energy.

Magnetron amplifiers usually employ a common screened electron gun, similar in design to that of devices of the O-type. Electron-optical systems with a transverse magnetic field are more common as the source of electron beam in magnetron amplifiers with an injected electron stream; the simplest example of such systems is the *short-optics* magnetron gun shown schematically in Fig. 7.39. In this assembly the cathode is mounted parallel to the surface of a negative electrode with the control electrode (first anode) positioned above the cathode, and the entire assembly, as well as the interaction space, is subjected to the action of a static transverse magnetic field.

Electrons from the cathode move along cycloidal trajectories, as in an ordinary magnetron (Fig. 7.39). These electrons can be made to appear in the interaction space just at the peak of the cycloidal trajectory, when the transverse component of electron velocity $v_y = 0$ by adjusting the distance between the cathode and the entrance to the interaction space. Electron motion will thereafter be along recti-

linear trajectories by virtue of (7.48), provided the effects of discontinuities in the transition region can be neglected. This change in electron motion, with (7.52) allowed for, can be described as transfer of the electrons from the circumference of the rolling circle of radius R to the centre of another circle, whose velocity is twice higher than in

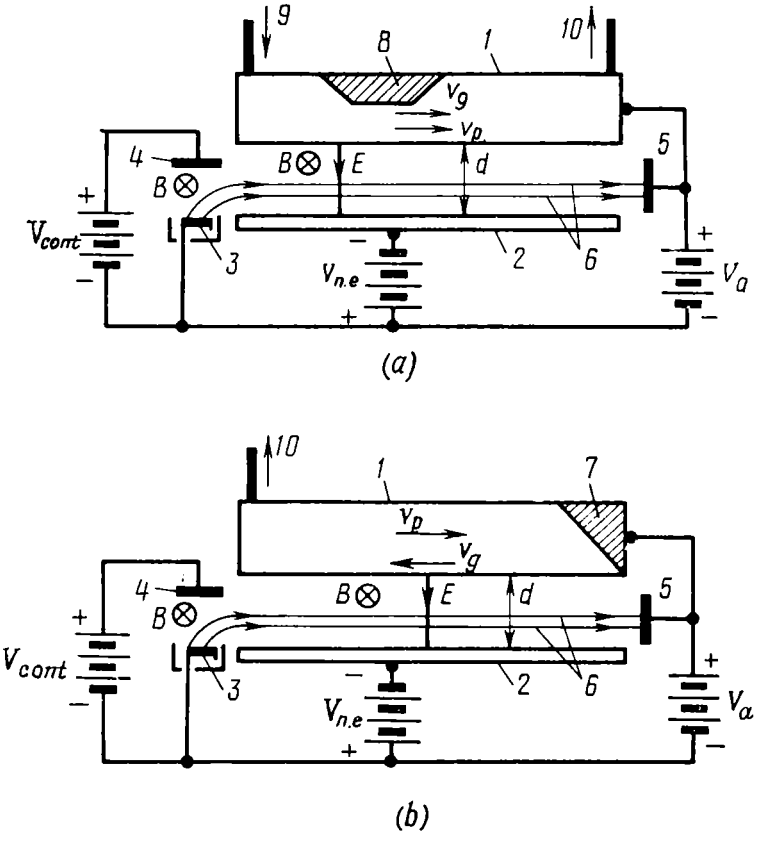

Fig. 7.40. Basic circuits of M-type TWT and BWO with injected electron beams
1—slow-wave structure; *2*—negative electrode; *3*—cathode; *4*—control electrode; *5*—collector; *6*—electron beam; *7*—matched load; *8*—dissipative pad; *9*—input; *10*—output

the region of the electron gun. To this end the intensity of the static electric field E_0 in the electron gun has to be exactly twice less than the electric field intensity E in the interaction space, provided the magnetic field B remains constant. The distance between the point, from which the electron was emitted by the cathode, and the entrance to the interaction space should be πR.

With a cathode of finite length (along the x axis), the electron trajectories are trochoidal; this effect can be eliminated by making the cathode in the form of a narrow strip, as illustrated in Fig. 7.39.

The design of an M-type forward-wave amplifier device (magnetron amplifier) with a short-optics gun is schematically shown in Fig. 7.40*a*. Backward-wave M-type tubes can be of similar design,

as illustrated in Fig. 7.40*b* depicting a BWO of the M-type. As in an O-type tube, a matched load is provided at the collector end of the slow-wave structure.

7.10b. Efficiency of M-Type BWO and TWT

The maximum electronic efficiency of M-type amplifiers and oscillators will be examined, the respective circuits being presented in Fig. 7.40. As in the case of magnetrons, the discussion will be based on energy relations. In the absence of cycloidal motion, the energy dissipated by an individual electron on the slow-wave structure or the collector is

$$W_{diss} = mv_c^2/2$$

where as before v_c is the electron velocity corresponding to the centre of the rolling circle in the interaction space; $v_c = E/B$. This velocity can be described in terms of the equivalent d.c. accelerating voltage V_0 on the accelerating electrode of an electron gun of the ordinary type (refer, for instance, to Fig. 7.37). The obvious relation of velocity v_c to this voltage is

$$V_0 = mv_c^2/2e \tag{7.54}$$

The energy dissipated by an individual electron on the slow-wave structure can be described as $W_{diss} = eV_0$. On the other hand, the maximum potential energy of the electron relative to the slow-wave structure is $W_{pot} = eV_a$, where V_a is the d.c. voltage between the cathode and the slow-wave system. Consequently, an electron arriving at the slow-wave system due to the presence of a microwave signal should give up to the radio-frequency field an amount of energy equal to

$$\Delta W = W_{pot} - W_{diss} = e\,(V_a - V_0)$$

Hence, the efficiency of a solitary electron

$$\eta_e = \frac{\Delta W}{W_{pot}} = 1 - V_0/V_a \tag{7.55}$$

The greater the distance between the surface of the slow-wave structure and the level of electron beam injection at a fixed spacing d (refer to Figs. 7.37 and 7.40), the greater is the potential energy of electrons and therefore, in principle, the higher is the electronic efficiency.

The voltage V_0 in (7.55) is closely related to the c/v_p ratio of the slow-wave structure. Indeed, under phase synchronism the electron velocity should be equal to the phase velocity of either the forward or the backward wave. Substituting v_p into equation (7.54) and apply-

ing definition (7.55) result in

$$\eta_e = 1 - \frac{25.6 \cdot 10^4}{V_a} (v_p/c)^2 \tag{7.56}$$

Thus, as indicated by this relation, the greater the c/v_p ratio and the higher the voltage V_a, the higher the electronic efficiency of devices of the magnetron type. As with travelling-wave magnetrons, there are no principal limitations to the value of electronic efficiency. It should be remembered, however, that an increase in the voltage V_a has to be accompanied by a correspondingly higher static magnetic field intensity B, so as to ensure an unaltered velocity of the rolling circle.

If the electron movement is along trochoidal trajectories instead of rectilinear paths, the electronic efficiency is reduced. This is due to the fact that the maximum energy dissipated by electrons when striking the surface of the slow-wave structure is the higher, the greater is the distance r from the centre of the rolling circle. As an example, consider the case when electrons are emitted by the negative electrode instead of the cathode: at zero initial electron velocities their trajectories are cycloidal, as in an ordinary magnetron oscillator. Electron velocities at the peaks of the cycloidal paths are twice higher than the velocity of the centre of the rolling circle and therefore the energy dissipated is four times greater than when the electrons travel along rectilinear paths. In this case the electronic efficiency of an amplifier or oscillator of the magnetron type is

$$\eta_e = 1 - 4V_0/V_a \tag{7.57}$$

With trochoidal trajectories, which are an intermediate case between rectilinear and cycloidal paths, the electronic efficiency of a BWO or a TWT of the M-type can be described as

$$\eta_e = 1 - kV_0/V_a \tag{7.58}$$

where k is a numerical factor which can vary in the range from 4 to unity. Note, that V_0 denotes an imaginary (equivalent) voltage corresponding to the average velocity of electrons equal to v_c. The physical meaning of relations (7.55) and (7.58) is similar to that of (7.41) for the electronic efficiency of a magnetron oscillator.

In case of rectilinear electron trajectories the electronic efficiency of a TWT or a BWO of the M-type theoretically can be even higher than that of a similar magnetron oscillator. However, the requirements that have to be met by the cathode of the electron-optical system, employed in M-type devices with an injected electron beam, are somewhat specific and even more stringent than those imposed upon a cathode of an ordinary magnetron. This is the reason why the extremely high efficiencies inherent in devices of this kind are ordinarily impracticable. Experimental data prove the overall efficiency

of high-power devices of the M-type with injected electron beams to be about 40 to 50 per cent; thus, in efficiency values these devices are similar to modern magnetron oscillators.

7.10c. Peculiarities of Electronic Tuning of Backward-Wave Tubes of the M-Type

The principles of electronic tuning, discussed in Section 6.6 for the case of O-type BWO's, are equally applicable to backward-wave oscillators of the M-type. Only one of the peculiarities, which determines the dependence of the oscillation frequency on the value of the supply voltage, will now be examined.

In the interaction space of a BWO of the magnetron type the electron velocity is E/B. Since the intensity of the static electric field E is in direct proportion to the d.c. voltage V_a (refer to Fig. 7.40*b*), the electron velocities also turn out to be directly proportional to the anode voltage. (Note, that in tubes of the O-type the electron velocity is proportional to the square root of the d.c. accelerating voltage.)

Suppose for simplicity the dispersion characteristic of the slow-wave structure to be linear, i.e. the phase velocity of the fundamental backward wave to be a linear function of frequency. In this case the electronic tuning of tubes of the M-type, as determined by the condition of synchronism of the electron beam with the fundamental backward wave, should also feature a linear pattern

$$f = k_1 V_a$$

Here k_1 is a proportionality factor, whose magnitude depends on the geometry of the slow-wave structure and the intensity of the static magnetic field.

Under the same conditions the electronic tuning of devices of the O-type is described as

$$f = k_2 V_0^{1/2}$$

Thus, crossed-field backward-wave oscillators exhibit not only a higher electronic efficiency than tubes of the O-type, but a wider range of electronic tuning at one and the same variation of the supply voltage. It should be mentioned, however, that BWO's of the M-type have also one disadvantage in common with BWO's of the O-type and voltage-tunable magnetrons, namely, to vary the frequency it is imperative to control the voltage of an electrode which carries a significant current. This drawback is especially pronounced if these devices are compared with reflex klystrons, for instance, in which the repeller circuit consumes no power.

Figure 7.41 shows schematically the BWO of the M-type with a slow-wave interdigital structure rolled for convenience in an open ring. In such a form the M-type BWO bears a still greater resemblance to a magnetron oscillator. However, as seen from Fig. 7.41, the

electron stream and the slow-wave structure of the BWO are *non-reentrant*. The collector end of the slow-wave structure terminates in a matched load whose function is usually performed by an absorbing composition applied to the digits of the slow-wave structure.

The typical parameters of a BWO of the M-type designed for use in radio countermeasures equipment, are listed in Table 7.3 (No. 1). This particular tube has an output power of several hundred watts and is capable of covering a frequency range in excess of 20 per cent of the middle frequency without any mechanical tuning. Backward-wave tubes with c.w. power levels of the order of several kilowatts are also available. Pulsed BWO's of the M-type provide output powers ranging from hundreds of kilowatts to several megawatts.

M-type BWO tubes operating under *synchronized oscillation* conditions constitute a group of devices of some interest. In these devices the collector end of the slow-wave structure is equipped with a signal input, while the power output as before is at the injector gun end of the slow-wave system. A small microwave signal with a frequency near to the natural frequency of oscillations is applied to the tube input and provides frequency locking (synchronization) of the BWO oscillations in an instantaneous frequency band of about 0.5 to 1 per cent.

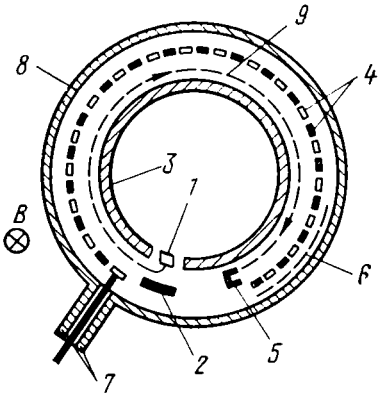

Fig. 7.41. M-type BWO with a cylindrical slow-wave system of the interdigital kind
1—cathode; *2*—control electrode; *3*—negative electrode; *4*—digits of slow-wave system; *5*—collector; *6*—dissipative pad; *7*—coaxial power output; *8*—metal envelope of the tube; *9*—electron beam

Under such conditions the synchronized BWO may be considered as a narrow-band amplifier, reproducing the frequency and phase of the input signal within the locking band. The parameters of a typical synchronized oscillator of this kind are presented in Table 7.3 (No. 2). In this case the gain is defined by equation (3.32) with the power of the input locking signal being substituted for P_{in}.

7.10d. Gain of the M-Type Travelling-Wave Tube

The gain of amplifiers with injected electron beams (Figs. 7.37 and 7.40*a*) can be calculated with the aid of the linear theory, similar to that used for the analysis of travelling-wave tubes of the O-type. The analysis of magnetron amplifiers is peculiar in that it must take account of the two-dimensional character of electron motion in the interaction space as well as of the fact that electrons give up their potential energy when they are displaced relative to the axis of the undisturbed electron beam.

With a rectilinear electron beam of infinitesimal thickness the gain of an M-type TWT under small-signal conditions may be described as

$$G = A + BDN \text{ dB} \tag{7.59}$$

provided the effects of space charge are negligible; here N is the number of slow-wave lengths accommodated along the slow-wave structure axis, just as in the case of an O-type TWT, D is the gain parameter of a meaning similar to that of parameter C in the theory of O-type devices (refer to Section 6.2) equal to

$$D = \left[\frac{I_0 K}{E}\beta_e \operatorname{co\,th}(\beta_e d_0)\right]^{1/2}$$

where E is the intensity of the static electric field as determined by equation (7.50), d_0 is the coordinate of electron beam injection relative to the negative electrode, K and β_e are the coupled impedance at the level of the undisturbed electron beam and the phase constant of the electron beam ($\beta_e = \omega/v_0$), respectively.

The launching loss parameter A and the factor B in equation (7.59) under synchronism prove to be

$$A = -6 \text{ dB}; \quad B = 54.6 \text{ dB}$$

With realizable values of the coupled impedance, d.c. current and static field intensity, the value of parameter D turns out to be of the order of 0.02 to 0.2 and the gain at $N \approx$ 10-20, by equation (7.59), can be up to 30-50 dB and even higher. Such amplifiers would appear to be very attractive, especially when such high gains are accompanied by the wideband properties and high efficiencies, inherent in devices of the M-type.

Actually, however, there is a contradiction between high efficiency and high gain in a device of the M-type, this contradiction being due to that obtaining a high efficiency necessitates increasing the amount of potential energy stored by the electrons. To this end, the spacing between the slow-wave structure and the plane of electron beam injection has to be increased (at a fixed distance between the slow-wave structure and the negative electrode). However, such an increase results in a rapidly diminishing intensity of the radio-frequency electric field, and the electron bunching can be maintained at the previous level only by increasing the power of the microwave input signal; this sets an upper limit to the value of realizable gain.

There are also other factors which limit the value of gain practicable in TWT's of the M-type with injected electron beams. Employing a dissipative sever as in a TWT of the O-type (Fig. 7.40*a*) or utilizing two-stage designs is a means for obtaining gains of about 20 to 25 dB at efficiencies of the order of 40 to 60 per cent with TWT's of the M-type. These devices as yet prove to be inferior, as regards

the gain, to travelling-wave tubes of the O-type and multicavity klystrons; nevertheless, M-type devices are of considerable promise due to such advantages as high phase stability, small dimensions, low supply voltages, etc. High efficiencies in conjunction with high gains in a wide band of frequencies can be expected to result from further development of these and similar devices.

7.11. M-Type Amplifiers with Emitting Negative Electrode. Platinotron

In the forward-wave and backward-wave tubes of the M-type discussed above, the electron beam is injected into the space between the slow-wave structure and the non-emitting negative electrode ("cold cathode"). There is another version of electronic devices of the magnetron type, which differs from those previously examined in that the cathode is located directly in the interaction space and functions simultaneously as the negative electrode, just as in common magnetrons. Typical of this group of devices is the *platinotron*, which is a version of a backward-wave tube of the M-type with an emitting negative electrode.

7.11a. Platinotron Operating Principles

The design of a platinotron amplifier is schematically shown in Fig. 7.42; when used as a broad-band amplifier the device is also known as an *amplitron*.

The main units of a platinotron are a cylindrical anode structure, similar to the equicavity block of a magnetron oscillator and a cylindrical cathode. The device output is separated from its input by a freak in the ring straps. It is common practice to fabricate amplitrons with an *odd* number of cavities to eliminate the possibility of the device becoming self-excited at the π oscillation mode, which is typical of magnetron oscillators.

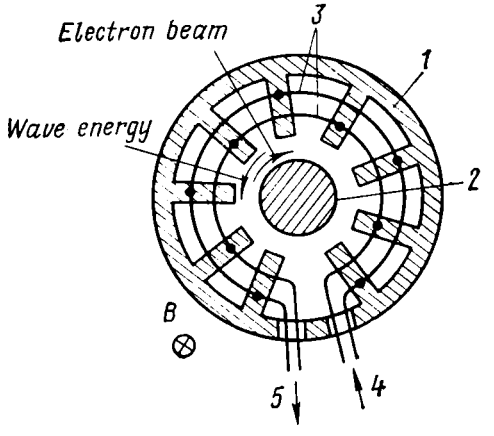

Fig. 7.42. Schematic of an amplitron

1—anode block with resonant cavities; *2*—cathode; *3*—straps; *4*—input; *5*—output

As in other devices of the magnetron type, a static magnetic field exceeding the critical value ($B > B_c$) is superimposed onto the entire assembly normal to the plane of the diagram. The direction of this static magnetic field is such that electron spoke rotation is *opposite* to the microwave energy flux, the latter propagating from the input

to the output of the amplifier. Note, that this peculiarity is common to all backward-wave tubes (Sections 6.6 and 7.10). The d.c. voltage is applied between the cathode and the multicavity anode block, as in a magnetron oscillator.

The mechanism of platinotron performance has much in common with that of a magnetron oscillator. Electrons from the cathode move in the interaction space along cycloidal trajectories, and space charge spokes, formed under synchronism conditions, interact with the tangential radio-frequency field. As a result, electrons give up their potential energy to this field. Owing to this, the platinotron retains

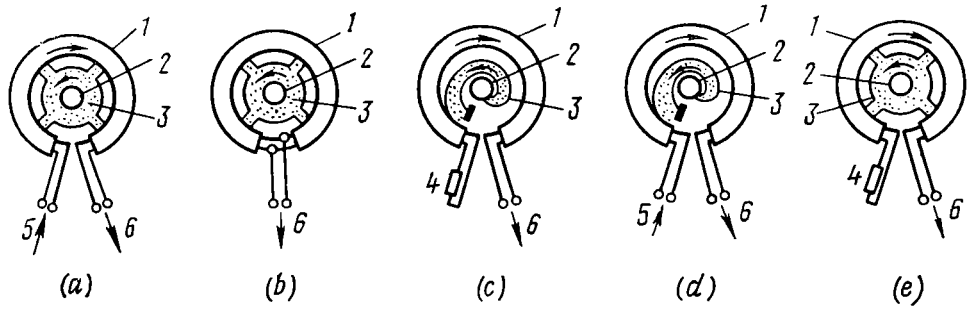

Fig. 7.43. Comparison of the circuits of an amplitron (*a*), magnetron oscillator (*b*), oscillator (*c*) and amplifier (*d*) backward-wave tubes of the M-type with injected electron beam and carmatron (*e*)

1—slow-wave system; *2*—cylindrical cathode or negative electrode; *3*—electron beam; *4*—matched load; *5*—input; *6*—output

an important advantage inherent in magnetron devices, a high efficiency along with the simplicity of design, small dimensions and comparatively low d.c. anode resistance, as in magnetron oscillators.

In principle, the platinotron can be considered as an amplifier of the backward-wave M-type rolled into a ring with an emitting negative electrode, in which the slow-wave structure is an open loop, while the electron beam is reentrant (Fig. 7.43*a*). In this respect the platinotron takes an intermediate position between a BWO of the M-type, in which both the slow-wave structure and the electron beam are non-reentrant, and a magnetron oscillator with a reentrant electron beam and reentrant radio-frequency system (refer to Fig. 7.43*b*, *c* and *d*). The absence of a reentrant oscillatory system defines the comparatively broad-band characteristics of the platinotron, as an amplifier of microwave signals.

The loss introduced when the microwave signal passes the "cold" slow-wave system of a platinotron is ordinarily not in excess of about 0.5 dB. When feeding the anode voltage the platinotron amplifies the input signal, but leaves the signal travelling from the device output towards its input practically unaffected. Thus, a platinotron functions as a twoport network with unidirectional amplification of the signal.

A mismatch at the platinotron input and output may cause self-excitation of the device, just as was the case with ordinary TWT's. To eliminate this possibility, ferrite isolators are usually provided both at the platinotron input and output. Since the gain of platinotrons is commonly not in excess of some 10 to 15 dB, excluding self-excitation by means of dissipative isolators in the slow-wave structure is considered inexpedient.

Still another form of a crossed-field oscillator—the *carmatron*—is presented in Fig. 7.43*e*; here various forms of M-type devices are compared. In the carmatron a non-reentrant slow-wave system terminates in a matched load, while a reentrant electron beam is provided by a solid cylindrical cathode. Thus, the carmatron combines the features of an ordinary backward-wave oscillator and a platinotron.

Amplitron self-excitation effects were put to good use in a high-power oscillator of highly stable frequency known as *stabilotron*. The design and circuit connection of stabilotrons are shown in Fig. 7.44. Essentially, a stabilotron is an amplitron with a phase shifter, matched load and high-Q tunable resonant cavity at the input. Reflections from the *ab* plane (Fig. 7.44) are present only at frequencies in the vicinity of the stabilizing cavity resonance, while in the rest of the operating frequency band this plane can be considered as reflectionless.

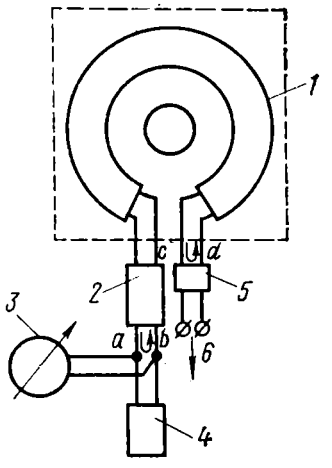

Fig. 7.44. Basic diagram of a stabilotron

1—amplitron; *2*—phase shifter; *3*—stabilizing resonant cavity; *4*—matched load; *5*—mismatcher; *6*—power output

At the stabilotron output (at plane *cd* in Fig. 7.44) a mismatching element is provided. The signal reflected from this discontinuity passes back to the device input without being either attenuated or amplified; re-reflection of this signal from the *ab* plane provides the required positive feedback at the operating frequency. The phase of this positive feedback is adjusted with the aid of the phase shifter.

Several advantages are obtained owing to that the stabilizing cavity is removed from the vacuum envelope of the tube. First of all, this results in a lower temperature coefficient at the operating frequency. Furthermore, because of the high loaded Q-factor of this cavity, it becomes possible to reduce frequency pushing effects significantly. At the same time, a considerable reduction of frequency pulling is obtained (as compared to a similar magnetron oscillator). Moreover, the stabilizing cavity is at the low-power end of the tube, so that it does not affect the overall efficiency and the output power of the device. Finally, the range of mechanical tuning of the stabilizing cavi-

ty and phase shifter can be quite wide, up to some 5 to 10 per cent of the middle frequency.

Other forms of devices of the platinotron type are also available. As an example the *ultron*, an amplifier of the M-type with a reentrant electron beam and non-reentrant slow-wave structure (as in the amplitron) can be mentioned. In contrast to the amplitron, the ultron utilizes interaction of the electron beam with the forward wave, so that this device may be considered as a version of the M-type TWT with an emitting negative electrode.

7.11b. Properties of the Platinotron Oscillatory System

A section of the slow-wave structure of a platinotron is shown in Fig. 7.45*a*. Adjacent vanes are alternately connected to a strapping arrangement, which can be considered as a two-wire transmission line

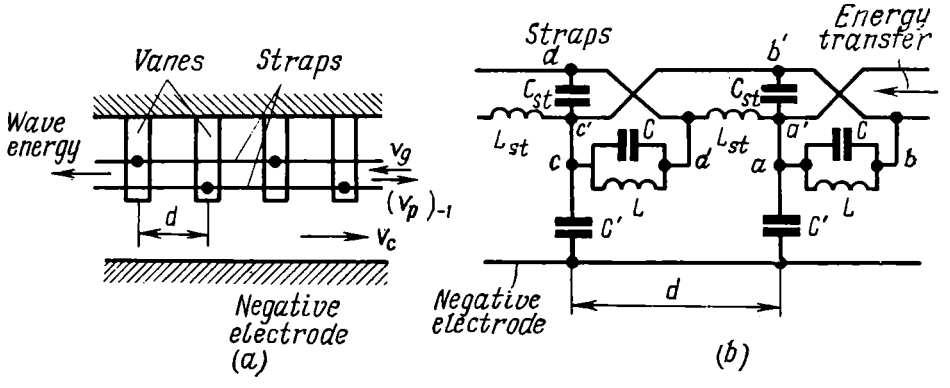

Fig. 7.45. Platinotron slow-wave structure with straps and the equivalent circuit

carrying the TEM propagation mode. The simplified equivalent circuit is presented in Fig. 7.45*b* where L and C are the equivalent inductance and capacitance of an individual cell (cavity), L_{st} and C_{st} are the inductance and capacitance of the straps per cavity and C' is the capacitance of a single segment relative to the cathode.

The microwave energy can be assumed to flow along the system from right to left, as indicated in Fig. 7.45. The phase shift of the TEM wave *along the straps* per cavity (between planes $a'b'$ and $c'd'$) will be designated as θ. Variation of the strap connections with individual cavities, shown as crossovers in Fig. 7.45*b*, results in an additional phase shift along the *interaction space* between planes ab and cd by 180°.

An observer moving in the interaction space parallel to the surfaces of the vanes with a speed v from right to left would encounter

a microwave field of constant phase if

$$\frac{\omega d}{v}=\theta+\pi+2\pi n; \quad n=0; \pm 1; \ldots \tag{7.60}$$

where d is the spacing between the middles of adjacent gaps, measured along the surface of the system. The additional third term in (7.60), i.e. an integer of 2π, does not affect the condition of the constant phase of the wave. Hence, the synchronous speed of the observer, which can be considered as the phase velocity of a spatial harmonic of the microwave field in the given slow-wave system, can be described as

$$v=(v_p)_n=\frac{\omega d}{\pi+\theta+2\pi n}$$

The argumentation presented, which is similar to the analysis of waves in a slow-wave structure of the interdigital type (refer to Section 6.6), may be used to determine the phase velocities of various spatial harmonics (at $\theta < \pi$) as

$$n = 0; \ (v_p)_0 = \omega d/(\pi + \theta) \tag{7.61}$$

$$n = +1; \ (v_p)_{+1} = \omega d/(3\pi + \theta) \tag{7.62}$$

$$n = -1; \ (v_p)_{-1} = -\omega d/(\pi - \theta) \tag{7.63}$$

. . . . . .

The first backward spatial harmonic ($n = -1$) has the highest (in absolute value) phase velocity; this harmonic, therefore, is the fundamental wave of the structure in question. Since in any slow-wave system the field of the fundamental wave has the maximum amplitude and the minimum rate of decay in the transverse direction, it is just this wave that is utilized in platinotron amplifiers and made to interact with the electron beam.

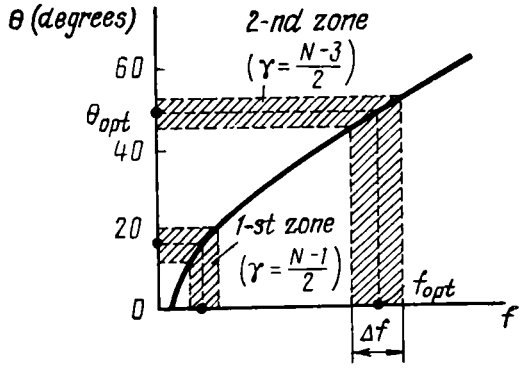

Fig. 7.46. Dispersion characteristic of platinotron slow-wave structure. Amplification zones are shown as shaded areas (refer to Section 7.11*c* for details)

The dispersion characteristic of the slow-wave system at $n = -1$ can be presented as the dependence $\varphi = \pi - \theta = f_1(\lambda)$ or as $\theta = f_2(\lambda)$. This characteristic can be obtained from examining the equivalent circuit of Fig. 7.45*b*. A typical pattern of the relation θ *versus* frequency is illustrated in Fig. 7.46; a zero value of the phase angle θ ($\varphi = \pi$) corresponds to the π oscillation mode in an ordinary magnetron

oscillator. The graph of Fig. 7.46 is thus similar to the graphs of oscillation modes in magnetrons treated earlier.

Figure 7.46 indicates that the slow-wave system of a platinotron displays anomalous dispersion. Indeed, with an increase in operating frequency the angle φ along the interaction space, equal to $(\pi - \theta)$, diminishes, while the phase velocity (which is related to the phase shift by $|\varphi| = \omega d / |v_p|$) increases. The negative sign in the right-hand member of equation (7.63) indicates that the dispersion is negative (backward). To ensure synchronism, the observer (electron beam) has to travel in a direction *opposite* to that of energy transfer in the system, i.e. from left to right in Fig. 7.45.

Note, that this circumstance is of absolutely no significance in magnetron oscillators, despite the fact that the oscillatory system provided with straps and carrying the same fundamental wave under π-mode conditions is a common feature of these devices [1]. The fact is that the oscillatory system of a magnetron is reentrant in the azimuthal direction and therefore supports discrete oscillation modes. The ring resonant system of a magnetron therefore supports two waves of identical phase velocity travelling in opposite directions. The condition of electron stream synchronism with the wave and, hence, the condition of magnetron self-excitation, are satisfied with any direction of electron beam rotation, in other words, with any direction of the static magnetic field.

In a platinotron, on the contrary, there is only one direction of electron beam rotation (opposite to the direction of energy transfer) at which the synchronism essential for signal amplification is possible, provided the input and output ports of the device are matched. This defines the unidirectional amplification of a platinotron and other devices of the travelling-wave type, which utilize the principle of synchronism. Reversion of the direction of the static magnetic field results in that the device practically no longer functions as an amplifier.

Another circumstance also merits consideration here. Magnetron oscillators feature only discrete values of the phase angle between adjacent cavities. On the contrary, in a platinotron the angle φ in principle can attain any value within the limits set by the dispersion characteristic $\varphi = f(\lambda)$ since the resonant system is non-reentrant and the input and output ports are matched. However, as will be shown later, the reentrant nature of the electron beam imposes additional limitations, this resulting in the appearance of preferential values of the phase angle φ.

---

[1] The fundamental wave of a slow-wave system provided with straps is a backward wave and designated as $n = -1$ in the present discussion; when treating magnetrons in Section 7.3 this wave was formally ascribed the zero subscript, with all the other harmonics given numbers correspondingly shifted by unity.

7.11c. Peculiarities of Electron Beam Interaction with the Microwave Field in a Platinotron. Amplification Zones

Synchronism of the electron beam with the fundamental backward wave is ensured when the average electron velocity (that is, the speed of the centre of the rolling circle v_c, examined in Section 7.2) is equal to the velocity $(v_p)_{-1}$, as defined by equation (7.63). Since v_c is constant at fixed values of V_a and B, while the phase velocity by (7.63) is a function of frequency and of the dispersion characteristic $\varphi = f(\lambda)$, variations of the input signal frequency around the middle frequency of the operating passband should lead to violation of the conditions of synchronism and thus result in lower gain. An increase in frequency should thus be accompanied by a higher phase velocity $|v_p|_{-1}$ and restoration of synchronism necessitates that the anode voltage V_a be somewhat increased. Practice confirms the operating bandwidth of platinotrons to be commonly not in excess of some 3 to 5 per cent of the middle frequency, if the anode voltage is not adjusted.

There is also another circumstance limiting the frequency band of an amplitron, associated with the reentrant character of the electron beam. Returning once again to Fig. 7.42, we find an *idler* cavity between the device input and output of the same geometrical dimensions as all the other (operating) cavities. The electron spokes rotating in a direction opposite to that of energy transfer pass unhindered from the device input to its output.

Spoke formation in a platinotron follows the same basic laws as in magnetron oscillators. As demonstrated in Section 7.4, to a first approximation, the middle of the space charge spoke may be considered to coincide with the maximum of the retarding tangential field. To obtain maximum transfer of energy to the microwave field it is therefore necessary to ensure that electron bunches arrive at the platinotron output at the same phase of the retarding microwave field after having accomplished a complete revolution. The time of a complete revolution of the electron spoke around the cathode should thus be an integer of radio-frequency oscillation periods with a small allowable lag or lead of $\pm \Delta t$:

$$\tau_{tot} = \gamma T \pm \Delta t; \ \gamma = 1; \ 2; \ 3; \ \ldots \tag{7.64}$$

On the other hand, the time of a complete revolution is a function of the rate of space charge spoke rotation; under synchronism this rate of rotation should be equal to the phase velocity $(v_p)_{-1}$. Taking into account the fact that the spacing d between the middles of adjacent cavities along the anode surface is $2\pi r_a/N$, by equation (7.63), we obtain

$$\tau_{tot} = \frac{2\pi r_a}{|v_p|_{-1}} = \frac{N}{\omega}(\pi - \theta) \tag{7.65}$$

where N is the total number of cavities (cells), including the idler cavity, and r_a is the radius of the anode structure.

Substitution of (7.64) into (7.65) results in

$$\theta = \pi(1-2\gamma/N) \pm \omega\Delta t/N \qquad (7.66)$$

Equation (7.66) is indicative of the existence of discrete values of $\theta = \theta_{opt}$ at $\Delta t = 0$ at which the most effective interaction of the electron beam with the microwave field takes place and at which the gain is at a maximum. The optimum values of the phase shift per cavity along the interaction space are

$$\varphi_{opt} = \pi - \theta_{opt} = 2\pi\gamma/N \qquad (7.67)$$

Condition (7.67) is similar to (7.27), which describes the discrete values of the phase shift φ in magnetron oscillators. In the present instance, however, the limitations imposed on the value of φ are of a different nature and are the result of a reentrant electron beam. This condition is less stringent than that imposed by a reentrant oscillatory system and thus certain deviations are possible, these admissible deviations being described by the term Δt in equation (7.66). To ensure that the space charge spokes be within the retarding phase of the field in the output cavity, the magnitude of Δt should not exceed $T/4$ and in any case be less than $T/2$ in order that the spoke not arrive at a maximum accelerating tangential field.

The result is the appearance of *amplification zones* around optimum frequencies f_{opt} which correspond to optimum values of φ; these amplification zones are shown in Fig. 7.46 as shaded areas. In case of a 9-cavity platinotron ($N = 9$) there are four zones of amplification ($\gamma = 1; 2; 3; 4$), at $N = 15$ seven zones are present, and so on. The zone corresponding to the maximum value of γ, which in case of an odd number of cavities is equal to $(N - 1)/2$, is conventionally known as the first amplification zone. Operation at the first amplification zone corresponds to the lowest anode voltage because under these conditions the rate of spoke rotation should be the lowest. At the second zone, however, where $\gamma = (N - 3)/2$, the bandwidth Δf is the widest due to the dispersion characteristic being of a more sloping pattern (refer to Fig. 7.46), and for this reason most amplitrons are operated at the second amplification zone. The factor γ characterizing the amplification zone has a simple physical meaning: as was demonstrated earlier, this factor indicates the number of periods of microwave oscillations per one complete revolution of the space charge spoke. This factor also determines the number of space charge spokes in the interaction space of a platinotron, because the spokes are formed around each retarding halfwave of the radio-frequency field. The similarity of this factor γ to the number of oscillation mode in a magnetron oscillator can be noted, this latter also determining the number of rotating spokes of space charge.

7.11d. Platinotron Amplifier Characteristics and Parameters

One of the peculiarities of platinotron amplifiers is the pattern of the amplitude characteristic, i.e. the output power of the amplifier as a function of the input signal power. Practice shows that this characteristic features pronounced saturation as illustrated in Fig. 7.47*a*. At invariable supply power P_0 there is a minimum value of the input power P_{thresh}, below which the platinotron no longer reproduces the frequency and spectrum of the input signal. These

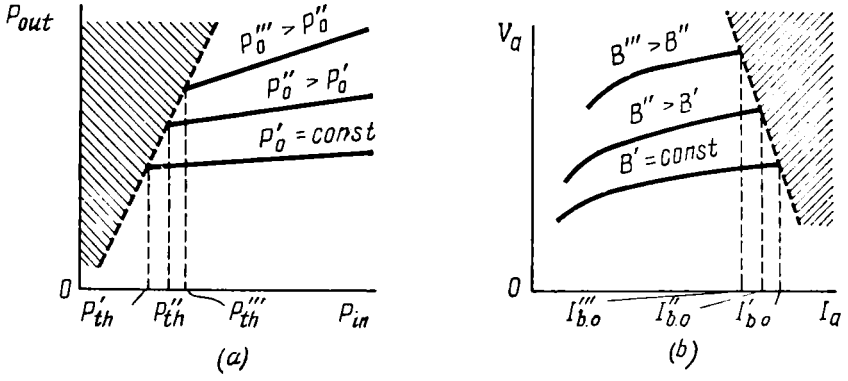

Fig. 7.47. Amplitude and voltampere characteristics of a platinotron amplifier; regions of zero gain are shown as shaded areas

conditions, shown as a shaded area in the figure, correspond to the platinotron generating a considerable amount of noise and becoming self-excited, with the output signal frequency no longer determined by the input signal.

This is one of the features of platinotron amplifiers in which they differ from other types of microwave amplifiers, which are capable of reproducing the amplitude of the input signal as well as its frequency (refer, for example, to Fig. 6.8). The amplification properties of platinotron amplifiers can be qualitatively compared with those of a synchronized magnetron, locked by an external signal.

Platinotron self-excitation in the absence of an input signal is of so great importance that in some cases special measures have to be taken to prevent this parasitic effect. When a chain of several platinotrons is used to provide the desired amount of signal gain, the pulses of anode voltage applied to each stage are usually made slightly shorter than the input microwave pulse.

Another important conclusion, which can be also drawn from Fig. 7.47*a*, is that the gain of a platinotron falls off rapidly with an increase in the power of the input signal. Under nominal operating conditions the gain of a platinotron is usually not in excess of some 10 to 15 dB and rapidly falls off to several decibels with a further

increase in input signal power. As a result, the output and input signal powers become commensurate. Since a platinotron introduces a small amount of loss, the overall efficiency has to be determined as

$$\eta_{tot} = (P_{out} - P_{in})/P_0 \qquad (7.68)$$

rather than by the ratio of output power to supply power. Here P_{out} is the power of the output signal, P_{in} is the input signal power and P_0 is the power drawn from a d.c. source.

Table 7.3

Parameters of Typical Backward-Wave Oscillators and M-Type Amplifiers

Nos	Tube type	Operating frequency range, GHz	Anode voltage, kV	Anode current, A	Output power	Efficiency, per cent	Gain, dB	Magnetic induction, tesla	Operating bandwidth per cent
1	C.w. M-type BWO of 10-cm band	2.5-3.1	2.0-5.1	0.4	250-330 W	25	—	0.12	—
2	C.w. amplifier M-type BWO of 5-cm band (synchronized oscillator)	5.925-6.425	0.9-1.5	—	500 W	35	17		1
3	Pulsed amplifier M-type TWT for decimetric range	—	64-90	—	3-8 MW	50-68	11-15	—	17
4	Pulsed 10-cm amplitron (Fig. 7.49)	2.9-3.1	50-54	66	3 MW	70-80	12 (at P_{out}= 50 kW)		7

A limited amount of gain is one of the gravest drawbacks of platinotron amplifiers, as compared to other kinds of microwave devices and, first of all, to multicavity klystrons and travelling-wave tubes of the O-type. However, an exceedingly high efficiency (up to 60 to 80 per cent) in conjunction with a comparatively wide bandwidth make the use of platinotrons a most attractive possibility.

The voltampere characteristic of a platinotron $V_a = f(I_a)$ at $B =$ =const is similar to that of a magnetron oscillator (refer to Section 7.7*a*). A peculiarity of platinotron voltampere characteristics is the existence of a break-off in amplification at heavy anode currents, as illustrated in Fig. 7.47*b*. The magnitude of this break-off current $I_{b.o}$ is to a considerable degree a function of the emissive properties of the cathode, first of all, of its secondary emission.

By analogy with electronic frequency pushing of magnetron oscillators, the performance of platinotron amplifiers can be characterized by *electronic phase pushing*, that is the change in phase of output

microwave signal per 1 A of anode current variation; often the phase stability of platinotron amplifiers is also evaluated by the amount of phase shift produced by a 1 per cent variation of the anode voltage or current, typical values being 0.1 to 0.3 degree per 1 per cent of anode current variation and 0.5 to 0.8 degree per 1 per cent of anode voltage variation.

7.11e. Typical Platinotron Designs

The design of the radio-frequency system and the external appearance of a typical high-power pulse amplitron of the 10-cm band are illustrated in Figs. 7.48 and 7.49, respectively; the main parameters of this device are listed in Table 7.3 (No. 4). This device is of the stacked design with an axial cathode assembly. As can be noted, the device is similar in design to magnetron oscillators.

A distinguishing feature of this particular amplitron is the structure of its waveguide input and output. A rectangular waveguide of a standard cross section is tapered to a ridge waveguide of the H-type; the double straps at the middle section of the anode block are connected at the input and output to the ridges of this waveguide.

The slow-wave system of this platinotron is of the ladder type and has straight cylindrical bars with rectangular vanes along the device axis, connected to the butt-end caps. These bars are made in the form of hollow copper pipes to carry a liquid coolant (water), this considerably enhancing power dissipation capability.

In the decimetric and centimetric wave bands at comparatively moderate power levels, coaxial inputs and outputs are widely used, with the inner conductor connected to one of the straps or the extreme vane of the slow-wave structure.

The input and output of a platinotron are often divided by a drift space in the form of a smooth anode surface several cavities in length to reduce the feedback *via* the electron beam, this drift space replacing the idler cavity mentioned earlier. In the interaction space between the cathode and this smooth section of anode block the spokes of space charge are partially disintegrated and consequently the limitations imposed on the operating bandwidth are somewhat relaxed; at the same time, this tends to increase decoupling between the input and output, leading to an increase in the value of obtainable gain.

In modern platinotron tubes, nevertheless, the combination of high gain with high efficiency and wide passbands has not been yet achieved. Typically, the gain does not exceed 20 dB at operating bandwidths (even with anode voltage adjustment) about 5 to 10 per cent of the middle frequency and efficiencies of the order of 50 to 60 per cent.

The pulse power levels attained with platinotron amplifiers are of the same order of magnitude as with magnetron oscillators, up to

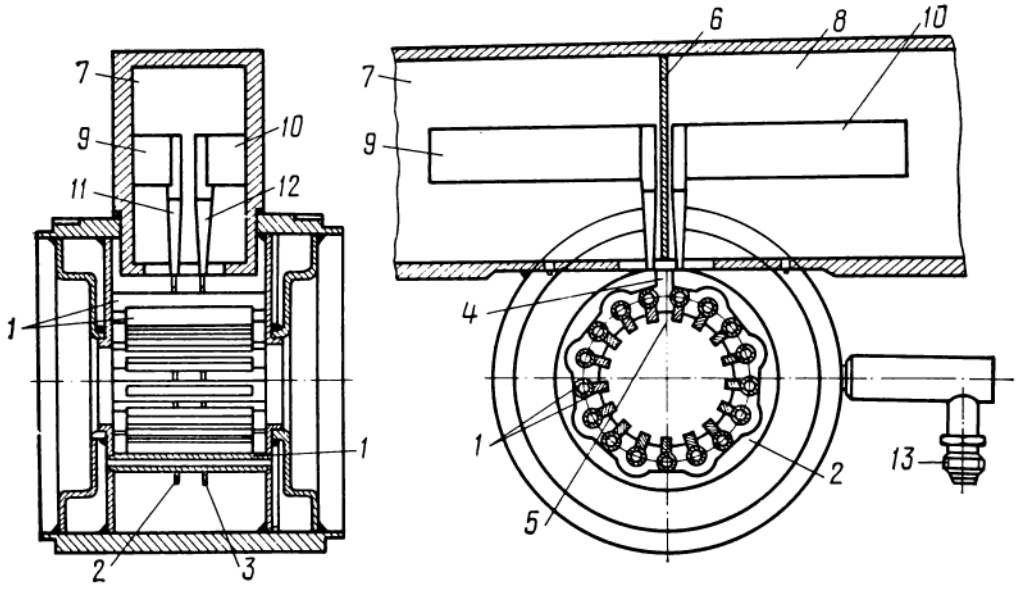

Fig. 7.48. Slow-wave structure of high-power platinotron

1—bars with vanes; *2*, *3*—straps; *4*—freak in strapping arrangement; *5*—idler cavity (cell); *6*—shorting wall; *7*, *8*—input and output rectangular waveguides; *9*, *10*—longitudinal ridges in waveguides; *11*, *12*—strap connections to waveguide ridges; *13*—pipe connection to water cooling system

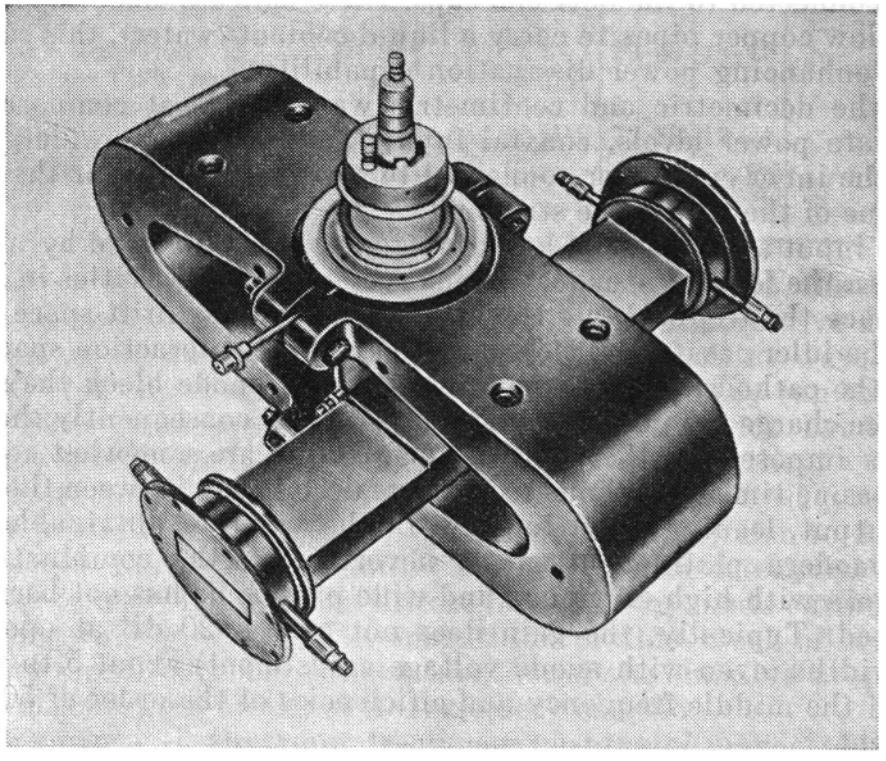

Fig. 7.49. Typical 10-cm pulse platinotron

10 MW in the centimetric wave band. At present the greatest c.w. power level is about 500 kW in the 10-cm band at an efficiency in excess of 70 per cent.

Employing cold cathodes (which provide the required anode current due to secondary emission) is very promising in platinotron designs. The great advantage of such devices is the possibility of excluding a modulator to provide the anode voltage pulses. The anode voltage is constantly applied in this case, and the device is "turned on" by the pulse microwave signals applied to the input, as a result of an avalanche-like increase in cathode bombardment by electrons. To stop the secondary emission current it is usually necessary to apply a control pulse to a special electrode mounted in the drift space between the input and output of the amplifier.

The main field of platinotron application is as the output stages (and as drivers of such output stages) in pulse transmitters of the centimetric and decimetric wave bands. Systems consisting of a master oscillator (usually, crystal-controlled), intermediate amplifier and output amplification stage are considered preferable to a power oscillator in that they make it possible to meet ever increasing requirements to frequency and phase stability of the output signal. Besides, platinotrons are also suitable for other applications, where their extremely high efficiency is of major importance; in particular, platinotrons may prove to be the most suitable for microwave energy transmission purposes, this branch of engineering opening up new interesting possibilities that are far outside the scope of pure radio engineering problems.

The availability of platinotron amplifiers has resulted in a certain narrowing down of the field of magnetron oscillator application. It should not be taken for granted, however, that in future magnetron oscillators can be expected to be completely replaced by platinotrons or other kinds of crossed-field amplifiers. As in other branches of microwave electronics, oscillator and amplifier devices of various kinds can be expected to co-exist during a long time, each satisfying some specific engineering requirement to the best of its ability.

7.11f. Other M-Type Devices with Emitting Negative Electrode

The operating bandwidth of M-type amplifiers can be widened by employing slow-wave structures operating on the fundamental mode, which displays normal positive dispersion. One of the versions of such amplifiers is the *dematron*, which differs from the M-type TWT of Fig. 7.37 in the absence of an electron gun of the injector type. A considerable portion of the negative electrode of dematrons is occupied by an emitting surface[1]. The instantaneous operating band-

[1] The first two letters in the term "dematron" stand for "distributed emission".

width of devices of this kind is up to 15 per cent of the middle frequency at gains of about 15 to 17 dB.

A further development of the same idea can be noticed in the design of the *bidematron* shown in Fig. 7.50. This device is actually a combination of an amplifier with an injected electron beam (bimatron) with the dematron mentioned above. The electron beam injected out of the first stage into the second functions as a peculiar "electronic synchronizer" providing beam control in the second stage by a small input signal applied to the first stage. An increase in efficiency and output power is provided by using an additional ("booster") electron beam in the second (dematron) stage. Bidematron gains up to 35 dB in the 10-cm band at efficiencies up to 70 per cent appear to be possible. The complicate design, as compared to that of other microwave devices, has hindered up to the present time the wide application of bidematrons.

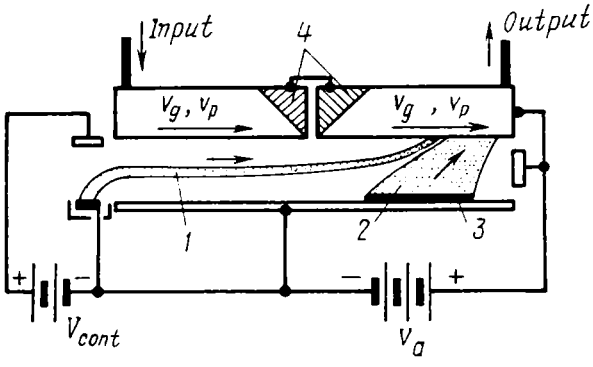

Fig. 7.50. Two-stage M-type amplifier with a forward wave and two electron beams
1—injected electron beam; *2*—"booster" electron beam; *3*—emitting section of negative electrode; *4*—matched load

We shall mention in conclusion still another amplifier of the M-type with an emitting negative electrode, the waveguide magnetron amplifier (or the electromagnetic amplifying lens, as it is also called) shown in Fig. 7.51. This amplifier features a reentrant ring-type multicavity anode structure similar to that of an ordinary magnetron oscillator; the axial length of this anode block can be up to 3-4 free space wavelengths and the block is provided with an even number of resonant cavities. A long cylindrical cathode is mounted along the axis of this system.

The signal input and output (not shown in this figure) should be matched to the anode block, which can be considered as a coaxial waveguide with the cathode as the central conductor. The wave propagating along this waveguide is of the fast (unslowed) kind and features the field distribution across the transverse cross section peculiar to the π oscillation mode.

Interaction of the electron beam with the field of this travelling wave takes place in just the same way as in a common magnetron, when synchronism in the azimuthal direction is ensured. The pattern of space charge spokes produced, with the variation of the phase of the microwave field along the axis of the system taken into account, is illustrated in Fig. 7.51.

The amplifier in question is thus to be listed among devices with *transverse interaction* of the electron beam and microwave field (relative to the direction of energy transfer). In contrast to TWT's, BWO's and other devices utilizing the principles of longitudinal

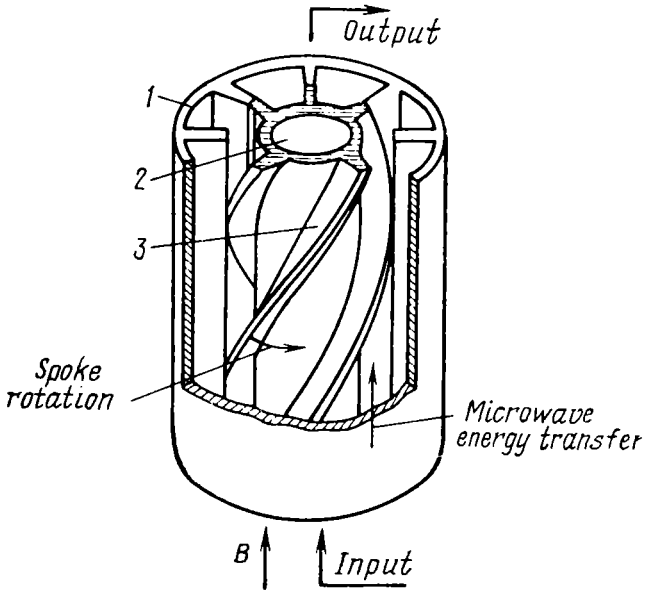

Fig. 7.51. Schematic of a waveguide magnetron amplifier
1—anode block; *2*—cathode; *3*—configuration of rotating space-charge spoke

synchronism, this device does not exhibit unidirectional amplification properties. An analogy can be drawn between the waveguide magnetron amplifier and a transmission line with a distributed negative resistance.

Owing to a considerable axial length of the cathode and anode, there is no principal limit to the amount of output power obtainable. However, the gain is not in excess of about 20 dB due to the absence of any preferable direction of amplification; such a low gain is the result of unavoidable instability and tendency to self-excitation of this device, caused by practically inevitable mismatches present at the input and output.

A further increase in the output power level may be obtained by employing the inverted design version of a waveguide magnetron amplifier.

7.12. Oscillators and Amplifiers Utilizing Cyclotron-Frequency Resonance

Electrons in a static magnetic field are capable of oscillating with an angular frequency equal to the cyclotron frequency ω_c. This frequency, treated earlier in Section 7.2*b*, by equation (7.11),

depends only on the intensity of the static magnetic field B and determines, in particular, the duration of a single cycloidal loop performed by electrons in a magnetron oscillator. The manner in which these cyclotron-frequency oscillations can be put to good use in microwave oscillators and amplifiers is now to be examined.

7.12a. Cyclotron-Frequency Oscillations in Magnetron Oscillators

In common multicavity magnetrons operating with the travelling-wave mode of oscillations, the frequency is mainly a function of the natural frequency of the resonant system and is only slightly related to the value of ω_c. The ratio of oscillation frequency to cyclotron frequency can be made to vary within very wide limits of from 0.5 to 5 and even more by changing the values of the static magnetic field B and anode voltage V_a. There are, however, specific operating conditions of a magnetron oscillator, characterized by the oscillation frequency approximately *equal* to the cyclotron frequency.

For simplicity, the case of a diode with a *solid* (uncut) anode, placed into a static magnetic field, will be examined. At $B \approx B_c$, i.e. when the operating conditions approach the cutoff region (refer to the curve $I_a = f(B)$ in Fig. 7.4*a*), the peaks of the cycloidal electron trajectories pass very close to the surface of the anode.

The time of electron transit from the cathode to the surface of the anode and back is the same for all electrons and is determined from equation (7.20). Consequently, the currents induced by these oscillating electrons in the anode-cathode circuit of a planar magnetron have a period T equal to

$$T = \tau = 2\pi m/eB \tag{7.69}$$

and the wavelength of the oscillations in the external circuit is therefore related to the intensity of the static magnetic field by a simple equation

$$\lambda B = \frac{2\pi cm}{e} = \text{const} \tag{7.70}$$

Substitution of the values of e, m and c results in

$$\lambda B \cong 1.07 \tag{7.70a}$$

where the wavelength is in centimetres, the magnetic induction, in tesla.

Suppose an oscillatory system to be connected between the anode and cathode of the magnetron under treatment. Tuning this system to the frequency of induced oscillations should be expected to result in oscillations with a wavelength determined by equations (7.70) and (7.70a); thus, at $B = 0.1$ tesla (10^3Gs) the wavelength should be in the 10-cm band, while a wavelength of about 1 cm should be

obtained at a static magnetic field intensity of approximately 1 tesla, which is also within the range of practicable values.

It was confirmed by experiment that magnetrons with solid anodes can oscillate at microwave frequencies at static magnetic fields in the vicinity of the critical value. As a first approximation, the operating wavelengths can be determined from equation (7.70a) and are not much dependent on the parameters of the external resonant system. The magnitude of the constant λB, as determined experimentally, is about 1.2 tesla·cm.

Note, however, that the periodic movement of electrons is inadequate to account for the effect of self-sustained oscillations. There

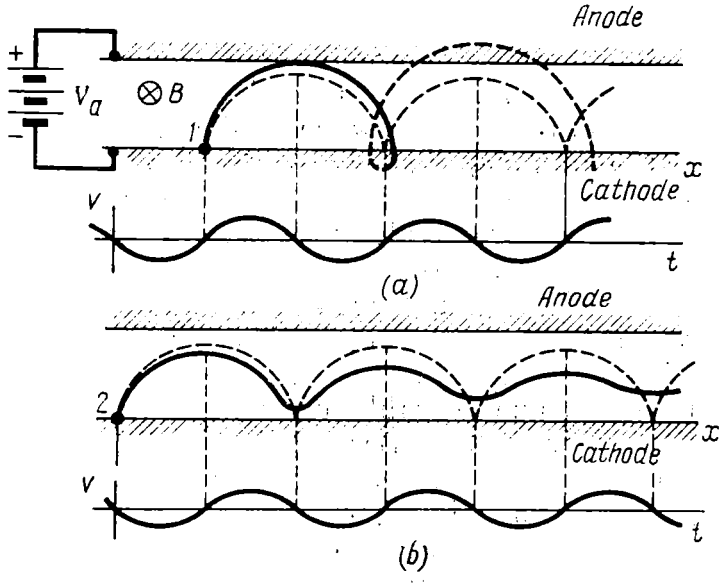

Fig. 7.52. Electron motion in a planar smooth-anode magnetron at cyclotron-frequency oscillation mode; the cycloidal trajectory of the same electron in the absence of a radio-frequency field is shown in dashed lines

has to be some kind of a mechanism of electron bunching (sorting) responsible for the preferential energy transfer from the electron beam to the radio-frequency field.

Assume radio-frequency oscillations with a period defined by equation (7.69) to be already present in the interaction space of the magnetron in question. Electron trajectories beginning at various phases of the microwave field will be examined, taking account of the fact that in a solid-anode magnetron the microwave field has but one component that is either added up with or extracted from the transverse static electric field.

Figure 7.52 illustrates the trajectories of two typical electrons that are emitted from the cathode at the instants of time the microwave field intensity goes through zero. Electrons of type *1*, which begin to

move in an accelerating field, are unfavourable from the viewpoint of self-excitation effects. The rotary energy of such electrons is increased and they begin to move along involuting trochoidal paths. As a result, electrons of type *1* are either brought into collision with the anode after a half-period of oscillations and thereafter cease taking part in beam formation, or, after being again accelerated by the radio-frequency field, strike the cathode and thus dissipate the energy acquired on this electrode (Fig. 7.52*a*). In either case, electrons of type *1* are removed from the interaction space after travelling in it for no longer than one period of microwave oscillations.

Electrons of type *2*, which begin their movement in a retarding transverse radio-frequency field, remain under the action of this field in all the subsequent sections of their trajectories, because at $\tau \approx T$ each field reversion is accompanied by a reversion of the direction of electron movement. These electrons continuously give up their rotary energy to the microwave field and cannot arrive either at the anode or the cathode, as shown in Fig. 7.52*b*. As a result, electrons of type *2* are forced to perform multiple oscillations, all the time remaining in a favourable phase relative to the microwave field.

The electron bunching (sorting) mechanism discussed results in an orderly character of electron motion, which ensures oscillation build-up starting from small initial magnitudes. These oscillations meet the condition that $\tau \approx T$, or what is the same, $\omega \approx \omega_c$. These effects can be noted to bear some resemblance to the drift effects in a retarding-field oscillator treated in Section 2.6.

Self-sustained oscillations in a magnetron at the cyclotron-frequency mode, as in any oscillator, are set up only if the conductance of the main gap (in the present case the anode-cathode space) is negative. Since electrons give up their energy to the microwave field effectively only when $\omega \approx \omega_c$, it is obvious that the electron conductance remains negative only in a very narrow band of frequencies around the cyclotron frequency ω_c. With this oscillation mode it is impossible to vary the operating frequency within any significant range by tuning the external resonant cavity. This explains why the magnetron appears to be insensitive to the parameters of the external cavity.

The cyclotron-frequency oscillation mode has not found wide application mainly because the efficiency at this mode is lower than with the travelling-wave mode. Ordinarily, cyclotron-frequency resonance in magnetron oscillators has to be taken into account as an undesirable effect, which tends to impair interaction of the electron beam with the field of the travelling wave at $\omega \approx \omega_c$ (refer to Section 7.5).

The progress made in microwave electronics has made it possible to re-examine the problem of utilizing cyclotron-frequency resonance effects in microwave oscillators and amplifiers. This problem will be given a more detailed treatment later.

7.12b. Cyclotron-Frequency Devices with Fast Waves. Cyclotron-Frequency Resonant Maser

A serious drawback of microwave devices utilizing electron beam interaction with a slow wave is the elaborate design of the slow-wave structure. The dimensions of the slow-wave structure become inconveniently small when designing devices for the millimetric and especially submillimetric wave bands. This makes their manufacture more difficult and imposes serious limitations on the amount of output power obtainable, stemming from the problem of power dissipation.

The possibility of avoiding the use of slow-wave structures and utilizing electron beam interaction with fast (unslowed) waves was

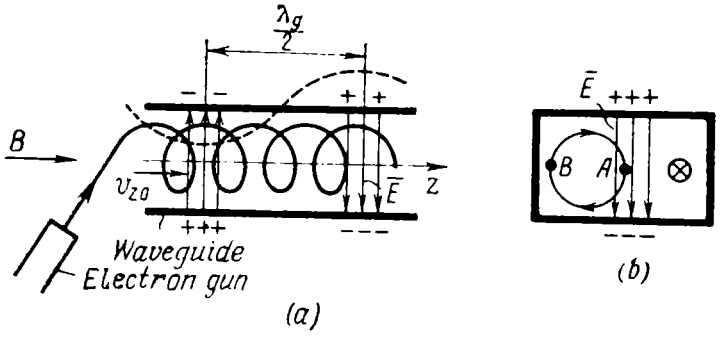

Fig. 7.53. Helical electron beam in a rectangular waveguide carrying the H_{10} propagation mode

pointed out in Section 2.4*d*. To this end, the path of the electron beam should be made *non-linear*, as shown in Fig. 2.14*a*. A periodical electron beam trajectory can be obtained, as by injecting the electron beam from an electron gun of the common kind at an oblique angle to the lines of force of a static magnetic field (Fig. 7.53*a*). It is also possible to use an electron gun of the magnetron type, directly producing an electron beam with helical electron trajectories.

Consider a helicoidal electron beam moving along the axis of a uniform waveguide of rectangular cross section, as illustrated in Fig. 7.53*a*. The duration of a single revolution of the electron beam is a function of the induction of the longitudinal magnetic field only and is equal to the period of cyclotron-frequency oscillations, as in the case of a magnetron

$$T_c = \frac{2\pi}{\omega_c} = \frac{2\pi m}{eB} \tag{7.71}$$

For simplicity, the waveguide will be supposed to support only the dominant propagation mode H_{10}. In the transverse section of the

waveguide the electron trajectories and microwave field distribution are as shown in Fig. 7.53*b*.

The condition of prolonged interaction of the electron beam with the field of the travelling wave at a constant phase of the microwave field may be deduced from the following argumentation. An electron located at a certain instant of time at point A, where the microwave field is of a retarding character, will appear at point B after half a revolution; this latter point is near to the waveguide wall and the radio-frequency field here is nearly zero. The length of the path travelled by this electron along the waveguide in the axial direction during a complete period T_c is a function of the axial component of velocity v_{z0}, and is equal to $v_{z0}T_c$. During the same time interval the wave travels a distance $l_2 = v_pT_c$, where v_p is the phase velocity of the propagation mode in question and is greater than the free space velocity of light. The condition that this electron at point A will again turn out to be in a maximum retarding field can be described as

$$l_2 = n\lambda_g \pm l_1;\ n = 1;\ 2;\ 3;\ \ldots \tag{7.72}$$

where λ_g is the guide wavelength and $l_1 = v_{z0}T_c$. The plus sign in this relation corresponds to the case of coincident directions of electron beam travel and energy transfer, the negative sign, to opposite directions, with the wave propagating in the $-z$ direction.

Taking into account that $\lambda_g = 2\pi v_p/\omega$ and applying condition (7.72) yield

$$\omega = n\omega_c/(1 \mp v_{z0}/v_p);\ n = 1;\ 2;\ 3;\ \ldots \tag{7.73}$$

This is the condition of phase synchronism of the electron beam with a travelling fast wave in a smooth rectangular waveguide. At v_{z0} much lower than v_p, prolonged interaction of the electron beam with the microwave field is obtained at frequencies approximately equal to the cyclotron frequency or its harmonics.

The conditions of synchronism at other propagation modes and other configurations of the waveguide cross section may be obtained in a similar way, taking into account the displacement of the axis of electron beam movement relative to waveguide axis.

When in the device of Fig. 7.53 the electron beam interacts with a backward-wave, the device behaves as a backward-wave tube. The optimum average velocity of electrons v_{z0} at which microwave amplification or oscillation will take place can be determined from equation (7.73). At the fundamental cyclotron frequency ($n = 1$)

$$v_{z0} = v_p\left(\frac{eB}{\omega m} - 1\right) \tag{7.74}$$

The interaction space of the device shown in Fig. 7.53 carries no static electric field normal to the static magnetic field B. However,

synchronism of a trochoidal electron beam with a travelling or standing wave in crossed static electric and magnetic fields can also be utilized; the condition of phase synchronism in this case is also described by relation (7.73). A device of this kind with a fast wave of the TEM mode first proposed by S. Tetelbaum in 1955, is termed the *phasochron*. Considerable progress in the development of this trend has been made due to the work of A. Gaponov and his collaborators. Oscillators and amplifiers of the cyclotron-frequency type, utilizing interaction of a helicoidal or trochoidal electron beam with a fast wave in a waveguide or resonant cavity are conventionally termed *cyclotron-resonance masers* (CRM).

One of the forms of a CRM-oscillator with a long cylindrical resonant cavity is shown schematically in Fig. 7.54. Here an injector

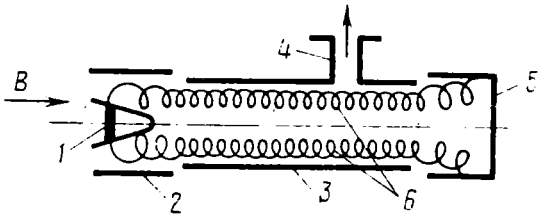

Fig. 7.54. Diagram of a cyclotron-resonance maser oscillator
1—emitting section of cathode; *2*—anode; *3*—cylindrical resonant cavity; *4*—output waveguide; *5*—collector; *6*—electron trajectories

electron gun of the M-type with a narrow emitting strip is used to provide the electron beam. The resonant cavity is excited at the H_{01p} oscillation mode, but oscillations at other modes are also possible. Analysis discloses that electron bunching in these devices is similar to the process typical of devices of the O-type.

Devices of the CRM type hold much promise for obtaining high-power levels in the millimetric wave band at high efficiencies of 25 to 30 per cent and even higher. The operating bandwidth of CRM-amplifiers is determined by the width of the cyclotron resonance line and may be up to several per cent of the middle frequency; electronic tuning can be obtained by varying the magnitude of the static magnetic field.

The shortest wavelength obtainable is limited by the magnitude of static magnetic induction realizable. Thus, at a 2 mm wavelength the magnetic induction B by (7.70a) should be greater than 5 tesla (50,000 Gs). Such high field intensities can be produced by using superconductive solenoids operating at liquid-helium temperatures. The magnitude of the required magnetic induction can be considerably reduced by operating at harmonics of the fundamental cyclotron frequency.

7.12c. Cyclotron Waves

The effects taking place in devices of the cyclotron-frequency type can be described with the aid of the concept of *cyclotron-frequency waves* in electron beams subjected to the action of a longitudinal static magnetic field. In contrast to space-charge waves treated in Section 2.9, cyclotron waves are of the transverse type and can be excited, for instance, by a pair of deflecting plates between which a transverse radio-frequency field is developed.

Consider the behaviour of an electron beam moving along the z axis in a static magnetic field directed along the same axis. At $E = 0$ the motion of electron will be governed by a modified equation of the (7.6) kind

$$m \frac{d\bar{v}}{dt} = -e [\bar{v}\bar{B}]$$

whence

$$\frac{\partial v_x}{\partial t} + \frac{\partial v_x}{\partial z} \frac{dz}{dt} = -\frac{eB}{m} v_y$$

$$\frac{\partial v_y}{\partial t} + \frac{\partial v_y}{\partial z} \frac{dz}{dt} = -\frac{eB}{m} v_x$$

$$\frac{\partial v_z}{\partial t} + \frac{\partial v_z}{\partial z} \frac{dz}{dt} = 0$$

At $\frac{dz}{dt} = v_0$ the first two of these equations reduce to

$$\frac{\partial v_x}{\partial t} + v_0 \frac{\partial v_x}{\partial z} = -\omega_c v_y \tag{7.75}$$

$$\frac{\partial v_y}{\partial t} + v_0 \frac{\partial v_y}{\partial z} = -\omega_c v_x \tag{7.76}$$

The transverse electron velocities can be described as a travelling wave with a propagation constant Γ

$$v_x = v_{x0} \exp(j\omega t - \Gamma z); \quad v_y = v_{y0} \exp(j\omega t - \Gamma z)$$

where ω is the angular frequency of induced oscillations. Substitution of these relations into (7.75) and (7.76) yields

$$\Gamma = j \frac{\omega \mp \omega_c}{v_0} \tag{7.77}$$

According to equation (7.77) this propagation constant is an imaginary quantity. Designating $\Gamma = j\beta = j\omega/v_p$, we obtain

$$v_p = v_0/(1 \pm \omega_c/\omega) \tag{7.78}$$

The relation thus obtained indicates that an electron beam in a static longitudinal magnetic field of finite induction B is capable

of supporting two transverse waves; the first of these waves corresponding to the plus sign in the denominator of (7.78) is termed the *slow* cyclotron wave, while the second is called the *fast* cyclotron wave.

By (7.78), the phase velocity of the fast cyclotron wave may exceed the velocity of electron travel along the z axis of the system. This can be used to provide synchronism between this wave and the fast waves propagating along smooth microwave transmission lines with phase velocities exceeding the speed of light in free space.

The cyclotron wave concept is used in the analysis of performance of certain types of microwave electron devices. An example of the direct application of these waves is the electron-beam parametric amplifier, which provides amplification of small microwave signals at very low levels of inherent noise. A more detailed description of these problems can be found in special publications.

CHAPTER EIGHT
MICROWAVE DISCHARGE DEVICES

8.1. Electron-Ion Plasma at Microwave Frequencies

The microwave devices discussed in the preceding Chapters, triodes, klystrons, travelling-wave tubes, magnetrons, etc., utilize the motion of electron beams under conditions of high vacuum. Under normal operating conditions the effects of residual gas ionization in these devices are so insignificant that they are treated as purely electronic.

However, there is another, though far less numerous class of microwave devices, whose performance is based on the effects of microwave current conduction by an electron-ion plasma; it is only natural to term these devices as *gas discharge*. The plasma utilized in these devices can be developed by a d.c. gas discharge or by a self-maintained microwave gas discharge.

There are a number of peculiarities specific to current conduction by an electron-ion plasma at microwave frequencies. Many of the problems encountered when treating phenomena in electron-ion plasma have not been solved as yet, and therefore the present discussion will be limited to a simplified treatment of only some of the main properties of electron-ion plasma at microwave frequencies.

8.1a. The Effect of Free Electrons and Ions

The peculiarities of electron and ion movement under the action of a low microwave field will be first examined, the electron-ion plasma being assumed to be developed *independently* of the source of microwave signal. This case is of interest not only when treating gas-filled devices; similar effects take place during radio wave propagation through the ionized layers of the atmosphere (the ionosphere), as well as through the plasma envelopes developed around missiles and spaceships when they enter the higher layers of the atmosphere.

Suppose that an electric field $E = E_m \sin \omega t$ is present in a certain volume filled by a uniform quasineutral[1] plasma. For simplicity

[1] Remember that a quasineutral plasma is characterized by an equal concentration of electrons and ions.

this field can be imagined to be set up with the aid of a parallel-plate capacitor, as shown in Fig. 8.1. At first the effects of electron collisions with neutral gas particles will be considered negligible. The equation describing the motion of a solitary electron (provided there is no external magnetic field) is of the usual form

$$m\frac{d^2x}{dt^2} = -eE_m \sin \omega t \tag{8.1}$$

Integrating this equation twice, we arrive at

$$\frac{dx}{dt} = v_0 + \frac{eE_m}{\omega_m}(\cos \omega t - \cos \omega t_0) \tag{8.2}$$

$$x = x_0 + v_0(t - t_0) + \frac{eE_m}{\omega^2 m}[\sin \omega t - \sin \omega t_0 - (\omega t - \omega t_0)\cos \omega t_0] \tag{8.3}$$

Here the initial electron velocity, corresponding to a point with a coordinate x_0 at the instant of time t_0, is designated as v_0.

Equation (8.2) can be used to determine the maximum energy taken by the electron from the radio-frequency field. The maximum velocity $v_{e.\,max}$ (absolute value) of the electron, acquired at a most favourable phase of the microwave field ωt_0, is

$$v_{e.\,max.} = 2eE_m/\omega m$$

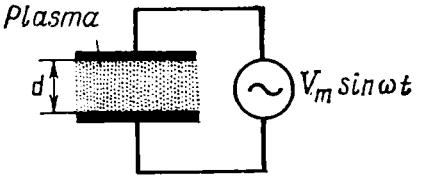

Fig. 8.1. Parallel-plate capacitor with electron-ion plasma filling

and therefore the maximum kinetic energy $W_{e.\,max.}$ delivered to this electron by the microwave field is

$$W_{e.\,max.} = 2e^2E_m^2/\omega^2 m \tag{8.4}$$

The greatest amplitude of electron oscillations $x_{e.\,max.}$ is easily determined from equation (8.3). Neglecting the rectilinear uniform motion which is superimposed onto the oscillatory process, we obtain

$$x_{e.\,max.} = 2eE_m/\omega^2 m \tag{8.5}$$

Similar equations can be used to describe the motion of ions, if the effects of ion collisions with neutral gas molecules can be considered negligible

$$W_{ion\,max.} = 2e^2E_m^2/\omega^2 M \tag{8.6}$$

$$x_{ion\,max.} = 2eE_m/\omega^2 M \tag{8.7}$$

where M is the ion mass, e is its electric charge (in the following discussion assumed to be the same as the charge of an electron).

At fixed frequency and electric field intensity, the ratio of maximum kinetic energies acquired by an electron and an ion, by equa-

tions (8.4) and (8.6), is

$$\frac{W_{e.\,\max.}}{W_{ion\,\max.}} = \frac{M}{m} \tag{8.8}$$

Therefore, the ions of even the lightest atoms (hydrogen) can acquire but an 1 : 1840 part of the energy delivered in the same field to an electron; with gases of greater atomic weights this ratio will be even higher.

Equations (8.5) and (8.7) indicate that there is a similar difference in the oscillation amplitudes of electrons and ions. It is of interest to evaluate the order of magnitude of the oscillation amplitude at actually encountered microwave field intensities. Suppose the value of E_m to be 100 V/cm and the wavelength to be 10 cm. The amplitude of electron oscillations by (8.5) will then be but $0.99 \cdot 10^{-2}$ mm; even at extremely high electric field intensities of 10^4 V/cm the maximum oscillation amplitude is only 0.99 mm and diminishes with an increase in oscillation frequency.

Thus, the oscillation amplitude of an electron under actually existing conditions is considerably less than the geometrical dimensions of discharge gaps or interelectrode spacings of microwave devices. This indicates that the *volume phenomena* are of predominant significance in gas-discharge plasma at microwave frequencies. All the surface effects, including processes taking place at the device electrodes, should be much less pronounced than in low-frequency gas-discharge devices.

The oscillation amplitude of ions is still lower by some three or four orders of magnitude due to the considerable mass of ions. If the oscillation amplitudes of electrons are assumed to be of the same order of magnitude as their mean path of free travel in gas, the ions can be considered as practically stationary; the energy, drawn by the ions from the microwave field can also be considered negligible. It follows, that microwave current conduction through electron-ion plasma is but slightly affected by the presence of ions and that the properties of electron-ion plasma at microwave frequencies are determined mainly by the presence and motion of free electrons.

8.1b. Electron-Ion Plasma Permittivity at Microwave Frequencies

Macroscopically, the plasma between the plates of the parallel-plate capacitor of Fig. 8.1 can be considered as a medium with a relative permittivity ε. This quantity shall be discussed from the viewpoint of the concept of current induction by electrons moving in the space between the conducting plates.

Oscillating electrons induce alternating charges on the capacitor plates, this resulting in an induced current in the external circuit along with a displacement current. In cases when electron collisions

with other particles may be neglected the electron velocities are given by equation (8.2). Since the exciting field is $E = E_m \sin \omega t$, this equation can be presented as

$$v = v_0 - \frac{eE_m}{\omega m} \cos \omega t_0 - \frac{e}{\omega^2 m} \frac{dE}{dt} \tag{8.9}$$

The radio-frequency current induced in the external circuit is determined by the variable component of electron velocity, that is by the last term in equation (8.9). Taking into account the fact that an electron carries a negative electric charge, the current induced by a solitary oscillating electron, by the general equation (2.31), is

$$i_{ind} = -\frac{ev}{d} = -\frac{e^2}{\omega^2 md} \frac{dE}{dt}$$

where d is the spacing between the capacitor plates (refer to Fig. 8.1).

The number of electrons per unit volume of the plasma will be denoted by N. The density of the induced current J_{ind} is a function of the total number of electrons oscillating in the volume between the capacitor plates per unit of the cross-sectional area, i.e., Nd. The density of the induced current will therefore be

$$J_{ind} = i_{ind} Nd = -\frac{Ne^2}{\omega^2 m} \frac{dE}{dt} \tag{8.10}$$

On the other hand, the capacitor under examination will conduct a displacement current, whether the electron-ion plasma is present or not. The density of this displacement current is

$$J_{dis} = \varepsilon_0 \frac{dE}{dt}$$

Thus, the density of the total current through the capacitor in the presence of electron-ion plasma will be

$$J_{tot} = \varepsilon_0 \left(1 - \frac{Ne^2}{\omega^2 m \varepsilon_0}\right) \frac{dE}{dt} \tag{8.11}$$

The field theory gives the total current density as

$$\operatorname{curl} \bar{H} = \bar{J}_{tot} = \sigma \bar{E} + \varepsilon \varepsilon_0 \frac{d\bar{E}}{dt}$$

this being valid in case of a negligible free space charge. Comparing the latter relation with (8.11), we note that the electron-ion plasma features a zero conductivity (i.e., $\sigma = 0$) due to the absence in (8.11) of a term directly proportional to the electric field intensity E. Physically, this statement is a natural consequence of the assumption that electron collisions with other particles produce a negligible effect, and therefore no energy dissipation should take place.

The factor at the dE/dt term in (8.11) should represent the relative permittivity of the medium; thus, the electron-ion plasma permittivity is given by

$$\varepsilon = 1 - \frac{Ne^2}{\omega^2 m \varepsilon_0} \tag{8.12}$$

The quantity $Ne^2/m\varepsilon_0$ in (8.12) is the square of the plasma frequency ω_p, known from the previous discussion (refer, for instance,

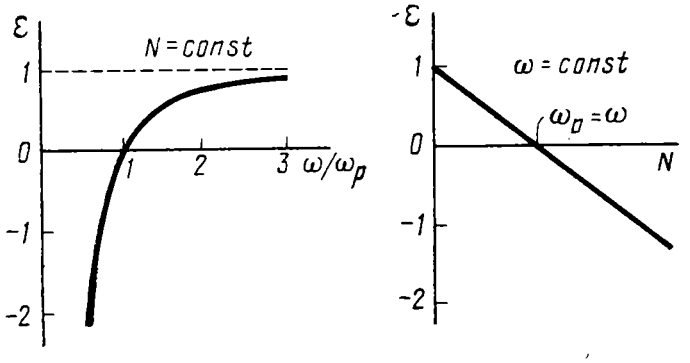

Fig. 8.2. Relative plasma permittivity as a function of frequency and electron concentration

to Section 2.9). Thus, the equation describing plasma permittivity may be reduced to

$$\varepsilon = 1 - (\omega_p/\omega)^2 \tag{8.12a}$$

The dependence of relative permittivity of plasma on the oscillation frequency and on electron concentration N is illustrated in Fig. 8.2. Under certain conditions the permittivity of electron gas proves to be negative; in any case the permittivity does not exceed unity.

Note, that equations (8.12) and (8.12a) do not allow for the effects of electrons colliding with gas molecules; this problem merits a more detailed treatment.

8.1c. Plasma Permittivity and Conductance Under Conditions when Electron Collisions with Gas Molecules Cannot Be Neglected

The problem becomes more complicate when the effects of electron collisions with other particles (mainly with molecules of neutral gas) have to be taken into account. A strict theoretical treatment of this problem presents considerable difficulties; the discussion will therefore have to be restricted to the macroscopic examination of electron motion at considerable gas pressures when each oscillation of an electron is accompanied by a great number of collisions

with gas molecules. Under these conditions the effect of collisions is similar to the effect of friction on a pendulum oscillating in viscous medium.

Again neglecting the motion of ions, electron collisions will be taken into account by introducing a second term into the left-hand side of equation (8.1), this term corresponding to the force of friction. This force is proportional to the velocity of the particle in question, and to a certain factor F, which should characterize the nature of the medium. In this case the motion of an electron in an alternating field should be described as

$$m\frac{d^2x}{dt^2}+F\frac{dx}{dt}=-eE_m\sin\omega t \tag{8.13}$$

The friction factor F can be related to the properties of the plasma taking account of the fact that with each elastic collision a complete electron momentum $\left(\text{equal to } m\frac{dx}{dt}\right)$ is lost. Thus, the change in momentum during a second will be $f_{eff}\frac{dx}{dt}m$, where f_{eff} is the effective rate of collisions, in other words, the ratio of the mean thermal electron velocity to the mean free path of electron travel.

On the other hand, this change in momentum should be equal to the power impulse of the friction force for 1 second, i.e.

$$m\frac{dx}{dt}f_{eff}=F\frac{dx}{dt}\cdot 1$$

Hence

$$F = mf_{eff} \tag{8.14}$$

Solution of equation (8.13) with respect to the electron velocity $v = dx/dt$ yields (for the case of steady-state conditions)

$$v=\frac{\omega meE_m}{F^2+\omega^2m^2}\cos\omega t-\frac{eFE_m}{F^2+\omega^2m^2}\sin\omega t \tag{8.15}$$

Further rearrangement of equation (8.15) can be similar to that performed earlier for the case of negligible collision effects. The density of the current induced in the capacitor by oscillating electrons proves to be

$$J_{ind}=\frac{Ne^2F}{F^2+\omega^2m^2}E-\frac{Ne^2m}{F^2+\omega^2m^2}\frac{dE}{dt}$$

and the density of the total current through the capacitor

$$J_{tot}=\frac{Ne^2F}{F^2+\omega^2m^2}E+\varepsilon_0\left[1-\frac{Ne^2m}{\varepsilon_0(F^2+\omega^2m^2)}\right]\frac{dE}{dt} \tag{8.16}$$

The first term in (8.16) corresponds to the conduction current, while the second describes the displacement current. Hence the

plasma conductance and the plasma permittivity may be described as

$$\sigma = \frac{Ne^2F}{F^2+\omega^2m^2} \quad \text{and} \quad \varepsilon = 1 - \frac{Ne^2m}{\varepsilon_0 (F^2+\omega^2m^2)}$$

Substitution of the coefficient of friction F, as defined by (8.14), into these relations after obvious rearrangements results in

$$\sigma = \frac{Ne^2f_{eff}}{m(f_{eff}^2+\omega^2)} = \frac{\omega_p^2\varepsilon_0 f_{eff}}{f_{eff}^2+\omega^2} \tag{8.17}$$

$$\varepsilon = 1 - \frac{Ne^2}{m\varepsilon_0 (f_{eff}^2+\omega^2)} = 1 - \frac{\omega_p^2}{f_{eff}^2+\omega^2} \tag{8.18}$$

These equations are the solution to the problem of the effect of elastic collisions of electrons with gas molecules on the properties of plasma at microwave frequencies. At f_{eff} approaching zero, equation (8.18) reduces to (8.12a) derived earlier. The specific plasma conductance tends to approach zero.

Sometimes equation (8.16) is given in a complex form

$$\dot{J}_{tot} = j\omega\varepsilon_0 \left[1 - \frac{Ne^2m}{\varepsilon_0 (F^2+\omega^2m^2)} - j\frac{Ne^2F}{\omega\varepsilon_0 (F^2+\omega^2m^2)}\right] \dot{E} =$$

$$= j\omega\varepsilon_0 (\varepsilon_1 - j\varepsilon_2)\dot{E}$$

with the quantities ε_1 and ε_2 describing the real and imaginary parts of the complex permittivity, respectively; these quantities are equal to

$$\varepsilon_1 = 1 - \frac{Ne^2}{m\varepsilon_0 (f_{eff}^2+\omega^2)} \tag{8.19}$$

$$\varepsilon_2 = \frac{Ne^2f_{eff}}{m\omega\varepsilon_0 (f_{eff}^2+\omega^2)} \tag{8.20}$$

The properties of the plasma can be also described in terms of a complex admittance with conductive and susceptive components if the total current is represented in a complex form as $j_{tot} = (\sigma_1 - j\sigma_2)\dot{E}$. The reader is invited to derive the simple equations describing σ_1 and σ_2.

The conductance of the electron-ion plasma should be considered in more detail. It can be easily shown, that this conductance is at a maximum when

$$f_{eff} = \omega \tag{8.21}$$

The frequency of collisions f_{eff} is directly proportional to the gas pressure p and, therefore, there should be a definite value of this pressure, at which microwave dissipation in plasma is at a

maximum at specified signal frequency and electron concentration. The behaviour of conductance as a function of gas pressure is qualitatively illustrated in Fig. 8.3; the higher the oscillation frequency, the greater is f_{eff}, which corresponds to maximum energy dissipation, and the higher should the gas pressure be.

At lower gas pressures the reactive component of the induced current becomes more pronounced. On the contrary, at very high gas pressures the plasma susceptance tends toward zero.

The conclusions made are of considerable interest to the discussion of plasma behaviour at comparatively low microwave signals, when electron collisions with gas molecules are of a purely elastic character and gas ionization effects due to the external microwave field can be considered negligible; such conditions are characteristic of a certain group of microwave discharge devices. In certain cases the susceptance of the plasma can be put to good use, for example, in controllable phase shifters. In other cases, microwave power absorption by the plasma is the most important property, as is the case of attenuators. The pressure of the gas filling should be chosen such as to correspond to maximum plasma conductance.

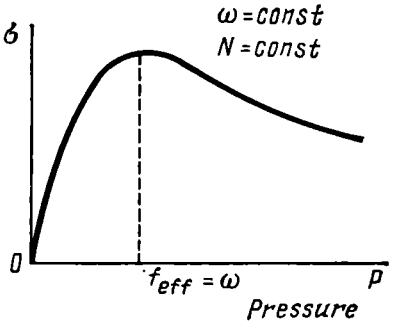

Fig. 8.3. Plasma conductance as a function of gas pressure (with equation (8.17) taken into account)

If the power of oscillations imposed on the plasma is increased, the non-linear properties must first become pronounced owing to a rise in electron temperature, these non-linear properties being due to a change in the number of collisions f_{eff}. With a further increase in power, the electron concentration N increases; as a result, the non-linear character of the processes taking place becomes still more complicate. Finally, a condition can be obtained at which self-maintained gas discharge may develop.

8.1d. Self-Maintained Microwave Gas Discharge

The phenomena examined above are independent of the amplitude of microwave oscillations, these conditions prevail as long as this amplitude is low enough and does not noticeably affect the mean thermal velocity of electrons and their concentration. Microwave current conduction through plasma in this case is somewhat similar to the behaviour of the non-self-maintained d.c. Townsend gas discharge at the initial section of the voltampere characteristic.

At considerable intensities of the radio-frequency field, an avalanche-like breakdown takes place and a self-maintained gas discharge is developed. Using again an analogy to d.c. gas discharge, this

effect may be compared to the transition from non-self-maintained discharge to self-maintained glow discharge.

It should be emphasized that the analogy between microwave and d.c. gas discharge phenomena is purely superficial and can not be extended to cover the physical processes taking place. The predominant role of volume effects and the insignificance of surface effects were already pointed out earlier. Experiments indicate, in particular, that the kind of the electrode metal is of no practical importance to the main characteristics of a microwave gas discharge. The discharge can even be *electrodeless*, i.e. can be developed and sustained in a volume without any external or internal electrodes. There are other interesting peculiarities of microwave gas discharge. Nevertheless, many of the characteristics of microwave gas discharge are similar to the characteristics of gas discharge at direct current, as will be shown later.

In contrast to d.c. gas discharge, there is yet no proper classification of microwave gas discharge and a universal terminology is still to be worked out.

The most common type of microwave gas discharge, which is utilized in many types of microwave discharge devices, is the so-called *arc* discharge. This kind of discharge is ordinarily developed in waveguides, resonant cavities and other kinds of microwave elements at the regions of excessive electric field intensities under conditions of reduced gas pressure. In appearance this discharge resembles the positive column of the common d.c. glow or arc discharge. At low gas pressures (units or fractions of mm Hg) the glow is of a uniform diffused character; an increase in gas pressure usually causes the discharge to be contracted into glowing bands or threads.

Another variety of microwave gas discharge is the *ring electrodeless* discharge that is developed in a radio-frequency magnetic field; this kind of discharge is encountered mainly in the longwave part of the microwave range. A similar ring discharge can be also developed at considerably lower frequencies, down to audio frequencies. The principle underlying this ring discharge can be easily understood by imagining an ordinary low-frequency transformer with a secondary in the form of a hollow toroid filled with a rarefied gas. The eddy electric field will cause electrons to move along ring trajectories, the discharge thus acquiring the form of a glowing ring. Microwave ring discharge has not yet found a wide field of practical application, except as a source of ions. At present the possibility of using microwave ring discharge in controlled fission reactions is being studied.

Besides the two types of discharge mentioned, *torch* and *spark* discharges are also phenomena sometimes encountered at high and microwave frequencies, with the spark discharge being somewhat more common and thus more thoroughly studied. This kind of dischar-

ge is evidenced as gas (air) breakdown even under normal gas pressure. The torch discharge is considerably rarer and has the appearance of a tongue of flame (torch) burning from the edge of some metal part, where the electric field gradient is the highest.

The microwave gas discharge of the most practical interest is the arc discharge and it will therefore be treated in some detail.

One of the peculiarities of this type of discharge is that it can be sustained by an electric field of quite low intensity: practice indicates that in most cases the intensity of discharge burning ranges from dozens to hundreds of volts per centimetre. The maximum energy acquired by free electrons in a field of such intensity, calculated

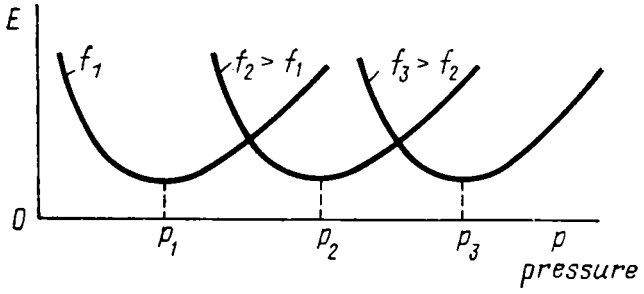

Fig. 8.4. Electric field intensity required to sustain a microwave gas discharge. Curve ordinates for different frequencies are conventionally reduced to one level

by (8.4), proves to be several orders of magnitude less than the energy of gas ionization. This proves that explanation of the mechanism of microwave gas discharge presents considerable difficulties. A strict analysis of the characteristics of microwave gas discharge falls outside the scope of subjects discussed in the present textbook.

Experiments point to the existence of a minimum in the intensity of the microwave electric field, at which a gas discharge is developed, as a function of the gas pressure; the behaviour of this function is similar to the Paschen curve at d.c. The field intensity corresponding to a self-sustained (burning) gas discharge as a function of the gas pressure is also of a similar appearance (Fig. 8.4). The optimum gas pressure, at which the discharge becomes self-sustained at the lowest electric field intensity, is directly proportional to the frequency at wavelengths shorter than 1 m. The corresponding shift of the curves for three different values of the frequency is illustrated in Fig. 8.4. Thus, for example, in the 10-cm band the optimum gas pressure for various kinds of gases is from 2 to 7 mm Hg, while in the 3-cm band it increases to 10-20 mm Hg.

Some authors have attempted to explain the peculiarities of microwave gas discharge by the resonant properties of the electron-ion plasma. From this standpoint, longitudinal or transverse waves propagating through the plasma interact with the free electrons

and provide the latter with energies sufficient to make the gas discharge self-sustained. Experimental findings confirm in the main the part played by wave processes in microwave gas discharge phenomena, at least at low gas pressures.

8.1e. Natural Oscillations in an Electron-Ion Plasma

Consider a uniform quasineutral plasma developed, for instance, by a d.c. arc discharge in rarefied gas; assume that random fluctuations have caused a certain number of electrons to be displaced relative to their equilibrium positions. Since the positive ions remain practically stationary, this will result in the appearance of an uncompensated space charge of positive and negative particles and thus in the formation of a peculiar electric dipole structure. The Coulomb forces, developed due to such a displacement, will tend to restore the initial equilibrium state, the nature of this force being essentially the same as that of the elastic force in any mechanical oscillator.

As known from mechanics, the existence of an elastic force is the cause of the appearance of discrete resonant frequencies. An electron-ion plasma should therefore be also expected to feature a certain frequency of natural resonance.

The radius-vector determining electron displacement relative to the equilibrium state will be designated as $\bar{r}$; the density of the space charge, developed as a result of electron displacement, will then be positive and equal to

$$\rho = \operatorname{div}(Ne\bar{r}) \tag{8.22}$$

This space charge will in turn develop a local electric field with an intensity $\bar{E}$, which can be described as

$$\operatorname{div}(\varepsilon_0 \bar{E}) = \rho \tag{8.23}$$

Substitution of (8.22) into (8.23) yields

$$\operatorname{div}(\varepsilon_0 \bar{E} - Ne\bar{r}) = 0$$

and with curl $\bar{E} = 0$ and curl $\bar{r} = 0$ the latter reduces to

$$\bar{E} = \frac{Ne}{\varepsilon_0}\bar{r} \tag{8.24}$$

Thus, the displaced electrons prove to be affected by a quasielastic force, which is directly proportional to the magnitude of electron displacement. The motion of electrons in this local field should thus be described as

$$m\frac{d^2\bar{r}}{dt^2} = -e\bar{E}; \quad \frac{d^2\bar{r}}{dt^2} + \frac{Ne^2}{m\varepsilon_0}\bar{r} = 0 \tag{8.25}$$

Solution of this equation describes harmonic oscillation of electrons with exactly the plasma frequency ω_p

$$\omega_p = e\,(N/m\varepsilon_0)^{1/2} \tag{8.26}$$

Thus, the plasma frequency, mentioned earlier in Section 2.9 and other parts of the present textbook, has a clear physical meaning—an electron-ion plasma behaves as an oscillatory system with an angular resonant frequency equal to ω_p.

The natural frequency of electron-ion plasma proves to be

$$f_p \approx 8980 N^{1/2} \tag{8.27}$$

if the electron concentration is in particles per cubic centimetre.

At realizable charge concentrations of the order of $(10^9\text{-}10^{14})$ cm^{-3}, the resonant plasma frequency turns out to be in the range of decimetric, centimetric and even millimetric waves.

The existence of a quasielastic interaction between particles and their oscillation with one and the same frequency f_p are by themselves inadequate to explain the orderly motion of great numbers of electrons and the transfer of oscillatory energy from this plasma to some external load. A similar situation was encountered when discussing the behaviour of a positive-grid triode (refer to Section 2.6). Nevertheless, experimental data show that under certain conditions electron-ion plasma is capable of sustaining orderly microwave oscillations with a frequency closely approximating the resonant frequency f_p.

It is of interest to note that the existence of plasma oscillations was discovered about 40 years ago when research was carried out into the so-called sonde method[1]. Numerous efforts to utilize this peculiarity of plasma behaviour for the development of practical microwave oscillators with a wide range of electronic tuning have been repeatedly made. The electronic tuning expected should be possible by controlling the electron concentration (by varying the conditions of a d.c. gas discharge). Up to the present time the mechanism governing these oscillations has not been explained, but the important role of a directive electron beam provided by a thermionic cathode and passed through the plasma has been established. The performance of microwave plasma oscillators is often accounted for by drawing analogies with the behaviour of klystrons and travelling-wave tubes.

---

[1] The discovery of plasma oscillations is due to the so-called "Langmuir paradox" consisting in an abnormal scattering of an electron beam provided by a thermionic cathode, when passed through plasma. The Maxwell distribution of electron velocities is determined at a distance about 1000 times shorter than predicted by kinetic theory.

8.2. TR and ATR Tubes

8.2a. Circuit Connection and Operating Conditions of Discharge Tubes

TR and ATR tubes constitute the most numerous type of microwave discharge devices and are designed for use in antenna duplexing assemblies (TR and ATR are abbreviations of "transmit-receive" and "anti-transmit-receive", respectively), utilizing the properties of self-maintained microwave gas discharge. At the same time, interaction of a low-density microwave signal with an electron-ion plasma, developed independently of this signal, also plays an important part in the performance of these devices.

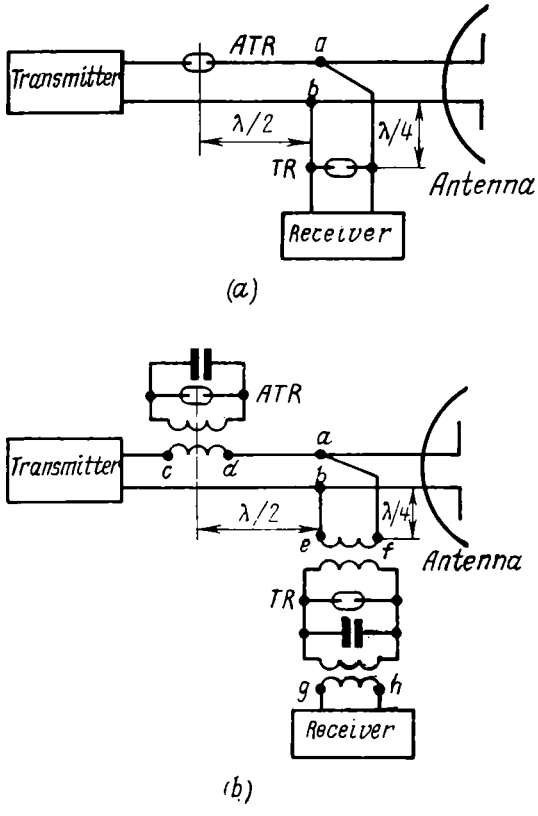

Fig. 8.5. Equivalent circuits of duplexing assemblies with non-resonant (*a*) and high-*Q* (*b*) TR and ATR tubes

The skeleton diagram of an antenna duplexing assembly with a TR and ATR switch is presented in Fig. 8.5*a*. In this circuit the ATR tube is connected into the main guide in series between the transmitter and the antenna; while the TR tube is connected in parallel to the same guide. The spacing between plane *ab* and the TR tube is set at a quarter of the guide wavelength, this ensuring that the transmitter is connected to the antenna and the receiver, disconnected from it during the transmit period (termed high power level conditions). Providing a spacing of half the guide wavelength between the ATR tube and plane *ab* is necessary to ensure an effective disconnection of the transmitter from the main guide during the receive period (low power level conditions) in the pauses between transmitter pulses.

To increase the efficiency of TR tube operation, the discharge device is usually housed inside a *resonant cavity*, this latter functioning as a step-up transformer of the resonant kind. A version of a duplexing assembly employing this type of tubes is shown in Fig. 8.5*b*. The design of a resonant TR tube with a coaxial input

and output is schematically shown in Fig. 8.6*a*; the functions of the auxiliary ("keep alive") electrode will be examined somewhat later. ATR tubes feature a similar design, differing only in the presence of a single coupling element.

During the transmit period both these tubes are fired and the microwave discharge across their gaps practically short-circuits the resonant cavities. The low impedance of this gas discharge is further transformed to a still lower impedance presented by the devices at the *cd* and *ef* planes (Fig. 8.5*b*). Thus, during the transmit period

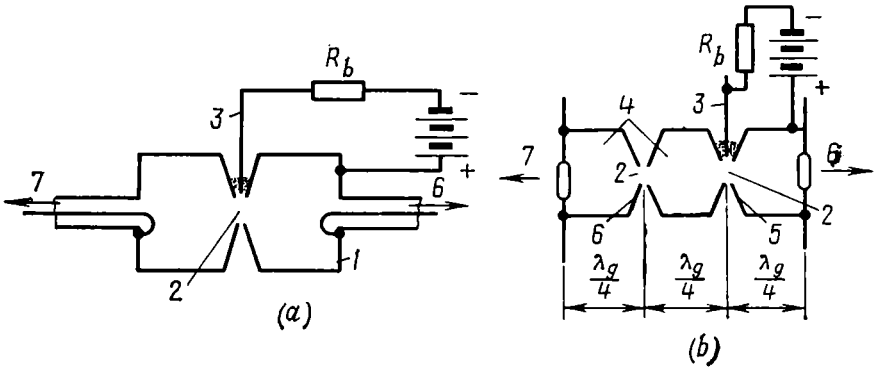

Fig. 8.6. Diagram and connection circuit of a high-Q (*a*) and bandpass (*b*) TR tube

1—resonant cavity; *2*—microwave spark gap; *3*—keep-alive electrode; *4*—rectangular waveguide; *5*—resonant gap; *6*—to receiver; *7*—to main guide

there is a practical short at the *cd* plane, while the circuit at the plane *ab* is open (recall the transforming properties of quarterwave sections of transmission lines) and all the signal from the transmitter is directed to the antenna without any significant amount of introduced loss or reflection. In so far as the receiver is concerned, the low impedance of the fired TR tube is transformed into a still lower impedance at the receiver input (plane *gh* in Fig. 8.5*b*), this ensuring that the part of transmitter signal leaking past this tube to the receiver input is considerably lower than in the circuit of Fig. 8.5*a*, where the switches shown are not provided with resonant cavities.

During the receive period both resonant cavities feature a high dynamic resistance, this leading to the main guide being practically disconnected from the transmitter (an open circuit at points *cd* in Fig. 8.5*b*); the input impedance of the transmitter branch of this duplexer tends to approach infinity and therefore does not affect signal transmission from the antenna to the receiver input. The low signal received is thus passed to the receiver without attenuation, except the small amount of loss introduced by the "cold" resonant cavity of the TR tube.

The main drawback of duplexing assemblies with *high-Q* TR tubes fitted with resonant cavities is their narrow band of operating frequencies, a change in the operating frequency necessitating mechanical retuning of the resonant cavities of both the TR and ATR tubes. *Wide-bandpass* tubes are therefore employed in radar equipment types where the frequency is to be variable, these tubes not requiring any mechanical tuning in a band of frequencies from about ± 3 to some $\pm$ (6-10) per cent of the middle frequency. A wide-bandpass tube employs a waveguide bandpass filter with two resonant windows and two or three spark gaps instead of a single resonant cavity. The spacing between the spark gaps and the resonant windows is set at a quarter of the middle guide wavelength (Fig. 8.6*b*); the input window also functions as a discharge gap, along with the resonant spark gaps. A bandpass ATR tube is of a simpler design, ordinarily consisting of a low-*Q* resonant cavity with a resonant input window functioning as an additional resonant gap. From the standpoint of waveguide techniques, these devices were treated in the textbook "Microwave Engineering", so that here only their main parameters and design features need be examined.

8.2b. Main Parameters Under Transmit Conditions

During the transmit period, when the high power pulse from the transmitter is to be passed to the antenna, a small fraction of this signal leaks past the duplexing assembly and appears at the receiver input; the time-dependence of this leakage power is illustrated in Fig. 8.7, showing the performance of a high-*Q* TR tube. Three main components of the leakage pulse can be distinguished:

(1) leakage power due to *direct* coupling between the tube input and output in the presence of a perfect short circuit across the radio-frequency spark gap; this component is therefore independent of the parameters of the microwave gas discharge;

(2) leakage power at the *top* of the pulse ("flat leakage power") passed by the tube after a steady-state microwave gas discharge has been established and due to a finite value of the voltage drop across a fired spark gap;

(3) power *peak* at the leading edge of the radio-frequency pulse, corresponding to transients during the firing of a microwave gas discharge, when the firing voltage is considerably higher than the voltage drop across the fired gap under steady-state conditions.

The sum of the first two components has to be kept lower than a certain specified value, which is a function of the characteristics of the receiver input. Thus, with most types of crystal mixer diodes the rated amount of leakage power is about 30 to 80 mW under long-term conditions and does not exceed 100 to 200 mW under short-term operation. Taking into account the transmitter power level,

which can be up to hundreds and thousands of kilowatts, the signal attenuation to be provided by the TR tube should be approximately some 60 to 80 dB. The problem of receiver protection against overloads is further complicated by that the spectrum of the transmitter signal is inevitably rich in harmonic content. Therefore, the TR tube is required to provide an adequate attenuation of these harmonics (evaluated by the harmonic leakage power) as well as of the fundamental.

The flat leakage power can be brought down to a minimum by selecting a proper gas filling with the lowest electric field intensity sustaining the microwave gas discharge. Physically, this means that monoatomic gases which feature a low electronic affinity, i.e. do not produce negative ions, should be employed. Neglecting all other factors, inert gases would seem most suitable for use in TR tubes from this viewpoint; gas pressure should be set to correspond to the minimum of the curve in Fig. 8.4*a*. As will be shown, this is usually contradictory to the requirement of a short recovery time and this latter has also to be taken into account when selecting the kind of gas filling.

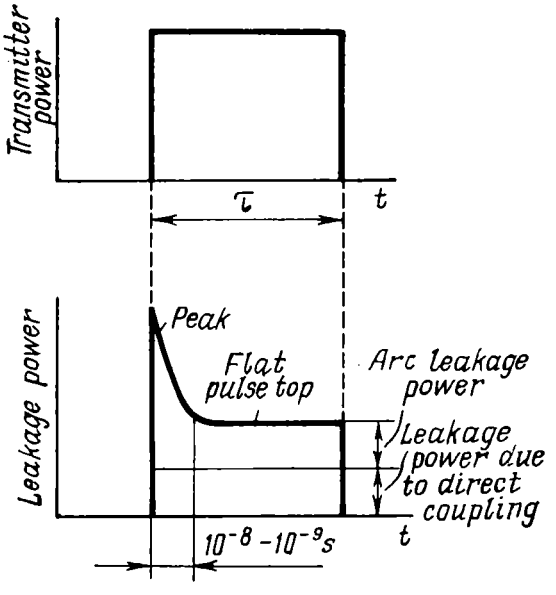

Fig. 8.7. Waveform of pulse leaking past a TR tube with a single discharge gap

The value of the flat leakage power is affected by the dimensions of the spark gap, because the intensity of the electric field remains approximately constant along the gap length. Ordinarily, it is advisable to employ short spark gaps so as to obtain a low firing voltage and a low voltage drop across the fired gap.

The time of establishment of a microwave gas discharge at the leading edge of each transmitter pulse usually is about 10^{-8} to 10^{-9} of a second and the power peak shown in Fig. 8.7 is of the same order of duration. Practice shows that just this peak is the most dangerous as it may cause mixer crystal damage because the thermal constant of the crystal contact features a duration of about the same magnitude. The heat dissipated by a small area of the contact surface does not therefore have time enough to be absorbed by the main mass of the crystal and this may result in burn-out of the crystal contact, despite the fact that the flat leakage power remains well within the limits of admissible values.

The waveform and the height of this power peak under such conditions are practically much less important than the amount of *total energy* contained in this peak; it is just this quantity determining the reliability of mixer crystal protection, that is one of the most important characteristics of TR tubes.

The maximum rated peak leakage energy depends on the type of crystal detector used in conjunction with the TR tube in question. Thus, with ordinary mixer diodes the peak leakage energy of high-Q TR tubes is required to be not in excess of 0.05 to 0.1 erg[1]. Such a low value of the rated leakage energy is one of the most stringent requirements that have to be met by TR tubes. Experience shows that this peak leakage energy is the most common source of crystal detector damage and consequent failure of the entire radar station[2].

In wide-bandpass tubes with several spark gaps (Fig. 8.6*b*) the duration of this leakage power peak is increased, while the typical flat leakage power is usually entirely absent. A greater duration of the peak tends to improve the operating conditions of the mixer diode and makes it possible to increase the rated peak leakage energy to 0.15-0.3 erg, sometimes even to several ergs. Note in passing, that the power leaking past these TR tubes due to direct coupling between the input and output is zero, this constituting an additional advantage of bandpass devices.

The value of the peak leakage energy is a function of several factors, namely, kind and pressure of the gas filling, the transformation ratio relative to the spark gap, the length and initial ionization conditions in the spark gap, etc. The effect of these factors is in the main the same as on the flat leakage power; the only factor that merits a more detailed examination is the initial ionization in the discharge gap.

As with d.c. discharge, the microwave electric field intensity at which the discharge is fired can be reduced by increasing the initial concentration of free electrons. This effect is utilized to reduce the amount of peak leakage energy by means of providing an auxiliary d.c. glow discharge, which is maintained in TR tubes by a separate *keep-alive electrode* (refer to Fig. 8.6). The required level of initial gas ionization is due to electrons diffusing out of the auxiliary discharge gap into the main spark gap.

The presence of such a keep-alive discharge leads to one of the numerous contradictions encountered in the development of resonant TR tubes. Indeed, the higher the intensity of this keep-alive discharge, the lower is the peak leakage energy. However, this is accompanied by a greater signal attenuation during the receive

[1] As an exception, the unit used to evaluate energy is here in the CGS system of units instead of the mksa. 1 erg $= 10^{-7}$ joule.

[2] A travelling-wave tube or parametric amplifier at the receiver input can make this requirement to the TR tube less stringent.

period due to the presence of a conducting gas discharge, this conductance being the higher, the greater the concentration of free electrons, as seen from equation (8.17). From this point of view, it would be necessary to keep the initial ionization of the discharge gas as low as possible. Still another consideration in favour of a low-intensity keep-alive discharge is that an intense discharge will reduce the life of these tubes. Thus, the problem of selecting a suitable intensity of the keep-alive discharge has to be ordinarily solved as a compromise between different and contradictory requirements; typical currents of this keep-alive discharge are some 100 to 200 μA.

Another problem, besides that of peak leakage energy, usually encountered in the development of TR tubes is that the microwave discharge is fired with a certain time delay relative to the radio-frequency pulses, this occurring when the transmitter is first turned on. Some TR tube types are provided with a small amount of radio-active matter contained in the tube body, this ensures the required initial ionization and thus reduces this delay. Such an initial ionization is useful in ATR tubes as well, despite the concept of peak leakage energy being applicable only to TR tubes.

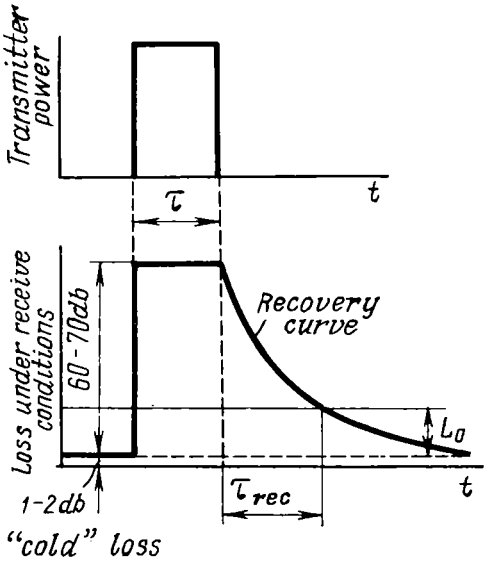

Fig. 8.8. Time dependence of microwave loss in plasma

Another very important parameter of resonant discharge tubes is the time of *gap recovery* after discharge extinction.

The free electrons present in the discharge gap after the transmitter pulse is over cause attenuation of the reflected signal which is to be passed to the receiver input.

The concentration of these free electrons gradually decreases due to diffusion and recombination effects. As a result, the received signal experiences a variable attenuation, as illustrated in Fig. 8.8.

The discharge gap conductance is determined only by free electrons and not by ions. Therefore the recovery process in resonant TR and ATR tubes can be considered as a consequence of the *de-electronization*, and not of the de-ionization of the discharge gap.

The recovery time of TR tubes is defined as the time required for a tube, after the transmitter pulse is over, to attain a specified value of attenuation L_0 of a low-level radio-frequency signal transmitted

through the tube, this value being referred to the attenuation presented by a completely recovered tube (Fig. 8.8). As the reference value, the 3 dB or 6 dB points are ordinarily specified; thus, the recovery time by the 6 dB level can be cited, for instance.

The greater the recovery time of TR and ATR tubes, the greater is the "dead time" during which the radar station in question is incapable of detecting and tracking objects (in other words, the wider is the zone of silence, within which objects cannot be detected). The radius of this zone of silence can be considered as directly proportional to this recovery time:

$$r_{\min.} = c\tau_{rec}/2 \tag{8.28}$$

where c is the free-space velocity of light. With a 5 microsecond recovery time the zone of silence around a station by (8.28) will be 750 m.

The recovery time cannot be reduced to as low a value as desired; in this respect the kind of the gas filling plays a significant part.

Physically, free electrons may be quickly withdrawn from the discharge gap by utilizing stepwise recombination effects with the development of negative ions. Obtaining a short recovery time, therefore, can be facilitated by the use of electronegative gases, which feature a pronounced electron affinity; negative ions in this case are the result of electrons adhering to neutral gas atoms and molecules.

Inert gases are known to be incapable of developing negative ions. The process of gap recovery in case of an inert gas filling is mainly due to diffusion. The most pronounced electron affinity is peculiar to water vapour, halogens, oxygen and similar gases. However, the same gases make the initiation and extinction of a microwave discharge more difficult, this resulting in a higher peak leakage energy, higher flat leakage power and higher loss in the discharge (this latter effect will be examined below). Thus, the requirement of a short recovery time is contradictory to other requirements that are to be met by a discharge device during the transmit period (high power level conditions).

In most TR tubes the gas filling is an inert gas (usually argon) with an admixture of electronegative gas, such as water vapour. A filling of this kind provides a recovery time of the order of several (2 to 5) microseconds, while with a pure argon filling the recovery time may be up to 1000 μs.

The use of water vapour as an admixture results in a series of undesirable side effects: the device parameters become sensitive to ambient temperature, the life span is reduced, etc. On the other hand, the recovery time obtained by using water vapour as an admixture is still too long for certain applications. Therefore, other methods

of reducing the recovery time, not necessarily involving the use of electronegative gas admixtures, are of considerable interest.

Diffusion methods can be used to reduce the recovery time to units or dozens of microseconds, while employing pure gas fillings. In essence, this diffusion technique consists in confining the microwave discharge to a comparatively small volume by mounting dielectric surfaces in the vicinity of the discharge (mica or ceramic wafers) or by introducing a dielectric of considerable surface area into the volume around the discharge gap (for instance, quartz batting). In this case the increase in the rate of free electron removal is a result of bipolar diffusion at the surface of the dielectric.

Another way of quickening the process of gap recovery without resorting to electronegative admixtures is based on pulse extraction of free electrons out of the discharge gap by applying an external electric field; to this end, the device is equipped with an auxiliary electrode. The drawback of this technique is the necessity of providing a separate pulse circuit.

The radical solution to the problem of a short recovery time is the development of purely electronic switching devices, which could be considered as non-inertial as compared to discharge devices. The main difficulty here is to provide extremely high convection current densities, which are necessary to obtain high microwave conductance values and thus to ensure adequate receiver protection.

One of the possible solutions to this problem is the utilization of *secondary-emission resonance effects* under high vacuum conditions, the secondary emission being caused by the microwave signal which is to be switched. Vacuum TR tubes utilizing secondary emission have already been developed and feature extremely short recovery times of the order of 10 nanoseconds; the degree of receiver protection obtained with these devices, however, is still considerably inferior to that provided by discharge tubes.

In the end of the present Section the problem of power loss in a fired tube will be briefly treated. Obviously, it is desirable to keep this loss at a realizable minimum so as not to reduce the amount of transmitter signal power radiated by the antenna. Another effect of no smaller importance is the tube gas hardening (a higher degree of vacuum being developed in the tube during its life span) as well as the thermal conditions of the tube itself, which can be damaged by excessive power dissipation.

At present there is no strict method available of calculating most of the characteristics of a gas discharge under high power level conditions, including loss in the discharge. The current through each of the switching tubes in Fig. 8.5, as in any transmission line, can be related to the pulse power by

$$I = k_1 P_{tr}^{1/2}$$

where I is the pulse current, P_{tr} is the transmitted power and k_1 is a proportionality factor, determined by the characteristic impedance of the line into which the tube in question is connected, and the transformation properties of this connection. At low impedance values of the plasma the magnitude of the discharge current I is practically independent of the properties and parameters of the microwave discharge.

The loss in signal power P_l which is dissipated by the discharge tube, is proportional to the product of discharge current I by the microwave voltage drop across the spark gap under steady-state conditions, i.e. in a fired tube. Therefore

$$P_l = k_2 VI$$

In case of the electron-ion plasma being developed independently of the microwave signal and therefore featuring a constant conductance, the voltage drop across the spark gap by Ohm's law would be directly proportional to the discharge current I and the power loss P_l would be a linear function of the transmitter signal power P_{tr}. Actually, however, the conductance of a self-maintained microwave gas discharge increases with a higher discharge current; the voltage drop across a fired tube proves to be almost independent of the discharge current and therefore of the power of the transmitter signal. Assuming for simplicity that $V \neq f(P_{tr})$,

$$P_l = k_1 k_2 V P_{tr}^{1/2} \cong k P_{tr}^{1/2} \tag{8.29}$$

where k is a constant for the type of discharge tube under consideration, with the properties of the gas filling, operating frequency, tube design and method of tube connection into the guide being taken into due account.

Thus, in contrast to an ordinary linear load, power loss in a discharge tube (under the approximations adopted) is proportional to the square root of the transmitter pulse power. Investigations disclose that in actual designs the loss introduced is $P_l \sim P_{tr}^m$, with m ranging from 0.5 to 0.8, depending on design peculiarities.

The loss introduced during the *transmit period* will be designated as L_{tr} and defined as

$$L_{tr} = 10 \log_{10} [P_{tr}/(P_{tr} - P_l)] \quad \text{or}$$

$$L_{tr} = -10 \log_{10} (1 - k/P_{tr}^{0.5}) \text{ dB} \tag{8.30}$$

this relation pointing to an increase in the absolute value of power loss with a higher transmitted power, but a lower introduced loss during the transmit period. This statement is in agreement with experimental findings.

The higher the current transformation ratio (refer to Fig. 8.5*b*), the lower is the constant k in (8.29) and (8.30), as a result, a consi-

derably lower loss is introduced by resonant TR and ATR tubes as compared to their wideband counterparts. A typical value of loss introduced by bandpass TR and ATR tubes is from 0.1 to 0.7 dB; despite these seemingly low values, the thermal operating conditions can be quite severe. For example, suppose $L_{tr} = 0.3$ dB and $P_{tr} = = 10$ MW at a pulse duration of 1μs and pulse recurrence rate of 1000 pps. Under such conditions the average power dissipated in the tube is about 660 W and normal tube performance necessitates the use of forced-air (or even water) cooling.

8.2c. TR Tube Parameters During Receive Period

The main parameters of resonant TR tubes under low power level (receive) conditions are the middle wavelength or range of mechanical tuning, the loaded Q and the introduced loss, as well as the loss in the branching arrangement. These parameters are determined by the "cold" characteristics of the oscillatory system and the manner of tube connection into the main guide. The parameters of the discharge tube during the receive period are, however, quite closely related to the parameters of the device during the transmit period, this interrelation excluding the possibility of selecting the "cold" parameters in the same arbitrary manner, as was the case with ordinary microwave circuits.

The loaded Q of high-quality resonant TR tubes is usually about 200 to 300 at non-loaded values of the order of 1000 to 2000. The operating bandwidth of these devices is therefore quite narrow and is from 0.3 to 0.5 per cent of the middle frequency (by the half-power points of the signal being transmitted). This makes it necessary to provide high-Q tubes with mechanical tuning facilities to make the device tunable in a range of some 10 to 15 per cent of the middle operating frequency.

With wide-bandpass tubes, the operating bandwidth corresponds roughly to the mechanical tuning range of modern high-power microwave oscillators (magnetrons, for instance) and is from ± 3 to $\pm$ (6-10) per cent of the middle frequency. Typical "cold" characteristics of bandpass TR and ATR tubes are presented in Fig. 8.9.

The *total loss* introduced by a TR switch will be denoted by L_{int} and defined as

$$L_{int} = 10 \log_{10} (P_1/P_2), \text{ dB} \tag{8.31}$$

where P_1 is the power delivered to the tube input from a matched signal source and P_2 is the power passed by the tube to a matched load. This total loss consists of the dissipative loss in the TR tube and the signal loss due to reflection. This latter will be denoted

by L_{ref} and defined by the obvious relation

$$L_{ref} = 10 \log_{10} 1/(1 - |\Gamma|^2), \text{ dB}$$

where $|\Gamma|$ is the modulus of the reflection coefficient.

In case of a high-Q tube with one resonant cavity by-passing the signal during the receive period the value of the total introduced loss is about 1 to 1.5 dB, while with wide-bandpass tubes of the type shown in Fig. 8.6*b* this value is commonly not in excess of 0.5 dB.

It is highly desirable to keep the total introduced loss at a realizable minimum so as not to reduce the level of received signal,

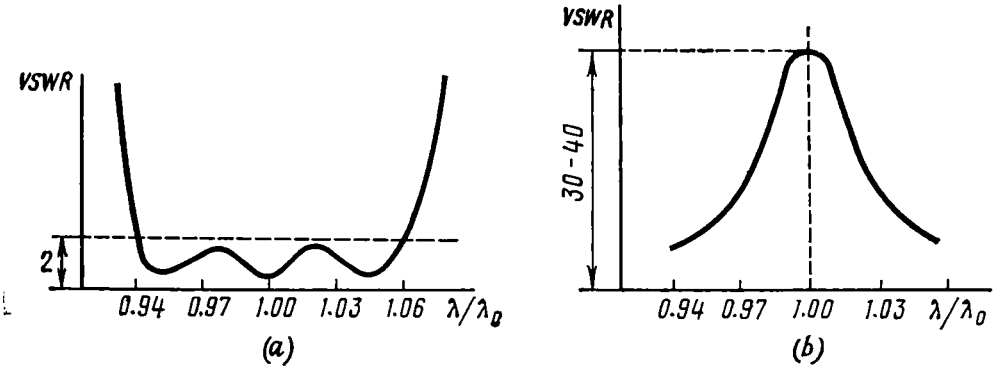

Fig. 8.9. Frequency characteristic curves of bandpass TR (*a*) and ATR (*b*) tubes under low power level conditions with the guide terminating in a matched load (VSWR not to scale)

as well as to keep the noise of the TR tube as low as possible. To a considerable degree, the value of L_{int} is a function of the loaded Q of the resonant elements employed in the tube, since a lower loaded Q tends to reduce L_{int}, but at the same time is accompanied by an increase in L_{tr}, higher peak leakage energy and higher flat leakage power. Once again the contradictions, characteristic of TR tubes, show up.

The introduced loss to a certain extent depends on the ionization level provided by the keep-alive discharge. This, along with a reduced life, prohibits the use of high-intensity keep-alive discharges to reduce the peak leakage energy during the transmit period[1].

Analysing the loss due to circuit branching is much more of a problem; this loss is defined as ten decimal logarithms of the ratio of power delivered by a matched antenna to the duplexing assembly

[1] It appears possible to employ a keep-alive discharge of greater intensity for this purpose by making this discharge a pulsed one and synchronizing it with the transmitter pulses. This technique, however, has not found any wide field of application due to the circuit complications involved, as well as the absence of automatic receiver protection from spurious microwave radiation.

to the power delivered from the duplexer output to the receiver input in case of a perfect TR tube. Physically, this loss is in part due to that the signal is partially branched away into the "cold" transmitter arm and in part to that the signal is reflected from the place of the branching arrangement (plane *ab* in Fig. 8.5). Under highly unfavourable conditions this loss may be quite high, up to 6-10 dB and even higher. In the absence of an ART tube the maximum branching loss tends to become infinite.

Omitting the calculations involved, the importance of the "cold" parameters of the ATR tube, and first of all the value of its loaded Q, should be emphasized. The lower the loaded Q, the wider the tube passband corresponding to a specified amount of branching loss (for instance, 1dB). For this reason the loaded Q of bandpass ATR tubes is made as low as practicable, about 5 and even less.

8.3. TR and ATR Tubes Design Problems

8.3a. High-Q Tubes

As a rule, resonant tubes are designed with a resonant cylindrical cavity fitted with truncated cones and excited at the E_{010} oscillation mode. During the transmit period a microwave gas discharge is developed between these cones and thus the resonant spark gap is practically short-circuited.

The design and appearance of a disc-seal high-Q glass tube are presented in Figs. 8.10 and 8.11*a*, respectively; in this design a removable external resonant cavity is used. Typical parameters of this tube are listed in Table 8.1 (No. 1). Tubes of this kind are employed both as TR and ATR switches; in the latter case the auxiliary keep-alive electrode is not used and sometimes is not provided.

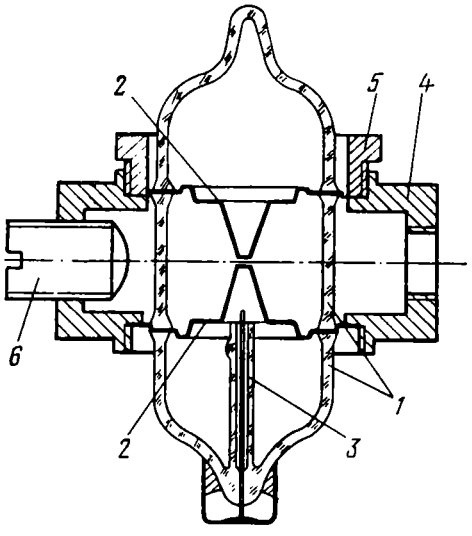

Fig. 8.10. Typical TR tube of the 10-cm band with removable cavity
1—glass envelope; *2*—copper discs; *3*—keep-alive electrode; *4*—outer part of cavity; *5*—clamping ring; *6*—tuning screw

In certain cases the keep-alive electrode is maintained at a voltage negative relative to the tube case (Fig. 8.6) and the discharge developed is of the abnormal glow type, this being accomplished by restricting the working area of the keep-alive electrode. The useful property of a discharge of this type is that it tends to eliminate the possibility

of relaxation oscillations in the circuit of the keep-alive electrode, because it features a rising voltampere characteristic. It is common to select the voltage applied to the keep-alive electrode to be in the range of 300 to 400 V, with a supply voltage of 800 to 1000 V.

The external cavities used with TR and ATR tubes are ordinarily inductively tuned to the operating frequency by means of screws (Fig. 8.10). In some cases capacitive tuning is considered to be more suitable and is accomplished by varying the spacing between

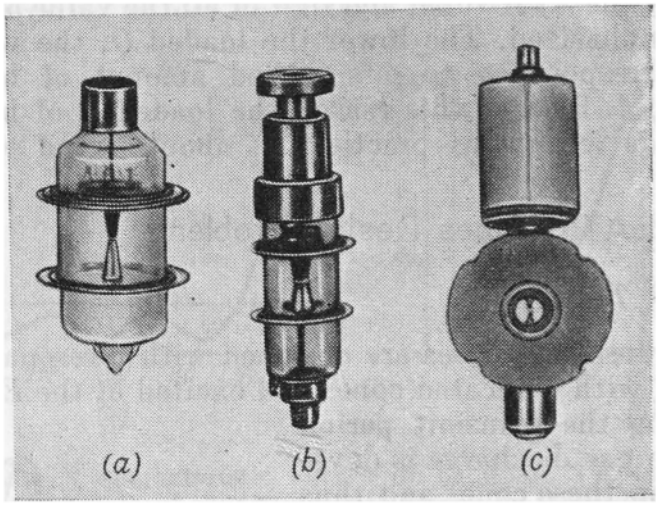

Fig. 8.11. Appearance of high-Q TR tubes for 10-cm band (a, b) and 3-cm TR tube with internal cavity (c)

the cones constituting the spark gap. The appearance of such a tube is shown in Fig. 8.11*b*, this particular type designed for use in an external cavity.

A high-Q TR tube with a built-in cavity is shown in Fig. 8.11*c*, here the cylindrical cavity with truncated conical electrodes is mounted inside the metal vacuum envelope of the tube. One of these electrodes is made movable by means of a screw gear differential, this providing the required capacitive tuning. The device is provided with two non-resonant glass windows sealed into the metal casing, for coupling to the receiver and the main guide. The parameters of this particular tube type are listed in Table 8.1 (No. 2).

8.3b. Bandpass Tubes

In contrast to resonant TR tubes, bandpass tubes feature three (rarely four) radio-frequency spark gaps instead of one, the input resonant window also functioning as one of these gaps and the rest being designed as resonant gaps with truncated conical electrodes

Table 8.1

Parameters of Typical Resonant Discharge Tubes

Nos	Discharge tube type	Operating frequency range, GHz	Maximum pulse power of transmitter, kW	Leaking arc power, mW	Peak energy, erg	Recovery time, 3 dB level, μs	Q_0	Q_L	Loss introduced during receive time, dB	Loss introduced during transmit time, dB	Type of tuning	Gas filling
1	High Q-factor glass discharge tube with external cavity for 10-cm range (Figs. 8.10 and 8.11*a*)	2.7-3.3	350	30-40	0.04	7	2000	—	1.5	—	Inductive	H_2 at 10 mm Hg H_2O at 10 mm Hg
2	High Q-factor discharge tube for receiver protection with internal cavity for 3-cm range (Fig. 8.11*c*)	8.5-9.6	100	10	0.02	4	3000	300	1.0	—	Capacitive	H_2 at 15 mm Hg H_2O at 15 mm Hg
3	Wide-bandpass 3-cm TR tube (Figs. 8.12*a* and 8.13*a*)	8.5-9.6	200	30	0.2	4	—	—	0.5	—	Fixed	Ar at 15 mm Hg H_2O at 4 mm Hg
4	Wide-bandpass 3-cm ATR tube (Figs. 8.12*b* and 8.13*b*)	8.5-9.6	250	—	—	5	—	5	—	0.7 dB at 4 kW	Fixed	Ar at 15 mm Hg H_2O at 4 mm Hg
5	Demountable tube	2.9-3.3	30,000	3 kW	—	50	—	5	—	0.1	Fixed	Ar at 40 mm Hg

or rods. The design and appearance of typical bandpass tubes are shown in Figs. 8.12*a* and 8.13*a*, respectively (refer also to Table 8.1, No. 3).

The spark gaps and the input windows are spaced from each other by a quarter of the guide wavelength at the H_{10} mode (Fig. 8.6*b*) so as to obtain the characteristics of a bandpass filter (Fig. 8.9*a*).

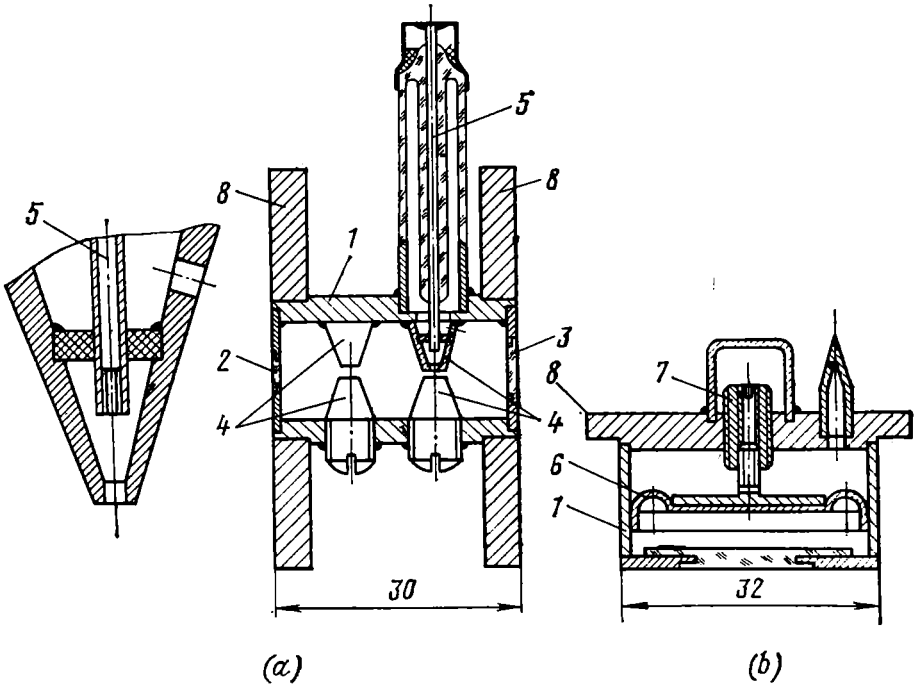

Fig. 8.12. Typical design of 3-cm bandpass TR tubes. The keep-alive electrode design shown at the left (enlarged view)

1—casing (rectangular waveguide); *2*, *3*—input and output resonant windows; *4*—resonant gap; *5*—keep-alive electrode; *6*—elastic membrane; *7*—preliminary tuning screw; *8*—waveguide flange

The resonant windows and spark gaps feature about one and the same resonant wavelength, the gaps being tuned to this wavelength during device manufacture. The loaded Q of the windows ranges from 1 to 3, while that of the spark gaps is ordinarily from 4 to 6. The waveguide casing and the resonant windows constitute the vacuum envelope of the tube.

The keep-alive electrode in bandpass TR tubes is always mounted at the discharge gap nearest to the input window, so that the microwave gas discharge is developed across this last gap first, after which all the other gaps break down one by one and finally a discharge across the input window is developed. The microwave power leaking past a discharge gap is insufficient to maintain the gas discharge across the next spark gap, this results in that the discharge across the last gap is extinguished and the gap begins to restore during

the transmit period, even while the transmitter pulse is still present. This effect is responsible for the inconsistent nature of the

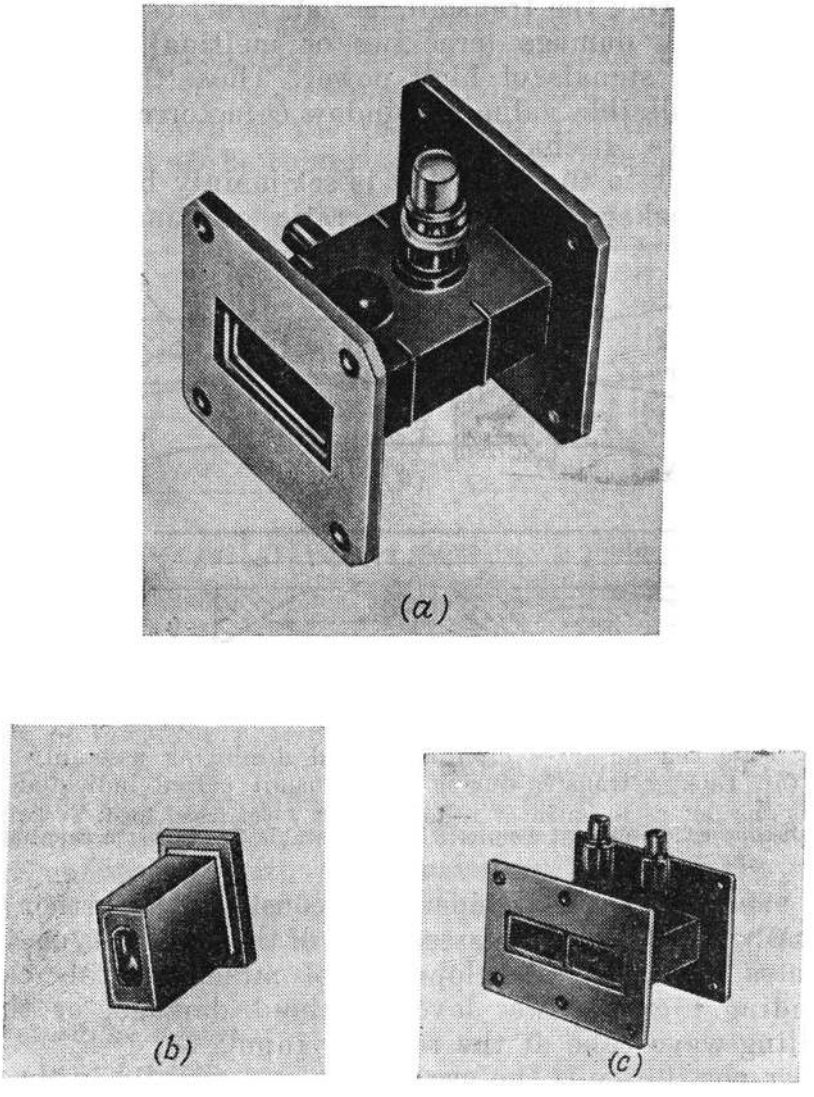

Fig. 8.13. 3-cm bandpass tubes

leakage power in bandpass TR tubes, mentioned earlier. In practice, the flat leakage power, averaged over the pulse duration, is usually cited as the device parameter.

The question of what limits a further widening of the passband of TR tubes is perhaps in order. As concerns the parameters at low power level conditions, the passband can easily be made wider by a further reduction of the loaded Q of the resonant gaps and windows. The main limitations are once again the deterioration of device parameters pertaining to high power level conditions.

Indeed, with a fixed design and technology, the loaded Q of a resonant window can be reduced only by increasing the geometrical dimensions of the aperture, which will inevitably result in a higher discharge loss during the transmit period. Practice shows the possibility of window damage (cracking or melting) when operating with transmitter signals of high power. Thus, there is a certain limit to the admissible value of window Q-factor due to power loss in the microwave discharge.

The lower limit to the loaded Q is set mainly by the admissible level of peak leakage energy. The ratio of bandwidth to peak

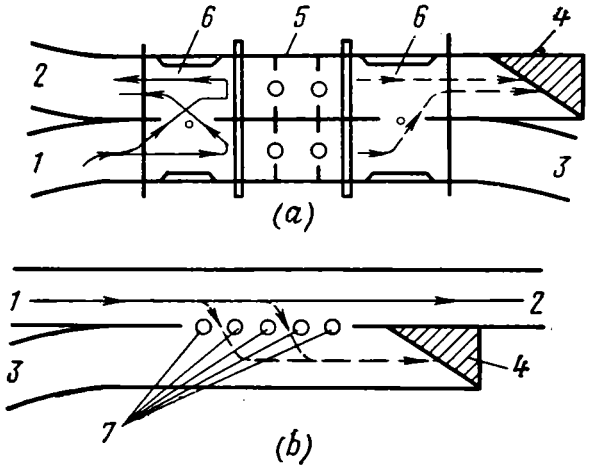

Fig. 8.14. Balanced duplexer circuit (*a*) and duplexing assembly with total coupling (*b*). Energy transfer during the transmit period indicated by arrows
1—from transmitter; *2*—to antenna; *3*—to receiver; *4*—matched load; *5*—twin TR tube; *6*—slot-coupled directional coupler; *7*—demountable TR tubes in coupling slots

leakage energy can be considered as constant; a further widening of the passband of duplexing assemblies of the coupler type, therefore, necessitates either the development of mixer crystals capable of withstanding higher power levels without damage, or the use of a travelling-wave tube at the receiver input.

Another possibility is the use of balanced circuits in the duplexer assembly with twin TR tubes and two slot-coupled waveguide directional couplers, as illustrated in Fig. 8.14*a*. In the ideal case such a circuit can provide a total elimination of both the peak leakage energy and the flat leakage power in the receiver arm. In actual designs the peak leakage energy is reduced by several times relative to the value provided by a single TR tube.

The appearance of a typical twin TR tube, designed for use in a circuit of this kind, is shown in Fig. 8.13*c*. The operating bandwidth of balanced duplexing assemblies is to a considerable extent determined by the bandwidth of the waveguide directional couplers and can be up to 6 to 10 per cent of the middle frequency.

The trends in the development of bandpass ATR tubes are mainly to employ single cavities, tightly coupled to the guide and thus featuring a low loaded Q. The design of a bandpass ATR tube is schematically shown in Fig. 8.15; the design, appearance and parameters of a typical ATR tube are presented in Figs. 8.12*b*, 8.13*b* and Table 8.1, respectively. This tube is made as a rectangular waveguide cavity with a resonant window at the open end. This window functions both as the tube input and the resonant spark gap. The other end of the tube is shorted by a plunger, as an elastic

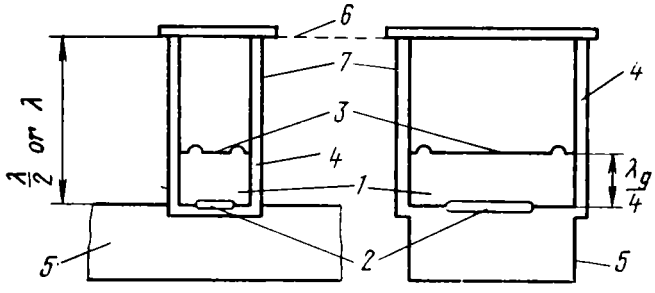

Fig. 8.15. Bandpass ATR tube mounted on main waveguide
1—rectangular quarterwave resonant cavity; *2*—resonant window; *3*—elastic membrane for tuning; *4*—choke gap; *5*—main waveguide; *6*—plane of mounting; *7*—socket for tube mounting

membrane. The tube is tuned to the operating frequency during the process of manufacture, after which the position of this tuning membrane is fixed. To obtain a minimum loaded Q, the tube has to be mounted onto the wide wall of the main waveguide with the resonant input window flush with the inner surface of this waveguide.

A choke connection with a halfwave gap between the external surface of the tube casing and the metal socket provided on the main waveguide for tube mounting, is shown in Fig. 8.15.

8.3c. Demountable Tubes

Demountable tube designs are widely used in the decimetric and centimetric wave bands at very high levels of pulse and average power of the transmitter signal. The design of such devices is schematically illustrated in Fig. 8.16; the tube here is detachable from the waveguide resonant structure.

Metal electrodes with truncated ends can be mounted inside a glass or ceramic envelope of a removable tube, as shown in Fig. 8.16*a*. These electrodes constitute a capacitive spark gap, which together with an inductive diaphragm or inductive bars, provides the entire assembly with resonant properties. The simplest is the design of an electrodeless tube, as shown in Fig. 8.16*b*. The demountable

tubes are versatile devices and this makes it possible to use them in balanced duplex circuits and in duplexer assemblies with total coupling as well as in duplexers of the directional coupler type.

An interesting feature of the design shown in Fig. 8.16*b* is the *dynamic choke*, which provides a means for a contactless connection of the electrodeless tubes to the walls of the main waveguide. In the presence of a microwave gas discharge the plasma thus developed

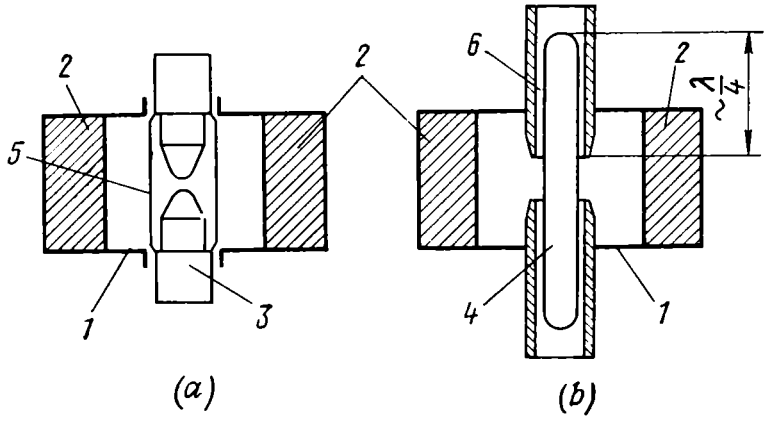

Fig. 8.16. Detachable TR and ATR tubes with inner electrodes (*a*) and of electrodeless design (*b*) mounted across a rectangular waveguide

1—waveguide; *2*—inductive iris; *3*—detachable tube with inner electrodes; *4*—electrodeless tube; *5*—vacuum envelope; *6*—dynamic choke gap

penetrates into the hollow metal cone and fills the volume of the tube, forming a peculiar central conductor of a coaxial line; the effective length of the choke gap should be set at approximately a quarterwave.

Detachable tubes are capable of meeting the severe requirements imposed upon modern duplexing assemblies. In particular, they can be used to provide the main receiver protection, while a pre-TR tube with a different gas filling and design can be mounted at the input of the branching structure of balanced and directional-coupler duplexers. An arrangement of this kind makes it possible to combine a high level of power switching with a short recovery time at adequate receiver protection from overloads (refer to Table 8.1, No. 5). The life and reliability of demountable tubes are considerably superior to those of ordinary TR and ATR tubes.

8.3d. Other Types of Microwave TR and ATR Tubes

At decimetric wavelengths and moderate power levels coaxial designs of non-resonant or slightly resonant tubes are used. The vacuum envelope of these devices is composed of a section of rigid

coaxial line with ring glass or ceramic non-resonant windows at one or both ends. In TR tubes this line is tapered, this providing a lower level of leakage power. It should be mentioned that the peak leakage energy and the flat leakage power in coaxial designs are considerably higher than in resonant and bandpass tubes. Bandpass coaxial TR tubes may be employed, therefore, in systems where the receiver input is an electron amplifier (triode, travelling-wave tube), but not a crystal mixer.

Another version of waveguide TR tubes, the *pre-TR tube*, should also be mentioned. Devices of this kind are used, for instance, in conjunction with high-Q TR tubes at high levels of pulse power. Pre-TR tubes are used generally to protect the TR tube from excessively high power levels, as well as to provide additional receiver protection at frequencies other than the fundamental. These devices are usually fabricated as sections of rectangular waveguide a quarter of the guide wavelength long with resonant windows at both ends. The input window functions also as a spark gap, just as in the bandpass tubes described above. During the transmit period the main TR tube encounters only the power leaking past this pre-TR tube, this not only improving thermal operating conditions of the TR tube, but reducing the leakage power as well.

TR tubes are developed for use with other types of microwave guides besides coaxial lines and waveguides. Among such unusual guides the circular waveguide operated at the symmetrical H_{01} propagation mode and the rectangular waveguide of increased cross-sectional dimensions (capable of propagating higher modes) can be cited as examples. Experiments show that duplexing assemblies designed with these unusual guides can be developed with about the same parameters as in available duplexer designs.

The constantly increasing power levels of transmitters, improved sensitivities of receivers, greater range of functions to be carried out by radar equipment and improvement of radar station parameters impose more and more stringent requirements on the characteristics of modern TR and ATR tubes. A trend of considerable promise is the use of gas discharge duplexing assemblies in conjunction with ferrite and semiconductor devices of the microwave band. In particular, the use of ferrite circulators in the design of duplexing assemblies proves to be a suitable combination. Furthermore, receiver protection can be improved by using additional semiconductor limiters designed with crystal diodes, mounted in the waveguide directly after the output window of the TR tube.

Further progress in TR and ATR tube design will be closely related to the general trends of microwave engineering and microwave electronics development.

8.4. Other Types of Microwave Discharge Devices

8.4a. Switches of High Power Level

The functions to be performed by microwave equipment often necessitate that a transmitter be switched from one antenna to another or one receiver be connected in turn to one of several antenna systems. In certain cases, when the required rate of switching is not excessive, this function can be carried out by waveguide or coaxial switches of the mechanical kind; in cases the power to be switched

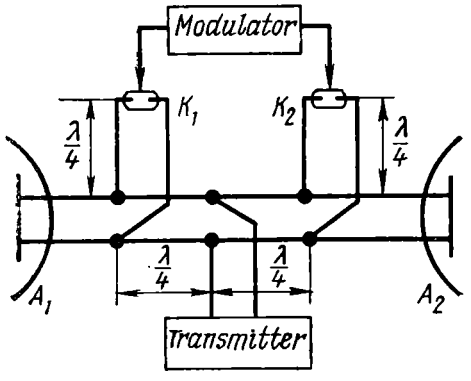

Fig. 8.17. Equivalent circuit of discharge commutator connection for transmitter switching between two antenna systems

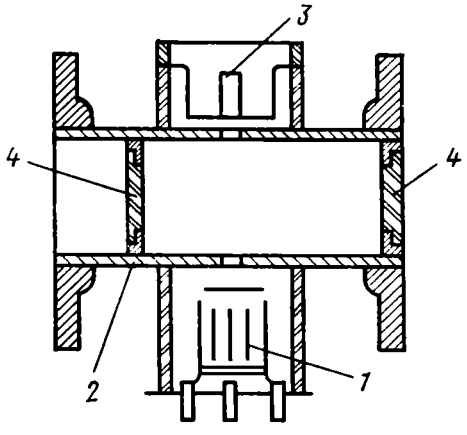

Fig. 8.18. Diagram of waveguide switch of thyratron type (10-cm band device)

1—cathode assembly; *2*—rectangular waveguide; *3*—anode; *4*—resonant vacuum-tight windows

is of a low level, the commutation can be performed with the aid of special types of semiconductor diodes. Fair results, especially at higher power levels, are obtained with the use of *controllable gas discharge switches*, in which the gas discharge is developed by external d.c. current pulses.

One of the possible versions of such a circuit with two switches connected at the ends of quarterwave stubs, is presented in Fig. 8.17; the switching elements here are discharge devices shorting the waveguide, when fired, by the plasma thus developed. These two devices (K_1 and K_2 in this figure) are fired alternately from an external pulse modulator. Firing device K_1 causes all the transmitter power to be delivered to antenna A_1 and vice versa, with fired K_2 and extinguished K_1 the transmitter load is antenna A_2.

To a certain extent, the development of such gas discharge switches is akin to the development of TR and ATR tubes, but with certain distinguishing peculiarities. These switches do not utilize a self-maintained microwave gas discharge, so that either very low or very

high gas pressures can be used, the value of the gas pressure being far removed from the minimum of the curve shown in Fig. 8.4. For instance, the gas discharge here can be developed between the device body and an auxiliary electrode with the aid of a separate pulse modulator.

High-power switches operating with low gas pressures (0.1-0.2 mm Hg) can be designed with thermionic cathodes mounted outside the discharge gap, this making the device somewhat similar in design to a hydrogen thyratron. The fuctions of the thyratron grid are in this case carried out by the metal waveguide, in which the microwave power is to be switched (Fig. 8.18).

The pulse current in the discharge fired across the waveguide (Fig. 8.18) can attain values up to 20 A at a voltage drop between the anode and cathode of about 100V. Power loss in such a discharge does not exceed some 0.2 dB, while the power handling capability in the 10-cm band is up to several megawatts.

8.4b. Discharge Noise Sources of Microwave Band

Tubes of the d.c. arc or glow discharge type at low gas pressures are widely used in measuring equipment as microwave noise sources with a "white" noise spectrum. The circuit connection of a discharge

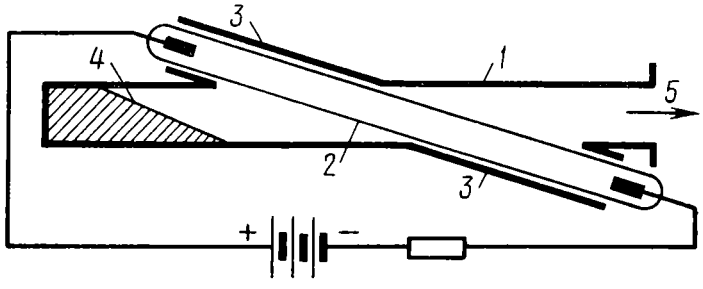

Fig. 8.19. Design of a discharge noise source
1—ordinary rectangular waveguide; *2*—discharge tube; *3*—section of cutoff waveguide; *4*—matched load; *5*—noise power output

noise generator is presented in Fig. 8.19; a glass gas discharge tube is mounted inside a waveguide at an oblique angle to the waveguide axis, this providing a fair match of the tube to the waveguide. The open end of the waveguide is the output of this noise generator, while the other end of the waveguide can terminate in a matched load of the dissipative kind. However, often both ends are left open and the device is inserted into the microwave plumbing for convenience of measurements.

The performance of a microwave noise generator is based on the laws of thermal radiation: by Kirchhoff's law the effective noise temperature T_n of a noise source is determined by the temperature

of that component of the medium, which absorps microwave energy at the frequency specified. As was demonstrated in Section 8.1, in the case under consideration the electron gas with a temperature T_e is the medium in question. The magnitude of T_e is usually tens of thousands of degrees in the non-isothermal plasma of positive columns of gas discharges at low pressures. This is one of the advantages of discharge noise generators over electron noise diodes, for instance (these devices are not treated in the present textbook).

Another advantage of discharge noise sources is the almost unlimited possibility of increasing the frequency of the section of noise spectrum being utilized. The upper frequency limit of the noise spectrum generated by an electron diode with a thermionic cathode can be shown to be set by the electron transit time. On the contrary, the frequency range of a discharge noise source is mainly limited not by the properties of the gas discharge, but rather by the dimensions of the cross section of the waveguide used. As a result, a complete series of noise sources covering all the microwave band of frequencies is available, the models differing from one another by the cross section of the waveguide and, as a consequence, by the diameter of the discharge tube.

The spectral density of the noise obtained is determined from equation (3.35). Taking the bandwidth as 1 Hz and assuming $T_n \cong \cong T_e \cong 2 \cdot 10^4$ (Kelvin degrees), the noise spectral density proves to be $3 \cdot 10^{-19}$ watts per unit bandwidth. Commercially available devices of this kind feature such or nearly such parameters.

This value is many orders of magnitude lower than that obtainable with high-power noise sources designed with TWT's and devices of the M-type. Despite this, the great advantage of discharge noise generators is the standard value of their output power, this being especially important in microwave measurement techniques.

8.4c. Plasma Amplifiers of Microwave Signals

The design of a plasma amplifier of the beam type is schematically shown in Fig. 8.20. Electron-ion plasma developed with the aid of d.c. gas discharge is pierced by an electron beam, which carries the microwave signal to be amplified. The plasma may also be developed directly by the electron beam, without the use of any additional electrodes.

The similarity between this plasma amplifier and a staged TWT amplifier or a drift klystron can be noted. The section of the helix shown in Fig. 8.20 is used to modulate the electron beam by the input signal, while another similar helix is used to couple out the amplified signal. The main part of signal amplification takes place in the drift space filled by electron-ion plasma. The pressure of the gas filling (argon, hydrogen, caesium vapour) should be kept quite

low about 10^{-3}-10^{-5} mm Hg. Maximum signal gain is obtained under conditions of approximate equality of the natural plasma frequency to the signal frequency, this necessitating the development of great electron concentrations if the operation is to be in the millimetric and especially submillimetric wave bands.

The main advantage of plasma amplifiers over the discussed earlier "purely electronic" amplifier tubes of the O-type is the greater gain per unit of drift space length, attaining values up to 20 dB/cm.

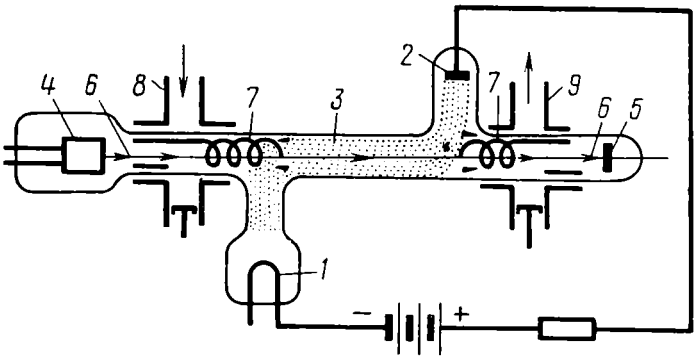

Fig. 8.20. Microwave plasma amplifier
1—cathode of gas discharge; *2*—anode; *3*—plasma-filled volume; *4*—electron gun; *5*—collector; *6*—electron beam; *7*—helical signal input and output; *8*, *9*—input and output waveguides

At the outset it was also assumed that utilizing direct interaction with electron-ion plasma will be a means for overcoming some of the limitations inherent in ordinary types of amplifier devices at the higher power levels in the millimetric, and even more so in the submillimetric wave bands.

Extensive research has resulted in the development of plasma amplifiers with pulse output powers up to 20 kW in the 10-cm band at efficiencies up to 40 per cent. The shortest wavelength obtained at present is 8 mm. However, plasma amplifiers also suffer from certain drawbacks, such as a considerable level of inherent noise, difficulty of stabilizing operating conditions due to gas "hardening", and some other. These and other drawbacks, as well as the indisputable progress in the development of "purely electronic" devices, have resulted in that plasma amplifiers are at present given considerably less attention. However, the possibility of research in the field of plasma amplifiers leading to a renewed interest in this problem at a higher level of knowledge should not be overlooked.

Still other applications of electron-ion plasma at microwave frequencies, besides the main types of microwave discharge devices examined above, are also possible. Among these the discharge detectors of microwave signals can be mentioned as an example, such devices featuring a considerably higher endurance to overloads

than the ordinary semiconductor diodes. Attempts to develop a controllable phase shifter with the aid of gas discharge have been made; here the variation of signal phase was expected to be due to variations of the plasma permittivity, which in turn may be controlled by varying the electron concentration, i.e. the direct current through the gas discharge. Similar effects can be utilized to control the frequency of low-power microwave oscillators, such as reflex klystrons, etc.

Self-maintained gas discharge is used for visual indication of the presence of microwave oscillations at power levels in excess of several watts. Plasma frequency multipliers are undoubtedly also of interest. The use of high-power microwave gas discharge for controlling fission reactions is an interesting possibility of a more remote future.

CHAPTER NINE
CONCLUSION

The discussion of microwave device types presented here cannot be considered as an exhaustive study of oscillator and amplifier devices for the microwave range, available at present and constantly supplemented by new types and versions of microwave devices. Among the yet rare tube types, the *ubitron* — a high power oscillator utilizing the interaction of a periodic electron beam with the field of a fast wave in a waveguide — may be mentioned as an example. The present treatment has not encompassed all the possible versions of retarding-field oscillators, for instance the *strophotron* has not been examined; the same is true of *parametric electron beam amplifiers* which are at present successfully competing with semiconductor parametric amplifiers and low-noise TWT's. Microwave diodes designed for *measurement* purposes and microwave *noise* diodes have been completely omitted, as well as microwave special-purpose cathode-ray tubes, and so on.

The present trend to develop devices of the so-called hybrid type, which occupy an intermediate place between, for instance, klystrons and TWT's or TWT's and magnetrons, has been practically only briefly mentioned in passing. Nevertheless, most new types of microwave devices operate on the general basic principles treated in the first three chapters, as well as in subsequent parts of this textbook; the development of these basic principles is demonstrated by the examples of devices of the greatest practical interest, such as triodes, drift and reflex klystrons, travelling-wave and backward-wave tubes, magnetron oscillators and platinotron amplifiers.

In certain cases one and the same function can be successfully carried out by microwave devices belonging to different device groups. For instance, a local oscillator may be designed as a reflex klystron, backward-wave oscillator of the O-type, triode oscillator or a voltage-tunable magnetron; magnetrons, M-type backward-wave tubes, stabilotrons and (at the longer wavelengths) triodes and tetrodes can be employed as high-power oscillators; the output stages of power amplifiers can be designed as multicavity klystrons, travelling-wave tubes of the O- or M-type, platinotrons, triodes, tetrodes, and so on.

Sometimes the choice of a particular device type for the task in hand is determined by the operating wavelength, some devices being more suitable for the frequency range specified than others. Thus, for instance, microwave power triodes are mainly used in equipment of the decimetric wave band, while magnetrons should be considered more suitable at centimetric and millimetric wavelengths. However, in most cases a strict demarcation is quite impossible and the practical choice of a suitable device type has to be based on a detailed examination of the characteristics and parameters of devices of similar application, while making allowance for cost, supply source requirements, dimensions, weight, cooling, etc. The possibility of a choice should not be taken as an indication that further progress will lead to the development of tubes of "general-purpose" character. In most cases the co-existence and further improvement of characteristics of various devices, designed to perform similar functions, is highly desirable, this facilitating satisfaction of diverse requirements imposed by actual practice.

Progress in the field of microwave electronics can be expected to lead to the improvement of such characteristics of modern microwave devices as higher frequencies and higher output power levels (pulsed and c. w.), reduced noise figures, wider bandwidths and wider tuning ranges, higher frequency stability, longer life, etc. The development of oscillators and amplifiers with pulse powers in the 1000 MW range at average power levels in excess of 1 MW can be expected in the immediate future, this being evident from data published at present.

The progress in the art of high-power electronics is so great that this branch of microwave engineering begins to outgrow the traditional boundaries of electronic industry, which is conventionally considered to deal mainly with information processing and transmission, as well as measurements and control. The power levels and efficiencies attained with magnetron oscillators, platinotrons, multicavity klystrons and TWT's make it already feasible to consider the possibilities of microwave energy application for industrial and commercial purposes. Among direct applications of microwave devices, microwave power sources for heating, drying, baking, welding etc., should be mentioned as examples of present-day equipment. A more remote but even more tempting aspect is the partial or even complete replacement of energy transmission systems operating at the mains frequency or direct current by microwave guiding systems for energy transmission over great distances with low loss. From the standpoint of transmission lines this already appears to be possible and economically feasible at power levels in excess of about 6000 MW.

However, this will require that a whole number of complicate scientific and engineering problems be solved, and, first of all,

the problem of efficient reverse conversion of microwave oscillations into mains or direct current. In principle, such a conversion is possible with the aid of almost all the existing microwave oscillator and amplifier devices, including magnetrons and klystrons. Up to now research in this direction was of a preliminary, exploratory character; direct utilization of microwave energy without intermediate conversion into direct or mains frequency current, is also a promising aspect of the same problem.

Solution of the problems of microwave energetics necessitates the development of microwave devices with even higher power levels and efficiencies. The present state of microwave electronics theory and engineering does not impose any principal restrictions in this respect. Development of super-high power oscillators and amplifiers is possible even now and is restrained mainly by the absence of demand for such giant devices.

In the immediate future the development of microwave electronics can be expected to be aimed at further improvements of the radio location, radio navigation, television and telecommunication services. Microwave electronics plays an increasing part in various space research programs, where electron devices have to meet some of the most stringent requirements. Besides having to satisfy the constantly increasing requirements of improved performance characteristics and parameters, electron devices now have to provide an extremely high reliability during a long life span, up to dozens of thousands of hours.

The progress in solid-state electronics and optical quantum devices at wavelengths longer than about 0.1 mm opens up new possibilities for microwave engineering. At present the frequency range covered by shortwave electron devices already overlaps that of the longwave quantum oscillators. Thus, BWO's with wavelengths of about 0.2 mm are already available, while lasers with operating wavelengths of 0.77 mm have also been developed. Solid-state oscillators designed with avalanche diodes, Gunn diodes and their modifications are capable of operating at millimetric wavelengths. Development of all-solid-state equipment, designed with microwave transistors and varactor diodes (these latter as frequency multipliers of the transistor signal), is a promising trend, widely recognized and applied in modern equipment.

The present state of art of microwave signal generation and amplification is illustrated in Fig. 9.1, where electronic, solid-state and quantum-mechanical devices are presented. The maximum power levels for c.w. conditions or the average values for pulsed duty are shown in a logarithmic scale.

As evident from this graph, the output power of electron devices begins to diminish at wavelengths shorter than about 3 cm; analysis discloses this decline in output power to be approximately proportional to the fifth power of the operating frequency. A similar trend

can be noticed with solid-state devices as well. The output power levels obtained with the best samples of solid-state devices can be noticed to be about four orders of magnitude lower than those provided by electron devices, the features intrinsic in solid-state devices imposing most serious restrictions on their application as high-power microwave sources. However, in the range of low power levels

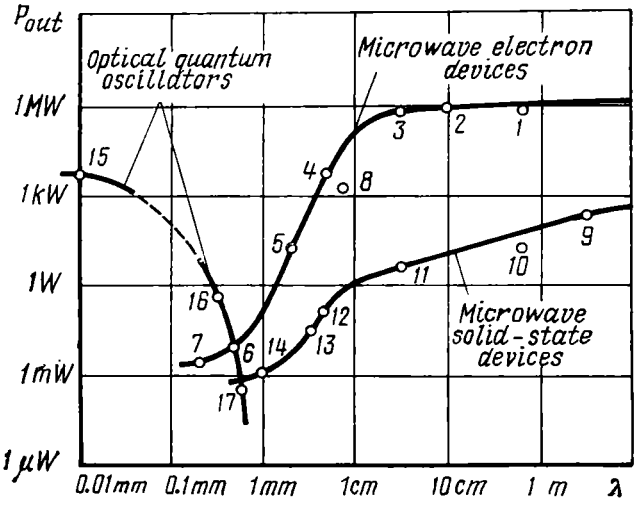

Fig. 9.1. Output power of microwave devices (1971 state of the art). Values cited are for c.w. conditions or average for pulsed duty

1—microwave tetrode; *2*—platinotron; *3*—klystron with distributed output cavity; *4, 5*—TWT of O-type; *6*—BWO of O-type; *7*—BWO of O-type; *8*—cyclotron-frequency resonance maser; *9, 10*—microwave transistor; *11, 12, 13, 14*—avalanche diode; *15*—gas laser (CO_2); *16*—gas laser (HCN); *17*—gas laser (ICN)

solid-state devices are quite capable of successfully competing with "purely" electronic devices.

The graph of Fig. 9.1 shows the existence of a significant reduction of the power level obtainable with the aid of all kinds of oscillators and amplifiers in the range of millimetric and submillimetric waves. The demand for output powers increased by several orders of magnitude compared to available values can be expected to result from the progress of application of these frequency ranges. Here again the most promising devices are electronic, in particular, cyclotron-frequency resonance masers. The competition between solid-state and electron devices in the low power range promotes further research and development. Miniaturization and microminiaturization tendencies play quite an important part in this respect.

Development of electron optics and emission techniques, as well as vacuum technology, is essential to the improvement of characteristics and parameters of microwave devices of all types. These trends, along with a further development of physical concepts and theory of microwave devices, can be expected to provide for the essential progress of microwave electronics.

INDEX

Amplification zone, 361, 364
Amplifier, 45, 112, 113
Amplifier, low-noise, 115, 255 265
Amplifier. M- type, 317, 369
Amplifier, non-resonant type, 230
Amplifier, O-type, 230
Amplifier, plasma, 414
Amplifier, power, 112
Amplifier, range of mechanical tuning of 113
Amplifier, regenerative, 276, 280
Amplifier, small signal, 113
Amplitron, 357, 367
Anode voltage, threshold 317
ATR tube, 392, 403
ATR tube, wide-passband, 394

Bandwidth. 112, 186, 249, 363, 394, 401, 407
Bandwidth, instantaneous, 113
Bidematron, 370
Bimatron, 355, 370
Buncher, 149
Bunching cascade, 176, 178, 182
Bunching parameter, 184
Bunching space, 68, 149, 197
BWO, 371, 282, 352
BWO, resonant, 284

Capacitor, blocking, 141
Carmatron, 359
Catcher, 149
Cathode, back bombardment of, 132, 323
Cathodes of microwave electron devices, 126, 337
Cavity, anode-grid, 137
Cavity, cathode-grid, 137
Cavity, multigap, 194
Characteristic, amplitude, 166, 365
Characteristic, amplitude-frequency, 168
Characteristic, dispersion, 305, 361
Characteristic, load, 102, 329
Characteristic, operating, 327
Characteristic, phase, 257, 367
Characteristic, transfer, 255
Characteristic equation, 79, 240, 246
Circuit, common cathode, 48, 125
Circuit, common grid, 125, 136
Coherence, 11
Collector, 39, 45, 150, 185, 190
Collision rate, 385
Compatibility, electromagnetic, 112
Conditions, critical, 263, 295
Conditions, large signal, 47, 122, 127
Conditions, small signal, 22, 123, 234
Continuity equation, 16
Control, dynamic, 51
Control, electrostatic, 47, 119
Control device, 45, 47
Convection current, perfect waveform of, 36
Coupling coefficient, 32, 33
Current, convection, 14, 30, 31, 33, 135, 154
Current, induced, 26, 28, 31, 58, 135, 238
Current, starting, 88, 211, 276
Current, total, 14, 26
Cutoff current, 294
Cyclotron frequency, 291, 294
Cyclotron resonance, 325, 372
Cyclotron resonance maser, 375

Dematron, 367
Device, M-type, 232, 324, 346
Device, non-resonant, 41, 71, 107
Device, O-type, 230
Diode, equivalent, 123, 127, 128
Diode, noise, 61, 117, 414
Discharge, arc, 388
Discharge, auxiliary, 396, 403
Discharge, electrodeless, 388
Discharge, spark, 388
Discharge, torch, 388
Dispersion, 43, 272, 277, 305, 362
Dispersion characteristic, 305, 361
Dispersion equation, 240, 246, 280
Dynamic control, 51
Dynamic range, 256

Effect, long-line, 104
Efficiency, 110, 159, 183, 208, 250, 322, 352
Electode, common, 48
Electrode, control, 194, 343, 350
Electrode, keep-alive, 396, 406
Electrode, negative, 343, 347
Electrode grounding, 141, 193, 226
Electron, favourable, 56, 312, 374
Electron, unfavourable, 55, 177, 184, 313, 374
Electron beam, dynamic control of, 51
Electron beam, matching to oscillatory system, 40
Electron beam, periodical, 44, 375
Electron beam, power coupling out of, 34, 254, 325, 363
Electron beam, underbunched, 161, 166
Electron beam bunching, 68, 151, 176, 236
Electron beam bunching parameter, 153, 180, 184, 203
Electron beam conductance, 84, 205
Electron beam conductance, negative, 60, 62, 86
Electron beam convergence, 192
Electron beam debunching, 161
Electron beam density modulation, 67, 313
Electron beam overbunching, 161, 166

Electron beam susceptance, 60, 84, 205
Electron beam velocity modulation, 52, 63, 71
Electron bunch, 37, 44, 47, 54, 156, 252, 314
Electron bunch center, 69, 71, 363
Electron bunching, 54
Electron charge, 15
Electron load conductance, 66
Electron transit angle, 21, 163
Electron transit angle, fictitious, 22
Electron transit angle, undisturbed, 21
Electron transit time, 18, 199, 294
Electron velocity, 17, 292
Electronic tuning, range of, 216
Electronic tuning, rate of, 214
Equation, characteristic, 79, 240, 246
Equation, continuity, 16
Equation, dispersion, 240, 246, 280
Equation, Hartree, 317
Equation, Maxwell, 13
Equation of velocity modulation, 64

Feedback, 45, 140, 169, 257, 274
Feedback factor, 138
Field, self-matched, 235, 240
Fields, crossed, 287, 346
Flow, double-stream, 296
Flow, single-stream (Brillouin), 296
Focussing, electrostatic, 193, 350
Focussing, phase, 73, 75
Frequency, Doppler shift, 110
Frequency, limiting, 113, 119, 128
Frequency, temperature coefficient of, 91
Frequency jump, 94, 106, 271
Frequency multiplier, 38, 40, 173
Frequency of oscillations, 90, 107, 276
Frequency pulling, 98, 329
Frequency pulling figure, 101, 330
Frequency pushing, 91, 320
Frequency stability, 93, 219, 335, 359

Gain, 112, 166, 181, 243, 248, 356, 365
Gain, condition of maximal, 167, 190
Gain parameter, 241, 251
Gap, 24, 31, 41, 57, 63
Gap, equivalent, 33, 66
Gap factor, 32, 64
Gap recovery time, 397
Gas discharge, microwave, 387
Gas discharge, self-sustained, 387
Gas discharge device, 380
Grid, perfect (ideal), 58, 123, 151

Hartree equation, 317
Hysteresis, electronic, 97, 208

Induced current, equation of, 26
Induction, critical, 294
Interaction, long-term (prolonged), 44, 71, 230
Interaction, short-term, 41
Interaction space, 288, 297, 346, 358, 360
Interdigital slow-wave structure, 278

Kinematic theory, 151, 178
Klystron, distributed interaction, 194
Klystron, drift (amplifier), 71, 149, 175, 191
Klystron, multibeam, 193
Klystron, multicavity, 175, 192
Klystron, optimal spacing of gaps in, 167, 192
Klystron, reflex, 196, 212, 221, 226
Klystron, two-cavity, 149, 163, 169

Laddertron, 285
Leakage power, 394, 407
Leakage power, flat, 394, 407
Lens, electromagnetic amplifying, 370
Lens, phase, 73
Loss under receive conditions, 397
Loss under transmit conditions, 397

Magnetron, 287, 310, 331
Magnetron, coaxial, 334
Magnetron, inverted coaxial, 335
Magnetron, multicavity, 297, 326, 331
Magnetron, oscillation modes, 287
Magnetron, rising sun, 309
Magnetron waveguide amplifier, 370
Maser, cyclotron resonant, 375
Maxwell's equations, 13
Miniaturization, 10
Mitron, 343
Modulation, amplitude, 226
Modulation, frequency, 219, 226
Monotron, 61, 116
Motion diagram, 23, 54, 68, 135, 146, 177, 198

Noise, 113, 228, 254
Noise factor, 113, 255
Noise source, 270, 413
Noise temperature, 114, 432

Operating conditions, pulsed, 193, 344
Oscillation mode, 93, 298
Oscillation mode separation, 94, 305, 307
Oscillation stability, 87
Oscillation type, 94
Oscillation zone, 171, 200, 275, 318
Oscillator, 45, 85
Oscillator, local, 110, 228, 281, 285
Oscillator, microwave diode, 62, 116
Oscillator, non-resonant type, 83, 230
Oscillator, positive-grid triode, 52
Oscillator, resonant type, 83
Oscillator, retarding-field, 52, 117
Oscillator, synchronized, 355, 365
Oscillator for measurements, 110, 228, 283, 285

Parameters, «cold», 84, 239, 401
Parameters, «hot», 167
Parameters, transformation of, 96
Peak leakage energy, 396, 408
Perveance, 189, 192
Phase characteristic, 257, 367
Phase pushing, 366
Phasochron, 377
Plasma, relative permittivity of, 382
Plasma amplifier, 414
Plasma frequency, 79, 384, 391
Plasma frequency reduction, 81
Plasma oscillations, 390
Plasma wavelength, 162
Platinotron, 357, 367
Power output, 95, 192, 223, 336

Q, external, 99
Q, loaded, 90, 401

Radiation, spurious, 110
Range, dynamic, 256

Recuperation (depressed collector operation), 185, 253
Relativistic correction factor, 17
Resnatron, 146
Resonance, secondary emission, 399
Retarding field, 35, 53, 312
Retarding field method, 67, 197
Retarding-field oscillator, 52, 117
Rieke diagram, 330

Self-excitation, 56, 86, 206, 257, 315, 374
Self-excitation, hard, 88
Self-excitation, soft, 86
Sever, 259, 266
Signal spectrum, 111
Slow-wave structure, 42, 71, 231, 261, 282, 367
Slow-wave structure, interdigital, 278
Slow-wave structure, periodic, 272
Sorting, anode, 56
Sorting, electron, 56, 310, 373
Space charge in microwave devices, 161, 245, 289
Space charge parameter, 247
Space charge spokes, 313
Space charge waves, 76, 80
Spatial harmonic, 231, 273, 315, 332
Stabilotron, 359
Strapping arrangement, 307
Switch, controllable gas discharge, 412
Switch, high power level, 412
Synchronism, 42, 230, 248, 311
Synchronism, phase, 42, 230
Synchronous tuning, 188

Tetrode, microwave, 116, 145
Transfer characteristic, 255
Triode, lighthouse, 143
Triode, microwave, 116, 119
TR tube, 392, 403
TR tube, bandpass, 404
TR tube, high-Q, 392
Tube, demountable, 409
Tube, double-stream electron-wave, 81
Tube, drift, 149
Tube, electrodeless, 409
Tube, electron-wave, 81
Tuning, electronic (voltage), 91, 172, 213, 278, 343, 354
Tuning, mechanical, 91, 192, 219, 220, 332, 404
Tuning, synchronous, 188
Twistron, 189
TWT, 230, 233, 346
TWT, velocity tapered, 253

Ultron, 360

Velocity, electron, 17, 292
Velocity modulation equation, 64
Velocity parameter, 246
Voltage, ideal waveform of modulating, 73, 75
Voltage-tunable magnetron (VTM), 343

Wave, backward, 231
Wave, cyclotron, 378
Wave, fast cyclotron, 379
Wave, fast space charge, 80
Wave, forward, 231
Wave, slow cyclotron, 379
Wave, slow space charge, 380
Wave, space charge, 76

TO THE READER

Mir Publishers welcome your comments on the content, translation, and design of the book.

We would also be pleased to receive any suggestions you care to make about our future publications.

Our address is:
USSR, 129820,
Moscow, I-110, GSP,
Pervy Rizhsky Pereulok, 2
Mir Publishers

Printed in the Union of Soviet Socialist Republics